Factors shaping the population structure and historical abundance of pinnipeds and penguins

LUKE BENJAMIN BRADFORD HECHT

Factors shaping the population structure and historical abundance of pinnipeds and penguins

Luke Benjamin Bradford Hecht

This thesis is submitted for the degree of
Doctor of Philosophy

Department of Biosciences
Durham University
2022

Abstract

The idea that there is a causal chain between ecological pressures, demographic trends, and the distribution of genetic variation in a population underlies the use of genetic markers to model biogeographic history and conservation priorities. Ecological traits are increasingly being linked to genetic loci in studies of natural selection, but are often only gestured at in studies using neutral markers to study population structure and demographic history. In this thesis, I investigate the modern population structure of the South American sea lion (*Otaria flavescens*) using SNPs derived from reduced-representation genome sequencing (RADseq) and mitochondrial loci, finding no evidence for nuclear structure, but confirming the existence of matrilineal (mitochondrial) structure and suggesting that it may have developed relatively recently. I then show that the populations of *O. flavescens* and a sympatric and ecologically similar penguin species, *Spheniscus magellanicus*, expanded at different times in the mid-to-late Holocene, paralleling recent dietary shifts indicated by analysis of stable isotopes (δ15N and δ13C), possibly towards more benthic prey.

To help identify populations with especially similar demographic histories and try to understand what ecological factors explain their similarity, I developed a program called 'align_stairwayplot.py', which quantitatively compares demographic histories based on a metric combining the magnitude of, and level of model support for, their growth or decline trajectories at aligned time points. With the support of this tool, I found that populations of pinniped and penguin species shared common patterns in their demographic histories that allowed them to be clustered with reasonable accuracy, even with low sample sizes. Antarctic and sub-Antarctic penguins had highly similar demographic responses to the last glacial maximum (LGM), but that the response was weaker in the most ice-tolerant species, the emperor penguin. Globally distributed pinniped species fell into clusters based on the similarity of their demographic histories; their relationships were best explained by differences in latitude from among the factors considered, but conclusions were limited by lack of diet information and small sample sizes with respect to some factors.

Table of Contents

Declaration

The material contained in this thesis has not previously been submitted for a degree at the University of Durham or any other university. The research reported within this thesis has been conducted by the author unless otherwise stated.

Acknowledgements

I am extremely appreciative to the people who have helped me through the process of preparing this thesis, directly and indirectly.

First, I thank my supervisor, Rus Hoelzel, for his advice, assistance, and most distinctly his flexibility as I progressed on my PhD while accommodating personal needs. I also appreciate the supportive lab environment Rus fostered. I particularly thank former lab members – Vania Fonseca, Daniel Moore and Menno De Jong – and my secondary supervisor, Andreanna Welch, all of whom offered invaluable assistance or advice on my project. Thanks also to my progression committee, including Adrian Brennan and Steve Willis, for their reassurance and moral support during setbacks, particularly around the Covid-19 pandemic. I also thank collaborators: Enrique Crespo and Rocio Loizaga De Castro who provided the South American sea lion and Magellanic penguin samples from which DNA was extracted and isotope composition was measured, and Darren Gröcke who carried out the stable isotope measurements.

For much of my PhD and through the present, I also worked at Wild Animal Initiative as a Researcher and Grants Manager. I thank Abraham Rowe, Mal Graham, Cameron Meyer Shorb, Vittoria Elliott, and Simon Eckerström Liedholm for their support as I balanced my work and PhD.

Before starting my PhD, my scientific thinking and confidence was greatly improved by the mentorship of Benjamin Rosenthal and Peter Thompson at the US Department of Agriculture. The fourth chapter of this thesis would not have happened without them.

Finally, I thank my wife, Lily. Being apart when I had to be in Durham for lab work was the hardest aspect of completing this degree.

List of Figures

List of Tables

Chapter 1: General introduction

Overview

This thesis seeks to understand changes in genetic diversity and population structure over time, and how they relate to demographic, behavioural and ecological processes. These relationships are important to understand for their scientific and practical value, especially because assumptions about them underly the use of population genetics tools and markers to model biogeographic history and conservation priorities. In particular, I aim to better understand whether the demographic histories of populations, as reconstructed from genetic data, can be informatively compared with each other or with other historical trends in their environment, and how consistent the patterns revealed are. This in turn should contribute to understanding how important various ecological and biological factors are or have been in determining the abundance and distribution of species, or even of groups of species with shared traits.

Processes controlling population dynamics

Wild populations are generally assumed to be in equilibrium with the pressures of their native habitat, in both the evolutionary sense of being as well-adapted as their available genetic variation allows and the demographic sense of their population size being relatively constant throughout their range. The concept of equilibrium implies a balance between the processes that add and remove individuals or genetic variation from a population. Populations grow by gaining individuals through births or through immigration from other populations, and they decline when a larger number of individuals are lost through mortality or emigration to other populations. These processes occur on the scale of individuals, but they can be quantified at a range of spatial and temporal scales. An equilibrium must also be defined and measured relative to a specific spatial and temporal scale. For example, in a hypothetical population where births occur in the spring and most deaths occur over winter, a monthly census over the course of a single year would suggest a population out of equilibrium. However, an annual census carried out over the course of a decade might show that, despite seasonal oscillations, the average population size is constant.

Similar logic applies to different spatial scales, and understanding the scale of equilibrium dynamics is critical for studying and managing populations. For example, Brzeziecki et al.

(2016) reported evidence of population decline and non-equilibrium age structure in multiple tree species across five transects totalling a few hectares each within the boreal coniferous forest of Poland's Białowieza National Park. From this, they concluded that strict protective management of the forest was actually leading to its decline by preventing the recruitment of younger trees. However, Jaroszewicz et al. (2016) showed that the area Brzeziecki considered was too small to draw useful conclusions about equilibrium states because forests of this type are expected to display distinct patch dynamics where a whole stand of trees may be composed of one or a few cohorts of similar age. Stands of old trees may be matched by stands of young trees elsewhere such that, over the forest as a whole, the population remains constant over generations.

Metapopulation theory describes how relatively consistent large-scale population dynamics can emerge from more varied dynamics within and among subpopulations that are demographically linked by varying rates of migration between them (Hanski 1998). Subpopulation dynamics may be purely stochastic, such as when only one subpopulation faces a disturbance event (e.g. flooding) in a given year, despite all subpopulations having an equal annual probability of disturbance. Different dynamics can also result when subpopulations differ in the quality of their habitat patch or the fitness of their inhabitants. For example, if excessive competition occurs in one subpopulation on prime habitat, less competitive individuals may be forced to emigrate to another subpopulation and live on poorer-quality habitat. Owing to its poor-quality habitat and the low relative fitness of its inhabitants, this subpopulation may receive more migrants from other subpopulations than it produces each generation. This is termed a source-sink dynamic (Figure 1.1).

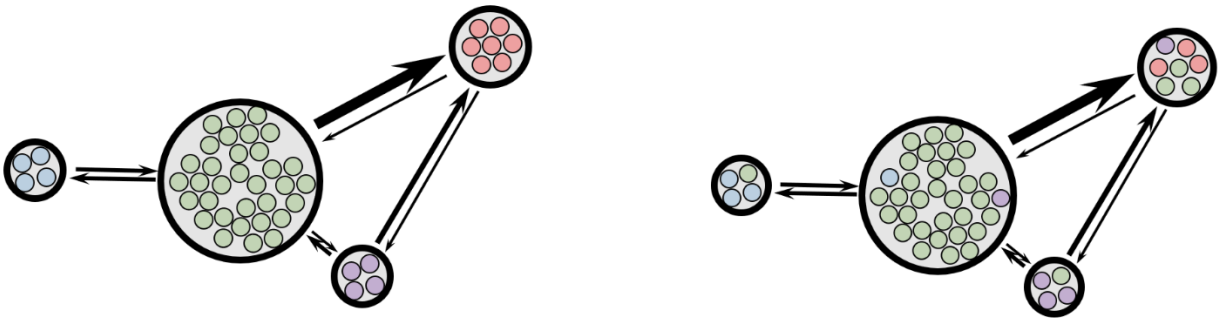

Figure 1.1. Four subpopulations connected by bidirectional migration (rates represented by arrow width). Left shows the population at the beginning of a generation, with individuals colour-coded by their subpopulation of birth. Right shows the population at the end of the generation, following reproduction, migration and death. The total size of the metapopulation and each subpopulation is maintained by density-dependent migration despite different growth rates (births-deaths) in each subpopulation. Most notably, the upper-right (red) subpopulation is a sink sustained by immigration from the central (green) and bottom-right (purple) subpopulations.

Source-sink dynamics are thought to be fairly common in the wild, such as between populations at the core and periphery of their species' range, and for species with non-contiguous ranges where habitat can vary significantly in quality (Furrer and Pasinelli 2015). With the expansion of human-dominated land-use types leading to range fragmentation, many wild animals are forced to transit increasingly hostile matrices (e.g. roads, suburbs) to reach suitable habitat and mates (e.g. Andreasen et al. 2012). Marine animals could also find their populations becoming more separated as a result of climate change or other human activity altering the distribution of their prey and/or breeding grounds, or the local reproductive surpluses that lead some individuals to emigrate (e.g. Carroll et al. 2020).

Linking population dynamics to population genetics

Similar to the dynamics of population size, a population's genetic diversity can grow, shrink, or achieve an equilibrium based on the relative strength of processes that add or remove variation. The diversity of gene combinations harboured within a population can increase through mutation, which produces novel gene variants ("alleles"); sexual recombination between the genomes of native individuals, which can produce novel allelic combinations; and immigration of

genetically distinct individuals from other populations. Populations lose genetic diversity through the death, emigration, or reproductive failure of individuals bearing rare alleles or allele combinations. Most of the time, the specific genetic makeup of these individuals has no influence on the outcome. In these cases, any effect on the frequencies of particular alleles is random, and the process is termed “genetic drift.” Many rare alleles are lost from populations by chance in this way. Sometimes, individuals die, emigrate (e.g. to “sink” populations), or fail to reproduce for reasons that are linked to their genetic makeup (natural selection). In these cases, specific alleles may fall in frequency or be lost from the population due to their effects or associations, while competing alleles of the same genes rise in frequency. In general, natural selection reduces the average number of offspring that individuals expressing certain alleles will contribute to future generations, relative to individuals with more beneficial genes. The effects of natural selection on specific genes are often subtle and difficult to predict, but the accumulation of mutations and the loss of alleles via random genetic drift can be quite predictable. Under conditions of long-term stability, a balance can be reached between these processes, leading to a relatively constant abundance of genetic variation known as mutation-drift balance (Schneider et al. 2016).

Demography is linked to the genetics of a population via the concept of effective population size (N_e). A population’s effective size is equivalent to the census size (i.e. the true number of individuals) that would be required for an idealised population to harbour the same level of genetic diversity. In this context, an “idealised” population is one where any individual has an equal probability of mating with any other individual, and which has maintained its current size long enough to reach an equilibrium between the addition of genetic variation by mutation and the loss of variation by genetic drift (Wright 1931; Fisher 1930). In such a population, merely counting the number of individuals (N) should be enough to predict the average number of genetic differences between any two of its members (nucleotide diversity θ), given a known mutation rate (μ), by solving the equation $\theta = 4N\mu$.

Effective population size

The complexity of these processes in the real world has motivated the use of the abstract metric of effective population size. In nature, N_e is almost always less than the census size, N_c (James and Eyre-Walker 2020). Many factors can lead to the violation of the simple condition of non-random mating. For example, some species have an unequal ratio of males to females, which

reduces the number of unique reproductive pairings possible in the population. Individuals may also leave unequal numbers of offspring to the next generation, whether by pure chance (genetic drift) or as a result of their heritable phenotypes (natural selection). A population's history can also skew its effective population size to be less than its census size. This occurs because genetic variation takes time to accumulate; moreover, the rate at which it accumulates is limited by the number of individuals and amount of genetic variation already present in the population. For example, if a population passes through a temporary bottleneck that reduces its population by an order of magnitude, many of the rarest alleles are likely to be lost by chance (random genetic drift). Even if the population recovers demographically fully by the next generation, those newly born individuals will all reflect the genetics of the small number who survived the bottleneck. The recovery of the population's genetic diversity - and therefore its effective population size - will depend on the occurrence of new mutations and the recombination of ancestral alleles that passed through the bottleneck, or on the introgression of alleles from immigrants. Because genetic diversity can be reduced much faster than it can be recovered, populations' effective sizes are most affected by the low points of their geologically recent history. Cheetahs represent a classic example of this. Their extant population, now located in Africa, have been affected by two severe bottlenecks, the first associated with migration out of North America approximately 100,000 years ago, and a second ~10,000 years ago at the same time as many other large mammals went extinct (Dobrynin et al. 2015). Despite demographically recovering to a size of hundreds of thousands of individuals at their recorded peak, their genetic diversity remains extremely depleted, leading to inbreeding effects such as harmful genetic conditions, susceptibility to infectious outbreaks, and relatively high juvenile mortality, even in captivity (O'Brien et al. 2017). The recovery of cheetahs' genetic diversity from this bottleneck has also been slowed by high variance in reproductive success among individuals (Kelly 2008). In general, effective population size is expected to be proportional to the harmonic mean of historical census sizes, all other conditions (e.g. random mating) being equal (Nei et al. 1975; Motro and Thomson 1982). For example, in species exhibiting cyclical population dynamics, their long-term effective population size is related to the low points their census size reaches during "crash" phases of their cycle. Chapuis et al. (2009) quantified the genetic diversity of migratory locust *Locusta migratoria* populations worldwide, some of which had recently undergone explosive, yet temporary growth in population size, and found that a population's outbreak history was not predictive of genetic diversity. On the other hand, Kaeuffer et al. (2007) found that feral sheep in an island population that experienced regular population crashes associated with winter weather had a higher effective population size than expected

based on the frequency and severity of these crashes, which the authors attributed to a reduction in variance in male reproductive success during those periods for surviving males. This sort of negative feedback loop, where one N_e-reducing factor is weakened during periods when another is strengthened, could buffer the effective population size against crashes.

Another factor that can limit a population's effective size relative to its census size is population structure. Geographic barriers or differences in foraging or mating behaviour may skew the probability of pairings between individuals. In the previous section, the concept of a metapopulation was introduced, where subpopulations exhibit partial demographic independence, exchanging migrants with other subpopulations at a certain rate (Figure 1.1). In a population genetic sense, subpopulations can be further defined as groups of individuals within a population that are more likely to mate with each other than with individuals from outside their group. Over time, this mating bias would be expected to lead to greater genetic similarity among individuals in the same subpopulation. Wright developed a system of indices to quantify the degree to which genetic variation is unequally distributed within populations, including among subpopulations. If two subpopulations host the same alleles at identical frequencies, their fixation index (F_{ST}) will be 0. At the opposite end of the scale, two subpopulations sharing no alleles in common will have an F_{ST} of 1. In practice, population structure can be assessed by comparing the genetic distance between individuals from different subpopulations to the nucleotide diversity among individuals within the same subpopulation.

What happens when the environment changes?

So far, I have introduced the concepts and processes that control the short-term dynamics and genetics of a population and how these in combination can shape a population's equilibrium state. Environmental change shifts the goalposts of any such equilibrium, and is therefore expected to induce demographic and/or evolutionary changes, including adaptation, migration, and population growth or decline. The precise effects of environmental change on a given population are in turn modulated by ecological and life history traits, such as reproductive rate and dispersal capability (Cayuela et al. 2018).

An outstanding question in ecology and evolution concerns the rate and frequency with which populations typically grow and decline over geological time. Do populations most often grow/decline gradually in response to continuous incremental changes in their environment

(abiotic and biotic), or is it more common for population sizes to remain relatively constant for centuries at a time, occasionally punctuated by rapid readjustments to new regimes?

Populations can adjust demographically very fast in response to an instantaneous change in their carrying capacity. For example, the population of the South American sea lion (*Otaria flavescens*) is estimated to be growing at up to 5.5% per year since the end of legal hunting in 1974. Assuming that rate was sustained, ~43 years would be required for the population to grow by an order of magnitude, i.e. a factor of ten (Romero et al. 2017). Based on the demographic vital rates (age-specific fecundity and survival) estimated for a healthy population of North American black bears (*Ursus americanus*) in Colorado, it would take an estimated ~68 years for their population to grow by an order of magnitude (Lewis et al. 2014). However, as we have seen, it can take much longer for N_e to catch up. Assuming a closed population, where mutation is the only source of new variation, it would take >1000 years for the effective size of the black bear population to approach its new census size (N_e~N_c). This is based on equations (based on the idea that effective population size can be approximated by the harmonic mean of a population's past census sizes; Wright 1938) from Nei et al. (1975), who modelled a scenario in which a *Drosophila* population takes more than one million generations for its average heterozygosity to recover after an extreme founder event by two individuals. It has also been estimated that, following the explosive growth of the human population over the past few centuries and millennia, it would take billions of years to generate the amount of genetic diversity commensurate with our current census size (Kliman et al. 2008). In many natural cases, a metapopulation structure with migration between local populations can help accelerate both demographic and genetic recovery through the introduction of foreign alleles by migrants (e.g. Ims and Andreassen 2005; Cammen et al. 2018). For example, that recovering population of black bears in Colorado will likely attract or come into contact with other, older and more stable black bear populations and mix with them genetically, which could rapidly accelerate the Colorado population's genetic recovery.

With exponential growth, populations can almost always grow or shrink rapidly (relative to geological time) in response to changing conditions to reach a new demographic equilibrium or carrying capacity. Therefore, whether changes in population size occur gradually or in a punctuated manner over a geological timescale may not be limited by population dynamics so much as ecosystem dynamics. A population's carrying capacity is shaped by its environment, including abiotic factors like climate and landscape (e.g. availability of suitable breeding sites),

and biotic factors like abundance of prey, competitors, and other density-related factors such as disease spread. Some of these variables are correlated or anti-correlated, and some may be independent. Some may change in the same direction, but at different rates. This heterogeneity has the potential to bring about abrupt changes in a population's equilibrium state. If carrying capacity changes gradually, then demographic change will be gradual. On the other hand, if there are 'tipping points' (Lenton 2013) or 'regime shifts' (Woolway et al. 2017) in climate, or a different resource becomes limiting (Jentsch and White 2019), or another species (prey, predator, competitor) is introduced or goes extinct (Parmesan 2006), or new habitat opens up (Matthiopoulos et al. 2005; de Bruyn et al. 2009), then the ability of the environment to support a population of a given size may change abruptly. How fast do carrying capacities typically change? As in the debate between "gradualism" and "punctuated equilibrium" in macroevolution, there is probably no universal answer, but rather a spectrum of context-dependent outcomes (Barnosky 1987). Ecological disturbances of these sorts occur frequently, implying that abrupt shifts in carrying capacity are common.Yet, as discussed above, the resulting demographic change will almost always leave a more gradual imprint on a population's genetic diversity (corresponding to the harmonic mean of past population sizes).

Ecological and life history toolkit

A species' ecological and life history traits can be thought of as an evolvable "toolkit" that constrains its range of possible responses to a given environmental change. Ecological traits, including their physiology and dietary preferences, largely determine the direction of their demographic response, whether changes in the environment are beneficial or deleterious. Life history traits then constrain the rate and mechanism(s) of that demographic response. For example, a species where reproductive adults disperse widely (owing to a combination of ecological and life history adaptations) may be able to exploit the opening of a remote new habitat (e.g. Southern sea lions: de Bruyn et al. 2009). On the other hand, in species with similar capabilities but stronger site fidelity behaviour or less intense density-dependent competition, suitable habitat may be left uncolonised for longer (Matthiopoulos et al. 2005; e.g. Adélie penguin *Pygoscelis adeliae*: Southwell et al. 2021). More fundamentally, species with a faster net reproductive rate (e.g. higher fecundity) can potentially complete their demographic response to an environmental change within fewer generations than another slower-living species would require (Romiguier et al. 2014; Healy et al. 2019). Even though a population's genetic response (change in N_e) will always lag behind its pure demographic response (change

in N), the rate of a demographic response may still have a significant effect on the time required for that genetic response, since a larger population means more mutation to regenerate variability after a bottleneck. Likewise, a reduced population, whether during a temporary bottleneck or at a new lower carrying capacity, takes time to lose the variation it previous harboured (Nei et al. 1975; Nei and Tajima 1981; Luikart et al. 2002; Romiguier et al. 2014). Species with high intrinsic reproductive rates are able to recover more rapidly from a population crash, allowing them to sustain higher average population sizes over time relative to a given disturbance frequency. This may help explain why highly fecund species are generally more diverse than slower-reproducing species (Romiguier et al. 2014).

While life history traits clearly influence the rate of demographic and genetic responses to perturbation, and may affect the mechanism(s) of those responses, it is less obvious whether life history traits influence the direction - growth or decline - of a population's response. One way this could happen is if a species' life history strategy allowed for reproductive investment/potential to be effectively stored up, buffering against downturns. Examples of this may be found in capital breeders, like Southern elephant seals and some bears which, among other taxa, have evolved a tactic of intermittent breeding (Desprez et al. 2017). North American black bear (*Ursus americanus*) mothers, for example, may defer reproduction in a given year if they have not reached a threshold of weight gain that will allow them to sustain their cubs and themselves through the winter and into spring (Robbins et al. 2012). This sort of effect would only buffer against hard times lasting less than a generation, but that could be significant for iteroparous species with late maturity and long generation times. This sort of effect would also not be able to convert a period of decline into a period of growth, it could merely stabilize the population against a weak downturn.

A third element potentially driving or moderating demographic change is a species' ecological dependencies. Environmental change need not directly impact the organisms in question (e.g. by causing them to freeze to death), but can be mediated by effects on other ecological dependencies, such as predators, prey, symbionts, hosts, or competitors. In general, the propagation of population dynamics from one species to another that feeds on or is fed upon by it is known as a trophic cascade or trophic shift (Madenjian et al. 2013). Decline in the population of a competitor, predator, or parasite can trigger a demographic "release" in a focal species (Torchin et al. 2003; Torchin and Lafferty 2009). On the other hand, decline in the abundance of prey, hosts or beneficial symbionts could cause the population of the focal

species itself to decline, with this effect being much stronger against highly specialised predators/pathogens than against generalists (e.g. Ferrer and Negro 2004).

Molecular ecology

The field of molecular ecology is preoccupied with the analysis of molecular markers - components of organisms' biochemical makeup, including their genetics and the isotopic composition of their tissues - to make inferences about their evolution, behaviour and history that might otherwise be difficult or even impossible to observe. This primarily owes to the fact that some types of molecular changes accumulate over time. For example, genetic differences between individuals and populations accumulate over generations, while chemical differences analysed in stable isotope biogeochemistry can accumulate over the lifetime of an individual. By understanding the processes that govern their variation and accumulation, researchers can make inferences about history even when they are limited to samples corresponding to a single slice of time. For example, the radio signals used by animal-borne telemetry devices are attenuated by water, reducing their effectiveness for tracking animals during dives. The devices also have short lifetimes in some species, including sea lions, due to being lost, removed, damaged, or their batteries expiring (Riet-Sapriza et al. 2013). However, some of the questions telemetry is intended to answer can also be addressed by molecular analyses. Juvenile dispersal distances could be inferred retrospectively by measuring the stable isotopes assimilated into the bodies of adult individuals (Zenteno et al. 2013). Or, they could be studied over a longer term, with coarser resolution, by quantifying gene flow between populations. All these methods can provide independent lines of evidence at different scales and resolutions, and with situational advantages and disadvantages. On the other hand, drawing accurate ecological inferences from molecular markers requires a strong theoretical foundation, with mechanistic models of the processes that shaped your observed markers.

One such theoretical foundation, coalescent theory, has been pivotal for enabling the reconstruction of historical demography from population genetic data. Coalescent theory essentially models population genetics in reverse, describing the distribution of ages of alleles in a population – the time since they shared a common ancestor, or "coalesce" (Kingman 1982a,b). The average time to coalescence for a randomly selected pair of alleles is defined as $2N_e$ generations (i.e. 2N generations in an idealised population; Wright 1931). Time to coalescence can be measured by creating gene trees from molecular data sampled from many

individuals. Just as species trees permit estimation of speciation rates over geological time, it is possible to recognise changes in coalescence rate from a gene tree based on the density of nodes (coalescence events) with respect to time (Rosenberg and Nordborg 2002; Kuhner 2009). Given that the average number of generations to coalescence is equal to twice the effective population size, it may be inferred that a population was effectively smaller during periods when the estimated rate of coalescence was higher. That is to say, assuming the null model of the coalescent, where a population is evolving by neutral genetic drift alone, a population's demographic history can be reconstructed from a genetic sample by analysing the interval between coalescences (i.e. genealogical nodes) over time under the mathematical expectation that coalescence to an ancestral allele occurs more rapidly in smaller populations. On the other hand, recent natural selection on the genes being analysed would violate the null model of the coalescent. Selective sweeps can leave coalescent signatures that are difficult to distinguish from population bottlenecks without examining many genetic loci (Galtier et al. 2000).

Demographic history reconstruction

Demographic history has most often been studied using model-constrained methods, which require researchers to hypothesize a specific demographic history (e.g. "stability, then a bottleneck, followed by rapid expansion"), the parameters of which (e.g. the timing and severity of the bottleneck) are estimated based on how well results simulated under a given set of parameter values correspond to the actual data. With growing computer power, model-free methods that test a much wider range of possible demographic histories than a human researcher could hope to come up with have become increasingly feasible. A leading method of this type is the Bayesian Skyline Plot (BSP), introduced in 2005 by Drummond et al. Earlier methods took as input a single consensus genealogy, rather than the nucleotide data that genealogy was based on, and inferred effective population sizes without accounting for uncertainty in any of the data or calculations, essentially because the computational impossibility of considering every possible outcome of the coalescent. The BSP's main innovation was the use of Markov chain Monte Carlo approximation to sample the range of possible histories given an input DNA alignment and nucleotide substitution model. This sampling procedure permits confidence intervals on each interval of the reconstructed demographic history, resulting in smoother and more accurate inference overall because uncertainty has been accounted for. The BSP has also been extended (Extended Bayesian

Skyline Plot; EBSP) to permit analysis of multiple loci simultaneously (Heled and Drummond 2008; Ho and Shapiro 2011).

This capability for multilocus analysis is extremely important for accurately and precisely reconstructing demographic history. Allele coalescence is an inherently stochastic process. For example, on average, in a population of constant size, the average time to coalescence of a randomly chosen pair of alleles is equal to $2N_e$ generations, while the expected coalescent time of all sampled alleles is less than $4N_e$ generations (Tajima 1983). Departure from this expected *average* rate is what coalescent-based methods use to infer historical departures from a constant population size. However, each locus is an independent roll of the dice, and some will depart from the average rate simply by chance (Figure 1.2). To avoid inaccurately calling a population size shift based on patterns observed in a single locus, methods like the BSP have to internalize this uncertainty, trading precision for accuracy in their reconstructions of demographic history in the form of wide confidence intervals. Therefore, it is preferable when possible to incorporate data from multiple independent loci, using capable methods like the Extended Bayesian Skyline Plot (EBSP).

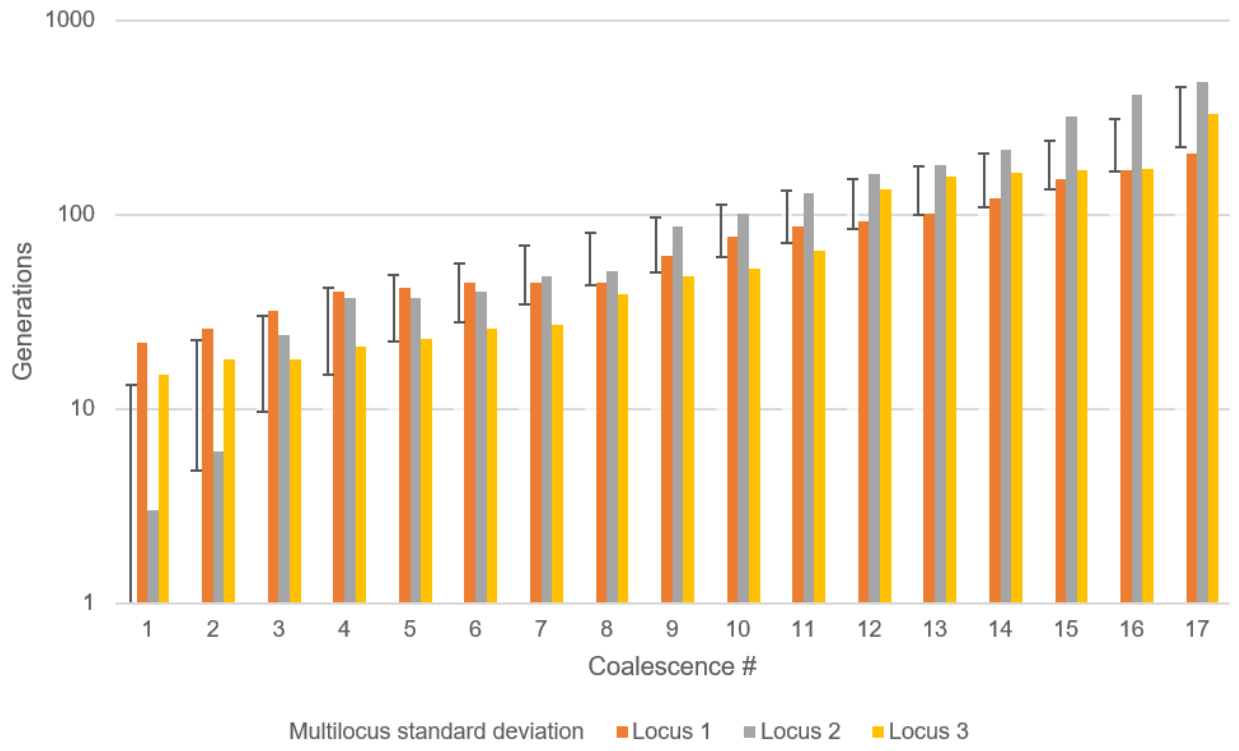

Figure 1.2. The average number of generations between coalescence events in a sample depends on the effective size of the population the samples were drawn from. However, because genetic loci are inherited more or less independently, the distribution of coalescence times can be quite different by chance, as if reflecting different demographic histories. In the Figure Bove, the error bars represent the standard deviation relative to the average number of generations to each sequential coalescence event up to 17, over 100 simulated loci. The coloured bars show the distribution of coalescence times for three randomly selected loci. These data were simulated using a custom program based on the simplest equations for the coalescent in a constant size population.

In addition to predicting the distribution of genetic differences among a sample of DNA sequences, the coalescent can also be used to predict the distribution of allele frequencies, known as the site frequency spectrum (SFS), of a population of constant or changing size. For example, a population that has very recently experienced a bottleneck is expected to have an excess of intermediate-frequency alleles, as rare alleles existing prior to the bottleneck will have been disproportionately lost via random genetic drift. As the population begins to genetically recover, an excess of very rare (singleton) alleles may be expected to appear, representing new

mutations. The Stairway Plot method takes advantage of this relationship, and the incredibly simple data structure of an SFS, to enable model-free inference of demographic history from whole-genome datasets based on hundreds of individuals (Liu and Fu 2015).

Linking demographic history to environmental factors

Population bottlenecks often result from major ecological events, such as glaciation, but there are other more consistent ecological determinants of population size and connectivity that thereby shape the coalescent process and demographic history. For example, Zhou et al. (2014) found that the demographic history of leaf-eating snub-nosed monkeys (*Rhinopithecus roxellana*) correlated much more closely with that of leaf-eating pandas than of its congeners, suggesting diet as a historically primary factor in how the population fared. Presumably, if this interpretation is correct, the demographic histories of the plants they eat would also be correlated. Groenen et al. (2012) showed that the effective population size of wild boar (*Sus scrofa*) grew after boar from Asia first colonised Europe, relatively free from competition. European and Asian populations both experienced bottlenecks around the time of the last glacial maximum (LGM, ~18-24 Kya), though the bottleneck was stronger in Europe, probably due to more extensive glaciation.

Demographic history reconstruction and phylogeography are two related population genetics-based approaches that have been used to predict populations' responses to contemporary climate change by extrapolating from the inferred responses of ancestral populations to similar environments. Such implications have been recognised with approval by many authors (e.g. Miller et al. 2012 and Alberto et al. 2013), although fewer have explicitly ventured predictions.

Galbreath et al. (2009) attempted to derive predictions from their analysis of the historical demography of American pika (*Ochotona princeps*) by comparing it with a model that predicts suitable habitat space based on climatic conditions. The pika is a small mammal that is typically confined to high-altitude, low-temperature environments characterised as 'sky islands' due to the lack of connectivity between different mountain peaks. These authors found that although – according to the ecological niche model – pika populations inhabiting different peaks were often isolated during warm climate periods, genetic populations were primarily differentiated by mountain range, with smaller-scale peak-to-peak differences presumably being swamped out by gene flow during cooler periods that allowed the populations inhabiting adjacent peaks to

reconnect. This history bodes well for the preservation of genetic variability in this species, so long as warming temperatures do not force its habitat off even the tops of mountains. BSP analysis indicated effective population size decline over the Holocene interglacial period in all studied lineages, from northern and southern mountain ranges of North America, and suggested a stronger positive effect of the LGM in more northern populations, as expected. However, contrary to the authors' expectations of very recent population growth in the north, in response to northward range expansion, none was evident in the demographic history plots. Instead, northern and southern populations all appeared to have declined recently.

It is not always clear whether situations like this demonstrate the importance of coalescent-based demographic history analysis as a line of evidence or reveal its limitations. In this case, the disagreement could be due to the countervailing effect of population structure, as several simulation and modelling studies (Heller et al. 2013; Mazet et al. 2016) have shown that demographic histories reconstructed based on samples from only a small fraction of the subpopulations ('demes') within a metapopulation can inaccurately suggest that the population declined when in fact it remained stable. A more "scattered" sampling scheme, where only one or few samples are taken from each subpopulation, can avoid this problem, but results in less power to resolve recent demographic history because recent coalescence events among the sample's ancestors will be relatively rare unless migration is very frequent

Ancient DNA

As remarkably effective as coalescent modelling can be at reconstructing the historical relationships among modern samples, the inferred demographic history is susceptible to certain biases and uncertainties. Accuracy and precision can be dramatically improved by the inclusion of true ancient DNA samples as calibration points for coalescence and mutation rates, and to directly estimate the genetic diversity ($=4N_e\mu$) present at a specific point in history. Mutation rate calibration is especially important for reconstructing relatively recent demography, because long-term mutation rates tend to appear lower than short-term ones due to processes such as slow sorting by selection of nearly neutral alleles, and homoplasy (Orlando and Cooper 2014). This emphasises the need for accurate dating of ancient samples. Several coalescent simulation programs have been specially designed or modified to incorporate ancient, time-calibrated samples. A pioneer in this regard was SerialSimCoal, which tests user-defined models of demographic history (Hadly et al. 2004). Since then, the program BEAST has

accommodated ancient DNA in its model-flexible EBSP method (Heled and Drummond 2008; Ho and Shapiro 2011).

Prost et al. (2010) applied Bayesian coalescent methods to a combination of ancient and modern DNA to reconstruct the demographic history of a small arctic mammal, the collared lemming (*Dicrostonyx torquatus*). They found a general population decline associated with climate warming following the LGM, with a particularly strong impact around the Greenland Interstadial 1 period, ~14.5 Kya. They also infer more recent local population bottlenecks from a relative paucity of heterozygosity and net extinction of haplotypes (from seven at the dawn of the Holocene to three in the modern population). On the basis of these apparent impacts of historical climate change, the authors warn of further declines in genetic diversity resulting from future climate change against a species that has already lost much of its raw material for adaptation.

Ancient DNA is also required for inferring local extinctions, since by definition, no contemporary samples exist (Chang and Shapiro 2016). Even with ancient samples, the signal of extinction can still be challenging to interpret. For example, if the structure of an ancient metapopulation is neglected or misunderstood, the genetic signal of extinction could be masked. If all subpopulations decline in concert, a decrease in population size may be accompanied by a decrease in subpopulation connectivity (migration rates). This can lead to greater pairwise genetic distance between individuals and the illusion of a growing population, which may drown out the signal of overall population decline. Orlando and Cooper (2014) showed that geographic sampling bias can fundamentally alter the shape of a species' inferred demographic history curve, while the analyses of de Bruyn et al. (2009) highlight the importance of meaningfully grouping samples into populations in order to reconstruct true demographic history.

The most significant challenges specific to ancient DNA analysis come from chemical damage and contamination that can accumulate over the centuries prior to its analysis (Dabney et al. 2013; Orlando et al. 2021). It is common for DNA strands to break into ever smaller fragments over time, limiting the maximum length of sequencing reads. More perniciously, some types of damage can be misinterpreted as genuine genetic differences, such as when cytosine bases are deaminated to uracil, which may then be misinterpreted as a C-to-T substitution. This can potentially bias reconstructions of demographic history, especially when the true variability of the ancient population is low relative to the amount of damage (Axelsson et al. 2008). Programs

have been developed to account for the likelihood of these changes in variant-calling (e.g. Zhou et al. 2017), and results are mixed on how much ancient DNA damage skews results in different datasets (Rambaut et al. 2009). For example, Axelsson et al. (2008) addressed this question by removing transitions (C-to-T and G-to-A substitutions) from an ancient bison dataset and checking how that affected the resulting inference of demographic history. They found that the resulting demographic history was constant, which they interpreted as showing that the apparent population expansion and recent decline that featured in the original reconstruction were artefacts of aDNA damage. However, the signal of this demographic history could have been lost simply because the discarding of transitions resulted in a loss of statistical power. Even though it is not possible to distinguish specific transitions that were caused by post-mortem damage from true transition mutations, it is unlikely to be the case that all transitions were caused by damage (Rambaut et al. 2009). To test this, Rambaut et al. (2009) simulated DNA damage and evolution jointly, and found that after a plausible rate of post-mortem damage was accounted for (as opposed to writing off *all* transition substitutions), the original demographic history was largely unchanged.

Contamination is not uniquely a problem of ancient DNA, and is usually easy for next-generation sequencing read-mapping software to recognise when it comes from distantly related species, such as bacteria (Peyrégne and Peter 2020). However, in poorly preserved ancient samples, the concentration of exogenous (contaminating) DNA may exceed the concentration of endogenous (native) DNA. All of this non-target noise makes the process of amplifying and sequencing the target DNA less efficient. The level of sequencing effort that is therefore required to obtain usable data from target ancient DNA also has the potential to amplify minute amounts of contaminating DNA from other ancient or modern samples being analysed in the same vicinity (Peyrégne and Prüfer 2020). This kind of contamination would not be easy for standard software to recognise and exclude, and so steps must be taken to mitigate cross-contamination of samples during laboratory methods when working with ancient DNA (Orlando et al. 2021), such as using separate workspaces for modern and ancient samples, frequent cleaning of pipettes and surfaces, and even combining multiple DNA extractions and amplifications to make apparent mutations introduced by damage or contamination more obvious (e.g. as apparent heterozygosity in a haploid marker like mtDNA).

Study system

This thesis focuses on the coastal ecosystem of Argentina; specifically, as experienced by the South American sea lion *Otaria flavescens* and the Magellanic penguin *Spheniscus magellanicus*. I adopt a historical perspective, considering how these species have responded to a changing environment since the Last Glacial Maximum, through the Holocene, to the present.

Ecological similarities and differences of *Otaria flavescens* and *Spheniscus magellanicus*

The South American sea lion and Magellanic penguin both depend on the marine ecosystem for food, while also keeping one flipper on land so to speak, as they haul out onto beaches to breed. Terrestrially, the species also exhibit different habitat preferences. For example, the penguins select sites on slopes with dense, ideally clay-based substrate, into which they build burrows (Stokes and Boersma 1991). Gravel and sand beaches support less stable burrow constructions, so chick mortality by flooding and collapse can be common. In contrast, the sea lions favour relatively flat open beaches of gravel or sand, ideally with tidal pools for thermoregulation (Campagna and Le Boeuf 1988; Fernández-Juricic and Cassini 2007). These differences in terrestrial habitat preference lead to the two species occupying different sites for breeding along the coast of Argentina, and could cause their populations to respond differently to environmental changes affecting the availability of habitat with these characteristics.

Considering that we are comparing a mammal and a bird, there are also dramatic differences in life history and breeding system between the two species. For example, social monogamy is common among Magellanic penguins, with pairs of penguins cooperating to raise chicks year after year; though extra-pair mating is also common (Marasco et al. 2020). Most South American sea lions, in contrast, have a generally polygynous mating system, where males strive to defend beach territories within which they control and mate with multiple females, while males who have failed to claim territory of their own occasionally form groups and raid beaches to seize them or individual females (Campagna and Le Boeuf 1988; Soto and Trites 2011; Franco-Trecu et al. 2015). These differences in life history and breeding system may lead to differences in the proportion of the population who manage to breed in a given year (N_e:N_c), as well as the sensitivity of the species' population growth rates to different life history parameters, such as juvenile survival (Finkelstein et al. 2010; Maniscalco et al. 2015; Gownaris and Boersma 2019).

In particular, the polygynous breeding system of the sea lion, where a large proportion of pups receive their paternal DNA from relatively few males, is expected to lead to a lower N_e:N_c ratio than in the penguin, and therefore slower genetic response to demographic changes, all else being equal.

Modern climate change is already affecting the Magellanic penguin through extreme weather events that have directly increased juvenile mortality (Boersma and Rebstock 2014). Extreme pup mortality was also documented in *Otaria flavescens* following intense El Nino events, such as the one in 1997 (Soto et al. 2004; Oliveira et al. 2012). Juvenile mortality has also been increased indirectly by climate change, as parent penguins are required to travel increasing distances from their historic breeding colonies to find prey that are already shifting their range in response to climate-induced changes in the marine environment (Boersma and Rebstock 2009). If Magellanic penguins and South American sea lions are tracking the same prey, the sea lions may suffer similar effects.

Coastal Argentina since the Last Glacial Maximum

The Last Glacial Maximum (LGM), around 18-24 Kya, saw extensive glaciation at high latitudes. An ice sheet covered inland Patagonia and extended to Tierra del Fuego at the southern tip of the continent (Waldmann et al. 2009). However, the Atlantic coast of Argentina north of Tierra del Fuego was never glaciated. The coast did, however, still experience a global drop in sea level and temperature, and altered sedimentation due to altered precipitation and the glaciation occurring further inland. During the LGM, much of the continental shelf was exposed; thus the actual palaeo-coastline was farther east into what is now the Atlantic, a conclusion supported by sedimentation, landscape modeling, and palaeoclimatic indicators (Ponce et al. 2011; Violante et al. 2014; Berman et al. 2016) (Figure 1.3).

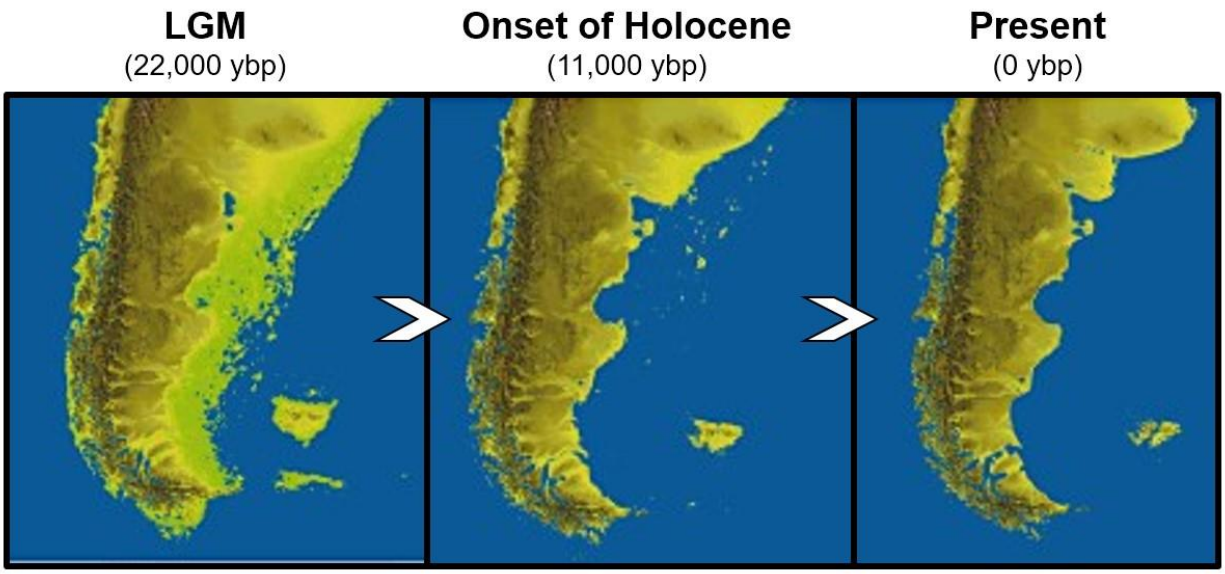

Figure 1.3. Evolution of the Argentine coastline from the LGM to present. Adapted from Ponce et al. (2011). The coastline during the LGM was more broken up, but its large-scale profile straighter and connected than it has been since the Holocene onset, with the modern coast featuring more distinct bays separated by various peninsulas.

The transition from the LGM into the early Holocene was characterised by global warming, glacial retreat and sea level rise (Jouzel et al. 2007; Berman et al. 2016). Warm temperatures, with increasing humidity, prevailed in the region during the early-mid Holocene (>6 Kya), but the climate has cooled over the most recent 6,000 years (Waldmann et al. 2009; Kaplan et al. 2016).

The Atlantic coast of Argentina has a broad continental shelf, which - under modern conditions - intersects several major marine fronts. Marine fronts are features where water bodies with different properties mix while maintaining sharp boundaries (Acha et al. 2004). These boundary waters tend to be very productive, due to the high nutrient content of upwelling waters and the way the currents concentrate plankton, attracting fish and higher predators. For example, Mauna et al. (2011) sampled benthic organisms along a transect intersecting the highly productive shelf-break front off the coast of northern Argentina, near Mar del Plata. They found that sampled organisms differed in their carbon and nitrogen isotopic signatures according to their proximity to the front boundary, specifically becoming more enriched in δ13C and depleted

in δ15N nearer the front, consistent with phytoplankton being concentrated by marine conditions along the front.

Because fronts are defined by sharp transitions in conditions such as temperature and salinity, they can define the range of small prey and possibly serve as reference points for navigation of larger fish (Acha et al. 2004; Alemany et al. 2014). Thus, marine fronts become important even to the marine mammals and birds who predate these smaller animals. For example, elephant seals from northern Patagonia travel far to forage along the Antarctic Polar Front and the front formed far from shore along the continental shelf of South America (Campagna et al. 1998). Marine fronts also occur nearer to shore. For example, fronts occur east and north of the Valdés Peninsula, creating distinct bodies of water in the San Matías Gulf (Figure 1.4) (Pisoni et al. 2015). Other fronts occur to the south, including from the southern edge of the San Jorge Gulf. While all of these fronts are characterised by elevated biological productivity, the precise species and community dynamics differ (Acha et al. 2004). For example, Valdés Peninsula coastal front (Figure 1.4) hosts large numbers of anchovy, hake and squid, while the San Jorge Gulf coastal front is specifically abundant in hake. The continental shelf front that the elephant seals of Campagna et al. (1998) focused on is notable for the abundance of squid.

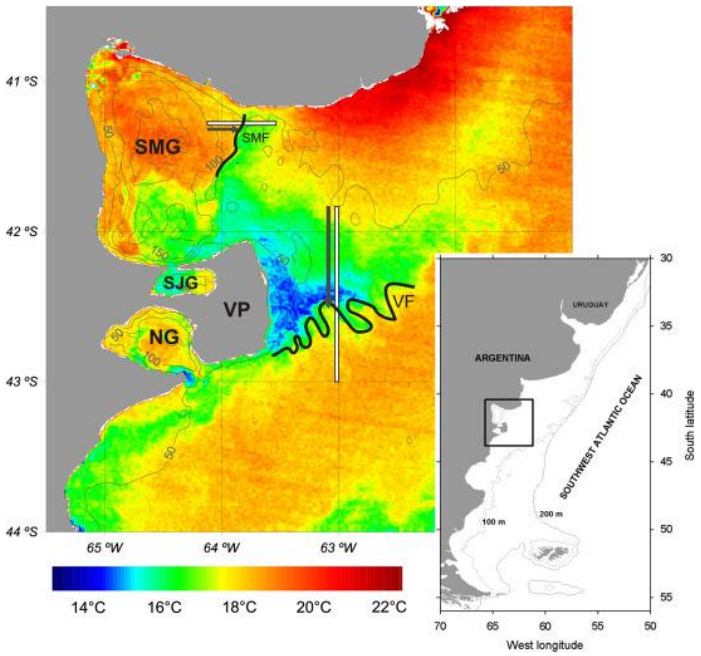

Figure 1.4. Marine fronts adjacent to the Valdés Peninsula defined by abrupt change in sea surface temperature. Reproduced from Pisoni et al. (2015). VP = Valdés Peninsula, NG = Golfo Nuevo, SJG = Golfo San Jorge, SMG = Golfo San Matias, VF = Valdés Front.

The changes in temperature, precipitation and sedimentation (including freshwater runoff from the melting of glaciers), as well as the reshaping of the Argentine coastline, would have dramatically altered the strength and position of marine fronts during the LGM and the subsequent Holocene transition (Berman et al. 2016). This in turn could have shifted the ranges of fish hunted by marine mammals and birds such as *Otaria flavescens* and *Spheniscus magellanicus*.

Objectives and outline

The central theme of this thesis is the role of ecological traits and dependencies in shaping populations' responses to environmental change. To address these questions, I combine genetic and ecological information to infer and attempt to explain population structure and demographic history. These analyses initially focus on the South American sea lion (*Otaria flavescens*) and the Magellanic penguin (*Spheniscus magellanicus*), before widening to include a global range of pinniped and other populations.

In Chapter 2, I present the highest-resolution genetic data yet available for *Otaria flavescens*, including a SNP dataset and full mitochondrial genomes, and use them to investigate the relationships between individuals from geographically distinct colonies. The observed patterns are then interpreted in the context of previous evidence for sex differences in dispersal proclivity. Most notably, although previous studies have not detected geographic structure using a handful of nuclear microsatellite markers, I will test whether a large SNP dataset produced by ddRADseq is able to detect more subtle structure.

In Chapter 3, I add ancient DNA samples to the modern genetic datasets from the Chapter 2 and use them to improve inferences about the demographic histories of *Otaria flavescens* and *Spheniscus magellanicus*. To better understand possible influences on their histories, I also use the stable isotope composition of some of the same animals to test whether their species' typical diet varies geographically or has varied over time, and whether change in diet has been related to past population growth or decline.

In Chapter 4, I investigate on a larger taxonomic and geographic scale whether patterns of similarity and difference in demographic histories across populations and species can be informative about their ecology. I also test and what factors (e.g. taxonomy, geographic range, life history, diet) explain the composition of clusters of species that appear to have experienced similar demographic histories. Specifically I investigate whether and how species of penguin were affected by historical climate change around the LGM, whether breeding strategy has shaped the demographic histories of pinnipeds, and whether the demographic histories of silverside fish species have been shaped by their habitat or range. To enable these analyses, I also describe and test a new program for quantitatively comparing demographic histories inferred by the program Stairway Plot 2 from SNP datasets.

In Chapter 5, I revisit the broad questions raised in this introduction in light of the results presented in the previous chapters. The results of Chapters 2 and 3 will enable me to describe an updated view of the modern population structure of *O. flavescens* and how it came to be that way through the combined influences of diet, climate, breeding strategy, and demographic change. Also based on the results of Chapter 3, I will describe the demographic history of *S. magellanicus* in relation to its dietary history and informed by ancient DNA calibration. Having reconstructed the demographic and isotopic (i.e. dietary) histories of these two distantly related

but ecologically similar and sympatric species, I will begin to address broader questions about the consistency and comparability of demographic histories across species, and the biological factors that influence them. These broader questions will be the focus of Chapter 4, which tests them quantitatively within species, within clades (pinnipeds, penguins), and between clades.

Chapter 2: Population structure of modern *Otaria flavescens*

Introduction

Background

South American sea lions (*Otaria flavescens*) may be found almost anywhere off of the Atlantic coast of Argentina. Males have been known to undertake very long migrations to mate in breeding colonies hundreds of kilometres from their usual haul-out and foraging grounds (Giardino et al. 2016). Based on this continuous distribution of individuals and potential for long-distance dispersal, one might expect that all *Otaria flavescens* in Argentina make up a single large population; perhaps with a gradual decline in migration rate between more distant colonies, but no hard boundaries. This is what has been found by most genetic research to date when considering markers inherited from both parents via the nuclear genome. As early as 1999, Szapkievich et al. were unable to distinguish between Argentine and Uruguayan populations using allozymes. However, this could have been a matter of the capacity of the markers to display variation that could be used to statistically distinguish populations. Feijoo et al. returned to the question in 2011 using thirteen microsatellite markers and found no evidence of differentiation between regions within Argentina or between Argentina and the Falklands or Uruguay based on the fixation indices F_{st} and Φ_{st}. Using ten microsatellite loci and a much larger sample of 111 individuals, Oliveira et al. (2017) found similar results, with no statistically significant differentiation between Argentine and other Atlantic populations (including the Falklands and Uruguay), though differentiation from Pacific populations was well supported.

The long-distance dalliance of males is in stark contrast to the philopatry, or birth-site fidelity, of female sea lions (Campagna et al. 2001). While the evidence so far points to an absence of overall population structure, based on the nuclear genomes of *Otaria flavescens*, mitochondrial DNA (mtDNA) markers that are almost exclusively inherited from the female parent do show differentiation between some populations in Argentina. The earliest reported mtDNA work in Atlantic *Otaria flavescens* was by Tunez et al. (2007), who found strong differentiation between Argentina and Uruguay, and within Argentina between the Patagonian provinces of Chubut or Santa Cruz and Buenos Aires province, based on only three polymorphic sites in a 445-bp fragment of the cytochrome *b* gene. Subsequent work by Tunez et al. (2010) focused in to look for finer-scale genetic structure by using a more variable marker, a 508-bp fragment including

the hypervariable D-loop region of the mitochondrial genome featuring 12 polymorphic sites across 49 individuals. This dataset exposed statistically significant differentiation between colonies from the Valdes Peninsula of northern Chubut and colonies in northern Santa Cruz, but not within those regions. Feijoo et al. (2011) also expanded on Tunez' mitochondrial analysis with samples from additional colonies, and analysed their structure hierarchically, by region, rather than merely pairwise between colonies. Feijoo reported significant differentiation in the mitochondrial D-loop between the north and south sides of the Valdes Peninsula; they did not report tests for differentiation with the south Chubut-Santa Cruz region, grouping these colonies *a priori* based on demographic information compiled by Tunez et al. (2008) suggesting that they make up a single population based around focal colonies.

If structure exists within the Argentine population of *Otaria flavescens*, it is most likely delineated by features of breeding behaviour or geography. According to Tunez et al.(2008), the localization of focal colonies is determined over a large geographic scale by the tidal range, with sea lions favouring beaches for breeding where the water line does not change too dramatically with the tides. This preference has led to relatively few breeding colonies being formed in southern Chubut and Santa Cruz; therefore, individuals sampled from diverse haul-outs and foraging grounds may come from a smaller set of breeding communities. A much larger number of breeding colonies are found in northern Chubut and Rio Negro, where the tidal range is smaller and fish are more abundant (Tunez et al. 2008).

There are also ecological and behavioural differences between sea lions from different regions. For example, on a small geographic scale, sea lions foraging on the northern side of the Valdes Peninsula, in the Golfo San Matias, mainly fish prey out of the pelagic waters, whereas sea lions on the south side of the peninsula, foraging in the Golfo Nuevo, primarily feed on benthic animals (Jarma et al. 2019). Benthic prey have a lower lipid content than pelagic prey, and therefore have lower energetic value, requiring more individual prey to be caught, while also potentially requiring more energy due to the challenges of diving (Hückstädt et al. 2016). In modern times, *Otaria* colonies on the north side of the peninsula are growing more rapidly than those in the south, despite (or perhaps because of) greater anthropogenic disturbance, and this dietary difference is one plausible factor (Jarma et al. 2019). The difference in accessibility of pelagic versus benthic prey in these local water bodies is influenced by differences in key environmental variables, such as seafloor depth (bathymetry) and nutrient availability. They are

also separated by marine fronts that concentrate smaller prey - and therefore sea lion foraging activity - in specific areas.

Given these demographic and environmental mechanisms that might be expected to produce signatures of genetic structure in both sexes, the lack of evidence for it in past work involving nuclear DNA markers requires explanation. There are four main possibilities. First, gene flow mediated by males dispersing between the colony clusters identified by Tunez (2008) may simply be prevalent enough to overcome contemporary forces of differentiation (genetic drift or positive selection) and swamp any signature of historical differentiation. There are strong indications that this is at least partially true, between evidence of long-distance male dispersal and reproduction (e.g. Giardino et al. 2016) providing the mechanism and the contrasting results between strong differentiation in maternally inherited mtDNA markers yet very weak differentiation in nuclear (biparental) DNA markers, even between other countries in the South Atlantic, such as Uruguay and the Falkland Islands territory. This contrasts with the Magellanic penguins (*Spheniscus magellanicus*), who face similar ecological pressures and barriers, but have a different breeding system and life history. They also show weak genetic structure, but this structure is actually better supported by microsatellite markers (Bouzat et al. 2009; Dantas et al. 2018). This may be because Magellanic penguins do not have such sexually dimorphic breeding behaviour as sea lions, and so the greater statistical power of multi-locus microsatellite markers is decisive here, whereas it is overpowered by the effect of female-specific philopatry on mtDNA markers in *Otaria*. There is also less evidence of long-distance mating dispersal in these penguins; individuals roam far, and it is possible that some copulate before settling down with a permanent mate, but members of both sexes tend to return to their place of birth to settle and raise offspring year on year (Boersma 2008).

Another explanation for the apparent lack of genetic structure in Argentine sea lions is that the populations have not been in the current regime for long enough to differentiate. Due to the lower mean sea level that prevailed from the LGM into the early Holocene, the coastline of Argentina was much farther out on the continental shelf and many of its modern contours, such as the Valdes Peninsula, along with its adjacent bays and their ecological differentiation, did not exist (Ponce et al. 2011; Figure 1.3). As a result, what we now see as semi-independent populations in the different regions could have been even more linked than they are today. The mitochondrial genome has an effective population size one quarter that of the nuclear genome, due to it being haploid and inherited from only one parent. As a result, differentiation would be

expected to develop more rapidly if the populations are separated, due to stronger genetic drift in allele frequencies. This scenario may also apply to the Magellanic penguin, which are thought to have expanded their range into northern Patagonia relatively recently. However, multilocus markers, such as microsatellites, are expected to better record recent demographic and migratory history. This has been true for the Magellanic penguin, with only microsatellites providing evidence of recent differentiation between northern and southern Patagonia (Dantas et al. 2018), but as noted, microsatellites have so far not revealed any finer-scale differentiation in *O. flavescens*.

There may also simply not be enough genetic variation in the population(s) to discern the shallow level of genetic structure that does exist. Our understanding of the variability of the nuclear genome of *Otaria flavescens* is so far limited to a handful of microsatellite loci, between studies by Feijoo et al. (2011) and Oliveira et al. (2017). The levels of allelic richness and heterozygosity they reported for these markers, which did not show evidence of genetic structure, were not unusual (Garner et al. 2005; Hoffman et al. 2009; Pinsky and Palumbi 2013). Similarly, mitochondrial nucleotide diversity reported at the cytochrome *b* gene (Tunez et al. 2007) and the mitochondrial D-loop (Feijoo et al. 2011: π=0.014; Oliveria et al. 2017: π=0.010) have been within the typical range for a mammal (Santamaria et al. 2007; Nabholz et al. 2008) and geographic genetic structure has been detectable with these markers.

A final possibility is that evidence of population structure in the nuclear genome has eluded previous studies not because of an innate lack of variation in the markers used, but because the number of markers has been insufficient. The number of alleles determines the number of different genotypes that can be distinguished at a single locus, and the use of multiple independent loci allows genotypes to be defined combinatorially, exponentially increasing the number of possible genotypes that can be resolved (Sunde et al. 2020). More importantly, multiple loci should represent independent outcomes of genetic drift, which is the random process expected to be chiefly responsible for allowing allele frequencies to diverge between populations with limited gene flow. Single loci are more susceptible to chance events that could produce misleading pictures of the relatedness between populations. For example, due to incomplete lineage sorting, the mitochondrial genome of the European bison (*Bison bonasus*) implies that the species is most closely related to cattle, despite the overwhelming majority of gene trees putting it closer to the bison and yak (Wang et al. 2018).

The characterization of a dozen or so microsatellite loci between Feijoo et al. (2011) and Oliveira et al. (2017), with each locus featuring multiple alleles, was a great advancement over the sole reliance on mtDNA. However next-generation sequencing technologies now allow for thousands of loci to be analysed. One method that is especially efficient for studies focusing on population structure and demography in non-model species is RADseq, or restriction site-associated DNA sequencing. This method uses restriction enzymes to cut the genome at homologous sites across many individuals of the same species. Fragments within a certain size range can then be concentrated and sequenced, yielding a catalogue of loci from across the genome without the need for a high-quality, species-specific reference genome to map them to (Davey and Blaxter 2011; Peterson et al. 2012). Studies bringing RADseq datasets to bear on species where prior work has been done with microsatellites have commonly reported finer levels of population structure than had previously been detected (though this could be affected by publication bias) (McKinney et al. 2017). For example, Hodel et al. (2017) found that RADseq datasets resolved a biogeographic margin that was not apparent in microsatellites from the same samples. Jeffries et al. (2016) found that a RADseq data set of 13,189 single-nucleotide polymorphisms (SNPs) supported roughly the same population structure for Crucian carp (*Carassius carassius*) as 13 microsatellite loci, but the RADseq dataset facilitated assignment individuals to their correct population with greater confidence, despite being based on less than 20% as many individuals as microsatellite dataset. Similarly, from a direct comparison between RADseq and microsatellite datasets containing the same samples, Bohling et al. (2019) reported that RADseq more confidently consistently assigned samples to while also providing finer estimates of the amount of admixture between populations. This owes to the fact that SNPs may be fixed for one of their two alleles in certain populations, allowing admixed individuals to be identified from their heterozygous genotypes at many such loci. Fixation of a single allele is less common with microsatellites, as one of their strengths is the generation of many alleles.

Objectives

Aiming to better understand the nature of population structure of *Otaria flavescens* within Argentina and the reasons why it has not been evident in nuclear genetic data thus far, I analysed 2,497 SNPs from across the nuclear genomes of 49 individuals. These samples were concentrated in northern Patagonia, but extend into southern Santa Cruz. This dataset was used to characterise the degree of genetic variability present in the nuclear genomes of

Argentine *Otaria* and test for genetic structure and natural selection. I hypothesized that some level of population structure would be found in the nuclear genome, owing to the far greater power afforded by ddRADseq data compared to microsatellites.

This chapter also describes innovation in the use of mitochondrial DNA markers for this species. Whole mitochondrial genomes of 53 individuals were sequenced to obtain a much larger number of segregating sites than were available with previous analyses using only cytochrome *b* or the mitochondrial control region. These mitogenome sequences were also combined with control region sequences from additional samples, both novel and previously published, to obtain a new alignment that retains a large number of segregating sites while maximizing geographic coverage and number of individuals. The novel samples from this study include a large number from Rio Negro - specifically the northern shore of the Golfo San Matias - which had been largely absent from previous studies. I hypothesized that the mitochondrial control region will exhibit significant population structure and that this will persist when looking at full mitogenomes, which may also reveal finer levels of structure by more finely distinguishing individuals.

Materials and Methods

Data generation

Sample preparation

A total of 132 modern samples from *Otaria flavescens* were processed for population genetics analysis. The vast majority of these (125) were obtained via skin biopsy, while the remaining 7 were bone. To prepare samples for DNA purification, tissue was minced using surgical scissors and approximately 30 mg was then digested for three hours at 55 °C in proprietary TL (digestion) buffer and added proteinase K, according to the recommended protocol of the EZNA Tissue DNA kit (Omega Bio-Tek). Bone samples were cut into small (~1 mm^3) pieces with a Dremel manual drill, and these pieces were pulverized into a fine powder using ball bearings in a steel capsule, vibrated at high speed as part of a Mixer Mill MM 200 system. Approximately 30 mg of bone powder was then dissolved overnight at 55 °C, in 400 µl of solution composed of 50% TL buffer and 50% 0.5 M EDTA (final concentration 0.25 M EDTA), plus 25 µl of proteinase

K. Following the digestion step, DNA from tissue and bone samples was extracted and purified using silica binding columns according to the manufacturer's instructions.

Mitogenome sequencing

Seventy-five modern *Otaria flavescens* samples were selected for sequencing of the full mitochondrial genome. Illumina libraries were prepared closely following the BEST protocol (Carøe et al. 2017; Mak et al. 2017), which is optimised for degraded DNA. For samples with a borderline low DNA concentration, the input sample volume was increased from the recommendation of 32 µl to achieve as close to 500 ng DNA as possible. First, genomic DNA was sonicated to fragment it into pieces of 200-600 bp and an initial end-repair step was performed on all samples to give them blunt ends for adapter ligation. Then, Illumina barcode (P5) and index (P7) adapters were ligated and libraries were amplified, quantified, and cleaned of excess adapters and other reagents using a size-selection protocol with magnetic beads.

A hybridisation capture approach was selected to make downstream high-throughput sequencing as cost-effective as possible by maximizing the proportion of reads mapping to the mitogenome. This was especially important for archaeological samples (to be discussed in chapter 4), which could contain large amounts of microbial contamination, resulting in inefficient sequencing of endogenous DNA. Hybridisation capture is based on the strong affinity of biotin for streptavidin. Biotin can be attached to a DNA probe with a custom sequence and hybridised with complementary "target" DNA. Streptavidin-coated magnetic beads can then be added to the solution, to which only DNA molecules which have hybridised with a "bait" probe will bind. The mixture can then be separated by applying a polarised magnetic field, allowing non-target molecules to be preferentially removed in the supernatant while target molecules remain bound to the beads via their hybridised biotinylated probes. Subsequently, the bound DNA can be released back into solution, yielding a sample enriched in target molecules.

The mitochondrial reference genomes of *Otaria flavescens* (accession NC049152; Tian et al. 2019) and *Arctocephalus australis* (accession NC063561; Tian et al. 2021) were used as templates for probe tiling design by masking an especially repetitive stretch of the mitochondrial control region (D-loop/origin of replication) known from related species (Hoelzel et al. 1993, 1994). These masked reference sequences were sent to Arbor Biosciences, who returned a custom version of their MyBaits® (Arbor Biosciences) kit containing a set of custom probes

designed to tile across Otariid mitochondrial genomes. All libraries were processed according to the manufacturer's instructions for degraded samples, including extended hybridization time (48 hours). The resulting enriched libraries were again amplified by PCR and quantified by qPCR. At this stage, eleven libraries displaying the lowest concentrations were discarded. Finally, 64 libraries - each bearing uniquely identifying adapter sequences - were pooled in approximately equimolar concentrations and sequenced on a single lane of an Illumina HiSeq 2500 shared with samples from another project.

The resulting reads were demultiplexed and cleaned using the process_shortreads command in Stacks (version 2.2). This command was set to discard reads with any uncalled bases or average phred quality scores of less than 20, or trim sections of reads where the quality score drops below 20 within a sliding window of 30% of the read's total length. This typically leads to trimming at the 3' end of reads, where quality tends to decline. Forward and reverse read pairs were then mapped to the indexed *Otaria flavescens* mitogenome reference sequence using the 'mem' command in BWA (version 0.7.12), with default settings. Samtools (version 1.2) was used to filter out reads with a MAPQ, or mapping score, of less than 20, and produce a sorted .bam file for further analyses. MAPQ is a metric of how specifically a read aligns to its inferred position on the reference relative to alternative alignments, and a MAPQ of >20 means that there is a <1% chance that the read is mapped to the wrong position. Potential duplicate reads were then removed using the 'MarkDuplicates' command of Picard (version 1.141). Eleven assemblies with less than 90% reference coverage were excluded from further analyses, as inclusion of these additional samples was not thought to be worth the loss of informative sites from the mitogenome alignment. Although a multi-sequence alignment covering less than 90% of the mitogenome would still have been very useful, the combination of them would have rapidly reduced the coverage of the final alignment because each was missing coverage in different areas of the mitogenome.

Site-specific genotype probabilities were estimated using bcftools (version 1.13) 'mpileup' into bcftools 'call' for each site represented in the reference mitogenome. A Python script by Ortiz (2019) was then used to convert these genotype calls into a consensus sequence alignment limited to sites called in 100% of these 53 high-quality assemblies, resulting in an alignment of 14554 bp (Appendix A). The assemblies were also analysed in Geneious v6.1.8, where significant heteroplasmy (multiple mitochondrial genotypes in the same individual) or propagation of PCR errors was ruled out based on the fact that at every called site across all

samples a single base was represented in >50% of reads; that is to say, the 50% consensus sequences lacked any ambiguous base calls.

Mitochondrial D-loop sequencing

An additional 18 modern *Otaria flavescens* samples were sequenced in the D-loop only. These were all samples from the south of Chubut province, which had uniformly yielded low DNA concentrations. For this procedure, primers needed to be designed with the objectives of amplifying a sequence that would overlap with several previously published datasets (Tunez et al. 2010; Artico et al. 2010; Feijoo et al. 2011) and obtaining a high density of variable sites. Density of variable sites was especially important here due to the constraint of needing to amplify degraded DNA from archaeological samples with the same primers, which would likely be highly fragmented, resulting in exponentially fewer molecules containing both primer binding sites as the length of the target region increases. Ultimately, a set of four primers was selected. Primers F1 (AATCCCACCACCAACACCC)/R3 (ACAAGGGTTGCTGGTTTCTC) were used to amplify a 300-bp fragment of the D-loop. Successful amplification of the target fragment size was verified by gel electrophoresis. Excess primer was removed using ExoSap Express-IT. The cleaned amplicons were then sequenced using Sanger technology. The resulting electropherograms were analysed in Geneious and aligned with sequenced mitogenomes to validate base calls and determine consensus sequences (Appendix A).

Published datasets

These mitochondrial D-loop sequences were supplemented with overlapping sequences published in two prior studies. Forty-nine sequences came from Tunez et al. (2010): 19 from northern Chubut (Valdes Peninsula), 20 from southern Chubut, and 10 from northern Santa Cruz. Fifteen sequences were taken from Feijoo 2011: 11 from northern Chubut and 4 from southern Santa Cruz. A subset of 145 overlapping base pairs (within the 300-bp fragment described above) was selected to contain as many variable sites as possible while being present in the published datasets and being sequenced to a good quality in all individuals novel to this study, including ancient samples which will be discussed in the next chapter (Chapter 4). The resulting alignment comprised a total of 141 sequences from modern *Otaria flavescens* (Appendix A).

Nuclear genome sequencing

Double digest restriction-site associated DNA sequencing (ddRADseq) was also performed to complement the single locus of the maternally inherited mitochondrial genome with numerous independent loci from the biparental nuclear genome. ddRADseq uses a pair of endonucleases to cleave the genome at numerous sites that are mostly homologous among members of the same species, allowing for a fraction of the genome to be sequenced at the same sites across many individuals, facilitating population genetics analysis in species without reference genomes at a lower cost than whole-genome sequencing. For application to *Otaria flavescens*, the endonucleases MspI and HindIII were selected. This pair of enzymes is good for SNP discovery as it is expected to cut the genome into a larger number of fragments for sequencing than many alternative pairs, with the trade-off of obtaining lower read depth per fragment (Jiang et al. 2016).

Sixty-four modern tissue samples were selected for ddRAD sequencing following the ddRADseq protocol described by Peterson et al. (2012). This number was selected based on the number of barcode combinations available and to achieve decent coverage per individual within a single Illumina HiSeq 2500 lane. The template DNA of each sample was digested by MspI and HindIII simultaneously. Then, Illumina barcodes were ligated to the ends of the digested fragments and samples with different barcodes were pooled. Each pool was size-selected using a Pippin Prep machine to select fragments of approximately between 250 and 400 bp long (mean 325 bp), to obtain a reduced pool of fragments that would be shared among individual samples. Each selected pooled library was divided into triplicates to reduce the impact of PCR duplicates, then amplified using pool-specific index primers, leaving each sample with a unique combination of barcode and index. Next, the libraries were quantified by both qPCR and TapeStation (Agilent), and all pooled in approximately equimolar concentrations for sequencing on a single lane of an Illumina HiSeq 2500.

The resulting reads were demultiplexed using the ‘process_radtags’ command of Stacks v2.2. The settings were the same as those previously described for the mitogenome reads using ‘process_shortreads’ (i.e. minimum average phred quality score of 20 across the whole read or in any 30% sliding window), except that the ddRADseq reads were also truncated to a uniform length of 110 bp for downstream applications. Samples with less than 500,000 reads retained at this stage were excluded. The reads were then mapped to the reference genome of *Otaria flavescens* (accession CNP0000758; Yuan et al. 2021) using the ‘mem’ command of BWA

v0.7.12. Variant sites were then called using Stacks' ref_map.pl. Each site was required to be present in at least 70% of individuals in every pre-defined population to be included in the overall SNP catalogue. Only the first SNP encountered per locus was included in the final catalogue to avoid close physical linkage.

Data analysis

Geographic structuring

Samples were grouped by region, reflecting an initial hypothesis of structure. Defined regions included Rio Negro (RN), North Peninsula Valdes (NPV), South Peninsula Valdes (SPV), North Santa Cruz (NSC), South Santa Cruz (SSC), and Tierra del Fuego (TdF) (Figure 2.1). Some regions were combined *a priori* to compensate for weaknesses in geographic coverage of each genetic dataset. For the mitochondrial analyses, North Santa Cruz, South Santa Cruz, and a small number of samples from the southern end of Chubut province (within the Golfo San Jorge) were analysed together as Santa Cruz (SC) because of low numbers of whole-mitogenome sequences available from each of these regions compared to the others, which would otherwise lead to inaccurate and imprecise estimates of regional haplotype frequencies. Pooling of samples from these regions also follows one of the most recent papers to address genetic population structure within Argentina (Feijoo et al. 2011). For the ddRADseq analyses, samples from southern Chubut were not available, however the division between North Santa Cruz (NSC) and South Santa Cruz (SSC) was kept. ddRADseq data from the Valdes Peninsula was also relatively sparse in comparison with other regions, and so North Peninsula Valdes and South Peninsula Valdes were treated together as North Chubut (NCh). Only a few samples were sequenced from Tierra del Fuego, and so these will be considered exclusively in the next chapter, alongside additional archaeological samples from the same region. Final sample sizes per region or site are shown in Figure 2.2. All samples and datasets they were included in are detailed in Appendix A.

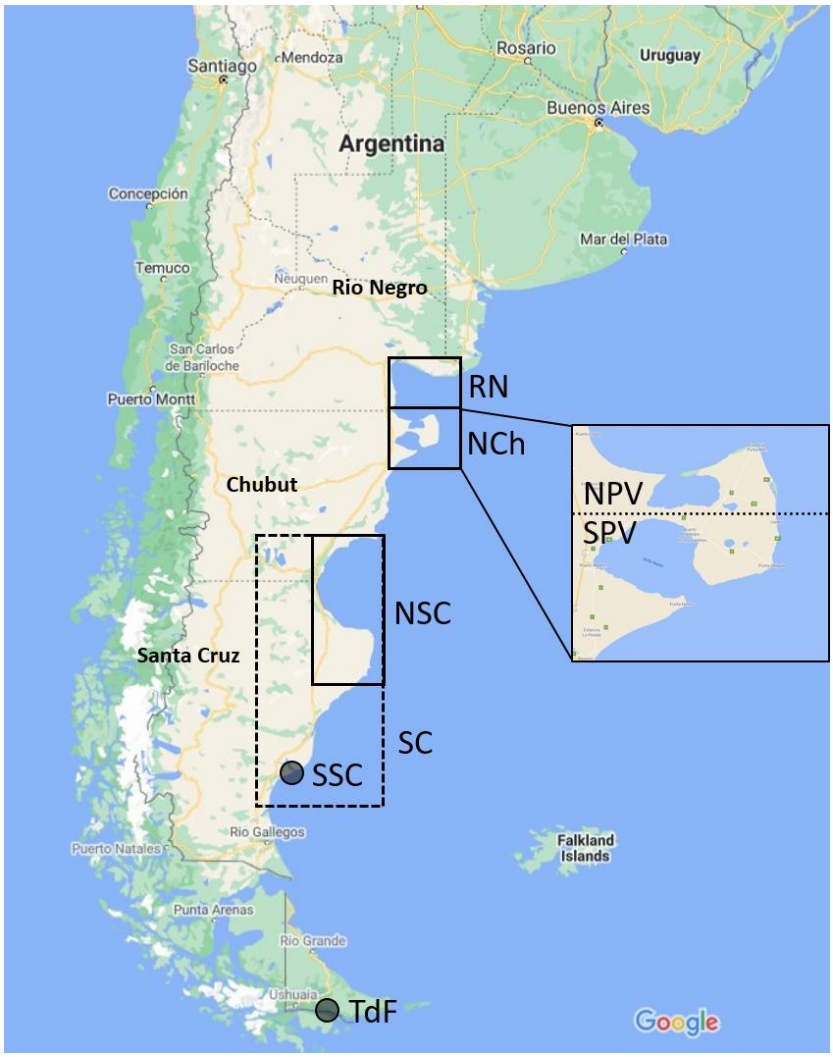

Figure 2.1. Identification of geographic groupings of samples and their abbreviations. RN=Rio Negro, NCh=North Chubut. North Chubut comprises North Peninsula Valdes (NPV) and South Peninsula Valdes (SPV). The water body, Golfo San Matias, is located between RN and NPV. North Santa Cruz (NSC) comprises the northern part of Santa Cruz province (including specific haulout sites at Monte Loayza and Isla Pinguino), as well as the southern end of the Chubut province. NSC contains the water body Golfo San Jorge. Santa Cruz (SC) combines NSC with a southern population at Cerro Bayo (SSC). Modern samples from Tierra del Fuego (TdF) were scarce and were not analysed quantitatively in this chapter.

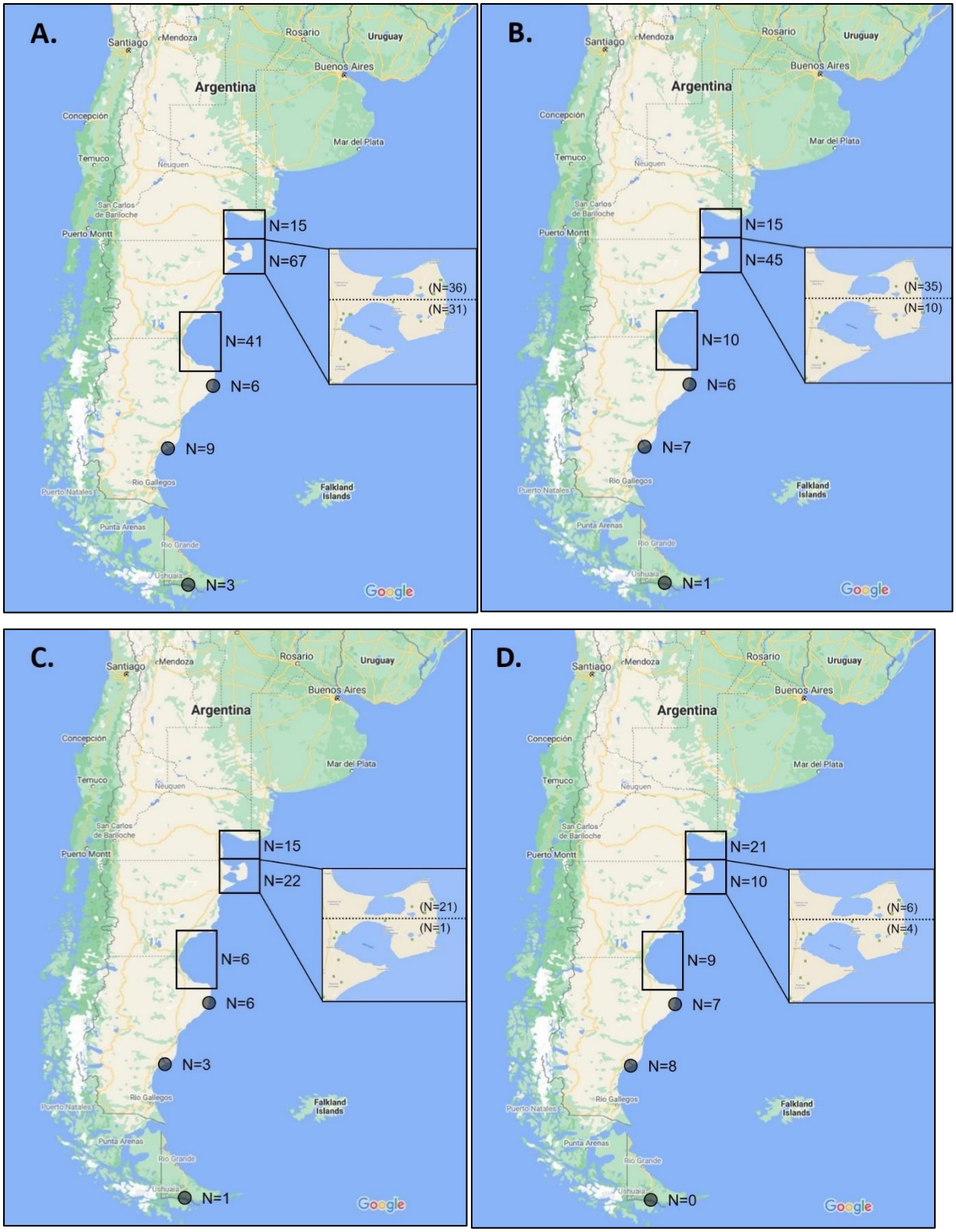

Figure 2.2. Geographic distribution of modern *Otaria flavescens* samples considered in this study that are included in the 145-bp mtDNA alignment (A), 409-bp mtDNA alignment (B), full mitogenome alignment (C), or the final RADseq dataset (D).

mtDNA analyses

Three mitochondrial DNA alignments were built for population structure analyses. First, a full mitogenome alignment, optimizing for the largest total sequence length (53 individuals x 14554 bp). The amount of variability present in the full-length mitogenomes allowed for very few shared haplotypes, and so a second version of this alignment was constructed by clustering similar haplotypes into ten haplogroups based on principal components analysis (PCA) guided by a Bayesian information criterion and using each haplogroup's consensus sequence in the alignment. Third, a short D-loop alignment was constructed including all available samples (141 individuals x 145 bp), including the sequences published by Tunez 2010 and Feijoo 2011. A fourth alignment struck a balance between D-loop sequence length and sample size (84 individuals x 409 bp), also including published sequences.

Arlequin was used to calculate regional and global summary statistics for genetic diversity (Excoffier and Lischer 2010). Fixation indices based on differences in haplotype frequencies (F_{st}) and their degree of similarity (Φ_{st}) were calculated between all pairs of regions, using 10,000 permutations to test statistical significance. The program SAMOVA2 (spatial analysis of molecular variance; Dupanloup et al. 2002) was used to search for the best-supported higher-level groupings of regional and/or local populations, which were tested for statistical significance by performing analyses of molecular variance (AMOVA) in Arlequin. A median-joining network was also generated in Popart to help visualise the phylogeographic relationships among mitochondrial haplotypes (Leigh and Bryant 2015).

Nuclear SNP analyses

Variable call format (VCF) files generated by Stacks following variant-calling on the ddRADseq data were filtered using VCFtools to remove individuals containing missing genotype calls at >50% of variable sites, then sites missing genotype calls in >5% of individuals, and finally, sites where the minor allele was observed only once (i.e. as heterozygous in a single individual).

Diversity statistics were calculated and visualised using the SambaR package in R (de Jong et al. 2021). Fixation indices (Φ_{st}) were calculated in Arlequin as described for the mtDNA alignments above (Excoffier and Lischer 2010). Discriminant analysis of principal components (DAPC) implemented in the R package Adegenet (Jombart and Ahmed 2011) was also used to

test for structure in the genetic data by identifying the most parsimonious number of clusters (K). DAPC combines principal components analysis (PCA) to identify clusters of individuals within the data, with discriminant analysis (DA) to identify combinations of characters (in this case, segregating nucleotide sites) that most clearly differentiate those clusters (Jombart et al. 2010). The find.clusters() function was run using the maximum number of principal components and the optimal number of clusters (K) was selected as that at which the value of the Bayesian information criterion (BIC) reached a minimum plateau. A DAPC analysis was then performed on these clusters after selecting the most parsimonious and stable number of principal components to use to separate the clusters without overfitting (using a-score optimization). The resulting genetic clusters were compared with *a priori* expectations based on geography. DAPC was also used to evaluate the support of the data for the *a priori* geographic relationships based on the amount of data (number of principal components) required to discriminate the pre-defined clusters.

Further analyses of population structure could be applied to the nuclear SNP dataset thanks to it being composed of numerous independently segregating loci. First, the snmf function of the R package LEA was used to complement DAPC, implementing a STRUCTURE-like approach to detect genetic structure and admixed individuals through Bayesian clustering (Frichot and Francois 2015). In LEA, K was tested over a range of 2-6 with up to 10,000 iterations, tolerance set to $1e^{-10}$, and alpha set to 10. The tolerance parameter defines how stable the result of the optimization algorithm must be across iterations before the optimization procedure is halted. The parameter alpha is a regularization parameter that is intended to control over-fitting. Ten is the default value, with smaller values leading to a more generally accurate but less precise model, and vice versa for larger values (Frichot et al. 2014). A minimum plateau of the cross-entropy criterion signalled the optimal value of K. The program STRUCTURE was also used to round out this selection of tools for detecting population structure and for direct comparability with previous studies (Pritchard et al. 2000). STRUCTURE was run with a burn-in of 5,000, followed by 10 replicates of the MCMC chain. K values 1 to 4 were tested, and the optimal K was identified as the one where the estimated likelihood of the data plateaued.

PCAdapt (Prive et al. 2020) was used to scan for evidence of positive selection. In contrast to most tools for detecting selection, such as OutFLANK and Bayescan, PCAdapt does not require populations to be pre-defined. Instead, PCAdapt uses principal components analysis (PCA) to identify clusters in the data, similar to the first stage of DAPC. The essence of PCA is to

summarise the underlying structure of a dataset with few variables (components). Most neutral loci, those whose frequencies are determined entirely by chance and demographic processes, would be expected to follow the trends represented by the principal components. PCAdapt identifies outlier loci potentially under selection as those whose SNP frequencies are not well predicted by the selected principal components (i.e. display a large error when regressed against the components). As a result of this flexibility, the results of PCAdapt are not seriously compromised by the presence of admixed individuals or misidentification of populations, such as might occur when biogeographic structure is shallow (Luu et al. 2016). PCAdapt was ultimately run with K=2 and potential outlier SNPs were identified using the using the Bonferroni correction method.

Results

Sequence data quality control

Mitogenome filtering and assembly

A total of 172,225,412 reads were obtained bearing the assigned barcodes of the 64 *Otaria flavescens* mitogenome libraries, of which 99% passed filters. After read mapping, a median of 1655x mean coverage was achieved across all libraries, with a minimum of 0.7x. Forty-six assemblies had 100% coverage of the reference sequence by at least one high-quality base call, while fifty-four assemblies had >90% reference coverage. Eight assemblies had a reference coverage of 90-99%, and the median of mean coverage among them was 17x with a minimum of 8x. Individuals missing genotype calls at >10% of sites and sites that were uncalled in any of the remaining individuals were filtered out. One additional individual (CB10, P509-N711) that passed this filter was nevertheless excluded as an outlier, as it exhibited many nucleotide variants not found in any other sample. These variants appeared to be genuine, but were not parsimony-informative and had the potential to obscure population structure. At the conclusion of these filtering steps, a consensus sequence alignment was obtained containing 14554 bp each from 53 individuals (Appendix A).

Mitochondrial D-loop dataset

Eighteen additional modern *Otaria* samples were successfully sequenced over the 300-bp D-loop fragment defined by the primers. These sequences were trimmed and integrated with the

145-bp alignment made up of fragments from other mitogenome sequences and published alignments (Appendix A).

ddRADseq filtering, assembly, and SNP calling

A total of 307,316,720 reads were obtained across 64 libraries, a median of 3,713,674 reads per sample. Of these, 188,206,808 (63%) reads were retained after filtering for quality and radtag presence, leaving a median of 1,945,232 per sample. On the basis of low read count, 13 samples were excluded, leaving 51. Seventy-four percent of reads mapped with a MAPQ score >20; the remainder were filtered out. This left a final total of 145,721,886 high-quality mapped reads, with a median of 1,770,581 per sample. These allowed for an average effective per-sample coverage of 12.4x across 859,468 loci identified by Stacks. After initial filtering in Stacks, 44,575 loci composed of 10,534,779 sites were retained, including 14,514 variable sites genotyped in all regional populations. Further filtering for population structure analyses (maximum proportion missing data per individual = 0.5, maximum proportion missing data per locus = 0.05, minimum minor allele count = 2) resulted in a dataset containing 49 individuals and 2,497 biallelic SNPs. These individuals were split over four geographic populations: 10 from North Chubut (primarily the Valdes Peninsula), 10 from northern Santa Cruz, 23 from Rio Negro, and 6 from southern Santa Cruz (Appendix A).

Nuclear genome diversity

The greatest total genetic diversity was found in the northern (RN) population, and the least was found in the southern (SSC) population (Figure 2.3). However, this was driven by the larger number of individuals sampled in RN. For an equally small sample size, slightly fewer segregating sites were identified in the RN population than in the other three populations (Figure 2.4). The rarefaction curve of SNP discovery suggests that none of the regional populations were exhaustively represented, but the number of sites shows signs of stabilizing in RN. The ratio between the number of segregating sites (Waterson's theta) and nucleotide diversity indicates that there is consistently an excess of rare alleles, resulting in a negative value of Tajima's D in every population (RN: D=-0.21; NCh: D=-0.20; NSC: D=-0.19; SSC: D=-0.19) (Figure 2.5).

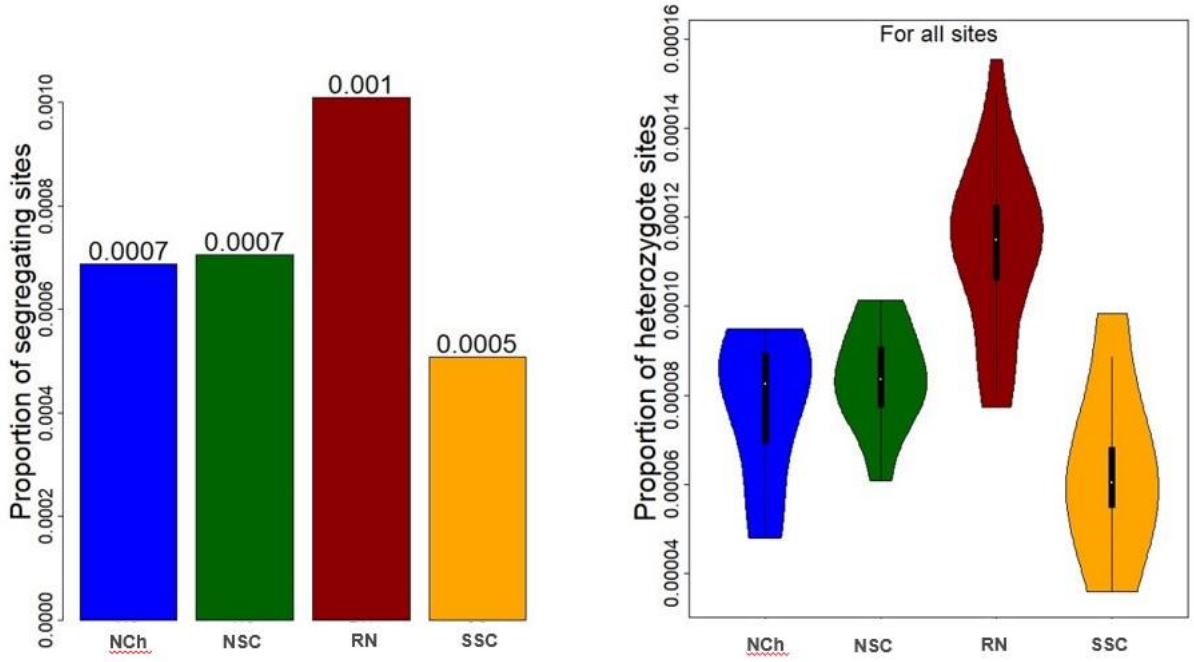

Figure 2.3. Left: The proportion of all sequenced sites that were found to be segregating in each population. Right: The proportion of all sequenced sites that were genotyped as heterozygous, on average, per individual, in each population.

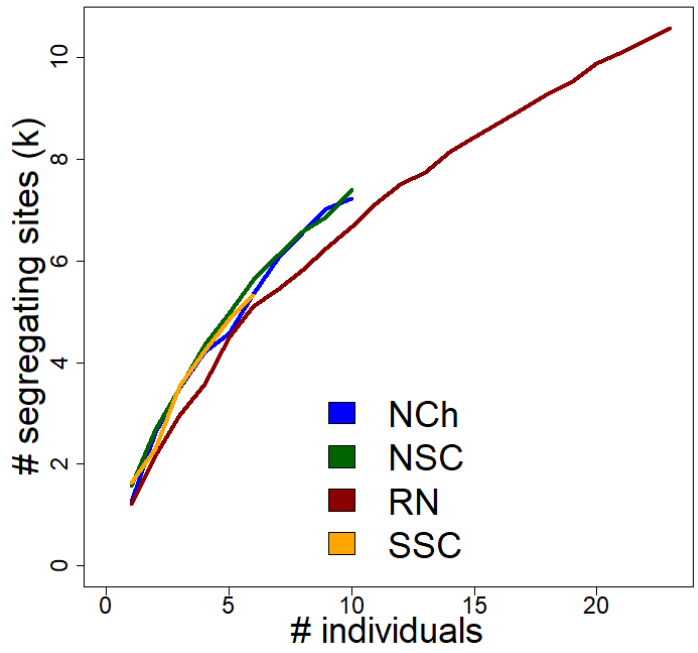

Figure 2.4. The total number of sites found to be segregating in each population, as a function of the number of individuals genotyped.

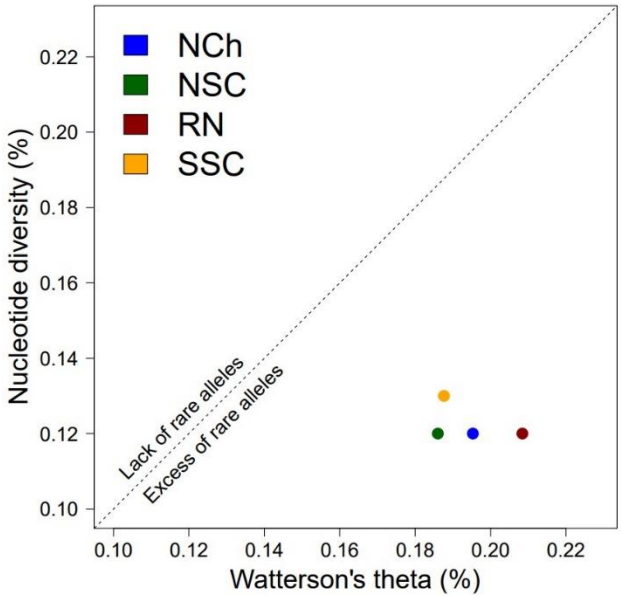

Figure 2.5. The ratio between nucleotide diversity and Watterson's theta for each population. Nucleotide diversity refers to the frequency of differences (in this case, considering only segregating sites) between randomly drawn pairs of samples. Watterson's theta is an estimator of the number of segregating sites. A low ratio of nucleotide diversity to the number of segregating sites indicates an excess of rare alleles.

Mitochondrial diversity

Only 154 variable sites were identified across the 14554-bp mitogenome alignments of 53 individuals, leading to a mean nucleotide diversity (π) of 22.215 differences between any pair of individuals on average, or $1.53e^{-3}$ per site. The D-loop alignment of 141 individuals was only 0.1% as long (145 bp), but contained 16.2% as many (25) variable sites, leading to 2.415 average pairwise differences between individuals (π) or $1.67e^{-2}$ per site (Figure 2.6). The ratio between π and the number of variable sites is much closer between the two alignments, with a higher value in the mitogenome (0.144) compared to the D-loop alignment (0.097). This is probably because the number of variable sites found would be expected to scale with both the number of individuals and the number of sites sequenced. However, adding individuals has strong diminishing returns for variant discovery; although the D-loop alignment includes 2.57x as many individuals as the mitogenome alignment, alleles found uniquely in this sample set and not in the 53-individual mitogenome sample set would have to occur at a frequency of less than 2%, limiting their contribution to nucleotide diversity.

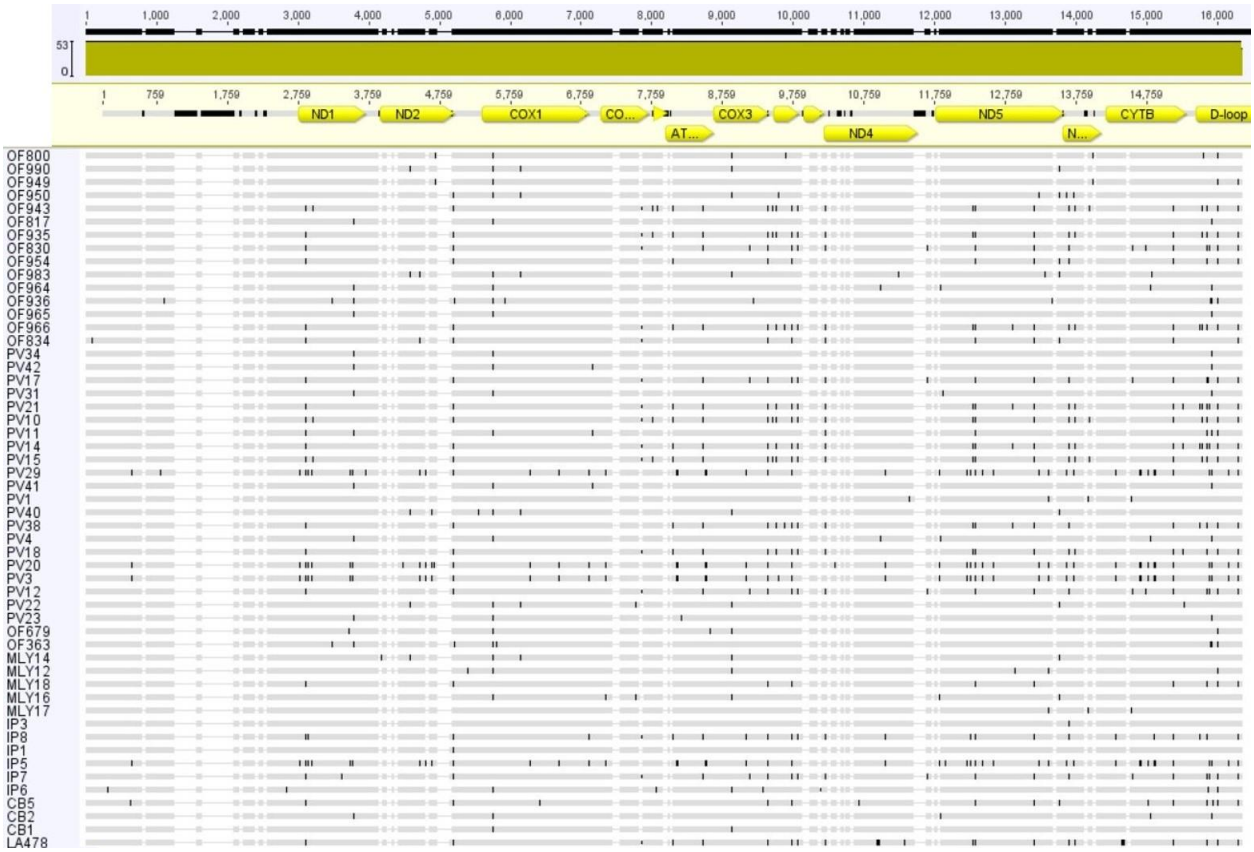

Figure 2.6. Overview of the distribution of variable sites across the mitochondrial genome. Gene annotations are shown at the top. The density of variable sites is greatest in the D-loop region (far right).

Nuclear population structure

Evidence of genetic structure in this nuclear SNP dataset was first assessed by DAPC in the R package Adegenet, using the find.clusters() function to identify the most parsimonious number of clusters in the data, without any *a priori* population assignments, based on a Bayesian information criterion (BIC). This returned an optimal K of 1, indicating little correlation among SNPs in their presence or absence across individuals. This test was repeated on variations of the dataset with filtering strategies, all yielding qualitatively the same result (Figure 2.7). Forcing the program to separate individuals into four clusters resulted in very imbalanced clusters, which had no correlation to the samples' geographical origin (Figure 2.8). Finally, DAPC was used to test whether the data supported the pre-defined geographic structure of the samples. Six principal components were selected, based on the a-score, as the optimum amount of information to use for discriminating these populations without overfitting. However, even with

prior assumptions about population structure, the analysis was unable to separate the clusters (Figure 2.9).

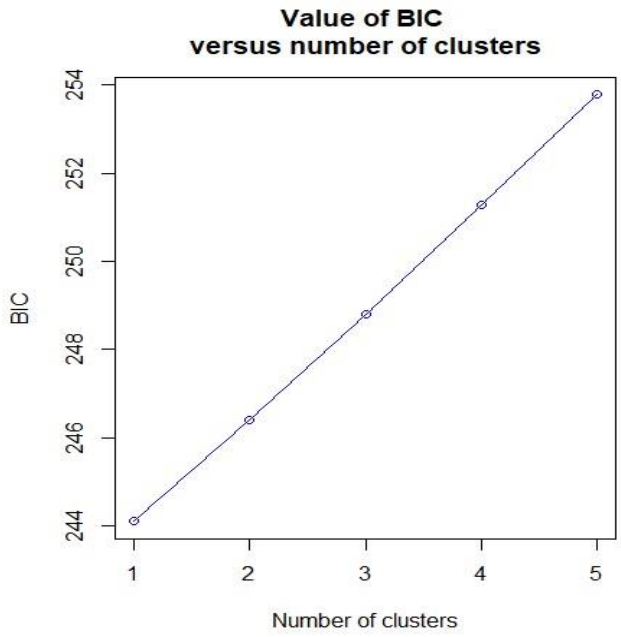

Figure 2.7. Bayesian information criterion as a function of number of clusters (K) assumed for DAPC. The optimal value of K is that at which BIC is minimized or plateaus after an initial sharp decline. Here, BIC is minimized at K=1, suggesting a lack of discernible population structure. Qualitatively the same result was obtained for other levels of SNP filtering, both more and less stringent (not shown).

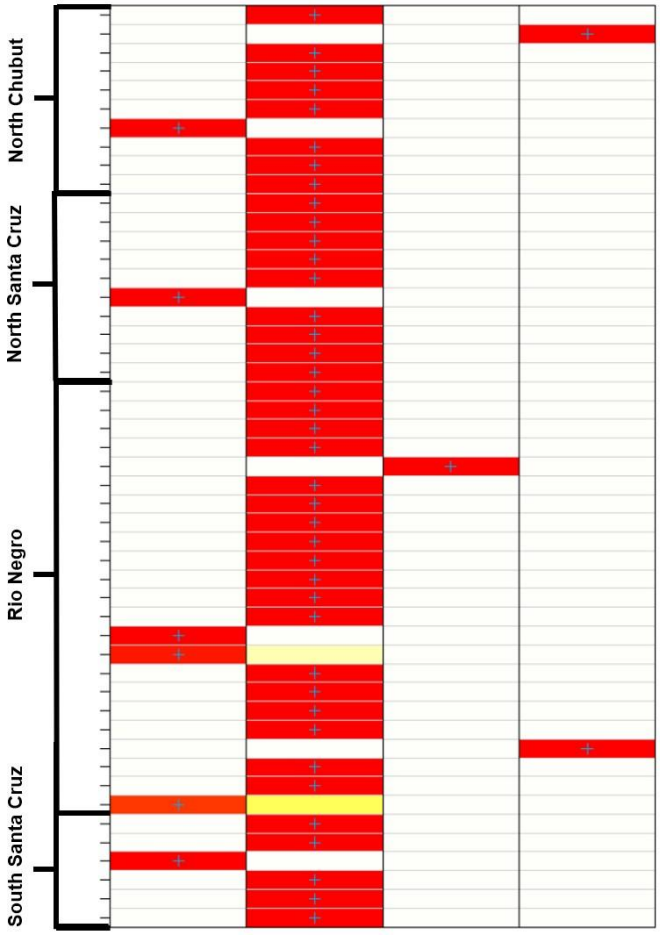

Figure 2.8. When forced to define multiple clusters (in this case, four clusters) despite its suboptimality according to the Bayesian information criterion, the resulting clusters identified by DAPC are not related to regional proximity, but rather defined by the distinctiveness of a few specific samples. Each of four columns represents a different cluster that samples (rows) were statistically assigned to. Sample origins are given on the left side.

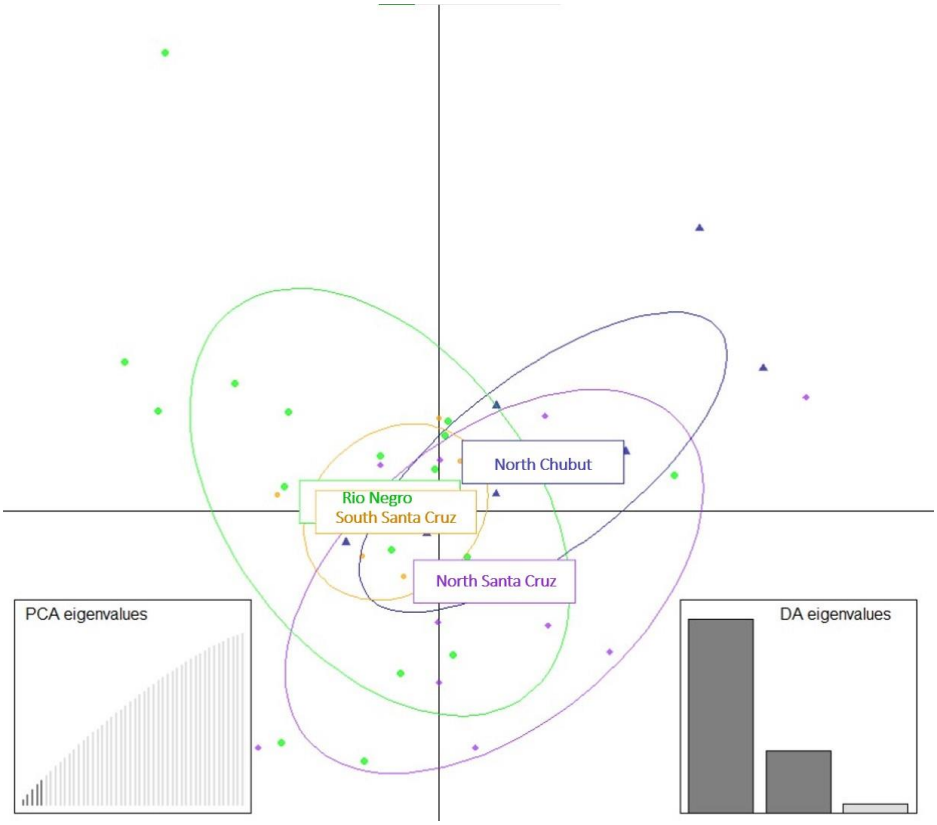

Figure 2.9. When DAPC is run with the a-score-indicated optimum of 6 principle components (PCs), the *a priori* geographic clusters are not distinguished. The two axes of this plot reflect the two most significant discriminant analysis eigenvectors (the first two shaded columns in the bottom right inset). The bottom left inset shows the proportion of total variance accounted for by the top 6 PCs (shaded bars). Although the 6 only account for a small proportion of total variance (~10%), the a-score optimisation procedure identified that number as an optimal balance between under-fitting and over-fitting to the data. The relatively monotonic increase in variance that would be accounted for by additional PCs (the lighter bars) is also consistent with the lack of genetic structure.

Similar results were returned by LEA. The program's cross-entropy criterion indicated that a single ancestral population most parsimoniously explained the data (Figure 2.10). When the assumption of higher levels of structure was imposed, the resulting clustering of individuals did not reflect their geographic source (Figure 2.11).

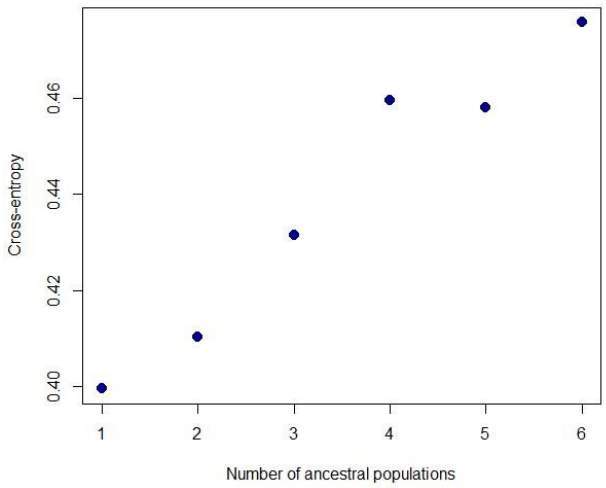

Figure 2.10. Cross-entropy statistic from LEA used to determine the optimal number of clusters (K). As with DAPC, the test statistic is minimized at K=1, suggesting a lack of structure to the genetic variation.

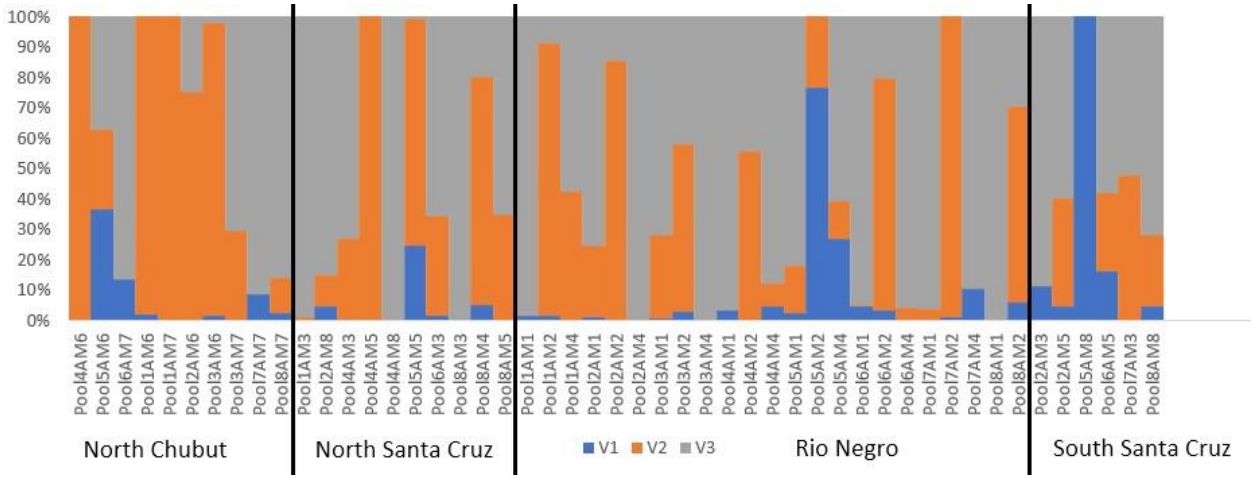

Figure 2.11. LEA result with K=3 selected. Most individuals are inferred to have significant ancestry from multiple clusters, and there is no correlation with the regional sources of the samples.

The genetic significance of geographically-based sample groupings was also tested using F-statistics in Arlequin. This analysis also returned no evidence of population structure, as Φ_{st} was extremely low and not statistically significant between samples from any pair of regions (Table 2.1). An AMOVA testing a possible north-south division, with Rio Negro and North Chubut

grouped against North and South Santa Cruz, also returned a low and non-significant value of F_{st} (-0.00507, p=0.89).

Table 2.1. Pairwise fixation indices between regional populations based on the ddRADseq dataset. F_{st} is shown above the diagonal and Φ_{st} below. RN=Rio Negro, NCh=North Chubut, NSC=North Santa Cruz, SSC=South Santa Cruz.

	RN	**NCh**	**NSC**	**SSC**
RN		0.018 (p=0.694)	0.017 (p=0.695)	0.019 (p=0.757)
NCh	0.000 (p=0.362)		0.027 (p=0.654)	0.035 (p=0.719)
NSC	-0.002 (p=0.417)	-0.003 (p=0.499)		0.033 (p=0.719)
SSC	-0.012 (p=0.928)	-0.007 (p=0.624)	-0.008 (p=0.672)	

Given the lack of genetic structure identified by these other methods, PCAdapt also did not identify distinct clusters of individuals (Figure 2.12). This afforded relatively little power to detect outlier SNPs. Thirty-five outliers were detected using the Bonferroni correction method. However, these were distributed relatively uniformly across the genome, suggesting that they do not represent hotspots of recent divergence or adaptation (Figure 2.13).

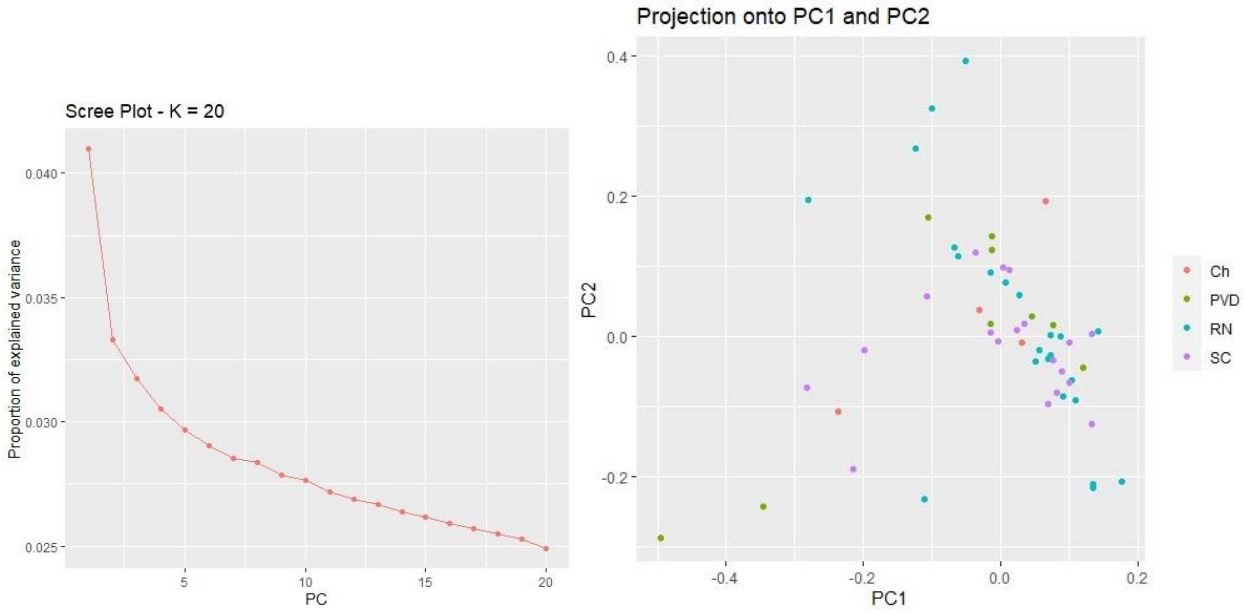

Figure 2.12. Left: Proportion of variance explained per additional principal component. The optimal number of PCs to retain should be the point at which the line stabilizes. Here, the line does not stabilize. The first PC accounts for a much greater share of variance than later PCs do individually, but collectively they still account for significant variance. Right: PCs 1 and 2 do not separate individuals into distinct clusters, whether linked to geography or not.

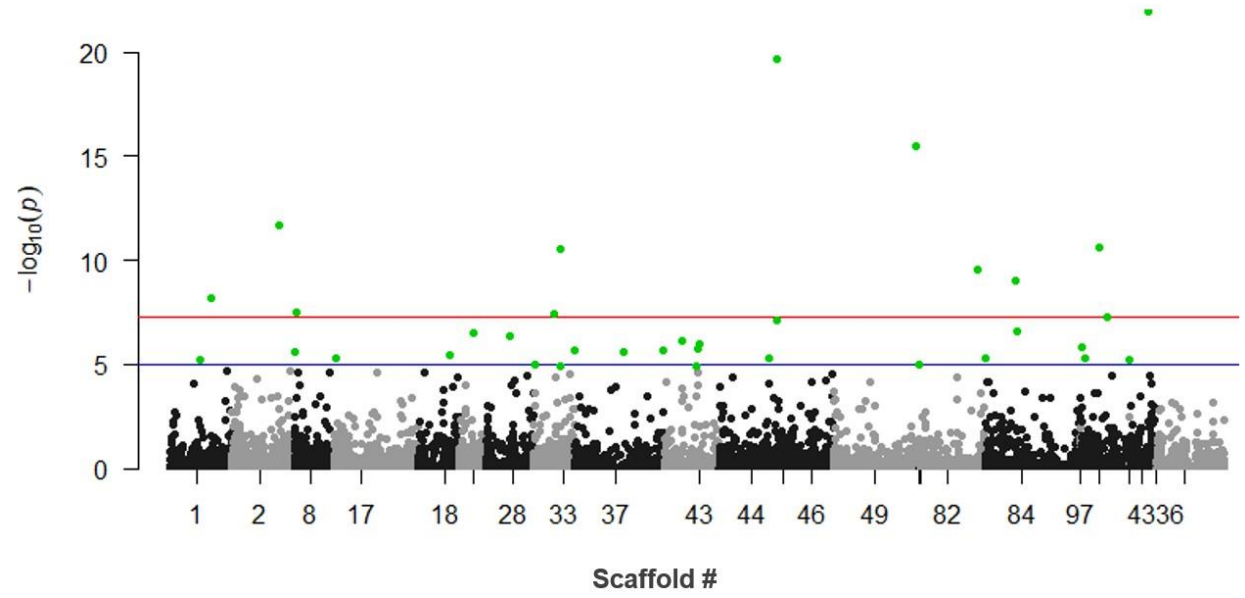

Figure 2.13. Manhattan plots showing the location in the *O. flavescens* draft genome (accession CNP0000758; Yuan et al. 2021) scaffold of putative outlier SNPs (green) identified by the Bonferroni correction method. The blue and red horizontal lines represent 10% and 0.1% thresholds of expected false discovery rate, respectively.

Mitochondrial population structure

Initial exploratory analysis of mitochondrial population structure was carried out by generating haplotype networks to visualize the distribution of variation in the mitogenome (Figure 2.14) and D-loop (Figure 2.15) alignments.

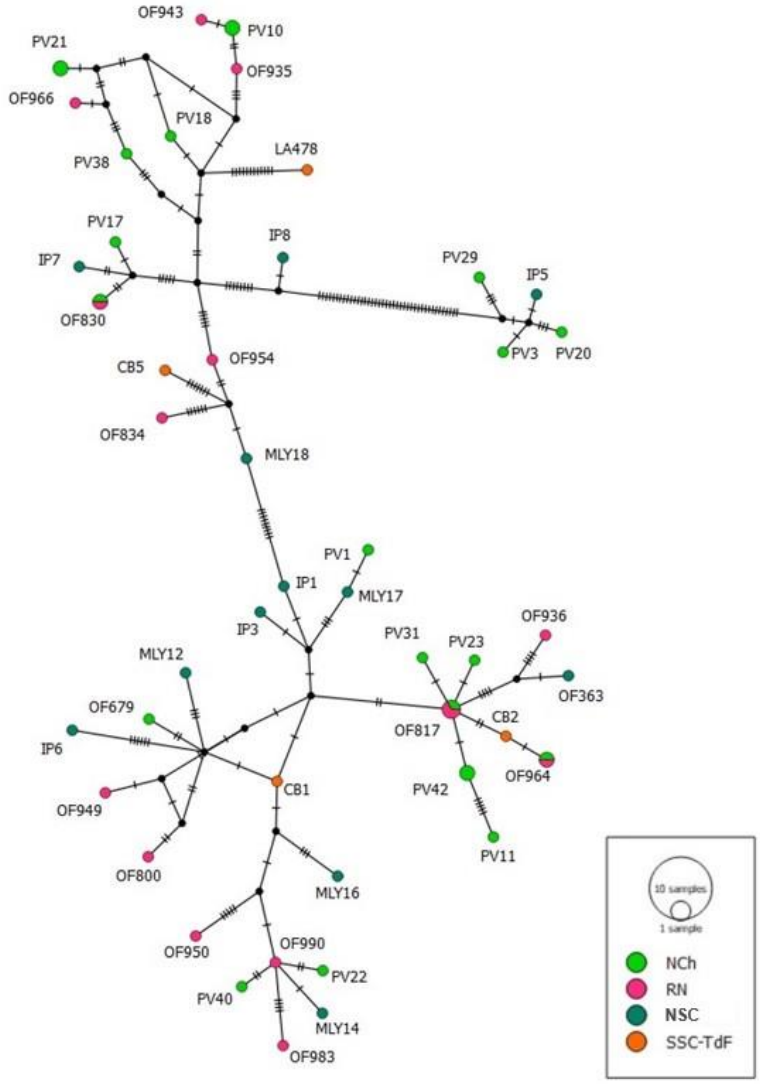

Figure 2.14. Median-joining network of mitogenome haplotypes. Samples are coloured by population assignment, with samples from South Santa Cruz (SSC) and Tierra del Fuego (TdF) pooled together (refer to Figure 2.1 for region definitions). Notably, at the scale of the whole mitogenome, most samples displayed unique haplotypes.

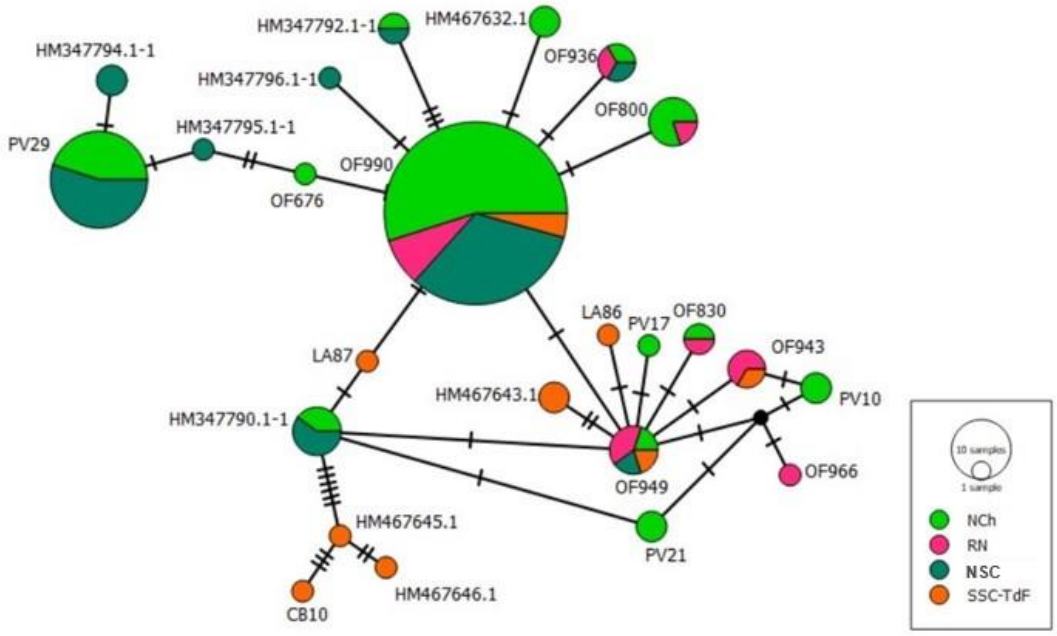

Figure 2.15. Median-joining network of mitochondrial D-loop haplotypes. Samples are coloured by population assignment, with samples from South Santa Cruz (SSC) and Tierra del Fuego (TdF) pooled together (refer to Figure 2.1 for region definitions). At the much smaller genetic scale of the mitochondrial D-loop, most haplotypes were shared, and arrayed around a single most common haplotype.

Discriminant analysis of principal components was also applied to the mitochondrial alignments to assess haplotype clustering and see whether there was evidence of geographic structure in the evolutionary history of the haplotypes (i.e. whether closely related haplotypes are associated with the same regions. For both the mitogenome (Figure 2.16) and D-loop (Figure 2.17), three clusters were identified as optimal. These clusters corresponded to the haplotype networks of their respective datasets, but the geographic makeup of the clusters differed greatly between the datasets (Figure 2.18). In the case of the whole mitogenomes, two main clusters were identified that appeared to be evenly represented across samples with respect to latitude. The third cluster was much smaller, composed of four samples from the Valdes Peninsula and northern Santa Cruz. In the D-loop analysis, one main cluster was identified, including most samples from across the geographic range. However, the other two clusters appeared to have geographic associations: cluster 1 contained more samples from the middle of the range

(Chubut and northern Santa Cruz), while cluster 3 was primarily composed of samples from the northern and southern extremes (Rio Negro and southern Santa Cruz) (Figure 2.18).

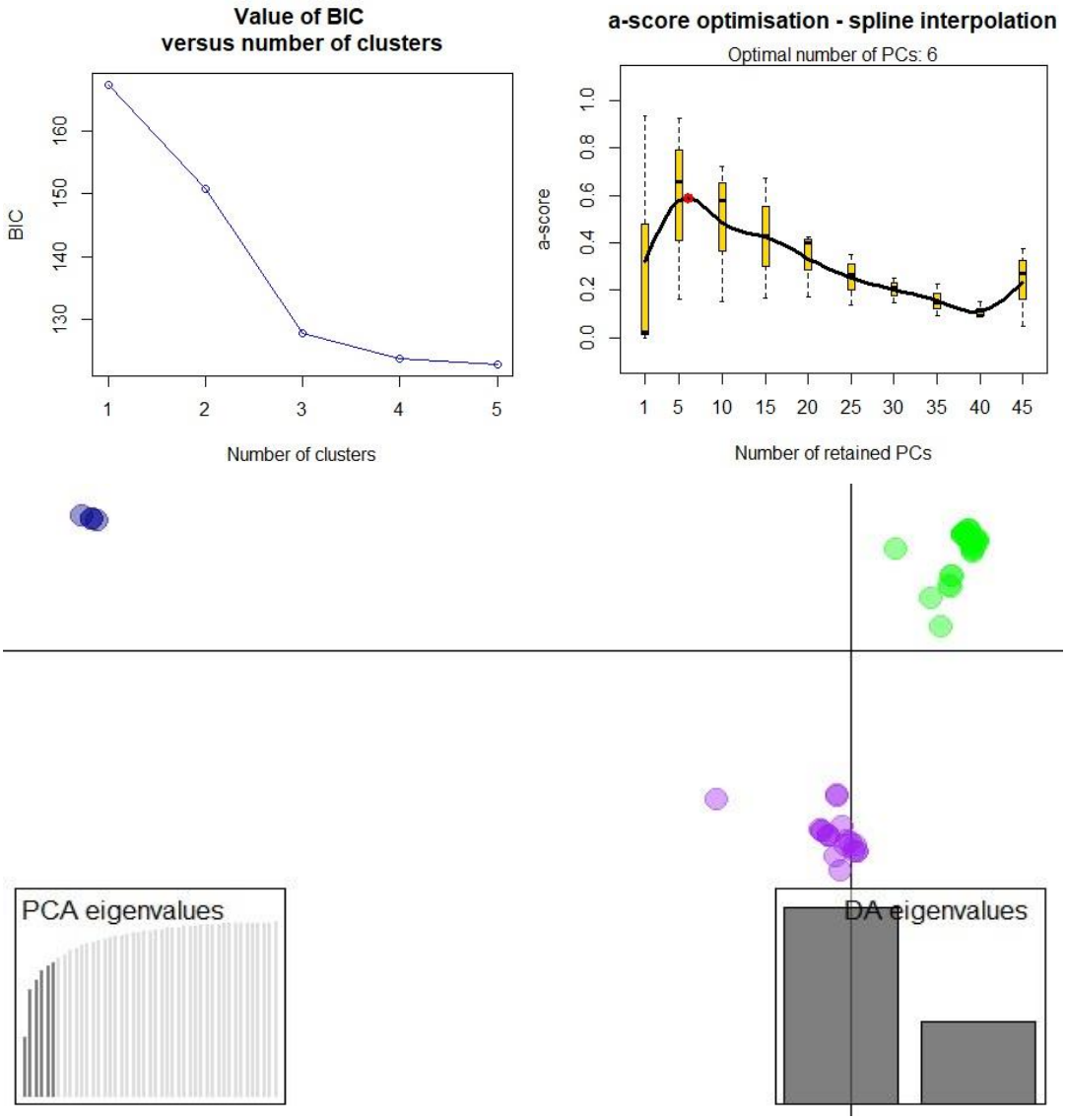

Figure 2.16. DAPC analysis of whole mitogenomes. Three clusters were identified as optimal based on BIC score (top left), and 6 principal components were identified as optimal based on a-score (top right). The two axes of the main plot reflect the two most significant discriminant analysis eigenvectors (the first two shaded columns in the bottom right inset), while the bottom left inset shows the proportion of total variance accounted for by the top 6 principal components (shaded bars).

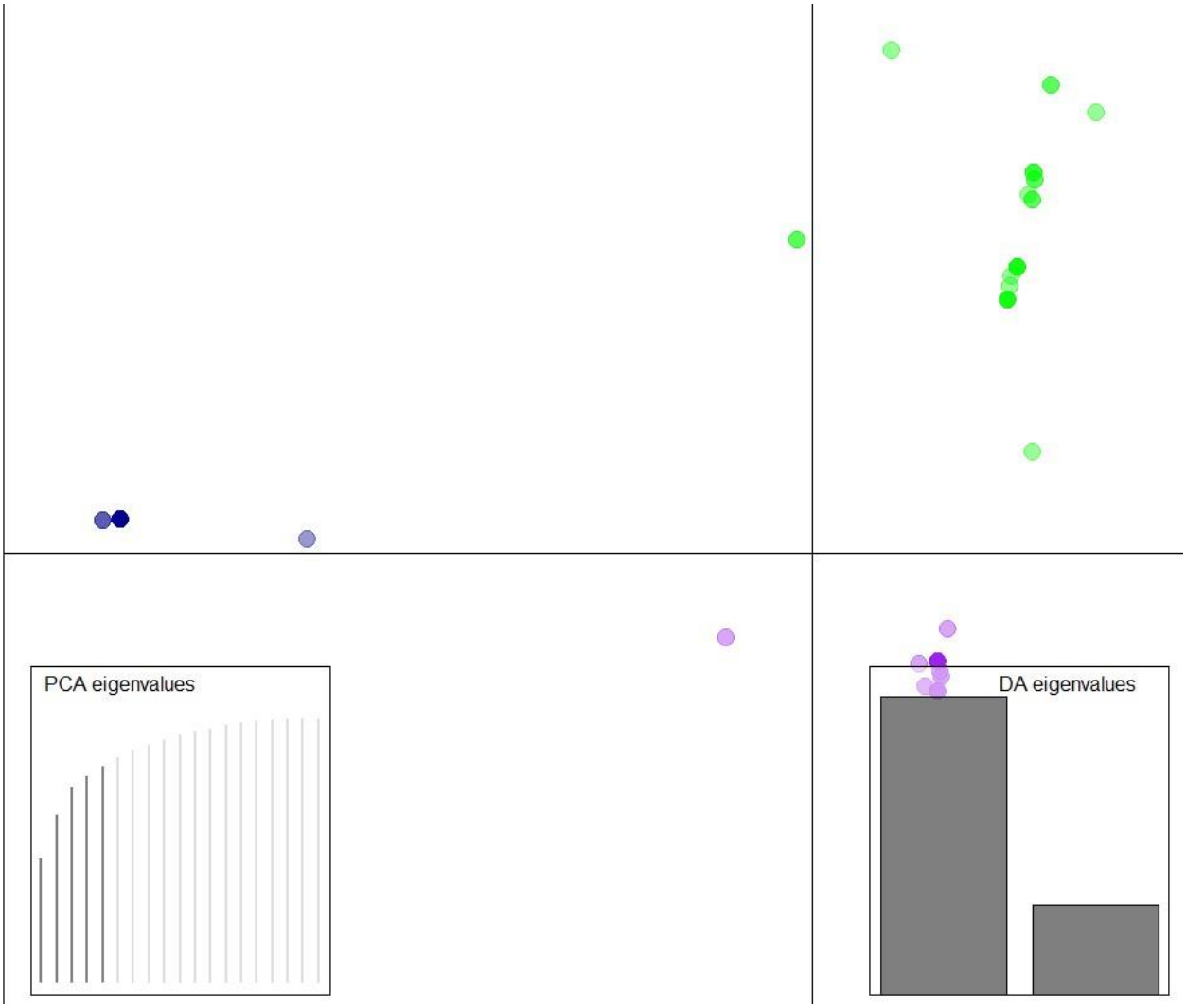

Figure 2.17. DAPC analysis of mitochondrial D-loop sequences. Again 3 clusters were identified as optimal, based on an a-score optimised number of 4 principal components (bottom left inset). However, the sample makeup of these clusters was entirely different from those identified in the mitogenome analysis (Figure 2.16).

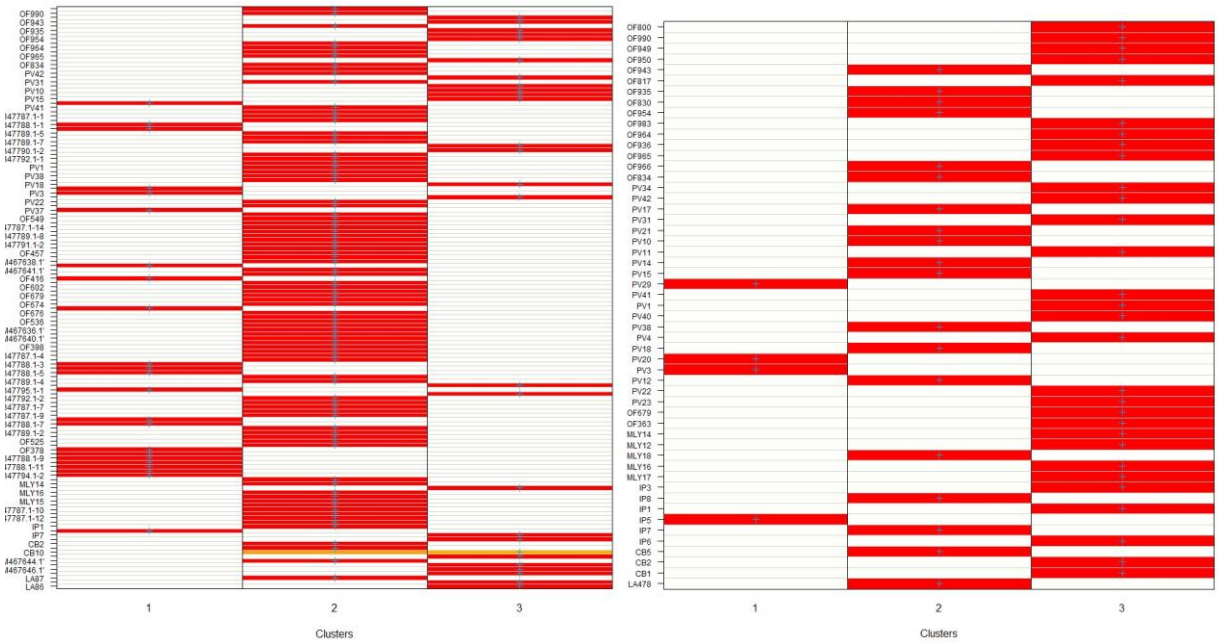

Figure 2.18. Assignment plots for 3 clusters identified by DAPC in the mitochondrial D-loop (left) and whole-mitogenome (right) datasets. The sample order is sorted by latitude, with samples from Rio Negro at the top and South Santa Cruz-Tierra del Fuego at the bottom. Clusters 1 and 3 of the D-loop set appear to disproportionately involve samples from the centre and extremes of the range, respectively. However, no geographic pattern is apparent in membership of the mitogenome clusters.

Following the exploratory analyses with DAPC, population structure was formally assessed using F-statistics (F_{st}/Φ_{st}) and AMOVA. In general, pairwise F_{st} values were much higher and more often statistically significant than pairwise Φ_{st} values. Pairwise Φ_{st} was small and non-significant for all populations based on the mitogenome dataset, while pairwise F_{st} was significant in all cases (Table 2.2). F_{st} was significant in all cases for the 145-bp D-loop dataset, and Φ_{st} was also significant between Rio Negro and South Peninsula Valdes and Santa Cruz (Table 2.3). The 409-bp D-loop alignment gave intermediate results, with F_{st} being significant in all cases and Φ_{st} being non-significant in all cases (but nearly significant for Rio Negro x Santa Cruz) (Table 2.4).

Table 2.2. Pairwise fixation indices between regional populations based on the mitogenome alignment with 10 haplogroups. F_{st} is shown above the diagonal and Φ_{st} below. RN = Rio Negro, NPV = North Peninsula Valdes, SPV = South Peninsula Valdes, SC = Santa Cruz.

	RN	**NPV**	**SPV**	**SC**
RN		0.149 (p<0.001)	0.079 (p<0.001)	0.081 (p<0.001)
NPV	-0.006 (p=0.382)		0.145 (p<0.001)	0.144 (p<0.001)
SPV	0.006 (p=0.403)	-0.041 (p=0.562)		0.075 (p<0.001)
SC	-0.029 (p=0.768)	0.029 (p=0.226)	-0.035 (p=0.403)	

Table 2.3. Pairwise fixation indices between regional populations based on the 145-bp mitochondrial D-loop alignment. F_{st} is shown above the diagonal and Φ_{st} below. RN = Rio Negro, NPV = North Peninsula Valdes, SPV = South Peninsula Valdes, SC = Santa Cruz.

	RN	**NPV**	**SPV**	**SC**
RN		0.258 (p<0.001)	0.312 (p<0.001)	0.233 (p<0.001)
NPV	0.018 (p=0.212)		0.367 (p<0.001)	0.293 (p<0.001)
SPV	0.130 (p=0.004)	0.041 (p=0.062)		0.332 (p<0.001)
SC	0.087 (p=0.014)	0.020 (p=0.132)	0.022 (p=0.087)	

Table 2.4. Pairwise fixation indices between regional populations based on the 409-bp mitochondrial D-loop alignment. F_{st} is shown above the diagonal and Φ_{st} below. RN = Rio Negro, NPV = North Peninsula Valdes, SPV = South Peninsula Valdes, SC = Santa Cruz.

	RN	**NPV**	**SPV**	**SC**
RN		0.086 (p<0.001)	0.084 (p<0.001)	0.081 (p<0.001)
NPV	-0.168 (p=0.656)		0.075 (p<0.001)	0.072 (p<0.001)
SPV	0.021 (p=0.229)	-0.002 (p=0.399)		0.070 (p<0.001)
SC	0.026 (p=0.160)	0.006 (p=0.307)	0.002 (p=0.379)	

The program SAMOVA was used to assess evidence for higher-level population structure (i.e. differentiation among regions) in the mitochondrial markers. SAMOVA operates by using a simulated annealing algorithm to locate the population structure hypothesis that yields the highest F_{ct} value (measuring the proportion of genetic variation accounted for by membership in different population groupings) according to a Φ_{st}-based AMOVA implemented in Arlequin. The results showed that no higher-level grouping of the regional populations was statistically significant. Although not statistically significant, both D-loop alignments gave the most support for grouping geographically adjacent populations, while the mitogenome alignment supported grouping Rio Negro and South Chubut-Santa Cruz to the exclusion of the Valdes Peninsula (Table 2.5).

Table 2.5. SAMOVA assessments of super-regional population structure. The best-scoring structure is shown, along with its support values. RN = Rio Negro, NPV = North Peninsula Valdes, SPV = South Peninsula Valdes, SC = Santa Cruz.

	K=2	**K=3**
Mitogenome	(RN + SC) x (NPV + SPV) F_{ct}=0.030; p=0.315	(RN + SC) x NPV x SPV F_{ct}=0.031; p=0.165
409-bp D-loop	(RN + NPV + SPV) x SC F_{ct}=0.025; p=0.257	(RN + NPV) x SPV x SC F_{ct}=0.032; p=0.160
145-bp D-loop	RN x (NPV + SPV + SC) F_{ct}=0.053; p=0.258	(RN + NPV) x SPV x SC F_{ct}=0.036; p=0.167

Discussion

A sequence alignment with a large number of segregating sites affords greater power to distinguish individuals or to more accurately group individuals, while a larger number of individuals allows for population-specific allele frequencies to be estimated more accurately and precisely. These virtues must inevitably be traded off against one another, by sequencing a greater number of individuals or a larger amount of their genomes. In the present study, there is a tension between utilizing the power of full mitogenome sequences to distinguish individuals and using the many published sequences that are available for *O. flavescens*, supplemented by novel sequences, to achieve better geographic representation. The full mitogenomes almost over-distinguished individuals, with few instances of complete haplotypes being shared by multiple individuals. This made direct estimation of F_{st} impossible, so similar haplotypes were clustered into families, or haplogroups, and mitogenome F_{st} was calculated based on differences in the frequencies of these haplogroups across regions. With this correction, the mtDNA analyses confirmed previous findings of geographic structure in matrilineages, finding significantly different alleles frequencies (F_{st}) between all regional pairs. This result was consistent regardless of which mtDNA alignment was used, ranging from 145 sites represented across 141 individuals to 14554 sites represented across 53 individuals.

Despite far greater power to recognise geographic differences than nuclear (microsatellite) markers used by previous studies (Feijoo et al. 2011; Oliveira et al. 2017), the ddRADseq analyses presented here still do not reveal any geographic structuring of nuclear genomic variation. Although consisting of a large number of SNPs and broad geographic representation, the dataset is far from exhaustive, as indicated by the rarefaction curves of new SNP discovery per individual added (Figure 2.4), which continue to increase approximately linearly at the sample sizes available for central-southern Patagonian populations (NCh, NSC, SSC) and only begin to level off in the northern-most population (RN), at twice the sample size. However, rare alleles are also necessarily less likely to diagnose major divisions among populations. The most parsimonious explanation at this point, considering the consistency of this result across studies, is that there is indeed no meaningful geographic structure to be found in the variation of the nuclear genome writ large.

The main explanation for geographic structure in mtDNA but not nuclear markers is based on female philopatry, the tendency of females to return to the place they were born during each mating season (Tunez et al. 2010; Feijoo et al. 2011). In contrast, male Otaria typically haul out near their feeding grounds and mate with local females. This may result in long-distance nuclear gene flow being common while introgression of maternally transmitted mtDNA haplotypes from other regions remains rare. Female philopatry and male-biased dispersal has been observed in *O. flavescens* (e.g. Oliveira et al. 2017) and is reasonably common across pinniped species (e.g. *Mirounga leonina*, Fabiana et al. 2003; *Arctocephalus galapagoensis*, Lopes et al. 2015). Grandi et al. (2018) have suggested that female *O. flavescens* do move between adjacent colonies within range of key foraging sites, with regional-scale philopatry being related to familiarity with ideal foraging grounds that will allow them to reliably sustain themselves and their pups during the breeding season.

Historical population dynamics could also contribute to explaining why the nuclear genome does not show geographic structure while the mitochondrial genome does. Structure would develop over time, as regional populations differentiate. The effective population size of the mitochondrial genome is approximately half that of the nuclear genome, since only females pass on their mtDNA. While this would mean that the mitochondrial genome should evolve half as quickly as the nuclear genome, it is outweighed by the fact that the mitochondrial mutation rate of vertebrates is on average ~20x faster than the nuclear mutation rate (Allio et al. 2017). Moreover, the strength and rate of genetic drift, which is generally the most common force

behind allele frequency divergence, is inversely proportional to effective population size. Therefore, if regional differentiation has begun only recently (on an evolutionary timescale), we would expect to see mtDNA divergence sooner than divergence in the nuclear genome.

Shallow differentiation

The sequencing of full mitogenomes afforded far greater power to discriminate individual haplotypes and count the nucleotide differences between them, allowing for the calculation of Φ_{st}. This revealed that while the frequencies of specific haplogroups differ between regions, the most common haplotypes in each region are not especially closely related. Therefore, F_{st} is significant while Φ_{st} is not, because population identity does not explain much of the absolute genetic distance between individuals even if it does predict which precise haplotypes they are likely to carry. There were not extended haplotype families associated with particular Argentine regions, in contrast to the level of differentiation that has been found for Atlantic versus Pacific lineages (Oliveira et al. 2017). Mutation, which is required for the generation of families of similar haplotypes from single ancestral haplotypes, typically occurs over a longer period than is required for genetic drift, which would be the process responsible for regional differentiation in the frequencies of shared haplogroups. This is consistent with the idea that regional matrilineal differentiation has developed relatively recently within a historically mixed population (i.e. the Atlantic lineage).

The nuclear SNP data actually display a similar pattern despite no indication of regional structure. They include an excess of low-frequency SNPs (low nucleotide diversity despite a high number of segregating sites, i.e. negative Tajima's D; Tajima 1989). Rare alleles are most likely to have been derived relatively recently, and a negative Tajima's D is normally interpreted as reflecting geologically recent population expansion. The demographic history of *O. flavescens* will be investigated in more detail in the next chapter.

A possible environmental mechanism for bringing about reduced connectivity between regional populations of *O. flavescens* was the large-scale crenulation of the coastline of Argentina, the formation of distinct gulfs and proximal foraging grounds associated with marine fronts. These changes began after the LGM and stabilized around the beginning of the Holocene after thousands of years of post-glacial sea level rise (Ponce et al. 2011). During the LGM and for several thousand years after, the coastline was likely a sprawling coastal plain that would have

been more homogeneous in characteristics like tidal width and rockiness (substrate type), factors which in modern times contribute to the heterogeneous distribution of *O. flavescens* colonies (Tunez et al. 2008). The Golfo San Jorge is thought to have formed ~15 kya, while the gulfs surrounding the Valdes Peninsula (San Matías, San José and Golfo Nuevo formed ~12 kya (Ponce et al. 2011). These gulfs are associated with different marine fronts (Acha et al. 2004; Pisoni et al. 2015) – ideal foraging grounds – and, as we have seen, they now define regional populations that exhibit partial mtDNA differentiation.

Chapter 3: Environmental influences and demographic history of *Otaria flavescens* and *Spheniscus magellanicus*

Introduction

Populations of the same species have some degree of demographic dependence, given an ongoing exchange of migrants and their genes (e.g. White et al. 2011). This means that growth or decline in one population is likely to be either mirrored or contrasted in other populations. One of the main practical applications of understanding population structure, as discussed in the previous chapter, is to recognise partially differentiated groups that have the potential to respond differently to changes in their environment. At the extreme end of this are separate biological species, defined by a complete absence of gene flow and full demographic independence. However, even distantly related species also have the potential to respond similarly to environmental change in a shared environment. Individuals' ecological traits determine aspects of the environment to which they and their population are vulnerable to change. For example, a population of dietary specialists is likely to decline when the species they feed on becomes more rare, and grow when their food source proliferates. This means that predators are also dependent on the environmental conditions and resources required by their prey.

The main species of interest in this chapter are the South American sea lion (*Otaria flavescens*) and the Magellanic penguin (*Spheniscus magellanicus*). These species coexist along the Atlantic coast of Patagonia, foraging in the same waters and breeding on the same beaches (Hernández-Orts et al. 2017). Sea lions and penguins both take prey from the ocean along the coast of Patagonia. Marine conditions, such as depth, temperature and overall biological productivity, vary along the length of this coastline. The width of the continental shelf also differs, determining how far individuals must travel to reach certain prey. Both species are capable of travelling great distances on foraging trips (e.g. >500 km in *S. magellanicus*; Kochi et al. 2018), potentially allowing them to access preferred prey species that do not occur near their home colony.

Diet

The diet of wild animals can be studied through direct observation of their foraging behaviour or through analysis of their stomach or scat contents. The dietary history of an individual can also be reconstructed through analysis of the stable isotope composition of their tissues, including bone (Ben-David and Flaherty 2012). Nitrogen isotope composition (δ15N) is associated with trophic level, with the tissue of predators typically being enriched in δ15N relative to their prey. However, δ15N values of a marine consumer can also be influenced by the distance from shore and depth at which they or their prey forage, because intertidal plants may assimilate nitrogen from terrestrial runoff, and there are differences between typical native marine and terrestrial nitrogen values (Sealy et al. 1987; Griffin and Valiela 2001). This difference can propagate up to higher trophic levels to also affect the δ15N composition of predators who feed on nearshore fish or molluscs, for example. Carbon isotope composition (δ13C) can also be affected by trophic level, but for marine vertebrates, differences in δ13C values are mainly thought to reflect differences in water depth and distance to shore at which they forage (e.g. Hückstädt et al. 2007; Barros et al. 2010; Zenteno et al. 2015a; Szpak and Buckley 2020). Sulphur isotope composition (δ34S) is thought to be the most sensitive of these isotopes to distance from shore, because terrestrial sulphates have dramatically lower δ34S values than marine sources. However, because δ34S is specifically so strongly influenced by terrestrial/freshwater input to the marine ecosystem, it may be especially sensitive to local conditions along the shore (e.g. river interfaces), not simply proximity to shore (Gorski et al. 2015; MacAvoy et al. 2014). At the same time, δ34S is thought to be the least sensitive to variations in trophic level (Szpak and Buckley 2020). Measuring each of these isotopes can provide clues to overall diet composition and foraging behaviour (Ben-David and Flaherty 2012).

O. flavescens diet

The most consistent message from past research on the diet of *Otaria flavescens* is that individuals adapt their diet to what is available in their environment, with a preference for demersal-pelagic prey, including anchovy (*Ergraulis anchoita*), when available (Alonso et al. 2000). Bustos et al. (2012, 2014) used fecal analysis to study the diet of sea lions in Rio Negro and its seasonal variability. They found that during the summer breeding season this population forage on fish, especially the eel *Raneya brasiliensis*, followed by cephalopods, with a lower amount and diversity of prey being consumed in the winter.

In general, benthic prey (those living on the seafloor) are less densely aggregated than pelagic prey (those living in the water column), and as a result are less efficient targets for foraging. Benthic prey also physiologically have lower energetic value, due to having lower lipid content on average than pelagic prey (Hückstädt et al. 2016). Through analysis of the stomach contents of accidentally killed and stranded individuals, Alonso et al. (2000) found that females consumed a greater proportion of benthic prey than males, suggesting that females fed closer to shore in shallower waters. This is consistent with the findings of a GPS tracking study by Campagna et al. (2001), which showed that members of both sexes disperse widely, but lactating females took shorter trips on average that did not allow them to reach the edge of the continental shelf where pelagic prey would be more abundant. The tracking also showed that most female dives were “U-shaped”, meaning that they spent a significant amount of time moving horizontally along the seafloor, indicative of benthic feeding (Campagna et al. 2001). Based on a combination of their own stable isotope analysis and previous stomach content analyses, Zenteno et al. (2015a) described that males primarily ate demersal fish, with a shift towards more pelagic fish in Patagonia in recent decades, potentially as a reaction to the rise of bottom-trawling fisheries in the area, which has depleted some of their preferred prey. They also found that juvenile *O. flavescens* consume more pelagic prey than adults on average.

Evidence of geographic differences in sea lion diet is mixed, and has been explicitly addressed by relatively few studies. For example, Alonso et al. (2000) did not find differences in stomach contents in a large-scale comparison between Rio Negro/north Chubut and south Chubut/north Santa Cruz. However, Jarma et al. (2019) found differences in diet on a much smaller scale between sea lions of the Golfo San Matias and the Golfo Nuevo on the north and south sides of the Valdes Peninsula, respectively. Based on stomach samples, they found that pelagic fish were central to the diet of sea lions in the Golfo San Matias, while those in the Golfo Nuevo ate more benthic prey. This is consistent with the higher overall productivity of the Golfo San Matias’ waters, but may be more directly related to the presence of human fishing boats that gather fish, making them more accessible to the sea lions. These waters have been fished by humans for thousands of years, but the scale has grown dramatically since industrialisation. Based on analysis of carbon and nitrogen isotopes, Baylis et al. (2016) found dietary differences between the West and East Falkland Islands among female sea lions. This, despite substantial individual variability in diets within colonies. They also found that a colony’s main foraging areas were not simply determined by geographic proximity, suggesting a role for individual preferences, perhaps informed by prior experience of foraging in different areas.

S. magellanicus diet

The diet of Magellanic penguins in northern Patagonia appears to be dominated by anchovy (Yorio et al. 2017; Castillo et al. 2019). They even follow the anchovy north to Uruguay and Brazil during the winter, between breeding periods (Marques et al. 2018). Juveniles also eat anchovies, but also eat a much larger share of cephalopods (e.g. *Doryteuthis sanpaulensis*) (Marques et al. 2018).

Areas with high competition among penguins or between penguins and human fisheries exhibit lower average individual consumption of anchovies (Ramirez et al. 2014). For example, when anchovies are hard to find, juveniles and females may shift focus to other prey (Castillo et al. 2019). Yorio et al. (2017) found that anchovies were the most important prey for penguins in the Golfo San Jorge, based on stomach content and stable isotope analysis. However, older chicks, arguably weak competitors, were the only group to have a different main item, shortfin squid (*Illex argentinus*). Forero et al. (2002) determined based on carbon and nitrogen isotopes that chicks who were being provisioned by parents ate more anchovies than adults, and that anchovy proportion in diet was predictive of chick body condition. Independent yearlings, on the other hand, ate less anchovy than adults. It is not clear how large of a role competition plays in these age and sex differences. Females and juveniles are both smaller than males on average, which could make them less competent competitors. However, they may also have dietary needs and different behaviours or diving capabilities. It may simply be a matter of smaller and/or less experienced individuals being less competent at catching their preferred prey.

While anchovies form the bulk of the penguin diet in northern Patagonia, Scolaro et al. (1999) found that Magellanic penguins from farther south (Santa Cruz) ate little anchovy, but instead had a more diverse diet including silverside fish (*Odontesthes smitti*), squid and other fish. Notably, these were all fish that are also commercially hunted by humans. In the far south, Tierra del Fuego, Magellanic penguins mainly consumed sprat, lobster and squid, with adults eating more lobster while juveniles ate more sprat (Scioscia et al. 2014; Dodino et al. 2020). Similarly, Otley et al. (2004) found squid to be the main food of chicks in the Falkland Islands.

Interspecific dietary overlap

Overall, previous studies suggest that *Otaria flavescens* and *Spheniscus magellanicus* have overlapping trophic niches (e.g. both consume pelagic fish), but they are not identical. Throughout Patagonia, *O. flavescens* consume far more benthic prey than penguins. In contrast, penguins seem to be somewhat more specialised on anchovy or other pelagic fish.

South American sea lions and Magellanic penguins also co-occur with other potential competitors. Magellanic and gentoo penguins (*Pygoscelis papua*) coexist in Tierra del Fuego, where gentoos focus on diving for benthic prey while Magellanics prioritise pelagic or other opportunistically acquired prey, similar to the relationship that seems to exist with sea lions (Sabrina et al. 2020). In sympatric Uruguayan populations, breeding females of *O. flavescens* and the fur seal *Acrocephalus australis* have largely distinct trophic niches, with sea lions mainly foraging in the intertidal zone nearer to shore while fur seals forage in the water column farther from shore (Franco-Trecu et al. 2012).

Life history and behaviour

Life history traits are also potentially important mediators of demographic history. They affect the rate at which a species adapts to changing circumstances (demographically or evolutionarily), shape habitat preferences (breeding site requirements), and influence which environmental variables species are sensitive to.

Females belonging to species that follow a “capital” breeding strategy, such as Southern elephant seals (*Mirounga leonina*), accumulate most of the energy they will use for sustaining themselves and their offspring until the offspring is weaned in their bodies prior to giving birth. Therefore, proximity to optimal foraging areas does not need to be an important factor in selection of the site where they will actually nurse their pup(s). In species that follow an “income” breeding strategy, which includes both *O. flavescens* and *S. magellanicus*, breeding sites need to be as close as possible to good foraging grounds because a juvenile’s survival and fitness depends on their mother’s ability to efficiently provide food for both of them during the nursing period. This strategy also means that the availability of prey during the breeding season is especially important for setting offspring up for healthy lives. For example, Soto et al. (2004) reported that interannual variation in pup recruitment in Peruvian *O. flavescens* was strongly correlated with anchovy biomass during the summer breeding season, which was in

turn related to the El Niño climatic oscillation. Intuition and modelling suggests that populations of income breeders are generally more sensitive to short-term (e.g. seasonal) disturbance than populations of capital breeders, since capital breeders can accumulate and retain resources for breeding (i.e. body mass) over a longer period of time (Jonsson et al. 1997; Simmons et al. 2010; McHuron et al. 2016; Holser et al. 2021).

Otaria life history and behaviour

Mating system, the process by which individuals find and select mates, also influences genetic diversity (i.e. N_e) and adaptive potential by determining what proportion of the population actually contributes to the genetic makeup to the next generation. *Otaria* generally practice a polygynous mating system, in which males may mate with multiple females and defend them as a "resource" against rival males. To do this, males strive to defend beach territories where they can guard their harem, while other males (typically younger) who have failed to claim territory of their own occasionally form groups and raid beaches to seize individual females (Campagna and Le Boeuf 1988; Soto and Trites 2011; Franco-Trecu et al. 2015). The intensity of territoriality and polygyny appears to be flexible to environmental conditions, with at least one population of *Otaria flavescens*, in Peru, having a lek-like breeding system, emphasizing female choice in mates (Soto and Trites 2011). This is thought to have come about locally, in part due to a warm climate driving females to require more access to the ocean than they need in the cooler climate of modern Patagonia, where tidal pools or limited shoreline access are usually sufficient to keep females content in a male's territory, where the females can be prevented from coming into contact with competing males, ultimately limiting the role of female choice in mate selection.

While male sea lions are largely occupied with territorial defence during the breeding season, females continue to make journeys out to sea to forage in order to sustain themselves and their pup. Sea lion pup mortality is strongly affected by fluctuations in prey availability, such as those that result from El Nino events on the Pacific coast (Soto et al. 2004; Oliveira et al. 2012). Variation in the frequency or intensity of extreme weather events in the past or present, due to climate change, might especially impact juvenile survival rate (Sepúlveda et al. 2020), which could have secondary effects on population size and growth rate, as well as generation time if disproportionate reduction in juvenile survival were to push the population's age structure and median age higher. Pups are also threatened by predation (e.g. by orcas: Vila et al. 2008) and

infanticide (Campagna et al. 1988; Cassini 1998). Individual females and pups receive less harassment from males in large breeding groups, with males spending more time simply corralling and securing their harem of females against other males (Cappozzo et al. 2008).

Outside of the breeding season, males and females both hunt for food in open waters, but females generally return each breeding season to the same area where they were born, while males are much less loyal to place, prioritising areas where they are most likely to be able to defend a territory (Giardino et al. 2016). Early arrival could give them an advantage in this regard, and so, many males may end up breeding at beaches near the preferred feeding grounds.

Spheniscus life history and behaviour

In contrast to sea lions' polygynous breeding system, social monogamy is common among *Spheniscus magellanicus*, with pairs of penguins cooperating to raise chicks year after year. Despite social monogamy, extra-pair mating is also common (Marasco et al. 2020). All else being equal (e.g. excluding recent population bottlenecks), this more egalitarian breeding system should lead to Magellanic penguins having a higher genetic diversity (N_e) relative to their numbers (N_c) than sea lions, thanks to reproductive output being distributed more evenly across individuals.

Penguin parents share the responsibilities associated with caring for their chicks. Barrionuevo et al. (2018) analysed a spectrum of factors that could plausibly affect hatchling growth and survival rate. They found that parents' body condition was related to hatchling growth rate and survival, presumably reflecting the ability of the parent(s) to provide food. The nutritional quality of food provided was also highly predictive of chick growth and survival. As noted previously, benthic prey have a lower lipid content than pelagic prey on average, and therefore have lower energetic value, requiring more prey – in terms of count and bulk mass – to be caught, while also potentially requiring more energy due to the challenges of diving (Hückstädt et al. 2016).

Across breeding seasons (as opposed to within breeding seasons or geographically), hatchling survival was also inversely related to chlorophyll-a concentration. Chlorophyll-a is a proxy of primary productivity near the ocean surface, but differences from one breeding season to the next may also reflect differences in weather, such as more severe weather leading to churned-

up oceans leading to greater abundance of chlorophyll-bearing phytoplankton at the surface. Nest-flooding and hypothermia, which would be more likely during periods of severe weather, are important causes of chick mortality. Modern climate change is already affecting the Magellanic penguin through extreme weather events that have directly increased juvenile mortality (Boersma and Rebstock 2014). Juvenile mortality has also been increased indirectly by climate change, as parent penguins are required to travel increasing distances from their historic breeding colonies to find prey that are already shifting their range in response to climate-induced changes in the marine environment (Boersma and Rebstock 2009). If Magellanic penguins and South American sea lions are tracking the same prey, the sea lions may suffer similar effects.

In contrast to the female philopatry and male dispersal that characterises *Otaria flavescens*, Magellanic penguins of both sexes are more-or-less equally philopatric. This leads to much greater consistency between their nuclear and mitochondrial DNA markers (Dantas et al. 2018). It could also imply that their colonies are more demographically independent, which could leave them with more distinct genetic signatures of past demographic change as well as leaving their colonies more vulnerable to local collapse.

Environmental influences in Patagonia since the LGM

During the last glacial maximum (LGM; ~18-22 kya), lowered global sea levels led to much of the Atlantic continental shelf of Argentina being exposed. During this period, the modern coastal front systems – hotspots of primary productivity over the continental shelf – would not have existed. Modern examples include the Peninsula Valdes tidal front and the Atlantic Patagonia cold estuarine front (Acha et al. 2004; Zangrando and Tivoli 2015). Other coastal fronts could have existed, but their existence is facilitated in modern times by the unusually broad continental shelf, which provides space for the development of distinct water bodies and diverse local conditions (Acha et al. 2004). On the other hand, for shoreline-dwelling species such as *Otaria flavescens* and *Spheniscus magellanicus*, this would have meant that their haul-out and breeding sites were closer to the edge of the continental shelf (the shelf break), which generally hosts even more productive fronts. For example, some modern *O. flavescens* and *S. magellanicus* make long foraging trips out towards the shelf edge (Campagna et al. 2001; Boersma et al. 2009). The net effect of these changes on penguin and sea lion populations is unclear, but would mainly depend on the resulting change in two factors. First, foraging journey

distance, as long journeys waste energy and keep parents away from offspring for longer, reducing their survival (e.g. Boersma and Rebstock 2014). Second, changes in forage quality, such as a shift towards even more benthic feeding (e.g. due to lower sea level), or less benthic and more pelagic feeding (e.g. due to closer proximity to the deep ocean waters of the shelf break). Implied by the question of how these two species would have responded to the minimum sea level during the LGM is also the question of how they would have responded to sea level rising again for ~6,000 years before a coastline approximating the modern one was reached in the early Holocene.

Previous evidence on demographic history

Otaria flavescens

Existing evidence on the prehistoric demographic histories of *O. flavescens* and *S. magellanicus* has mainly come from population genetics work based on mtDNA markers. Tunez et al. (2007) sequenced the mitochondrial cytochrome *b* gene (445 bp) of 60 individuals of *O. flavescens*. They then used an estimated rate of sequence divergence of $2e^{-8}$ nucleotide substitutions per site per year (s/s/y) to estimate the timing of the common ancestor of all haplotypes currently circulating in the population. They estimated a divergence time of ~110 kya, and suggested that the Atlantic lineage of *O. flavescens* had undergone a bottleneck around that time that limited the diversity from which all extant haplotypes could have been derived. A major limitation of their study was that they only identified six distinct haplotypes in their cytochrome *b* alignment. Tunez et al. (2010) followed up on this work by sequencing the hypervariable D-loop region of the mtDNA, which revealed 10 haplotypes. This alignment was subject to mismatch distribution analysis, which can indicate whether a population has expanded in the geologically recent past based on the distribution of the frequency of genetic distances between pairs of haplotypes. Histograms of pairwise genetic difference for populations that have expanded from a bottleneck are expected to show a single peak at a number of pairwise differences corresponding to the amount of time (scaled by mutation rate) elapsed since the population began to expand. This is similar to the expectation of a star-shaped haplotype network, as the existence of a single common number of pairwise differences suggests that all haplotypes have been evolving independently for approximately the same amount of time, presumably from a single ancestral haplotype that became very common in the population due to genetic drift during a bottleneck. Tunez et al. (2010) did find such a peak. Using a mitochondrial mutation rate estimated for Steller sea lions (*Eumetopias jubatus*) of $2.745e^{-7}$ s/s/y (Phillips et al. 2009), they estimated that

the peak corresponded to ~64 kya, suggesting that the north-central Patagonian population of *O. flavescens* began to expand around that time. Feijoo et al. (2011) performed a nearly identical analysis, except with a larger and more geographically disparate population sample. Their mismatch distribution analysis suggested that the population expanded around ~23-27 kya, but that this expansion was concentrated in north Patagonia.

More recent work has taken advantage of the Skyline Plot family of methods for inferring demographic history (Oliveira et al. 2017). These methods use coalescent theory to model the genealogical branching pattern among sampled DNA sequences as a function of population size (Ho and Shapiro 2011). Many coalescence events (i.e. common ancestry events between sampled haplotypes) occurring within a small space of time suggests that the population was relatively small during that time, whereas coalescence events are expected to have occurred less frequently when a population was relatively large, and to occur at a consistent rate across the whole genealogy if the sampled population maintained a constant size (large or small) (Figure 3.1).

Oliveira et al. (2017) used the Extended Bayesian Skyline Plot (EBSP) to reconstruct the history of *O. flavescens* from Argentina, southern Chile, and Peru based on 147 sequences of the mitochondrial D-loop. Their analysis indicated that all three regional populations of *O. flavescens* had grown dramatically, by two orders of magnitude, since ~10 kya. They found no evidence of population growth or decline within the prior ~40 kya. These results contrast sharply with those of Tunez and Feijoo. Oliveira et al. assumed a much slower mutation rate than Tunez et al. (2010) and Feijoo et al. (2011) had used, at $5.8e^{-8}$ s/s/y compared to $2.745e^{-7}$ s/s/y. This slower rate was based on a comparison by Dickerson et al. (2010) of northern fur seals (*Callorhinus ursinus*) against Steller sea lions and California sea lions (*Zalophus californianus*), using estimates of the divergence times between the species. In contrast, the faster rate reported by Phillips et al. (2009) for *E. jubatus*, and used by Tunez and Feijoo, was based on a survey of populations within the single species and homoplasy was controlled for by also sequencing a slower-evolving locus on the same mtDNA haplotypes. In general, rates based on interspecific divergence times are likely to underestimate the mutation rates that apply to the shorter timescales of population genetics because homoplasy (mutation of the same site) is more likely to occur over these timescales and be missed in the analysis (Hoffman et al. 2011).

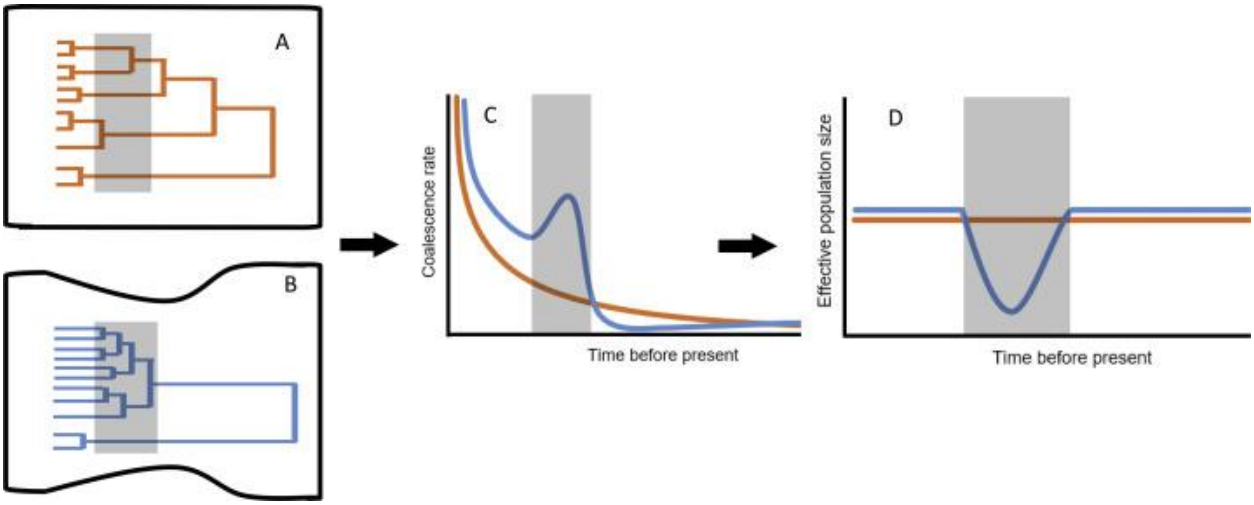

Figure 3.1. Figure taken from Hecht et al. 2020. The frequency of inferred coalescent events with respect to time can be indicative of historical population sizes. In particular, populations that experienced a bottleneck during a given period (blue), and then recovered, are expected to show a higher density of branching events in their genealogy around the time of the bottleneck, and a lower density after the bottleneck as the population grew, relative to a population that remained at a constant size (orange) (Eriksson et al. 2010).

The most recent work on *O. flavescens* demographic history has come from Peralta et al. (2021). They built on these prior studies by using the arguably more appropriate, faster mutation rate in conjunction with a large and geographically broad sample to supplement the dataset previously published by Tunez et al. (2010). Their BSP analysis showed no clear evidence of population growth or decline over the past million years, albeit very weak evidence for modest growth, specifically in the Patagonian population, sometime within the last 200,000 years. However, this analysis was based exclusively on modern samples, which would have provided less power to reveal past demographic change than if they had been able to use ancient DNA to more directly represent historical coalescences. This null finding is at odds with all prior work on the demographic history of *O. flavescens*, but is based on the most comprehensive dataset and arguably the most plausible set of assumptions that have been used in published studies.

Spheniscus magellanicus

The literature on the prehistoric demography of *S. magellanicus* is much smaller than the literature on *O. flavescens*. Several studies have discussed the penguins' modern demographic history, including the fact that new colonies have been founded farther north since the 1920s (e.g. Boersma 2008; Bouzat et al. 2009). However, only one study seems to have used population genetics to reconstruct the species' demographic history. Dantas et al. (2018) applied EBSP analysis to a mitochondrial D-loop alignment of 210 individuals from the Beagle Channel in the far south to the Valdes Peninsula in northern Patagonia. They found strong evidence for historical population growth, which they estimated to have begun ~17.5 kya in parallel to the warming of the region and possible exposure of additional breeding sites along the coast. This time estimate was based on an assumed mutation rate of $8.6e^{-6}$ s/s/y, originally estimated for the same locus in Adélie penguins (*Pygoscelis adeliae*) by Millar et al. (2008). The methodology behind this mutation rate estimate was very good, utilising ancient DNA samples to follow change in a single population over thousands of years. However, this rate was derived for Adélie penguins, who are thought to have last shared a common ancestor with *S. magellanicus* ~20 million years ago (Vianna et al. 2020).

Objectives

In this chapter, I aim to update knowledge of the demographic histories of *O. flavescens* and *S. magellanicus*, drawing for the first time in the study of either species on ancient DNA samples to improve the accuracy of estimates of the timing of key demographic events by providing direct evidence of historical coalescence events and serving to calibrate estimates of mutation rate, which directly determines how far back in time a given coalescence event (and associated demographic change) is inferred to have taken place. For *O. flavescens*, I will also present the first demographic reconstruction based on nuclear genomic data, as opposed to mitochondrial data, potentially offering greater temporal resolution and a completely distinct line of evidence. These historical demographic trends and the population genetics they are inferred from will be interpreted in the context of time referenced stable isotope data, which give insight into possible shifts in foraging behaviour, and the environmental history of the region. The timing of features of their demographic histories will be compared with any shifts in SI composition of ancient samples and other aspects of environmental history. This chapter will also investigate genotype-by-environment associations with SI data and other environmental variables.

Methods

Data generation

Sample processing

In addition to the tissue samples of modern *O. flavescens* described in the previous chapter, 38 additional bone samples were processed, ranging from modern bone to archaeological samples up to 7,000 years old. In addition, bone from 25 individuals of *S. magellanicus* up to 5,845 years old were processed. The data from some these novel samples was ultimately combined with published mtDNA sequences from 84 individuals of *O. flavescens* from three studies (Artico et al. 2010; Feijoo et al. 2011; Tunez et al. 2010) and 195 of *S. magellanicus* from one study (Dantas et al. 2018). Metadata for all of these samples is given in Appendix A.

DNA extraction and sequencing

To prepare samples for DNA purification, tissue was minced using surgical scissors and approximately 30 mg was then digested for three hours at 55 °C in proprietary TL (digestion) buffer and added proteinase K, according to the recommended protocol of the EZNA Tissue DNA kit (VWR). Bone samples were cut into small (~2 mm^3) pieces with a Dremel manual drill, then pulverised into a fine powder using ball bearings in a steel capsule vibrated at high speed as part of a Mixer Mill MM 200 system. Approximately 30 mg of bone powder was then dissolved overnight at 55 °C, in 400 µl of solution composed of 50% TL buffer and 50% 0.5 M EDTA (final concentration 0.25 M EDTA), plus 25 µl of proteinase K. Following the digestion step, DNA from tissue and bone samples was extracted and purified using silica binding columns as part of the EZNA Tissue DNA kit (VWR) or the QIAquick PCR purification kit (Qiagen) according to the manufacturer's instructions. Bone samples (including ancient) were processed in a dedicated laboratory to minimise contamination from abundant modern DNA. This laboratory included separate fume hoods for sample preparation, DNA extraction and PCR preparation, which were cleaned regularly with diluted bleach. Tools for cutting and pulverising bone were also soaked in diluted bleach overnight between uses, or were disposed of. DNA extractions were carried out with negative controls to test for contamination during the process, including from reagents. All DNA amplifications were carried out in a separate, normal laboratory once the tubes had been filled and sealed in the ancient laboratory.

As described in Chapter 2, DNA isolated from 88 *O. flavescens* samples was amplified and sequenced at a 300-bp segment of the hypervariable D-loop of the mitochondrial genome. The full mitochondrial genome was sequenced using a target enrichment approach for 53 samples. Mitochondrial D-loop sequences successfully derived from either targeted or whole-mitogenome sequencing were ultimately combined with published samples into 145-bp and 409-bp alignments (Appendix A). Whole-mitogenome sequences (purely from this study) were also aligned. Homologous fragments of the nuclear genome were sequenced in a subset of samples using a RADseq reduced representation library approach. These methods, including bioinformatic processing and assembly of the mitogenome and RADseq reads, were described in more detail in Chapter 2. Original and previously published samples contributing to these datasets are identified in Appendix A.

DNA isolated from 22 *S. magellanicus* samples (including 13 ancient) was amplified and sequenced using a pair of primers which had previously been used by Dantas et al. (2018) to target a 376-bp fragment of the mitochondrial D-loop (F: CCTGCTTGGCTTTTYTCCAAGACC ["D-loop C"] R: CTGACCGAGGAACCAGAGGCGC ["D-loop D"]). These novel sequences were aligned with the previously published dataset of Dantas et al. (2018), comprising 195 modern samples (Appendix A).

Demographic history reconstruction

Nuclear genome

Single-nucleotide polymorphisms (SNPs) called in the *O. flavescens* RADseq dataset were used to estimate the folded site frequency spectrum (SFS) using the program easySFS (https://github.com/isaacovercast/easySFS). easySFS is essentially a wrapper for the program dadi (Gutenkunst et al. 2009), with additional features to inform user decisions. The main advantage of easySFS over similar tools is its convenient implementation of an algorithm for retaining as many SNPs and samples as possible while eliminating missing calls from the dataset. It does this in part by imputing the most likely SNP calls based on the observed frequencies at each site after eliminating sites and individuals with the most missing data.

The folded SFS is a summary of the distribution of minority allele counts in a population sample, represented by a vector of the number of alleles in each frequency class beginning with singletons (SNPs that are heterozygous in a single individual). A population's SFS can be

shaped by historical changes in demographic history. A population that has remained at a constant size forever is expected to maintain an equilibrium exponential distribution of allele frequencies based on a balance between mutation, which introduces new rare alleles, and genetic drift, which causes some alleles to randomly increase in frequency while others are lost. In comparison, a population that has recently grown from a much smaller size, for example, is expected to feature fewer rare alleles than expected due to chance loss of rare alleles from many sites and insufficient time for this variation to have been regenerated through mutation.

With the SFS estimated, the program Stairway Plot 2 was then used to estimate demographic history based on the folded SFS. Stairway Plot 2 implements model-flexible inference of a population's demographic history (Liu and Fu 2015; 2020). It begins by first estimating the single best-fitting average N_e of a population based on its SFS and supporting information such as sample size, mutation rate, and the total number of observed sites. This basic model is then elaborated upon several times through a genetic algorithm randomly proposing new "breakpoints" at times when N_e might have changed in the historical demographic model, and estimating the likelihood of the new model. If the new model passes a likelihood ratio test, it is accepted and the process continues. In its final form, a model specifies N_e at n historical time points, with up to (but usually significantly less than) n-1 distinct values of N_e separated by breakpoints that were accepted over the course of the model's evolution. This whole process is repeated from the beginning a number of times (default I=200 iterations), and all iterations are combined to give the final result of the Stairway Plot 2 run.

Previous studies have found Stairway Plot to be especially robust to differences in underlying genetic data, such as from different genome assembly strategies (e.g. Patton et al. 2019). However, this averaging over many replicates of much lower resolution gives a somewhat misleading impression of smoothness and continuity to stairway plots. The smoothness of the final plot does not necessarily reflect actual history, but it is still meaningful because it does reflect uncertainty about that history in the underlying replicates. For example, uncertainty in the timing of an abrupt change could result in it being indistinguishable from a longer period of more gradual change.

In addition to the SFS, Stairway Plot 2 requires estimates of the population's generation time and per-generation mutation rate, and the total number of genomic sites analysed (i.e. the total number of sites that could have been identified as SNPs). For *O. flavescens*, a generation time

of 12 years was assumed, taken directly from Feijoo et al. (2011) and similar to other estimates for them and close relatives (e.g. 10.4 years; Peart et al. 2020). The genomic mutation rate has not yet been directly estimated for *O. flavescens* by any published study, so the per-generation nuclear genome mutation rate was assumed to be $2.5e^{-8}$ substitutions/site/year, a common ballpark estimate for mammals (e.g. Li and Durbin 2011; Foote et al. 2021) which is comparable (on the scale of mutation rate variation; Hodgkinson and Eyre-Walker 2011) to that estimated by Peart et al. (2020) for the closely related genus of *Arctocephalus* ($1.31e^{-8}$ s/s/y). . The total number of genomic sites analysed was given by the "all sites" line in the "populations.log" file produced by Stacks, which was then multiplied by the proportion of the original SNP count remaining after the aforementioned down-projection by easySFS.

Mitochondrial genome

The matrilineal demographic history of both *O. flavescens* and *S. magellanicus* was reconstructed via the Extended Bayesian Skyline Plot method implemented in BEAST v2.6 (Heled and Drummond 2008; Boukaert et al. 2014). Both analyses used an HKY substitution model with rate parameters estimated as part of the BEAST run.

For *O. flavescens*, two alignments were analysed. First, the 145-bp alignment, which maximises the number of samples (especially ancient samples) at the expense of sequence length, was analysed to estimate the annual mutation rate of the mitochondrial D-loop, using the time calibration afforded by archaeological samples. This rate was then assumed in a subsequent analysis of the 409-bp alignment consisting of only modern samples, which contained the 145-bp segment from the original alignment and was also located within the hypervariable region of the mitogenome. This EBSP was taken to be the best estimate of the matrilineal demographic history.

For *S. magellanicus*, the 277-bp alignment was analysed by EBSP, and the included ancient samples were used to estimate the mitochondrial D-loop mutation rate simultaneously as part of the analysis. Although the final rate was estimated from the data, a rate of $8.6e^{-5}$ substitutions/site/year was used as the prior, following Dantas et al. (2018).

Stable isotope analysis

Analysis of carbon (δ13C), nitrogen (δ15N) and sulphur (δ34S) isotopes was carried out on bone and tissue samples. Sections of samples used for isotope analysis were removed by drill (bone) or scalpel (tissue) as described above for DNA extractions. Collagen and lipid extraction, and quantification of stable isotope composition, was subsequently carried out by Darren Gröcke at the Stable Isotope & Biogeochemistry Laboratory (SIBL) of Durham University. Collagen was extracted from bone using a modified Longin method (Longin 1971). The bone was digested in 0.5 M hydrochloric acid, gelatinised in pH3 HCl at 75°C overnight, and then then the collagen residue was freeze-dried for analysis (King et al. 2018). Tissue samples were subjected to lipid extraction to isolate the signal of protein δ13C composition (lipids are relatively depleted in δ13C through their biochemical manufacture; Elliott et al. 2017). Isotope concentrations were quantified using a ECS 4010 elemental analyser (Costech, Valencia, CA, USA) connected to a Delta V Advantage isotope ratio mass spectrometer (Thermo Scientific, Bremen, Germany) (Gröcke et al. 2021).

Values of δ13C and δ15N measured from ancient samples were corrected for changes in the isotopic baseline by the addition of factors based on the results of Zenteno et al. (2015b). Zenteno et al. (2015b) measured δ13C and δ15N in the shells of ancient molluscs (limpets and mussels) off the coast of Patagonia, which are expected to reflect the isotopic composition of food sources in their area at the lowest trophic level. Some of the samples in the present study do not come from the same archaeological strata as any of the samples analysed by Zenteno et al. (2015b), with several being older than any of the samples they considered. For samples in this study belonging to different strata within the age range of those published, a correction factor was imputed by taking the weighted average of nearest known correction factors (i.e. assuming that the isotopic baseline changed linearly between the two time points). This is the same approach Zenteno et al. (2015b) followed for sea lion samples that were not from the same strata as their mollusc shells. For samples falling outside of the age range of the mollusc shell data, a correction factor was estimated by extrapolation of the best-fit line through all of the other younger correction factors.

Archaeological samples from the same or similar (temporally and geographically) sites were grouped for statistical analysis of temporal and geographic trends in stable isotope values. Unfortunately, latitude and age were highly correlated (R^2=0.77, p<0.001) among the ancient *O. flavescens* samples represented in this study, making it impossible to confidently disentangle

change over time from potential geographical variation in isotope values. To partially get around this, because most samples came from the north or south ends of each species' range (Appendix A), changes over time were tested for the north and south separately. Samples were considered "northern" if they were from north of the Golfo San Jorge (>-45° latitude), "mid" if they were from the Golfo San Jorge or northern Santa Cruz province (-45° to -50° latitude), or "southern" if they were from southern Santa Cruz province or Tierra del Fuego (<-50° latitude). This scheme was applied for both *O. flavescens* and *S. magellanicus*. Difference of means between pairs of sample sets grouped by age and latitude was tested using Welch's t test implemented in R v4.0.3. Welch's variant of the test was selected because it does not assume equal variance between the groups, which would often not be met given the small sample sizes that result from dividing the data up by both age and latitude (Welch 1947). Effect size of the t tests was quantified using Cohen's d (Cohen 1998), which standardises the difference in means (if any) by the standard deviation of both groups combined.

Of the samples analysed for stable isotope composition, sex metadata was only available for modern skin samples from Golfo San Matias (N = 7 female, 10 male). A multivariate analysis of variance (MANOVA) was used to test for sex-associated differences in trophic niche (δ15N and δ13C) in this population. MANOVA was also used to test interspecific overlap in trophic niche between *O. flavescens* and *S. magellanicus*.

Environmental data

Bathymetric data was obtained as a product of the GEBCO project (GEBCO 2020). Sea surface temperature (SST) and chlorophyll A (ChlA) concentration data were downloaded from NASA Goddard Space Flight Center via the MODIS spectroradiometer aboard the Aqua satellite (NASA 2018, 2019). From these global datasets, values were assigned to samples by averaging within one degree of latitude and longitude of the sample location.

Genotype-by-environment associations

Redundancy analysis (RDA) was used to detect SNPs associated with stable isotope values or specific environmental variables within the *O. flavescens* genomic SNP dataset. RDA essentially combines PCA with GLM by first regressing the SNPs against the predictive model of environmental variables, resulting in a matrix of new fitted values (i.e. the mean value that would be predicted based on the model, as opposed to the actual observed value), which are

then subjected to PCA to identify covarying combinations of SNPs associated with factors in the model. The factors initially considered in this analysis were δ13C, δ15N, ChlA, SST, and latitude. In order to not violate the assumptions of the GLM, only one factor was retained out of pairs of factors that were correlated at $r > 0.7$.

Relationship between demographic history and diet

To test whether historical change in diet had been associated with changes in population size, stable isotope measurements of ancient samples were paired with the age of the sample whose bone collagen were measured from, and with the effective size (N_e) of the population at that time according to the Stairway Plot 2 reconstruction (*O. flavescens*) or EBSP reconstruction (*O. flavescens* and *S. magellanicus*). A generalized additive model (GAM) was fit, using the R package "mgcv" (Wood 2011), to model N_e as a smooth function of δ15N and δ13C. The complexity of the curve was limited to no more than three degrees of freedom, and automatically optimized within this range by the restricted maximum likelihood (REML) method. This was a conservative tactic to limit overfitting while acknowledging the potential for some non-linearity. In addition to testing whether there was a statistically significant relationship between diet (stable isotope composition) and demographic history overall, the absolute value of the residuals of this model were themselves modelled as a function of time (sample age) to investigate whether the strength of the modelled relationship between diet and population size had varied over time.

Sample geography (latitude) was not considered in this analysis because of the aforementioned multicollinearity between age and latitude among the ancient samples, particularly of *O. flavescens*. Although it would have been good to control for any effect of latitude (i.e. geographic variation) on historical isotope values, to do so properly would have required a vastly more comprehensive dataset, with multiple localities represented at each time point to account for the strong possibility that any latitudinal gradient in isotope values (diet) would have itself changed over time due to Holocene climate change and recent anthropogenic impacts. Demographic history is, by definition, about change over time at the population scale. Therefore, for the purpose of this specific analysis, the assumption is made – out of necessity and with uncertainty – that the isotope values of samples over time are representative of the whole population and not just their locale.

Results

Demographic history analyses

Otaria flavescens

The demographic history of the Atlantic/Patagonian lineage of the South American sea lion as inferred by Stairway Plot 2 analysis suggests that the population underwent a major expansion around 40 kya, but has since remained relatively stable with an N_e of approximately 20,000, except for a temporary low during the mid-Holocene, ~1-6 kya, during which it was reduced to an N_e of ~4,000 (Figure 3.2).

EBSP analysis of the 409-bp D-loop alignment was not able to rule out the hypothesis of a constant population size, but did suggest that population has grown since ~2,000 years ago (Figure 3.3). The inclusion of ancient DNA made it possible to directly estimate the mutation rate of a portion of the hypervariable region of the mitochondrial D-loop for *O. flavescens*. Based on the 145-bp alignment, BEAST estimated a rate of $1.84e^{-6}$ [95% CI: $1.69e^{-7}$–$3.69e^{-6}$] s/s/y. Repeating the EBSP analysis of the 409-bp alignment (which itself includes no ancient samples) with this faster rate yields a result that only covers the past ~3,000 years, but matches the Stairway Plot reconstruction over the same period (Figure 3.2).

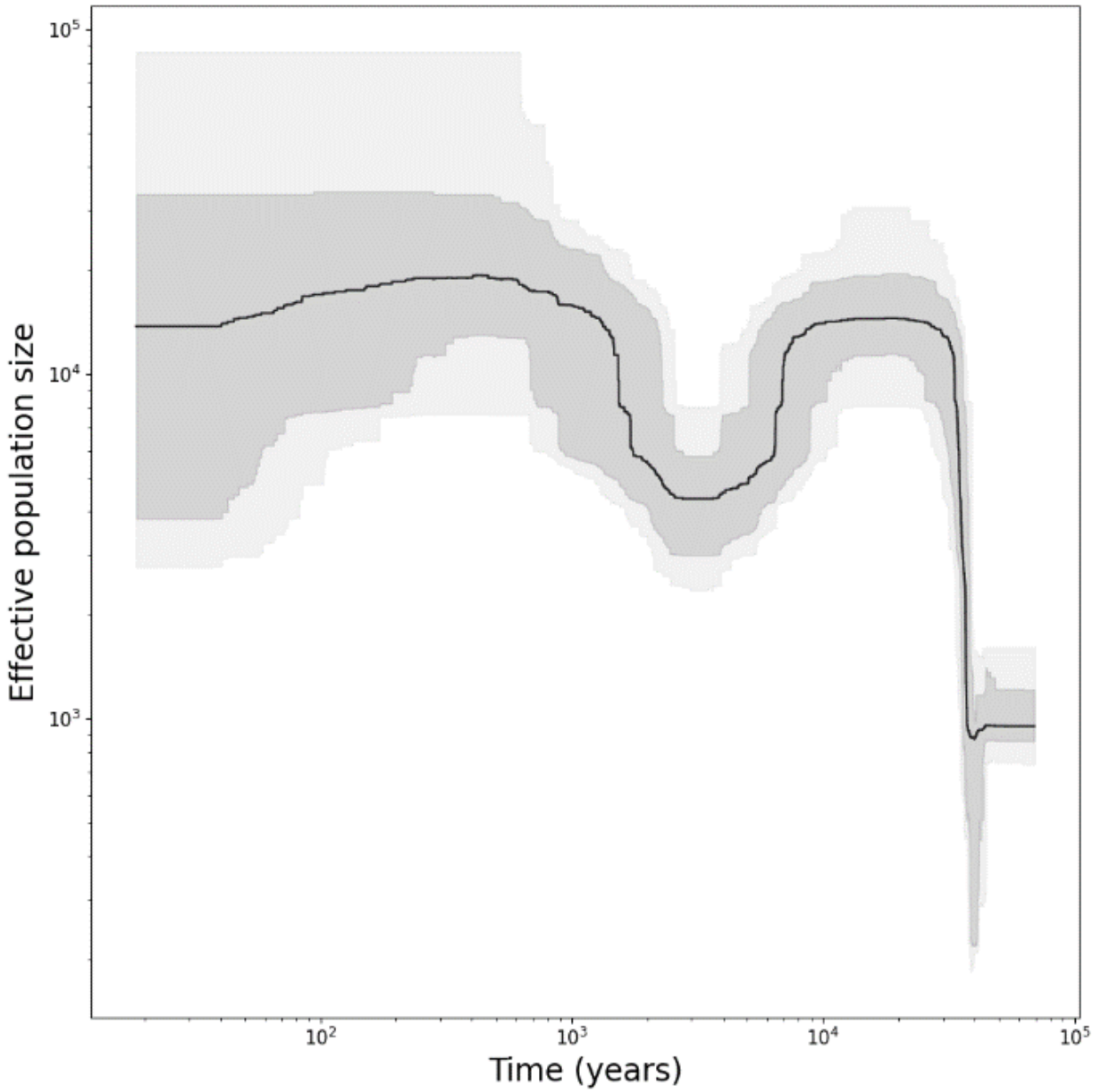

Figure 3.2. Demographic history of *Otaria flavescens* reconstructed by Stairway Plot 2 analysis based on RADseq data. The central line represents the median time-specific N_e estimate while the inner (darker) shaded area represents the 12.5^{th}-87.5^{th} percentiles of N_e estimates and the lighter shaded area represents the 2.5^{th}-97.5^{th} percentiles of N_e estimates over 200 Stairway Plot iterations. Note that these are not equivalent to formal confidence intervals, but rather comparable to bootstraps, showing the robustness of the analysis to variation in the data.

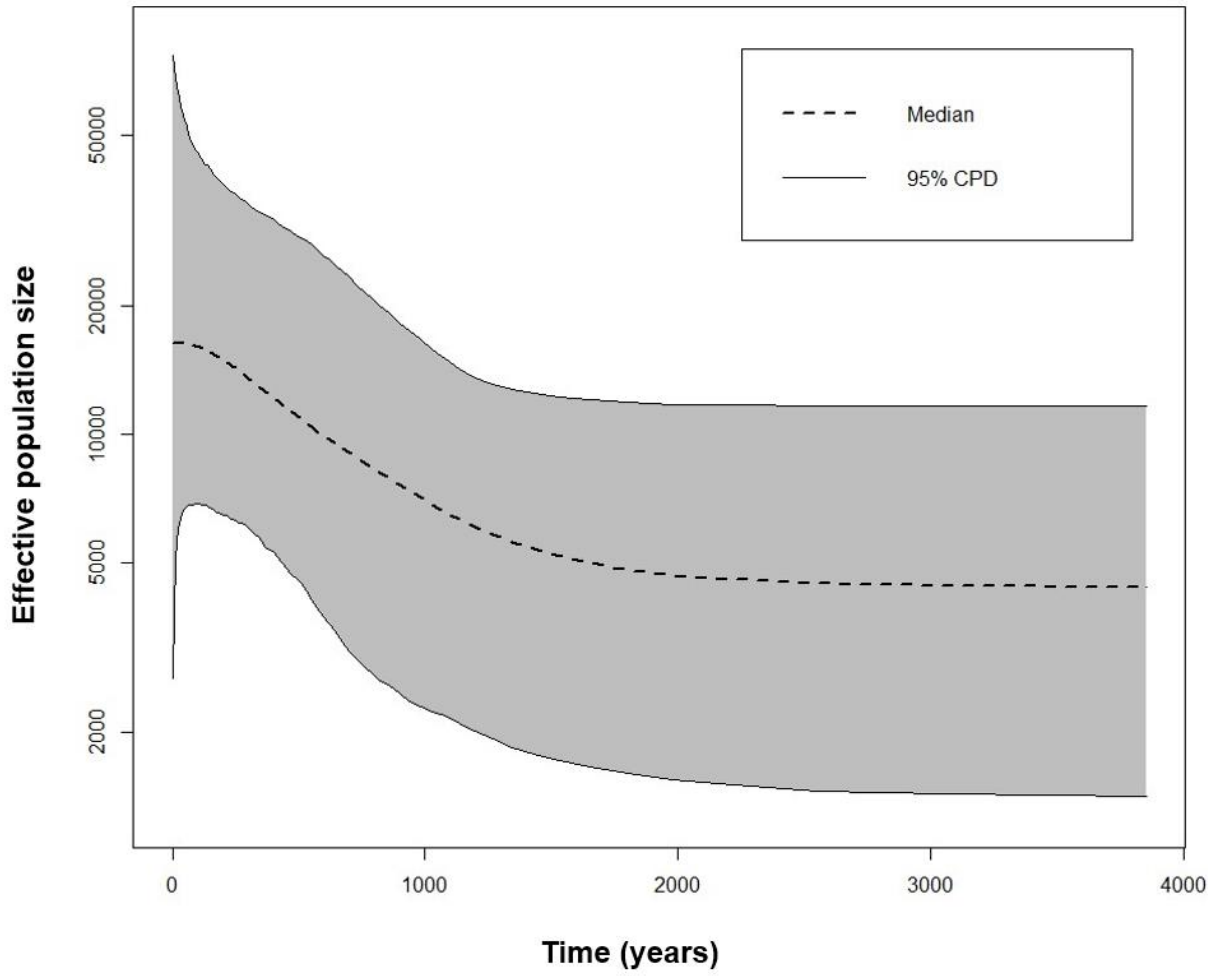

Figure 3.3. Demographic history of *Otaria flavescens* reconstructed by EBSP analysis based on mitochondrial D-loop sequences. This uses a mutation rate calibrated following a separate analysis that used a shorter alignment including ancient DNA sequences. The dotted line shows the central estimate of N_e over time, while the shaded area represents the 95% confidence interval.

Spheniscus magellanicus

The demographic history of the Magellanic penguin reconstructed by the EBSP method strongly indicates that the population grew during the Holocene, with the best estimate being that the population grew by a factor of ~20, beginning around 5,000 ybp. This estimate of timing was based on a new estimate of the annual mutation rate for the mitochondrial D-loop of *S.*

magellanicus, $2.3e^{-6}$ [95% CI: $1.19e^{-6}$–$3.52e^{-6}$] s/s/y, which was calibrated by incorporating ancient samples of known ages (Figure 3.4).

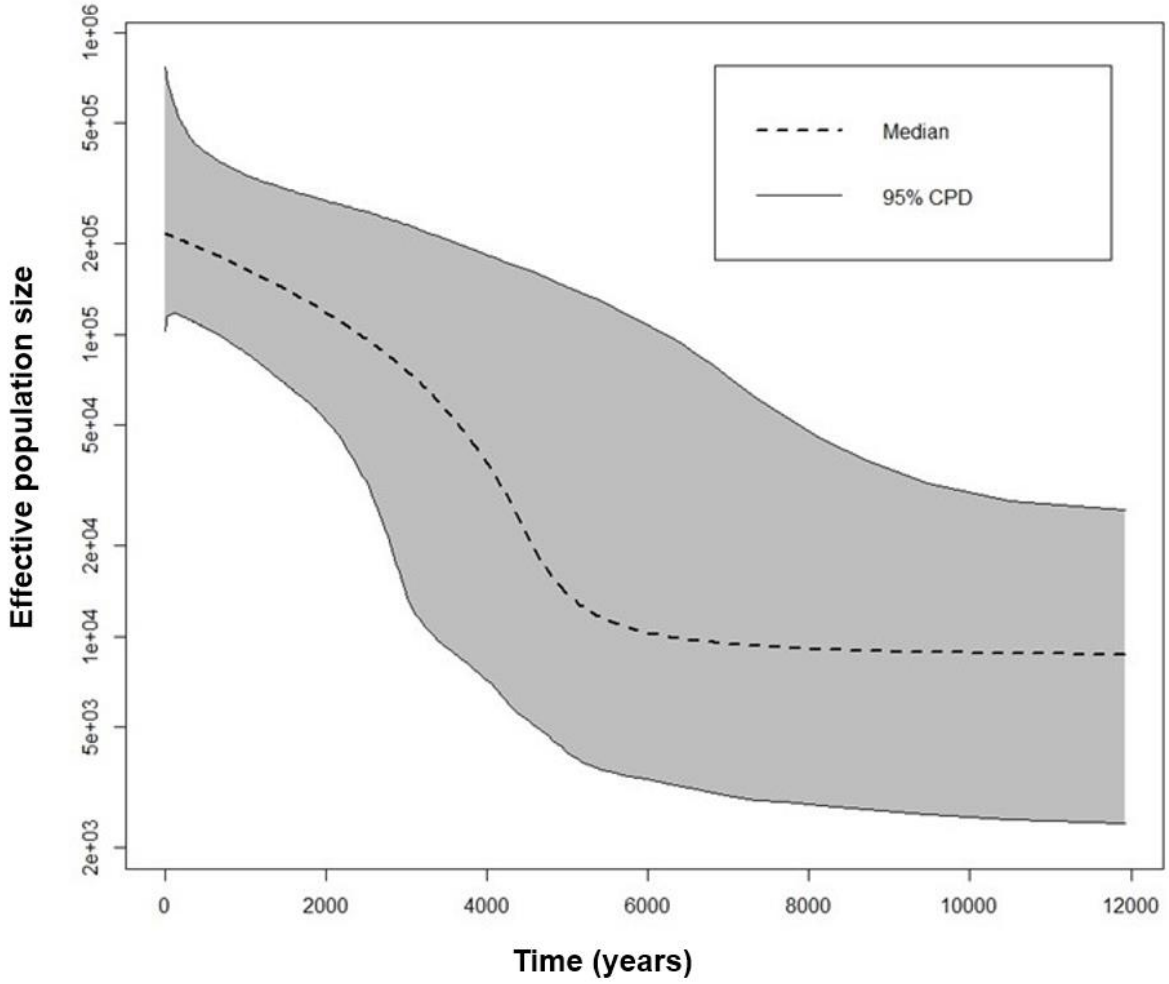

Figure 3.4. Demographic history of *S. magellanicus* reconstructed by EBSP analysis based on mitochondrial D-loop sequences, including 15 ancient samples (specified in Appendix A). The dotted line shows the central estimate of N_e over time, while the shaded area represents the 95% confidence interval.

Stable isotope analyses

Otaria flavescens

δ15N

Significant differences were found between the mean δ15N values of ancient samples from the north and south, with northern samples displaying higher d15N values ($p<0.001$, Cohen's $D=2.68$) (Figure 3.5). The samples from each region did not belong to exactly the same time periods, but there was no significant difference between the means of oldest northern samples from ~7,000 ybp and ~2,188 ybp ($p=0.60$, $D=-0.34$), or between the means of southern samples from ~1,234 ybp and ~580 ybp ($p=0.115$, $D=-1.06$). The δ15N profiles of modern samples were not significantly different between the north and south ($p=0.08$, $D=1.33$), but there was a respectable effect size. The modern mean was lower than the mean of ancient samples from the north ($p<0.001$, $D=-1.91$), and higher than the mean of ancient samples from the south ($p=0.002$, $D=1.55$). If samples are assumed to represent only their local region (this cannot be determined from the data because the ages of northern and southern samples are too distinct), these results imply that δ15N profiles were regionally distinct but locally stable until at least as recently as ~2,000 ybp, but that their trophic levels have converged in recent times, with δ15N decreasing in the north and increasing in the south.

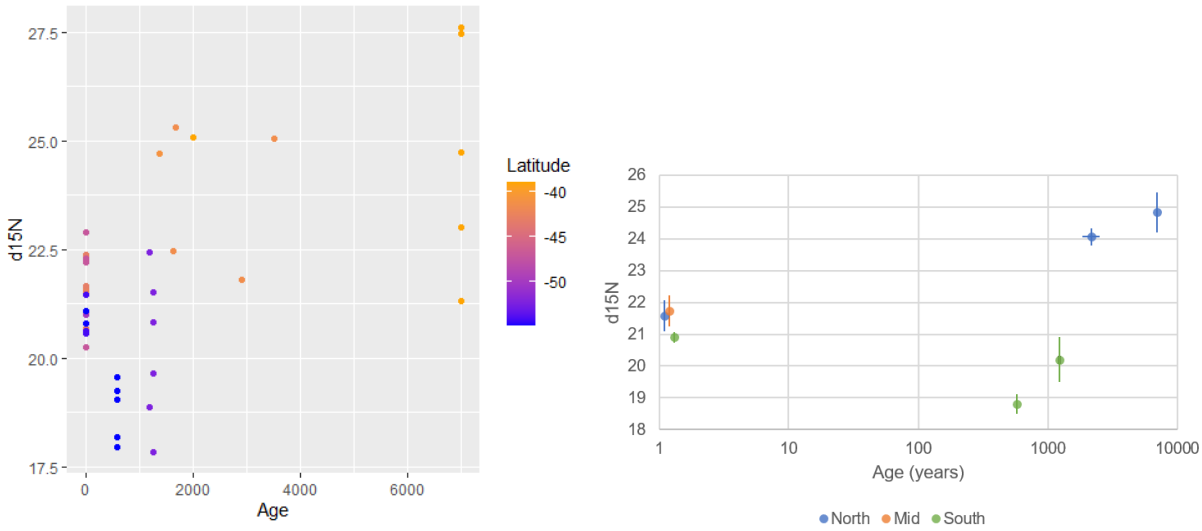

Figure 3.5. (left) Measured δ15N in *O. flavescens* bones with respect to the age and latitude of the sample. (right) Average δ15N values of samples from the same or similar sites.

δ13C

Modern samples from the north and south did not differ in δ13C profiles (p=0.24, D=0.81) (Figure 3.6). Younger ancient samples from the north (~2,188 ybp) and south (~580 bp) did not significantly differ in δ13C values relative to each other (p=0.93, D=-0.05) or to modern samples (p=0.89, D=-0.06). However, the δ13C values of younger ancient samples were higher were significantly higher than those of the oldest ancient samples within both regions (p<0.001, D=3.42). Taken together, these results suggest that similar changes in δ13C profile occurred asynchronously in the north and south, but have remained relatively stable over at least the past ~500-2000 years.

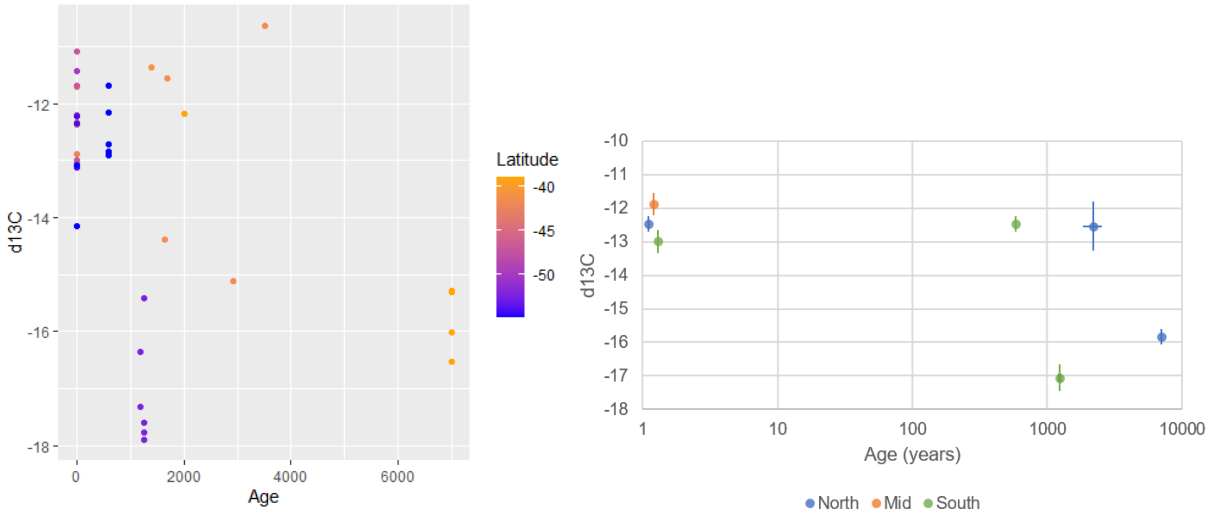

Figure 3.6. (left) Measured δ13C in *O. flavescens* bones with respect to the age and latitude of the sample. (right) Average δ13C values of samples from the same or similar sites.

δ34S

There does not appear to have been significant change over time in δ34S values, irrespective of region (p=0.065, D=-0.712), but the effect is on the margin of significance (Figure 3.7). However, there does appear to be a latitudinal gradient in δ34S values among modern samples, with northern samples significantly higher in δ34S (p=0.008, D=2.79). There is also a significant linear relationship between δ34S and latitude (AdjR^2=0.63, p<0.001), considering only modern samples (Figure 3.8).

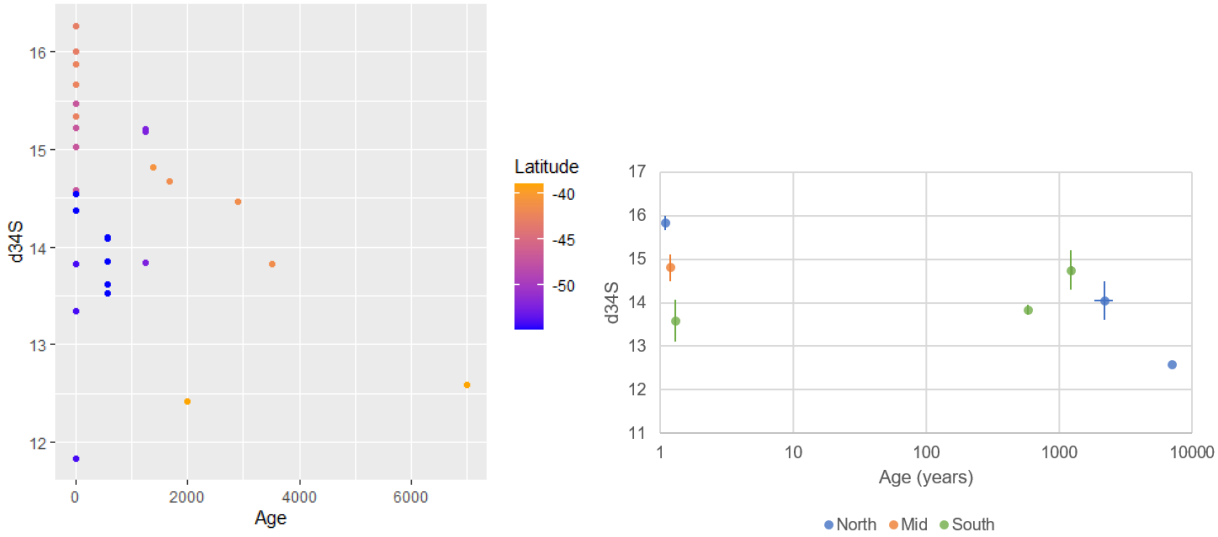

Figure 3.7. (left) Measured δ34S in *O. flavescens* bones with respect to the age and latitude of the sample. (right) Average δ34S values of samples from the same or similar sites.

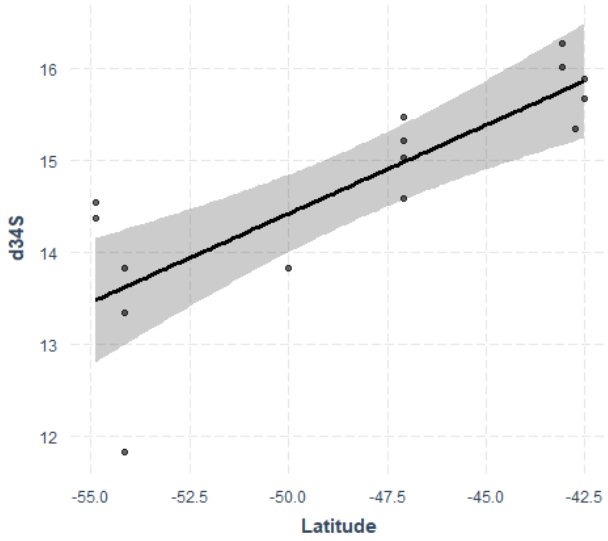

Figure 3.8. δ34S of modern *O. flavescens* bone samples with respect to latitude.

Trophic niche

Considering δ15N and δ13C isotopes together, it is clear that modern samples from a range of latitudes cluster together at lower δ15N and higher δ13C (Figure 3.9). There were also no statistically significant differences related to sex in δ15N (p=0.52, D=-0.34) or δ13C (p=0.54, D=-0.32), or their combination (MANOVA: p=0.61, effect size η_p^2=0.07), found among modern

O. flavescens, although this analysis was limited to samples from Rio Negro and the Valdes Peninsula, located in the north (Figure 3.10).

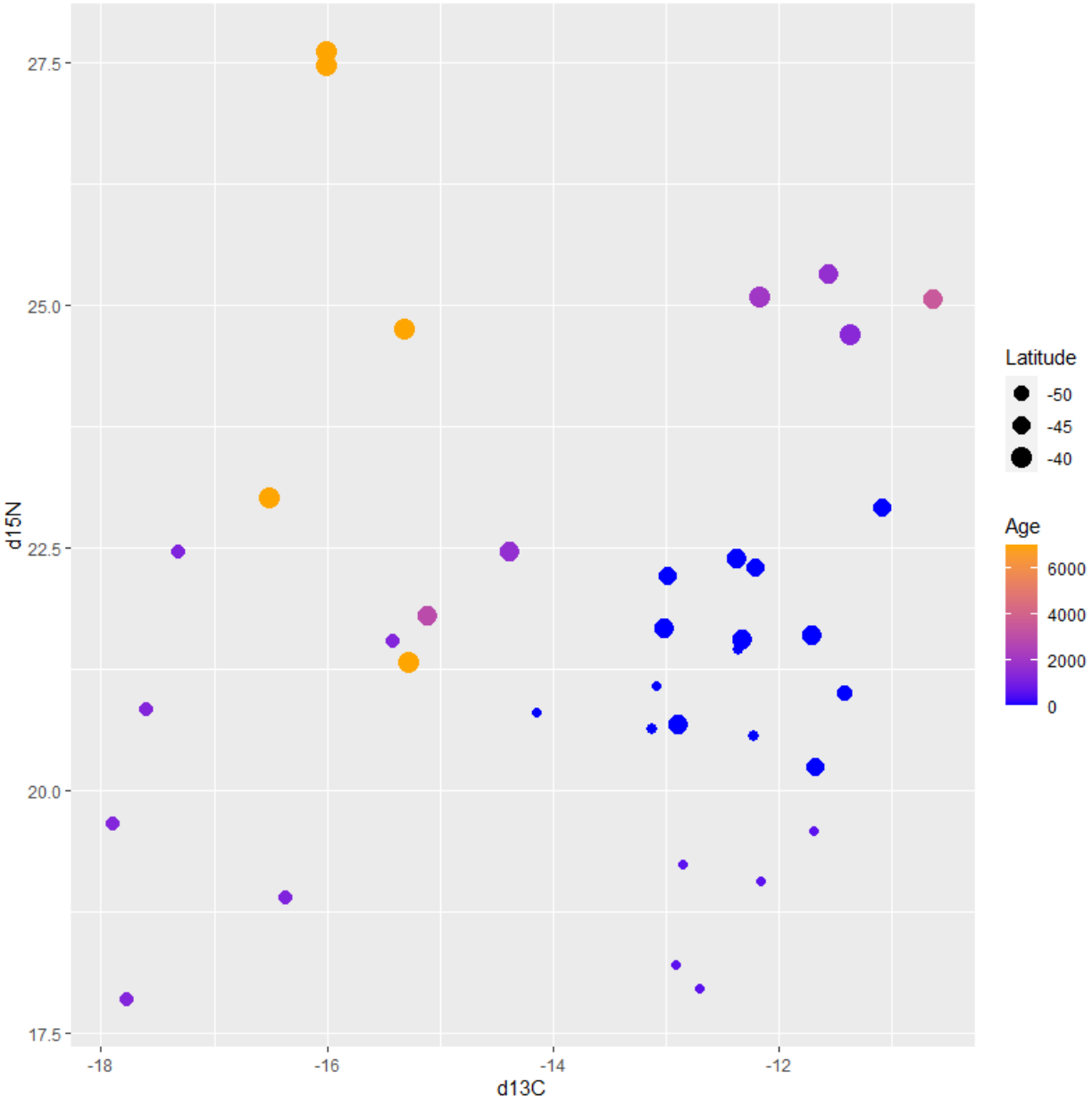

Figure 3.9. Isotopic niche plot of δ15N and δ13C from *O. flavescens* bone samples with respect to age and latitude.

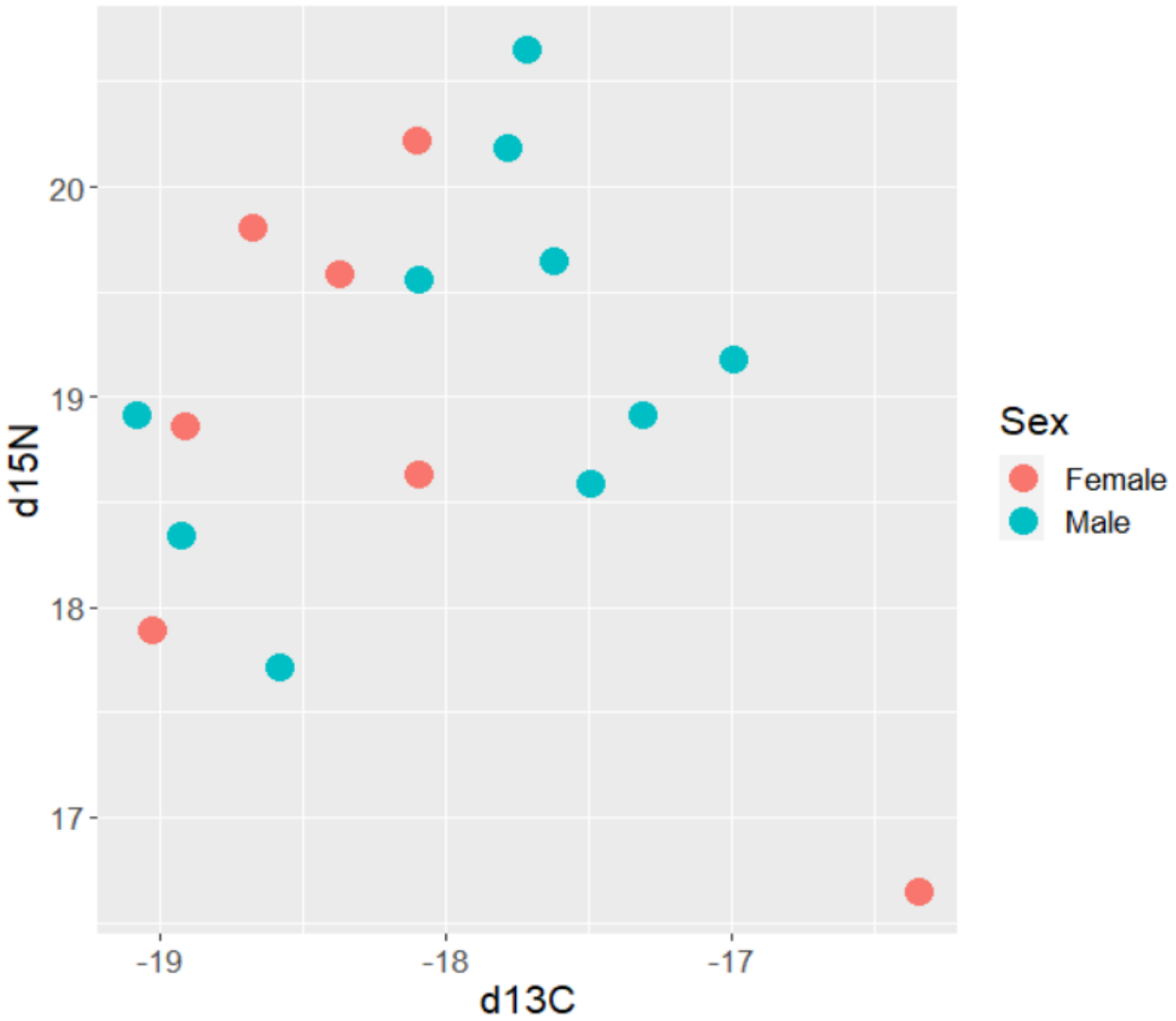

Figure 3.10. Isotopic niche plot of δ15N and δ13C from modern tissue samples of *O. flavescens* from the Rio Negro province, with respect to sex.

Spheniscus magellanicus

δ15N

There was no statistically significant difference in the δ15N values of early ancient samples from north and south (p=0.74, D=0.22) (Figure 3.11). There was also no significant regional variation in modern samples (p=0.18, D=1.56), although the effect size was large. However, the mean δ15N of early ancient samples (north and south considered together) was slightly higher than that of modern samples (p=0.049, D=0.89). δ15N may have declined prior to modern times,

based on samples from 500-1220 ybp which show δ15N values even lower than those of modern samples (p=0.022, D=-2.27).

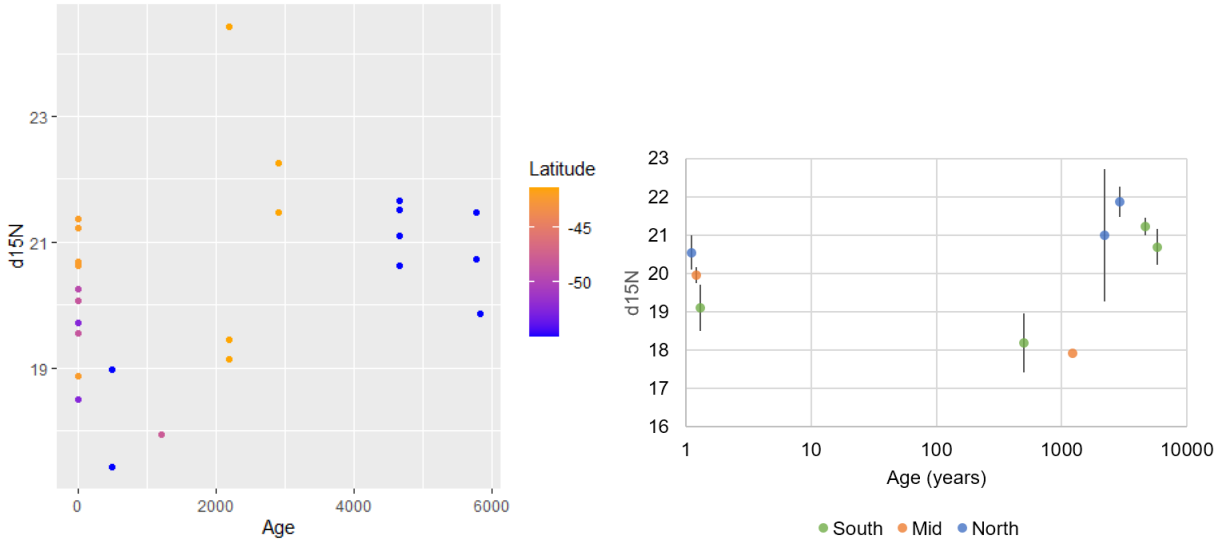

Figure 3.11. (left) Measured δ15N in *S. magellanicus* bones with respect to the age and latitude of the sample. (right) Average δ15N values of samples from the same or similar sites.

δ13C

There were large and statistically significant differences in δ13C between early ancient samples of the north and south (p<0.001, D=4.31), with higher values found in the north compared to the south (Figure 3.12). On the other hand, no difference was found in the mean δ13C values of modern samples (p=0.205, D=1.25). Two more recent ancient samples (500 ybp) from the south showed higher δ13C values, suggesting that the history of δ13C in this population may have been more complex than is able to be inferred from the majority of the samples, which otherwise show that higher values in the ancient north and lower values in the ancient south converged on less variable intermediate values in modern times.

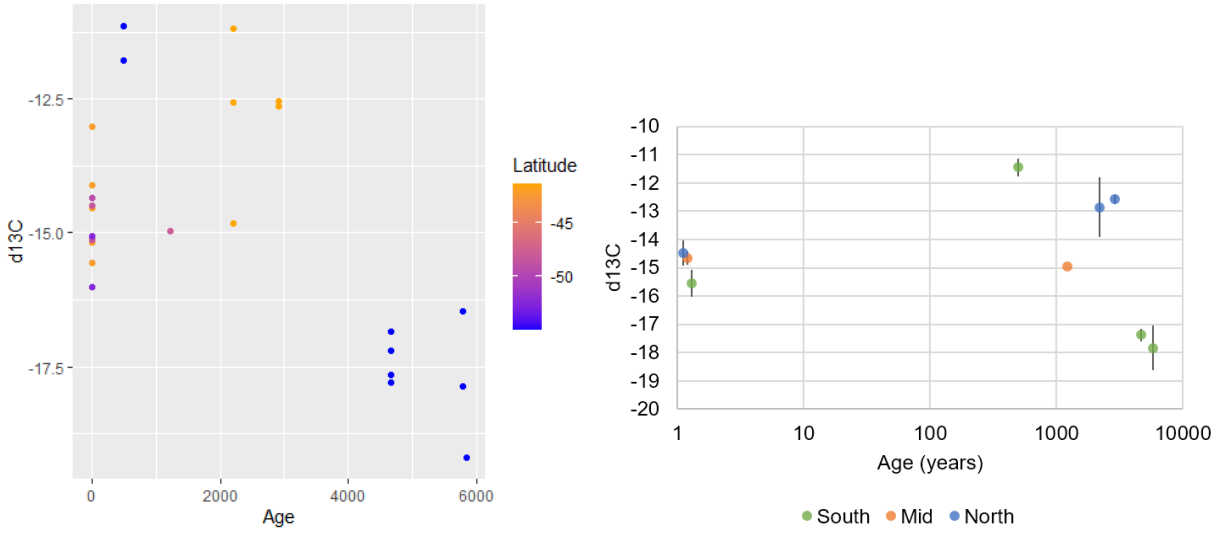

Figure 3.12. (left) Measured δ13C in *S. magellanicus* bones with respect to the age and latitude of the sample. (right) Average δ13C values of samples from the same or similar sites.

δ34S

The variability of δ34S in *S. magellanicus* with respect to time or latitude appears to be very low, with all samples falling between 15 and 16.5 per mil (Figure 3.13). There were negligible differences between the δ34S values of ancient samples from the north and south (p=0.98, D=-0.01), and between ancient and modern samples (p=0.73, D=-0.16).

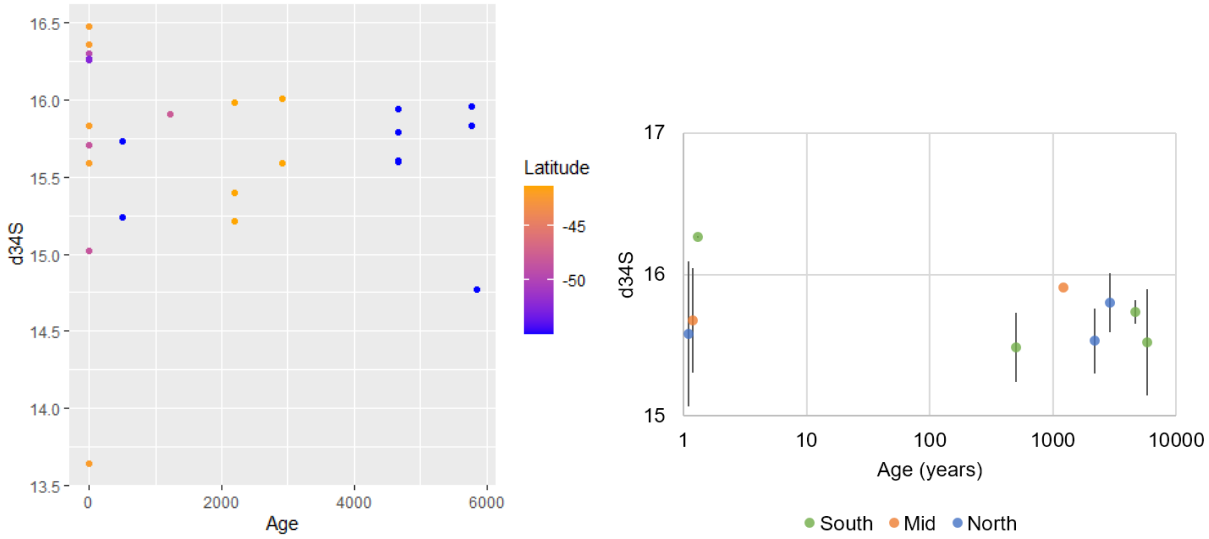

Figure 3.13. (left) Measured δ34S in *S. magellanicus* bones with respect to the age and latitude of the sample. (right) Average δ34S values of samples from the same or similar sites.

Trophic niche

Considering δ15N and δ13C isotopes together, samples from the oldest samples (>4000 ybp) from the far south (<-52 degrees latitude) seem to cluster separately at lower δ13C, while later samples (including modern samples) from all latitudes are more mixed together at higher δ13C values and across a greater range of δ15N values (Figure 3.14).

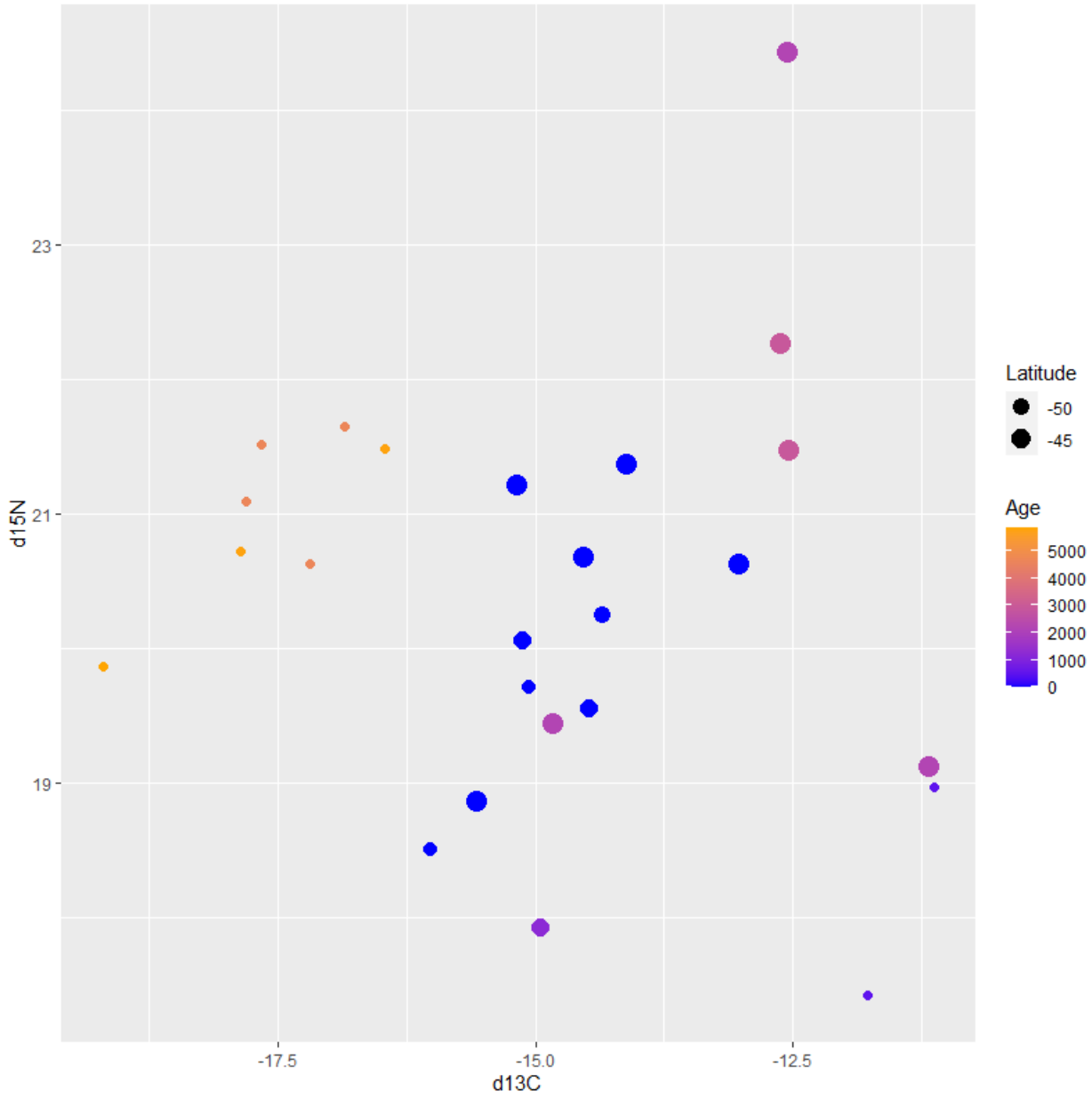

Figure 3.14. Isotopic niche plot of δ15N and δ13C from *S. magellanicus* bone samples with respect to age and latitude.

Interspecific comparison

There was a clear difference in isotopic niche between modern bone samples of *O. flavescens* and *S. magellanicus*, with *O. flavescens* being significantly higher in δ15N (p=0.002, D=1.52), δ13C (p<0.001, D=2.83), and their combination (MANOVA: p=0.006, effect size η_p^2=0.16) (Figure 3.15).

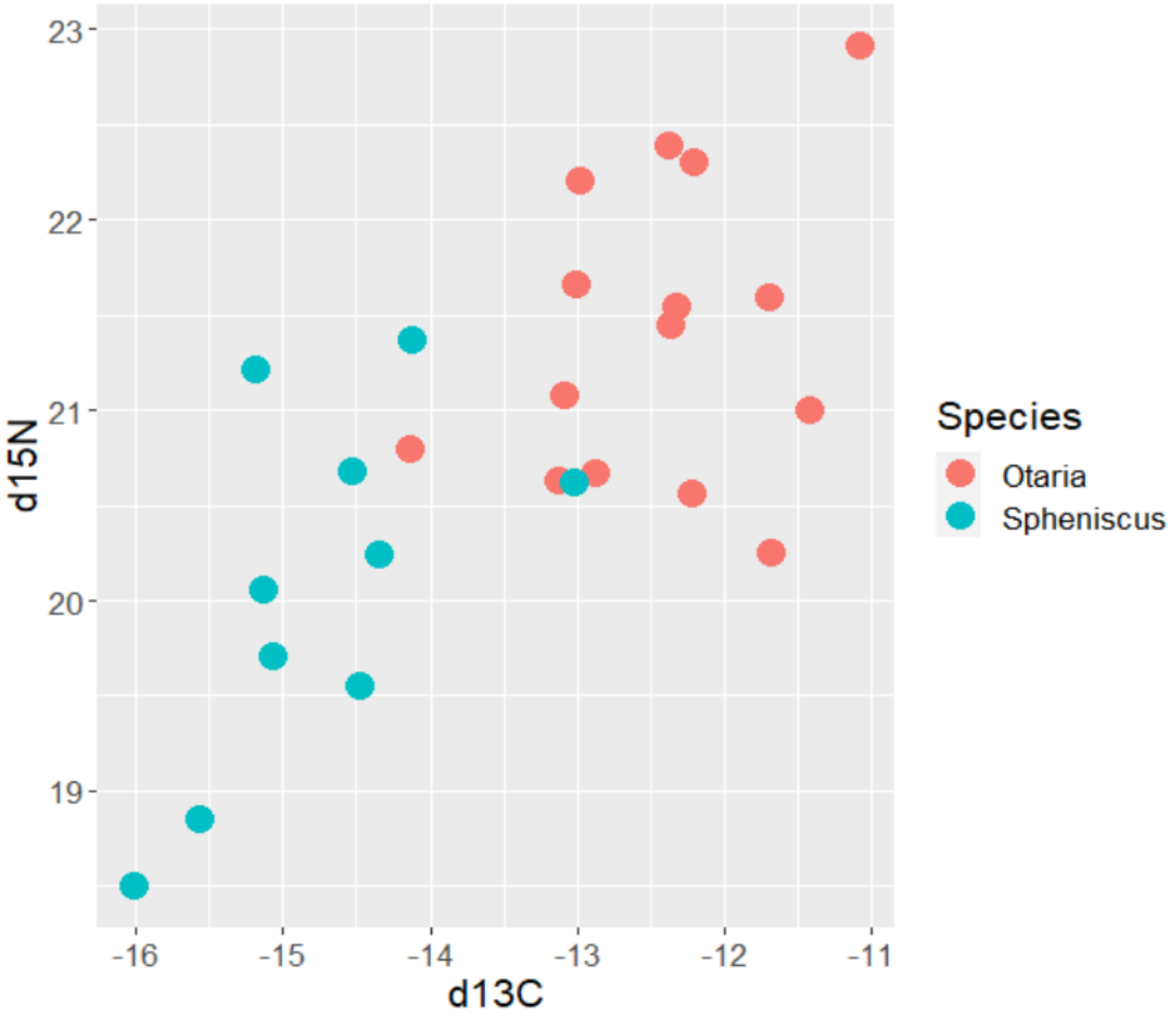

Figure 3.15. Plot showing the partial differentiation of isotopic niche in modern bone samples between *O. flavescens* and *S. magellanicus*.

Genotype-by-environment associations

Preliminary to the RDA of the *O. flavescens* genomic SNP dataset, SST was excluded as a factor because it was correlated with latitude at $r = 0.9$. ChlA was also correlated with latitude, but it was retained because the correlation coefficient was lower ($r = 0.7$) and it appeared to show a novel pattern, with higher values at the far south of the species' range, as well as the north. The remaining factors, which were considered, were δ13C, δ15N, latitude, and ChlA. The adjusted-R^2 value of the final model was -0.008, indicating that the factors included in the model

explained a trivial and statistically non-significant (p=0.923) proportion of the variance in SNP calls among individuals. A total of 461 candidate outlier SNPs were identified, defined by their fitted values falling >1 SD from the mean for one or more factors. The bulk of these (N=351) were associated with δ13C. However, given the statistical weakness of the model, these outliers are overwhelmingly likely to be artefacts of chance and not truly environmentally-associated SNPs. This is further suggested by their roughly symmetrical distribution around the edges of the 'cloud' of SNPs (Figure 3.16).

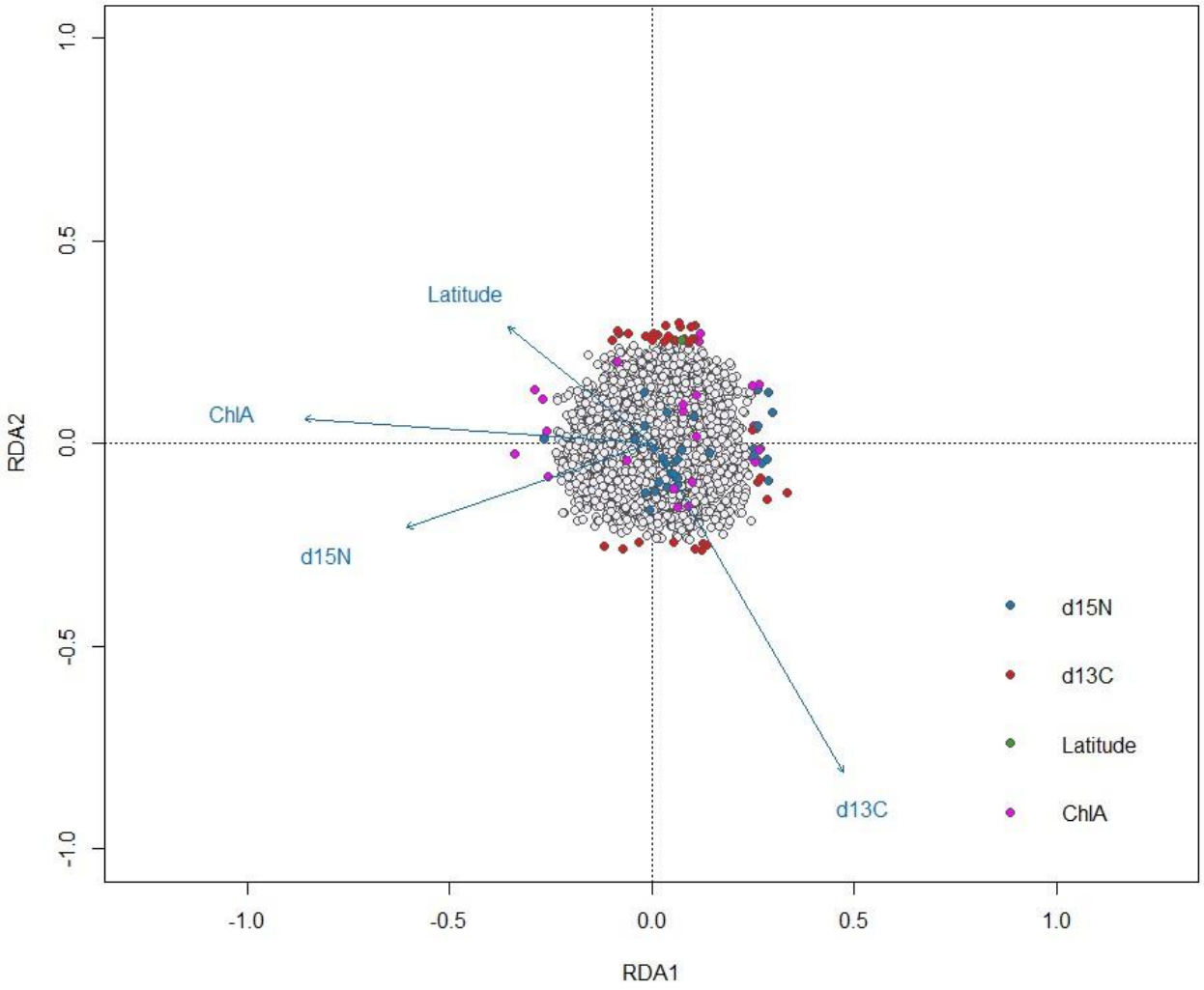

Figure 3.16. RDA triplot with putative outlier SNPs colour-coded according to their association with the four explanatory variables. However, as the model explained a trivial and statistically non-significant (p=0.923) proportion of the variance in SNP calls among individuals, these outliers are very likely to be due to chance.

Relationship between demographic history and diet

Otaria flavescens

Considering isotope values across time for the whole Patagonian population of *O. flavescens*, δ15N remained roughly stable from ~7000 ybp to ~2000 ybp. According to the Stairway Plot 2 results (Figure 3.2), population growth beginning ~2,000 ybp appears to have coincided with a decline in sample δ15N values (Figure 3.17). Both trends reached an inflection at ~500 ybp, then began to reverse slightly up to the present. However, this recent downturn in population size is only apparent in the Stairway Plot reconstruction; the EBSP reconstruction (Figure 3.3), while similar, was simpler, with less temporal resolution, and did not reflect this apparent recent event.

The history of δ13C was more dynamic in the ~1000-4000 ybp period. Although δ13C trended upwards alongside population size, it appears to have been less consistent, with some high-δ13C samples preceding population growth and some low-δ13C samples coming after the population had grown (Figure 3.18).

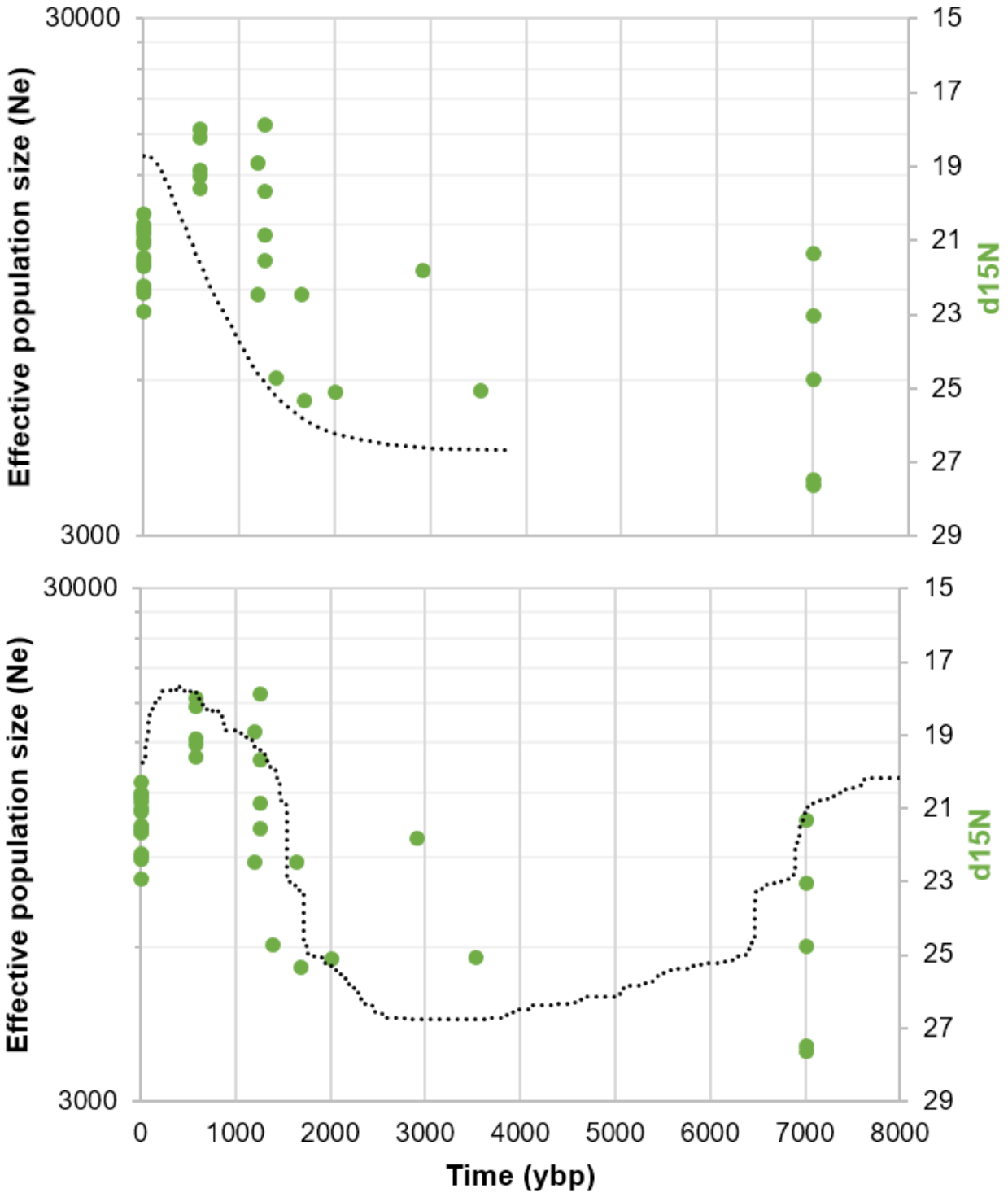

Figure 3.17. *O. flavescens* demographic history (black dotted line) reconstructed by EBSP (top) and Stairway Plot 2 (bottom), against δ15N (green; note inverted axis) values from ancient bone samples over the past 7,000 years.

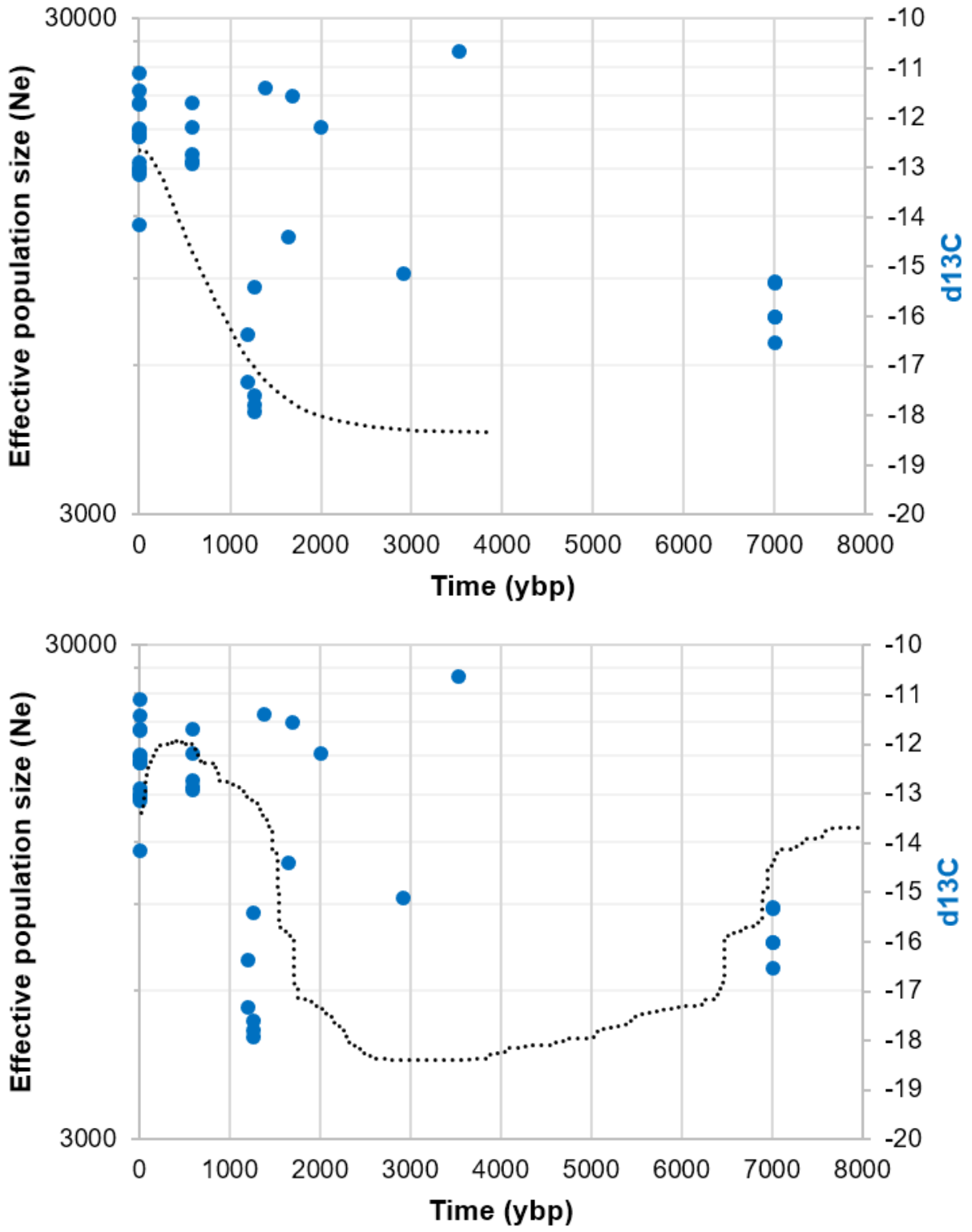

Figure 3.18. *O. flavescens* demographic history (black dotted line) reconstructed by EBSP (top) and Stairway Plot 2 (bottom), against δ13C (blue) values from ancient bone samples over the past 7,000 years.

The relationship between effective population size and trophic niche over time was tested using a GAM with both isotopes. Given the greater resolution and timescale of the Stairway Plot reconstruction, and considering its overall similarity to the EBSP reconstruction, only the Stairway Plot values of N_e were modelled for *O. flavescens*. The model explained 52.5% of deviance. The δ15N term was significant ($p<0.001$; Figure 3.19), while the δ13C term was not ($p=0.446$; Figure 3.20). N_e was generally inversely related to δ15N, although high values of δ15N (>23) were not associated with any change in N_e within the scope of this dataset (Figure 3.19). The absolute value of the residuals of the model exhibited a parabolic shape with respect to time, peaking at ~3000 ybp (Figure 3.21), although sample age was not overall a statistically significant factor in explaining the absolute residuals ($p=0.435$, deviance explained=6.53%). This makes sense, as the population size was apparently stable at this time, while there was still some variation in δ15N (Figure 3.17) and several major outliers in δ13C (Figure 3.18).

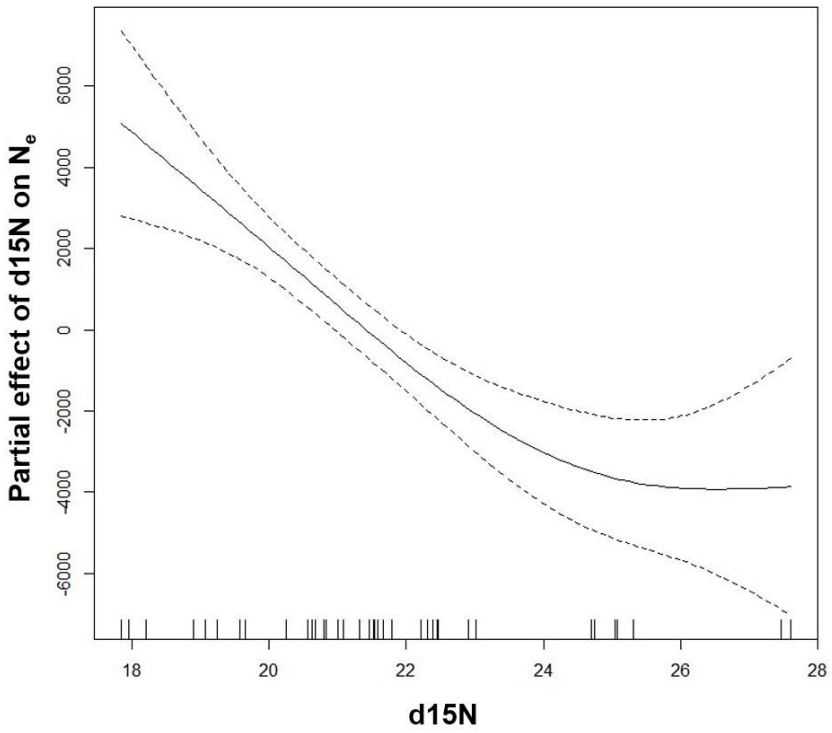

Figure 3.19. The relationship between δ15N and *O. flavescens* population size over the last 7,000 years, modelled in a GAM alongside δ13C. Interior ticks on the horizontal axis indicate the presence of actual data points at those values.

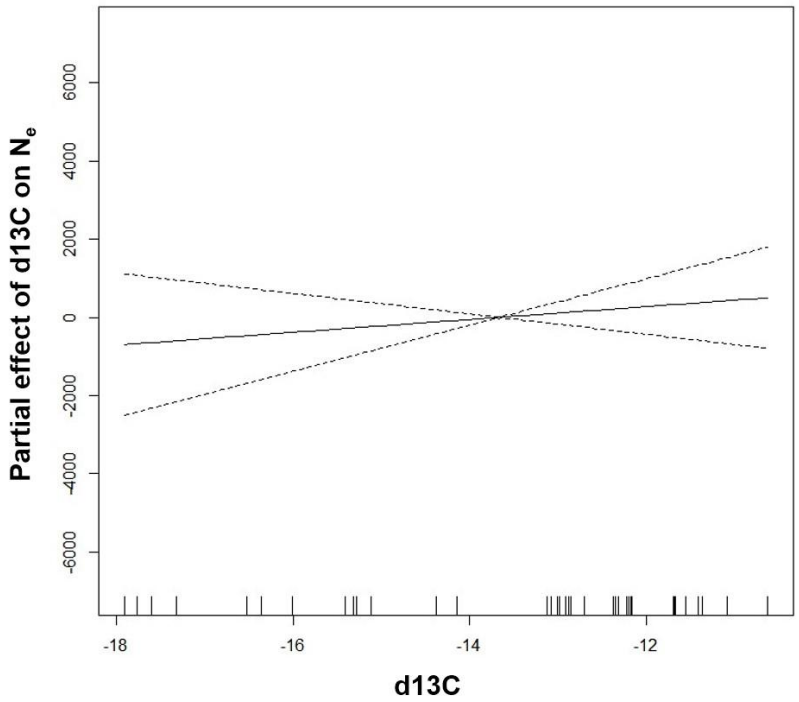

Figure 3.20. The relationship between δ13C and *O. flavescens* population size over the last 7,000 years, modelled in a GAM alongside δ15N.

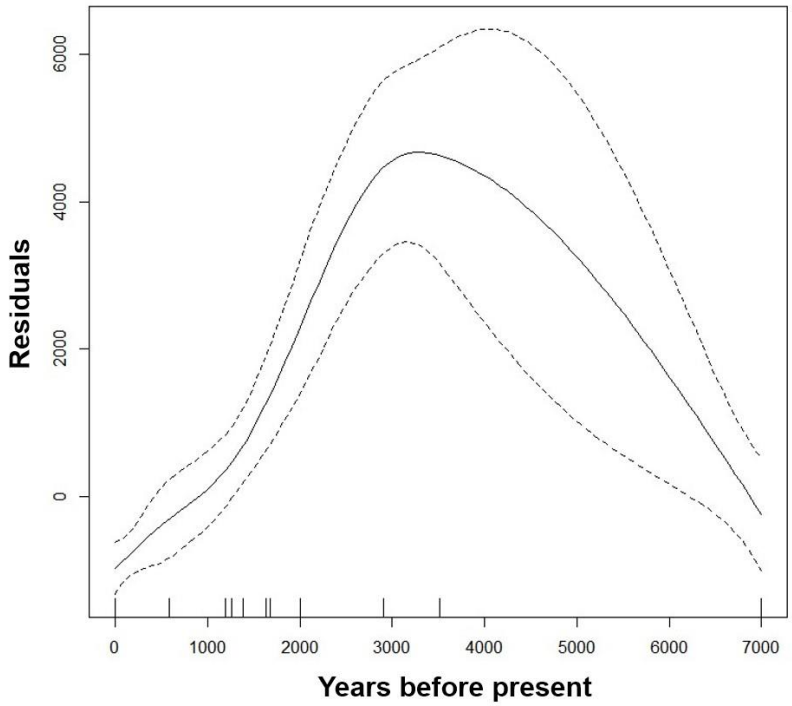

Figure 3.21. The absolute value of the residuals with respect to sample age, for the GAM fitting δ15N and δ13C to the *O. flavescens* population size.

Spheniscus magellanicus

Among *S. magellanicus*, little to no change occurred in population-wide average δ15N values over the last 6,000 years, while the population apparently grew by a factor of ~20 over the same period (Figure 3.22). On the other hand, δ13C values increased dramatically sometime between 3,000 and 4,500 ybp, following the initiation of population growth ~5,000 ybp (Figure 3.23).

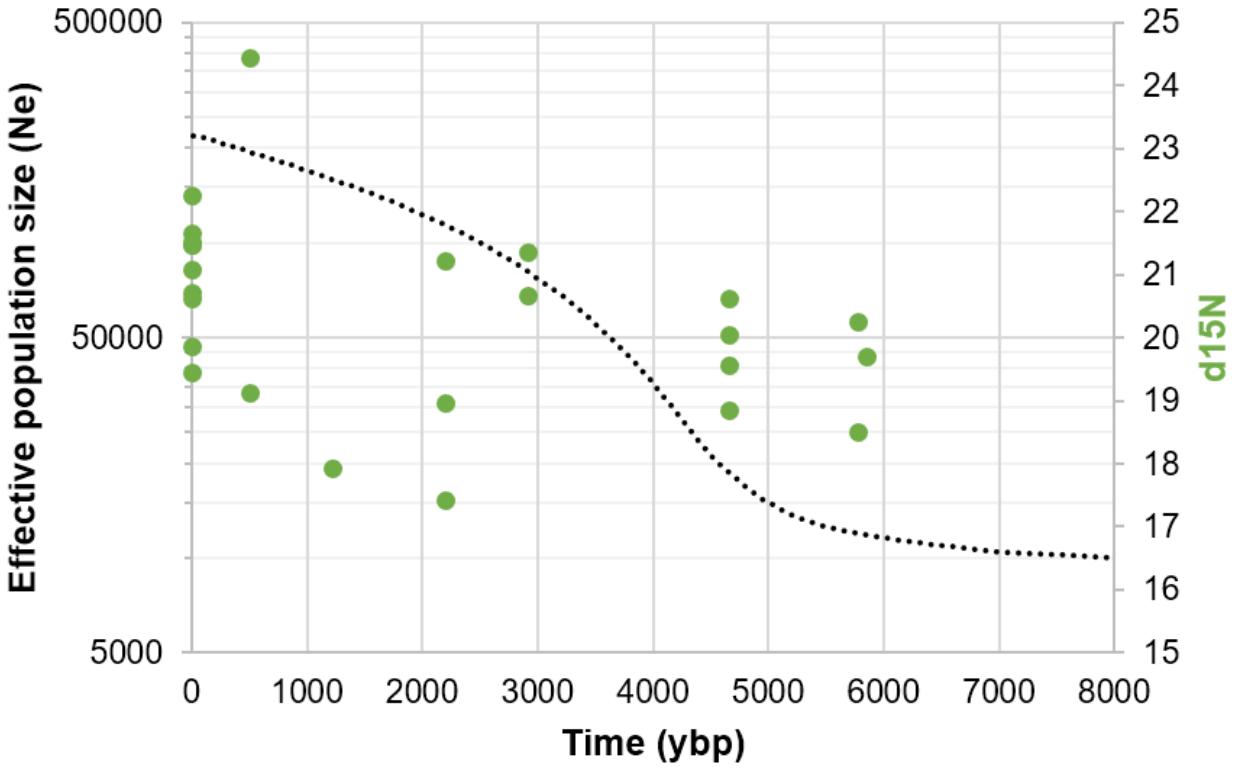

Figure 3.22. *S. magellanicus* demographic history (black dotted line) reconstructed by EBSP, against δ15N (green) values from ancient bone samples over the past 6,000 years.

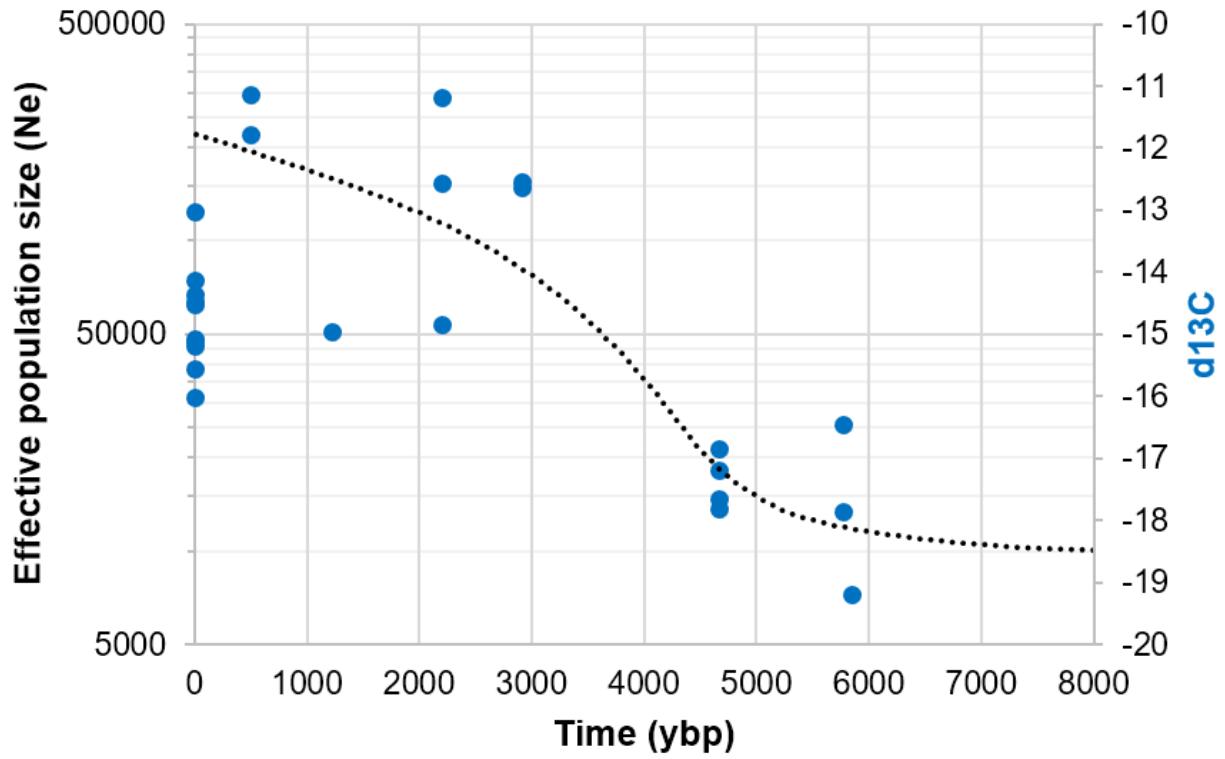

Figure 3.23: *S. magellanicus* demographic history (black dotted line) reconstructed by EBSP, against δ13C (blue) values from ancient bone samples over the past 6,000 years.

The GAM considering both isotopes as predictors of N_e (EBSP reconstruction) explained 56.9% of deviance. The δ15N term was not significant (p=0.24; Figure 3.24), while the δ13C term was significant (p=0.002; Figure 3.25). N_e had a positive relationship with δ13C, peaking around values of -14, which correspond to modern times (Figure 3.25). There was no relationship – statistically significant or otherwise – between the absolute value of the residuals of the model and sample age (p=0.465, deviance explained=2.34%), implying that the correlation between δ13C and N_e held over the last 6,000 years, at least as far as the data are capable of showing (Figure 3.26).

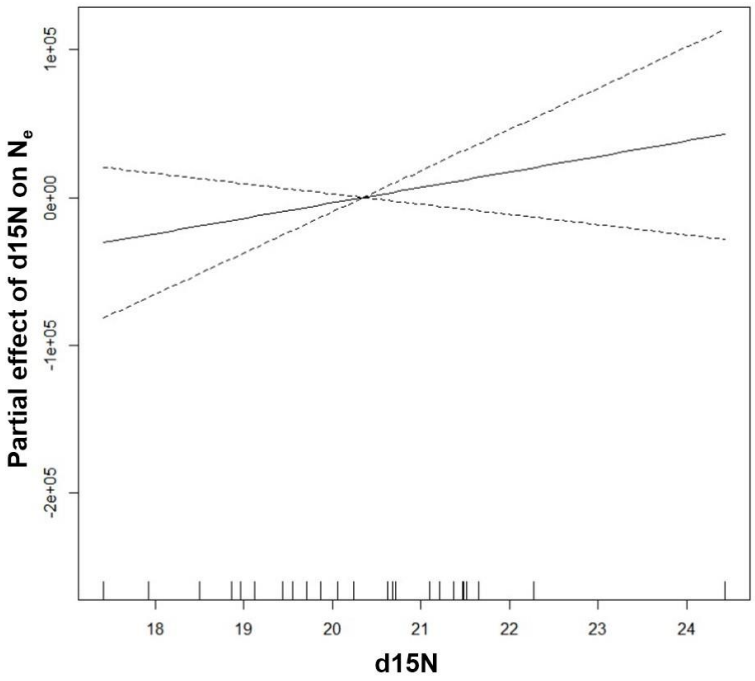

Figure 3.24. The relationship between δ15N and *S. magellanicus* population size over the last 5,845 years, modelled in a GAM alongside δ13C. Interior ticks on the horizontal axis indicate the presence of actual data points at those values.

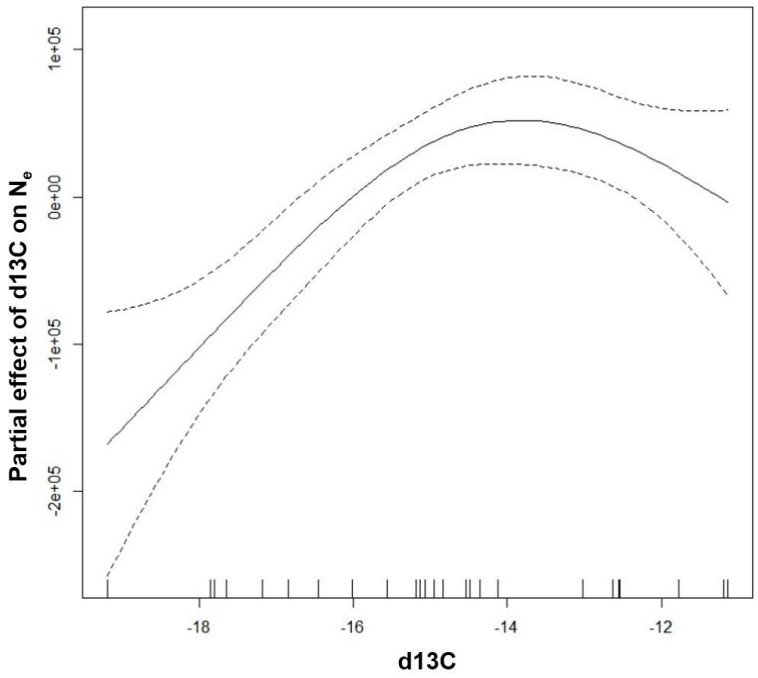

Figure 3.25. The relationship between δ13C and *S. magellanicus* population size over the last 5,845 years, modelled in a GAM alongside δ15N.

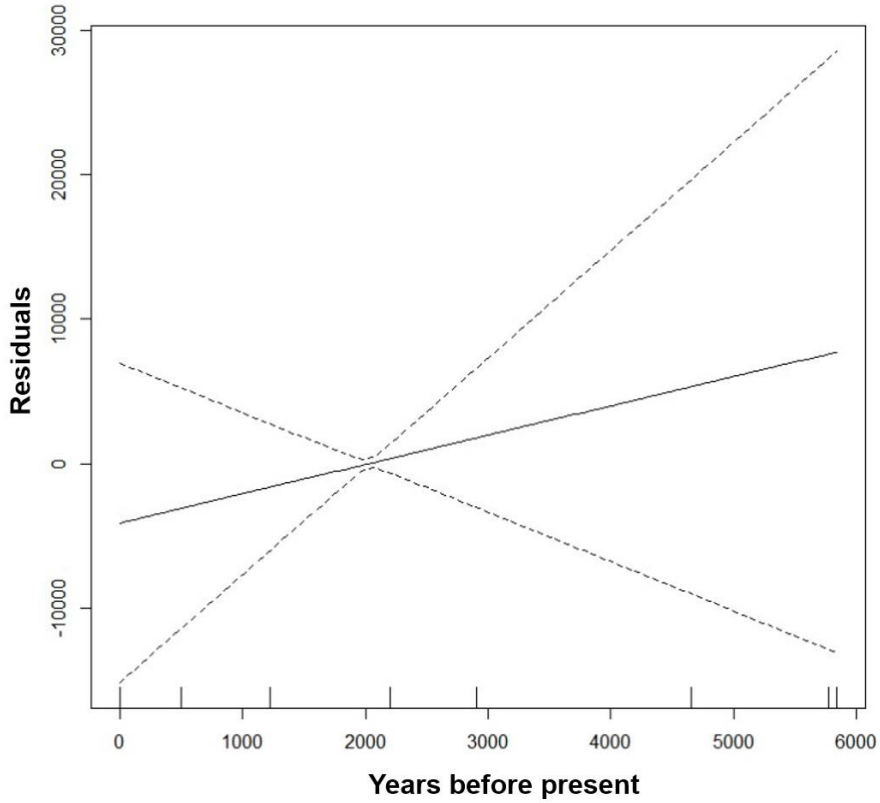

Figure 3.26. The absolute value of the residuals with respect to sample age, for the GAM fitting δ15N and δ13C to the *S. magellanicus* population size.

Discussion

Modern trends in stable isotopes

Previous reports on the diet of *O. flavescens* have not indicated regional differences in diet (Alonso et al. 2000), but rather suggested that differences in diet occur mainly on a local scale (Baylis et al. 2016; Jarma et al. 2019). Similarly, the present results do not clearly indicate any geographic trends in δ15N or δ13C among modern *O. flavescens*. However, they do suggest a geographic trend in δ34S, with δ34S values decreasing southward from Rio Negro to Tierra del Fuego. Variation in sulphur isotope ratios in marine animals are generally thought to reflect varying freshwater input to animals' diets, with freshwater sources being more depleted in 34S (MacAvoy et al. 2015). For a marine predator like *O. flavescens*, this could be mediated by foraging on anadromous fish, who rely on both marine and freshwater resources over the

course of their lives. One possibility is that the latitudinal gradient in δ34S in *O. flavescens* reflects increased foraging on anadromous fish in the south, anadromous salmonids having been introduced to Tierra del Fuego and southern Patagonia by humans in the early 20th century for economic reasons (Fernández et al. 2010; Tagliaferro et al. 2020). Predation by *O. flavescens* on farmed salmonids has been documented in southern Chile (Sepúlveda and Oliva 2005; Vilata et al. 2009), with this behavior leaving chemical signatures in the tissues of the predators (Guerrero et al. 2020). In Chile, populations of the anadromous fish *Galaxias maculatus* living farther south rely more on marine resources, and therefore presumably spend a larger share of their time in a marine environment, where they could be potential prey for *O. flavescens* (Gorski et al. 2015). Notably, this has resulted in a latitudinal gradient in δ34S among the fish oriented opposite to that of *O. flavescens*, with higher δ34S values in the south. However, these values are still lower than typical marine sources. The reasons for this trend among the fish in Chile are thought to be climatic, with warmer rivers in the north being able to more consistently support the fish over time. If the same pattern holds for other anadromous fish (including *G. maculatus*) on the Atlantic coast of Patagonia, it could explain the observed correlation between δ34S and latitude in modern Argentine *O. flavescens*. Moreover, the lack of evidence for such a correlation among ancient samples of *O. flavescens* may point to an anthropogenic influence, perhaps increasing the share of anadromous fish within the diet of *O. flavescens*, whether by increasing supply through the introduction of new species and/or causing aggregation of fish (e.g. farming), or by increasing demand and competition with human fisheries, which might limit the availability of other potential prey. A major complication to this story is that incorporating more anadromous fish in the diet should have also resulted in a lower level of δ13C in modern southern *O. flavescens* (Smith et al. 1996). Southern samples did appear to have the lowest δ13C values, but their difference to northern samples was not statistically significant (Figure 3.6).

Differences in diet have also been reported between demographic groups of *O. flavescens*, including sexes (Alonso et al. 2000) and age classes (Zenteno 2015a), as sex and age influence how far from shore and how deep in the water individuals forage. Demographic data were missing for most of the samples considered in this chapter. However, sex identifications were available for modern skin samples from the north, around Golfo San Matias. Among these, no evidence was found for significant sex differences in carbon or nitrogen isotope values. This is moderately surprising, given that at least one previous study (Alonso et al. 2000) found that females consumed a greater proportion of benthic prey than males, consistent with other

evidence that males travel farther than females on average (Campagna et al. 2001). This may simply be an issue of statistical power, because there does appear to be some separation between the male and female clusters in Figure 3.10, but only 17 samples from one region had sex identification and had their stable isotopes measured. However, a potential biological explanation for the discrepancy with previous findings would be that stable isotope measurements are expected to integrate diet over a period of months or longer (Dalerum and Angerbjörn 2005), whereas Alonso et al. (2000) were only able to determine what individuals had eaten shortly before death, in most cases analysing fishing bycatch. It may be, for example, that female and male diets only differ during certain periods, such as when females are nursing.

That explanation for the discrepancy between stable isotope analysis and the results of more traditional diet research seems to be validated in Magellanic penguins (Silva et al. 2013). In contrast to *O. flavescens*, previous studies have indicated regional differences in the diet of *S. magellanicus*, with anchovies being the overwhelmingly preferred prey in the north, while a more diverse diet including other fish species, as well as squid and lobster, is typical of penguins in Santa Cruz and Tierra del Fuego (Scolaro et al. 1999; Scioscia et al. 2014; Dodino et al. 2020). However, the present stable isotope results show no statistically significant differences in δ13C, δ15N or δ34S values between modern samples from the north and south. This fits with the findings of Silva et al. (2013), who pointed out that previous studies had focused on snapshots of the birds' diets during the breeding season, through stomach content analysis. However, the demands of parental care (which are shared between both parents in *S. magellanicus*) constrain how far the penguins can travel to forage, causing them to focus on locally abundant prey (which do vary regionally) and prey species that are especially good for chicks. Outside of the breeding season, however, the adult diet may be more varied and with more regional overlap in foraging grounds (Silva et al. 2013).

Historical and/or geographic trends in stable isotopes

In the present study, latitude and age covaried among the archaeological samples representing both species. This makes it difficult to draw firm conclusions about whether observed trends were related to history or simply to sampling from different regions. For example, if we were to assume that *O. flavescens* never exhibited regional differences in δ15N, we would conclude from the results that δ15N values had declined steadily from ~7,000 ybp to ~600 ybp, before rising again to their modern intermediate values (Figure 3.5). This scenario would be consistent

with the data. However, we cannot be certain of it because the early (high δ15N) values of that apparent historical trend all come from northern samples, while the late (low δ15N) values all come from southern samples. Therefore, an equally valid conclusion would be that the population-wide mean value of δ15N has not changed over time, but that in the past δ15N values followed a latitudinal gradient which has since collapsed, with both regions converging on the intermediate values that are observed in modern samples. This would imply that the average δ15N of individuals declined in the north and increased in the south within the past few hundred years (Figure 3.5).

Whereas this interpretation suggests opposite historical trends for δ15N in the north and south for *O. flavescens*, applying the same framework to δ13C values implies that they followed the same pattern in the north and south, albeit asynchronously, having increased suddenly at some point in the past. The shift seems to have occurred first in the north (by ~2000 ybp) and later in the south (by ~600 ybp). By those times, regional δ13C values were approximately equal to their present values, suggesting that they may have remained relatively stable for hundreds of years, although we do not have data throughout the intervening years to confirm that.

The δ13C values of *S. magellanicus* follow a similar pattern to the δ15N values of *O. flavescens*, with higher values in the ancient north and lower values in the ancient south converging on intermediate values in modern times which no longer display any regional variation. However, unlike *O. flavescens*, both very old (>4000 ybp) and less old (~500 ybp) samples are available to represent southern *S. magellanicus*, bookending northern samples of intermediate age (2000-2500 ybp). This is not ideal, but may go some way towards disentangling age and latitude because it suggests that southern δ13C values moved in the direction of and even beyond those of northern samples, with the average δ13C of the whole population increasing from approximately -18 to -12 from ~6000 to ~500 ybp, before declining again to intermediate modern values. On the other hand, there is no suggestion that ancient δ15N values may have varied regionally. Instead, δ15N seems to have been relatively stable, but decreased slightly over the last ~6000 years.

If differences among ancient samples are interpreted as at least partially reflecting regional differences, then the results suggest that the trophic niche of both species has become more limited in recent history, with less variation in δ13C and δ15N among modern samples compared to ancient samples from most time periods. Whereas no statistically significant

differences were found between the mean carbon or nitrogen isotope values of modern samples from the north and south in either species, the results were consistent with the existence of greater historical differences in trophic niche between the north and south, based on δ15N and δ13C of *O. flavescens* and δ13C of *S. magellanicus*. On the other hand, if ancient samples are interpreted as being representative of the whole population at their respective age, then the variance in δ15N and δ13C may have increased or decreased over time (e.g. Figure 3.5, left), but most time points were not represented by enough samples to properly quantify this (Figure 3.9, 3.14).

Zenteno et al. (2015b) previously analysed trends over time in the trophic niche of *O. flavescens* through a lens of geographic differences. The present results for the southern population of *O. flavescens* broadly agree with those described by Zenteno et al. (2015b; Figure 3.27). This is probably because the southern population is represented by samples from similar times and locations in both studies. On the other hand, the northern population described by Zenteno et al. (2015b) is mainly represented by samples less than ~1500 years old and sourced from the Chubut region (south of the Valdes Peninsula), while in the present dataset the ancient northern population is represented by samples from Rio Negro (Golfo San Matias, north of the Valdes Peninsula) that are almost all >1,500 years old. Considering the differences in both sampling and results, the northern population described by Zenteno et al. (2015b) can really be treated as a third geographically distinct population, which I will refer to as “Central Patagonian” going forward. This actually highlights the general conclusion that the trophic niche of *O. flavescens* has contracted in recent history, as despite their differences in sampling and evident historical trajectory, all three populations still converge on similar isotope values in modern samples.

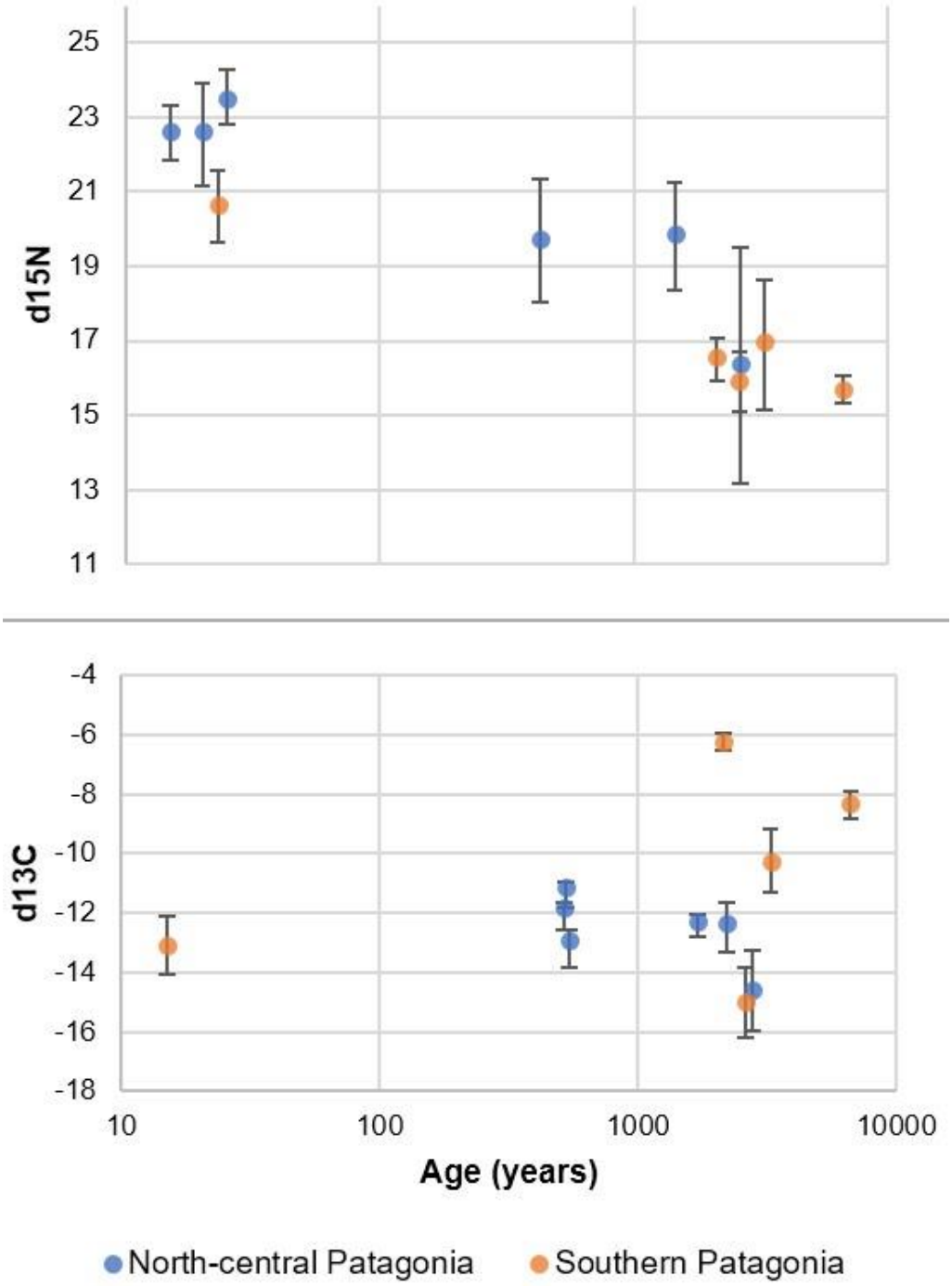

Figure 3.27. Regional and historical δ15N and δ13C results of Zenteno et al. (2015b) for *O. flavescens*. They found no consistent trend in δ13C values over time in north-central or southern Patagonia. However, their data clearly indicated an increase in δ15N values since ~3000 ybp in both north-central and southern Patagonia. Figure modified from Zenteno et al. (2015b).

Comparing the isotopic trends in different sample sets could help isolate the effects of either species membership or geography on populations' isotopic niches (Figure 3.28). For example, all *O. flavescens* populations show little evidence of change in δ13C values since the late Holocene, while both northern and southern *S. magellanicus* populations had higher δ13C values in the late Holocene relative to modern samples, suggesting that they have shifted to prey that are lower in δ13C within the last ~500 years. Likewise, a significant shift in δ15N values was observed for central and southern *O. flavescens* from the late Holocene. This could be significant in terms of the population's overall performance and demographic history, although it is difficult to attribute demographic history to a single cause.

		d15N		d13C	
		mid Holocene	late Holocene	mid Holocene	late Holocene
O. flavescens	northern	+	+	-	0
	central (Zenteno)		-		0
	southern		-		0
	southern (Zenteno)	-	-	+ *	0
S. magellanicus	northern		+ *		+
	southern	+ *	- *	-	+

Figure 3.28. Historical δ15N and δ13C values for the mid Holocene (>4.2 kya) and late Holocene (~0.5-4.2 kya) relative to modern values, broken down by region and by species. 0/grey = modern values, +/red = values above modern, -/blue = values below modern, black = no data.

Demographic history

The EBSP and Stairway Plot results for *O. flavescens* were highly consistent in both relative and absolute terms, for as long as they overlapped in time. Specifically, both methods suggested that the population grew from an effective size of ~4000 individuals ~3 kya to a present size of ~15,000-20,000 individuals. The Stairway Plot extended further back in time than the EBSP, and showed that this growth actually followed a decline of equal magnitude that apparent began ~8 kya. This short-lived low population phase was apparently centred on ~4 kya. Numerous palaeoclimate proxies suggest that the global climate temporarily became cooler around 4.2 kya, and this is recognised as the boundary between the middle and late Holocene,

with evidence from Australia and South America suggesting that the El Niño Southern Oscillation (ENSO) was stronger during this period (Walker et al. 2012). Modern El Niño events have been well documented to cause extremely high pup mortality in *O. flavescens* due to reduced prey availability (e.g. Soto et al. 2004; de Oliveira et al. 2012), potentially driving this feature of *O. flavescens*' demographic history.

Several previous studies have suggested that the population of *O. flavescens* expanded throughout the Holocene, but have generally placed the beginning of this expansion around 10-15 kya, coinciding with the post-glacial sea level rise that formed the Patagonian coastline into its modern shape and may have increased access to foraging in shallow continental shelf waters (Ponce et al. 2011; Oliveira et al. 2017). The EBSP analysis by Oliveira et al. (2017) also indicated that the population grew by ~100-fold, which is much greater than the ~4-fold growth indicated by the present Stairway Plot and EBSP results. However, another recent paper, by Peralta et al. (2021), found no evidence for population growth or decline based on a Bayesian Skyline Plot (BSP) analysis of the mitochondrial control region.

The Stairway Plot extends much further back in time, and suggests that substantial population growth occurred ~40 kya. This is roughly consistent with previous suggestions (based on mismatch distribution analysis) of a bottleneck ~64 kya (Tunez et al. 2010), and a subsequent population expansion ~27 kya (based on population divergence time analyses) (Feijoo et al. 2011). The Stairway Plot does not provide clear evidence of that ancient bottleneck, but it does suggest that the population was much smaller around that time. Such a bottleneck could have eliminated or distorted genomic variation that might otherwise have allowed the analysis to infer that demographic history from deeper in time.

The EBSP analysis of *S. magellanicus* suggests that the population has grown by a factor of ~20x since ~4-6 kya. As with *O. flavescens*, the one previous analysis (Dantas et al. 2018) suggested that this growth began around the onset of the Holocene, ~10-15 kya. However, the inclusion of ancient DNA for calibration suggests a much faster mutation rate (mean $2.3e^{-6}$ s/s/y compared to $0.86e^{-6}$ s/s/y). The previously used, slower, rate was based on a very strong analysis of the same locus (mitochondrial HVRI) in Adelie penguins (*Pygoscelis adeliae*) (Millar et al. 2008), and a similar rate was reported by Lambert et al. (2002), also for Adelies. However, the mutation rate could well vary between genera (*Pygoscelis* to *Spheniscus*), and the effective mutation rate may also vary with timescale, particularly in rapidly evolving loci like this one,

where multiple mutations at the same site may be missed and interpreted as one (Ho et al. 2005). Still, this new aDNA-based rate of $2.3e^{-6}$ s/s/y is not staggeringly faster than those previously used, as the upper confidence interval of Millar's and Lambert's estimates for Adelie were $1.17e^{-6}$ s/s/y and $1.43e^{-6}$ s/s/y, respectively. Notably, the addition of ancient samples to the Dantas et al. (2018) dataset did not change the shape of the EBSP curve in any perceptible way; they only updated the estimates of the absolute size of the population and the timing of its growth phase.

Relating demographic history to isotopic trends

The demographic history of *O. flavescens* seems to have closely paralleled changes in δ15N in the population (Figure 3.17). δ13C followed a comparable pattern, but fit less well to demographic history and did not emerge as a statistically significant factor. The correlation between N_e and δ15N was negative, meaning that the population grew at the same time as the average trophic level at which they foraged decreased. Such a reduction in trophic level could represent, for example, a shift from fish towards crustaceans (Cherel and Hobson 2007). That dietary shift would also likely bring about an increase in δ13C, since crustaceans tend to dwell more on the seafloor compared to fish. Although the relationship between N_e and δ13C was not significant, average δ13C of samples did also increase around the same time (Figure 3.18).

In *S. magellanicus*, it was δ13C that better paralleled demographic history (Figure 3.23). This relationship is less striking than in *O. flavescens* because only an EBSP reconstruction of demographic history was possible for *S. magellanicus*, and this provided less temporal resolution. The population began to grow around 5 kya and its growth began to slow (but apparently continued) around 3 kya. The change in δ13C over time was also not complex. Average δ13C increased from around -18 to around -14 sometime between 3 and 4.5 thousand years ago, around the same time as the population growth rate apparently peaked. In contrast, average δ15N of *S. magellanicus* increased only very gradually or remained stable over the last ~6000 years (Figure 3.22). Enrichment in δ13C could suggest either a shift to feeding farther north, at lower latitudes (Cherel and Hobson 2007), or to foraging at deeper depths, nearer the sea floor, or closer to shore (Polito et al. 2011). As with *O. flavescens*, such a change in diet would also be likely to be reflected somehow in δ15N, but there is no evidence of a recent shift in δ15N in *S. magellanicus*. One possibility is that the identity of the species comprising the diet of *S. magellanicus* (and hence their trophic level, indicated by δ15N) did not change, but they

changed the areas in which they hunted, focusing closer to shore or at greater depth. This may not reflect a change in dietary choice from *S. magellanicus*, but merely tracking of a shifting prey distribution.

The timing of these isotopic and demographic shifts apparently differs between *O. flavescens* and *S. magellanicus*, with the former beginning ~2-3 kya and the latter ~4-6 kya. However, these are not dramatically different; well within the range of plausible uncertainty, considering, for example, the alternative mutation rates that have been used in previous studies for both species. For either or both species, one possible environmental cause for shifting to more benthic or inshore foraging – whether this was an active change in behaviour or merely the predators following their prey – is the global mid-latitude aridification and cooling associated with the aforementioned 4.2-ka event (Walker et al. 2012; Bender et al. 2013), and the long-term gradual decline in relative sea level along the Patagonian coast that began ~6 kya (Prieto et al. 2017). Coastal aridification and sea level decline could have made demersal or benthic prey more accessible, gradually unlocking an additional food source. An increase in the variety of foraging sites where the sea floor was within diving range may have been especially valuable to individuals caring for pups or chicks, as they struggle to afford the costs in energy and time away from their offspring to forage (e.g. Campagna et al. 2001). Changes in sea level and/or temperature may have also altered the position of coastal fronts or larger ocean currents, such as the Brazil-Malvinas Confluence (BMC) (Aguirre 1993; Gu et al. 2019). These currents and their confluences are relatively far from the Patagonian coast, but Patagonian *S. magellanicus* have been known to overwinter in Brazil and utilise the Malvinas Current (Silva 2022), so its southward shift during the mid-Holocene could have been a boon to their population, and increased utilisation of lower-latitude food could have contributed to an increase in their average δ13C (Cherel and Hobson 2007).

Chapter 4: Comparative demographic history

Introduction

Background

Comparing the demographic histories of different populations may be enlightening, not only of facts about those populations' histories, but about the relative importance of processes and constraints influencing their demography, such as ecological dependencies and life history traits. There has been significant interest in identifying species that are exceptionally sensitive to specific environmental variables so that they can be used as "indicator species", whose population trends may serve as proxies for those environmental variables and predictors of demographic trends in other species that are also ultimately dependent upon, but may respond less rapidly to, the same features of the environment. Studied examples include earthworm taxa being used as indicators of geological change (e.g. in soil type), with their demographic histories appearing to be influenced by such events in the Mediterranean region (Fernánde et al. 2013), and the frog *Rana uenoi* being used as an indicator of climate change on the Korean peninsula due to the sensitivity of its breeding season to winter temperatures (Jeon et al. 2021). Some species create environmental conditions that help or hinder the survival of others, potentially defining entire communities of species (Jones et al. 1994; Wright and Jones 2006).

These concepts imply that we might expect to see suites of species exhibiting similar demographic histories as a result of being dependent upon each other or on the same environmental variable(s). For example, sea lions, seals and penguins should not be intrinsically very sensitive to parameters of the marine environment such as temperature and salinity; their large, well-insulated bodies and endothermy allow them to maintain homeostasis during their trips to sea to find food. However, their smaller and fully marine prey are highly sensitive to these parameters, and their abundance in a given area is strongly influenced by water temperature and chemistry (Acha et al. 2004; Alemany et al. 2014). As a result of their dietary dependence on these more sensitive animals, the demographic trends that have occurred in the marine mammals and birds of coastal Argentina and elsewhere might be similar to each other and to those of their local fish and cephalopods.

Numerous authors have described demographic histories from multiple species and highlighted similarities and differences between them, sometimes using their disjunction to infer divergence times (e.g. Rogers et al. 2019; Li et al. 2020). However, relatively few have made comparing demographic histories an explicit aim of their study, and fewer have used quantitative approaches to compare demographic histories. An early example was the comparison of snub-nosed monkeys and giant pandas performed by Zhou et al. (2014). They found that three of four species of snub-nosed monkey exhibited similar demographic histories according to the pairwise sequentially Markovian coalescent (PSMC) method (Li and Durbin 2011). However, a fourth species, the golden snub-nosed monkey (*Rhinopithecus roxellana*), had a different demographic history. For at least the last million years, its population size appeared to have more closely paralleled that of the giant panda (*Ailuropoda melanoleuca*), with which it shares a similar folivorous diet, rather than the population sizes of other snub-nosed monkeys. They quantified these findings by calculating Pearson's correlation coefficient between the demographic history curves of each pair of species (among *Rhinopithecus* spp. and *A. melanoleuca*).

Hecht et al. (2018) used PSMC to compare the demographic histories of host and symbiont pairs, including the nematode parasite *Trichinella spiralis* and their pig (*Sus scrofa*) hosts, and the malaria disease system, including humans, the other great apes, *Anopheles* mosquitoes, and the agent of malaria *Plasmodium falciparum*. They quantified the PSMC results similarly to Zhou et al.(2014), but rather than calculate correlation coefficients between the curves, Hecht et al. (2018) focused exclusively on the direction of change in effective population size between each pair of time points. The reason for this was that the correlation coefficient is heavily influenced by the relative magnitude of population size through time, but that is arguably not as relevant to understanding ecological relationships as simply whether the population is growing, shrinking, or remaining stable at a given point in time. Hecht et al. (2018) also allowed for a degree of uncertainty in the inferred timing of each population's demographic history based on model error and imprecise estimates of mutation rate and generation time. Finally, they reported that the demographic history curves of "true" host-symbiont pairs (e.g. *Trichinella* x pigs) differed significantly less on average than the demographic history curves of arbitrary pairings (e.g. *Trichinella* x gorillas).

The comparative approaches by Zhou et al. (2014) and Hecht et al. (2018) both focused on demographic histories inferred from the pairwise sequentially Markovian coalescent (PSMC),

which is a model-flexible method that estimates effective population sizes throughout a population's history, up to the time of the oldest recombination event detectable in the genome of sampled individual(s) (Li and Durbin 2011). All methods for reconstructing demographic history based on the coalescent are most accurate and precise in their estimates when dealing with a large number of coalescence events. Most coalescence events are expected to have occurred within the last 2N generations, but this means that within the most recent few generations (depending on the magnitude of N), and in the very distant past, few coalescence events will be detected from which to infer the size of the population during those periods (Fu and Li 1999). In their analysis of human genomes with PSMC, Li and Durbin (2011) suggested that reconstructions of the most recent 20,000 years (~800 generations) and points older than 3,000,000 years (~120,000 generations) should be regarded as untrustworthy. However, PSMC is expected to recover fewer coalescences in the recent past than most other coalescent-based methods, like the EBSP (Heled and Drummond 2008; Ho and Shapiro 2011) and Stairway Plot (Liu and Fu 2015) introduced in the previous chapter. This is because, in lieu of a population sample, PSMC takes the genome of a single diploid individual and detects recombination points where the flanking genomic regions have different genealogical histories. However, this means that it is also limited by the recombination rate in order to recover a sufficient number of distinct genomic regions that coalesce in the recent past, leaving PSMC with less power to resolve recent demographic history than a Stairway Plot (or similar) analysis using a modest sample of individuals from the same population.

Some other methods are simpler and less informative, but offer alternative lines of evidence and may be more robust in certain circumstances. Cole et al. (2019) investigated the demographic histories of six penguin species across three genera (*Eudyptes, Pygoscelis, Aptenodytes*) using genomic data derived from a DArT-seq strategy. To analyse specifically their recent demographic histories, Cole et al. used three distinct methods: 1) the common test statistic known as Tajima's D (Tajima 1989), which can indicate recent population expansion or contraction (alternatively, selective sweep or balancing selection) based on the frequency of rare alleles relative to expectations; 2) a genealogy-based method called SNAPP (Bryant et al. 2012) that infers population size changes from the density of recent lineage-coalescence events; and 3) a model-flexible method called CubSFS (Waltoft and Hobolth 2018) that reconstructs historical population sizes by fitting a model that best explains the full distribution of allele frequencies. They found a high level of consistency across these methods' indications of the direction of recent demographic change, with all agreeing in four cases of recent decline or

stability, and each method disagreeing with the others in one instance across seven cases of recent population growth. Overall, they concluded that macaroni, eastern rockhopper, Adélie, gentoo, king and emperor penguins showed evidence of recent population growth, while northern rockhopper, western rockhopper, fjordland and snares penguin populations had declined or remained stable.

Cristofari et al. (2018) also investigated the demographic history of two of these species, king penguins and emperor penguins. In agreement with Cole et al., their results suggested that the king penguin population had grown significantly since the last glacial maximum, though it was static over most of the Holocene. In contrast, the emperor penguin population appeared to have been relatively stable for tens of thousands of years. The authors interpreted this as indicating that the fluctuations in the king penguin population were not driven by changes in overall productivity of the Southern Ocean, which likely would have affected both species, but rather changes in habitat requirements peculiar to the king penguin, such as the proximity of sea ice and the Antarctic Polar Front to lower-latitude king penguin colonies. For their demographic history reconstruction, Cristofari et al. (2018) used Stairway Plot (introduced in the previous chapter) which - like CubSFS - uses the distribution of allele frequencies in a population sample to infer changes in effective population size.

As seen in the previous chapter, inference of a single population's demographic history based on population genetics is complicated, and there is inevitably uncertainty over whether a population grew/shrank or remained stable during a specified period. Moreover, the inference is of *effective* population size (N_e), which is influenced by more factors than just the number of individuals in the population (census size; N), such as the sex ratio, variance in reproductive success or offspring survival, and the demographic-genetic history of the population (i.e. if the size of the population has recently changed and genetic diversity has not yet caught up). For example, migration within a subdivided population can leave a genetic signature of the population having grown (if multiple subpopulations are sampled) or contracted (if only one subpopulation is sampled) even if the overall metapopulation actually remained at a stable size throughout (Mazet et al. 2015). Still, if our objective is to learn about demographic similarities and differences between populations, then changes in their degree of population structure could also be considered a legitimately interesting aspect of demographic history, rather than merely a confound. However, this assumes that we can either disentangle population size from population structure based on other information (e.g. circumstantial evidence from

environmental history) that lends greater plausibility to one scenario or another, or that we can gain useful insights from the overall similarity/difference of populations' genetically-inferred demographic histories. For example, separation of a population into refugia during episodes of glaciation would be expected to increase population subdivision and therefore skew the ratio between its inferred effective population size and its true historical census size, yet both population size and structure could contribute to a signature, diagnostic feature of the demographic histories of populations that were affected by a particular environmental upheaval, assuming consistent sampling strategies could be applied bearing in mind the cautionary simulations of Mazet et al. (2015). Considering the numerous forces shaping demographic trends, how likely is it that a pair of species selected at random from around the world will have a very similar demographic history? Furthermore, how likely is it that the independently generated genetic signatures of such similar demographic histories will lead to similar demographic histories being inferred by genomics-based methods?

In this chapter, I outline an approach for quantitatively comparing demographic histories, and use it to investigate how consistent patterns of demographic history are among related or sympatric species based on Stairway Plot analyses of published sequence data and the novel genomic data for the South American sea lion (*Otaria flavescens*) introduced earlier in this thesis. I use clustering-type analyses to assess what ecological, geographic, biological or historical factors could explain the patterns of similarity and difference among demographic histories. I apply this novel method to population genomic datasets of pinnipeds, penguins, and silverside fish, chiefly from South America and the Southern Ocean.

Methods

Data sources

Simulated populations

Three sets of populations were simulated using Hudson's 'ms' program (Hudson 2002) in order to test the reliability of demographic history comparisons under different conditions (Table 4.1). These simulations follow a lineage of simulations used in previous papers to validate new programs for use in demographic history reconstruction. For example, the "Standardsim" command found in Table 4.1 was previously used to validate PSMC (Li and Durbin 2011) and

Stairway Plot (Liu and Fu 2015; Liu and Fu 2020). Populations within each set had a common structure to their history and similar genome sizes, mutation rates and generation times. However, the timing and scale of each step in their population history was permuted by up to 2% and their genome size, mutation rate and generation time (demographic scaling parameters) were allowed to vary by up to 20%. These permutations were meant to represent actual variation that might be expected between the demographic histories of populations of the same species or similar species in the same environment, as well as noise introduced by different sample sizes and genome coverage. A novel program called “align_stairwayplot.py” was developed and tested to be able to correctly cluster these sets, before moving on to real data.

Table 4.1. The ‘ms’ command to generate the base version of each of the simulation sets, from which permutations were generated and tested. Clearly, SimBr is much more complex than Standardsim or Modsim. It is also unique in controlling N_e gradually by modifying population growth rate through “-eG” commands, while the other two rely on instantaneous changes in N_e set by “-eN” commands.

“Standardsim”	ms 80 200 -t 2732 -r 2179 30000000 -eN 0.01 0.05 -eN 0.0375 0.5
“Modsim”	ms 80 200 -t 2732 -r 2179 30000000 -eN 0.01 1.5 -eN 0.0375 0.5
“SimBr”	ms 80 200 -t 2688.000000 -r 2150.4 10000000 -G 9.032530 -eG 0.089286 0.0 -eN 0.214286 0.857143 -eN 0.334821 0.178571 -eG 0.334821 -2.700260 -eG 0.513393 0.752006 -eG 0.625000 0.0

Natural populations

Published RADseq reads from a wide taxonomic and geographic range of populations were downloaded from the NCBI GenBank database. Table 4.2 lists the populations that were ultimately used and their metadata.

In the case of penguins, multiple studies, including the source of the genomes used here, have reported extremely shallow genetic differentiation between modern populations of these species, discernible only with the use of geographic priors. Therefore, I analysed them first as full species (all individuals pooled) and then as separate populations to check for inconsistencies, whether due to error (reduced sample size) or distinct regional histories. For

pinnipeds, most species could only be represented with adequate sample size (10+ individuals) by a single population.

Mutation rates for most pinniped species were taken from Peart et al. (2020), who estimated them from the same genomes analysed here, by summing genomic differences relative to estimated divergence times between species. The commonly used vertebrate mutation rate of $2.5e^{-8}$ substitutions/site/generation (s/s/g; Nachman and Crowell 2000) was assumed for *O. flavescens* and *Leptonychotes weddellii*, as no species-specific estimate was available. For *O. flavescens*, this is not far from the rate estimated for close relatives by Peart et al. (2020). The 2.5^{-8} s/s/g mutation rate was also used for silverside fish, as it has been used for other ray-finned fish (e.g. *Sebastes* spp., Xu et al. 2019). The rate assumed for penguins in the literature is more variable. For example, Cole et al. (2019) used an extremely fast mutation rate of $2.6e^{-7}$ substitutions/site/generation for all penguins, which was originally estimated from king penguin RADseq data by Trucchi et al. (2014), who remarked that they did not trust the very high result to be generally applicable. They suggested that it was influenced by their selection of RAD enzyme, SbfI, which focused on GC-rich regions that may have unusually high mutation rates due to a high density of hypermutable CpG sites (Webster et al. 2006). The estimate was also made by analysing RAD loci jointly with mitogenomes. However, genealogical incongruity between the single maternally inherited locus of the mitogenome and the many nuclear RAD loci could also distort the result. At the other end of the spectrum, Li et al. (2014) estimated an implausibly slow rate of $8.11e^{-9}$ based on assumptions about generation time that are now regarded as incorrect (Cristofari et al. 2018). Cristofari et al. (2018) arrived at an estimate of $1.08e^{-7}$ using the approach of Trucchi et al. (2014), but also applied their refined approach to the data of Li et al. to yield a corrected rate of $4.55e^{-8}$, which is closer to the rate expected for a vertebrate. This mutation rate of $4.55e^{-8}$ substitutions/site/generation was assumed for all penguin species in the present study.

Generation times for most pinniped species were taken from Peart et al. (2020) and range from 8.7 years (*Mirounga angustirostris*) to 18.6 years (*Pusa hispida*). A generation time of 9 years for *L. weddellii* was taken from Curtis et al. (2009). A generation time of 12 years was used for *O. flavescens*, based on Hernandez-Camacho et al. (2008) and followed by Feijoo et al. (2011) and Oliveira et al. (2017). For all silverside fish, a generation time of 2.9 years was taken from Garcia et al. (2014), who used it for analyses on several of these exact species, and Cortinhas et al. (2016), who used the rate for analyses of *Atherinella brasiliensis* from the same family.

Penguin species-specific generation times were taken from Forcada and Trathan (2009), with estimates ranging from 8 years (*Pygoscelis* spp.) to 14 years (*Aptenodytes forsteri*).

Table 4.2. Natural populations considered in this study. All sequence data were originally obtained via RADseq or ddRADseq from the stated data source reference. They were then assembled to the closest reference genome available. NCBI accession numbers for the samples and associated RADseq reads of published data can be found in Appendix A.

Species	Location (population)	Mutation rate (/site/gen)	Generation time (yrs)	N	Data source	Genome reference accession
Otaria flavescens	Argentina	$2.5e^{-8}$	12	40	Original data	CNA0007262 (Yuan et al. 2021)
Arctocephalus australis	Brazil	$1.42e^{-8}$	11.7	11	Peart et al. 2020	GCA_900642305.1 (*A. gazella*)
Arctocephalus forsteri	Cape Foulwind, NZ ("CFoulwind")	$1.2e^{-8}$	9.9	8	Peart et al. 2020	GCA_900642305.1 (*A. gazella*)
Arctocephalus forsteri	Open Bay, NZ ("OBay")	$1.2e^{-8}$	9.9	7	Peart et al. 2020	GCA_900642305.1 (*A. gazella*)
Arctocephalus forsteri	Ohau Point, NZ ("OhauP")	$1.2e^{-8}$	9.9	6	Peart et al. 2020	GCA_900642305.1 (*A. gazella*)
Arctocephalus forsteri	Victory Beach, NZ ("VictoryB")	$1.2e^{-8}$	9.9	6	Peart et al. 2020	GCA_900642305.1 (*A. gazella*)
Arctocephalus galapagoensis	Isabela Island, Galápagos	$1.21e^{-8}$	10	12	Peart et al. 2020	GCA_900642305.1 (*A. gazella*)
Arctocephalus gazella	South Georgia	$1.1e^{-8}$	9.1	80	Peart et al. 2020	GCA_900642305.1
Mirounga leonina	Sea Lion Island, Falklands	$4.94e^{-9}$	9.5	11	Peart et al. 2020	GCA_004023865.1 (*M. angustirotris*)
Mirounga angustirostris	California	$4.52e^{-9}$	8.7	15	Peart et al. 2020	GCA_004023865.1
Phoca vitulina	Svalbard	$7.99e^{-9}$	14.8	12	Peart et al. 2020	GCA_004023865.1 (*M. angustirotris*)
Pusa hispida	Svalbard	$1.00e^{-8}$	18.6	14	Peart et al. 2020	GCA_004023865.1 (*M. angustirotris*)
Erignathus barbatus	Svalbard	$7.42e^{-9}$	13.4	11	Peart et al. 2020	GCA_004023865.1 (*M. angustirotris*)
Zalophus californianus	El Golfo de Santa Clara, MX ("GCal1")	$6.67e^{-9}$	14.5	12	Peart et al. 2020	GCA_004024565.1

Zalophus californianus	Isla Ángel de la Guarda, MX (“GCal2”)	$6.67e^{-9}$	14.5	11	Peart et al. 2020	GCA_004024565.1
Zalophus californianus	Isla San Pedro Nolasco, MX (“GCal3”)	$6.67e^{-9}$	14.5	21	Peart et al. 2020	GCA_004024565.1
Zalophus californianus	Isla del Espiritu Santo, MX (“GCal4”)	$6.67e^{-9}$	14.5	14	Peart et al. 2020	GCA_004024565.1
Zalophus californianus	Isla Santa Margarita, MX (“SMargarita”)	$6.67e^{-9}$	14.5	14	Peart et al. 2020	GCA_004024565.1
Zalophus wollabaeki	Baltra Island, EC	$4.6e^{-9}$	10	10	Peart et al. 2020	GCA_004024565.1 (*Z. californianus*)
Zalophus wollabaeki	Espanola Island, EC	$4.6e^{-9}$	10	10	Peart et al. 2020	GCA_004024565.1 (*Z. californianus*)
Zalophus wollabaeki	Fernandina Island, EC	$4.6e^{-9}$	10	19	Peart et al. 2020	GCA_004024565.1 (*Z. californianus*)
Zalophus wollabaeki	Genovesa Island, EC	$4.6e^{-9}$	10	9	Peart et al. 2020	GCA_004024565.1 (*Z. californianus*)
Zalophus wollabaeki	Isabela Island north, EC (“IsabelaB”)	$4.6e^{-9}$	10	15	Peart et al. 2020	GCA_004024565.1 (*Z. californianus*)
Zalophus wollabaeki	Isabela Island south, EC (“IsabelaV”)	$4.6e^{-9}$	10	8	Peart et al. 2020	GCA_004024565.1 (*Z. californianus*)
Zalophus wollabaeki	Pinta Island, EC	$4.6e^{-9}$	10	7	Peart et al. 2020	GCA_004024565.1 (*Z. californianus*)
Zalophus wollabaeki	Santa Fe Island, EC	$4.6e^{-9}$	10	8	Peart et al. 2020	GCA_004024565.1 (*Z. californianus*)
Leptonychotes weddellii	Erebus Bay	$2.5e^{-8}$	9	19	Miller et al. 2021	GCA_000349705.1
Aptenodytes patagonicus	Falkland Islands + Crozet Archipelago	$4.55e^{-8}$	9	30	Clucas et al. 2018	GCA_010087175.1
Aptenodytes patagonicus	South Georgia Island	$4.55e^{-8}$	9	16	Clucas et al. 2018	GCA_010087175.1
Aptenodytes patagonicus	Macquarie Island	$4.55e^{-8}$	9	12	Clucas et al. 2018	GCA_010087175.1
Pygooscelis antarcticus	South Shetland	$4.55e^{-8}$	8	10	Clucas et al. 2018	GCA_010078415.1
Pygooscelis antarcticus	Orne Harbor	$4.55e^{-8}$	8	10	Clucas et al. 2018	GCA_010078415.1

Pygooscelis antarcticus	Bouvet & South Sandwich Islands	$4.55e^{-8}$	8	10	Clucas et al. 2018	GCA_010078415.1
Pygoscelis adeliae	West Antarctica (Antarctic Peninsula & South Sandwich Island)	$4.55e^{-8}$	8	42	Clucas et al. 2018	GCA_000699105.1
Pygoscelis adeliae	East Antarctica (Welch, Bechervaise and Petrels Islands & Blakeney Point)	$4.55e^{-8}$	8	37	Clucas et al. 2018	GCA_000699105.1
Pygoscelis papua	Falkland Islands	$4.55e^{-8}$	8	10	Clucas et al. 2018	GCA_010090195.1
Pygoscelis papua	Antarctic Peninsula	$4.55e^{-8}$	8	34	Clucas et al. 2018	GCA_010090195.1
Pygoscelis papua	Kerguelen Island	$4.55e^{-8}$	8	11	Clucas et al. 2018	GCA_010090195.1
Aptenodytes forsteri	Amanda Bay & Pointe Geologie	$4.55e^{-8}$	14	27	Clucas et al. 2018	GCA_000699145.1
Aptenodytes forsteri	Fold Island & Auster	$4.55e^{-8}$	14	27	Clucas et al. 2018	GCA_000699145.1
Aptenodytes forsteri	Gould Bay & Halley Bay	$4.55e^{-8}$	14	22	Clucas et al. 2018	GCA_000699145.1
Aptenodytes forsteri	Cape Roget & Cape Washington	$4.55e^{-8}$	14	17	Clucas et al. 2018	GCA_000699145.1
Odontesthes argentinensis	Uruguay	$2.5e^{-8}$	2.9	28	Hughes et al. 2020	GCA_014825785.1
Odontesthes regia	Chile	$2.5e^{-8}$	2.9	17	Hughes et al. 2020	GCA_014825785.1
Odontesthes mirinensis	Brazil	$2.5e^{-8}$	2.9	10	Hughes et al. 2020	GCA_014825785.1
Odontesthes mauleanum	Chile	$2.5e^{-8}$	2.9	33	Hughes et al. 2020	GCA_014825785.1
Odontesthes ledae	Brazil	$2.5e^{-8}$	2.9	12	Hughes et al. 2020	GCA_014825785.1
Odontesthes bonariensis	Uruguay	$2.5e^{-8}$	2.9	15	Hughes et al. 2020	GCA_014825785.1
Odontesthes hatcheri	Uruguay	$2.5e^{-8}$	2.9	15	Hughes et al. 2020	GCA_014825785.1

Genome assembly and SNP-calling

Genomic DNA reads were assembled to an appropriate reference genome using the 'mem' command of BWA v0.7.12 (Li and Durbin 2009). For penguins, precise reference genomes were accessible for each species. For pinnipeds and silverside fish, a reference genome from within the same genus was usually relied upon (Table 4.2). The resulting assemblies were then converted to .bam file format with samtools 'view', ignoring alignments with mapping quality <20 (Danecek et al. 2021). Variant sites were called using Stacks' ref_map.pl pipeline (Catchen et al. 2011; Catchen et al. 2013). In an initial run, no limit on missing data (per site or per individual) was applied, but based on the results, individuals missing a genotype at >70% of all sites (i.e. sites genotyped in at least one individual) were excluded from subsequent analysis. Stacks' populations module was then run again, requiring any sites to be present in at least 95% of the remaining individuals in order to be included in the final SNP dataset.

Demographic history reconstruction

Folded site frequency spectra (SFS) were estimated for each population using the program easySFS (https://github.com/isaacovercast/easySFS). As explained in more detail in Chapter 3, the SFS is a vector of the number of alleles observed in each frequency class (beginning with singletons, SNPs that are heterozygous in a single individual) in a population sample. The SFS is expected to reflect – and therefore provide evidence of – demographic history because changes in population size have characteristic effects on the distribution of allele frequencies. For example, a population that has recently experienced a bottleneck is expected to feature fewer rare alleles than a long-term stable population would due to chance loss of rare alleles from many sites and insufficient time for this variation to have been regenerated through mutation.

The SFS was then analysed by the program Stairway Plot 2 (Liu and Fu 2015; 2020) to reconstruct the general shape of the population's demographic history. Stairway Plot 2 also requires specified values of generation time (years), mutation rate (substitutions/site/generation), and the total number of nucleotide sites observed (including invariant sites), to scale the demographic history in terms of years and N_e.

It is important, in the context of this chapter, to understand some of the inner workings of Stairway Plot 2. It begins by estimating the single best-fitting average N_e for the full history of a population as determined by the SFS of length n, where n is the number of diploid individuals sampled for the population. This basic model is then elaborated upon several times through a genetic algorithm, where new "breakpoints" are randomly proposed at time points in the historical demographic model when N_e might have changed, and the likelihood of the new model is estimated. If the new model passes a likelihood ratio test, it is accepted, and the process continues. In its final form, a model specifies N_e at 2n-1 historical time points, with up to (but usually far fewer than) 2n-2 distinct values of N_e separated by breakpoints that were accepted over the course of the model's evolution. This whole process is repeated from the beginning for a default of 200 iterations, and all iterations are combined to give the final result of the Stairway Plot 2 run.

Previous studies have found Stairway Plot to be especially robust to differences in underlying genetic data, such as from different genome assembly strategies (e.g. Patton et al. 2019). However, this averaging over many replicates of much lower resolution gives a somewhat misleading impression of smoothness and continuity to Stairway Plots. The smoothness of the final plot does not necessarily reflect actual history, but it is still meaningful because it does reflect uncertainty about that history in the underlying replicates. For example, uncertainty in the timing of an abrupt change could be represented as a longer period of gradual change.

Comparing Stairway Plot curves

I developed a method for quantitatively comparing many Stairway Plots simultaneously, to perform clustering analyses with the aim of identifying patterns uniting or distinguishing the demographic histories of the populations in question. Although this method is designed for analysing results of Stairway Plot 2, much of the approach would be applicable to any other model-flexible method for inferring demographic history (Hecht et al. 2020), and a similar approach has been applied to results of PSMC (Hecht et al. 2018).

The program, align_stairwayplot.py, takes as input the final demographic models from each iteration of a Stairway Plot 2 analysis. The time-specific N_e values in the final model are converted into one fewer "binary slope" values, reflecting the direction of change (if any) in N_e between one time point and the next. If the final model did not infer a breakpoint between a pair

of time points, such that their inferred N_e is the same, the slope of that pair is considered to be 0. A decline in N_e produces a slope of -1, and an increase in N_e produces a slope of 1. Proceeding on the assumption that the time points were contemporaneous across each model/iteration, the "binary slope" models from each iteration are combined into a composite model reflecting the proportion of iterations in which N_e was supposed to have been increasing, decreasing, or constant at a given point in time. For example, if 74% of models had N_e increasing (slope=1) at time t, 25% left N_e constant (no breakpoint; slope=0), and 1% had N_e decreasing (slope=-1), the composite slope at time t would be (0.74*1)+(0.25*0)+(0.01*-1) = 0.74-0.01 = 0.73. This composite slope value would then be further refined by multiplying it by the log of the magnitude of the suggested change in N_e at that time interval relative to others. For example, in a Stairway Plot analysis where the average time interval saw a change (growth or decline) of N_e=100, the composite slope value of a time interval where growth of only N_e=10 took place would be multiplied by 0.5 [log(10)/log(100)].

Although it is reasonable to treat time points as being contemporaneous across iterations within a single Stairway Plot 2 run for a single population (they must at least occur in the same order and with the same average age, being based on the same genetic parameters), the timescales of the reconstructed demographic histories of other populations can differ by orders of magnitude. Therefore, to align and compare multiple demographic histories, they must all be projected onto a common set of time points. In align_stairwayplot.py, these standardized time points are user-definable, depending on the period(s) of history and types of questions that are of interest, and the range of timescales covered by the sampled populations. For each specified time point, the program uses the nearest-in-time composite slope value for each population. If one of the standardized time points is more recent or more ancient than the earliest or oldest time points in the composite slope model of a given population, then a composite slope of -9 is assigned, representing "missing data". Pairs of populations' demographic histories are then compared by taking the average of the absolute value of the difference between the arrays of their contemporaneous composite slope values. Time points with a composite slope of -9 (missing data) in either of the populations are ignored in this calculation.

The resulting matrix of pairwise differences between populations' demographic histories can then be analysed with any method one might apply to a phylogenetic distance matrix. The main recommended avenue for further analyses (and the one I used in this chapter) directed at identifying clusters of populations with distinct types of demographic histories is

multidimensional scaling (MDS) and non-parametric PERMANOVA, which can be performed using the ‘adonis’ function in the R package ‘vegan’ (Oksanen et al. 2019). MDS attempts to project the distance matrix onto two dimensions while approximately preserving the relative distance between each pair of populations. Non-parametric multivariate analysis of variance (PERMANOVA) can be used to assess the statistical significance of models hypothesising that certain groups of populations cluster separately from others. PERMANOVA works by calculating a test statistic (F) representing the ratio of distances between the means of different groups and the average distance from each population to the mean of its assigned group (Anderson 2001; Anderson et al. 2014). The statistical significance of the test statistic can then be determined by randomly shuffling group assignments (“permutations”, the origin of the method’s name) among populations and repeating the test many times on these ‘incorrect’ groupings to determine how often their resulting test statistic exceeded that of the original, ‘true’ hypothesised groups (Anderson 2001). These groups can be categorical (e.g. continent of origin), or they can be based on a continuous variable (e.g. latitude), in which case group membership is more of a weighting rather than populations being strictly defined as in or out.

While the preceding paragraphs summarise the basic approach, another key feature of align_stairwayplot.py is relative evolutionary rate (RER) realignment. Demographic history curves frequently show periods when populations’ sizes are temporarily reduced or elevated, and then return to their long-term average. Up-down-up (and vice versa) curves are often important and distinctive features of demographic histories; for example, reflecting glacial cycles. However, even slightly inaccurate assumptions about the scaling factors of mutation rate and generation time, or simply noise/error in bioinformatic pipelines (including Stairway Plot itself), can lead to clearly related demographic histories being identified as very different under strict assumptions due to these features being out of phase. In previous work, the appearance of slight differences in timing may have led to single shared demographic events being identified as distinct (e.g. Oaks et al. 2020), even though this may have been accounted for by modest error in assumed rates and/or noise in the processes of mutation, reproduction, or bioinformatic analysis. At the same time, some constraint is clearly necessary to prevent a pair of demographic history curves from simply being stretched and compressed and shifted indefinitely until they achieve a perfect match.

In align_stairwayplot.py, users are able to define a plausible range of variation (‘RERrange’) in the timing of the demographic histories inferred in their Stairway Plot analyses. For example, an

RERrange set to 2 instructs the program to use the best alignment of each demographic history curve to each other curve based on time values of one half (1/2x) to twice (2x) the values from original Stairway Plot. The RERrange should reflect the uncertainty in the scaling factor estimates used for the Stairway Plot runs, namely mutation rate, generation time, and the total number of monomorphic sites in the genomic dataset. However, while confidence intervals in estimates of mutation rate and generation time would theoretically by easy to come by, estimates of either parameter may not be available for the exact species of interest, and it is not to scientifically quantify the credence that should be given to different methods of estimation, which can produce very different results. Moreover, generation time in particular is also known to vary between populations and even over time within a single population as a result of changes in juvenile survivorship and age of first reproduction (Hadley et al. 2006). On the bioinformatic side, the number of monomorphic sites depends on the parameters used in the SNP-calling pipeline, which inevitably allows for some rate of spurious SNP calls (e.g. misaligned reads, poor-quality base calls) as well as missed SNPs (e.g. insufficient read depth or quality). While standard SNP-calling pipelines, such as Stacks, should report a reasonably accurate number of observed sites, this can be further muddled when down-projection to a smaller sample size is required to deal with a large amount of missing calls in the SNP dataset.

Seeking a non-arbitrary way to select RERrange amid these layers of uncertainty, I developed a heuristic for estimating the optimal RERrange for a given set of populations to be analysed. The process described above is repeated with RERrange increasing incrementally from 1.0 to a user-defined value (e.g. 4.0), and the distance matrix resulting from each RERrange value is subtracted from the original distance matrix. From this, the average, 75th percentile, and 90th percentile reductions in pairwise differences across population pairs are calculated for each RERrange. In the case where two similar curves are slightly out of phase at their original scaling (RER=1), a modest increase in flexibility (RERrange) should lead to a large reduction in their pairwise difference score. Therefore, the expected behaviour is that high percentile reductions in pairwise differences should rapidly increase with RERrange, and then plateau (while RERrange continues to increase) as out-of-phase curves are able to find their place. The point at which the line(s) (especially the 90th percentile line) begin to plateau can be taken as the optimal RERrange to use for the analysis, notwithstanding other arguments to justify a more conservative or liberal RERrange in a particular case. This heuristic is referred to in this chapter as an RER robustness analysis. The approach is comparable to how plateauing of the cumulative variance explained by principal components (PCs) may be used to determine the

optimal number of PCs to retain for analysis in discriminant analysis of principal components (DAPC) (Jombart et al. 2010). As RERrange increases, most of the information for the clustering comes from the relative time between growth/decline phases, rather than the absolute timing of those phases, so a collection of populations with more complex histories should form more clear and stable clusters than one with fewer distinct phases in their reconstructed histories.

The Python code and more information on the usage of align_stairwayplot.py can be found at https://github.com/lbbhecht/align_stairwayplot.git.

Demonstration analyses

In this chapter, I will use the align_stairwayplot.py program to compare demographic histories among the simulated and natural populations described in Tables 4.1 and 4.2. These are generally exploratory analyses, without clear *a priori* expectations about how the populations' histories may or may not intersect. I expect that this would be a common-use case for align_stairwayplot.py or any similar tool, required when hypothesis-testing based on taxonomic, geographic or ecological factors is not practical due to inadequate data. In these cases, I focus on identifying distinct clusters of populations/species and any distinguishing features of their demographic histories. For example, it was not possible to test whether the demographic histories of Atlantic freshwater and marine silverside fish species are different on average because I was only able to obtain adequate data for a single Atlantic Ocean-dwelling species (*O. argentinensis*; Table 4.2). It was also not practical to assess penguin species in any formal statistical framework, due to the small number of species and lack of genetic differentiation among populations (Clucas et al. 2018). However, the variety of pinniped species was minimally sufficient to potentially investigate the importance of specific taxonomic, geographic and ecological factors in their demographic histories, depending on the level of structure found among those histories.

Factors that were considered to explain the relationships among pinniped demographic histories included family (otariid or phocid), geographic coordinates of the sampled population, typical breeding substrate (land or ice), marine foraging range (coastal vs oceanic), and parental care strategy (Table 4.3). Data on typical breeding substrate came from Schulz and Bowen (2005),

and lactation duration was used as a proxy for parental care strategy, following Schulz and Bowen (2005) and Stephens et al. (2014).

Table 4.3. Factors that could relate to differentiation in pinniped demographic histories. *A latitude of 53° is used for *M. angusirostris* despite the breeding population being sampled at latitude ~38° because the higher latitude better reflects its foraging range according to Robinson et al. (2010).

Species	**Family**	**Geographic range**	**Marine range**	**Breeding substrate**	**Lactation length (days)**	**Latitude (°)**	**Longitude (°)**
O. flavescens	Otariidae	South America (Atlantic)	Coastal	Land	548	-43	-64
P. vitulina	Phocidae	Arctic	Coastal	Land	26.7	79	18
A. galapagoensis	Otariidae	South America (Pacific)	Coastal	Land	540	0	-91
E. barbatus	Phocidae	Arctic	Oceanic	Pack ice	24	79	18
M. angustirostris	Phocidae	North America (Pacific)	Oceanic	Land	25.8	53*	-123
P. hispida	Phocidae	Arctic	Oceanic	Fast ice	39	-54	-38
A. gazella	Otariidae	Antarctic	Coastal	Land	116	-43	171
A. forsteri	Otariidae	Australasia	Coastal	Land	285	30	-111
Z. californicanus	Otariidae	North America (Pacific)	Coastal	Land	330	0	-90
Z. wollebaeki	Otariidae	South America (Pacific)	Coastal	Land	–	-31	-51
A. australis	Otariidae	South America (Atlantic)	Coastal	Land	365	-77	166
L. weddellii	Phocidae	Antarctic	Oceanic	Fast ice	50.3	79	18
M. leonina	Phocidae	Antarctic	Oceanic	Land	22.9	-53	-59

Results

Simulated populations

Multiple SNP datasets derived from each of the three sets of ms simulations were analysed with Stairway Plot 2. The results were then compared using align_stairwayplot.py to test the ability of the program to correctly group demographic histories known *a priori* to be similar and distinguish them from ones that were known to be different.

When all simulations were analysed together, the RER robustness heuristic indicated that the most extreme pairwise slope differences were minimized with an RERrange factor of 2.0, with higher values making little difference (Figure 4.1). The distance matrix generated with this RER range was then subject to MDS. Three fully separate clusters were apparent, comprising the predefined simulation sets (Figure 4.2). The PERMANOVA test was highly significant ($F=50.0$, $p<0.001$) for the three-group overall model. A pairwise test between the modsim and simBr groups specifically was still significant ($F=27.8$, $p=0.02$), but only narrowly so due to the substantial variance among simBr, with the simBr3 family being closer to the average of the modsim group than that of simBr. The variability of simBr in comparison with the other simulation sets is explained by the fact that its simulated histories are based on changes in population growth rate rather than instantaneous changes in population size, resulting in more ambiguity about when demographic shifts took place and how large they were. Slight changes in growth rate though minor permutation of the parameters could bring about much larger changes in this case, thanks to controlling an exponential growth rate, than in the other simulation sets where simpler histories were controlled by instantaneous shifts in population size.

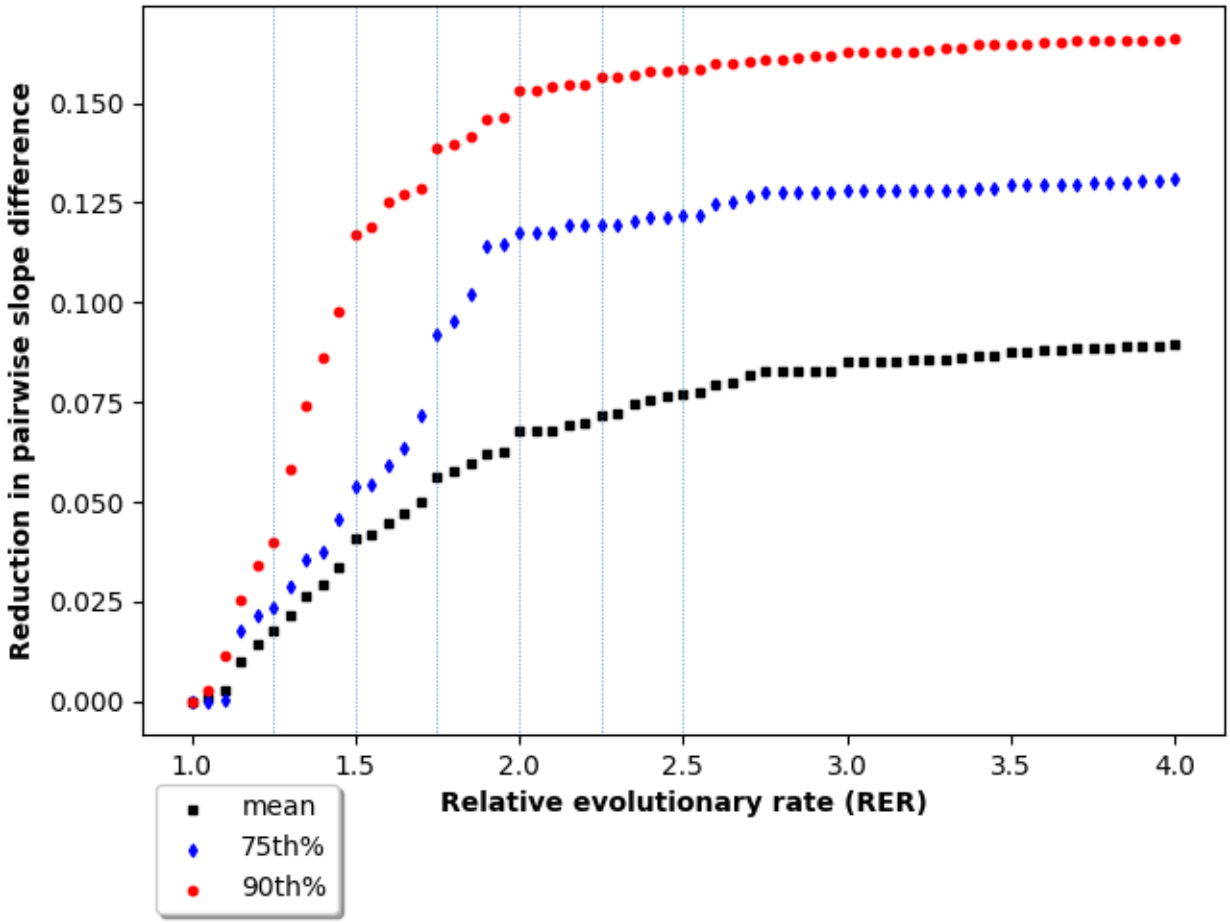

Figure 4.1. Reduction in the mean (black square), 75th percentile (blue diamond), and 90th percentile (red circle) of composite slope differences between pairs of simulated populations as RERrange is increased from 1.0 (i.e. no flexibility). The reduction plateaus around RER=2.0.

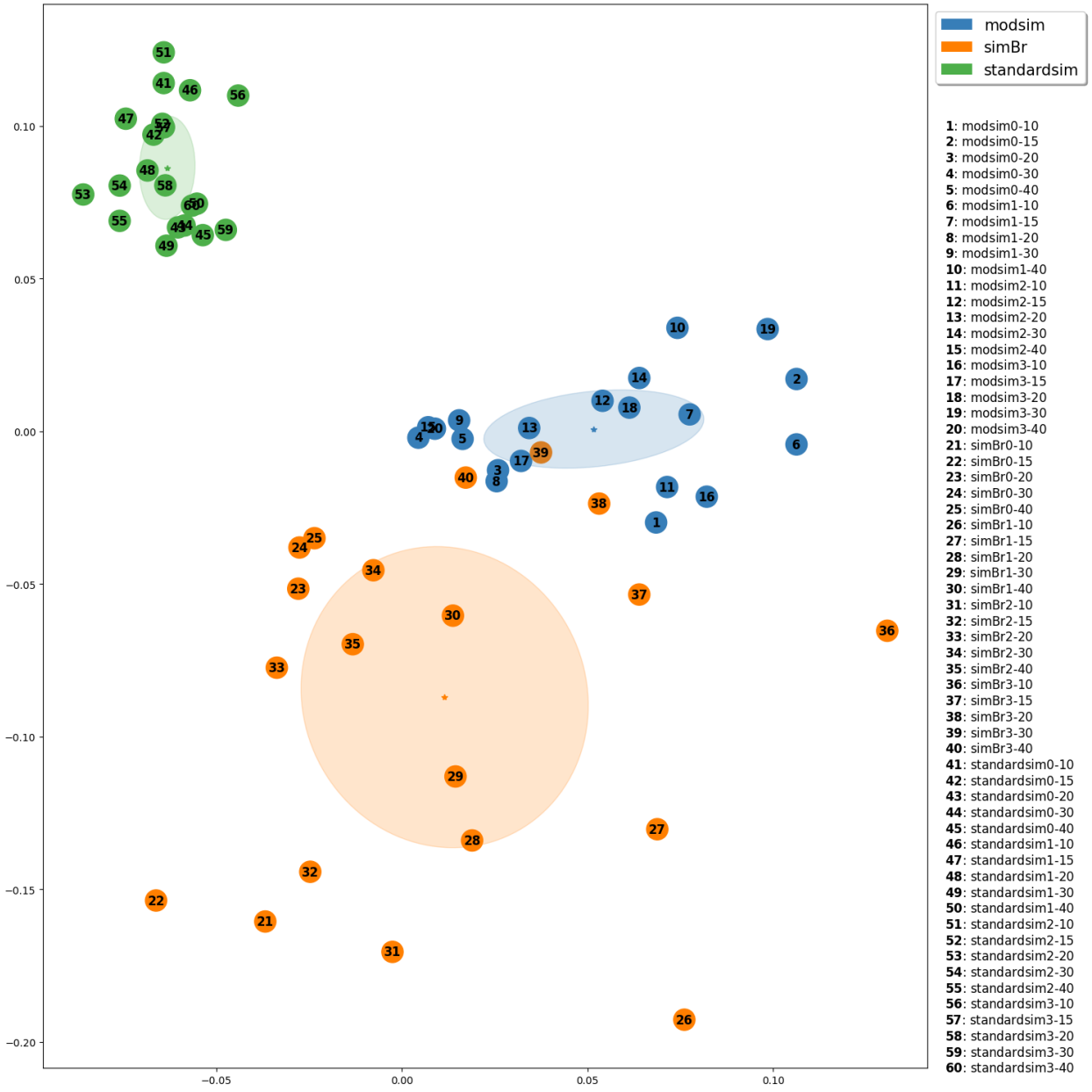

Figure 4.2. MDS plot summarising the difference among the demographic histories of populations simulated in ms (Table 4.1). The axes are unitless, and only used to visually represent the pairwise difference score between populations. Ellipsoids represent the group mean and average distance of populations from the mean on either dimension. Numbers (10-40) at the end of population names refer to the simulated sample size.

Over the sample size range tested (N=10-40), the number of individuals on which the SFS was based had no effect on the rate at which these simulated populations were correctly clustered. Average pairwise differences declined slightly with increasing sample size, both within and between groups (Figure 4.3).

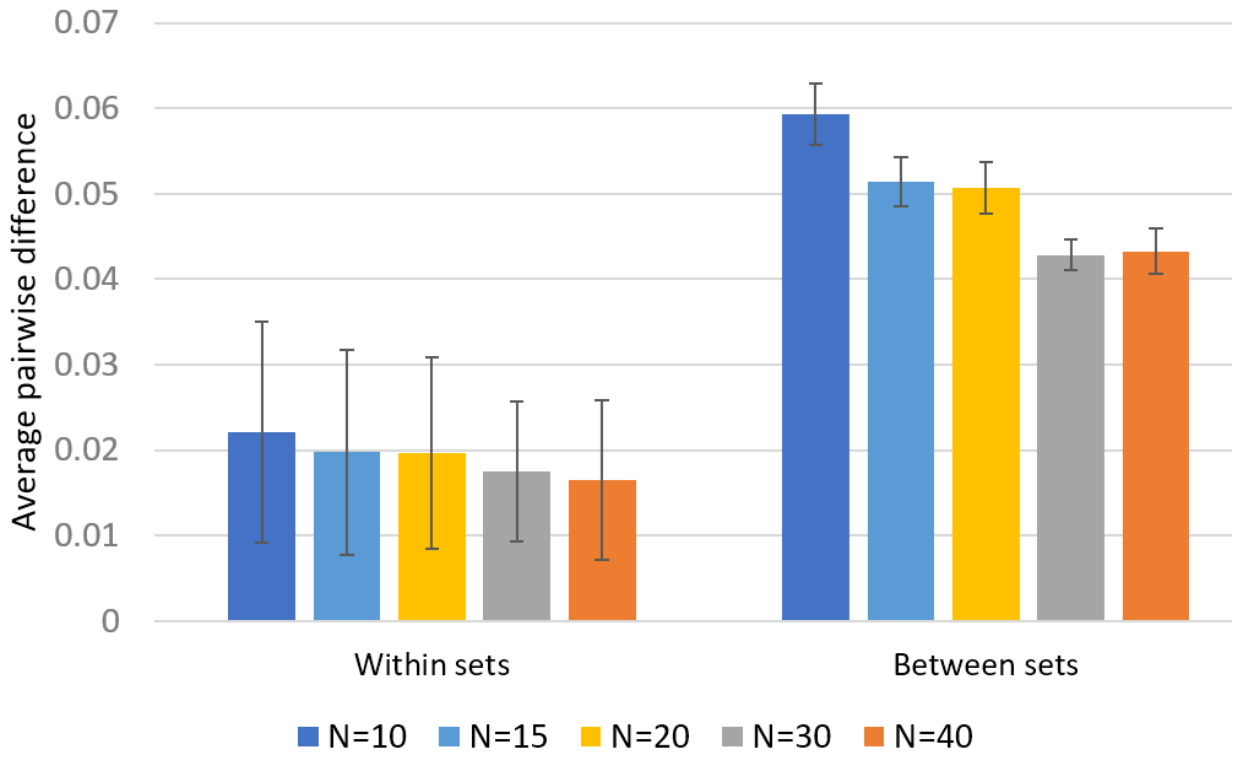

Figure 4.3. Increasing sample size from 10 to 40 was associated with only a slight decrease in average pairwise difference between simulation sets. These trends may be specific to different 'shapes' of demographic history curve, but with these simulated populations, a Stairway Plot based on 10 diploid individuals was sufficient to assign populations to their correct groups, as shown in Figure 4.2.

Natural populations

Comparing penguin species

Analysis of the Stairway Plots of penguin species at their originally assumed relative evolutionary rates (RERs) showed that the chinstrap (*Pygoscelis antarcticus*), gentoo

(*Pygoscelis papua*), king (*Aptenodytes patagonicus*) and Adélie (*Pygoscelis adélie*) penguins all had episodes of decline followed by growth between 10-30 kya (Figure 4.4). However, these episodes did not align, except in chinstrap and gentoo. The chinstrap and gentoo populations both apparently declined between ~17-25 kya, and grew between ~10-17 kya. This would fit with the timing of LGM (~18-22 kya) and likely post-glacial expansion. However, the king and Adélie penguin analyses indicated different timings. The king penguins apparently declined between ~25-35 kya and grew between ~17-25 kya. This would imply that the king penguins proliferated during the LGM, at the same time as the chinstraps and gentoos were declining. The Adélie penguins apparently declined between ~30-45 kya and grew between ~25-30 kya, both episodes occurring prior to the LGM. The emperor penguins (*Aptenodytes forsteri*) apparently declined weakly between ~10-18 and ~18-27 kya, suggesting a different and overall less dynamic demographic history than the other four species. In particular, it is less clear whether emperor penguin numbers were affected by the LGM or post-glacial warming.

Allowing for flexibility, or prior uncertainty, in RER to a factor 1.5 is enough to eliminate nearly all disagreement in the composite slope values of these penguin species that is based on potential misalignment of their demographic history curves (i.e. the absolute timing of events), as opposed to differences in curve shape (i.e. the occurrence and relative timing of events) (Figure 4.5).

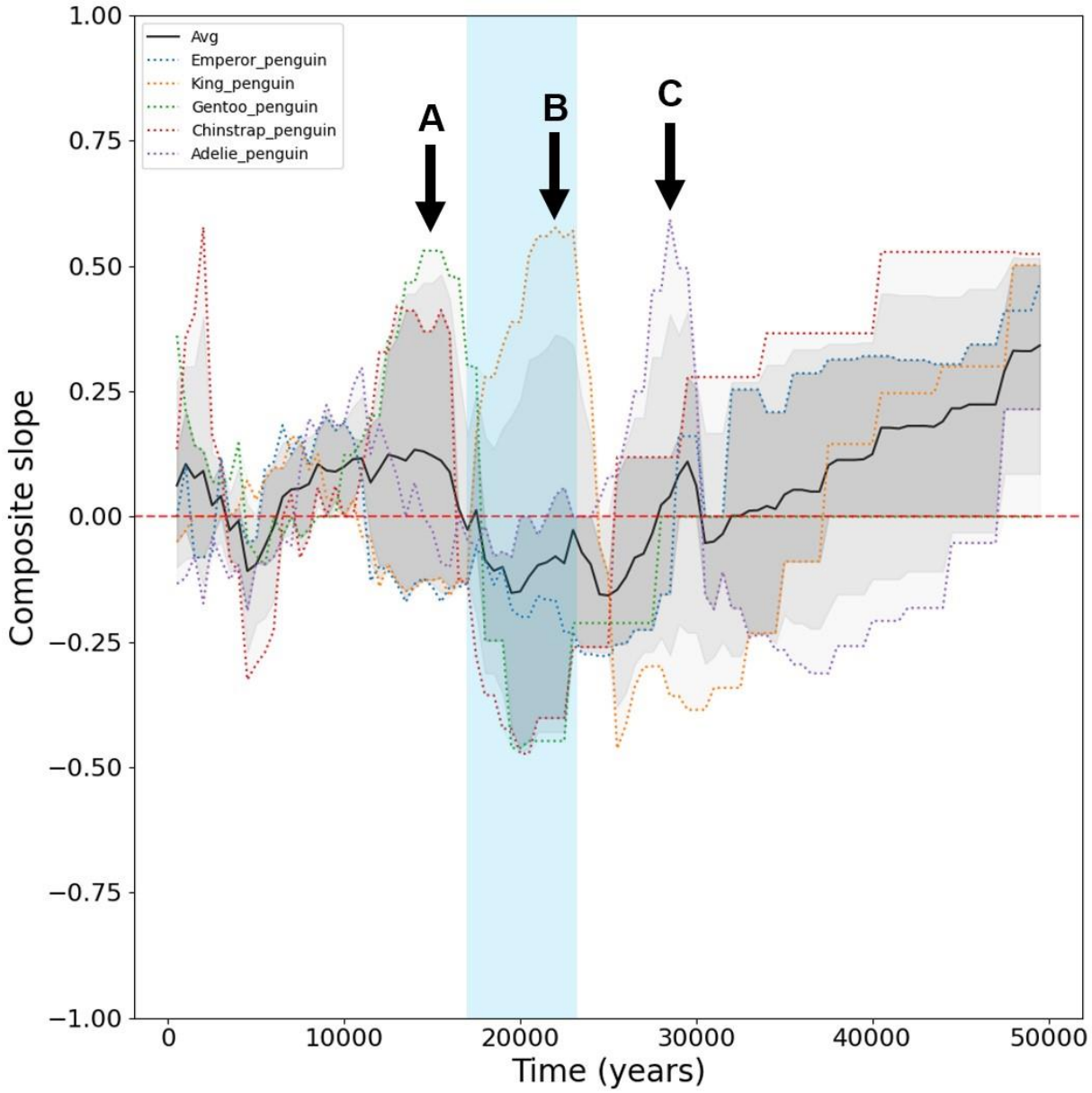

Figure 4.4. Time-specific composite slopes of penguin species at their original assumed evolutionary rates (i.e. generation time, mutation rate, genotyping rate). The black solid line traces the mean composite slope value of all five penguin species considered, while the shaded areas represent the interquartile range, interdecile range, and total range (i.e. maximum and minimum), respectively, in descending intensity of shading. The specific history of each species is shown by uniquely coloured dotted lines (but see Figures 4.6-4.7 for a less obstructed view of each). The approximate timing of the LGM is identified by a light blue bar. Lettered arrows identify distinct growth peaks represented at three different times across four species: A) Growth in the chinstrap and gentoo penguins, ~10-17 kya. B) Growth in the king penguins, ~17-25 kya. C) Growth in the Adélie penguins, ~25-30 kya.

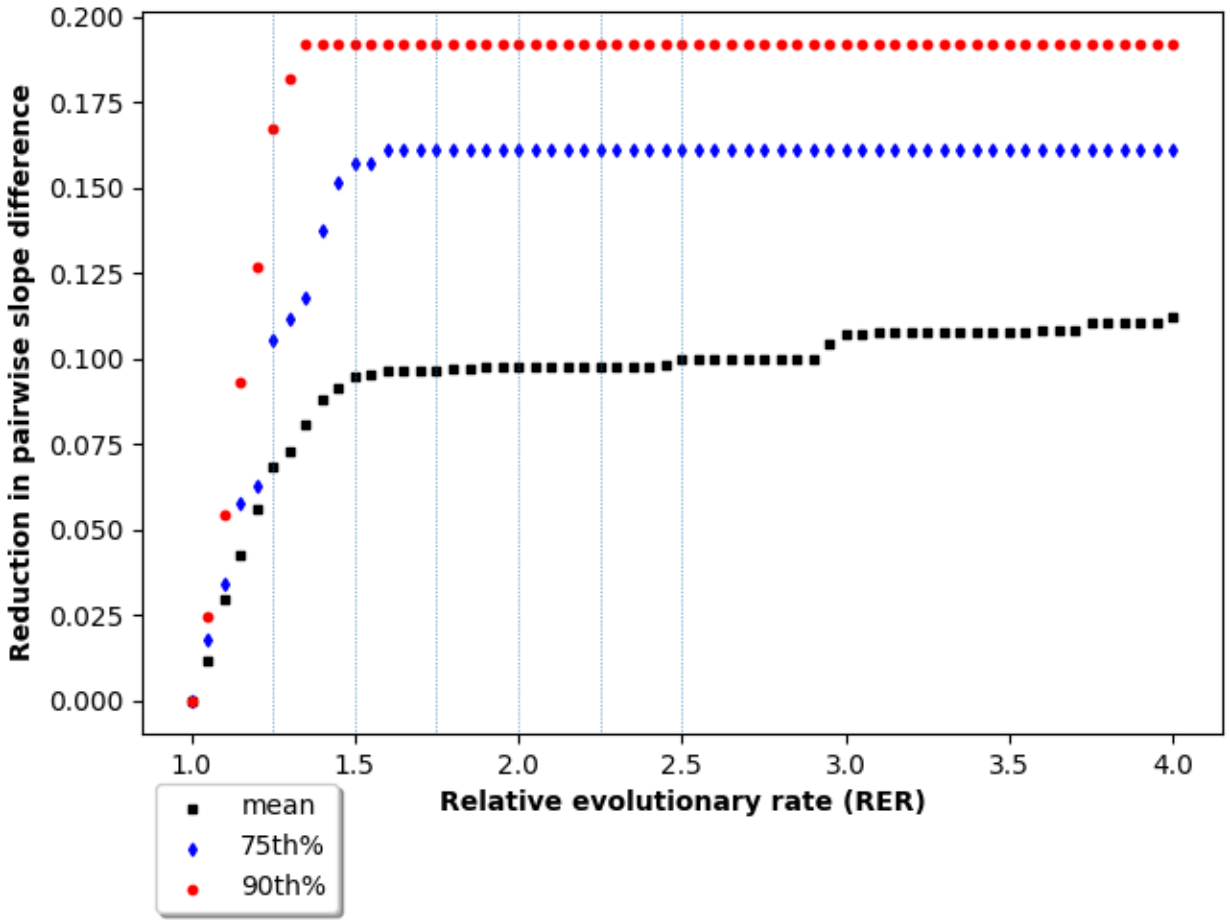

Figure 4.5. Reduction in the mean (black square), 75th percentile (blue diamond), and 90th percentile (red circle) of composite slope differences between pairs of penguin species as flexibility in RER is increased from 1.0 (i.e. no flexibility). The reduction plateaus around RER=1.5.

With this flexibility, the demographic histories of all five species are optimally aligned to the king penguin and the putative timings of its growth and decline (Figure 4.6). These timings are between those of the Adélie and chinstrap/gentoo, so they require less RER flexibility than aligning to Adélie or chinstrap/gentoo (Figure 4.4). The king penguin demographic history also shows the lowest average pairwise slope difference from the other species with RER flexibility of 1.5 (Table 4.4) or higher, albeit by a narrow margin. On the other hand, the gentoo and chinstrap penguins' demographic history curves were already naturally quite well aligned to each other even without RER adjustment. However, aligning all five species to chinstrap or gentoo would require positing a higher level of flexibility/error in RER. The fit of other species to

the chinstrap penguin is shown in Figure 4.7. The arguments for and against each fit will be considered in more detail in the Discussion section.

Table 4.4. Pairwise slope difference between the demographic histories of penguin species under an RERrange of 1.5.

	Adélie	Chinstrap	Emperor	Gentoo	King	**Average**
Adélie	0.00	0.24	0.13	0.19	0.11	**0.17**
Chinstrap	0.24	0.00	0.17	0.22	0.14	**0.19**
Emperor	0.13	0.17	0.00	0.17	0.16	**0.16**
Gentoo	0.19	0.22	0.17	0.00	0.17	**0.19**
King	0.11	0.14	0.16	0.17	0.00	**0.14**

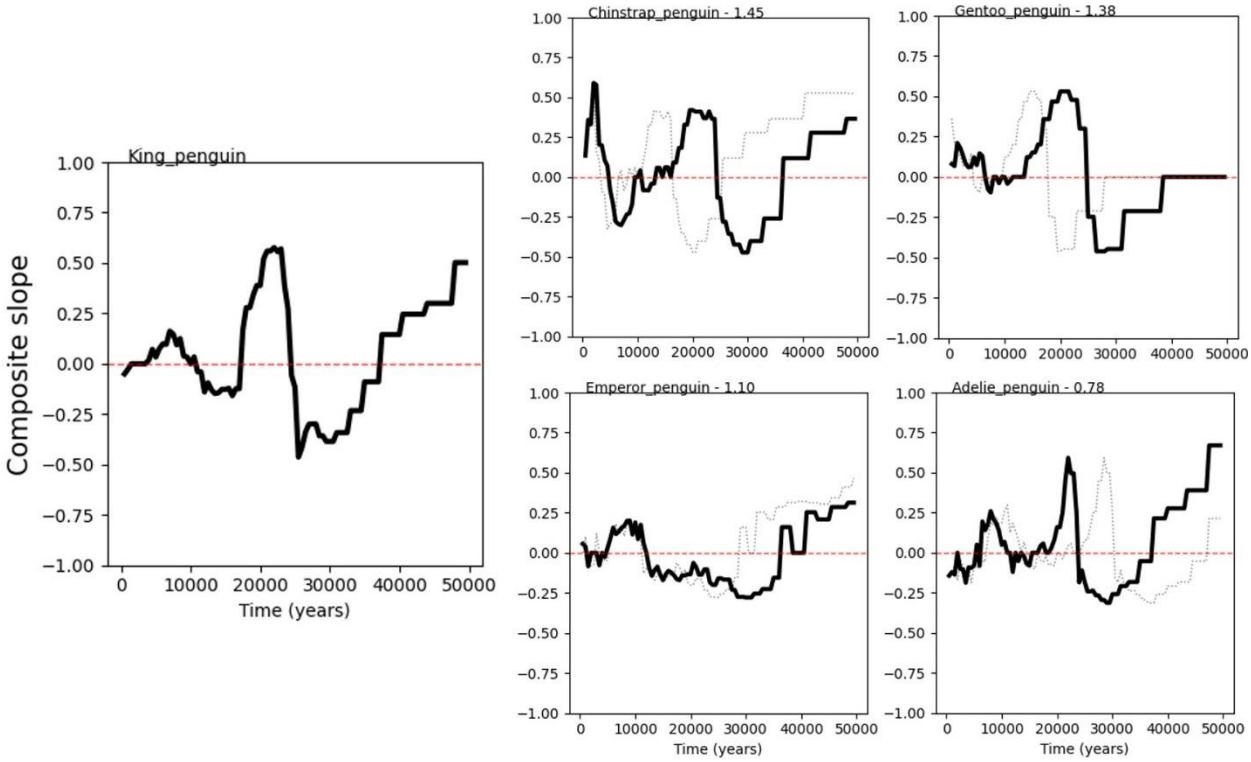

Figure 4.6. The fit of penguin species' demographic histories to the king penguin, under RER rescaling. Solid lines show the time-specific composite slope values of each species at their optimal fit to king penguin, based on the RER factors annotating the top of each plot after the species name. The dotted lines show the original timings of the species' histories, which were multiplied by the RER factor to yield the solid lines.

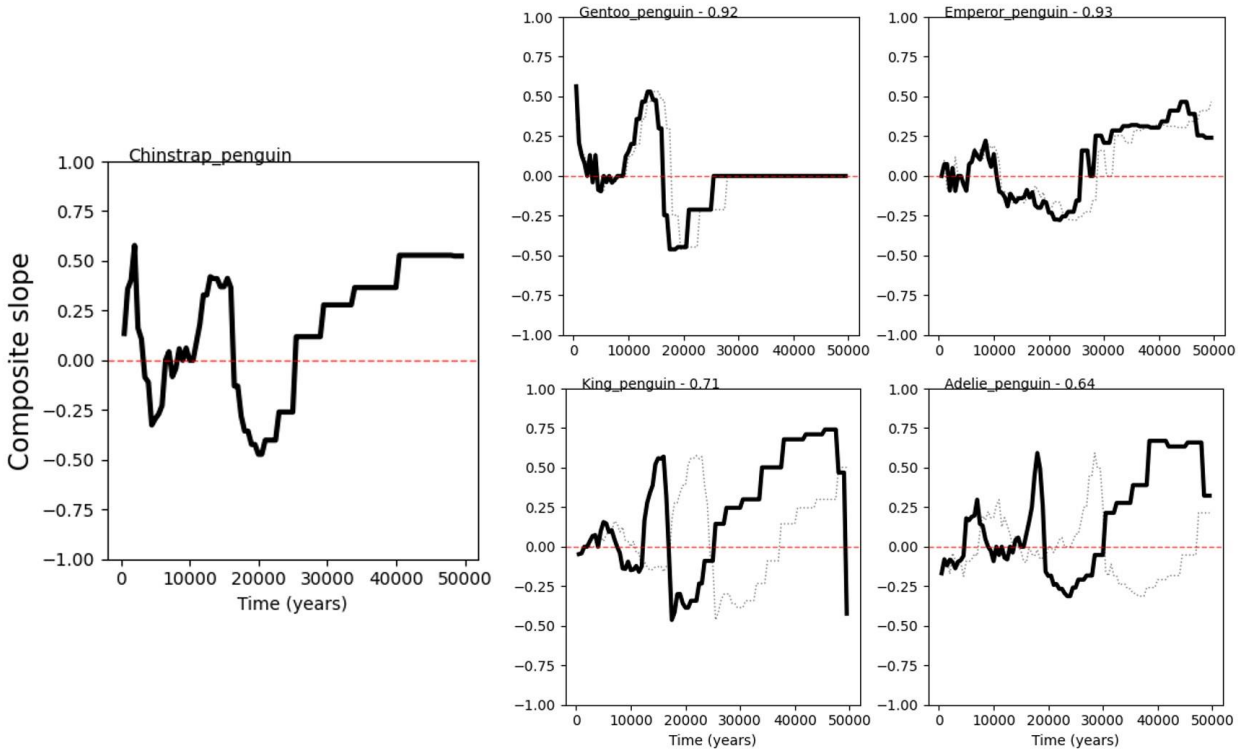

Figure 4.7. The fit of penguin species' demographic histories to the chinstrap penguin, under RER rescaling. Solid lines show the time-specific composite slope values of each species at their optimal fit to king penguin, based on the RER factors annotating the top of each plot after the species name. The dotted lines show the original timings of the species' histories, which were multiplied by the RER factor to yield the solid lines.

Comparing penguin populations

Within species, penguin populations showed varying levels of consistency amongst themselves and with the Stairway Plot reconstructions based on their whole species. Chinstrap penguin populations were the most consistent in both respects, with all three represented populations mirroring the species-level history with population decline peaking ~20 kya and population growth peaking ~10 kya (Figure 4.8). The two Adélie populations, representing east and west Antarctica, are highly consistent with each other from ~15 kya to the present, but prior to that point they show opposite patterns during critical periods. The eastern population grows in the period of ~15-20 kya while the western population remains static or possible declining, and conversely the western population was apparently growing prior to ~30 kya while the eastern population was declining (Figure 4.9). The mean of the composite slopes of the three gentoo penguin populations was consistent with their whole-species history, but there was significant

disagreement among populations, particularly prior to 10 kya, when the Kerguelen population was apparently growing while the Falklands population declined (Figure 4.10). The emperor penguin populations were highly consistent amongst themselves, indicating mainly growth until ~17 kya, followed by decline peaking ~5 kya and followed by recent growth (Figure 4.11). This is qualitatively similar to the history reconstructed for the whole species, but with the timeline approximately halved, as in the whole-species reconstruction, growth transitions to decline at ~30 kya and recent growth begins ~9 kya. Two out of three king penguin populations (South Georgia and Macquarie) were largely consistent with the whole-species reconstruction, showing decline up to ~25 kya, followed by growth peaking ~22 kya, followed again by decline from ~9 kya to the present (Figure 4.12). The period of this growth phase is longer than in the whole-species reconstruction, and there is no recent growth/stasis, which is also seen in the whole-species reconstruction (Figure 4.6). These discrepancies may be due to direct conflict between the populations' apparent histories, as the Falklands-Crozet population was apparently growing until ~25 kya, followed by decline peaking ~22 kya, followed by another growth phase peaking ~10 kya, and subsequent decline until the present. The Falklands-Crozet population, therefore, matches the demographic history of the chinstrap penguins (Figure 4.7; 4.8) and presents the mirror image of the South Georgia and Macquarie king penguin populations up to the Holocene.

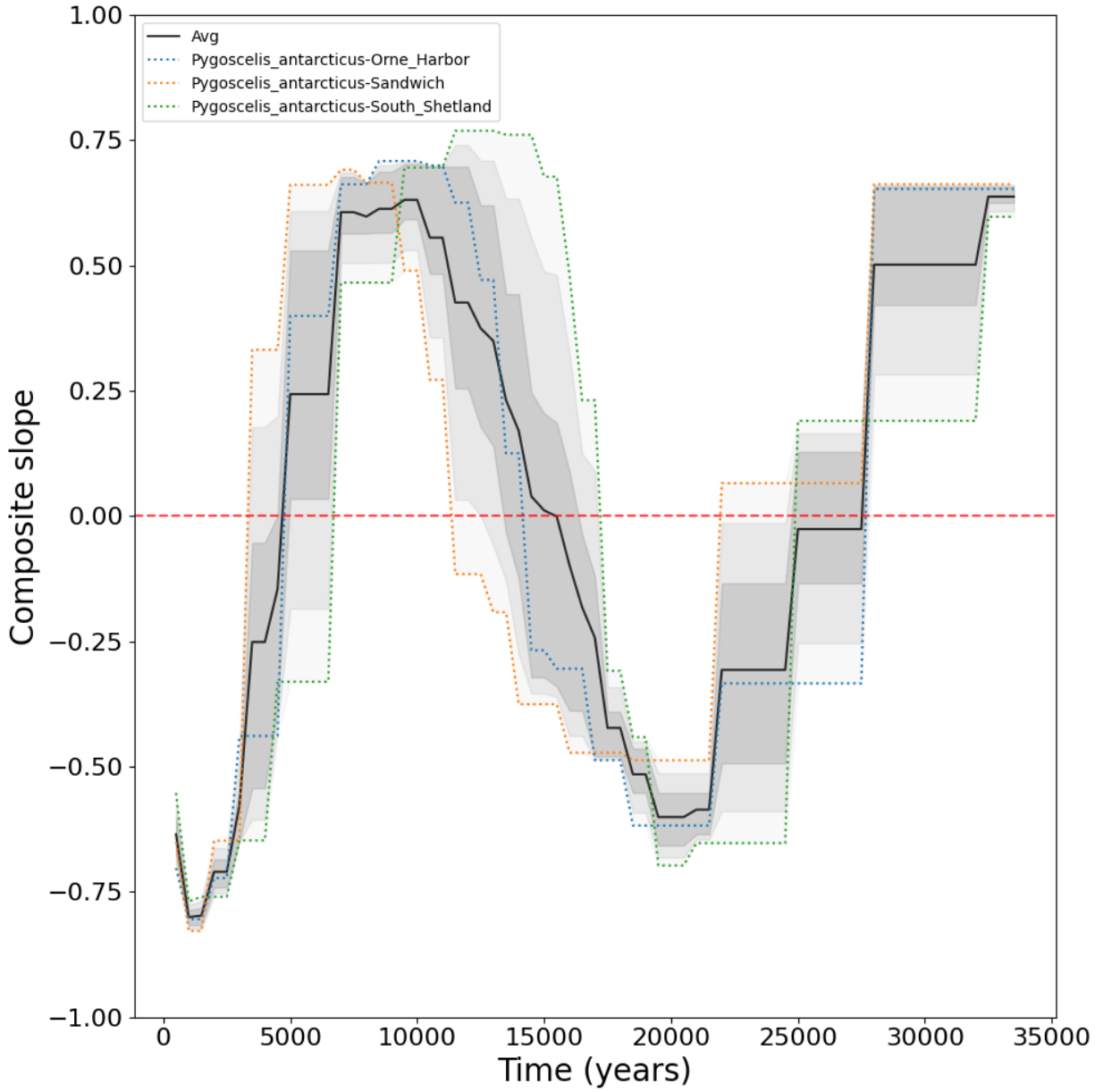

Figure 4.8. Time-specific composite slopes of chinstrap penguin populations at their original assumed evolutionary rates (i.e. RER=1). The black line traces the mean composite slope value of all populations considered, while the shaded areas represent the interquartile range, interdecile range, and total range (i.e. maximum and minimum), respectively, in descending intensity of shading. The specific history of each population is shown by uniquely coloured dotted lines. All chinstrap penguin populations decline around ~20 kya and grow ~10 kya.

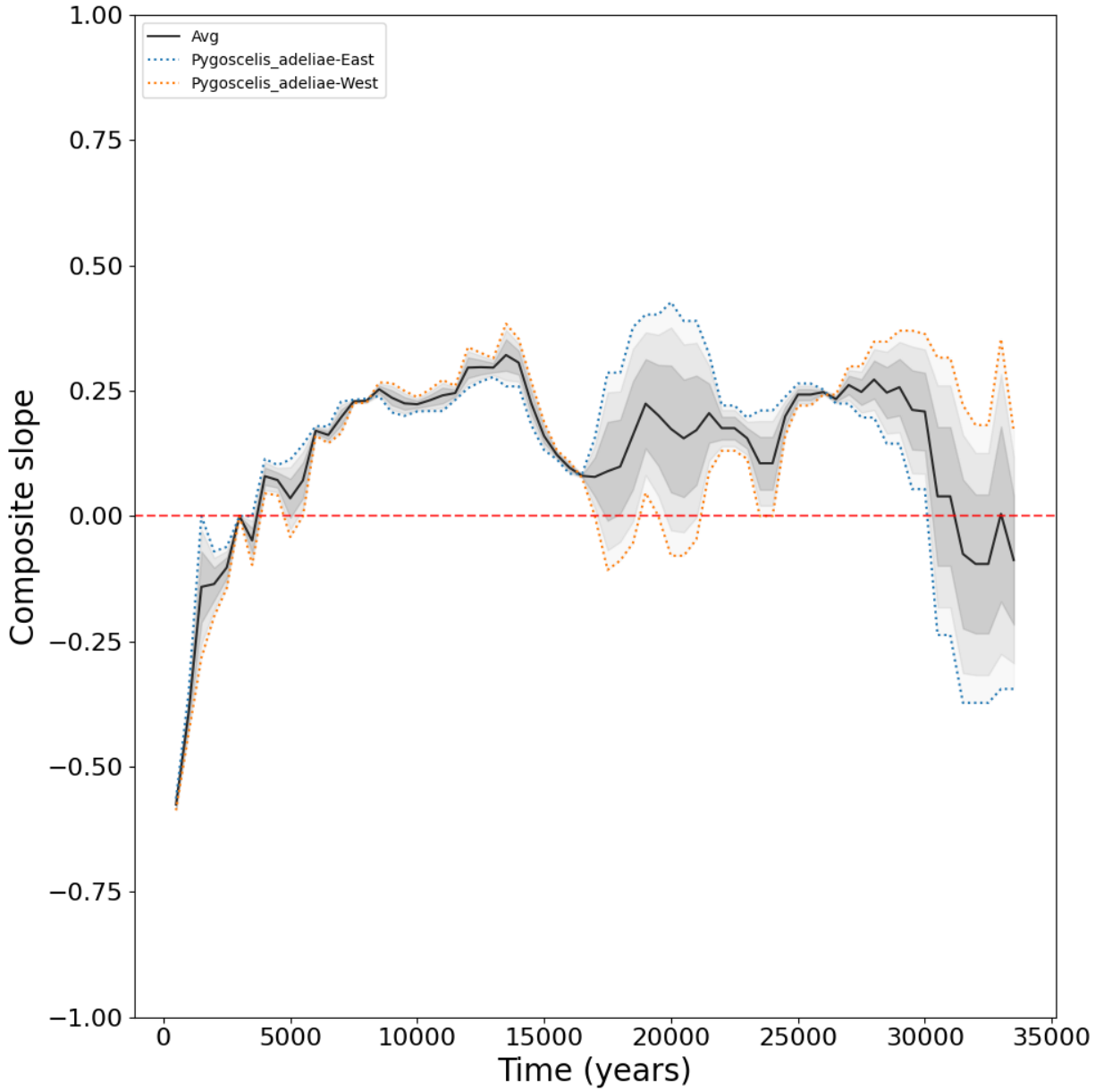

Figure 4.9. Time-specific composite slopes of Adélie penguin populations at their original assumed evolutionary rates (i.e. RER=1). The black line traces the mean composite slope value of all populations considered, while the shaded areas represent the interquartile range, interdecile range, and total range (i.e. maximum and minimum), respectively, in descending intensity of shading. The specific history of each population is shown by uniquely coloured dotted lines. The histories of the two Adélie populations are extremely similar after ~15 kya, but are partially inverted prior to that point.

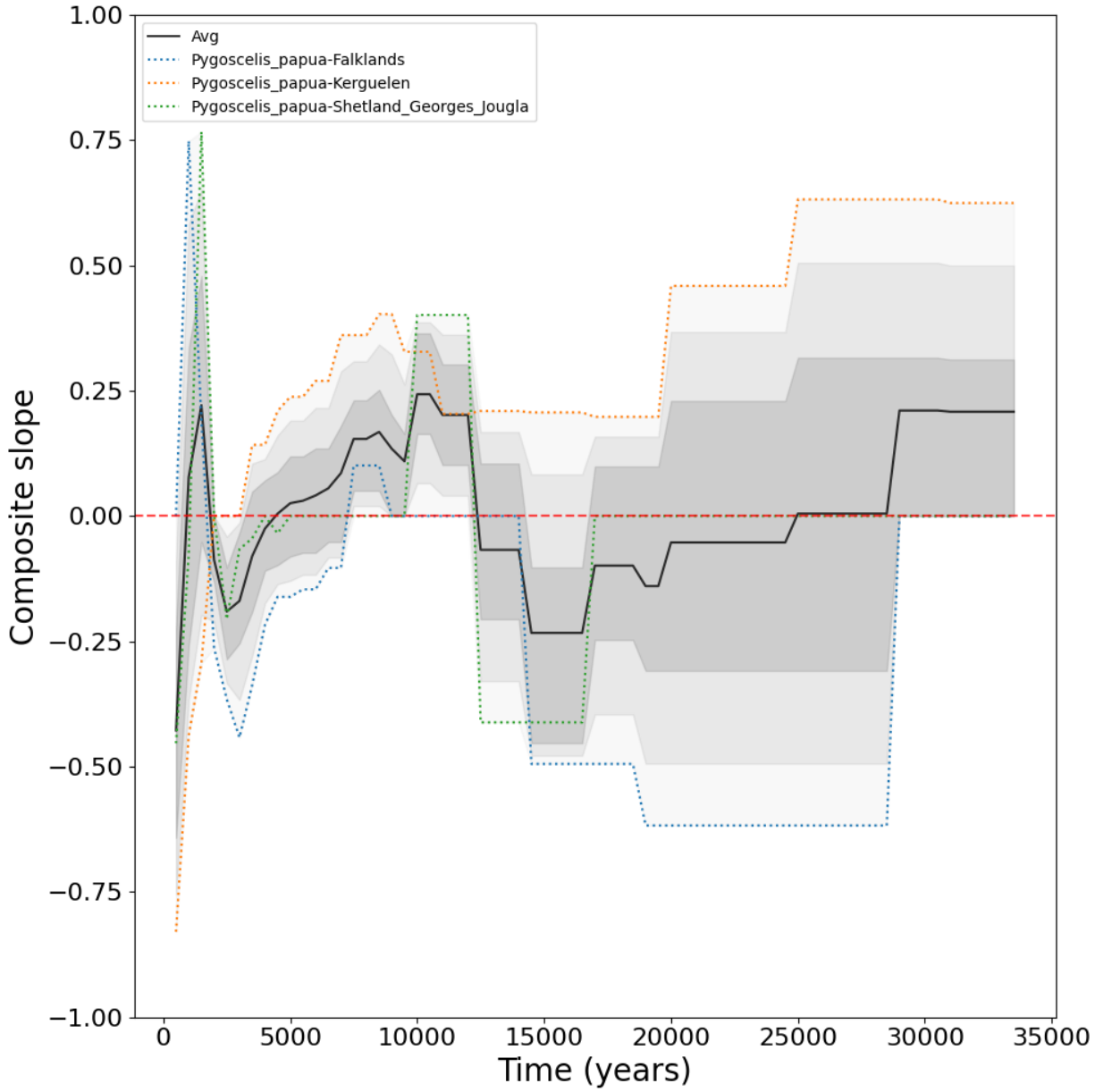

Figure 4.10. Time-specific composite slopes of gentoo penguin populations at their original assumed evolutionary rates (i.e. RER=1). The black line traces the mean composite slope value of all populations considered, while the shaded areas represent the interquartile range, interdecile range, and total range (i.e. maximum and minimum), respectively, in descending intensity of shading. The specific history of each population is shown by uniquely coloured dotted lines. Their histories appear highly consistent beyond ~12 kya, but prior to that time the three exhibit large differences ranging from growth to decline.

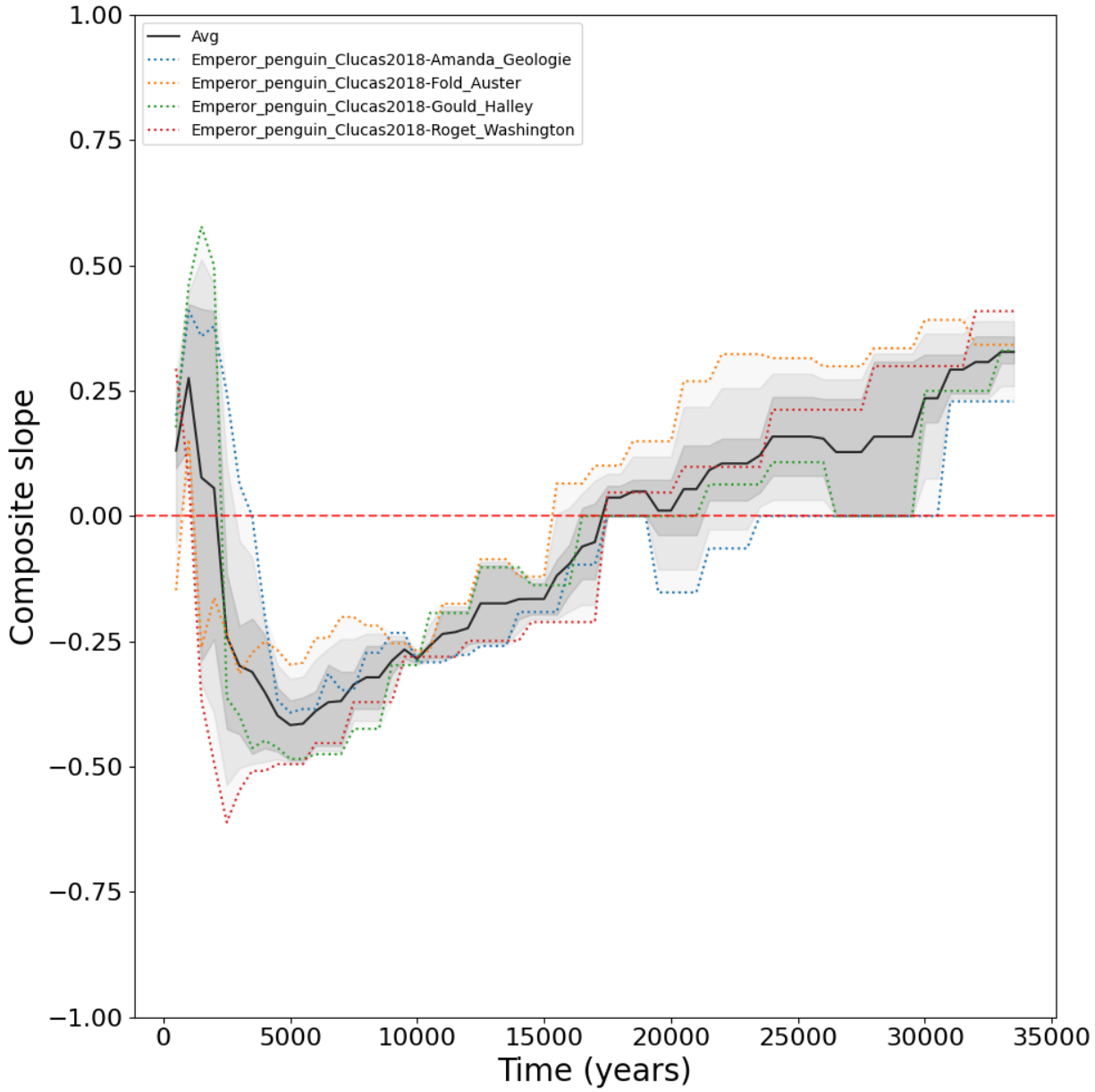

Figure 4.11. Time-specific composite slopes of emperor penguin populations at their original assumed evolutionary rates (i.e. RER=1). The black line traces the mean composite slope value of all populations considered, while the shaded areas represent the interquartile range, interdecile range, and total range (i.e. maximum and minimum), respectively, in descending intensity of shading. The specific history of each population is shown by uniquely coloured dotted lines. The trends across all four populations are highly consistent

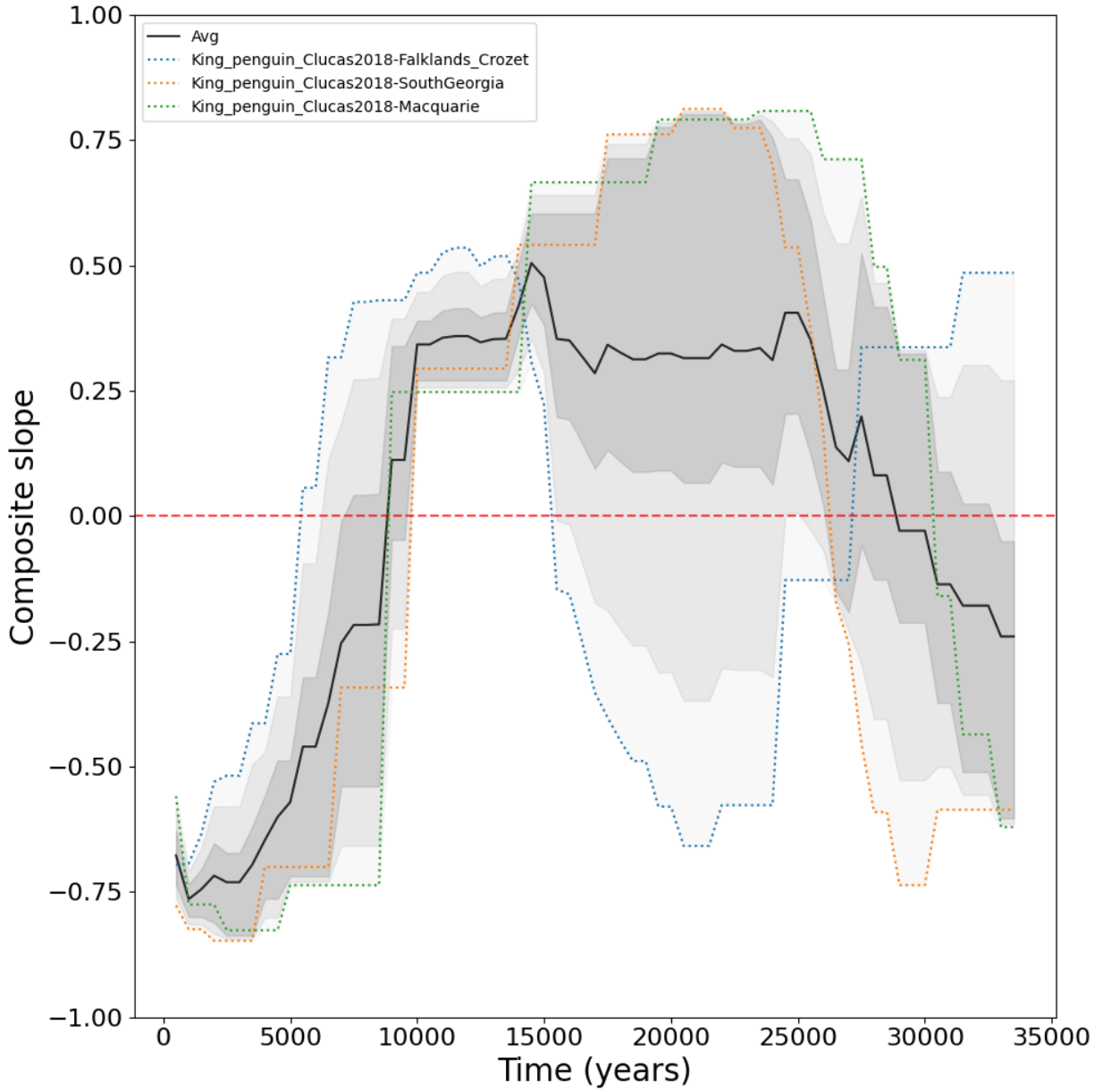

Figure 4.12. Time-specific composite slopes of king penguin populations at their original assumed evolutionary rates (i.e. RER=1). The black line traces the mean composite slope value of all populations considered, while the shaded areas represent the interquartile range, interdecile range, and total range (i.e. maximum and minimum), respectively, in descending intensity of shading. The specific history of each population is shown by uniquely coloured dotted lines. The Falklands-Crozet population exhibited opposite behaviour to the others until the Holocene, during which all three populations have apparently declined.

When the distance matrix based on pairwise comparisons of penguin populations' composite slope values is visualised via MDS, the chinstrap, emperor, and Adélie populations form clearly coherent clusters based on their similar demographic histories (Figure 4.13). The gentoo penguin populations are more disparate, with the Kerguelen population, in particular, being more similar to certain populations from other species, particular Adélie. The king penguin Macquarie and South Georgia populations clearly cluster together, but the Falklands-Crozet population clusters with the three chinstrap penguin populations on the opposite side of the plot, more distant than the gentoo, emperor and Adélie clusters. The trends in the Adélie, emperor and gentoo penguins were more subtle and/or less consistent, leading to the intermediate position of those species in the plot. On the other hand, as seen in figures 4.8 and 4.12, the apparent demographic trends of these two king penguin populations prior to the Holocene were almost precisely opposite those of the chinstrap penguins and the Falklands-Crozet population of king penguin.

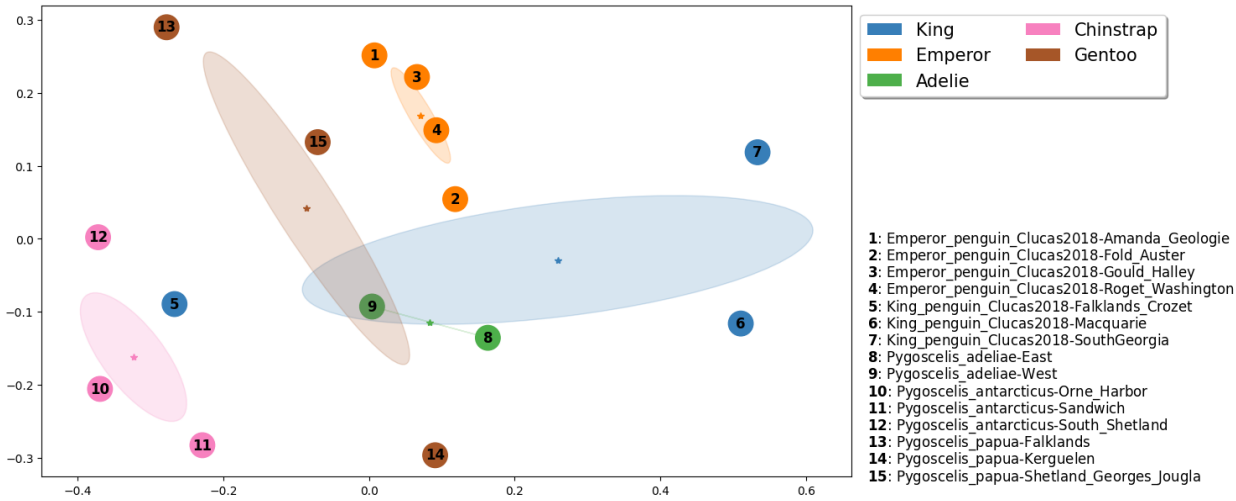

Figure 4.13. MDS plot comparing penguin populations grouped by species, with their original assumed scaling (i.e. RER=1.0). Three groups are apparent: chinstraps and one king penguin population in the lower left, the other two king penguin populations on the right, and the rest of the penguins in the middle displaying intermediate or completely distinct demographic histories (Figures 4.8-4.12). According to the PERMANOVA, the species groupings were overall not significant (F=3.89; p=0.07). Pairwise separations between the emperor penguin populations and Adélie (F=27.3; p=0.005), chinstrap (F=49.9, p=0.007), and gentoo (F=7.31; p=0.03) were significant; all other species comparisons were non-significant.

To investigate the scope of possible misalignment between king and chinstrap penguin demographic histories due to natural variation in or incorrect assumptions about rates, the same robustness test applied to whole penguin species in Figure 4.5 was used. This test indicated that the reduction in pairwise slope difference with increasing RERrange began to stabilise at a factor of ~1.75 (Figure 4.14). Allowing an RERrange of 1.75 resolved clearer differences among the penguin species clusters (Figure 4.15). There was little change in the position of emperor, gentoo or Adélie populations, except to slightly emphasise the affinity of the Kerguelen gentoo population for the Adélies, the similarities of which were subtle but recognisable in their time-specific composite slopes (Adélie: Figure 4.9; gentoo: Figure 4.10). However, the flexibility in RER allowed the king and chinstrap populations to all cluster together, implying that the shapes of their demographic histories are extremely similar, even though their apparent timing (based on the original assumptions, i.e. RER=1) was different.

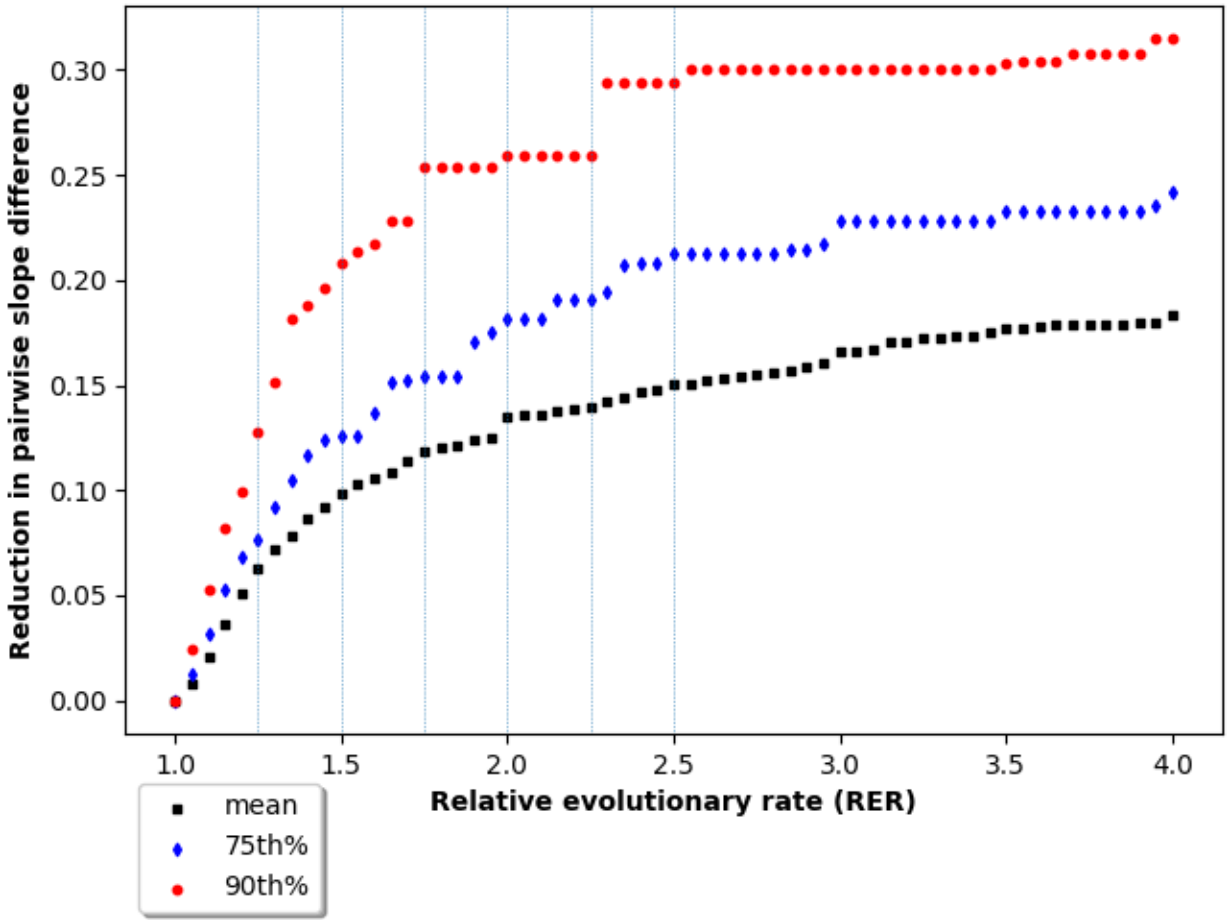

Figure 4.14. Reduction in the mean (black square), 75th percentile (blue diamond), and 90th percentile (red circle) of composite slope differences between pairs of penguin populations as flexibility in RER is increased from 1.0 (i.e. no flexibility). The reduction begins to plateau around RER=1.75.

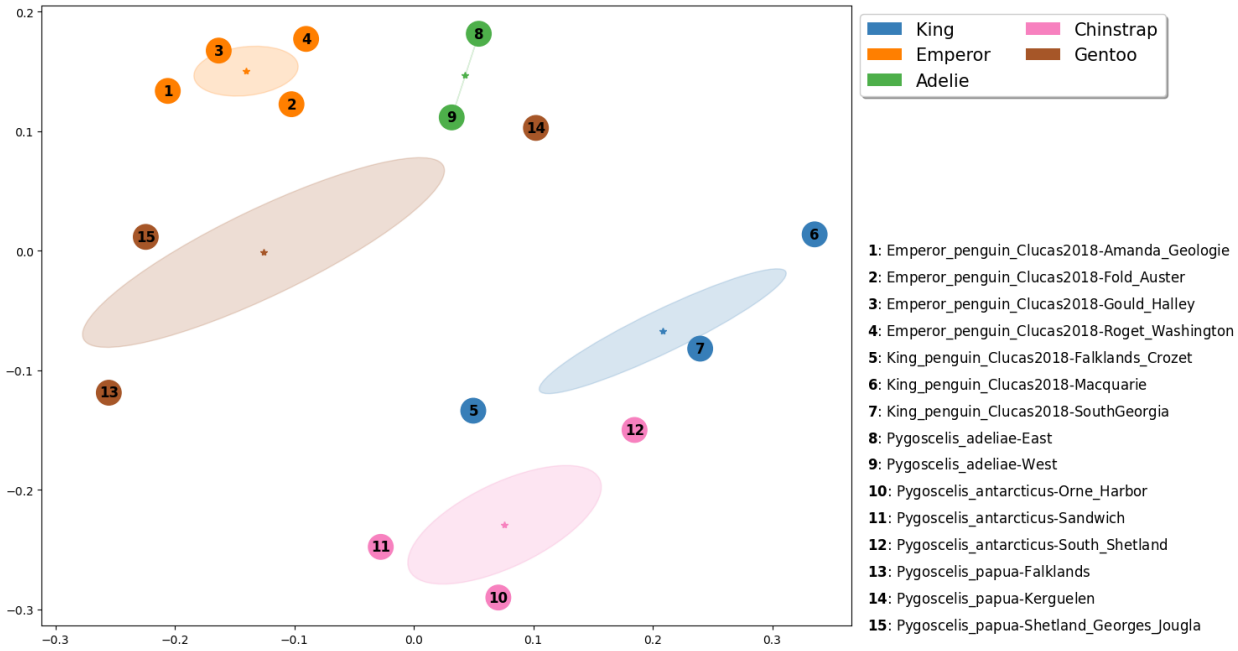

Figure 4.15. MDS plot comparing penguin populations grouped by species, with an RERrange factor of 1.75. Two main groups are apparent: the king and chinstrap populations in the lower right, and the emperor, Adélie, and gentoo populations in the upper left. According to the PERMANOVA, the overall grouping of populations by species was, with this newly permitted rescaling, highly significant (F=12.13; p=0.001). Only the distinct clustering of emperor penguins and king (F=32.0, p=0.03) and chinstrap (F=50.0, p=0.03) populations was significant; other species pairs were not statistically differentiable.

Comparing pinniped populations

Most pinniped species were only represented by a single population (Table 4.2). However, three species – *A. forsteri*, *Z. californianus*, and *Z. wollebaeki* – were represented by multiple populations, and previous studies had indicated recent genetic differentiation between some of their populations. Therefore, the consistency of the demographic histories of these pinniped populations was assessed both for scientific interest and to assess whether it would be reasonable to pool them for subsequent analysis as a single species. A major motivation for this was that some of these individual populations were represented by as few as 6 individuals (Table 4.2).

Pairwise differences between the populations began to stabilize (although continuing to decrease) at an RERrange factor of ~2.25 (Figure 4.16), so this level of flexibility was used to assess clustering of the populations with MDS (Figure 4.17).

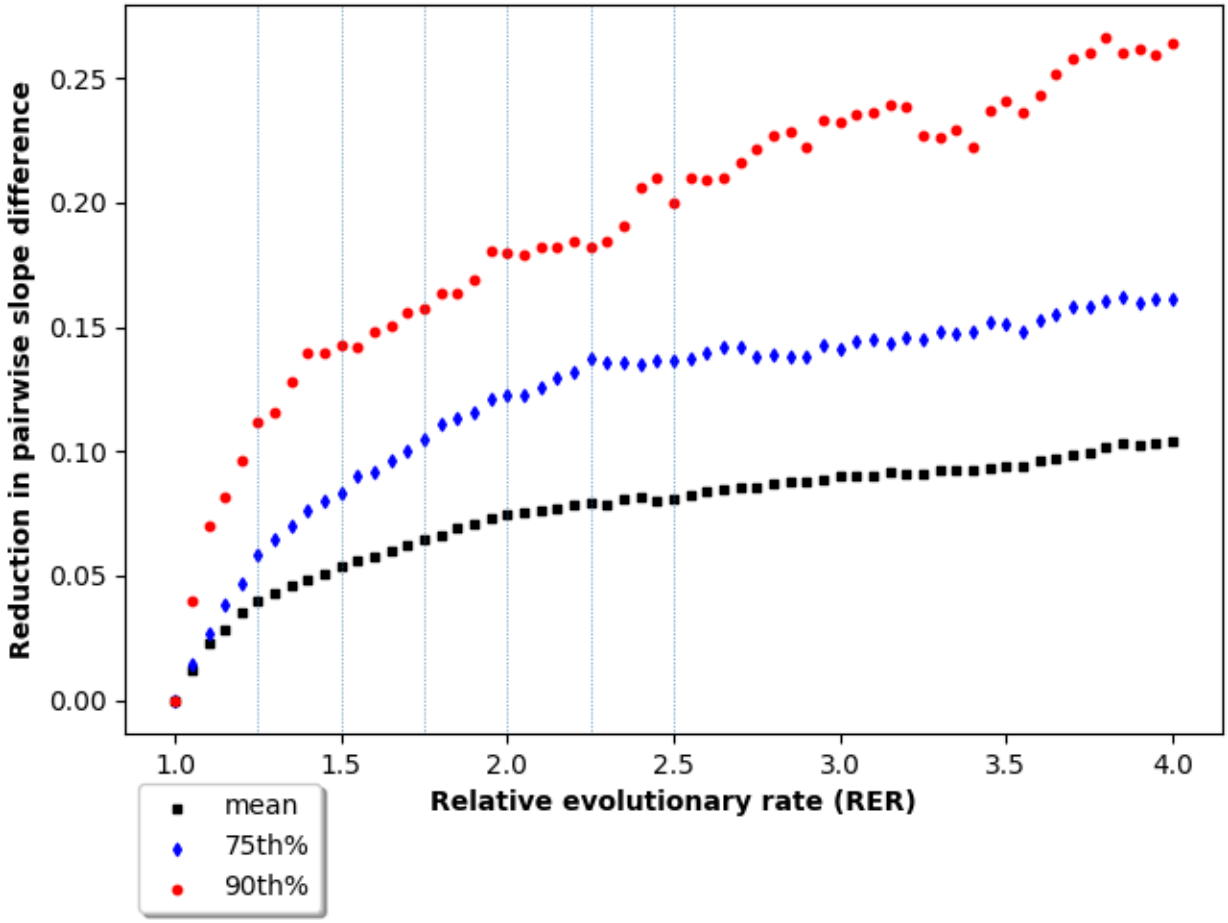

Figure 4.16. Reduction in the mean (black square), 75th percentile (blue diamond), and 90th percentile (red circle) of composite slope differences between pairs of pinniped populations of *A. fosteri*, *Z. californicanus*, and *Z. wollebaeki* as flexibility in RER is increased from 1.0 (i.e. no flexibility). The reduction in 90th-percentile differences slows slightly at an RER range of ~1.5, but continues to increase almost linearly. However, the 75th-percentile differences appear to stabilize around 2.25.

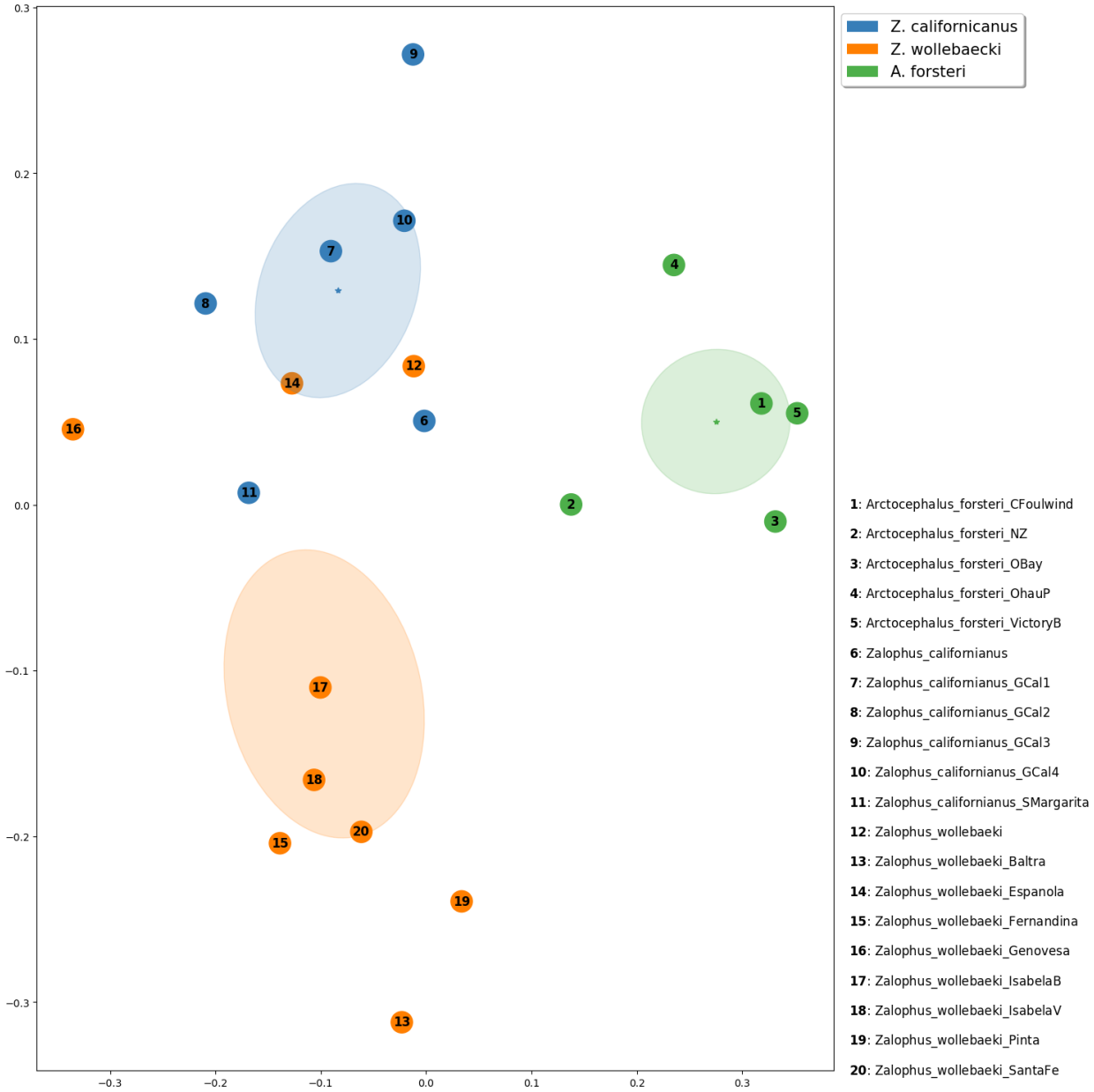

Figure 4.17. MDS plot comparing pinniped populations grouped by species, with an RERrange factor of 2.25. Most populations clearly clustered according to species (F=14.6, p<0.001). Populations #2, 6, and 12 were formed by pooling all the individuals from the other populations of their respective species.

MDS clustering and PERMANOVA indicated that, on average, populations of the same species were more similar to each other than to populations of other species. The basis for this can be seen in the distribution of their composite slopes. Based on their original scaling (i.e. RER=1),

all the *A. forsteri* populations represented here grew prior to ~50 kya and have evidently declined since then (Figure 4.18). During the last ~100,000 years, most *Z. californianus* populations appear to have been on relatively consistent growth trajectories, but with 2-3 periods of peak growth centred on ~70 kya, ~30 kya, and ~20 kya (Figure 4.19). Most *Z. wollebaeki* populations grew between ~100-175 kya, declined ~50-100 kya, grew again between ~10-50 kya, and finally declined again over the last ~10 kya (Figure 4.20). The precise timings of these episodes differ in the Stairway Plots of each population; for example, the most recent growth phase of the Espanola and Genovesa populations appears to be centred ~18 kya, while it appears to have been closer to ~35 kya in the Baltra population (with original RER scaling).

These results overall suggest that the histories of the populations are consistent enough to treat them as a single species. However, a potential cause for caution is that the whole-species (pooled) history of each of these species was quantitatively more similar to the whole-species histories of the other species than to the average population-level history of its own species (Figure 4.17), even though they qualitatively match their conspecific populations (Figures 4.18-4.20). This may be an artefact of differences in sample size; specifically, larger sample size biasing the Stairway Plot towards lower composite slope values. In each case (Figures 4.18-4.20), the absolute value of the mean composite slope value of the whole-species reconstruction was lower than for the other populations (i.e. the curve was flatter).

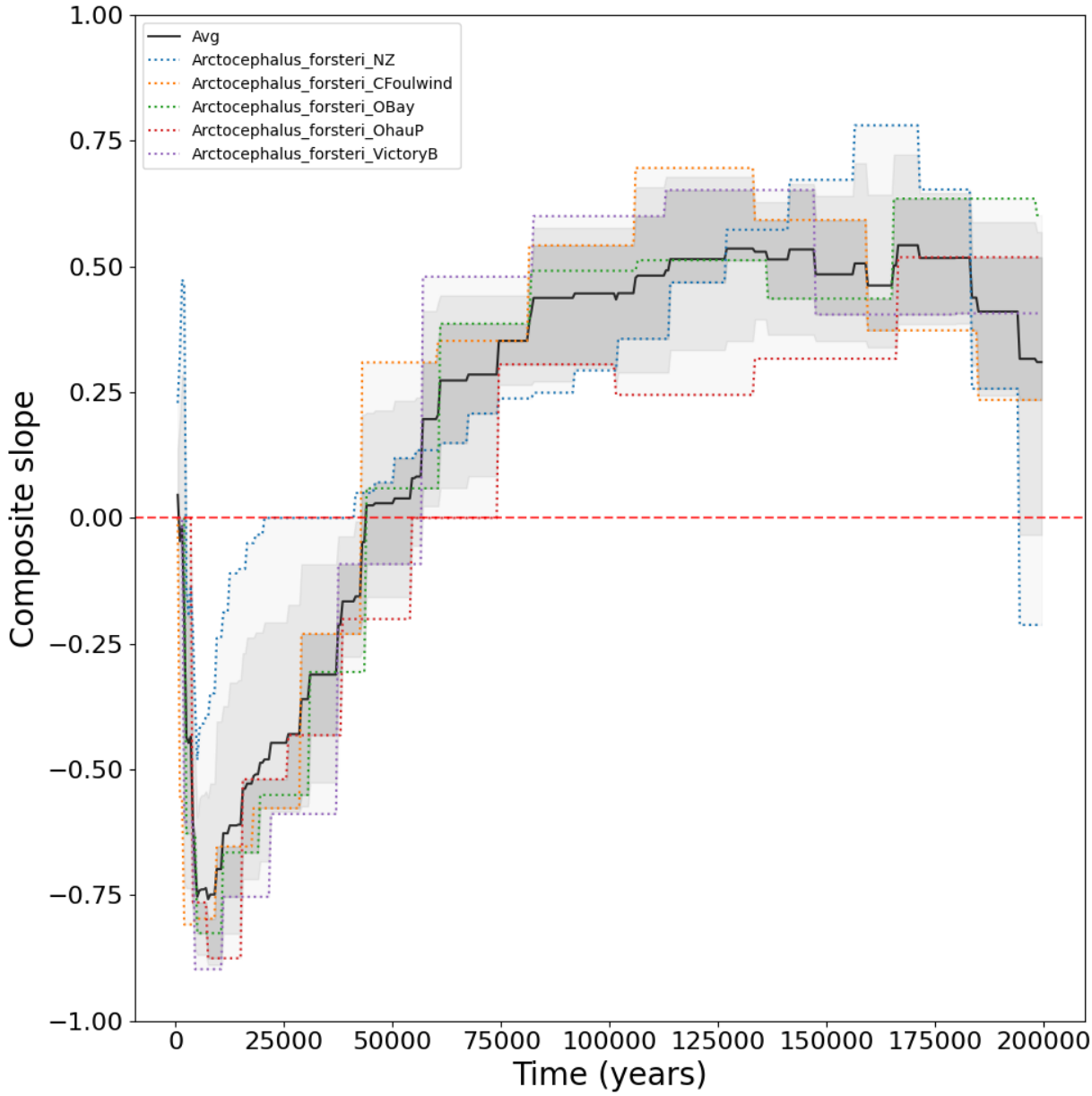

Figure 4.18. Time-specific composite slopes of *A. forsteri* populations at their original assumed evolutionary rates (i.e. RER=1). The population named *Arctocephalus_forsteri_NZ* was formed by pooling all the individuals from the other populations. The black line traces the mean composite slope value of all populations considered, while the shaded areas represent the interquartile range, interdecile range, and total range (i.e. maximum and minimum), respectively, in descending intensity of shading. The specific history of each population is shown by uniquely coloured dotted lines.

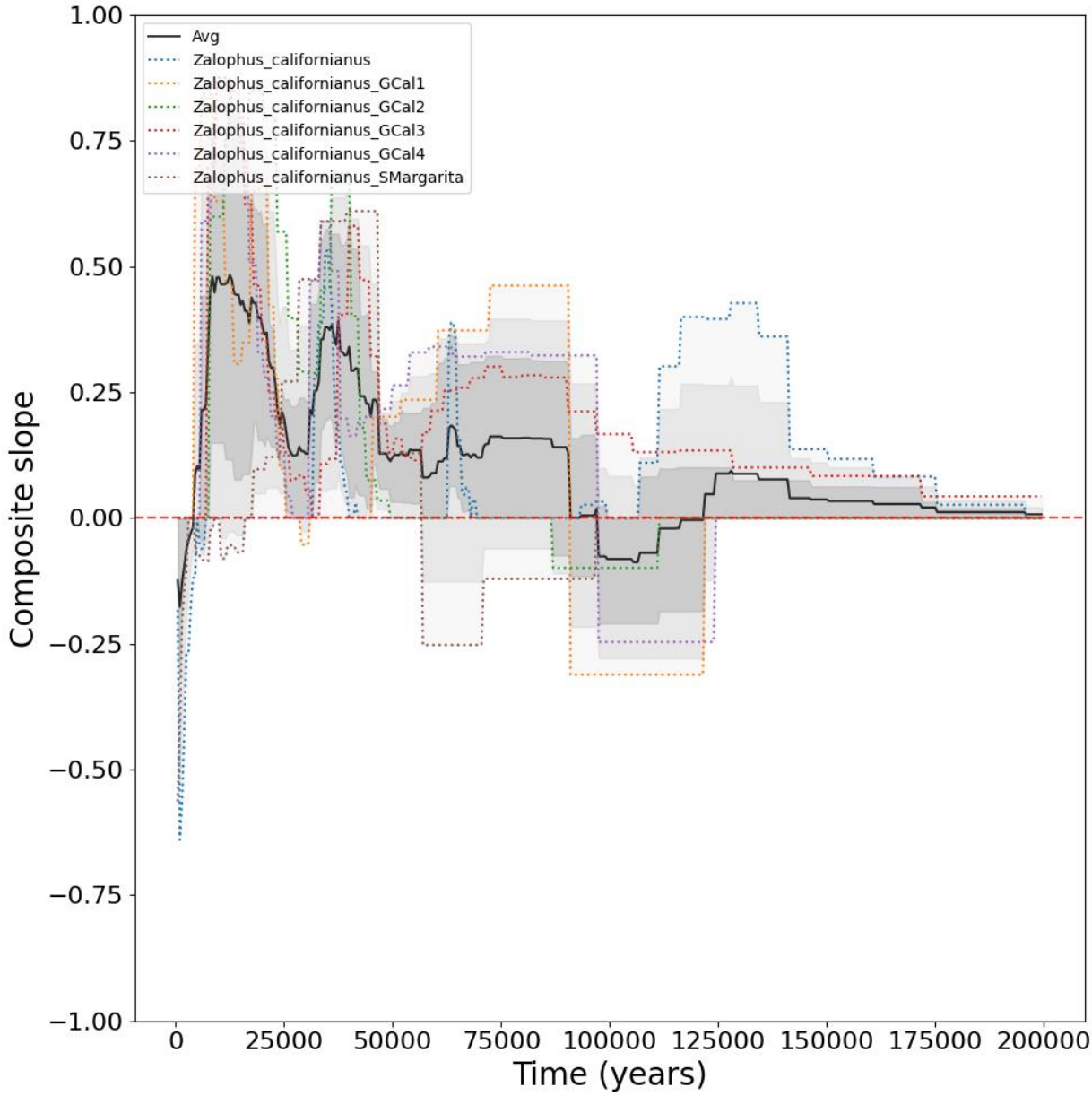

Figure 4.19. Time-specific composite slopes of *Z. californianus* populations at their original assumed evolutionary rates (i.e. RER=1). The population named *Zalophus_californianus* was formed by pooling all the individuals from the other populations. The black line traces the mean composite slope value of all populations considered, while the shaded areas represent the interquartile range, interdecile range, and total range (i.e. maximum and minimum), respectively, in descending intensity of shading. The specific history of each population is shown by uniquely coloured dotted lines.

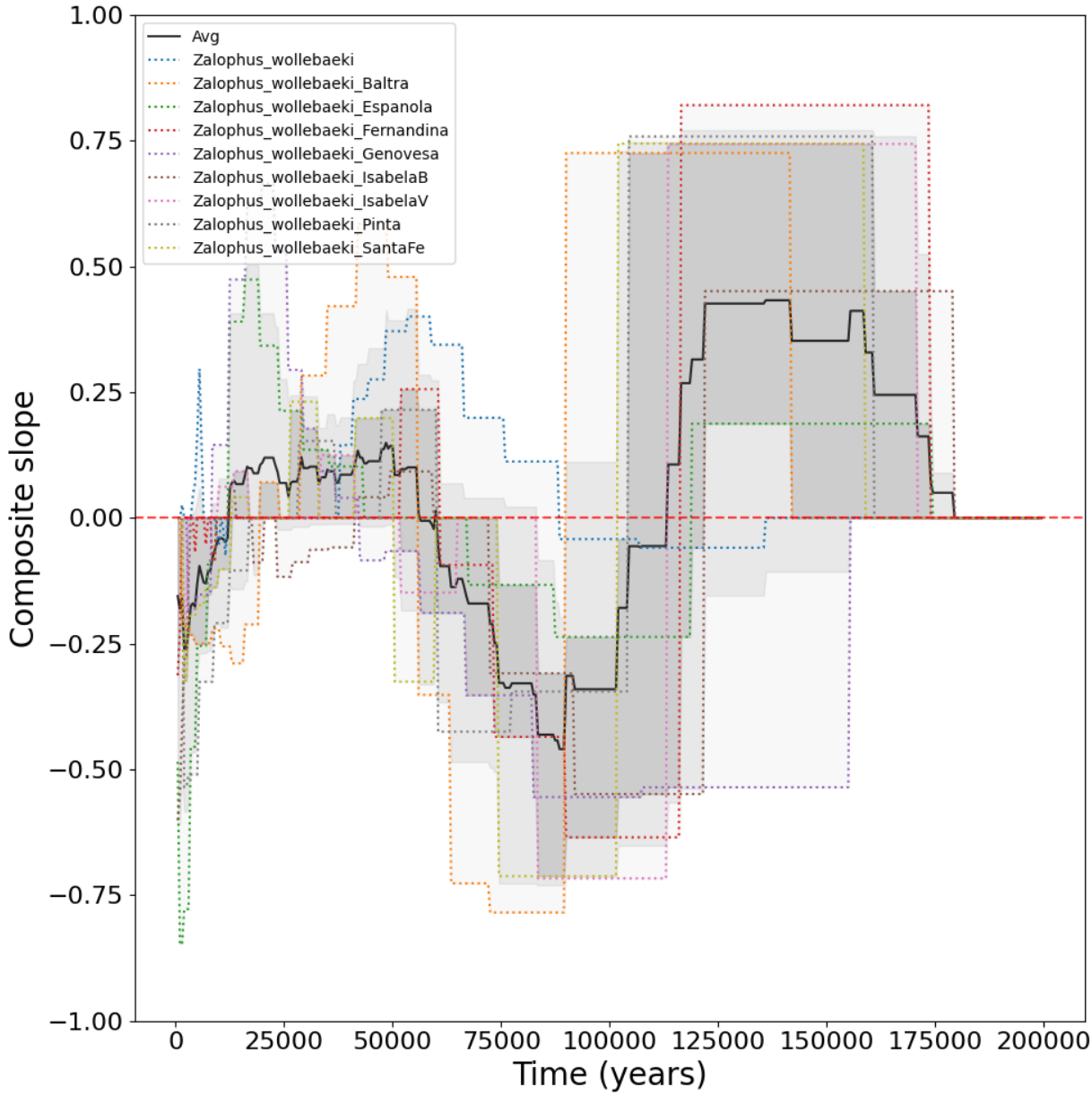

Figure 4.20. Time-specific composite slopes of *Z. wollebaeki* populations at their original assumed evolutionary rates (i.e. RER=1). The population named *Zalophus_wollebaeki* was formed by pooling all the individuals from the other populations. The black line traces the mean composite slope value of all populations considered, while the shaded areas represent the interquartile range, interdecile range, and total range (i.e. maximum and minimum), respectively, in descending intensity of shading. The specific history of each population is shown by uniquely coloured dotted lines.

Comparison of pinniped species

Pairwise slope differences between 13 pinniped species declined rapidly up to an RER range of ~2.25, where the 90th percentile stabilized (Figure 4.21). Approaching the associated MDS plot without prior assumptions, three main groups were visually identifiable (Figure 4.22). A complete table of the pairwise slope differences between all populations is found in Table 4.5.

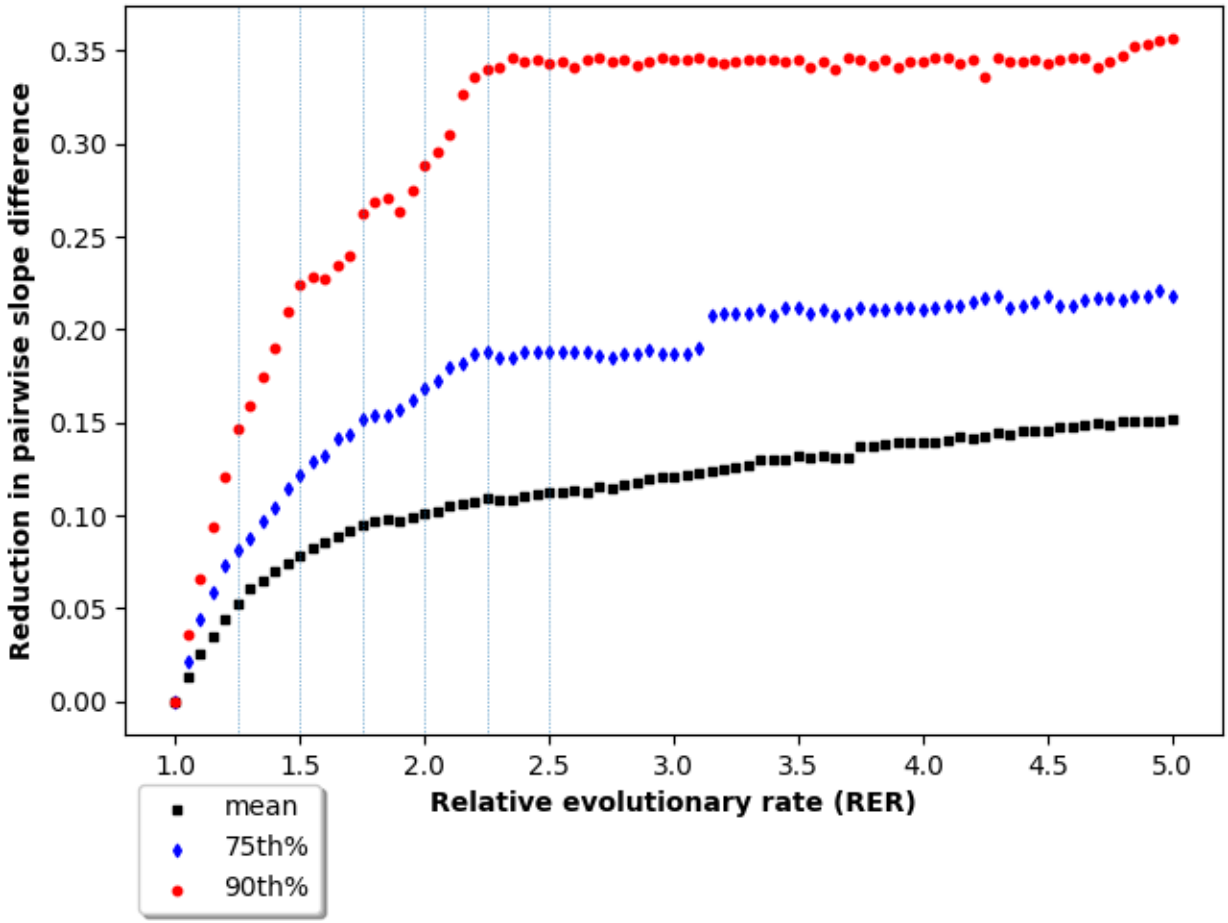

Figure 4.21. Reduction in the mean (black square), 75th percentile (blue diamond), and 90th percentile (red circle) of composite slope differences between pairs of pinniped populations as flexibility in RER is increased from 1.0 (i.e. no flexibility). The reduction plateaus around RER=2.25.

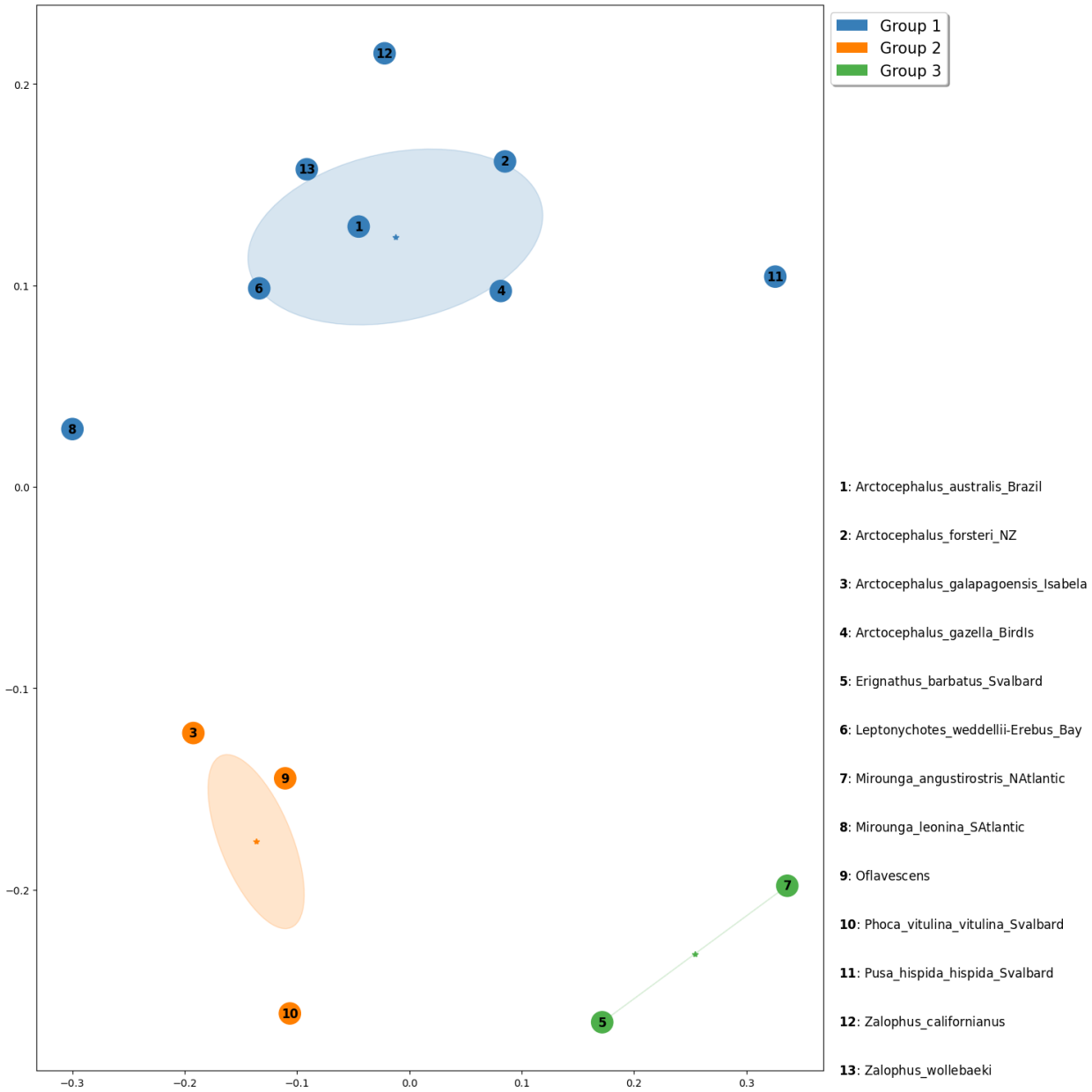

Figure 4.22. MDS plot of the demographic history dissimilarity among pinniped species using an RERrange factor of 2.25. The clusters shown were identified *a posteriori*, with the significance of the groupings confirmed by a PERMANOVA test ($F=11.9$, $p<0.001$).

Table 4.5. Pairwise slope difference between the demographic histories of pinniped populations under an RERrange factor of 2.25. The row/column corresponding to linchpins of pinniped species groups 1 and 2, *A. australis* and *P. vitulina*, are highlighted in olive green and the values corresponding to the species associated with their respective clusters are bolded. Note that *A. australis* is actually more similar to *P. vitulina* than *M. angustirostris* is to *P. vitulina*, but they find themselves in different clusters due to major differences in their similarity to other populations (e.g. *P. vitulina* x *A. forsteri* = 0.5 while *A. australis* x *A. forsteri* = 0.19).

	A.aus	A.for	A.gal	A.gaz	E.bar	L.wed	M.ang	M.leo	O.fla	P.vit	P.his	Z.cal	Z.wol
A.aus	0.00	**0.19**	0.35	**0.18**	0.42	**0.11**	0.52	0.32	0.44	0.33	0.39	**0.21**	**0.12**
A.for	0.19	0.00	0.43	0.08	0.34	0.20	0.63	0.30	0.35	0.50	0.21	0.25	0.18
A.gal	0.35	0.43	0.00	0.35	0.49	0.24	0.48	0.33	0.20	**0.18**	0.48	0.26	0.30
A.gaz	0.18	0.08	0.35	0.00	0.42	0.25	0.31	0.33	0.30	0.43	0.28	0.11	0.17
E.bar	0.42	0.34	0.49	0.42	0.00	0.56	0.24	0.29	0.42	**0.28**	0.37	0.48	0.61
L.wed	0.11	0.20	0.24	0.25	0.56	0.00	0.56	0.29	0.17	0.30	0.50	0.13	0.10
M.ang	0.52	0.63	0.48	0.31	0.24	0.56	0.00	0.66	0.42	**0.47**	0.35	0.51	0.48
M.leo	0.32	0.30	0.33	0.33	0.29	0.29	0.66	0.00	0.41	0.38	0.50	0.47	0.31
O.fla	0.44	0.35	0.20	0.30	0.42	0.17	0.42	0.41	0.00	**0.21**	0.64	0.32	0.22
P.vit	0.33	0.50	0.18	0.43	0.28	0.30	0.47	0.38	0.21	0.00	0.55	0.49	0.35
P.his	0.39	0.21	0.48	0.28	0.37	0.50	0.35	0.50	0.64	0.55	0.00	0.38	0.45
Z.cal	0.21	0.25	0.26	0.11	0.48	0.13	0.51	0.47	0.32	0.49	0.38	0.00	0.07
Z.wol	0.12	0.18	0.30	0.17	0.61	0.10	0.48	0.31	0.22	0.35	0.45	0.07	0.00

The first group consists of *L. weddellii*, *A. gazella*,, *A. australis*, *A. forsteri*, and both *Zalophus* species, as well as *M. leonina* and *P. hispida* as apparent outliers on opposite fringes of the cluster. The second group includes *P. vitulina*, *O. flavescens*, and *A. galapagoensis*. The third group contains only a pair of species, *E. barbatus* and *M. angustirostris*. The demographic histories of most populations within these groups are shown aligned in Figures 4.23, 4.24, and 4.25, respectively.

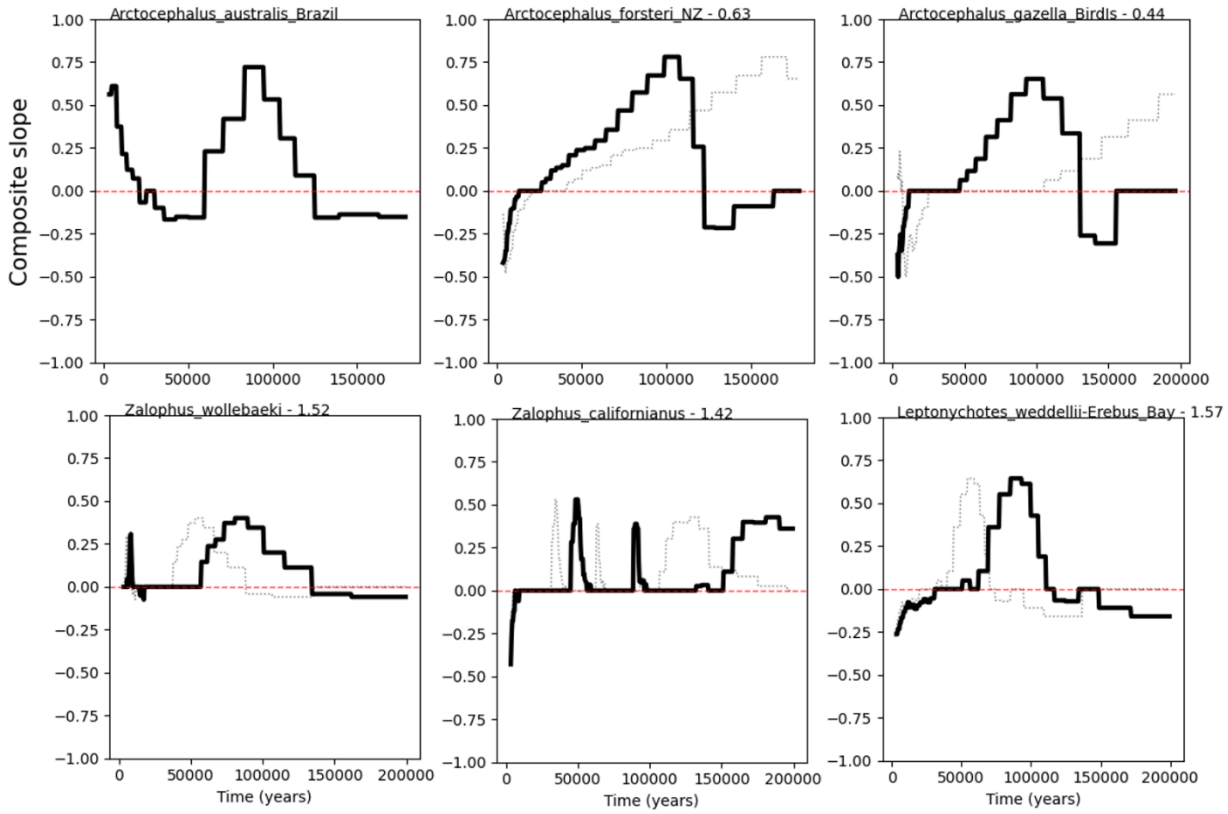

Figure 4.23. The fit of the demographic histories of pinniped species belonging to Group 1 to that of *A. australis*, under RER rescaling. Solid lines show the time-specific composite slope values of each species at their optimal fit to *A. australis*, based on the RER factors annotating the top of each plot after the species name. The dotted lines show the original timings of the species' histories, which were multiplied by the RER factor to yield the solid lines. The fit of *Z. californianus* is clearly not very good, but it is pulled into the cluster based on its relatively low average slope values (i.e. low amount of demographic change).

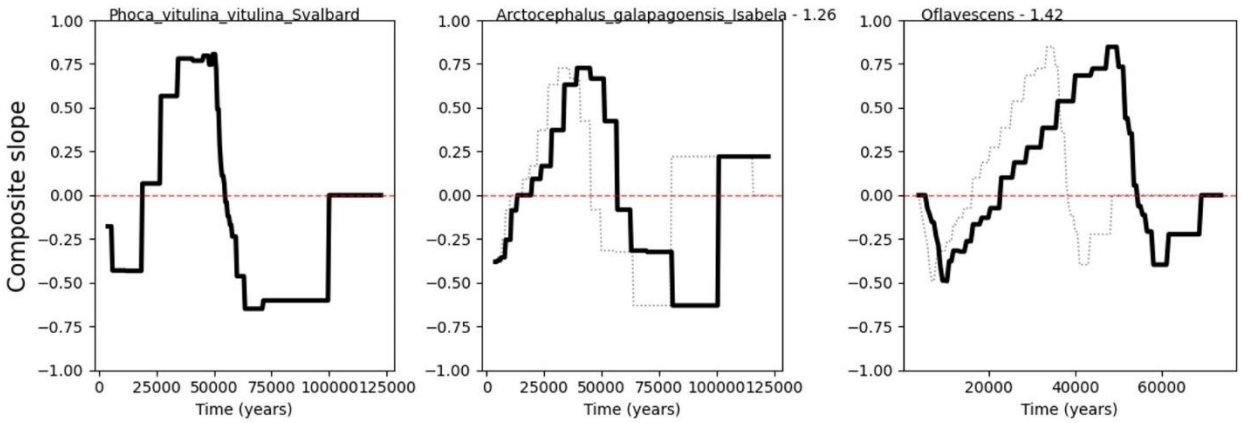

Figure 4.24. The fit of the demographic histories of pinniped species belonging to Group 2 to that of *P. vitulina*, under RER rescaling. Solid lines show the time-specific composite slope values of each species at their optimal fit to *P. vitulina*, based on the RER factors annotating the top of each plot after the species name. The dotted lines show the original timings of the species' histories, which were multiplied by the RER factor to yield the solid lines.

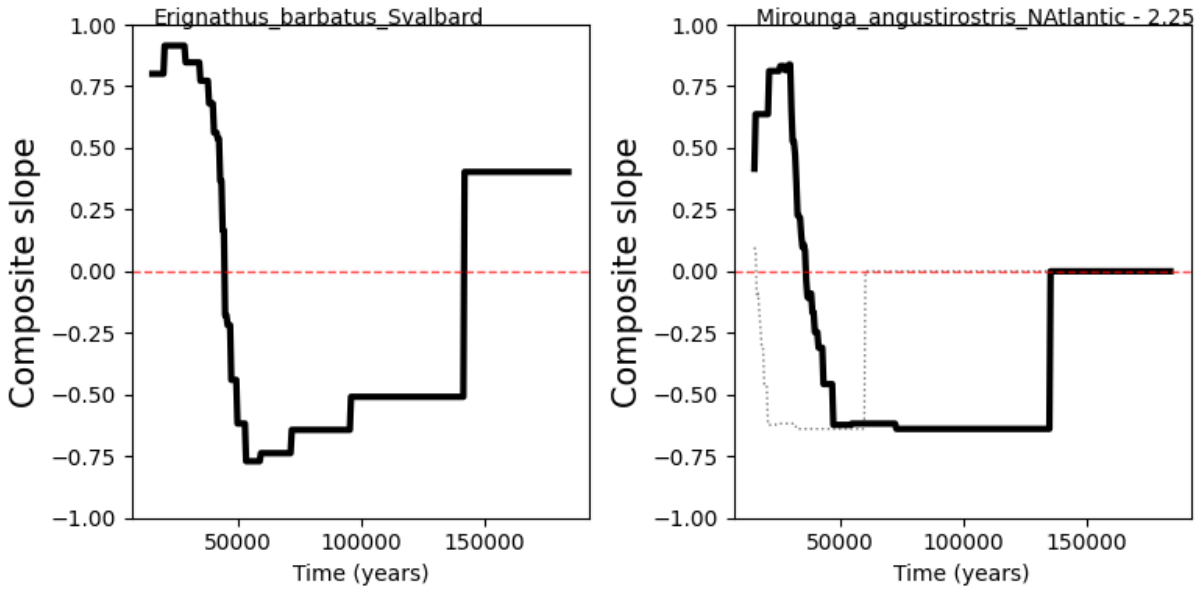

Figure 4.25. The fit of the demographic histories of pinniped species belonging to Group 3 to that of *E. barbatus*, under RER rescaling. Solid lines show the time-specific composite slope values of each species at their optimal fit to *E. barbatus*, based on the RER factors annotating the top of each plot after the species name. The dotted lines show the original timings of the species' histories, which were multiplied by the RER factor to yield the solid lines.

Factors were considered that might explain the composition of these groups, including family (otariid or phocid), geographic coordinates of the sampled population, typical breeding substrate (i.e. land or ice), marine foraging range (i.e. coastal vs oceanic), and parental care strategy (using lactation duration as a proxy). Data on typical breeding substrate came from Schulz and Bowen (2005), and lactation duration was used as a proxy for parental care strategy, following Schulz and Bowen (2005) and Stephens et al. (2014). The population metadata for each of these factors was given in the Methods, in Table 4.3.

Treated as a categorical factor based on its latitudinal limit (>50°: northern/arctic, -50°–50°: temperate, <-50°: southern/Antarctic), species range was a statistically significant predictor of average pairwise differences in composite slope values (Figure 4.26) based on PERMANOVA ($F=3.29$, $p=0.013$, $R^2=0.397$). Treated as a continuous factor, latitude was also significant ($F=3.54$, $p=0.022$, $R^2=0.244$). The three southern species clustered near to each other (Figure 4.26), although their histories differed in some important ways. *M. leonina* and *L. weddellii* both declined from at least ~140 kya to ~100 kya, but the population of *A. gazella* may have been growing over this same period (Figure 4.27). *L. weddellii* and *M. leonina* then grew between ~20-100 kya, while the population of *A. gazella* was static.

Three of the northern species (*E. barbatus*, *M. angustirostris* and *P. vitulina*) clustered near to each other, while the third (*P. hispida*) stood apart (Figure 4.26). The demographic histories of *P. vitulina* and *E. barbatus* were most similar, with both declining between ~50-100 kya, growing between ~15-50 kya, and finally declining during the Holocene (Figure 4.28). *M. angustirostris* followed a similar pattern, though apparently later (under the assumed generation time and mutation rate). *P. hispida* followed the same early decline, but apparently continued it throughout the entire late Pleistocene (i.e. the last ~125,000 years).

The demographic histories of the “temperate” species were much more variable, unsurprising given their comparatively diverse geographic origins (Figure 4.26). They fell into at least two groups; one with *A. australis*, *A. forsteri* and the two *Zalophus* species, and one consisting of *O. flavescens* and *A. galapagoensis*. Other factors, including taxonomic family (i.e. otariid vs phocid; Figure 4.29), breeding platform (i.e. land vs ice; Figure 4.30), marine foraging range (i.e. coastal vs oceanic; Figure 4.31), and lactation duration were not found to be statistically significant (Table 4.6).

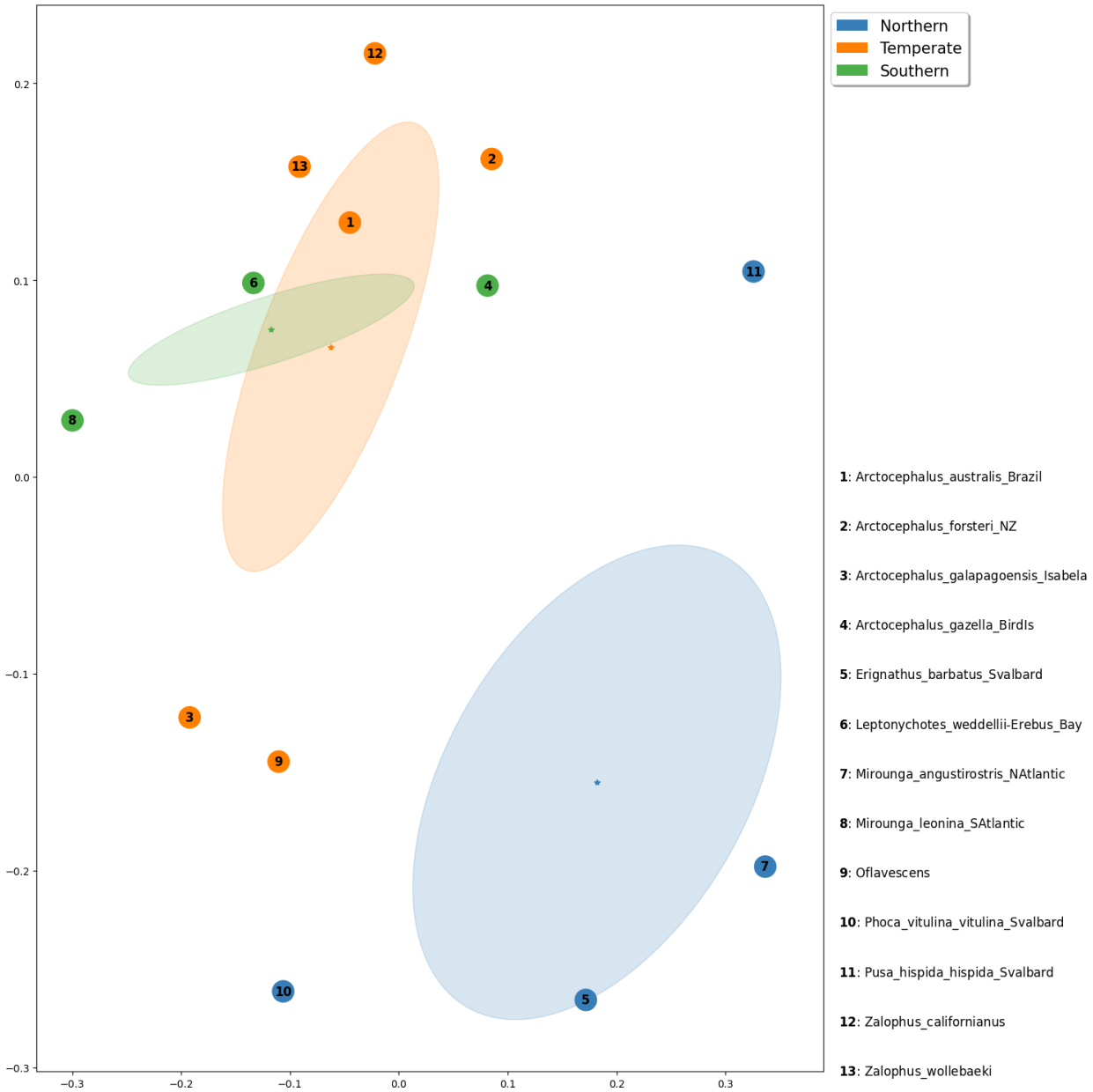

Figure 4.26. MDS plot comparing northern (~arctic), southern (Antarctic), and temperate-region pinniped populations using an RERrange factor of 2.25. PERMANOVA test indicates that the factor is statistically significant overall (F=3.29, p=0.013), but this is driven by the distinctiveness of northern demographic histories; the temperate and southern groups are not distinguishable from each other (F=7.51, p=0.431).

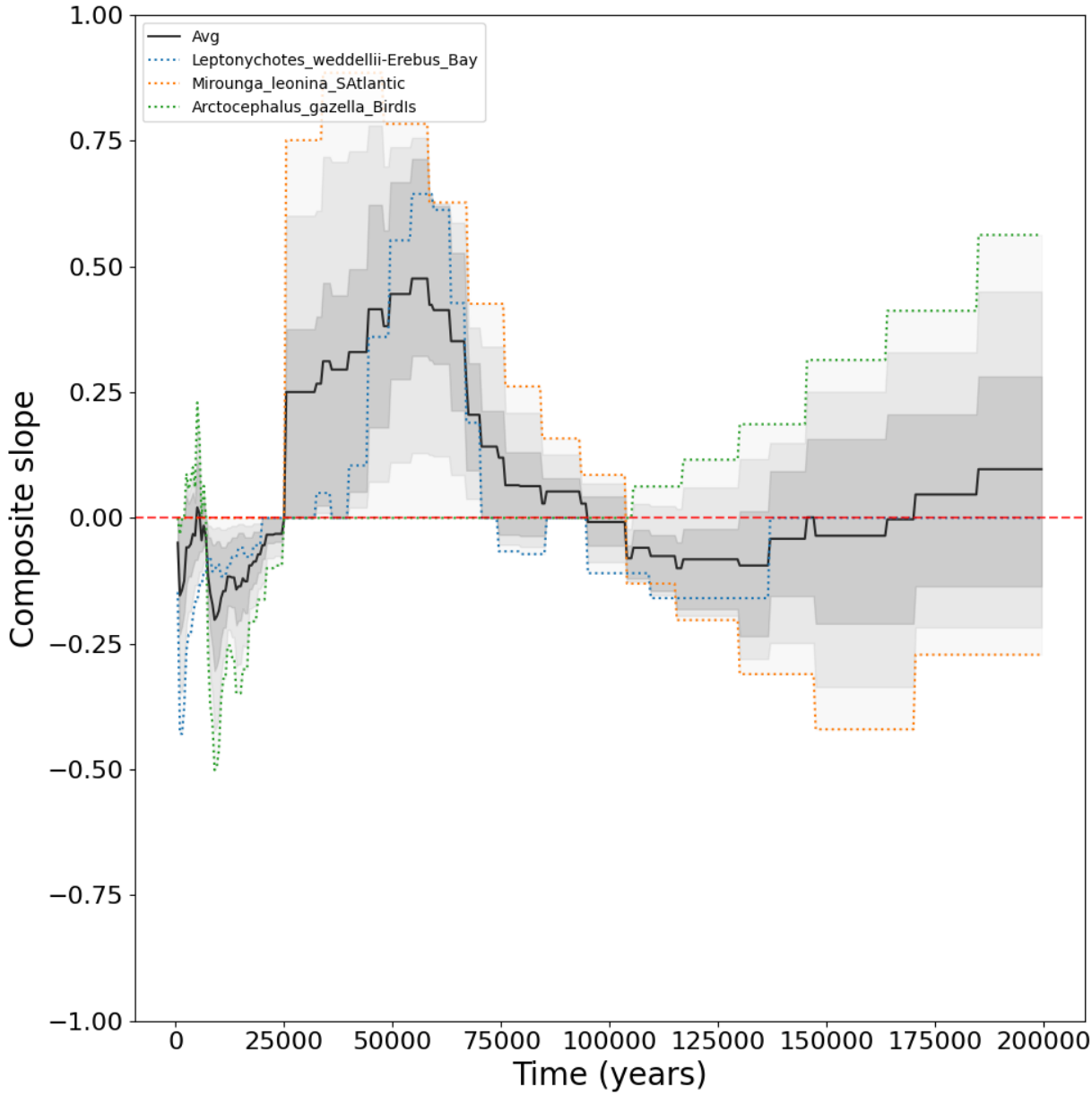

Figure 4.27. Time-specific composite slopes of southern (Antarctic) pinniped populations at their original assumed evolutionary rates (i.e. RER=1). The black line traces the mean composite slope value of all populations considered, while the shaded areas represent the interquartile range, interdecile range, and total range (i.e. maximum and minimum), respectively, in descending intensity of shading. The specific history of each population is shown by uniquely coloured dotted lines.

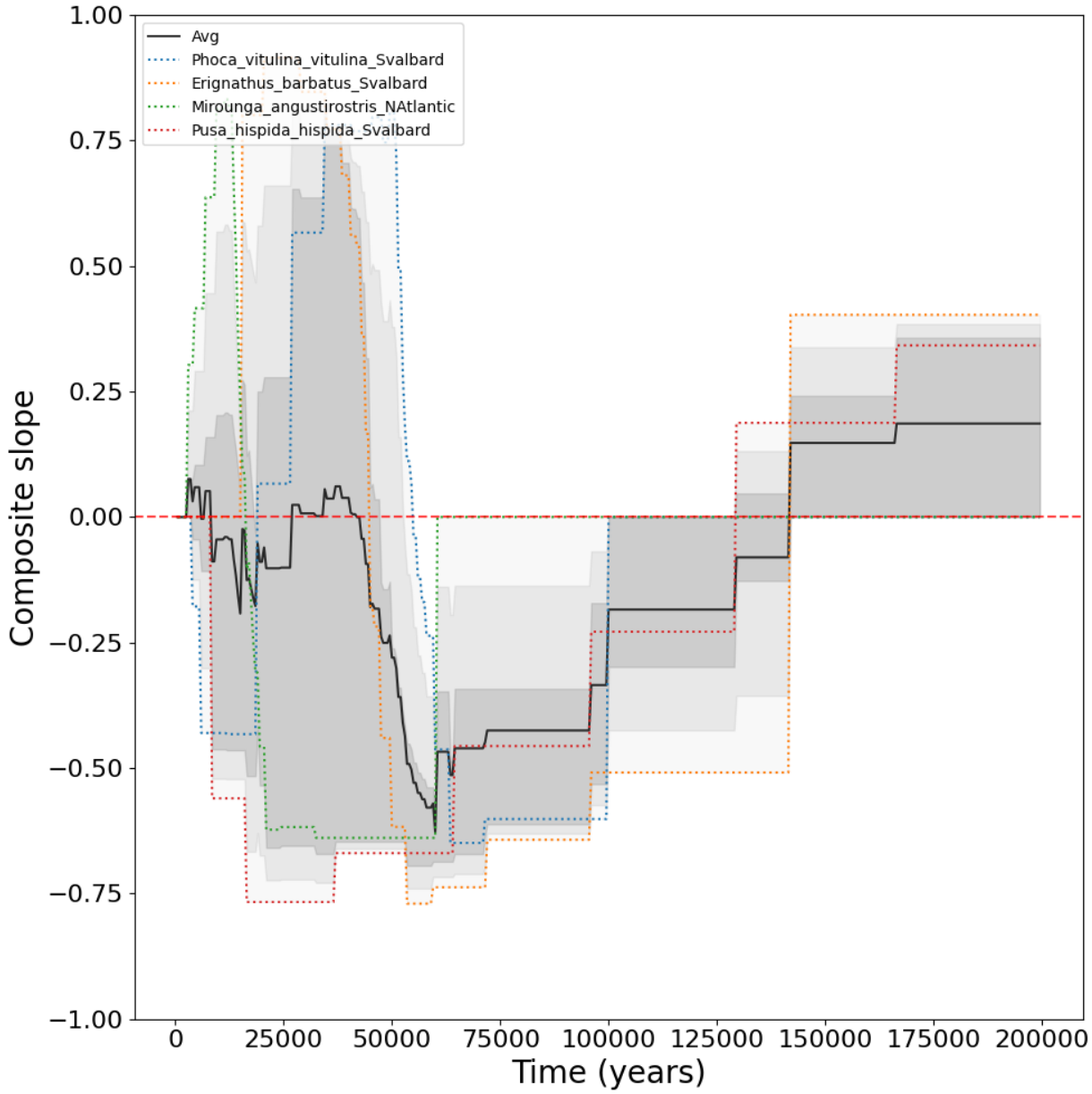

Figure 4.28. Time-specific composite slopes of northern (~arctic) pinniped populations at their original assumed evolutionary rates (i.e. RER=1). The black line traces the mean composite slope value of all populations considered, while the shaded areas represent the interquartile range, interdecile range, and total range (i.e. maximum and minimum), respectively, in descending intensity of shading. The specific history of each population is shown by uniquely coloured dotted lines.

Table 4.6. Factors considered to explain the pairwise differences among pinniped populations (Table 4.5). R^2 represents the percentage of total variance explained by the factor, with p being a measure of statistical significance based on an F test. Latitude was the only factor that was statistically significant ($p<0.05$), and it explained the largest share of variance, followed by genus, family, and marine range. Genus explains a relatively large amount of variance while having a low p value. This is mainly because there were few populations represented per genus (average 1.86). On the other hand, the significance of latitude as a factor is mainly driven by the separation between the demographic histories of populations at its extremes (arctic and Antarctic). Lactation duration and family were considered separately, but were highly correlated (AdjR2=0.69, $p<0.001$), with otariids generally having far longer lactation times (Schulz and Bowen 2005).

Factor	**R^2**	**p**
Longitude	0.062	0.573
Latitude	0.244	0.022*
Family	0.177	0.118
Genus	0.216	0.940
Marine range	0.205	0.061
Lactation duration	0.154	0.160
Breeding substrate	0.077	0.506

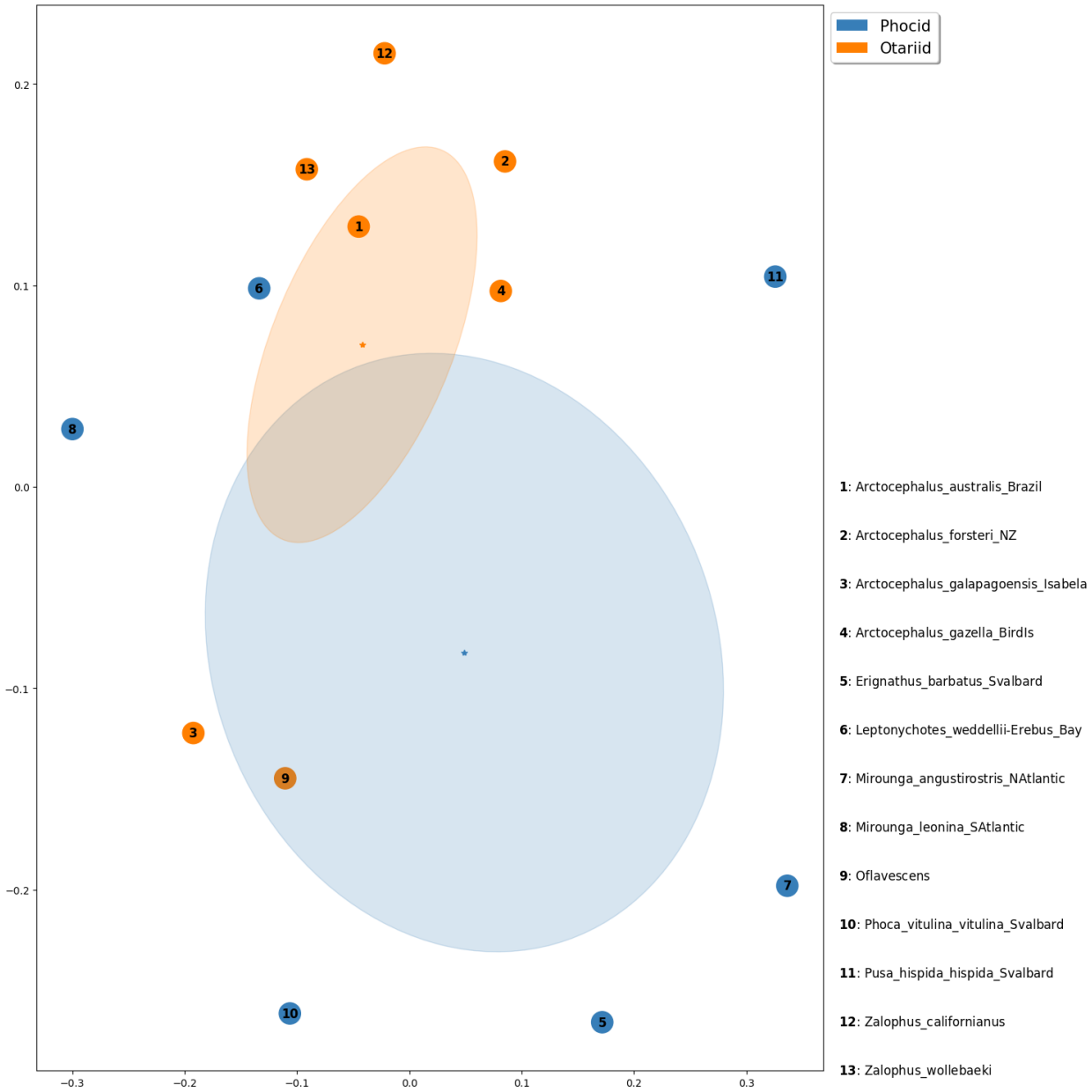

Figure 4.29. MDS plot comparing phocid and otariid species using an RERrange factor of 2.25. PERMANOVA test indicates that the factor is not statistically significant (F=2.37, p=0.118).

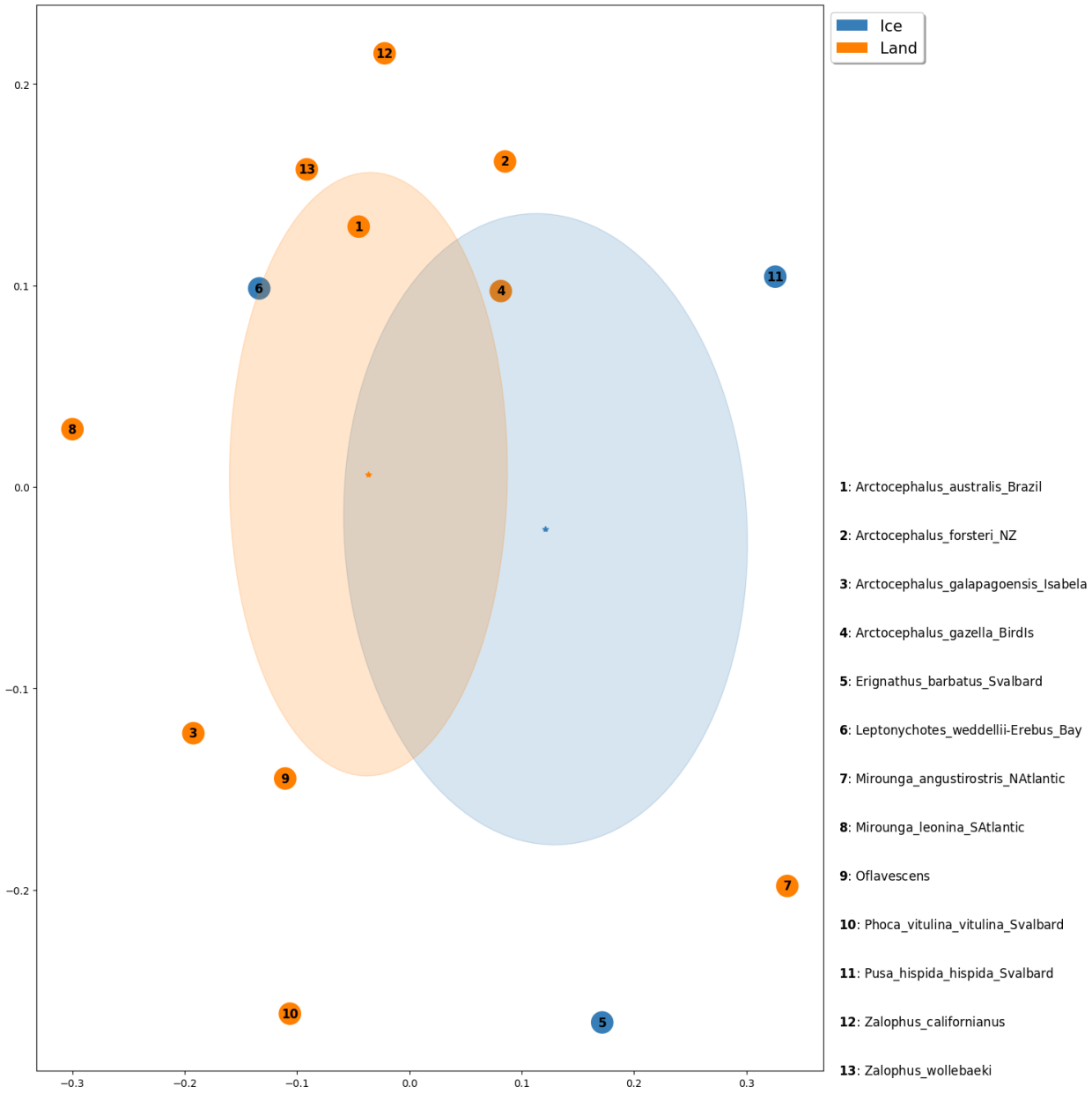

Figure 4.30. MDS plot comparing pinniped species based on their preferred breeding platform/substrate, using an RERrange factor of 2.25. PERMANOVA test indicates that the factor is not statistically significant (F=0.92, p=0.506). There were few predominantly ice-breeding species, weakening the power of this analysis.

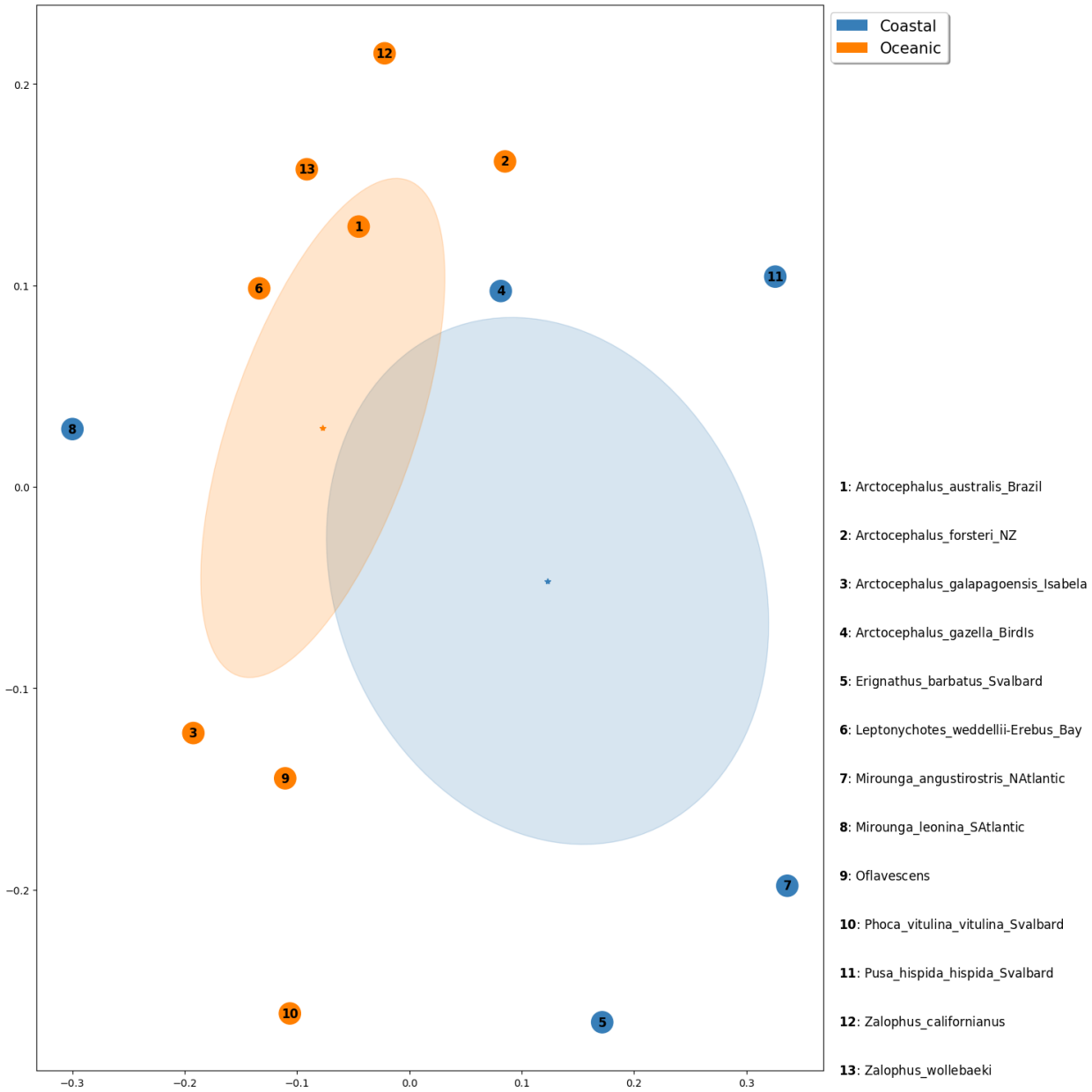

Figure 4.31. MDS plot comparing pinniped species based on their marine foraging range, using an RERrange factor of 2.25. PERMANOVA test indicates that the factor is not statistically significant (F=2.84, p=0.061).

Comparing pinnipeds and penguins

The same pinniped and penguin species and were aligned together with an RERrange factor of 2.25 (determined as optimal for previous pinniped species comparisons; Figure 4.21). In the resulting MDS analysis, penguins remained a distinct cluster (Group 1 x Penguins: F=18.1, p=0.013; Group 2 x Penguins: F=38.5, p=0.004; Group 3 x Penguins: F=56.6, p=0.01). The mean of the Group 1 pinnipeds was closest to the mean of the penguin group (Figure 4.32), but *O. flavescens* was the closest single pinniped species to the penguin group based on the distance matrix, being most similar to the gentoo and chinstrap (Figure 4.33).

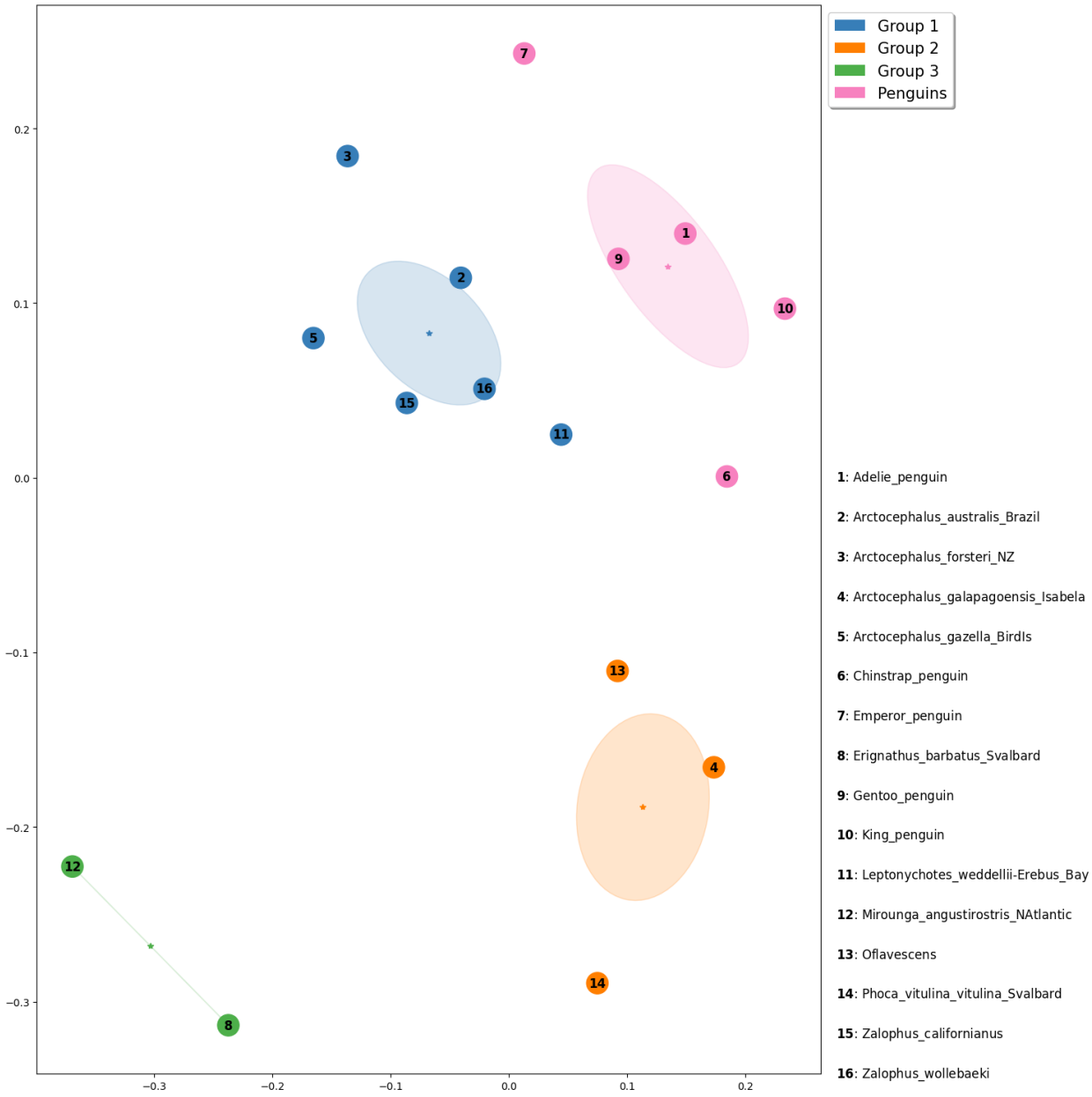

Figure 4.32. MDS plot comparing Northern Hemisphere and Southern Hemisphere pinniped populations with penguin species (Southern Hemisphere) using an RERrange factor of 2.5. Penguins clustered among the southern pinnipeds and were barely distinguishable from the northern pinnipeds (F=8.9, p=0.04).

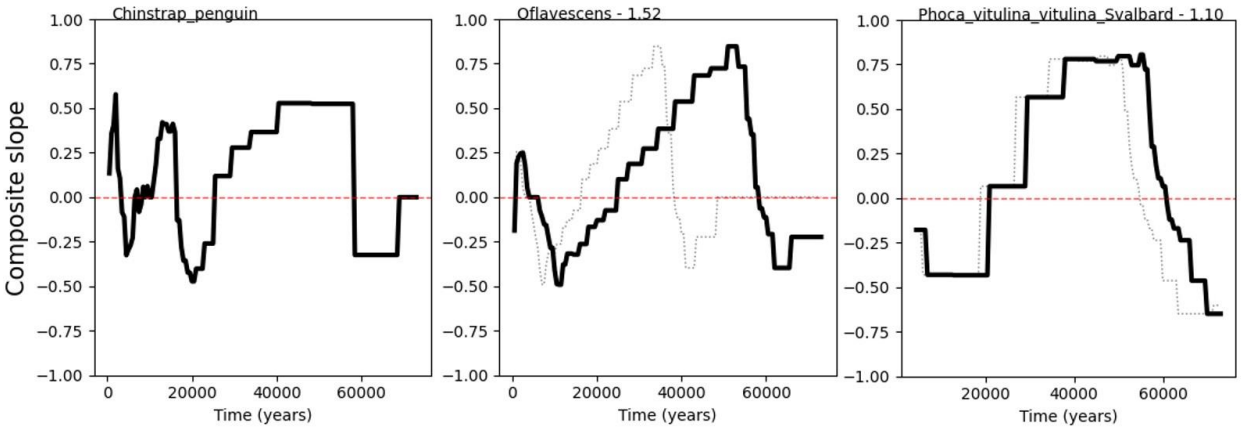

Figure 4.33. The fit of the demographic histories of pinnipeds *O. flavescens* and *P. vitulina* to that of the chinstrap penguin, under RER rescaling. Solid lines show the time-specific composite slope values of each species at their optimal fit to *E. barbatus*, based on the RER factors annotating the top of each plot after the species name. The dotted lines show the original timings of the species' histories, which were multiplied by the RER factor to yield the solid lines. According to this alignment, taking the chinstrap penguin's original scaling for granted, while the chinstrap penguin population expanded immediately following the LGM, *O. flavescens* continued to decline until the mid-Holocene.

Comparing South American pinnipeds and silverside fish

The demographic histories of six species of silverside fish (*Odontesthes*), distributed around the Pacific and Atlantic coasts of Patagonia, were compared with each other and with five potential pinniped predators using the same RER range of 2.25. In general, the demographic histories of silverside species were highly consistent (Figure 4.34). The MDS analysis indicated that the demographic histories of the silversides and these pinnipeds were not quite statistically distinguishable (PERMANOVA: F=5.3, p=0.07; Figure 4.35), due to *O. flavescens* (Argentina) and *A. galapagoensis* (Galapagos) being as or more similar to silversides than to the two other included pinniped populations, *A. australis* (Brazil) and *Z. wollebaeki* (Ecuador). Under optimal RER alignment to *O. ledae* (arbitrary selection from among the silverside species), *O. flavescens* clearly provided the most precise fit, followed by *A. galapagoensis* (Figure 4.36). The demographic history of *A. australis* appeared to bear no resemblance to that of *O. ledae* or the other silverside species.

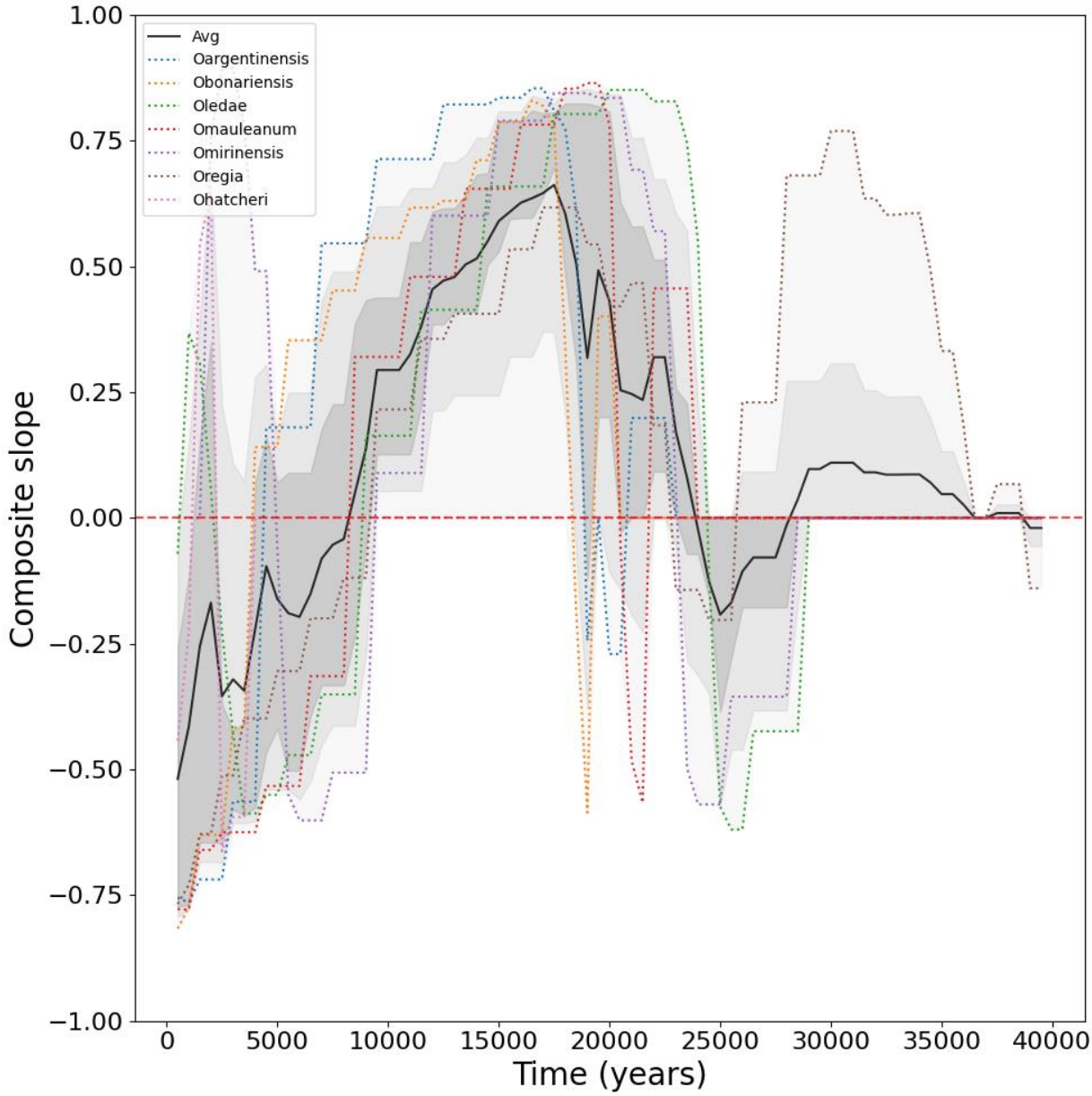

Figure 4.34. The demographic histories of silverside fish species were relatively consistent in overall shape, all indicating growth peaking at around 15 kya. Here, the black line traces the mean composite slope value of all populations considered, while the shaded areas represent the interquartile range, interdecile range, and total range (i.e. maximum and minimum), respectively, in descending intensity of shading. The specific history of each population is shown by uniquely coloured dotted lines.

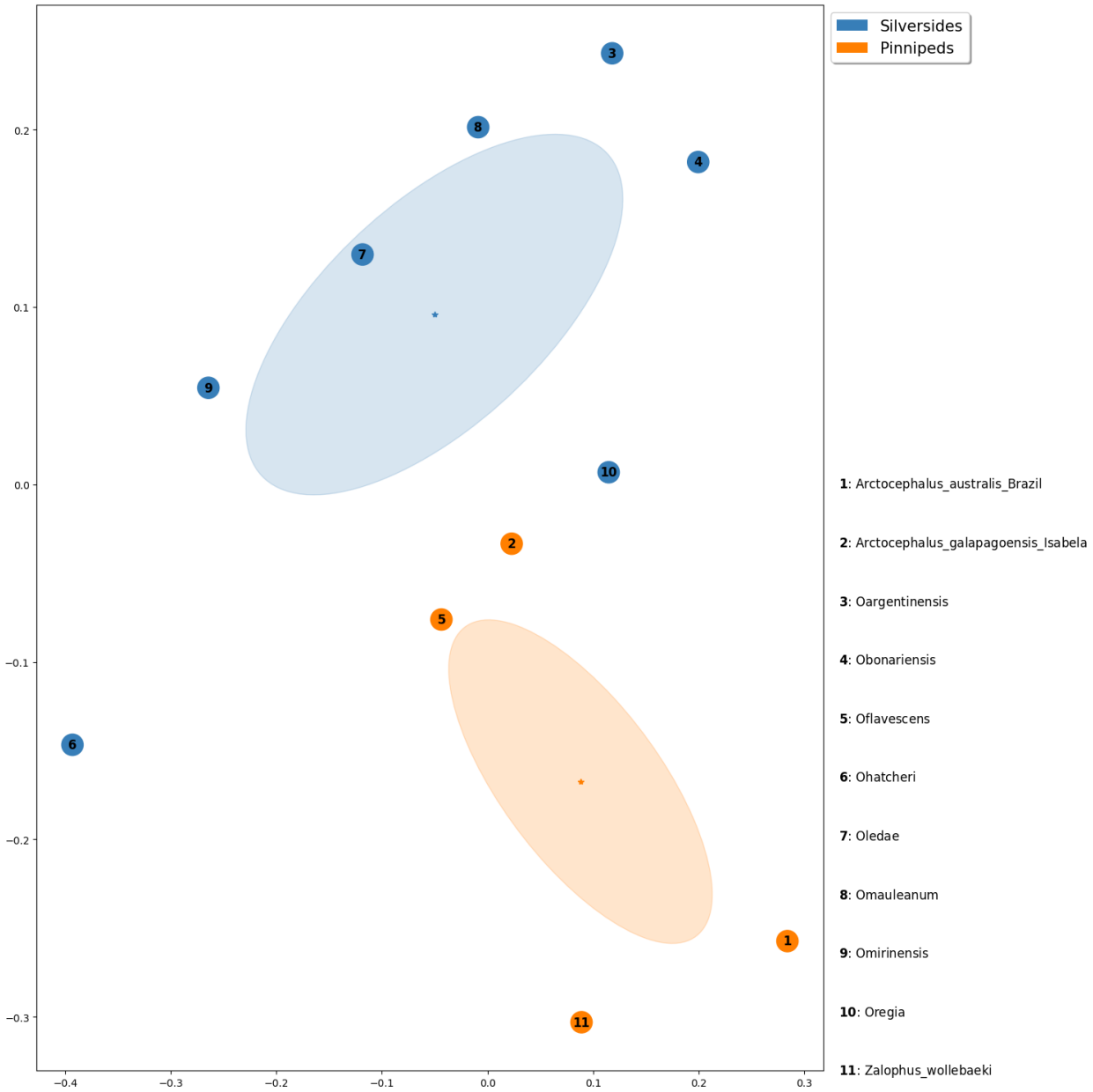

Figure 4.35. MDS plot comparing silverside fish and pinnipeds from the vicinity of South America. The two groups were not quite statistically distinguishable (PERMANOVA: F=5.3, p=0.07).

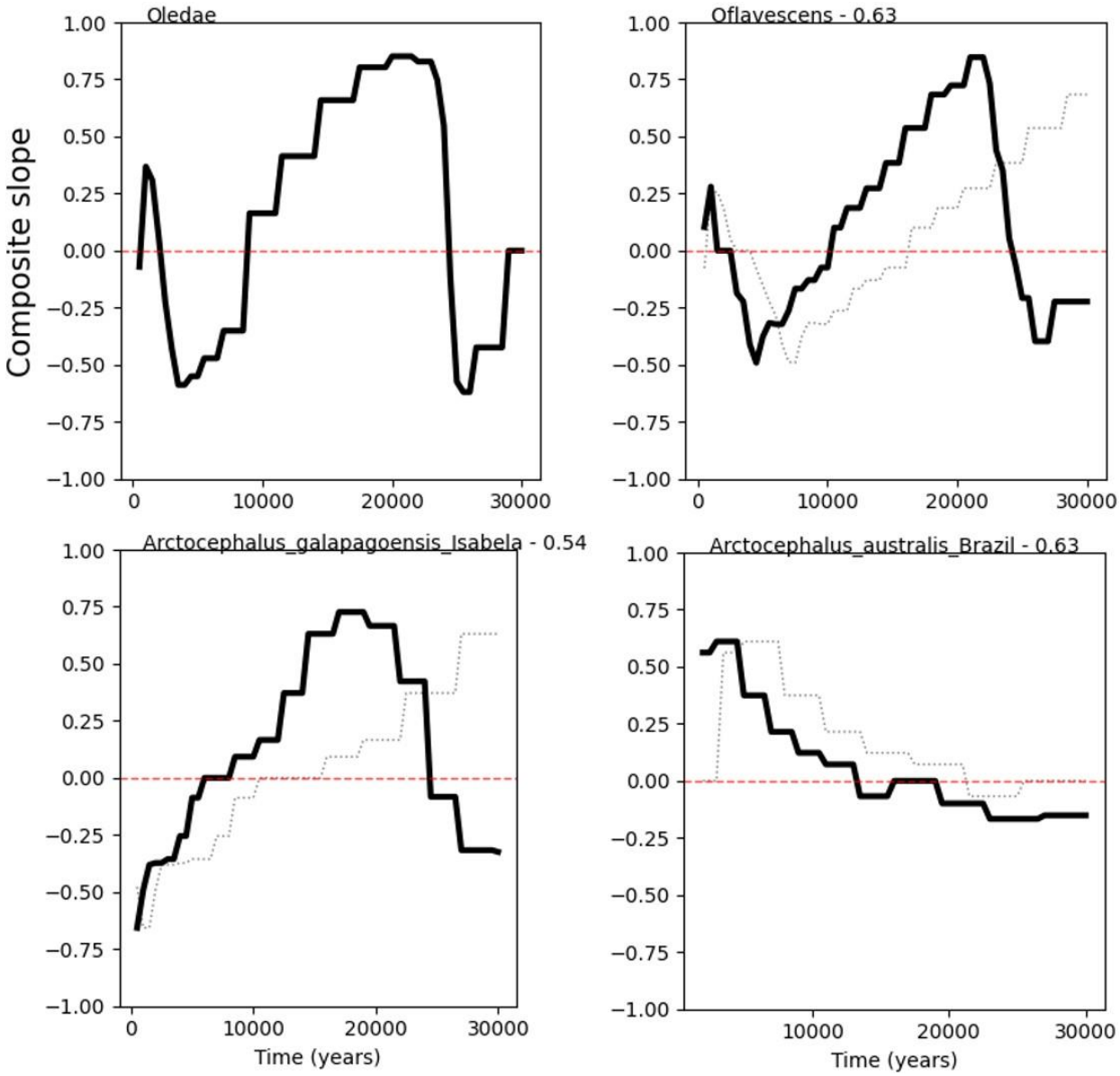

Figure 4.36. The fit of *O. flavescens*, *A. galapagoensis*, and *A. australis* demographic histories to that of the silverside fish *O. ledae* (arbitrary selection; see Figures 4.33-4.34 for similarity of *O. ledae* to other silversides), under RER rescaling. Solid lines show the time-specific composite slope values of each species at their optimal fit to king penguin, based on the RER factors annotating the top of each plot after the species name. The dotted lines show the original timings of the species' histories, which were multiplied by the RER factor to yield the solid lines.

Discussion

In this chapter, I have attempted to demonstrate the potential utility of a relatively neglected approach – quantitative comparisons of demographic history – by developing and applying a new tool (align_stairwayplot.py) to compare simulated data, as well as genomic datasets of relevance to the focal study system of this thesis, semiaquatic marine predators of Patagonia. Specifically, I have considered Antarctic and sub-Antarctic penguins, globally distributed pinnipeds, and South American silverside fish.

The analysis of simulated data demonstrated that align_stairwayplot.py can accurately identify sets of populations with very similar demographic histories. The consistency of clustering of those simulated population sets (Figure 4.2) was comparable to within-species clustering of natural populations considered here (Figure 4.17). However, predictably, the comparison of demographic histories across species produced less decisive clustering (e.g. Figure 4.22, 4.25, 4.27).

Even in the simulated data, there was a clear difference in the tightness of clustering of the 'modsim' and 'standardsim' sets and the 'simBr' set. simBr populations were less tightly clustered, and different iterations (i.e. simBr0 vs simBr3) were recognisably distinct even after RER realignment. This was most likely due to the fact that, in simBr, true N changed gradually through modification of the population growth rate, while the other two simulation sets were based on instantaneous changes in N (Table 4.1). These gradual rate changes in simBr resulted in more variability in the inference of when a shift took place and how large it was. Furthermore, minute changes in exponential growth rate with each slight randomization of the parameters could bring about much larger differences among replicates in their true demographic histories. Even though nothing unusual was apparent in the demographic history of any single simBr variant, it led to much lower consistency among the reconstructed histories of simBr variants compared to among variants of other simulations, translating into much looser clustering (Figure 4.2). This looser clustering better resembled that seen from ecologically similar or closely related natural populations in the later MDS results. This is consistent with the reality that natural populations grow and decline based on exponential rates (λ), but not instantaneously.

The align_stairwayplot.py tool was designed to consider both abrupt/dramatic and extended/gradual changes in N_e by quantifying the "slope" of population growth or decline in

terms of the degree of support for it found among replicate Stairway Plot models, the assumption being that large and sudden changes in N_e will receive high support at a few time points, while slower changes will receive low support, but spread over a larger number of time points. However, there was a potential issue with how this approach interacted with sample size. There was some indication from within-species population clustering in pinnipeds (Figure 4.17) that demographic histories based on large sample sizes had a tendency to cluster together on the basis of having lower absolute composite slope values on average. However, the same did not seem to occur with simulated populations (Figure 4.2), suggesting that it may have been due to an idiosyncrasy of these pinniped species or to the very low sample sizes of some of the pinniped populations clustered in Figure 4.17. If it is real, this 'flattening' of slopes may occur because Stairway Plot reconstructs demographic history by randomly inserting breakpoints where N_e is assumed to have changed, and using a likelihood ratio test to determine whether to keep or reject the new breakpoint. The number of potential breakpoint sites is equal to sample size minus one (n-1), so the average number of random breakpoint proposals per site would be lower for a population represented by a larger sample size. Align_stairwayplot.py uses the proportion of Stairway Plot iterations that include a breakpoint at time t in their final model to calculate the composite slope at time t, which could lead to the artefact seen here. A simple fix could be to account for this sample-size-related difference in null expectation of how many breakpoints will be observed. However, the number of these breakpoints retained following the likelihood ratio test would not necessarily match this expectation but should depend on the details of the SFS vector, so this issue requires further consideration. Fortunately, it does not appear to have been a major issue in the results of this chapter. It was only apparent in the clustering of pinniped populations alongside full-species reconstructions based on pooling of the populations (Figure 4.17, 4.18), where populations with sample sizes ranging from 6 to 83 were being considered simultaneously.

Overall, the largest challenge in comparing demographic histories comes from uncertainty about and natural variation in evolutionary rate (i.e. mutation rate, generation time), and error in other factors that determine the scaling of demographic histories into real time, such as the number of sites that were accurately genotyped, where a SNP would have been called if it had been present. Nearly all studies involving demographic history reconstruction adopt point estimates of mutation rate and generation time from the literature. However, these point estimates will generally come with confidence intervals. For example, Millar et al. (2008) estimated a mean rate of 0.55 mutations per site per million years for the HVRI region of the Adélie penguin

mitogenome, with a 95% confidence interval of 0.53-1.17. In historical terms, that confidence interval alone could mean the difference between an event occurring at 10 kya or 20 kya.

Different methods and populations also tend to yield different estimations of mutation rate and generation time. For example, it was challenging to select a base mutation rate to assume for penguins in this chapter, as estimates used by previous studies differ by orders of magnitude. Trucchi et al. (2014) estimated a very fast genomic mutation rate of $2.6e^{-7}$ substitutions/site/generation (s/s/g) for king penguins, which was subsequently used by Cole et al. (2019) to study and compare penguins' demographic histories. Cristofari et al. (2018) followed a similar approach to Trucchi et al. (2014) and arrived at an estimate of $1.08e^{-7}$ s/s/g, more than twice as slow, but still much faster than most vertebrate mutation rates are assumed to be (e.g. $2.5e^{-8}$ for humans and applied to many other mammals; Nachman and Crowell 2000). At the slow end of the spectrum, Li et al. (2014) arrived at an estimate of $8.11e^{-9}$ s/s/g, while in the middle of spectrum, Vianna et al. (2020) assumed a rate of $1.1e^{-8}$ s/s/g for king penguins based on chicken pedigrees, and Cristofari et al. (2018) offered an update of Li's (2014) estimate based on some corrected assumptions, yielding a rate of $4.55e^{-8}$ s/s/g. Even discounting the original estimate by Li et al. (2014), which was apparently based on some assumptions that are now thought to be incorrect, the slowest and fastest of these credible rates differ by a factor of ~24x, or the difference between an event occurring 10 kya or 240 kya. Although each of these estimates comes with some way of quantifying local uncertainty (e.g. a confidence interval or bootstrap distribution), it is not straightforward to quantify how much confidence should be placed in each of these estimates. Even if we think that one estimate was based on the best method, other estimates are not necessarily uninformative, because they are also based on different populations and timescales, and our confidence in the value of one method over another cannot reasonably be absolute. A similar story could also be told about generation times, which are not only estimated differently and naturally differ between populations, but even differ over time depending on the growth trajectory of the population in question (Cristofari et al. 2018).

For this chapter, I assumed for all penguin species the 4.55-8 s/s/g rate calculated by Cristofari et al. (2018) based on Li et al. (2014), because it was intermediate among the estimates and seemed to represent a consensus between two approaches by different authors. However, a major feature of this chapter and of the align_stairwayplot.py program it is based on is the realignment of demographic histories that are qualitatively similar but may be out of phase due

to variation or error in mutation rate, generation time, or other scaling parameters. This does not solve our uncertainty about the absolute timing of demographic-historical events that stems from uncertainty about mutation rate and generation time, but it may be useful for trying to make inferences despite this uncertainty by identifying groups of populations that have similar demographic histories, but which might otherwise be confidently interpreted as being very different due to variation in or misestimation of scaling parameters.

The shapes of demographic histories can be quite specific. Demographic histories with multiple peaks/valleys can be aligned almost like a lock and key because it is not only the presence of these features that is important, but the spacing (relative time) between them. That is why, in all of the RER robustness plots (Figure 4.1, 4.5, 4.14, etc.), the reduction in pairwise differences plateaus beyond a certain threshold of RERrange, yet clusters of populations in most cases remain as or even more distinct, rather than all coming to match each other perfectly. Of course, not all demographic histories are so specific; in this chapter, some, such as *A. gazella* and *L. weddellii*, showed little variation over time and ended up clustering together based on their mutual lack of distinct features. Another potential issue is autocorrelation. Although this RER realignment approach was developed to avoid the case where two histories were dismissed as being very different simply because they were out of phase, it is likely to be true sometimes that populations will mirror, rather than match each other. For example, ice-avoiding penguin species might decline at the same time as penguins who depend on sea ice proliferate. These scenarios are easier to interpret with complex demographic histories involving multiple distinct features to align, such as a stepwise series of bottlenecks.

Patterns of shared demographic history

Ice-avoiding penguins

Considering penguins, and turning to interpretation of the results of this chapter, a major cause of ecological shocks in the Antarctic and sub-Antarctic during the Pleistocene has been glaciation and changes in sea ice extent, which likely impacted the abundance and distribution of potential prey species, in addition to having more direct impacts on habitat availability. For example, king penguins primarily forage for fish in the vicinity of the Antarctic Polar Front (APF), but depend on ice-free sub-Antarctic islands for breeding grounds (Cristofari et al. 2018). The APF moves northward or southward during cooler or warmer climate periods, respectively, and the maximum extent of Antarctic sea ice expands or contracts with it. During the LGM, the

overall productivity of the Southern Ocean is thought to have stayed constant, but expanding sea ice is thought to have rendered many sub-Antarctic islands unusable for breeding by ice-avoiding penguins like the king penguin, while the northward movement of the APF put it within foraging range of at-the-time new and short-lived king penguin colonies on the Auckland and Campbell Islands of New Zealand, near Macquarie Island, which is still inhabited (Cristofari et al. 2018). The Falkland Islands likely served as a refuge for king penguins that had occupied – and occupy once again in the present – the South Georgia islands (Cristofari et al. 2018). Being concentrated on fewer sub-Antarctic islands would have meant access to a much smaller area of ocean forage within range (summed across the whole species), which likely would not have been able to support as large a population as existed before and after the LGM. According to previous studies, the net effect on king penguin demography was a sharp but brief decline during the LGM, followed by explosive growth as the Crozet archipelago and other sub-Antarctic islands were recolonised by the onset of the Holocene climatic optimum (Trucchi et al. 2014; Cristofari et al. 2018).

Similar late-Pleistocene histories, comprising LGM-associated decline and followed by population expansion amid post-LGM warming, have been suggested for the other ice-avoiding, sub-Antarctic penguins, including the chinstraps and gentoos (e.g. Clucas et al. 2014; Mura-Jornet et al. 2018; Cole et al. 2019), and even for Adélie penguins, which depend on ice-associated krill for food, but utilise ice-free land for breeding. In addition to terrestrial glaciation, the LGM also saw year-round sea ice extending much farther from the Antarctic coastline. This likely would have forced energetically costly travel from any ice-free terrestrial breeding sites that did remain, across the sea ice, to the edge of the open ocean. There is some evidence of sea ice negatively affecting inter-annual population dynamics via juvenile/subadult survival/recruitment in Adélie penguins (Jenouvrier et al. 2006), likely due to physiological stressors such as cold and the need to travel farther to find food. Ritchie et al. (2004) dated the most recent common ancestor of Adélie penguins to ~20-50 kya based on mtDNA with an evolutionary rate calibrated by ancient DNA, which is consistent with, but does not demonstrate, the idea that the species experienced a bottleneck within that timeframe. A BSP analysis by Younger et al. (2015b) on mtDNA of East-Antarctic Adélies also indicated a 135-fold increase in population size since ~15 kya. This pattern, featuring a net-negative effect of glaciation and net-positive effect of deglaciation, is intuitively what would have been expected penguins or any species living in the vicinity of Antarctica that required both ice-free land and proximity to productive open ocean.

In the present results, at their original scaling (i.e. RER=1), the gentoo and chinstrap penguins' demographic histories matched this expectation perfectly, with both species having apparently declined between ~18-25 kya around the LGM, and then proliferated ~10-15 kya, as the Antarctic sea ice was receding again (Figure 4.4). The histories of the king and Adélie penguins have approximately the same shape as those of the chinstraps and gentoos (Figures 4.6-4.7), but the timing of their decline and growth phases was completely different. At their original scaling, king penguin apparently grew during the LGM and declined afterwards, while Adélie penguin grew prior to the LGM but was then little affected by the LGM and later events.

As discussed, there is extreme uncertainty about penguin mutation rates. Although mutation rate should be relatively consistent among penguins, mutation rate and generation time can still vary considerably, even with genera. For example, Peart et al. (2020) found that mutation rate alone varied from $1.1e^{-8}$ to $1.42e^{-8}$ s/s/g among *Arctocephalus* species of pinnipeds, equivalent to an RERrange of 1.29. It would require no greater an RERrange than 1.5 to optimally align the decline and growth phases of all four penguin species (Figures 4.6-4.7), so it would not be reasonable to rule out the possibility that they all correspond to the same times. However, this also cannot be concluded.

If they do correspond to the same times, what are those times? Arguably, the strongest case can be made for the chinstrap/gentoo timing because those two already align, whereas the others are all different. Moreover, that timing (i.e. LGM decline/Holocene growth) conforms to biologically informed expectations and what most other studies have concluded. But why would the Stairway Plot reconstruction of the demographic history of any one of these species be precisely accurate while only the others were off to varying degrees? If this analysis is considered in isolation, it seems most likely that the true timing would be somewhere between them all, with chinstrap/gentoo and Adélie defining the early and late bounds, respectively. It is the king penguin that fits almost precisely between them, and would therefore require invoking both the lowest overall and the most consistent level of error in scaling parameters to align all four species' demographic history curves (Figure 4.7). It is also possible that the originally mismatched growth/decline timings of the king, chinstrap/gentoo, and Adélie penguins reflect their true histories and that rather than growing and declining in parallel, a changing environment sometimes had opposite net impact on each species (Figure 4.4).

Given their present-day requirement for ice-free breeding habitat near good foraging grounds, it would seem surprising for the populations of sub-Antarctic penguins to have actually increased in number during the LGM. One possibility is that the genomic evidence of population decline has been distorted by an even more powerful signature of admixture between genetically differentiated populations, which could appear as a spike in effective population size. This might have occurred around the LGM if emigrants from several partially differentiated populations converged on one or a few refugia and a mixed genetic stock went on to recolonise modern sites, as has been suggested for gentoo penguins based on phylogeographic analyses (e.g. Peña M et al. 2014). This scenario is beyond the scope of the present results to test, but studies of contemporary populations of these species have found little to no genetic differentiation (Clucas et al. 2018; Cole et al. 2019). The species with the most modern genetic differentiation (F_{st}) between colonies is the gentoo penguin. Owing to their flexible diet and coastal, benthic foraging strategy, gentoo penguins may have been relatively insulated from sea-ice-driven changes in the distribution of krill in the open waters of the Southern Ocean (Wolff et al. 2006; Kohfeld et al. 2013). This has been suggested as a reason for why gentoo penguins are now proliferating under anthropogenic climate warming while chinstrap penguins and others are declining (Clucas et al. 2014). Yet, it is the gentoo and chinstrap penguins whose Stairway Plots' original scaling shows them having declined during the LGM.

Scenarios could also be developed to explain how the populations of ice-avoiding penguins really could have increased during the LGM. While ice-free habitat is crucial for the breeding of sub-Antarctic penguins, it is not clear that they would have been a limiting factor controlling their population size. For example, Adélies, who also depend on ice-free land for breeding, currently colonise only a fraction of the suitable ice-free sites available to them (Ainley et al. 1995; Cimino et al. 2016). It is also possible that some Adélies colonised off-shore (sub-Antarctic) refugia (Roeder et al. 2001; Fraser et al. 2012). This scenario would have left Adélie penguins in a similar predicament to king and chinstrap penguins, whose populations do appear to have declined during the LGM. However, a crucial differentiator is that Adélie penguins are adapted to spending long periods of the non-breeding season living on sea ice, so they could have had larger foraging ranges and would not have had to make the energetically-costly repeat foraging trips made by king and chinstrap penguins (e.g. Ropert-Coudert et al. 2000; Le Vaillant et al. 2013). If the challenges posed by an extended sea ice shelf could be overcome by ice-avoiding penguins by maintaining enough of an ice-free range to maintain their population, they may have reaped some benefits from the LGM's expanded sea ice coverage. Sea ice margins are

also important as a nursery for juvenile krill, which undergird the productivity of the Southern Ocean ecosystem and are a primary food source for chinstrap penguins (Trivelpiece et al. 2011).

Although possible, these scenarios to explain why ice-avoiding penguin species might have grown (or appeared to grow) during the LGM strain credulity in some way, such as by proposing untested or untestable hypotheses about ancient genetic structure or short-lived lower-latitude colonies. Moreover, they only explain one aspect of the penguins' complex and demographic history at a time. There are actually at least three phases to the history that all align very well across the four ice-avoiding penguin species: early growth (>25 kya in chinstrap; this phase is absent in gentoo penguin due to truncated Stairway Plot), decline (~15-25 kya in chinstrap), growth (~10-15 kya in chinstrap), and recent stasis or growth (Figure 4.7). Any hypothesis about their timing should be able to explain all of these phases and their qualitative similarity (even if not simultaneity) across ice-avoiding species. Under the chinstrap/gentoo timing, these phases fit well with the glacial cycle. The beginning of the stadial phase that ended with the LGM began ~30 kya, glaciation and sea level reached their LGM levels by ~26.5 kya (Clark et al. 2009). This period corresponds to the transition from growth to decline in the chinstrap penguin. The Antarctic ice sheet began to recede ~15 kya, corresponding to the transition between decline and growth in the chinstrap penguin, which last until ~10 kya. The most recent period, corresponding to the Holocene epoch, is much more idiosyncratic among the penguin species. If, instead of adopting this chinstrap/gentoo timeline, we assume that the original timings of the king or Adélie penguin Stairway Plots were accurate, then perhaps the caveats offered in the previous paragraphs could account for their populations growing or remaining stable during the LGM, but this timing would also require an explanation for the pre-LGM decline and post-LGM decline or stasis that would be implied by the shift in timing (Figure 4.6).

Ultimately, the balance of the evidence and ecological plausibility seem to support the original idea, that the LGM had a net-negative effect on the demography of sub-Antarctic and ice-avoiding penguins, and that these species subsequent rebounded as the Antarctic sea ice edge retreated around the onset of the Holocene. Comparative demographic history contributes a valuable line of evidence to settling this question by constraining any historical scenario and accompanying explanation to be applicable to multiple species and multiple episodes of demographic change that appear to align so precisely. Moreover, the 'composite slope' approach to quantification used by align_stairwayplot.py resolves some of these events and

cross-species similarities that would not be obvious by looking at the standard Stairway Plot 2 summary plots (Appendix B).

Ice-dependent penguin(s)

The Stairway Plot analyses of the emperor penguin for this chapter stood out somewhat from the consistent pattern seen in the other species. Like the chinstrap and gentoo penguins (and most likely also king and Adélie, based on the evidence discussed in the previous section), the emperors apparently declined during the LGM, although the decline is less well supported and/or may have been more modest, as it is based on slightly lower absolute composite slope values than in other species (Figure 4.7). Unlike the other penguin species, this decline apparently continued into the early Holocene. Cristofari et al. (2018) also reported a very stable demographic history for emperor penguins based on their own Stairway Plot and PSMC analyses of emperor penguin RADseq and whole-genome datasets from a different set of emperor penguin samples. A Bayesian Skyline Plot analysis by Younger et al. (2015a), based on mtDNA, recorded no significant changes in N_e for emperor penguins during the LGM, but did suggest that the population grew over the last 5-10 ka, in line with Holocene warming. Their analysis of matrilineal population structure also led them to suggest that glaciation had isolated a population of emperor penguins in the Ross Sea area around a hypothetical polynya (a patch of open water that remains unfrozen). However, the productivity of such a polynya likely would have been significantly lower than the open ocean, so it is unlikely that they could have sustained a population of similar size to that of warmer, interglacial times (Ritchie et al. 2004). As for the suggestion that a Ross Sea population was isolated during the LGM, extended sea ice shelves would likely have made it more difficult for adult emperor penguins to reach the sea from where they over-winter with chicks. However, given that emperor penguins breed on ice, it has been suggested that most colonies may have simply migrated northward, over the generations approaching the LGM, as required to maintain a practical distance to the open ocean (Thatje et al. 2008). If the overall productivity of the Southern Ocean did not change during the LGM, but was merely redistributed towards lower latitudes along with the new sea ice edge (Cristofari et al. 2018), this tolerance for sea ice may have enabled emperor penguins to maintain a stable population through the LGM, since they could follow the productive areas more easily than other species who required ice-free land adjacent to foraging hotspots. Still, any increase in the energy investment required to reach the open ocean, even if it was possible, may have had a negative impact on the rate of recruitment to the population (c.f. Adélie

penguin: Jenouvrier et al. 2006, king penguin: Bohec et al. 2008), which could have edged the species into a slow decline.

The Adélie penguin is an interesting case to consider in the context of these comparative demographic history results, because Adélies live alongside emperor penguins on the Antarctic continent and have been considered an ice-dependent species like the emperor penguin (e.g. Lescroël et al. 2014; Hinke et al. 2017). It is interesting, then, that the Adélies' demographic history better matched the sub-Antarctic penguins, suggesting that the species should mainly be classified as ice-avoiding like the king penguin. On the other hand, tolerance, dependence and avoidance are all relative. The levels of sea ice seen during the LGM were extreme, and so may have simply exceeded the optimum for Adélies, which may still be much higher than the optimum for other species, like the king penguin (Younger et al. 2015a). This idea of a threshold effect, with species-specific optima, could help explain why the penguins' demographic histories seem to have become less consistent (while being overall more stable) during the Holocene after have been being so strikingly similar over the previous ~25,000 years of more extreme climate.

While this chapter contains the first quantitative comparisons of penguins' demographic histories, there are at least two comparable analyses in the literature involving qualitative comparisons of penguin demographic histories. The first was by Cristofari et al. (2018), who also described striking contrast between the stable demographic history of emperor penguins and the dynamic, apparently glacially-influenced demographic history of king penguins. Vianna et al. (2020) also compared the demographic histories of numerous penguin species, using PSMC. Their results suggested a completely opposite pattern, appearing to link emperor with chinstrap and king with Adélie based on the past one million years of their demographic histories. It is not intuitive how these groupings could be explained ecologically. However, PSMC estimates are known to be unreliable within the past ~1000 generations of a species' history (Li and Durbin 2011), which would suggest that the results of Vianna et al.'s analysis as they pertain to the LGM are likely not as reliable as the results of Stairway Plot and other methods based on the SFS.

Pinnipeds

Among the pinniped populations considered here, at least three broad types of demographic history seem to be represented. These were referred to in the results as Groups 1-3 (Figure 4.27). In terms of qualitative features, or shape, of their demographic histories, Group 2 species generally exhibited an ancient (~50-100 kya) decline phase, followed by a growth phase, followed by a recent decline phase, each with similar levels of support. Group 3 species exhibited almost the opposite pattern, with a decline phase (~50-150 kya in *E. barbatus*) followed by more recent growth. Group 1 species were less consistent on the whole, but most showed a single growth phase, flanked by stasis or slight decline. *A. forsteri* and *A. gazella* were the most coordinated, with both also showing recent (Holocene) decline, while the Brazilian *A. australis* population showed recent growth. More specifically, *A. gazella* and *A. forsteri* populations appear to have declined somewhat ~2-5 kya. Both species are strongly generalistic in their diet, and likely respond to changes in overall ocean productivity, although the New Zealand fur seal has a more localised distribution and coastal foraging niche in contrast to the circumpolar distribution of the Antarctic fur seal. Notably, *O. flavescens*, as discussed in the previous chapter, also features a dip in N_e ~2-5 kya. Numerous palaeoclimate proxies suggest that the global climate temporarily became cooler around 4.2 kya, and this is recognised as the boundary between the middle and late Holocene (Walker et al. 2012). The effect on other climatic variables, such as humidity and sedimentation, seems to have varied regionally. However, evidence from Australia and South America suggest a strengthening of the El Niño Southern Oscillation (ENSO) during this period. Modern El Niño events have been well documented to cause extremely high pup mortality in *O. flavescens* due to reduced prey availability (e.g. Soto et al. 2004; de Oliveira et al. 2012). This could explain the mid-late Holocene dips observed in all three of these species. However, while *O. flavescens* quickly recovered from this dip to its previous population size, the fur seals seem to have only partially covered, ultimately stabilising at a lower stable population size during the late Holocene. It is possible that this recent phase reflects the history of intense human hunting of (and competition with) fur seals (e.g. Boyd 2004).

Although MDS does not quantify components of variation like PCA, it is clear by eye that the most general feature distinguishing the histories of pinniped populations belonging to Group 1 from Group 2 and Group 3 was a lack of well-supported (i.e. high absolute value of composite slope) decline phases (Figure 4.23). In contrast, all the Group 2 and Group 3 pinnipeds have decline phases with composite slopes below -0.5, which apparently extended for tens of

thousands of years in some species (Figures 4.24-4.25). Another factor distinguishing Group 1 from Groups 2 and 3 was timing. For example, the demographic histories of *O. flavescens* and *A. forsteri* appear qualitatively similar, but the RER required to align the peak growth phase in *O. flavescens* with that of *A. forsteri* would be a factor of ~5, far higher than is required to align it to other the other Group 2 species. Even if an RERrange of 5 were tolerated to align the peak growth phases, the other features of the curves – ancient and recent decline – would be misaligned (not shown).

Demographic histories are likely to be shaped by the combination of environmental exposures (e.g. glaciation within historical geographic range) and ecological dependencies (e.g. diet, habitat requirements). However, the biological significance of these groups of pinniped demographic histories is not obvious; the combination of factors must be complex and subtle. For example, both Group 1 and Group 3 included a species that breeds on ice and specialises in diving for their food (*L. weddellii* and *E. barbatus*; Casaux et al. 2006; Kovacs 2018).

Although diet is potentially a very important factor, and seems to have been very influential over at least the Holocene demographic history of *O. flavescens* as shown in Chapter 3, information on diet is lacking for many of the other species considered here. What information is available tends to show just how flexible their diets are, with more specialisation at the level of individuals than species (e.g. *L. weddellii*: Casaux et al. 2006; *O. flavescens*: Baylis et al. 2015; *A. forsteri*: Hume et al. 2004; multiple species: Franco-Trecu et al. 2022). The variety of historical patterns observed among these pinnipeds, even within Group 1, is potentially reflective of that. Dietary specialism can be difficult to define for a species, and may simply not be useful, especially amid significant individual and temporal variation in diet. For example, modern Adélie penguins feed primarily on krill, to the extent that, in the absence of historical data, Adélies as a species might be classified as krill-specialists. However, stable isotope analysis of ancient Adélie egg shells suggests that this is a recent development, most likely owing to the anthropogenic decline of competitors, such as baleen whales and seals. Prior to ~200 ybp, fish apparently constituted a much larger proportion of the Adélie penguin diet (Emslie and Patterson 2007). Here, I attempted to use marine foraging range as a very imprecise proxy for diet, reasoning that species that typically ventured into deep water (i.e. beyond continental shelves) to forage would likely have a more pelagic diet on average than species that tended to feed closer to shore. This factor was not found to be statistically significant, but it was the second strongest factor in terms of variance accounted for. More precise and methodologically consistent quantification of

species' diets seems promising to explore as a factor explaining similarities and differences across pinniped demographic histories. Diet could also be tested as a factor linking demographic histories across major taxa, such as sympatric pinnipeds and penguins.

Parental care strategy is another factor that could be explored to explain the observed distribution of demographic history differences. Although this seems very narrow on its face, the way that pinniped species have adapted to care for their offspring has probably been shaped by interactions between geography, diet, and phenotype (Schulz and Bowen 2005). Phylogenetic analysis by Schulz and Bowen (2005) and modelling by Stephens et al. (2014) has suggested that high food availability, and in particular, high seasonality of food availability, may drive the evolution of capital versus income breeding strategies in pinnipeds. This is because capital breeding requires mothers to stock up massive fat reserves period to breeding, that can sustain themselves and their pup for an adequate lactation period, without the mother needing to leave the pup to forage as they would under an income breeding strategy. These strategies exist on a continuum, related to traits such as duration of lactation, or offspring provisioning. A shorter lactation period is more energetically efficient in the context of a capital breeding because it means that less energy needs to go into sustaining the mother during the period when she is concentrating on giving her pup a head start and foraging less than usual or not at all (Stephens et al. 2014). It is also potentially safer for the mother and pup, considering that capital breeding may be associated with less stable environments (Schulz and Bowen 2005). Given these advantages, abbreviated lactation is a defining trait associated with capital breeding strategies. Here, I hypothesised that lactation time might be a key factor shaping different demographic histories of pinniped species due to its relationship with food availability and environmental seasonality. However, it was not statistically significant and also could not be disentangled from other traits distinguishing phocids and otariids (i.e. it is highly correlated with taxonomic family). This exploratory analysis was not ideal for testing the hypothesis, given the small number of species considered and underrepresentation of phocids (which tend to have short lactation times).

Ultimately, the only factor that emerged as statistically significant, and the one that accounted for the most variance, was latitude. The significance of latitude as a factor was mainly driven by the separation between the demographic histories of populations at its extremes (i.e. arctic and Antarctic). It makes sense that temperate-latitude species would have more varied demographic histories and would face more varied limiting factors to their populations. For one thing,

temperate environments are more varied, with different ecological pressures likely associated with each continent's coastline and shelf ecosystem. Temperate species considered here spanned the Atlantic and Pacific coasts of South America, the Pacific coast of North America, and the coastline of New Zealand (Table 4.3). Temperate-latitude species also typically exist within a more diverse ecosystem, with a wider range of food sources (e.g. Yurkowski et al. 2016), owing to higher mid-latitude productivity and diversity. While latitude was the most strongly supported of the factors considered, for the species and populations considered, it is not entirely satisfactory, accounting for about a quarter of the total variance in pinniped demographic histories and lacking a clear mechanistic explanation as might come with another factor, such as diet or lactation time.

Silverside fish

Six species of South American silverside fish were also considered in this study, including one Pacific freshwater species (*Odontesthes mauleanum*), one Pacific marine species (*O. regia*), one Atlantic marine species (*O. argentinensis*), and three Atlantic freshwater species (*O. ledae*, *O. bonariensis*, *O. mirinensis*). According to phylogeographic modelling by Hughes et al. (2020), the freshwater species most recently diverged from their marine counterparts on the same side of the continent. These oceanic and freshwater colonisation events are thought to have occurred at least one million years ago, while their Stairway Plots constructed for this study only extend back to ~30 kya, implying that inferred demographic histories of each species should be based on their present environment. However, the results indicate no systematic differences in demographic history between silverside species from different habitats or oceans. Their demographic histories are remarkably consistent, as all show evidence of growth between ~10-20 kya. One of the most significant impacts of the LGM on these silverside fish, given their coastal range, probably would have been the emergence of a large area of the continental shelf of Argentina due to lowered sea level (Ponce et al. 2011). However, this does not seem to have caused a split between the histories of Atlantic and Pacific species. An explanation for the silversides' universal population growth between the onset of the LGM to deglaciation could be the increase in terrigenous sedimentation which is known to have washed out from Patagonia (Noble et al. 2012), which could have stimulated primary production in the region's coastal waters.

Despite the lack of broad ecologically based differences, there were some subtle patterns that may have more idiosyncratic explanations. For example, *O. ledae* and *O. mirinensis* were most similar to each other, and in fact these species are known to have recently exchanged genes, calling into question their status as separate species (Hughes et al. 2020) (Figure 4.35). Similarly, evidence for weak introgression between *O. argentinensis* and *O. bonariensis* has been reported (Hughes et al. 2020), and *O. argentinensis* is thought to be basal to the Atlantic silverside radiation, which would imply a relatively close relationship to *O. mauleanum*.

Silverside fish are known to be preyed upon by South American pinnipeds and penguins (e.g. Hernández-Orts et al. 2019). The abundance of specialist predators might be expected to track the abundance of their prey, both in the short term (e.g. arctic hare cycle; Krebs et al. 2017) and long term. In turn, the prey may be affected by other environmental variables (e.g. krill and sea ice; Brierley et al. 2002). This is part of the explanation for why the distribution and abundance of marine predators is thought to be so influenced by marine fronts; they are generally too large to be strongly affected by the accompanying changes in temperature and salinity, but their prey are not (Bost et al. 2009). In this case, although silverside fish are part of the diet of most South American pinnipeds, the pinnipeds have highly flexible diets, so they should not necessarily track silverside abundance unless silverside abundance is indicative of overall ocean productivity, which there is no particular reason to expect.

When the demographic histories of the silversides were compared with those of four potential pinniped predators from the vicinity of South America, the results suggested a reasonably good fit with *O. flavescens* and *A. galapagoensis* (from pinniped Group 2), but not with *A. australis* or *Z. wollebaeki* (from Group 1) (Figures 4.35-4.36). However, it is impossible to say whether this similarity is related to a trophic relationship. It may simply result from the species occupying a similar region. Fitting the curves together also requires an RERrange of ~1.6, although that seems plausible given that the mutation rates for *Odontesthes* spp. were unknown and so their histories were simulated under a default (and likely on the fast end) vertebrate mutation rate (Nachman and Crowell 2000).

Potential applications, pitfalls, and next steps for comparative demographic history

For now, the main scientific application for comparative demography using align_stairwayplot.py is hypothesis-generation by looking to explain patterns of clustering among populations of

interest. If the range of populations is too broad, especially if their demographic history profiles are not very specific (i.e. have few distinguishing features), spurious associations are more likely. This approach is analogous to the commonly used NCBI BLAST tool for identifying similar DNA sequences. Querying the entire NCBI database with a single mitochondrial gene from *O. flavescens*, for example, would return many spurious hits from bacterial and environmental genomes. However, querying a longer, more distinctive sequence, or limiting BLAST to consider only sequences associated with pinnipeds, can allow a user to identify the source of their DNA sequence of interest to species level.

The main practical application of comparative demography, for conservation and welfare biology, would be identifying the environmental variables to which particular species are (at least historically) most sensitive in order to predict the effects of future ecological change. This is essentially an approach to identifying indicator species, but from the opposite direction. Common approaches involve predicting whether a specific species will be sensitive to a given environmental variable or process based on detailed knowledge of its ecology and biology (Ricotta et al. 2020), or based on the species' modern abundance and distribution. However, using the comparative demography approach, one could determine which species have experienced similar histories and attempt to explain them by looking at what characteristics those species have in common, and how they differ from other species with different histories.

Challenges in identifying true correlations among demographic histories

It may be difficult to distinguish true correlations between demographic histories from spurious ones, and vice versa. This is fundamentally due to uncertainty in the scaling parameters that must be assumed for demographic history reconstruction, including mutation rate, generation time, and the total number of observed alleles (including monomorphic). Not recognising this uncertainty in inputs, as well as outputs, of the demographic model, may lead to what is in fact a single demographic event shared among several populations being interpreted as multiple discrete events (e.g. Oaks 2020). On the other hand, acknowledging too much uncertainty, and translating it into flexibility in the analysis, could render discrete demographic events impossible to distinguish. This is especially problematic when demographic history curves display high autocorrelation, such that multiple alternative timings of a demographic feature (e.g. a population bottleneck and recovery) could align a pair of demographic history curves approximately equally well, as long as the requiring scaling parameters are deemed plausible.

Where possible, comparative demographic history studies should employ rates of mutation and generation estimated using similar methods across each species, or ideally inferred from the exact dataset or source population itself. This issue could benefit from systematic literature reviews quantifying the confidence intervals associated with mutation rate and generation time estimates by different methods and for different species.

Insufficient sample size is another potential reason that true correlations between populations' demographic histories may be difficult to detect. The temporal resolution of Stairway Plot or any other SFS-based method is strictly limited by the length of the SFS vector (i.e. the number of different allele frequency classes), which is determined by the number of individuals in a population sample. If the sample size is too low, it may be mathematically impossible for models to infer an adequate summary of a population's history. However, this is unlikely to be a major issue unless a very small sample size (i.e. <10) is depended upon to infer a very complex demographic history (Bhaskar and Song 2014; Lapierre et al. 2017). In the analysis of simulated populations, I found that sample sizes down to 10 individuals did not affect clustering with align_stairwayplot.py at all (Figures 4.2-4.3). The models tested were relatively simple, though not exceptionally so compared to some of the demographic histories inferred for natural populations. Still, it should be considered that SFS-based methods may struggle to reconstruct more complex demographic models with small sample sizes.

One mitigating factor is that the way Stairway Plot identifies historical breakpoints means that additional epochs that are only identified with larger samples are likely to be ones that receive less support (i.e. appear in a smaller proportion of models and/or are associated with smaller changes in Ne) and therefore contribute less to clustering with align_stairwayplot.py. This would be more of an issue if missing one breakpoint/epoch led to incorrect estimation of the timing of another epoch, e.g. because two smaller episodes of demographic change were combined into a single one at an intermediate time.

The single largest concern about small sample sizes (of N>=10) is that a small sample may be more strongly affected by rare mistakes and sampling biases. Stairway plot, like all methods for inferring demographic history, assumes that the genetic sample is representative of a panmictic population. Excessive sampling of close relatives, for example, would violate this assumption and skew the estimated frequency of alleles (e.g. potentially identifying rare alleles as moderately common). This can happen with any sample size, but a smaller sample is more

sensitive to a given number of mistakes. Align_stairwayplot.py could potentially be used to validate population samples for demographic history analysis by running Stairway Plot on a handful (e.g. 10) of random subsamples equal to some fraction (e.g. 0.5x) of total sample size, and then quantifying the average pairwise distance among these Stairway Plot replicates as a metric of the sample's robustness. Although the subsampling was not random, this is similar to within-species comparisons of pinniped and penguin populations done in this chapter (penguins: Figures 4.8-4.13; pinnipeds: Figures 4.17-4.20). These analyses found a surprisingly good level of consistency, even with subsample sample sizes as low as six individuals. However, no minimum standard was established.

Another issue is that it is unclear what maximum level of gene flow between geographically distinct populations should qualify them as distinct for purposes of comparative demographic history. This is important both for determining which individual samples should be grouped together for accurate demographic history reconstruction, and for applying fair statistical tests to the results of align_stairwayplot.py by determining which populations' histories should be considered statistically independent data points. Taking any significant F_{st} as determining that populations should be analysed separately may be too aggressive, considering that allele frequency differences can develop over a very short timeframe, and so the populations' demographic histories may be similar not only due to ecological similarity but actual shared genetic history. A better, but much more time-consuming approach could be to estimate divergence time (or find estimates in the literature) and combine populations with estimated divergence times more recent than the earliest time point considered in the comparative analysis (e.g. 200 kya). This question could benefit from simulation studies to better understand the effect of minor or recent genetic divergence (i.e. low F_{st}) on demographic histories inferred based on the SFS.

As whole-genome sequencing becomes more affordable so population-scale resequencing project more common, and computational methods are developed to compensate for low depth of coverage (Lou et al. 2021), tools like SMC++ (Terhorst et al. 2017) are likely to see wider use for inferring demographic histories. SMC++ utilises the information from both recombination graphs and the SFS, combining the advantages of SFS-based methods in inference of recent history with the advantages of SMC-based methods in inference of deep history (Patton et al. 2019). This will ultimately lead to more accurate demographic history models and therefore a greater ability to distinguish true correlations among demographic histories.

A promising program for explicitly testing hypotheses of shared demographic history is multi-dice (Xue and Hickerson 2017), which uses the aggregate allele frequency spectrum (aSFS) of multiple populations to test for simultaneous demographic “pulses”. Cole et al. (2019) applied multi-dice to test for a concerted post-LGM population expansion in penguin species. Multi-dice requires the user to know in advance that a set of populations exhibit similar demographic histories, so it cannot fulfil the same exploratory role as something like align_stairwayplot.py can in conjunction with model-independent tools like Stairway Plot (or others, e.g. PSMC). However, even in this role, a tool like multidice could be potentially useful for statistically validating relationships suggested by an initial align_stairwayplot.py analysis.

Challenges in identifying factors associated with correlated demographic histories

Assuming that correlations among demographic histories can be accurately identified, the next challenge is to determine the ecological, biological, or geographical factors associated with them. This is complicated somewhat by the difference between census population size (N_c) and effective population size (N_e), where apparent N_e excursions can be caused by things such as changes in population structure, not only changes in population size (Mazet et al. 2016).
For purely comparative purposes, the fact that coalescent-based models cannot distinguish between changes in population size and population structure may not be very important because both processes represent meaningful information about what has happened to a species, and the same combination of processes may or may not have occurred to other similar (e.g. sympatric or related) species, potentially determining whether their demographic histories cluster together. For example, in many species, the LGM caused both population declines and subdivision of populations into refugia. A regional drought might similarly reduce population size and increase subdivision in many species occupying the same region, e.g. by concentrating them around water sources or reducing the energy they can afford to spend on dispersal. However, while the same combinations of processes may lead to recognisably similar results and keep populations correctly clustered together, it would be impossible to assess the relative amount of population decline or subdivision. Moreover, because the effects of population subdivision are not necessarily additive with population decline (for example), a set of populations that experienced both population decline and population subdivision may not be more similar to populations that only experienced population decline than to populations that experienced neither process. Ideally, population size and structure could be mostly disentangled

prior to analysis by being relatively conservative in the grouping of individuals into populations for demographic analysis, considering factors like estimated divergence time as suggested above.

In the present analyses, MDS and non-parametric PERMANOVA were used to identify distinct clusters of historically similar pinniped species, and a linear model was then used to assess the contribution of taxonomy versus life history trait (lactation duration) to determining cluster assignment. Given plentiful data on the ecology and life history of all populations, one could potentially use redundancy analysis (RDA) or latent factor mixed model (LFMM) (Frichot et al. 2013) to test for associations with a range of traits simultaneously, and with reference to specific time points. Normally, LFMM would be performed using a genotype matrix indicating the number of each allele present at each locus in each individual. The “composite slope” values calculated by align_stairwayplot.py could be coded in a similar manner, with growth and decline coded as alternative alleles and a heterozygous state representing stasis, at loci representing historical time points, and populations replacing individuals. This demographic history-based “genotype” matrix could then be fed into the same analyses. However, this approach would not be able to take advantage of ‘RERrange’ optimization for each population.

A known weakness of the indicator species concept is the difficulty in disentangling causation from mere correlation (Fleming et al. 2020). Causal relationships are not the only ones of interest, but an understanding of causation is important for determining how robust a particular correlation is likely to be in other environmental contexts, such as under climate change. For example, the paradigm that ice coverage *per se* is of singular importance to the demographic prospects of sub-Antarctic penguins might lead to surprise at the fact that chinstrap penguins have been on the decline in recent decades despite receding Antarctic ice, most likely due to declining abundance of krill, because krill depend on winter sea ice as a nursery for juveniles (Trivelpiece et al. 2011). In other words, although ice-free breeding habitat is important to chinstrap penguins, ice per se is not necessarily their most important demographic driver, and too little ice can begin to exert opposite effects. The comparative study of demographic histories could help address this issue of the robustness of ecological sensitivities and indicators by detecting such changes over time and relating them to threshold models of habitat suitability (Fordham et al. 2016; Cristofari et al. 2018; Hecht et al. 2020).

Chapter 5: Synthesis and conclusions

The first and most direct question to be addressed by this thesis was to do with the historical population dynamics of South American sea lions (*O. flavescens*) and Magellanic penguins (*S. magellanicus*) in Patagonia. A more general objective was to understand how consistent inferences of demographic history are within and between species. Understanding the level of consistency that may be found at different scales is interesting in its own right, but is also important for determining how surprised we should be if two populations do or do not exhibit similar demographic histories, and therefore whether a special explanation is warranted. One general issue encountered in this thesis was uncertainty about populations' evolutionary rates (mainly mutation rate/generation time), which are required to scale inferences of demographic history from mutational units into absolute time. This will be addressed as it comes up below. The ultimate purpose of reconstructing and comparing demographic histories is to understand the causes behind historical shifts. Such an understanding could facilitate prediction of population trends under future scenarios, including climate change, fishing, or even more intentional and positive interventions to improve the resilience and total welfare of populations.

Historical population dynamics of Patagonian marine predators

Otaria flavescens

The first and most direct question to be addressed by this thesis was to do with the historical population dynamics of South American sea lions (*O. flavescens*) and Magellanic penguins (*S. magellanicus*) in Patagonia. Analyses of the population structure of *O. flavescens* presented in Chapter 2 revealed abundant evidence for both local and regional-scale differentiation in the mtDNA, but no evidence of population structure within Argentina based on nuclear DNA markers. These results confirm the consensus that has emerged from all previous studies of Patagonian *O. flavescens*, but also extends and adds some nuance to this view. Previous studies have been limited to fragments of the mitochondrial genome (the cytochrome *b* gene [Tunez et al. 2007] or hypervariable D-loop region [Tunez et al. 2010; Feijoo et al. 2011; Oliveira et al. 2017]) and a handful of nuclear microsatellite loci (Feijoo et al. 2011; Oliveira et al. 2017), but this thesis presented the first sequences of the full mitochondrial genome for *O. flavescens*, and a substantial SNP dataset (2497 biallelic SNPs after filtering) derived by ddRADseq. These

analyses offered significantly greater power to genetically distinguish individuals compared to previous markers, which contained fewer variable sites/loci (e.g. mitochondrial D-loop: 39 sites, mitogenome: 154 sites; microsatellites: 10 loci [Oliveira et al. 2017], RADseq: 2497 SNPs). Consequently, the continued lack of evidence for nuclear genomic structure among colonies and regions of Argentina is all the more striking, and all the more convincing that it reflects a true approximation of nuclear panmixia among Argentine *O. flavescens* and not merely a lack of data.

That being said, the present RADseq dataset could certainly be improved. Rarefaction curves suggested that the number of individuals in the dataset was not sufficient to capture all of the segregating sites that could be detected given the number of loci sequenced (Figure 2.4). This was particularly true as one looks to southern Patagonia. At the southern tip of the continent – Tierra del Fuego – Peralta et al. (2021) recently provided evidence of weak gene flow between the Atlantic and Pacific lineages of *O. flavescens*. Previous work has shown that, despite the lack of within-lineage nuclear genetic structure, these oceanic lineages are distinguishable, even with microsatellites (Oliveira et al. 2017). ddRAD or even whole-genome sequencing of the samples used by Peralta et al. (2021), for example, still has the potential to identify genetic differentiation between northern and southern Patagonia, perhaps driven by a trickle of gene flow from the Pacific. A powerful nuclear dataset might even reveal that the rate of inter-oceanic gene flow is much higher than reported by Peralta et al. (2021) based on mtDNA, considering that the maternally inherited mtDNA haplotypes are thought to be less mobile in *O. flavescens* due to female philopatry (Oliveira et al. 2017).

The sequencing of full mitogenomes, and with it the increased ability to distinguish individuals and quantify the similarity of their haplotypes, added a new dimension to the understanding of matrilineal structure in Argentine *O. flavescens*. It showed that although groups of closely related mitogenome haplotypes (haplogroups) occur at different frequencies in different regions (i.e. moderate and significant F_{st}), the average similarity among haplotypes within regions was not higher than across the population as a whole (i.e. low and non-significant Φ_{st}). Because regional frequencies of established haplogroups can diverge by genetic drift much faster than new haplogroups become established by mutation and drift, this suggests that the regional matrilineal structure is quite shallow, perhaps because it is recently developed.

The demographic history of *O. flavescens* indicates a potential mechanism for the only recent emergence of regional structure. The results for *O. flavescens* indicated that the Patagonian population had recently grown by approximately a factor of five, within the last 2-4 thousand years. This recent expansion was indicated by both Stairway Plot analysis of SNPs and EBSP analysis of a mtDNA alignment using a mutation rate calibrated with ancient DNA. The Stairway Plot reveals deeper history, indicating that this recent growth followed a short-lived bottleneck from ~4-8 kya, and that the population had also experienced a ~15-fold expansion ~30 kya. Previous studies have also proposed that *O. flavescens* recently expanded from a bottleneck, with estimates of the timing ranging from ~110 kya (Tunez 2007) to ~64 kya (Tunez 2010) to ~25 kya (Feijoo 2011) to ~10 kya (Oliveira 2017) based on different methods. In the context of previous estimates, the new estimate suggests that other methods, with less temporal resolution, may have been detecting different events, or even combining the signal from both events into a single Frankenstein estimate.

If matrilineal population structure has only been (re)established since the apparent bottleneck(s), that may explain the shallowness of the regional differentiation. Although differentiation of mtDNA haplogroup frequencies has progressed, most of these haplogroups were probably common before the bottleneck(s). With the passage of time, further drift in haplogroup frequencies and the creation of new haplotypes by mutation would be expected to bring mitochondrial Φ_{st} up towards F_{st}, assuming the fundamentals of the population remain the same. A similar interpretation of the discrepancy between F_{st} and Φ_{st} was made by Bohonak et al. (2006) in relation to populations of freshwater copepods (*Eudiaptomus graciloides* and *E. gracilis*) that underwent population expansions at different times. *E. gracilis* expanded longer ago and its Φ_{st} is now similar to F_{st}, while Φ_{st} is much lower in the more recently expanded *E. graciloides*.

Spheniscus magellanicus

The demographic history of *S. magellanicus* was previously described by Dantas et al. (2018) using only modern samples. The novel inclusion of ancient DNA in the reconstruction of *S. magellanicus* demographic history did not change the overall shape of the inferred history relative to this previous study. However, the evolutionary rate calibration facilitated by ancient DNA did shift the history forward in time. Whereas Dantas et al. (2018) suggested that the population began to expand ~15 kya, the analysis in this thesis (Chapter 3) suggested that that

expansion began ~6 kya. This places it within the Holocene interglacial period, suggesting that it was not an immediate response to deglaciation at the end of the LGM. It also places the expansion within the timeframe for the most recent bottleneck and/or expansion of *O. flavescens*.

Comparability and consistency of demographic histories

Sympatric species

O. flavescens and *S. magellanicus* are extremely distantly related, but are nevertheless ecologically similar and sympatric. They breed on some of the same beaches in Patagonia and forage on or near the continental shelf. Their diets overlap, but their preferred food differs, with *S. magellanicus* preferring small pelagic fish, such as anchovies (Yorio et al. 2017; Castillo et al. 2019), while *O. flavescens* tend to be more generalist, consuming pelagic fish, but also more squid and benthic prey (Jarma et al. 2019) depending on the region. The demographic history analyses in Chapter 3 showed that both species' populations had expanded around the mid-to-late Holocene boundary (4.2 kya). However, the estimated timing of these expansions differed, with the most recent growth phase initiating ~2 kya in *O. flavescens* and ~5 kya in *S. magellanicus*, and the growth was also more dramatic in *S. magellanicus* (20x vs 5x). The mitochondrial mutation rate used for the *S. magellanicus* reconstruction was estimated directly from the data using ancient DNA, but the upper bound of the 95% confidence interval was approximately three times the lower bound. It would require a true mutation rate right at the upper bound to align the two species' growth phases. Of course, it is also possible that the rates used for *O. flavescens* were also not precisely accurate. However, the present alignment of both species' demographic histories with their stable isotope trends (discussed later) suggests that their assumed rates are not far from the truth. This would imply that, in these sympatric and ecologically similar species, the answer to whether their demographic histories are consistent with each other depends on timescale. Over the Holocene, yes; they both expanded. Their expansions may even have had the same ultimate causes, related to aridification and cooling around the mid-late Holocene. However, in detail, their expansions seem to have occurred at different times and with different immediate causes.

Populations of the same species

I developed a new program called 'align_stairwayplot.py' based on principles from some of my prior work (Hecht et al. 2018; Hecht et al. 2020) to quantitatively compare demographic history curves estimated by Stairway Plot 2, and also find their optimal alignment within an accepted range of uncertainty about their true evolutionary rates ("RERrange"). The results shown in Chapter 4 established that the program could, for the most part, correctly cluster populations belonging to the same species based on their demographic histories.

Simulated populations representing variants of one of three archetypal simulated histories (Table 4.1) were easily distinguishable when considered together. However, it was evident that the rate of population growth that took the simulated populations from one stable population state to another affected distinguishability. In the set of populations that used simulated growth rates over generations, as opposed to instantaneous changes in population size, there was much higher within-cluster variability, and some populations appeared to be more similar to those belonging to another group that theoretically had a different history.

The increased within-species variability of those simulated populations with more gradual population growth rates turned out to be more reflective of the variance among populations in natural species. Populations of the pinnipeds *Zalophus wollebaeki*, *Z. californicanus*, and *Arctocephalus forsteri* were also distinguishable on the whole; that is to say, intraspecific variation in demographic histories was significantly lower than interspecific variation on average. *A. forsteri* populations were completely distinct, all more similar to conspecific populations than to any *Zalophus* population. In contrast, a few populations of *Z. wollebaeki* clearly clustered with *Z. californicanus*. This is not necessarily surprising, because *Z. wollebaeki* and *Z. californicanus* are sister species, and *Z. wollebaeki* has even been considered a subspecies of *Z. californicanus*. Although genetic analysis of population structure has now led to their classification as distinct species (Wolf et al. 2008), it is likely that they recently exchanged genes or may continue to do so at low levels. Although not surprising, then, this result is still interesting as it suggests that recent introgression could potentially be recgonised by inconsistencies in populations' demographic histories as reconstructed from their genetics. The species boundary between *Z. californicanus* and *Z. wollebaeki* warrants more investigation using stronger genetic markers, and it would be interesting to see if the populations that were out of place in this analysis (Espanola and Genovesa) showed elevated rates of introgression.

Intraspecific consistency was also tested with the demographic histories of penguins. Emperor, Adélie, and chinstrap penguin populations were highly consistent amongst themselves. Gentoo penguin populations displayed much greater differences, though these variations were mostly unique and did not show greater similarity to another species, as the *Z. wollebaeki* populations had. This result was consistent with previous findings that all of the Arctic and sub-Antarctic penguin species considered here are nearly panmictic, but with the strongest evidence of population differentiation being for gentoo penguins, possibly due to their coastal foraging niche (Clucas et al. 2018). The king penguin also stood out in this analysis, with one population (Falklands/Crozet) initially clustering among the chinstrap penguins. It emerged that this population's demographic history was anti-correlated with that of the other two king penguin populations, and fit more comfortably with the other king penguin populations (though all were similar to the chinstrap populations) under RER rescaling. This analysis of penguin populations again brought up the potential for gene flow (or the lack thereof) to influence and be detectable in intraspecific comparisons of demographic history. It also highlighted the potential for populations to appear highly distinct from each other due to minor differences in scaling, especially when their demographic histories are relatively complex, as in the case of the king penguin.

Related species

The importance of taxonomic relatedness at approximately the family level was investigated in both penguins and pinnipeds by internally comparing the demographic histories of species of penguins (Spheniscidae), seals (Phocidae), and sea lions (Otariidae).

The shapes of the relatively recent (<50 kya) demographic histories of chinstrap, gentoo, king and Adelie penguins were found to be very similar, likely representing similar demographic responses to the same historical events. These events and responses most plausibly correspond to decline around the LGM and post-glacial (early Holocene) growth, which has been proposed by previous studies (e.g. Trucchi et al. 2014; Cristofari et al. 2018; Clucas et al. 2018; Cole et al. 2019). However, profound uncertainty about the nuclear genomic mutation rate of penguins makes it difficult to pin down an absolute timeline (Cristofari et al. 2018).

Most Otariid pinnipeds clustered close together, but *O. flavescens* and *A. galapagoensis* formed a distinct pair. Phocids were much more individually variable, with no clusters as distinct as the

two sets of Otariids. Therefore, membership in either family clearly did not determine a species' demographic history and demographic history was not sufficient to diagnose family membership, though demographic histories did seem to take one of only two broad forms among the Otariidae considered here.

Disparate taxa

Consistency of demographic histories was also tested across disparate taxa, including pinnipeds, penguins, and silverside fish (*Odontesthes* spp.). At this scale, there may be so many complex synergies between different aspects of phenotype, behaviour and habitat/range that it would require much deeper investigation to identify causes of similarity and difference among demographic histories.

When the demographic histories of pinnipeds and penguins were compared, all five penguin species formed a single distinct cluster, and the previously identified groups of pinniped species also remained distinct. This analysis confirmed the impression that there is much less variation among penguin demographic histories than among pinniped demographic histories, at least of those considered in this study. It was also notable that the variability within the groups did not interact; that is to say, while penguin species' histories varied, they did not vary in ways that made them especially more similar to certain pinnipeds, and vice versa.

In contrast, when a subset of four pinnipeds (potential predators of South American silverside fish) were compared with silverside fish (*Odontesthes* spp.), two of the pinnipeds – *O. flavescens* and *A. galapagoensis* – were drawn away from the other two pinnipeds towards the cluster of fish. Whether by cause or coincidence, the demographic histories of these two species more closely resembled that of the typical silverside fish than of *A. australis* or *Z. wollebaeki*.

Ecological drivers of population dynamics

Diet

The impact of diet as a potential driver of population dynamics was investigated in the most detail with *O. flavescens* and *S. magellanicus*. Stable isotope analysis of the two species confirmed that their modern isotopic niches are distinct, though similar. On average, *O.*

flavescens samples were slightly higher in δ15N, suggesting that they feed at a higher trophic level. They were also higher in δ13C, suggesting that they partake of a more benthic diet. Correlation between the age and latitude of samples made it impossible to fully disentangle the impacts of these two factors on the species' isotopic histories, but it was clear that there had been change between the past and the present mean isotopic composition of samples from both species. The most historically dynamic isotopes were δ15N in *O. flavescens* and δ13C in *S. magellanicus*, which both exhibited similar patterns, interpretable as either declining values in the north and increasing values in the south, or as population-wide decline then increase (*O. flavescens* δ15N) and population-wide increase (*S. magellanicus* δ13C).

These isotopes – δ15N in *O. flavescens* and δ13C in *S. magellanicus* – also correlated with the demographic history of the respective species. Over the past 7000 years, the effective size (N_e) of the *O. flavescens* population has apparently been inversely related to its average δ15N. Meanwhile, over the past ~6000 years, the N_e of *S. magellanicus* has been positively correlated with the population's average δ13C. The causes of these relationships are not clear, but both could be related to a decline in relative sea level that occurred in the area beginning ~6 kya, and a global mid-latitude aridification event ~4.2 kya. This would have increased the accessibility of deeper-water prey on the continental shelf, such as benthic crustaceans or demersal fish, which, respectively, could account for *O. flavescens*' apparent decrease in trophic level and *S. magellanicus*' apparent increase in demersal-benthic feeding (but without an accompanying change in trophic level) (Cherel and Hobson 2007; Woodland and Secor 2013).

As discussed earlier with respect to the similar dynamics of these species, scale may be important to consider. The results suggest that Holocene fluctuations in their demographic histories have paralleled changes in diet, but we cannot currently know whether this pattern would have held over a longer timescale or during a less moderate climate period than the Holocene. Among the penguins and pinnipeds considered in Chapter 4, diet did not seem to be an important determinant in the overall similarity of their demographic histories on a timescale of tens of thousands of years, although it was not evaluated explicitly. A detailed study considering isotopic change in samples over time in parallel to their genetics, as was done In Chapter 3 for *O. flavescens* and *S. magellanicus*, may be required to address this question properly given the potential for diet flexibility. Most pinniped species are highly generalist, consuming fish, cephalopods and crustaceans from both pelagic and demersal-benthic contexts. However, a few of the species considered specialised in benthic foraging (though this was still not their

exclusive diet), including *M. angustirostris*, *M. leonina*, and *L. weddellii*. The latter two species had relatively similar demographic histories, but they were very different from that of *M. angustirostris*. Among penguins, the emperor penguin and king penguin (genus *Aptenodytes*) could both be regarded as pelagic fish-specialists in comparison to the krill-specialist chinstrap penguin and generalist gentoo penguin (Adams and Klages 1987; Polito et al. 2015). However, the demographic histories of the king and emperor penguins were not especially similar. Obviously, diet is of ultimate importance in the sense that food must be consumed to support survival and reproduction. However, it may be that, at the timescale considered, with the temporal resolution provided by Stairway Plot at that timescale, and the large-scale environmental changes such as the LGM that seem to dominate the demographic history of these penguins, precise dietary needs may not be important at the margin relative to overall habitat productivity and other requirements.

Habitat requirements and geography

The one factor that did seem to account for some difference among penguin demographic histories, despite the relatively little overall variation among them, was whether a species was considered “ice-avoiding” (gentoo, king, chinstrap) or “ice-dependent” (Adélie, emperor) (Trivelpiece et al. 2011; Lynch et al. 2012; Cristofari et al. 2018). Adélie penguins, a continental Antarctic species, are classified as ice-dependent based on their needs relative to the modern environment, in contrast to the ice-avoiding sub-Antarctic penguins (Trivelpiece et al. 2011). Adélies depend on sea ice for foraging, but also require ice-free breeding sites. Too much sea ice surrounding their colonies can obstruct access to the open ocean from their breeding sites. The net effect is a tolerance range of between 15-80% local sea ice cover (Emmerson et al. 2011; Younger et al. 2015a). That Adélies seem to have responded similarly to king penguins and others to the greatly expanded sea ice of the LGM reflects the fact that even this tolerance range was exceeded. Emperor penguins were the species that stood out the most, likely reflecting the fact that they breed on sea ice and may have effectively unlimited tolerance for it over the long-term, since they can shift the locations of their breeding colonies over time to follow the sea ice edge. The more stable demographic history inferred for emperor penguins was consistent with previous studies, including Cristofari et al. (2018) using different samples from different emperor penguin colonies. Interpretation of the true consistency of penguin demographic responses was limited by the omission of important penguin groups, including the genera *Spheniscus* and *Eudyptes*, from this analysis due to a lack of comparable genomic data.

Although the Holocene demographic history of *S. magellanicus* was considered in detail, its response to the LGM remains uncertain. It seems likely that they and other penguin species already living north of the LGM sea-ice limit would have been less affected (Cole et al. 2019), although the previous study by Dantas et al. (2018) had placed the expansion *S. magellanicus* at ~15 kya, matching the expansion of Adélie penguins presented by Younger et al. (2015b).

There was little variation in breeding habitat requirements among the pinniped species considered, with only *E. barbatus*, *P. hispida*, and *L. weddellii* preferring to breed on ice platforms as opposed to barren beaches. However, geography in terms of latitude emerged as the most significant predictor of similarity among pinniped demographic histories. This was mainly driven by differentiation of northern/arctic and southern/Antarctic populations' demographic histories, while mid-latitude populations overlapped both groups. It is not surprising that demographic histories would vary with latitude, since latitude covaries with climate and also reflects simple geographic distance between populations, with populations that are more distant from each other naturally being less likely to face the same demographic pressures. However, it is somewhat surprising that basic latitude and not the absolute value of latitude – i.e. how close a population is to one of the Earth's poles – is what was significant, since the poles are more similar to each other in terms of climate than they are to the tropics of their respective hemisphere. The comparative demographic analyses presented here are not sufficient to draw any firm conclusions, but this result may suggest that it is not latitude per se, but geographic distance that predicts differentiation in pinniped demographic histories.

Life history

The final ecological factor considered was life history. This was specifically tested across pinnipeds, as some pinniped species are known for defining the extremes of "capital breeding" strategies, where females gain as much body fat as possible prior to giving birth and nurse their pups on milk produced mainly from these prior foraging excursions. In contrast, income breeders continue to make foraging excursions to sustain themselves and their young pups. The duration of the nursing period of pup dependency (lactation) has been used as a proxy for this spectrum of breeding strategy. This is because capital breeders are expected to evolve to shorten the period of lactation in order to minimize maternal overhead and thereby the amount of energy that goes to sustaining the mother while she is not foraging, as opposed to accelerating the growth of the pup (Schulz and Bowen 2005; Stephens et al. 2014).

Although the specific resource requirements of capital and income breeding species may vary, capital breeding is thought to be an adaptive strategy to cope with extreme seasonality in resource availability. Similar ideas about seasonality and other forms of habitat stability have been proposed to explain other life history trade-offs (Healy et al. 2019). It is easy to imagine how such a strategy of "putting all their pups in one season", so to speak, while more efficient in good times, could cause a population to be more vulnerable to ecological disturbances, resulting in different long-term demographic histories. However, among the pinnipeds considered here, no statistically significant relationship was found between lactation time or taxonomic family (which is highly correlated with lactation time, otariids tending to be income breeders) and the similarity of species' demographic histories.

Concluding remarks

Beyond the focal system of Patagonian pinnipeds and penguins, this thesis has contributed to understanding how ecological traits and dependencies shape populations' responses to environmental change, and how reliably we can compare populations' demographic histories to answer that question more thoroughly in other systems. The results highlight the potential of combining species-specific ecological data with demographic history to better understand both broad similarities in deep history, across groups of species (Chapter 4), and the potentially more idiosyncratic drivers of recent demographic history in individual species (Chapter 3). The thesis also echoes the importance of understanding population structure as context for understanding a species' past demography (Chapter 2).

Appendix A: Sample metadata tables

This appendix includes three tables of metadata (and stable isotope values where available) for *O. flavescens* samples novel to this study (Table A.1), *S. magellanicus* samples novel to this study (Table A.2), and samples belonging to either species, whose mtDNA sequence was obtained from previous publications (Table A.3). Whether a sample was included in a given genetic dataset is given as true (T) or false (F). NA indicates that information is "not available".

All physical samples, listed in Tables AA.1 and AA.2, were obtained from Argentinian collaborators. All archaeological samples and most modern tissue samples came via Enrique Alberto Crespo and Rocío Loizaga de Castro at Laboratorio de Mamíferos Marinos, Centro para el Estudio de los Sistemas Marinos (CENPAT-CONICET). For each archaeological sample, the original researcher(s) involved are credited in the tables below, where specific individuals are known. No information was available to us or our Argentinian collaborators concerning the collection date of the archaeological samples. Additional modern tissue samples came from Claudio Campagna (Wildlife Conservation Society).

Published genetic data accession numbers for NCBI are given in Table A.3 (mtDNA sequences used in Chapters 2 and 3) and Table A.4 (RADseq reads used in Chapter 4).

Table A.1. All samples of *Otaria flavescens* processed for this study. Note that ancient (i.e. Age>0) samples were not included in any genetic analyses from Chapter 2, but a "T" indicates that they were used in Chapter 3.

Sample ID	Sample type	Age (ybp)	Latitude (°)	Longitude (°)	δ15N	δ13C	δ34S	145-bp alignment	409-bp alignment	mitogenome alignment	RADseq	Collection date	Source
LO-502	Bone	7000	-39	-61.4	27.61	-16.01	NA	F	F	F	F	NA	G. Politis, C. Bayón
LO-S1-209	Bone	7000	-39	-61.4	24.75	-15.31	12.59	F	F	F	F	NA	G. Politis, C. Bayón

LA1300	Bone	7000	-39	-61.4	27.46	-16.01	NA	F	F	F	F	NA	G. Politis, C. Bayón
BLD1323	Bone	7000	-39	-61.3	NA	NA	NA	T	F	F	F	NA	G. Politis, C. Bayón
BLD1868	Bone	7000	-39	-61.3	23.02	-16.52	NA	T	F	F	F	NA	G. Politis, C. Bayón
LA2971	Bone	3520	-41.4	-64.5	21.32	-15.28	NA	T	F	F	F	NA	F. Borella
LA1150	Bone	2910	-41.4	-64.5	25.05	-10.63	13.83	T	F	F	F	NA	F. Borella
PF176/69	Bone	2000	-39	-61.4	21.80	-15.11	14.47	F	F	F	F	NA	R. Frontini, C. Bayón
LA1344	Bone	1680	-41.5	-65	25.08	-12.17	12.42	F	F	F	F	NA	F. Borella
LA3039	Bone	1638	-41.4	-64.5	25.31	-11.56	14.68	T	F	F	F	NA	F. Borella
LA1152	Bone	1380	-40.8	-64.7	22.46	-14.38	NA	F	F	F	F	NA	F. Borella
LA1335	Bone	1256	-52.3	-68.4	24.69	-11.37	14.82	T	F	F	F	NA	J.B. Belardi
LA1338	Bone	1256	-52.3	-68.4	19.65	-17.90	NA	T	F	F	F	NA	J.B. Belardi
LA1333	Bone	1256	-52.3	-68.4	20.82	-17.59	15.21	F	F	F	F	NA	J.B. Belardi
LA1337	Bone	1256	-52.3	-68.4	17.84	-17.77	13.84	F	F	F	F	NA	J.B. Belardi
LA1331	Bone	1190	-52.3	-68.4	21.53	-15.41	15.19	T	F	F	F	NA	L. Borrero
LA1330	Bone	1190	-52.3	-68.4	18.89	-16.36	NA	F	F	F	F	NA	L. Borrero
LA563	Bone	580	-54.9	-67.9	22.45	-17.32	NA	F	F	F	F	NA	L. Orquera, E. Piana,

													P. Zangrando
LA564	Bone	580	-54.9	-67.9	19.06	-12.16	14.09	T	F	F	F	NA	L. Orquera, E. Piana, P. Zangrando
LA565	Bone	580	-54.9	-67.9	19.24	-12.85	13.85	F	F	F	F	NA	L. Orquera, E. Piana, P. Zangrando
LA572	Bone	580	-54.9	-67.9	18.20	-12.92	14.10	T	F	F	F	NA	L. Orquera, E. Piana, P. Zangrando
LA577	Bone	580	-54.9	-67.9	17.96	-12.71	13.53	T	F	F	F	NA	L. Orquera, E. Piana, P. Zangrando
OF800	Tissue	0	-40.7	-65	19.18	-17.00	NA	T	T	T	T	20/06/2006	E.A. Crespo, R. Loizaga de Castro
OF990	Tissue	0	-40.8	-65	18.63	-18.10	NA	T	T	T	T	02/01/2012	E.A. Crespo, R. Loizaga de Castro
OF996	Tissue	0	-40.8	-64.9	17.89	-19.02	NA	F	F	F	T	28/05/2010	E.A. Crespo, R. Loizaga de Castro
OF949	Tissue	0	-40.8	-65	18.91	-19.08	NA	T	T	T	T	09/05/2008	E.A. Crespo, R. Loizaga de Castro
OF984	Tissue	0	-40.8	-65.1	19.80	-18.67	NA	F	F	F	T	16/08/2010	E.A. Crespo, R. Loizaga de Castro

OF969	Tissue	0	-40.9	-64.4	20.18	-17.78	NA	F	F	F	T	28/08/2008	E.A. Crespo, R. Loizaga de Castro
OF950	Tissue	0	-40.9	-64.8	20.66	-17.72	NA	T	T	T	T	24/05/2008	E.A. Crespo, R. Loizaga de Castro
OF943	Tissue	0	-41	-65	18.58	-17.49	NA	T	T	T	T	05/11/2007	E.A. Crespo, R. Loizaga de Castro
OF817	Tissue	0	-41	-64.9	NA	NA	NA	T	T	T	T	18/09/2006	E.A. Crespo, R. Loizaga de Castro
OF801	Tissue	0	-41	-64.1	19.56	-18.09	NA	F	F	F	T	18/07/2006	E.A. Crespo, R. Loizaga de Castro
OF935	Tissue	0	-41	-64.1	NA	NA	NA	T	T	T	T	03/09/2007	E.A. Crespo, R. Loizaga de Castro
OF830	Tissue	0	-41.1	-63.1	16.64	-16.35	NA	T	T	T	T	25/01/2007	E.A. Crespo, R. Loizaga de Castro
OF954	Tissue	0	-41.2	-63.8	19.65	-17.62	NA	T	T	T	T	26/01/2008	E.A. Crespo, R. Loizaga de Castro
OF983	Tissue	0	-41.2	-63.4	18.86	-18.91	NA	T	T	T	T	13/04/2009	E.A. Crespo, R. Loizaga de Castro
OF964	Tissue	0	-41.4	-64.2	NA	NA	NA	T	T	T	T	30/09/2007	E.A. Crespo, R. Loizaga de Castro
OF936	Tissue	0	-41.4	-64.1	18.92	-17.31	NA	T	T	T	T	28/09/2007	E.A. Crespo, R.

													Loizaga de Castro
OF965	Tissue	0	-41.5	-64.2	17.71	-18.58	NA	T	T	T	T	30/09/2007	E.A. Crespo, R. Loizaga de Castro
OF966	Tissue	0	-41.5	-64.8	NA	NA	NA	T	T	T	T	09/10/2007	E.A. Crespo, R. Loizaga de Castro
OF834	Tissue	0	-41.8	-65	20.22	-18.10	NA	T	T	T	T	28/01/2007	E.A. Crespo, R. Loizaga de Castro
OF838	Tissue	0	-41.8	-65	19.59	-18.37	NA	F	F	F	T	28/01/2007	E.A. Crespo, R. Loizaga de Castro
OF944	Tissue	0	-41.9	-64.9	18.34	-18.93	NA	F	F	F	T	07/11/2007	E.A. Crespo, R. Loizaga de Castro
PV10	Tissue	0	-42.1	-63.8	NA	NA	NA	T	T	T	F	09/01/1996	C. Campagna
PV11	Tissue	0	-42.1	-63.8	NA	NA	NA	T	T	T	F	09/01/1996	C. Campagna
PV14	Tissue	0	-42.1	-63.8	NA	NA	NA	T	T	T	F	10/01/1996	C. Campagna
PV15	Tissue	0	-42.1	-63.8	NA	NA	NA	T	T	T	F	10/01/1996	C. Campagna
PV17	Tissue	0	-42.1	-63.8	NA	NA	NA	T	T	T	F	10/01/1996	C. Campagna
PV21	Tissue	0	-42.1	-63.8	NA	NA	NA	T	T	T	T	11/01/1996	C. Campagna

PV29	Tissue	0	-42.1	-63.8	NA	NA	NA	T	T	T	F	17/01/1996	C. Campagna
PV31	Tissue	0	-42.1	-63.8	NA	NA	NA	T	T	T	F	17/01/1996	C. Campagna
PV34	Tissue	0	-42.1	-63.8	NA	NA	NA	T	T	T	F	17/01/1996	C. Campagna
PV41	Tissue	0	-42.1	-63.8	NA	NA	NA	T	T	T	F	19/01/1996	C. Campagna
PV42	Tissue	0	-42.1	-63.8	NA	NA	NA	T	T	T	F	19/01/1996	C. Campagna
PV1	Tissue	0	-42.2	-64.3	NA	NA	NA	T	T	T	T	07/01/1996	C. Campagna
PV12	Tissue	0	-42.2	-64.3	NA	NA	NA	T	T	T	F	08/01/1996	C. Campagna
PV18	Tissue	0	-42.2	-64.3	NA	NA	NA	T	T	T	T	11/01/1996	C. Campagna
PV20	Tissue	0	-42.2	-64.3	NA	NA	NA	T	T	T	T	11/01/1996	C. Campagna
PV22	Tissue	0	-42.2	-64.3	NA	NA	NA	T	T	T	T	16/01/1996	C. Campagna
PV23	Tissue	0	-42.2	-64.3	NA	NA	NA	T	T	T	T	16/01/1996	C. Campagna
PV3	Tissue	0	-42.2	-64.3	NA	NA	NA	T	T	T	F	08/01/1996	C. Campagna
PV37	Tissue	0	-42.2	-64.3	NA	NA	NA	T	F	F	F	18/01/1996	C. Campagna

PV38	Tissue	0	-42.2	-64.3	NA	NA	NA	T	T	T	F	18/01/1996	C. Campagna
PV4	Tissue	0	-42.2	-64.3	NA	NA	NA	T	T	T	F	08/01/1996	C. Campagna
PV40	Tissue	0	-42.2	-64.3	NA	NA	NA	T	T	T	F	18/01/1996	C. Campagna
LA37	Bone	0	-42.5	-63.6	21.55	-12.32	15.88	F	F	F	F	NA	E.A. Crespo, R. Loizaga de Castro
LA38	Bone	0	-42.5	-63.6	21.59	-11.70	15.67	F	F	F	F	NA	E.A. Crespo, R. Loizaga de Castro
OF549	Tissue	0	-42.5	-63.6	NA	NA	NA	T	F	F	T	26/08/2000	E.A. Crespo, R. Loizaga de Castro
OF457	Tissue	0	-42.7	-65	NA	NA	NA	T	F	F	F	21/08/1996	E.A. Crespo, R. Loizaga de Castro
LA39	Bone	0	-42.7	-65	20.67	-12.88	15.34	F	F	F	F	NA	E.A. Crespo, R. Loizaga de Castro
OF574	Tissue	0	-42.7	-65	NA	NA	NA	T	F	F	F	27/03/2001	E.A. Crespo, R. Loizaga de Castro
OF416	Tissue	0	-42.8	-65	NA	NA	NA	T	F	F	F	28/09/1995	E.A. Crespo, R. Loizaga de Castro
OF601	Tissue	0	-42.8	-65	NA	NA	NA	T	F	F	F	07/02/2002	E.A. Crespo, R. Loizaga de Castro

OF602	Tissue	0	-42.8	-65	NA	NA	NA	T	F	F	F	13/02/2002	E.A. Crespo, R. Loizaga de Castro
OF400	Tissue	0	-42.8	-65	NA	NA	NA	T	F	F	F	20/08/1995	E.A. Crespo, R. Loizaga de Castro
OF265	Tissue	0	-42.8	-64.9	NA	NA	NA	T	F	F	F	08/1993	E.A. Crespo, R. Loizaga de Castro
OF674	Tissue	0	-42.8	-64.9	NA	NA	NA	T	F	F	F	11/10/2005	E.A. Crespo, R. Loizaga de Castro
OF675	Tissue	0	-42.8	-64.9	NA	NA	NA	T	F	F	T	11/10/2005	E.A. Crespo, R. Loizaga de Castro
OF676	Tissue	0	-42.8	-64.9	NA	NA	NA	T	F	F	T	11/10/2005	E.A. Crespo, R. Loizaga de Castro
OF679	Tissue	0	-42.8	-64.9	NA	NA	NA	T	T	T	T	11/10/2005	E.A. Crespo, R. Loizaga de Castro
OF456	Tissue	0	-42.8	-64.9	NA	NA	NA	T	F	F	F	19/08/1996	E.A. Crespo, R. Loizaga de Castro
OF536	Tissue	0	-42.8	-64.9	NA	NA	NA	T	F	F	F	04/05/2000	E.A. Crespo, R. Loizaga de Castro
LA36	Bone	0	-43.1	-64.5	21.66	-13.02	16.27	F	F	F	F	NA	E.A. Crespo, R. Loizaga de Castro
LA35	Bone	0	-43.1	-64.5	22.39	-12.37	16.01	F	F	F	F	NA	E.A. Crespo, R.

													Loizaga de Castro
OF398	Tissue	0	-43.3	-65	NA	NA	NA	T	F	F	F	29/03/1995	E.A. Crespo, R. Loizaga de Castro
OF524	Tissue	0	-45.2	-66.7	NA	NA	NA	T	F	F	F	29/11/1999	E.A. Crespo, R. Loizaga de Castro
OF525	Tissue	0	-45.2	-66.7	NA	NA	NA	T	F	F	F	29/11/1999	E.A. Crespo, R. Loizaga de Castro
OF363	Tissue	0	-45.3	-66.6	NA	NA	NA	T	T	T	T	06/1994	E.A. Crespo, R. Loizaga de Castro
OF378	Tissue	0	-45.3	-66.2	NA	NA	NA	T	F	F	F	09/1995	E.A. Crespo, R. Loizaga de Castro
LA26	Bone	0	-47.1	-66.2	22.91	-11.09	15.22	F	F	F	F	NA	E.A. Crespo, R. Loizaga de Castro
LA58	Bone	0	-47.1	-66.2	22.30	-12.21	15.47	F	F	F	F	NA	E.A. Crespo, R. Loizaga de Castro
MLY10	Tissue	0	-47.1	-66.2	19.54	-17.21	NA	F	F	F	T	02/2010	E.A. Crespo, R. Loizaga de Castro
MLY12	Tissue	0	-47.1	-66.2	NA	NA	NA	T	T	T	T	02/2010	E.A. Crespo, R. Loizaga de Castro
MLY13	Tissue	0	-47.1	-66.2	NA	NA	NA	T	F	F	T	02/2010	E.A. Crespo, R. Loizaga de Castro

MLY14	Tissue	0	-47.1	-66.2	NA	NA	NA	T	T	T	T	02/2010	E.A. Crespo, R. Loizaga de Castro
MLY15	Tissue	0	-47.1	-66.2	NA	NA	NA	T	F	F	T	02/2010	E.A. Crespo, R. Loizaga de Castro
MLY16	Tissue	0	-47.1	-66.2	NA	NA	NA	T	T	T	T	02/2010	E.A. Crespo, R. Loizaga de Castro
MLY17	Tissue	0	-47.1	-66.2	19.52	-17.75	NA	T	T	T	T	02/2010	E.A. Crespo, R. Loizaga de Castro
MLY18	Tissue	0	-47.1	-66.2	21.14	-17.17	NA	T	T	T	T	02/2010	E.A. Crespo, R. Loizaga de Castro
LA25	Bone	0	-47.1	-66.2	20.25	-11.68	15.03	F	F	F	F	NA	E.A. Crespo, R. Loizaga de Castro
LA59	Bone	0	-47.1	-66.2	22.21	-12.99	14.58	F	F	F	F	NA	E.A. Crespo, R. Loizaga de Castro
IP1	Tissue	0	-47.9	-65.7	16.97	-17.73	NA	T	T	T	T	02/2010	E.A. Crespo, R. Loizaga de Castro
IP3	Tissue	0	-47.9	-65.7	NA	NA	NA	T	T	T	T	02/2010	E.A. Crespo, R. Loizaga de Castro
IP4	Tissue	0	-47.9	-65.7	19.56	-17.46	NA	F	F	F	T	02/2010	E.A. Crespo, R. Loizaga de Castro
IP5	Tissue	0	-47.9	-65.7	NA	NA	NA	T	T	T	T	02/2010	E.A. Crespo, R.

													Loizaga de Castro
IP6	Tissue	0	-47.9	-65.7	NA	NA	NA	T	T	T	T	02/2010	E.A. Crespo, R. Loizaga de Castro
IP7	Tissue	0	-47.9	-65.7	16.44	-20.24	NA	T	T	T	T	02/2010	E.A. Crespo, R. Loizaga de Castro
IP8	Tissue	0	-47.9	-65.7	NA	NA	NA	T	T	T	T	02/2010	E.A. Crespo, R. Loizaga de Castro
LA16	Bone	0	-50	-68.5	21.00	-11.42	13.83	F	F	F	F	NA	E.A. Crespo, R. Loizaga de Castro
CB1	Tissue	0	-50.2	-68.6	18.47	-18.12	NA	T	T	T	T	01/2004	E.A. Crespo, R. Loizaga de Castro
CB10	Tissue	0	-50.2	-68.6	NA	NA	NA	T	F	F	T	01/2004	E.A. Crespo, R. Loizaga de Castro
CB2	Tissue	0	-50.2	-68.6	NA	NA	NA	T	T	T	T	01/2004	E.A. Crespo, R. Loizaga de Castro
CB3	Tissue	0	-50.2	-68.6	17.93	-18.77	NA	F	F	F	T	01/2004	E.A. Crespo, R. Loizaga de Castro
CB4	Tissue	0	-50.2	-68.6	NA	NA	NA	T	F	F	T	01/2004	E.A. Crespo, R. Loizaga de Castro
CB5	Tissue	0	-50.2	-68.6	17.16	-18.64	NA	T	T	T	T	01/2004	E.A. Crespo, R. Loizaga de Castro

CB7	Tissue	0	-50.2	-68.6	20.62	-17.36	NA	F	F	F	F	01/2004	E.A. Crespo, R. Loizaga de Castro
CB8	Tissue	0	-50.2	-68.6	17.99	-19.20	NA	F	F	F	T	01/2004	E.A. Crespo, R. Loizaga de Castro
CB9	Tissue	0	-50.2	-68.6	16.02	-19.06	NA	F	F	F	T	01/2004	E.A. Crespo, R. Loizaga de Castro
LA82	Bone	0	-54.1	-67.2	20.56	-12.23	13.83	F	F	F	F	NA	R. Natalie, P. Goodall
LA83	Bone	0	-54.1	-67.2	21.45	-12.36	13.35	F	F	F	F	NA	R. Natalie, P. Goodall
LA88	Bone	0	-54.1	-67.2	20.63	-13.13	11.83	F	F	F	F	NA	R. Natalie, P. Goodall
LA478	Bone	0	-54.9	-68.1	NA	NA	NA	T	T	T	F	NA	R. Natalie, P. Goodall
LA86	Bone	0	-54.9	-68.1	21.08	-13.08	14.54	T	F	F	F	NA	R. Natalie, P. Goodall
LA87	Bone	0	-54.9	-68.1	20.80	-14.14	14.37	T	F	F	F	NA	R. Natalie, P. Goodall

Table A.2. All physical samples of *Spheniscus magellanicus* processed for this study.

Sample ID	**Sample type**	**Age (ybp)**	**Latitude (°)**	**Longitude (°)**	**δ15N**	**δ13C**	**δ34S**	**277-bp alignment**	**Source**
LA544	Bone	5845	-54.9	-67.8	19.86	-19.19	14.77	T	A.M. Tivoli
LA545	Bone	5775	-54.9	-67.8	21.48	-16.46	15.83	T	A.M. Tivoli

LA546	Bone	5775	-54.9	-67.8	20.72	-17.86	15.96	T	A.M. Tivoli
LA547	Bone	4660	-54.9	-67.8	21.65	-16.85	15.94	T	A.M. Tivoli
LA548	Bone	4660	-54.9	-67.8	20.63	-17.19	15.79	T	A.M. Tivoli
LA549	Bone	4660	-54.9	-67.8	21.09	-17.80	15.61	F	A.M. Tivoli
LA550	Bone	4660	-54.9	-67.8	21.52	-17.65	15.60	F	A.M. Tivoli
LA3181	Bone	2910	-41.4	-64.5	21.48	-12.54	15.59	T	F. Borella
LA3182	Bone	2910	-41.4	-64.5	22.27	-12.63	16.01	T	F. Borella
LA1156	Bone	2197	-41.4	-64.5	19.44	-14.83	15.21	T	F. Borella
LA1157	Bone	2197	-41.4	-64.5	19.12	-11.19	15.40	T	F. Borella
LA1158	Bone	2197	-41.4	-64.5	24.43	-12.56	15.98	T	F. Borella
LA2191	Bone	1220	-47.9	-65.8	17.93	-14.96	15.91	T	E. Moreno
LA559	Bone	500	-54.9	-67.8	18.97	-11.14	15.24	T	A.M. Tivoli
LA560	Bone	500	-54.9	-67.8	17.42	-11.78	15.73	T	A.M. Tivoli
LA372	Bone	0	-42.1	-63.8	21.21	-15.18	15.83	T	NA
LA378	Bone	0	-42.1	-63.8	21.37	-14.12	15.59	T	NA
LA364	Bone	0	-42.2	-64	20.68	-14.53	16.48	T	NA
LA362	Bone	0	-42.2	-64.8	20.62	-13.03	13.64	T	NA

LA366	Bone	0	-42.2	-64.4	18.86	-15.57	16.36	T	NA
LA399	Bone	0	-48.4	-66.4	19.56	-14.48	15.71	T	NA
LA397	Bone	0	-48.4	-66.4	20.06	-15.13	15.02	F	NA
LA388	Bone	0	-49.3	-67.8	20.24	-14.35	16.30	T	NA
LA391	Bone	0	-52.3	-68.3	18.50	-16.02	16.26	T	NA
LA392	Bone	0	-52.3	-68.3	19.71	-15.07	16.27	T	NA

Table A.3. All samples of *O. flavescens* and *S. magellanicus* whose previously published genetic data was used in this study.

Sample Accession #	**Species**	**Source**	**Latitude (°)**	**Longitude (°)**	**145-bp alignment (Otaria)**	**409-bp alignment (Otaria)**	**277-bp alignment (Spheniscus)**
EU044835.1	*O. flavescens*	Artico 2010	-34.9	-54.7	T	F	F
EU044836.1	*O. flavescens*	Artico 2010	-34.9	-54.7	T	F	F
EU044837.1	*O. flavescens*	Artico 2010	-34.9	-54.7	T	F	F
EU044838.1	*O. flavescens*	Artico 2010	-34.9	-54.7	T	F	F
EU044839.1	*O. flavescens*	Artico 2010	-34.9	-54.7	T	F	F
EU044840.1	*O. flavescens*	Artico 2010	-34.9	-54.7	T	F	F
EU044841.1	*O. flavescens*	Artico 2010	-34.9	-54.7	T	F	F
HM467619.1	*O. flavescens*	Feijoo 2011	-34.9	-54.7	T	T	F

HM467620.1	*O. flavescens*	Feijoo 2011	-34.9	-54.7	T	T	F
HM467621.1	*O. flavescens*	Feijoo 2011	-34.9	-54.7	T	T	F
HM467622.1	*O. flavescens*	Feijoo 2011	-34.9	-54.7	T	T	F
HM467623.1	*O. flavescens*	Feijoo 2011	-34.9	-54.7	T	T	F
HM467624.1	*O. flavescens*	Feijoo 2011	-34.9	-54.7	T	T	F
HM467625.1	*O. flavescens*	Feijoo 2011	-34.9	-54.7	T	T	F
HM467626.1	*O. flavescens*	Feijoo 2011	-34.9	-54.7	T	T	F
HM467627.1	*O. flavescens*	Feijoo 2011	-34.9	-54.7	T	T	F
HM467628.1	*O. flavescens*	Feijoo 2011	-34.9	-54.7	T	T	F
HM467629.1	*O. flavescens*	Feijoo 2011	-34.9	-54.7	T	T	F
HM467630.1	*O. flavescens*	Feijoo 2011	-34.9	-54.7	T	T	F
HM467631.1	*O. flavescens*	Feijoo 2011	-34.9	-54.7	T	T	F
HM467635.1	*O. flavescens*	Feijoo 2011	-42.1	-63.8	T	T	F
HM347787.1-1	*O. flavescens*	Tunez 2010	-42.1	-63.8	T	T	F
HM347787.1-2	*O. flavescens*	Tunez 2010	-42.1	-63.8	T	T	F
HM347788.1-1	*O. flavescens*	Tunez 2010	-42.1	-63.8	T	T	F
HM347788.1-2	*O. flavescens*	Tunez 2010	-42.1	-63.8	T	T	F
HM347789.1-5	*O. flavescens*	Tunez 2010	-42.1	-63.8	T	T	F

HM347789.1-6	*O. flavescens*	Tunez 2010	-42.1	-63.8	T	T	F
HM347789.1-7	*O. flavescens*	Tunez 2010	-42.1	-63.8	T	T	F
HM347790.1-1	*O. flavescens*	Tunez 2010	-42.1	-63.8	T	T	F
HM347790.1-2	*O. flavescens*	Tunez 2010	-42.1	-63.8	T	T	F
HM347791.1-1	*O. flavescens*	Tunez 2010	-42.1	-63.8	T	T	F
HM347792.1-1	*O. flavescens*	Tunez 2010	-42.1	-63.8	T	T	F
HM347793.1-1	*O. flavescens*	Tunez 2010	-42.1	-63.8	T	T	F
HM467633.1	*O. flavescens*	Feijoo 2011	-42.4	-64.3	T	T	F
HM347787.1-13	*O. flavescens*	Tunez 2010	-42.6	-64.3	T	F	F
HM347787.1-14	*O. flavescens*	Tunez 2010	-42.6	-64.3	T	F	F
HM347787.1-15	*O. flavescens*	Tunez 2010	-42.6	-64.3	T	F	F
HM347789.1-8	*O. flavescens*	Tunez 2010	-42.6	-64.3	T	F	F
HM347789.1-9	*O. flavescens*	Tunez 2010	-42.6	-64.3	T	F	F
HM347791.1-2	*O. flavescens*	Tunez 2010	-42.6	-64.3	T	F	F
HM347793.1-2	*O. flavescens*	Tunez 2010	-42.6	-64.3	T	F	F
HM467634.1	*O. flavescens*	Feijoo 2011	-42.7	-65.0	T	T	F
HM467638.1	*O. flavescens*	Feijoo 2011	-42.7	-65.0	T	T	F
HM467639.1	*O. flavescens*	Feijoo 2011	-42.7	-65.0	T	T	F

HM467641.1	*O. flavescens*	Feijoo 2011	-42.7	-65.0	T	T	F
HM467632.1	*O. flavescens*	Feijoo 2011	-43.1	-64.5	T	T	F
HM467636.1	*O. flavescens*	Feijoo 2011	-43.1	-64.5	T	T	F
HM467637.1	*O. flavescens*	Feijoo 2011	-43.1	-64.5	T	T	F
HM467640.1	*O. flavescens*	Feijoo 2011	-43.1	-64.5	T	T	F
HM467642.1	*O. flavescens*	Feijoo 2011	-43.1	-64.5	T	T	F
HM347787.1-3	*O. flavescens*	Tunez 2010	-45.0	-65.5	T	F	F
HM347787.1-4	*O. flavescens*	Tunez 2010	-45.0	-65.5	T	F	F
HM347787.1-5	*O. flavescens*	Tunez 2010	-45.0	-65.5	T	F	F
HM347788.1-3	*O. flavescens*	Tunez 2010	-45.0	-65.5	T	F	F
HM347788.1-4	*O. flavescens*	Tunez 2010	-45.0	-65.5	T	F	F
HM347788.1-5	*O. flavescens*	Tunez 2010	-45.0	-65.5	T	F	F
HM347789.1-3	*O. flavescens*	Tunez 2010	-45.0	-65.5	T	F	F
HM347789.1-4	*O. flavescens*	Tunez 2010	-45.0	-65.5	T	F	F
HM347790.1-3	*O. flavescens*	Tunez 2010	-45.0	-65.5	T	F	F
HM347795.1-1	*O. flavescens*	Tunez 2010	-45.0	-65.5	T	T	F
HM347790.1-4	*O. flavescens*	Tunez 2010	-45.1	-66.5	T	F	F
HM347792.1-2	*O. flavescens*	Tunez 2010	-45.1	-66.5	T	F	F

HM347787.1-6	*O. flavescens*	Tunez 2010	-45.2	-66.5	T	F	F
HM347787.1-7	*O. flavescens*	Tunez 2010	-45.2	-66.5	T	F	F
HM347787.1-8	*O. flavescens*	Tunez 2010	-45.2	-66.5	T	F	F
HM347787.1-9	*O. flavescens*	Tunez 2010	-45.2	-66.5	T	F	F
HM347788.1-6	*O. flavescens*	Tunez 2010	-45.2	-66.5	T	F	F
HM347788.1-7	*O. flavescens*	Tunez 2010	-45.2	-66.5	T	F	F
HM347789.1-1	*O. flavescens*	Tunez 2010	-45.2	-66.5	T	F	F
HM347789.1-2	*O. flavescens*	Tunez 2010	-45.2	-66.5	T	F	F
HM347788.1-10	*O. flavescens*	Tunez 2010	-47.1	-66.3	T	F	F
HM347788.1-11	*O. flavescens*	Tunez 2010	-47.1	-66.3	T	F	F
HM347788.1-8	*O. flavescens*	Tunez 2010	-47.1	-66.3	T	F	F
HM347788.1-9	*O. flavescens*	Tunez 2010	-47.1	-66.3	T	F	F
HM347794.1-1	*O. flavescens*	Tunez 2010	-47.1	-66.3	T	T	F
HM347794.1-2	*O. flavescens*	Tunez 2010	-47.1	-66.3	T	T	F
HM347796.1-1	*O. flavescens*	Tunez 2010	-47.1	-66.3	T	T	F
HM347787.1-10	*O. flavescens*	Tunez 2010	-47.1	-66.2	T	F	F
HM347787.1-11	*O. flavescens*	Tunez 2010	-47.1	-66.2	T	F	F

HM347787.1-12	*O. flavescens*	Tunez 2010	-47.1	-66.2	T	F	F
HM467643.1	*O. flavescens*	Feijoo 2011	-50.3	-68.6	T	T	F
HM467644.1	*O. flavescens*	Feijoo 2011	-50.3	-68.6	T	T	F
HM467645.1	*O. flavescens*	Feijoo 2011	-50.3	-68.6	T	T	F
HM467646.1	*O. flavescens*	Feijoo 2011	-50.3	-68.6	T	T	F
KX037161.1	*S. magellanicus*	Dantas 2018	?	?	F	F	T
KX037162.1	*S. magellanicus*	Dantas 2018	?	?	F	F	T
KX037163.1	*S. magellanicus*	Dantas 2018	?	?	F	F	T
KX037164.1	*S. magellanicus*	Dantas 2018	?	?	F	F	T
KX037165.1	*S. magellanicus*	Dantas 2018	?	?	F	F	T
KX037166.1	*S. magellanicus*	Dantas 2018	?	?	F	F	T
KX037167.1	*S. magellanicus*	Dantas 2018	?	?	F	F	T
KX037168.1	*S. magellanicus*	Dantas 2018	?	?	F	F	T
KX037169.1	*S. magellanicus*	Dantas 2018	?	?	F	F	T
KX037170.1	*S. magellanicus*	Dantas 2018	?	?	F	F	T
KX037171.1	*S. magellanicus*	Dantas 2018	?	?	F	F	T

KX037172.1	*S. magellanicus*	Dantas 2018	?	?	F	F	T
KX037173.1	*S. magellanicus*	Dantas 2018	?	?	F	F	T
KX037174.1	*S. magellanicus*	Dantas 2018	?	?	F	F	T
KX037175.1	*S. magellanicus*	Dantas 2018	?	?	F	F	T
KX037176.1	*S. magellanicus*	Dantas 2018	?	?	F	F	T
KX037177.1	*S. magellanicus*	Dantas 2018	?	?	F	F	T
KX037178.1	*S. magellanicus*	Dantas 2018	?	?	F	F	T
KX037179.1	*S. magellanicus*	Dantas 2018	?	?	F	F	T
KX037180.1	*S. magellanicus*	Dantas 2018	?	?	F	F	T
KX037181.1	*S. magellanicus*	Dantas 2018	?	?	F	F	T
KX037182.1	*S. magellanicus*	Dantas 2018	?	?	F	F	T
KX037183.1	*S. magellanicus*	Dantas 2018	?	?	F	F	T
KX037184.1	*S. magellanicus*	Dantas 2018	?	?	F	F	T
KX037185.1	*S. magellanicus*	Dantas 2018	?	?	F	F	T
KX037186.1	*S. magellanicus*	Dantas 2018	?	?	F	F	T
KX037187.1	*S. magellanicus*	Dantas 2018	?	?	F	F	T

KX037188.1	*S. magellanicus*	Dantas 2018	?	?	F	F	T
KX037189.1	*S. magellanicus*	Dantas 2018	?	?	F	F	T
KX037190.1	*S. magellanicus*	Dantas 2018	?	?	F	F	T
KX037191.1	*S. magellanicus*	Dantas 2018	?	?	F	F	T
KX037192.1	*S. magellanicus*	Dantas 2018	?	?	F	F	T
KX037193.1	*S. magellanicus*	Dantas 2018	?	?	F	F	T
KX037194.1	*S. magellanicus*	Dantas 2018	?	?	F	F	T
KX037195.1	*S. magellanicus*	Dantas 2018	?	?	F	F	T
KX037196.1	*S. magellanicus*	Dantas 2018	?	?	F	F	T
KX037197.1	*S. magellanicus*	Dantas 2018	?	?	F	F	T
KX037198.1	*S. magellanicus*	Dantas 2018	?	?	F	F	T
KX037199.1	*S. magellanicus*	Dantas 2018	?	?	F	F	T
KX037200.1	*S. magellanicus*	Dantas 2018	?	?	F	F	T
KX037201.1	*S. magellanicus*	Dantas 2018	?	?	F	F	T
KX037202.1	*S. magellanicus*	Dantas 2018	?	?	F	F	T
KX037203.1	*S. magellanicus*	Dantas 2018	?	?	F	F	T

KX037204.1	*S. magellanicus*	Dantas 2018	?	?	F	F	T
KX037205.1	*S. magellanicus*	Dantas 2018	?	?	F	F	T
KX037206.1	*S. magellanicus*	Dantas 2018	?	?	F	F	T
KX037207.1	*S. magellanicus*	Dantas 2018	?	?	F	F	T
KX037208.1	*S. magellanicus*	Dantas 2018	?	?	F	F	T
KX037209.1	*S. magellanicus*	Dantas 2018	?	?	F	F	T
KX037210.1	*S. magellanicus*	Dantas 2018	?	?	F	F	T
KX037211.1	*S. magellanicus*	Dantas 2018	?	?	F	F	T
KX037212.1	*S. magellanicus*	Dantas 2018	?	?	F	F	T
KX037213.1	*S. magellanicus*	Dantas 2018	?	?	F	F	T
KX037214.1	*S. magellanicus*	Dantas 2018	?	?	F	F	T
KX037215.1	*S. magellanicus*	Dantas 2018	?	?	F	F	T
KX037216.1	*S. magellanicus*	Dantas 2018	?	?	F	F	T
KX037217.1	*S. magellanicus*	Dantas 2018	?	?	F	F	T
KX037218.1	*S. magellanicus*	Dantas 2018	?	?	F	F	T
KX037219.1	*S. magellanicus*	Dantas 2018	?	?	F	F	T

KX037220.1	*S. magellanicus*	Dantas 2018	?	?	F	F	T
KX037221.1	*S. magellanicus*	Dantas 2018	?	?	F	F	T
KX037222.1	*S. magellanicus*	Dantas 2018	?	?	F	F	T
KX037223.1	*S. magellanicus*	Dantas 2018	?	?	F	F	T
KX037224.1	*S. magellanicus*	Dantas 2018	?	?	F	F	T
KX037225.1	*S. magellanicus*	Dantas 2018	?	?	F	F	T
KX037226.1	*S. magellanicus*	Dantas 2018	?	?	F	F	T
KX037227.1	*S. magellanicus*	Dantas 2018	?	?	F	F	T
KX037228.1	*S. magellanicus*	Dantas 2018	?	?	F	F	T
KX037229.1	*S. magellanicus*	Dantas 2018	?	?	F	F	T
KX037230.1	*S. magellanicus*	Dantas 2018	?	?	F	F	T
KX037231.1	*S. magellanicus*	Dantas 2018	?	?	F	F	T
KX037232.1	*S. magellanicus*	Dantas 2018	?	?	F	F	T
KX037233.1	*S. magellanicus*	Dantas 2018	?	?	F	F	T
KX037234.1	*S. magellanicus*	Dantas 2018	?	?	F	F	T
KX037235.1	*S. magellanicus*	Dantas 2018	?	?	F	F	T

KX037236.1	*S. magellanicus*	Dantas 2018	?	?	F	F	T
KX037237.1	*S. magellanicus*	Dantas 2018	?	?	F	F	T
KX037238.1	*S. magellanicus*	Dantas 2018	?	?	F	F	T
KX037239.1	*S. magellanicus*	Dantas 2018	?	?	F	F	T
KX037240.1	*S. magellanicus*	Dantas 2018	?	?	F	F	T
KX037241.1	*S. magellanicus*	Dantas 2018	?	?	F	F	T
KX037242.1	*S. magellanicus*	Dantas 2018	?	?	F	F	T
KX037243.1	*S. magellanicus*	Dantas 2018	?	?	F	F	T
KX037244.1	*S. magellanicus*	Dantas 2018	?	?	F	F	T
KX037245.1	*S. magellanicus*	Dantas 2018	?	?	F	F	T
KX037246.1	*S. magellanicus*	Dantas 2018	?	?	F	F	T
KX037247.1	*S. magellanicus*	Dantas 2018	?	?	F	F	T
KX037248.1	*S. magellanicus*	Dantas 2018	?	?	F	F	T
KX037249.1	*S. magellanicus*	Dantas 2018	?	?	F	F	T
KX037250.1	*S. magellanicus*	Dantas 2018	?	?	F	F	T
KX037251.1	*S. magellanicus*	Dantas 2018	?	?	F	F	T

KX037252.1	*S. magellanicus*	Dantas 2018	?	?	F	F	T
KX037253.1	*S. magellanicus*	Dantas 2018	?	?	F	F	T
KX037254.1	*S. magellanicus*	Dantas 2018	?	?	F	F	T
KX037255.1	*S. magellanicus*	Dantas 2018	?	?	F	F	T
KX037256.1	*S. magellanicus*	Dantas 2018	?	?	F	F	T
KX037257.1	*S. magellanicus*	Dantas 2018	?	?	F	F	T
KX037258.1	*S. magellanicus*	Dantas 2018	?	?	F	F	T
KX037259.1	*S. magellanicus*	Dantas 2018	?	?	F	F	T
KX037260.1	*S. magellanicus*	Dantas 2018	?	?	F	F	T
KX037261.1	*S. magellanicus*	Dantas 2018	?	?	F	F	T
KX037262.1	*S. magellanicus*	Dantas 2018	?	?	F	F	T
KX037263.1	*S. magellanicus*	Dantas 2018	?	?	F	F	T
KX037264.1	*S. magellanicus*	Dantas 2018	?	?	F	F	T
KX037265.1	*S. magellanicus*	Dantas 2018	?	?	F	F	T
KX037266.1	*S. magellanicus*	Dantas 2018	?	?	F	F	T
KX037267.1	*S. magellanicus*	Dantas 2018	?	?	F	F	T

KX037268.1	*S. magellanicus*	Dantas 2018	?	?	F	F	T
KX037269.1	*S. magellanicus*	Dantas 2018	?	?	F	F	T
KX037270.1	*S. magellanicus*	Dantas 2018	?	?	F	F	T
KX037271.1	*S. magellanicus*	Dantas 2018	?	?	F	F	T
KX037272.1	*S. magellanicus*	Dantas 2018	?	?	F	F	T
KX037273.1	*S. magellanicus*	Dantas 2018	?	?	F	F	T
KX037274.1	*S. magellanicus*	Dantas 2018	?	?	F	F	T
KX037275.1	*S. magellanicus*	Dantas 2018	?	?	F	F	T
KX037276.1	*S. magellanicus*	Dantas 2018	?	?	F	F	T
KX037277.1	*S. magellanicus*	Dantas 2018	?	?	F	F	T
KX037278.1	*S. magellanicus*	Dantas 2018	?	?	F	F	T
KX037279.1	*S. magellanicus*	Dantas 2018	?	?	F	F	T
KX037280.1	*S. magellanicus*	Dantas 2018	?	?	F	F	T
KX037281.1	*S. magellanicus*	Dantas 2018	?	?	F	F	T
KX037282.1	*S. magellanicus*	Dantas 2018	?	?	F	F	T
KX037283.1	*S. magellanicus*	Dantas 2018	?	?	F	F	T

KX037284.1	*S. magellanicus*	Dantas 2018	?	?	F	F	T
KX037285.1	*S. magellanicus*	Dantas 2018	?	?	F	F	T
KX037286.1	*S. magellanicus*	Dantas 2018	?	?	F	F	T
KX037287.1	*S. magellanicus*	Dantas 2018	?	?	F	F	T
KX037288.1	*S. magellanicus*	Dantas 2018	?	?	F	F	T
KX037289.1	*S. magellanicus*	Dantas 2018	?	?	F	F	T
KX037290.1	*S. magellanicus*	Dantas 2018	?	?	F	F	T
KX037291.1	*S. magellanicus*	Dantas 2018	?	?	F	F	T
KX037292.1	*S. magellanicus*	Dantas 2018	?	?	F	F	T
KX037293.1	*S. magellanicus*	Dantas 2018	?	?	F	F	T
KX037294.1	*S. magellanicus*	Dantas 2018	?	?	F	F	T
KX037295.1	*S. magellanicus*	Dantas 2018	?	?	F	F	T
KX037296.1	*S. magellanicus*	Dantas 2018	?	?	F	F	T
KX037297.1	*S. magellanicus*	Dantas 2018	?	?	F	F	T
KX037298.1	*S. magellanicus*	Dantas 2018	?	?	F	F	T
KX037299.1	*S. magellanicus*	Dantas 2018	?	?	F	F	T

KX037300.1	*S. magellanicus*	Dantas 2018	?	?	F	F	T
KX037301.1	*S. magellanicus*	Dantas 2018	?	?	F	F	T
KX037302.1	*S. magellanicus*	Dantas 2018	?	?	F	F	T
KX037303.1	*S. magellanicus*	Dantas 2018	?	?	F	F	T
KX037304.1	*S. magellanicus*	Dantas 2018	?	?	F	F	T
KX037305.1	*S. magellanicus*	Dantas 2018	?	?	F	F	T
KX037306.1	*S. magellanicus*	Dantas 2018	?	?	F	F	T
KX037307.1	*S. magellanicus*	Dantas 2018	?	?	F	F	T
KX037308.1	*S. magellanicus*	Dantas 2018	?	?	F	F	T
KX037309.1	*S. magellanicus*	Dantas 2018	?	?	F	F	T
KX037310.1	*S. magellanicus*	Dantas 2018	?	?	F	F	T
KX037311.1	*S. magellanicus*	Dantas 2018	?	?	F	F	T
KX037312.1	*S. magellanicus*	Dantas 2018	?	?	F	F	T
KX037313.1	*S. magellanicus*	Dantas 2018	?	?	F	F	T
KX037314.1	*S. magellanicus*	Dantas 2018	?	?	F	F	T
KX037315.1	*S. magellanicus*	Dantas 2018	?	?	F	F	T

KX037316.1	*S. magellanicus*	Dantas 2018	?	?	F	F	T
KX037317.1	*S. magellanicus*	Dantas 2018	?	?	F	F	T
KX037318.1	*S. magellanicus*	Dantas 2018	?	?	F	F	T
KX037319.1	*S. magellanicus*	Dantas 2018	?	?	F	F	T
KX037320.1	*S. magellanicus*	Dantas 2018	?	?	F	F	T
KX037321.1	*S. magellanicus*	Dantas 2018	?	?	F	F	T
KX037322.1	*S. magellanicus*	Dantas 2018	?	?	F	F	T
KX037323.1	*S. magellanicus*	Dantas 2018	?	?	F	F	T
KX037324.1	*S. magellanicus*	Dantas 2018	?	?	F	F	T
KX037325.1	*S. magellanicus*	Dantas 2018	?	?	F	F	T
KX037326.1	*S. magellanicus*	Dantas 2018	?	?	F	F	T
KX037327.1	*S. magellanicus*	Dantas 2018	?	?	F	F	T
KX037328.1	*S. magellanicus*	Dantas 2018	?	?	F	F	T
KX037329.1	*S. magellanicus*	Dantas 2018	?	?	F	F	T
KX037330.1	*S. magellanicus*	Dantas 2018	?	?	F	F	T
KX037331.1	*S. magellanicus*	Dantas 2018	?	?	F	F	T

KX037332.1	*S. magellanicus*	Dantas 2018	?	?	F	F	T
KX037333.1	*S. magellanicus*	Dantas 2018	?	?	F	F	T
KX037334.1	*S. magellanicus*	Dantas 2018	?	?	F	F	T
KX037335.1	*S. magellanicus*	Dantas 2018	?	?	F	F	T
KX037336.1	*S. magellanicus*	Dantas 2018	?	?	F	F	T
KX037337.1	*S. magellanicus*	Dantas 2018	?	?	F	F	T
KX037338.1	*S. magellanicus*	Dantas 2018	?	?	F	F	T
KX037339.1	*S. magellanicus*	Dantas 2018	?	?	F	F	T
KX037340.1	*S. magellanicus*	Dantas 2018	?	?	F	F	T
KX037341.1	*S. magellanicus*	Dantas 2018	?	?	F	F	T
KX037342.1	*S. magellanicus*	Dantas 2018	?	?	F	F	T
KX037343.1	*S. magellanicus*	Dantas 2018	?	?	F	F	T
KX037344.1	*S. magellanicus*	Dantas 2018	?	?	F	F	T
KX037345.1	*S. magellanicus*	Dantas 2018	?	?	F	F	T
KX037346.1	*S. magellanicus*	Dantas 2018	?	?	F	F	T
KX037347.1	*S. magellanicus*	Dantas 2018	?	?	F	F	T

KX037348.1	*S. magellanicus*	Dantas 2018	?	?	F	F	T
KX037349.1	*S. magellanicus*	Dantas 2018	?	?	F	F	T
KX037350.1	*S. magellanicus*	Dantas 2018	?	?	F	F	T
KX037351.1	*S. magellanicus*	Dantas 2018	?	?	F	F	T
KX037352.1	*S. magellanicus*	Dantas 2018	?	?	F	F	T
KX037353.1	*S. magellanicus*	Dantas 2018	?	?	F	F	T
KX037354.1	*S. magellanicus*	Dantas 2018	?	?	F	F	T
KX037355.1	*S. magellanicus*	Dantas 2018	?	?	F	F	T

Table A.4. NCBI BioSample accessions of all published samples from which RADseq reads were used for comparative demographic analysis in Chapter 4.

Species	**Location (population)**	**Sample Accessions**	**Data source**
Arctocephalus australis	Brazil	SAMEA6648919, SAMEA6648981, SAMEA6648992, SAMEA6649030, SAMEA6649075, SAMEA6649096, SAMEA6649108, SAMEA6649132, SAMEA6649185, SAMEA6649220, SAMEA6649236	Peart et al. 2020
Arctocephalus forsteri	Cape Foulwind, NZ (“CFoulwind”)	SAMEA6649012, SAMEA6649052, SAMEA6649057, SAMEA6649102, SAMEA6649106, SAMEA6649144, SAMEA6649325, SAMEA6649349	Peart et al. 2020
Arctocephalus forsteri	Open Bay, NZ (“OBay”)	SAMEA6648922, SAMEA6648966, SAMEA6649015, SAMEA6649022, SAMEA6649156, SAMEA6649235, SAMEA6649240	Peart et al. 2020
Arctocephalus	Ohau Point, NZ	SAMEA6649028, SAMEA6649201,	Peart et al. 2020

forsteri	(“OhauP”)	SAMEA6649275, SAMEA6649287, SAMEA6649305, SAMEA6649322	
Arctocephalus forsteri	Victory Beach, NZ (“VictoryB”)	SAMEA6648926, SAMEA6648947, SAMEA6648990, SAMEA6649111, SAMEA6649115, SAMEA6649161	Peart et al. 2020
Arctocephalus galapagoensis	Isabela Island, Galápagos	SAMEA6648910, SAMEA6648939, SAMEA6648954, SAMEA6649018, SAMEA6649116, SAMEA6649162, SAMEA6649170, SAMEA6649209, SAMEA6649223, SAMEA6649226, SAMEA6649310, SAMEA6649317	Peart et al. 2020
Arctocephalus gazella	South Georgia	SAMEA6648914, SAMEA6648925, SAMEA6648929, SAMEA6648930, SAMEA6648932, SAMEA6648953, SAMEA6648956, SAMEA6648958, SAMEA6648961, SAMEA6648963, SAMEA6648965, SAMEA6648968, SAMEA6648970, SAMEA6648973, SAMEA6648980, SAMEA6648985, SAMEA6648988, SAMEA6648989, SAMEA6648993, SAMEA6649000, SAMEA6649006, SAMEA6649011, SAMEA6649019, SAMEA6649037, SAMEA6649038, SAMEA6649043, SAMEA6649044, SAMEA6649046, SAMEA6649051, SAMEA6649061, SAMEA6649062, SAMEA6649064, SAMEA6649067, SAMEA6649073, SAMEA6649079, SAMEA6649082, SAMEA6649086, SAMEA6649110, SAMEA6649119, SAMEA6649123, SAMEA6649131, SAMEA6649135, SAMEA6649136, SAMEA6649137, SAMEA6649150, SAMEA6649154, SAMEA6649164, SAMEA6649172, SAMEA6649191, SAMEA6649193, SAMEA6649200, SAMEA6649217, SAMEA6649230, SAMEA6649245, SAMEA6649247, SAMEA6649248, SAMEA6649249, SAMEA6649251, SAMEA6649253, SAMEA6649254, SAMEA6649257, SAMEA6649261, SAMEA6649262, SAMEA6649264, SAMEA6649277, SAMEA6649278, SAMEA6649283, SAMEA6649289, SAMEA6649295, SAMEA6649297, SAMEA6649299, SAMEA6649302, SAMEA6649307, SAMEA6649311, SAMEA6649313, SAMEA6649324, SAMEA6649327, SAMEA6649334, SAMEA6649335, SAMEA6649342, SAMEA6649351, SAMEA6649355, SAMEA6649358, SAMEA6649364	Peart et al. 2020
Mirounga leonina	Sea Lion Island, Falklands	SAMEA6648952, SAMEA6648996, SAMEA6648999, SAMEA6649002, SAMEA6649035, SAMEA6649059, SAMEA6649098, SAMEA6649114,	Peart et al. 2020

		SAMEA6649121, SAMEA6649138, SAMEA6649167	
Mirounga angustirostris	California	SAMEA6648943, SAMEA6648948, SAMEA6649103, SAMEA6649174, SAMEA6649175, SAMEA6649213, SAMEA6649221, SAMEA6649252, SAMEA6649260, SAMEA6649279, SAMEA6649281, SAMEA6649303, SAMEA6649309, SAMEA6649338, SAMEA6649363	Peart et al. 2020
Phoca vitulina	Svalbard	SAMEA6648912, SAMEA6648916, SAMEA6648934, SAMEA6648938, SAMEA6649047, SAMEA6649077, SAMEA6649112, SAMEA6649187, SAMEA6649196, SAMEA6649208, SAMEA6649270, SAMEA6649282, SAMEA6649308	Peart et al. 2020
Pusa hispida	Svalbard	SAMEA6649009, SAMEA6649068, SAMEA6649083, SAMEA6649092, SAMEA6649133, SAMEA6649141, SAMEA6649166, SAMEA6649177, SAMEA6649274, SAMEA6649280, SAMEA6649331, SAMEA6649337, SAMEA6649350, SAMEA6649361	Peart et al. 2020
Erignathus barbatus	Svalbard	SAMEA6648915, SAMEA6648972, SAMEA6649023, SAMEA6649041, SAMEA6649049, SAMEA6649070, SAMEA6649094, SAMEA6649178, SAMEA6649182, SAMEA6649234, SAMEA6649330, SAMEA6649332	Peart et al. 2020
Zalophus californianus	El Golfo de Santa Clara, MX (“GCal1”)	SAMEA6648964, SAMEA6648978, SAMEA6649029, SAMEA6649153, SAMEA6649181, SAMEA6649202, SAMEA6649227, SAMEA6649258, SAMEA6649296, SAMEA6649321, SAMEA6649345, SAMEA6649346	Peart et al. 2020
Zalophus californianus	Isla Ángel de la Guarda, MX (“GCal2”)	SAMEA6648974, SAMEA6648991, SAMEA6649014, SAMEA6649084, SAMEA6649113, SAMEA6649143, SAMEA6649163, SAMEA6649184, SAMEA6649207, SAMEA6649212, SAMEA6649268, SAMEA6649271, SAMEA6649323	Peart et al. 2020
Zalophus californianus	Isla San Pedro Nolasco, MX (“GCal3”)	SAMEA6648911, SAMEA6648927, SAMEA6648941, SAMEA6648949, SAMEA6648969, SAMEA6648975, SAMEA6649008, SAMEA6649016, SAMEA6649072, SAMEA6649080, SAMEA6649095, SAMEA6649122, SAMEA6649134, SAMEA6649186, SAMEA6649222, SAMEA6649238, SAMEA6649244, SAMEA6649276, SAMEA6649290, SAMEA6649333, SAMEA6649344, SAMEA6649357,	Peart et al. 2020

		SAMEA6649365	
Zalophus californianus	Isla del Espiritu Santo, MX (“GCal4”)	SAMEA6648931, SAMEA6648977, SAMEA6649004, SAMEA6649048, SAMEA6649056, SAMEA6649093, SAMEA6649124, SAMEA6649140, SAMEA6649195, SAMEA6649203, SAMEA6649259, SAMEA6649286, SAMEA6649315, SAMEA6649320	Peart et al. 2020
Zalophus californianus	Isla Santa Margarita, MX (“SMargarita”)	SAMEA6648955, SAMEA6648987, SAMEA6649060, SAMEA6649085, SAMEA6649117, SAMEA6649155, SAMEA6649169, SAMEA6649183, SAMEA6649204, SAMEA6649242, SAMEA6649267, SAMEA6649269, SAMEA6649301, SAMEA6649306	Peart et al. 2020
Zalophus wollabaeki	Baltra Island, EC	SAMEA6648924, SAMEA6648928, SAMEA6648935, SAMEA6648936, SAMEA6648942, SAMEA6649039, SAMEA6649040, SAMEA6649055, SAMEA6649089, SAMEA6649194	Peart et al. 2020
Zalophus wollabaeki	Espanola Island, EC	SAMEA6648946, SAMEA6648986, SAMEA6649003, SAMEA6649054, SAMEA6649105, SAMEA6649152, SAMEA6649180, SAMEA6649241, SAMEA6649291, SAMEA6649341	Peart et al. 2020
Zalophus wollabaeki	Fernandina Island, EC	SAMEA6648920, SAMEA6648945, SAMEA6648979, SAMEA6648995, SAMEA6648997, SAMEA6649017, SAMEA6649031, SAMEA6649033, SAMEA6649050, SAMEA6649058, SAMEA6649118, SAMEA6649176, SAMEA6649192, SAMEA6649216, SAMEA6649237, SAMEA6649266, SAMEA6649318, SAMEA6649326, SAMEA6649359, SAMEA6649366	Peart et al. 2020
Zalophus wollabaeki	Genovesa Island, EC	SAMEA6649074, SAMEA6649104, SAMEA6649139, SAMEA6649160, SAMEA6649173, SAMEA6649189, SAMEA6649246, SAMEA6649272, SAMEA6649329	Peart et al. 2020
Zalophus wollabaeki	Isabela Island north, EC (“IsabelaB”)	SAMEA6648933, SAMEA6648950, SAMEA6649020, SAMEA6649045, SAMEA6649069, SAMEA6649125, SAMEA6649151, SAMEA6649158, SAMEA6649188, SAMEA6649206, SAMEA6649265, SAMEA6649312, SAMEA6649343, SAMEA6649348, SAMEA6649354	Peart et al. 2020
Zalophus wollabaeki	Isabela Island south, EC (“IsabelaV”)	SAMEA6649042, SAMEA6649066, SAMEA6649081, SAMEA6649130, SAMEA6649142, SAMEA6649224, SAMEA6649229, SAMEA6649256,	Peart et al. 2020

		SAMEA6649292, SAMEA6649300	
Zalophus wollabaeki	Pinta Island, EC	SAMEA6648998, SAMEA6649025, SAMEA6649099, SAMEA6649126, SAMEA6649214, SAMEA6649231, SAMEA6649293, SAMEA6649314, SAMEA6649347, SAMEA6649362	Peart et al. 2020
Zalophus wollabaeki	Santa Fe Island, EC	SAMEA6648923, SAMEA6649026, SAMEA6649076, SAMEA6649090, SAMEA6649145, SAMEA6649243, SAMEA6649250, SAMEA6649273, SAMEA6649319	Peart et al. 2020
Leptonychotes weddellii	Erebus Bay	SAMN19069043, SAMN19069042, SAMN19069041, SAMN19069040, SAMN19069039, SAMN19069038, SAMN19069037, SAMN19069062, SAMN19069061, SAMN19069060, SAMN19069059, SAMN19069058, SAMN19069057, SAMN19069056, SAMN19069055, SAMN19069036, SAMN19069047, SAMN19069045, SAMN19069044, SAMN19069035, SAMN19069034	Miller et al. 2021
Aptenodytes patagonicus	Falkland Islands + Crozet Archipelago	SAMN05771907, SAMN05771908, SAMN05771909, SAMN05771910, SAMN05771911, SAMN05771912, SAMN05771913, SAMN05771914, SAMN05771915, SAMN05771916, SAMN05771917, SAMN05771918, SAMN05771919, SAMN05771920, SAMN05771921, SAMN05771922, SAMN05771923, SAMN05771924, SAMN05771925, SAMN05771926, SAMN05771927, SAMN05771928, SAMN05771929, SAMN05771930, SAMN05771931, SAMN05771932, SAMN05771933, SAMN05771934, SAMN05771935, SAMN05771936, SAMN05771937, SAMN05771938	Clucas et al. 2018
Aptenodytes patagonicus	South Georgia Island	SAMN05771875, SAMN05771876, SAMN05771885, SAMN05771886, SAMN05771887, SAMN05771888, SAMN05771889, SAMN05771890, SAMN05771877, SAMN05771878, SAMN05771879, SAMN05771880, SAMN05771881, SAMN05771882, SAMN05771883, SAMN05771884	Clucas et al. 2018
Aptenodytes patagonicus	Macquarie Island	SAMN05771891, SAMN05771892, SAMN05771894, SAMN05771895, SAMN05771896, SAMN05771898, SAMN05771899, SAMN05771900, SAMN05771901, SAMN05771902, SAMN05771903, SAMN05771904, SAMN05771905, SAMN05771906	Clucas et al. 2018
Pygooscelis	South Shetland	SAMN10140923, SAMN10140921,	Clucas et al. 2018

antarcticus		SAMN10140922, SAMN10140919, SAMN10140920, SAMN10140917, SAMN10140918, SAMN10140915, SAMN10140916, SAMN10140914, SAMN10140913	
Pygooscelis antarcticus	Orne Harbor	SAMN10140924, SAMN10140925, SAMN10140926, SAMN10140932, SAMN10140931, SAMN10140934, SAMN10140933, SAMN10140928, SAMN10140927, SAMN10140930, SAMN10140929	Clucas et al. 2018
Pygooscelis antarcticus	Bouvet & South Sandwich Islands	SAMN10140936, SAMN10140935, SAMN10140904, SAMN10140905, SAMN10140906, SAMN10140912, SAMN10140911, SAMN10140910, SAMN10140909, SAMN10140908, SAMN10140907, SAMN10140937	Clucas et al. 2018
Pygoscelis adeliae	West Antarctica (Antarctic Peninsula & South Sandwich Island)	SAMN10140885, SAMN10140865, SAMN10140866, SAMN10140886, SAMN10140857, SAMN10140883, SAMN10140888, SAMN10140887, SAMN10140890, SAMN10140889, SAMN10140892, SAMN10140891, SAMN10140879, SAMN10140880, SAMN10140877, SAMN10140878, SAMN10140881, SAMN10140882, SAMN10140893, SAMN10140852, SAMN10140851, SAMN10140853, SAMN10140847, SAMN10140850, SAMN10140849, SAMN10140856, SAMN10140855, SAMN10140861, SAMN10140862, SAMN10140863, SAMN10140864, SAMN10140858, SAMN10140859, SAMN10140860, SAMN10140870, SAMN10140869, SAMN10140868, SAMN10140867, SAMN10140874, SAMN10140873, SAMN10140872, SAMN10140871, SAMN10140876, SAMN10140875, SAMN10140884	Clucas et al. 2018
Pygoscelis adeliae	East Antarctica (Welch, Bechervaise and Petrels Islands & Blakeney Point)	SAMN10140894, SAMN10140836, SAMN10140835, SAMN10140834, SAMN10140833, SAMN10140832, SAMN10140831, SAMN10140830, SAMN10140829, SAMN10140828, SAMN10140827, SAMN10140896, SAMN10140895, SAMN10140826, SAMN10140825, SAMN10140822, SAMN10140821, SAMN10140824, SAMN10140823, SAMN10140818, SAMN10140817, SAMN10140820, SAMN10140819, SAMN10140897, SAMN10140899, SAMN10140900, SAMN10140901, SAMN10140902, SAMN10140903, SAMN10140843, SAMN10140844, SAMN10140841, SAMN10140842, SAMN10140839,	Clucas et al. 2018

		SAMN10140840, SAMN10140837, SAMN10140838, SAMN10140845, SAMN10140846	
Pygoscelis papua	Falkland Islands	SAMN10140965, SAMN10140966, SAMN10140959, SAMN10140960, SAMN10140958, SAMN10140963, SAMN10140964, SAMN10140961, SAMN10140962, SAMN10140968, SAMN10140967	Clucas et al. 2018
Pygoscelis papua	Antarctic Peninsula (Shetland, Georges, Jougla)	SAMN10141003, SAMN10141004, SAMN10141001, SAMN10141002, SAMN10140999, SAMN10141000, SAMN10140997, SAMN10140998, SAMN10140977, SAMN10140978, SAMN10140979, SAMN10140980, SAMN10140981, SAMN10140982, SAMN10140983, SAMN10140984, SAMN10140985, SAMN10140986, SAMN10140996, SAMN10140995, SAMN10140994, SAMN10140993, SAMN10140992, SAMN10140991, SAMN10140990, SAMN10140989, SAMN10140988, SAMN10140987, SAMN10140976, SAMN10140975, SAMN10140970, SAMN10140969, SAMN10140972, SAMN10140971, SAMN10140974, SAMN10140973	Clucas et al. 2018
Pygoscelis papua	Kerguelen Island	SAMN10141005, SAMN10141006, SAMN10141016, SAMN10141015, SAMN10141012, SAMN10141011, SAMN10141014, SAMN10141013, SAMN10141008, SAMN10141007, SAMN10141010, SAMN10141009	Clucas et al. 2018
Aptenodytes forsteri	Amanda Bay & Pointe Geologie	SAMN06830720, SAMN06830721, SAMN06830715, SAMN06830718, SAMN06830719, SAMN06830716, SAMN06830717, SAMN06830670, SAMN06830671, SAMN06830668, SAMN06830669, SAMN06830666, SAMN06830667, SAMN06830664, SAMN06830665, SAMN06830662, SAMN06830663, SAMN06830676, SAMN06830677, SAMN06830674, SAMN06830675, SAMN06830672, SAMN06830673, SAMN06830725, SAMN06830724, SAMN06830723, SAMN06830722, SAMN06830729, SAMN06830728, SAMN06830727, SAMN06830726	Clucas et al. 2018
Aptenodytes forsteri	Fold Island & Auster	SAMN06830740, SAMN06830741, SAMN06830736, SAMN06830737, SAMN06830738, SAMN06830739, SAMN06830732, SAMN06830733, SAMN06830734, SAMN06830735, SAMN06830691, SAMN06830690, SAMN06830689, SAMN06830688,	Clucas et al. 2018

		SAMN06830687, SAMN06830686, SAMN06830685, SAMN06830684, SAMN06830683, SAMN06830682, SAMN06830692, SAMN06830693, SAMN06830743, SAMN06830742, SAMN06830745, SAMN06830744, SAMN06830678, SAMN06830679, SAMN06830680, SAMN06830681, SAMN06830731, SAMN06830730	
Aptenodytes forsteri	Gould Bay & Halley Bay	SAMN06830771, SAMN06830770, SAMN06830767, SAMN06830766, SAMN06830769, SAMN06830768, SAMN06830763, SAMN06830762, SAMN06830765, SAMN06830764, SAMN06830751, SAMN06830750, SAMN06830760, SAMN06830761, SAMN06830758, SAMN06830759, SAMN06830756, SAMN06830757, SAMN06830754, SAMN06830755, SAMN06830752, SAMN06830753	Clucas et al. 2018
Aptenodytes forsteri	Cape Roget & Cape Washington	SAMN06830711, SAMN06830710, SAMN06830703, SAMN06830702, SAMN06830705, SAMN06830704, SAMN06830707, SAMN06830706, SAMN06830709, SAMN06830708, SAMN06830714, SAMN06830712, SAMN06830713, SAMN06830700, SAMN06830701, SAMN06830694, SAMN06830695, SAMN06830696, SAMN06830697, SAMN06830698, SAMN06830699	Clucas et al. 2018
Odontesthes argentinensis	Uruguay	SAMN12709423, SAMN12709422, SAMN12709421, SAMN12709346, SAMN12709343, SAMN12709345, SAMN12709342, SAMN12709341, SAMN12709439, SAMN12709431, SAMN12709430, SAMN12709429, SAMN12709427, SAMN12709426, SAMN12709425, SAMN12709428, SAMN12709424, SAMN12709344	Hughes et al. 2020
Odontesthes regia	Chile	SAMN12709332, SAMN12709331, SAMN12709330, SAMN12709329, SAMN12709328, SAMN12709327, SAMN12709326, SAMN12709340, SAMN12709339, SAMN12709468, SAMN12709337, SAMN12709336, SAMN12709335, SAMN12709334, SAMN12709325, SAMN12709338, SAMN12709333, SAMN12709324	Hughes et al. 2020
Odontesthes mirinensis	Brazil	SAMN12709386, SAMN12709385, SAMN12709384, SAMN12709383, SAMN12709381, SAMN12709380, SAMN12709379, SAMN12709382, SAMN12709378, SAMN12709377, SAMN12709376	Hughes et al. 2020

Odontesthes mauleanum	Chile	SAMN12709405, SAMN12709402, SAMN12709401, SAMN12709400, SAMN12709399, SAMN12709397, SAMN12709396, SAMN12709395, SAMN12709398, SAMN12709394, SAMN12709393, SAMN12709392, SAMN12709391, SAMN12709390, SAMN12709375, SAMN12709373, SAMN12709372, SAMN12709374, SAMN12709370, SAMN12709369, SAMN12709368, SAMN12709366, SAMN12709365, SAMN12709364, SAMN12709367, SAMN12709363, SAMN12709362, SAMN12709469, SAMN12709471, SAMN12709467, SAMN12709465, SAMN12709464, SAMN12709463, SAMN12709462, SAMN12709371, SAMN12709466, SAMN12709404, SAMN12709403	Hughes et al. 2020
Odontesthes ledae	Brazil	SAMN12709415, SAMN12709414, SAMN12709412, SAMN12709411, SAMN12709410, SAMN12709413, SAMN12709409, SAMN12709408, SAMN12709407, SAMN12709389, SAMN12709388, SAMN12709387, SAMN12709406	Hughes et al. 2020
Odontesthes bonariensis	Uruguay	SAMN12709487, SAMN12709486, SAMN12709484, SAMN12709483, SAMN12709485, SAMN12709482, SAMN12709481, SAMN12709480, SAMN12709479, SAMN12709477, SAMN12709476, SAMN12709475, SAMN12709478, SAMN12709474, SAMN12709473	Hughes et al. 2020
Odontesthes hatcheri	Uruguay	SAMN12709456, SAMN12709455, SAMN12709454, SAMN12709453, SAMN12709452, SAMN12709451, SAMN12709450, SAMN12709449, SAMN12709448, SAMN12709447, SAMN12709446, SAMN12709445, SAMN12709444, SAMN12709441, SAMN12709440, SAMN12709443, SAMN12709442	Hughes et al. 2020

Appendix B: Stairway Plot figures

This appendix contains the standard Stairway Plot 2 outputs for all of the populations listed in Table 4.2. In these figures, the central line represents the median time-specific estimate of effective population size (N_e) while the inner (darker) shaded area represents the 12.5^{th}-87.5^{th} percentiles of N_e estimates and the lighter shaded area represents the 2.5^{th}-97.5^{th} percentiles of N_e estimates over 200 Stairway Plot iterations. Note that the composite slope values presented in Chapter 4 (e.g. Figure 4.4) are not derived directly from the changes in median N_e shown here, but are instead based on the proportion of Stairway Plot 2 model iterations in which N_e increased, decreased, or remained constant between time points, as described in the Methods section of Chapter 4. This is important to understand because it is possible, for example, for all Stairway Plot iterations to agree that N_e increased between t0 to t1, yet vary widely in the magnitude of N_e that each iteration estimates for t0 and t1. Such a scenario could result in the appearance of large disparities in N_e during a particular time interval in one of these plots (i.e. wide shaded areas implying disagreement in N_e estimates across model iterations), while at the same time the composite slope values generated by the align_stairwayplot.py program and analysed in Chapter 4 may be high, reflecting agreement across most model iterations that N_e was on the rise during that time interval, irrespective of the absolute magnitude of N_e or of the change in N_e.

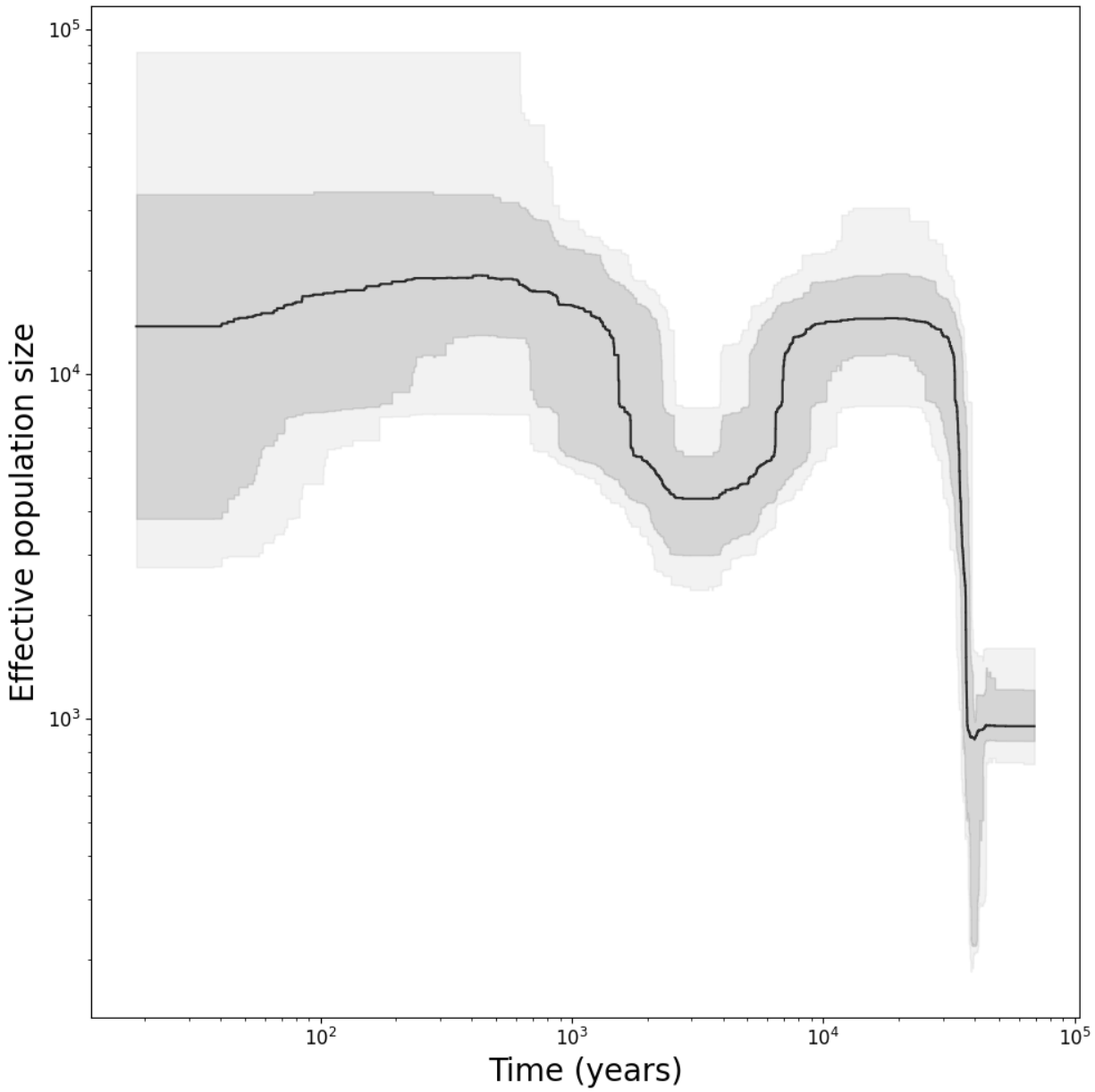

Figure B.1. *Otaria flavescens* (“Oflavescens”)

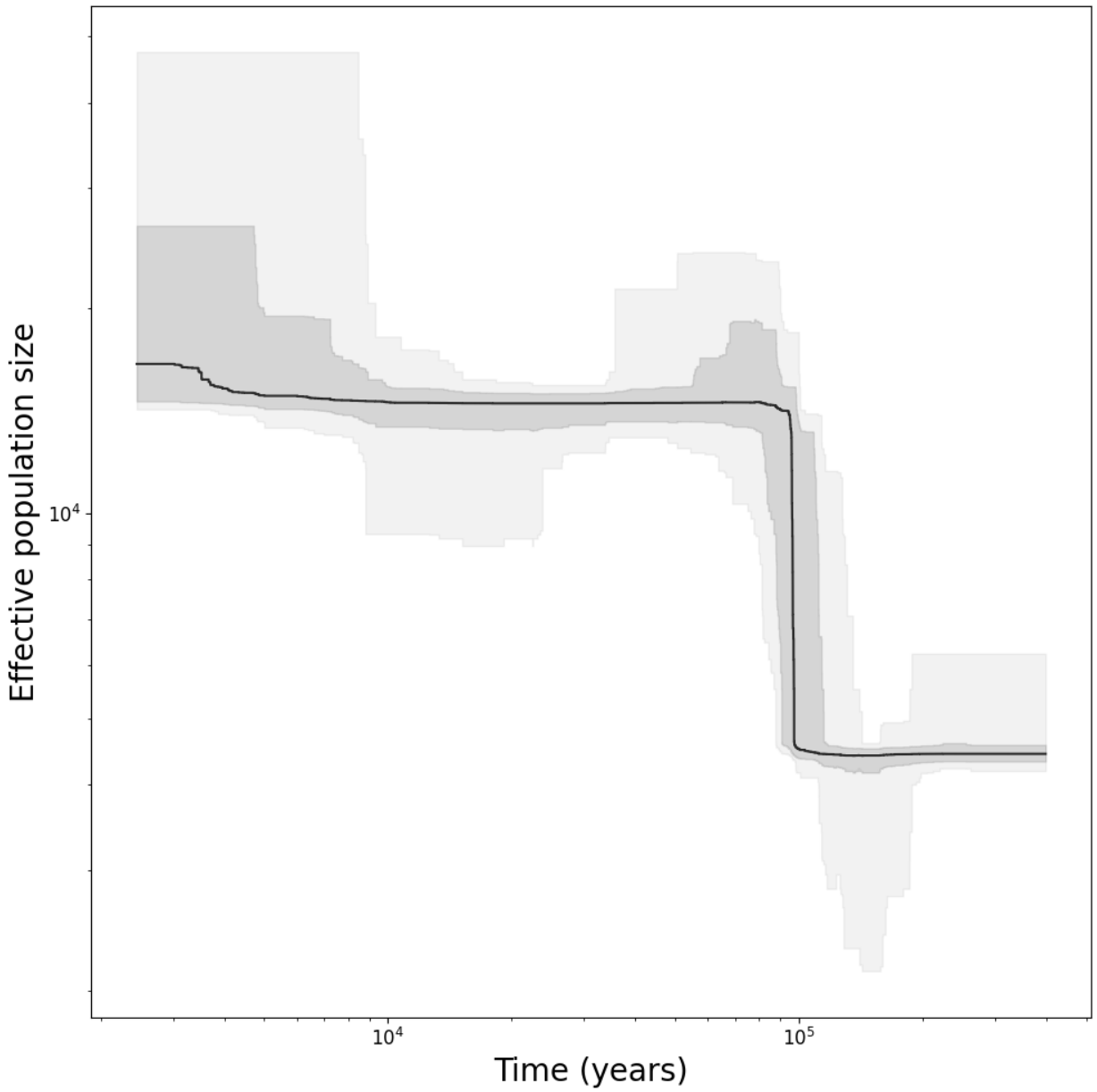

Figure B.2. *Arctocephalus australis* (“Arctocephalus_australis_Brazil”)

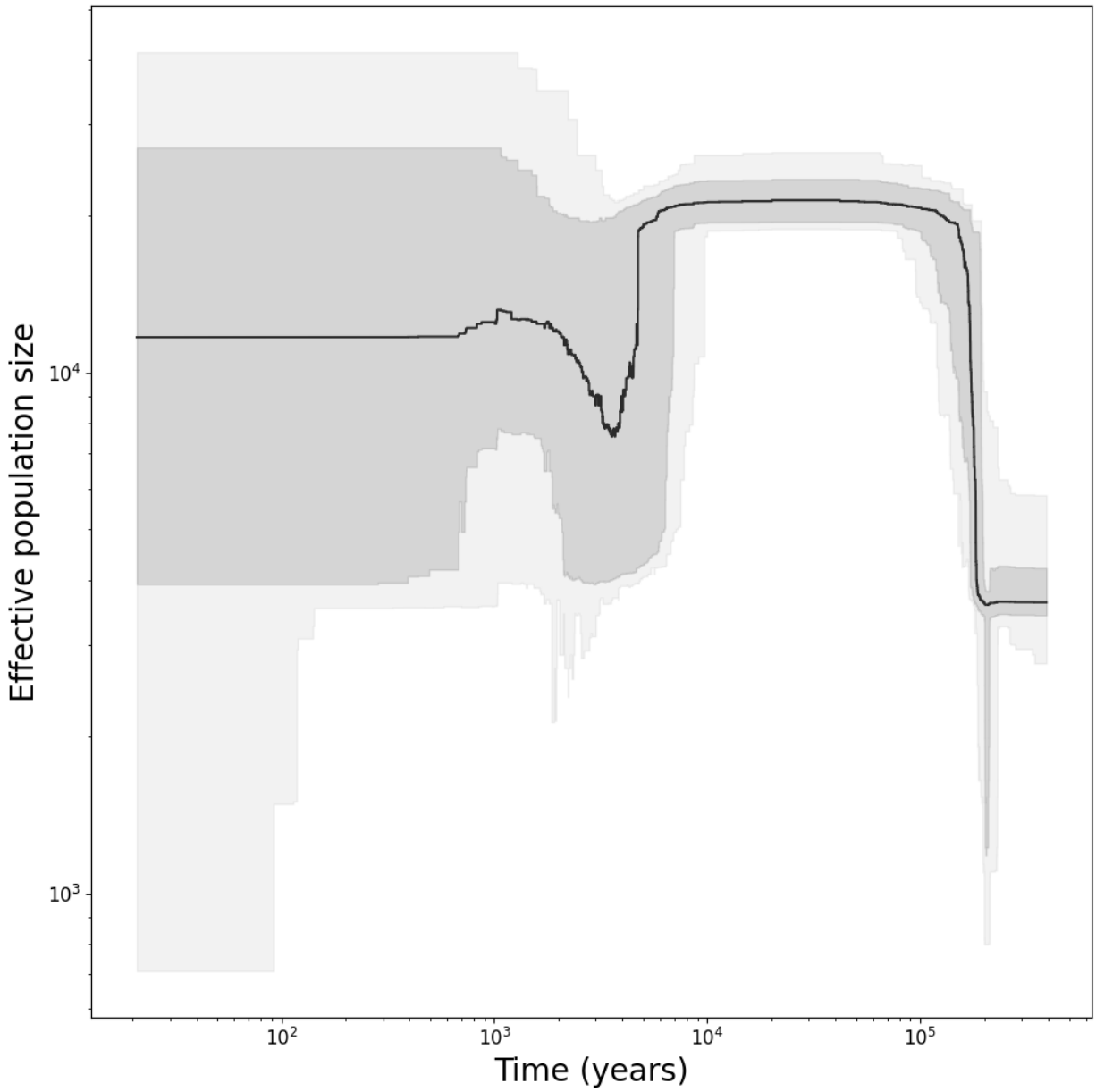

Figure B.3. *Arctocephalus forsteri* (“Arctocephalus_forsteri_NZ”)

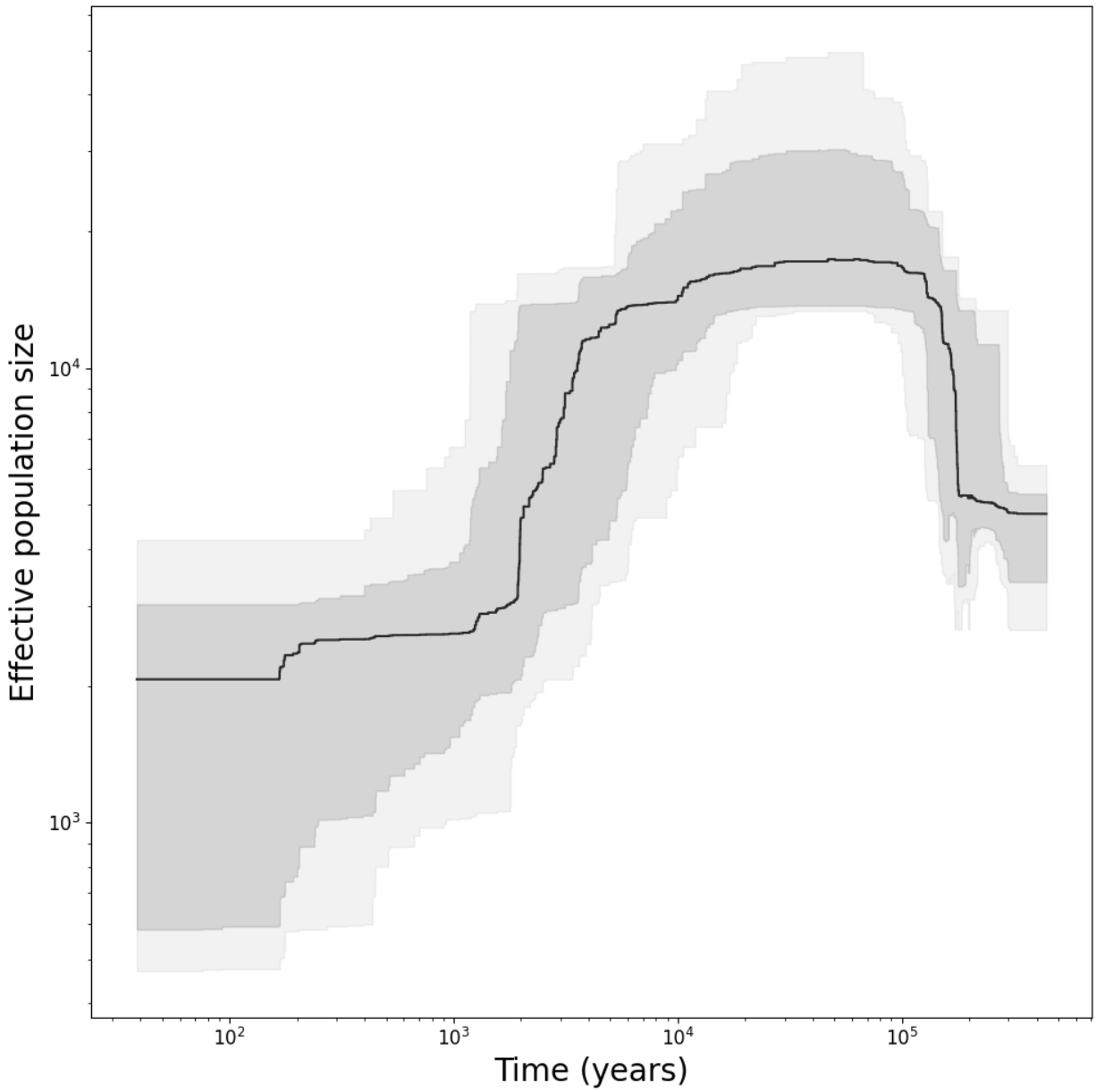

Figure B.4. *Arctocephalus forsteri* (“Arctocephalus_forsteri_CFoulwind”)

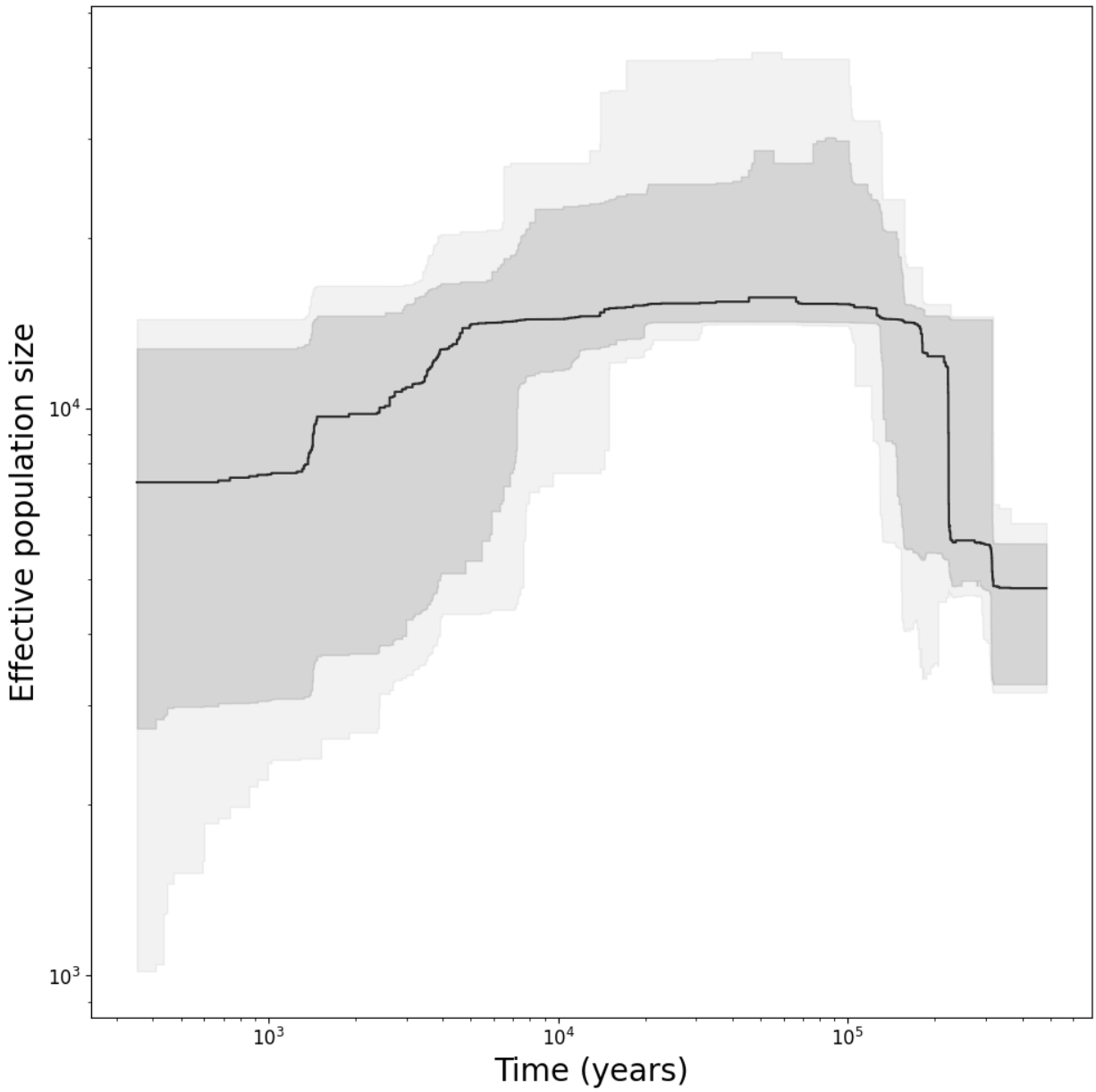

Figure B.5. *Arctocephalus forsteri* (“Arctocephalus_forsteri_OBay”)

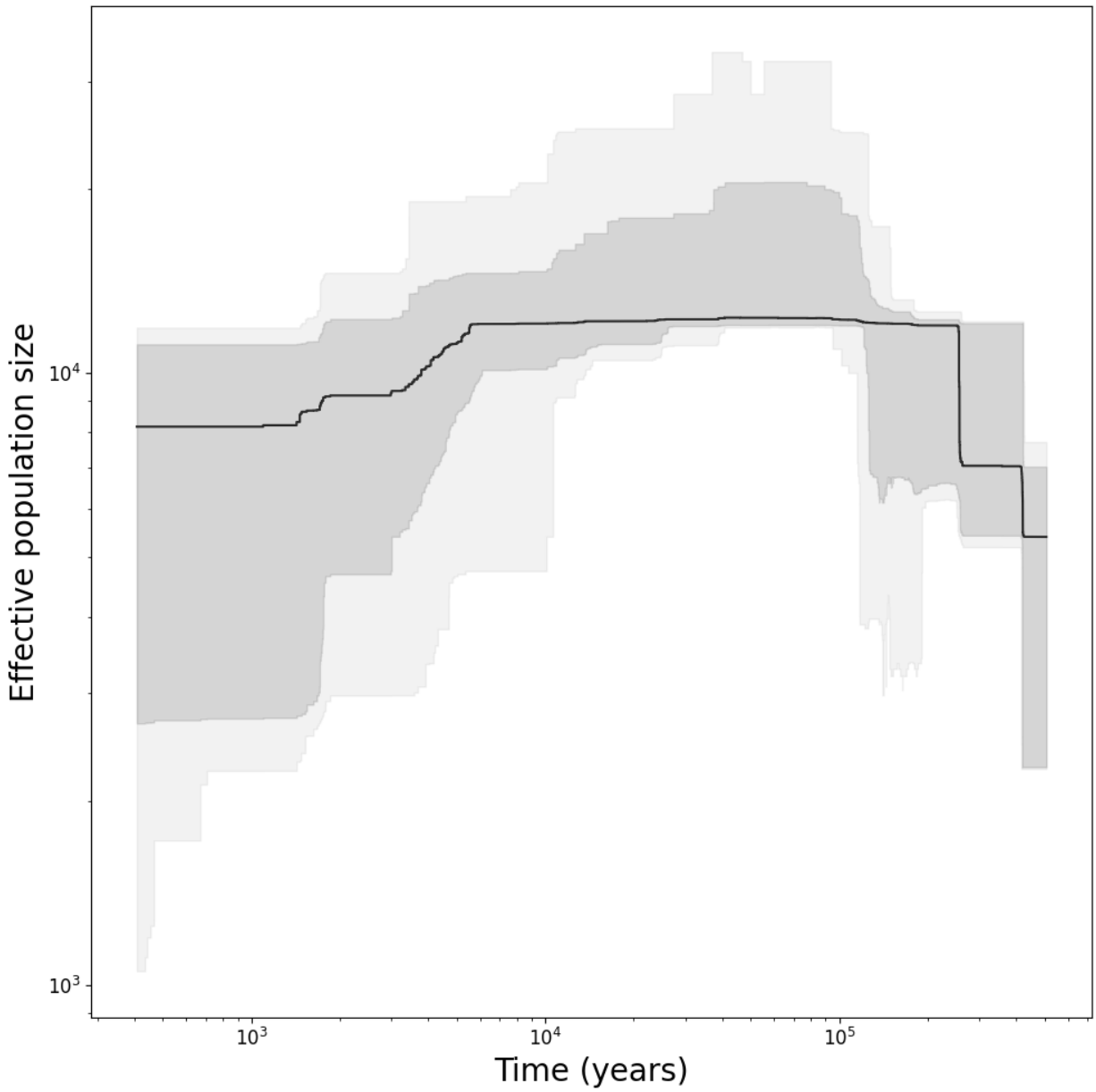

Figure B.6. *Arctocephalus forsteri* (“Arctocephalus_forsteri_OhauP”)

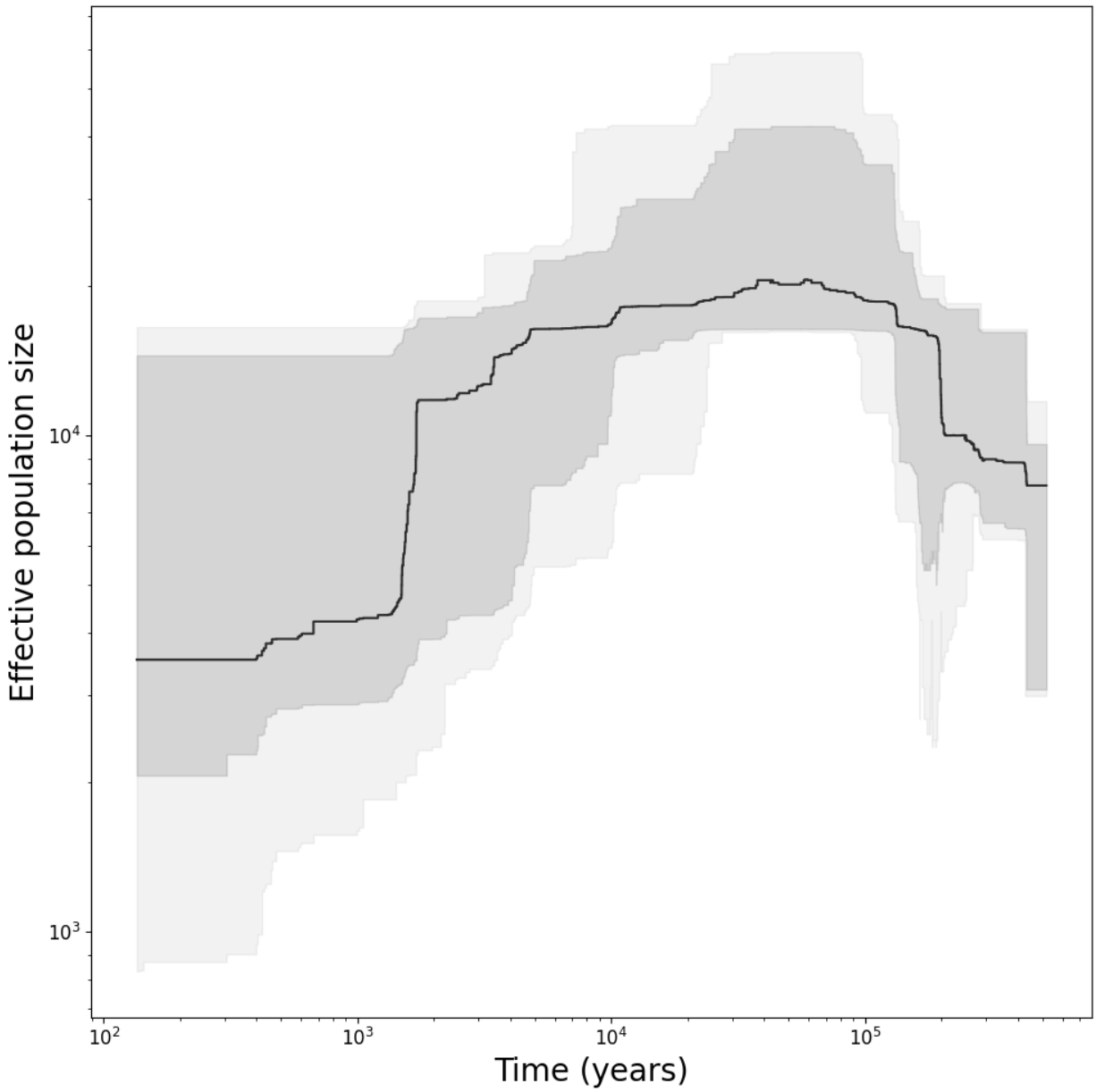

Figure B.7. *Arctocephalus forsteri* (“Arctocephalus_forsteri_VictoryB”)

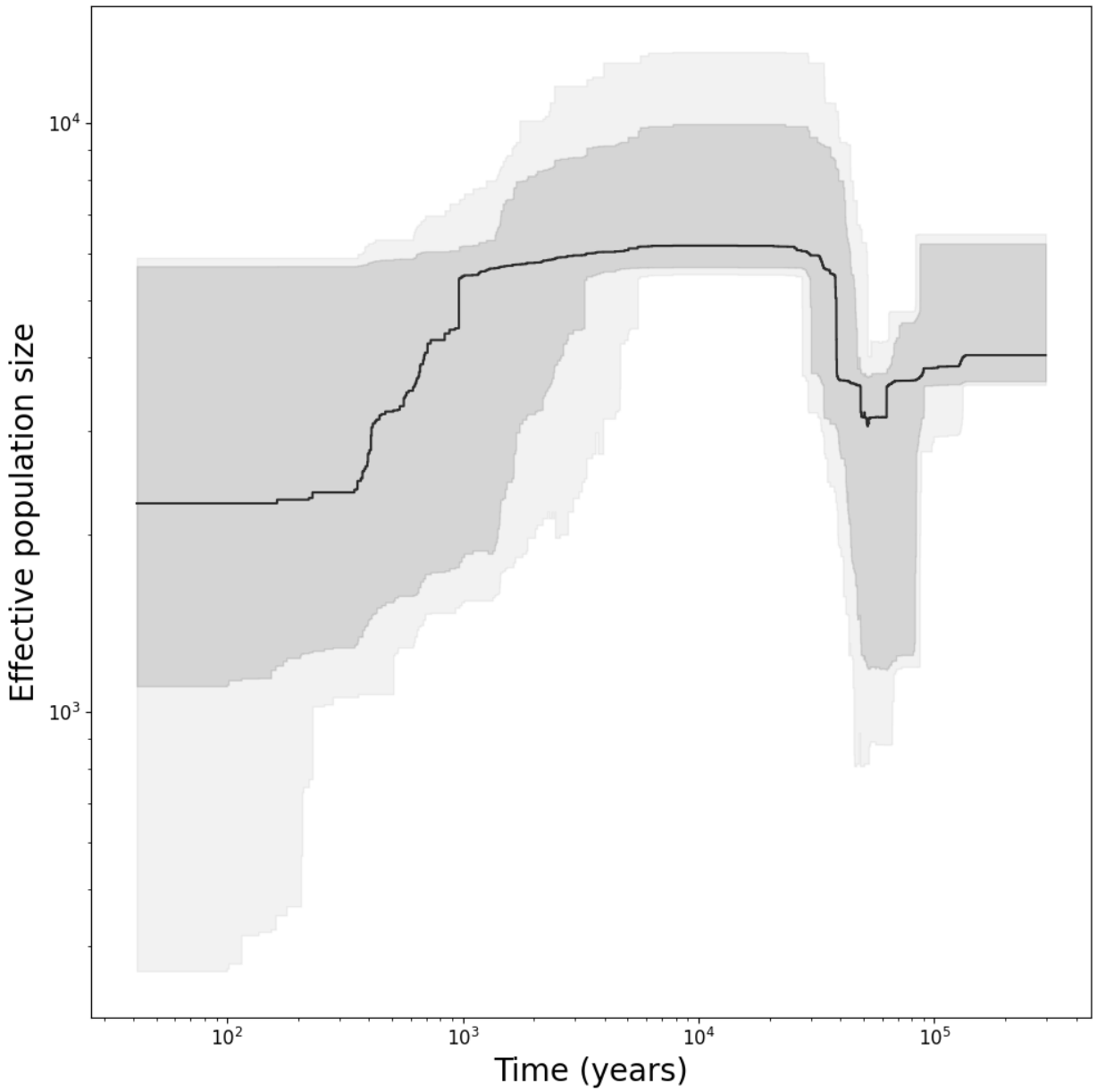

Figure B.8. *Arctocephalus galapagoensis* (“Arctocephalus_galapagoensis_Isabela”)

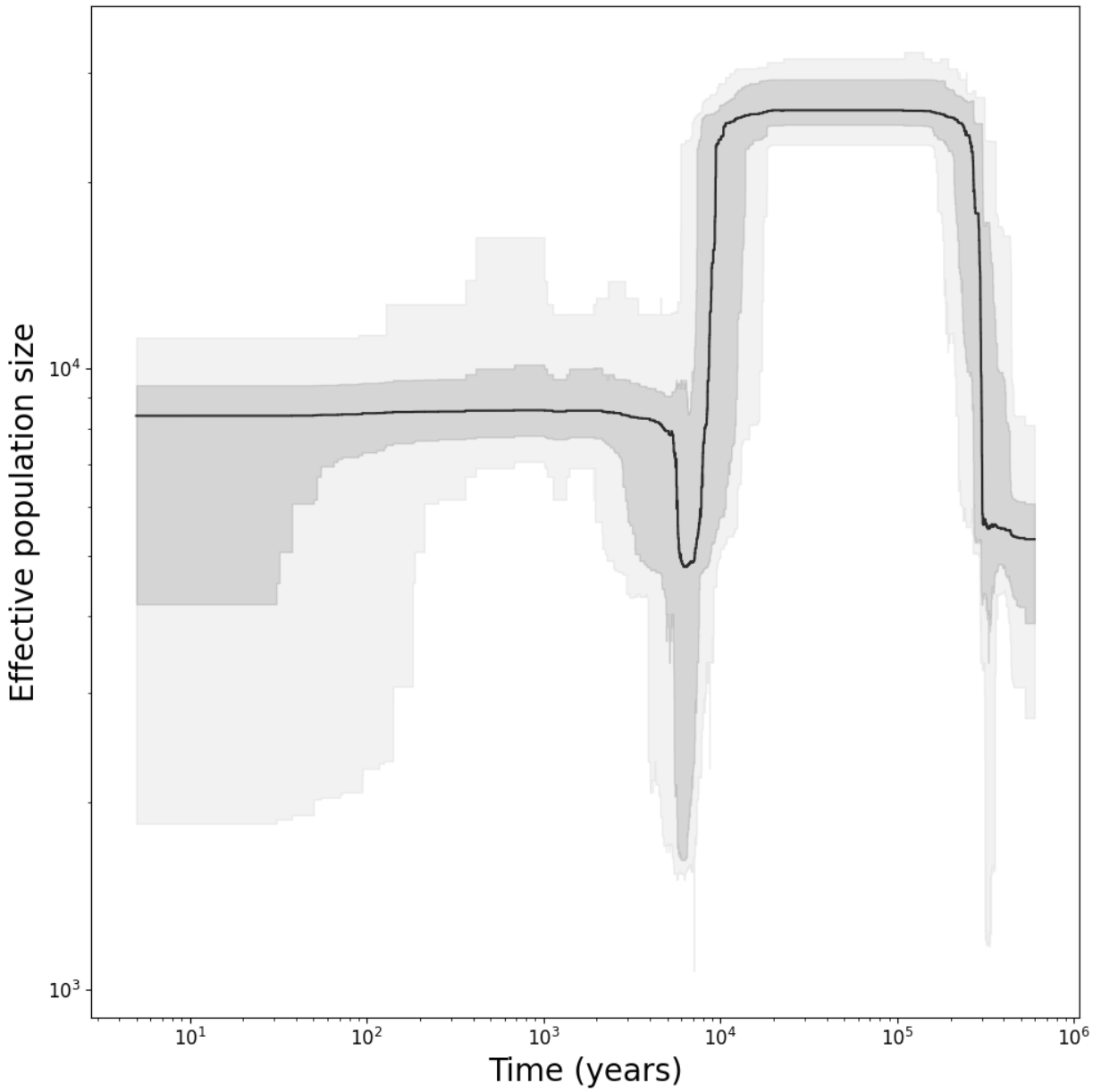

Figure B.9. *Arctocephalus gazella* (“Arctocephalus_gazella_BirdIs”)

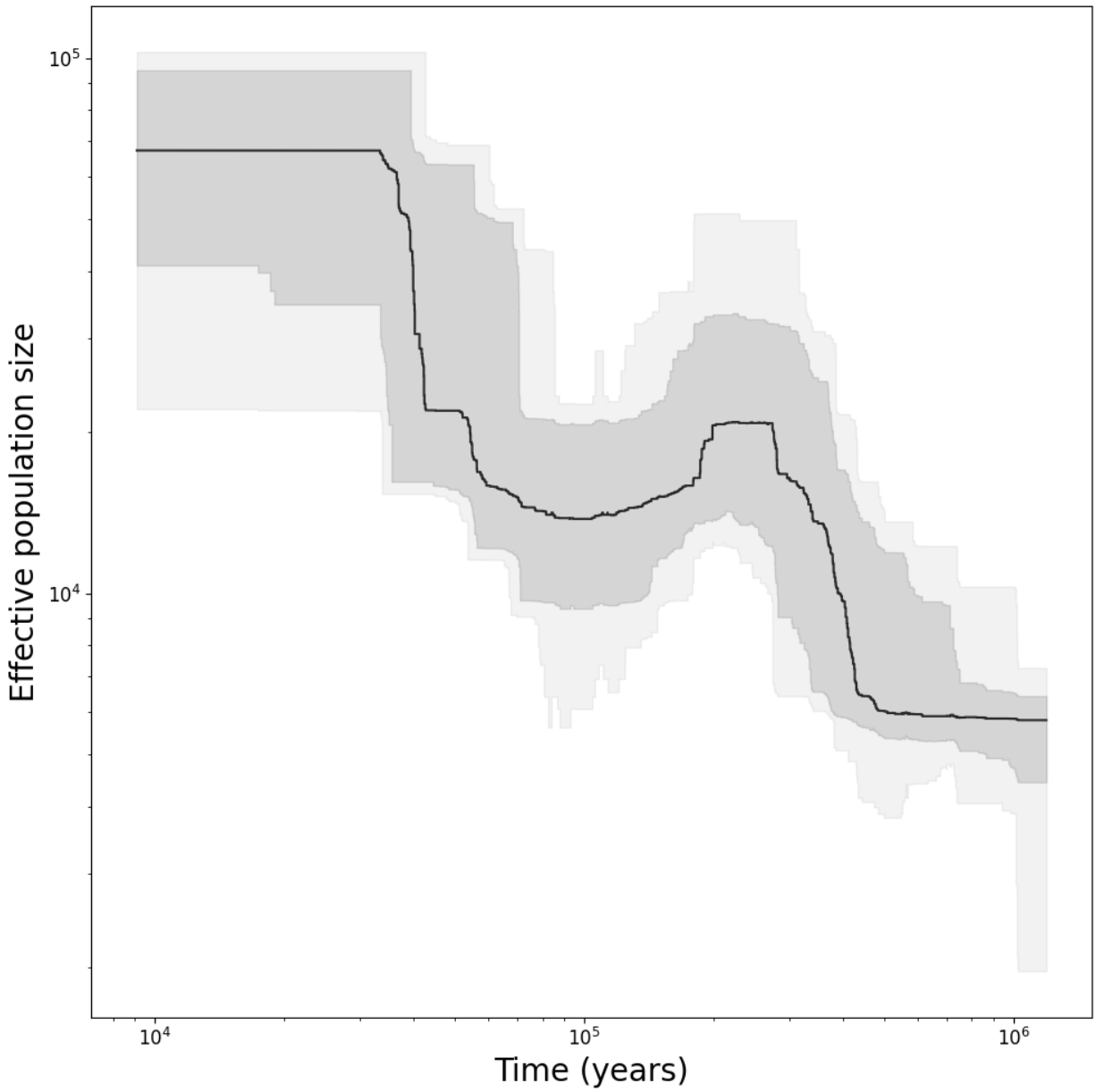

Figure B.10. *Mirounga leonina* (“Mirounga_leonina_SAtlantic”)

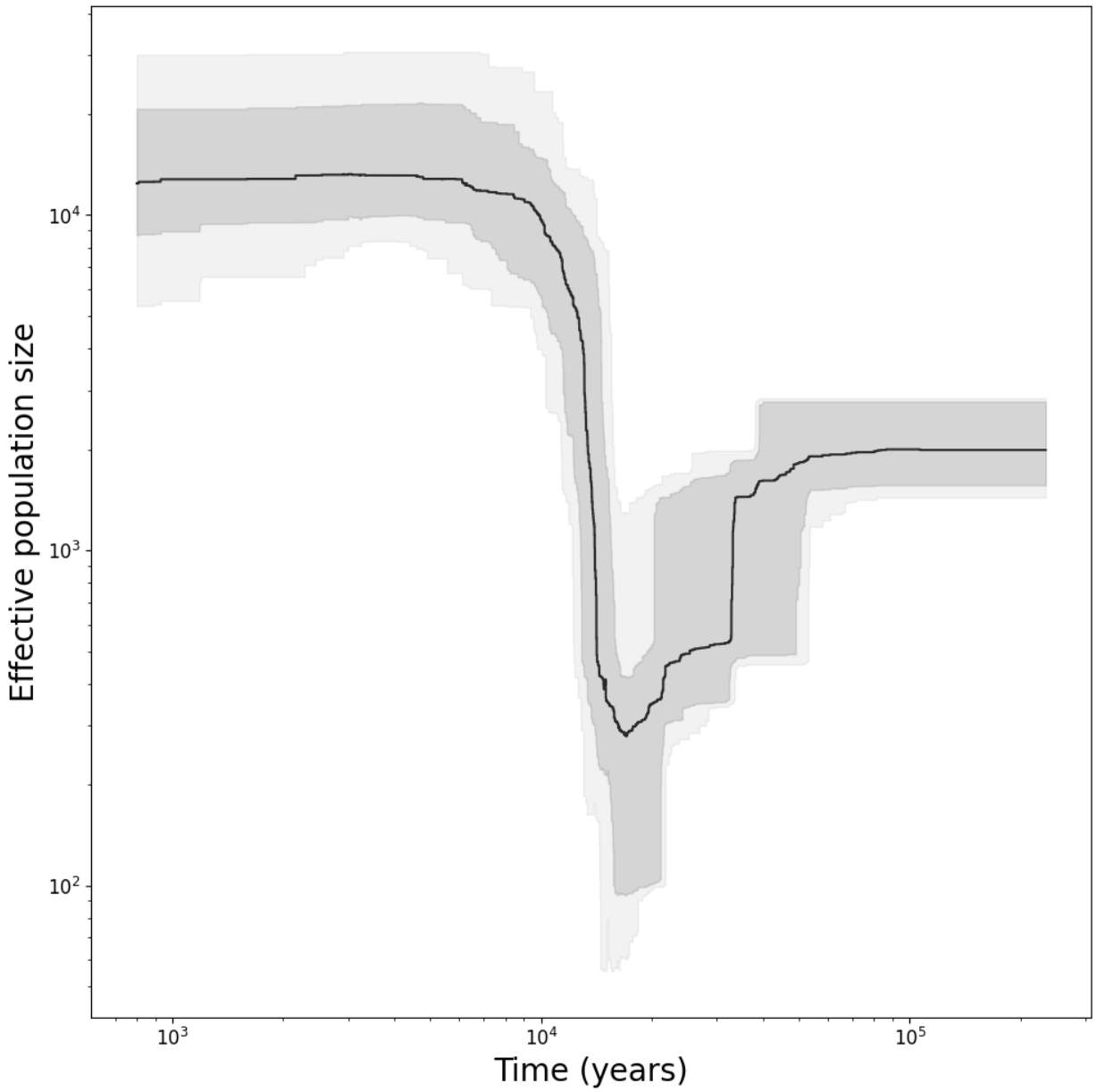

Figure B.11. *Mirounga angustirostris* (“Mirounga_angustirostris_NAtlantic”)

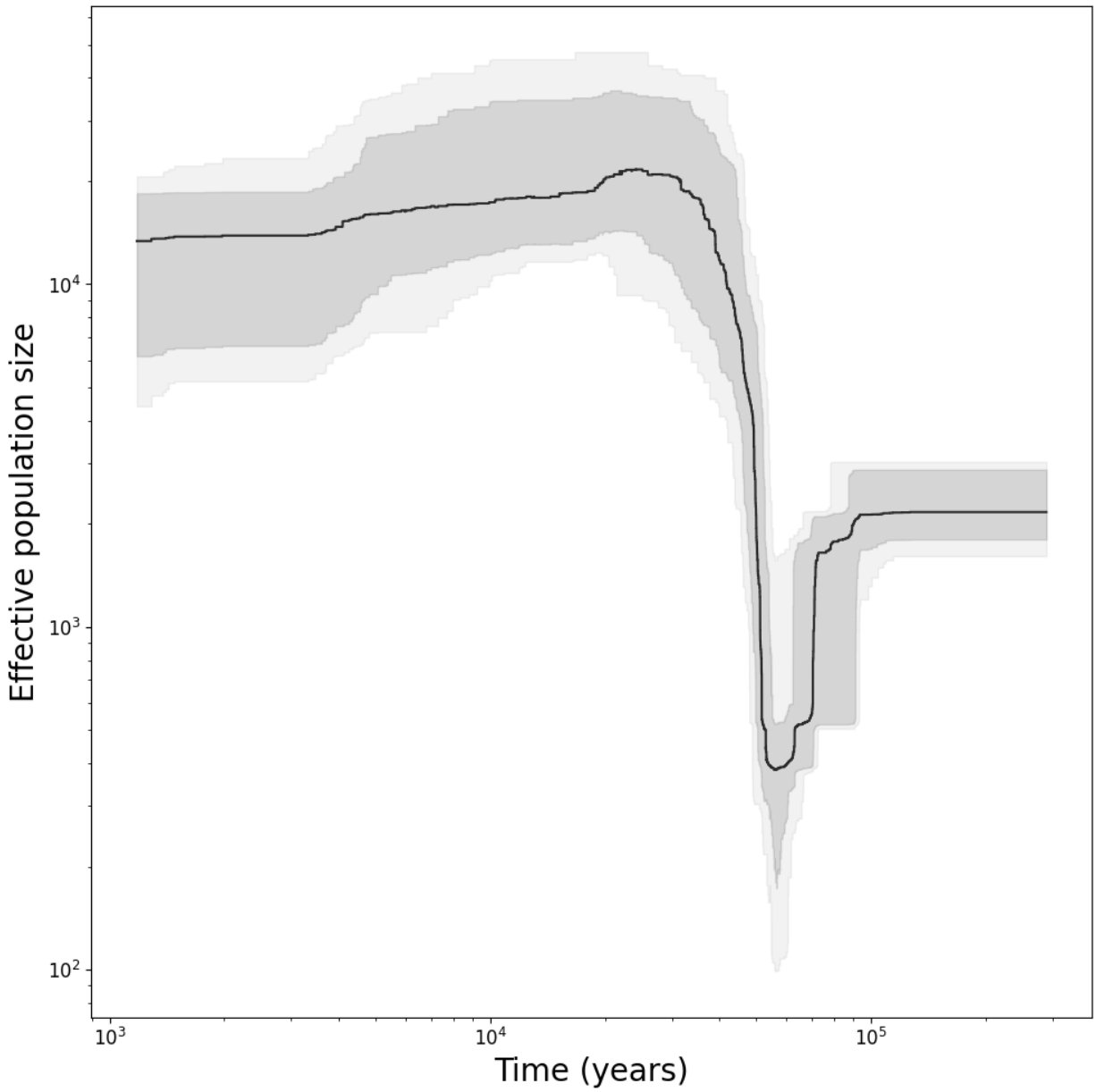

Figure B.12. *Phoca vitulina* (“Phoca_vitulina_vitulina_Svalbard”)

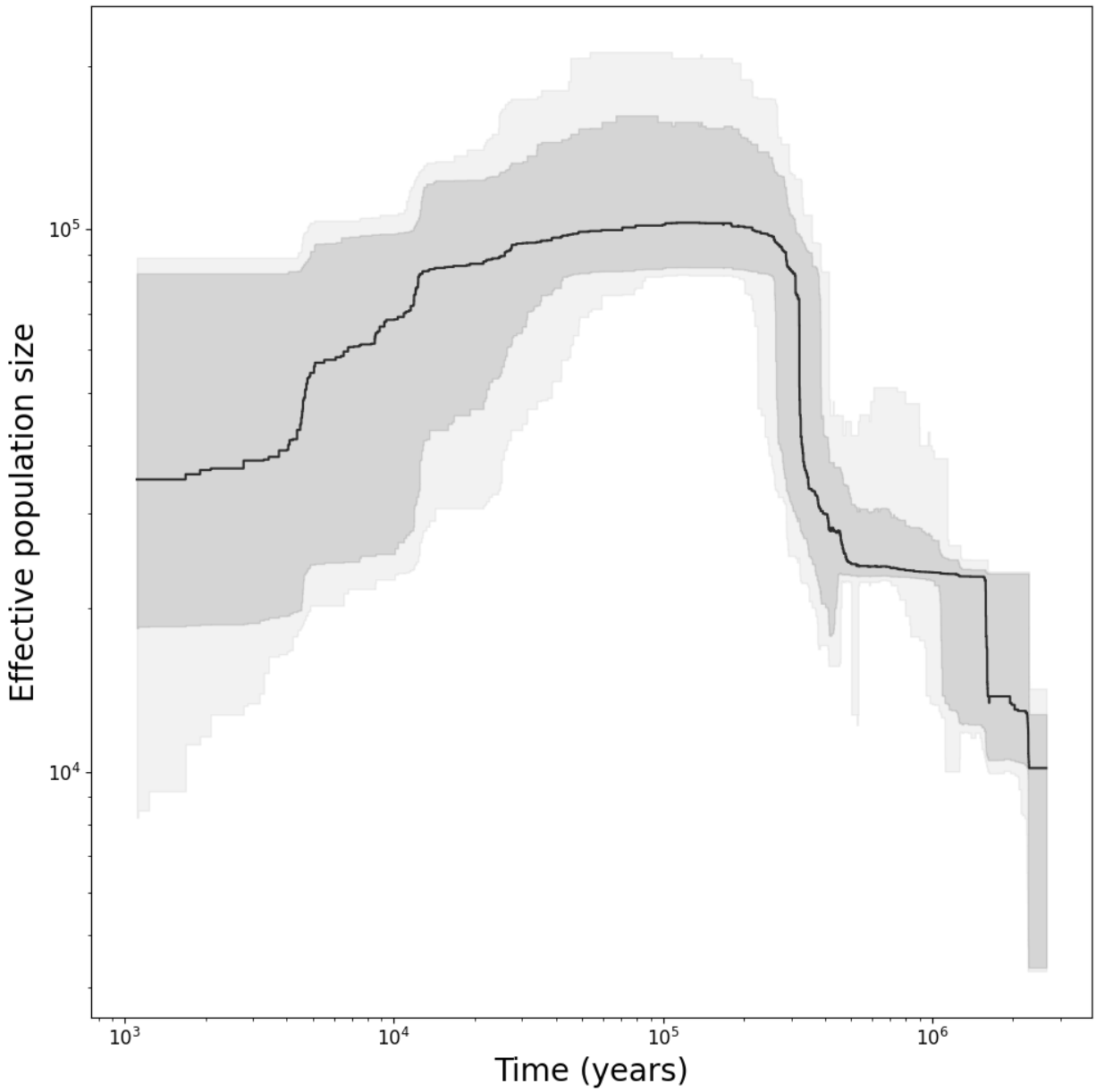

Figure B.13. *Pusa hispida* (“Pusa_hispida_hispida_Svalbard”)

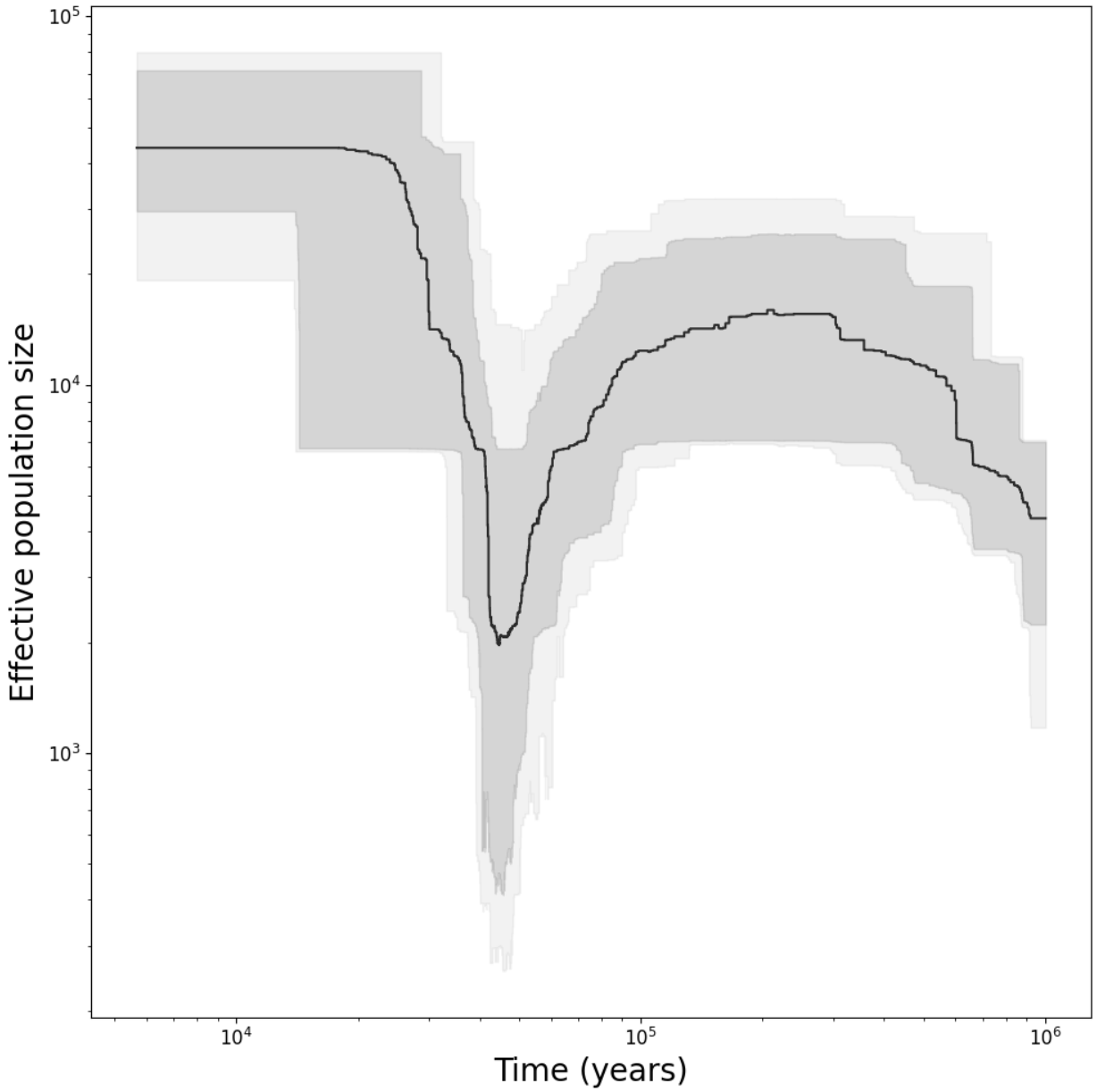

Figure B.14. *Erignathus barbatus* (“Erignathus_barbatus_Svalbard”)

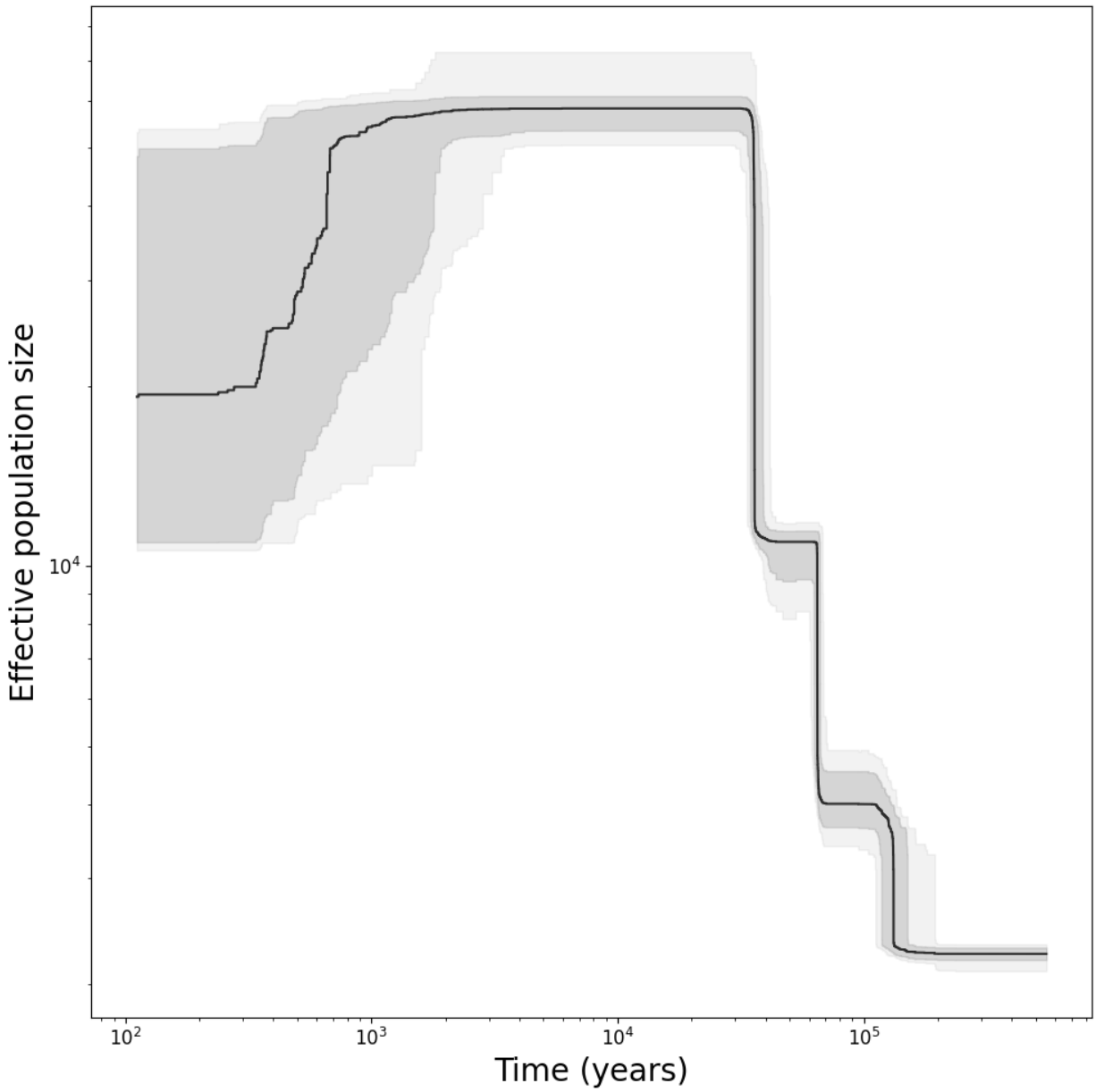

Figure B.15. *Zalophus californianus* (“Zalophus_californianus”)

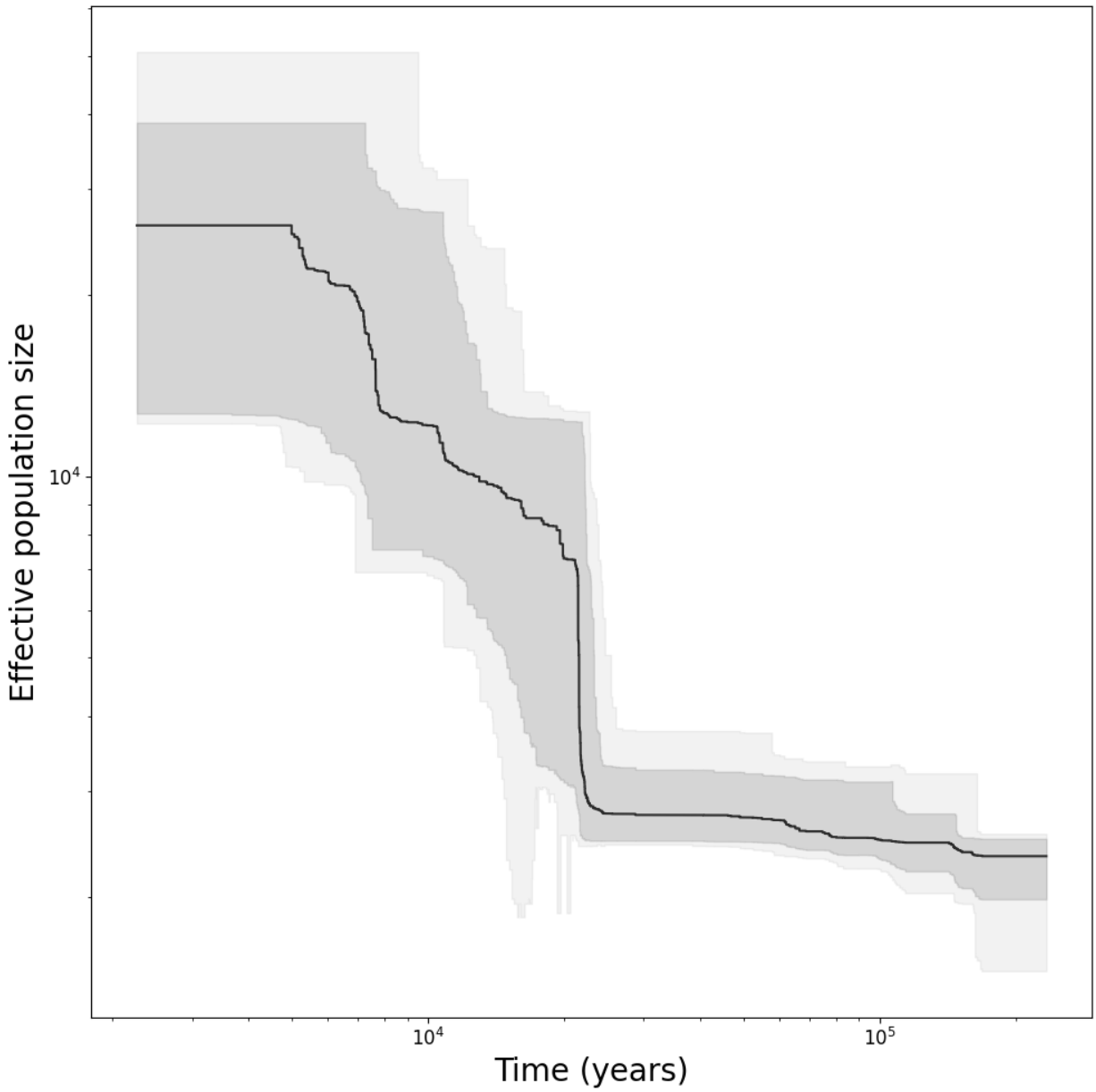

Figure B.16. *Zalophus californianus* (“Zalophus_californianus_GCal1”)

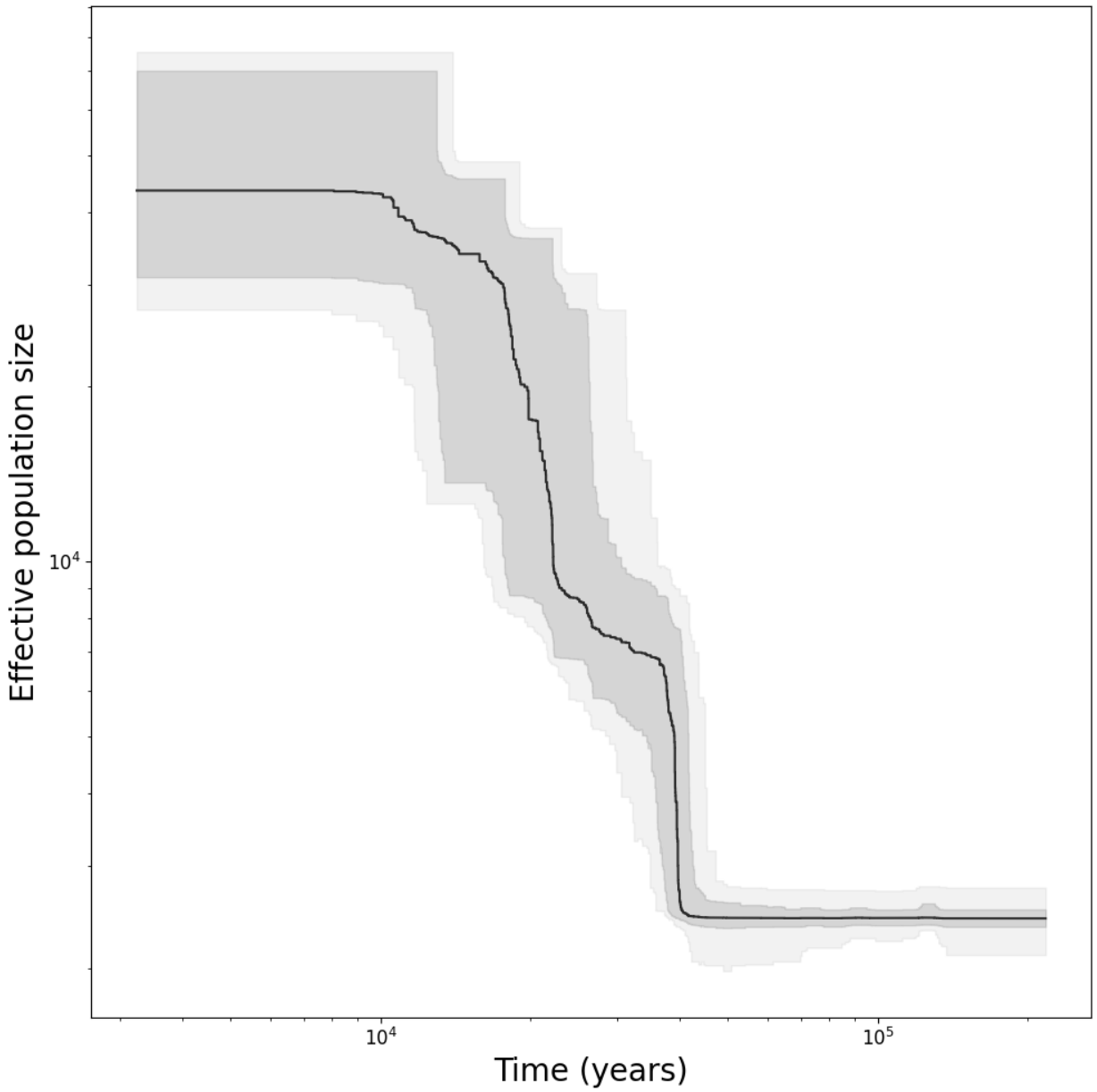

Figure B.17. *Zalophus californianus* (“Zalophus_californianus_GCal2”)

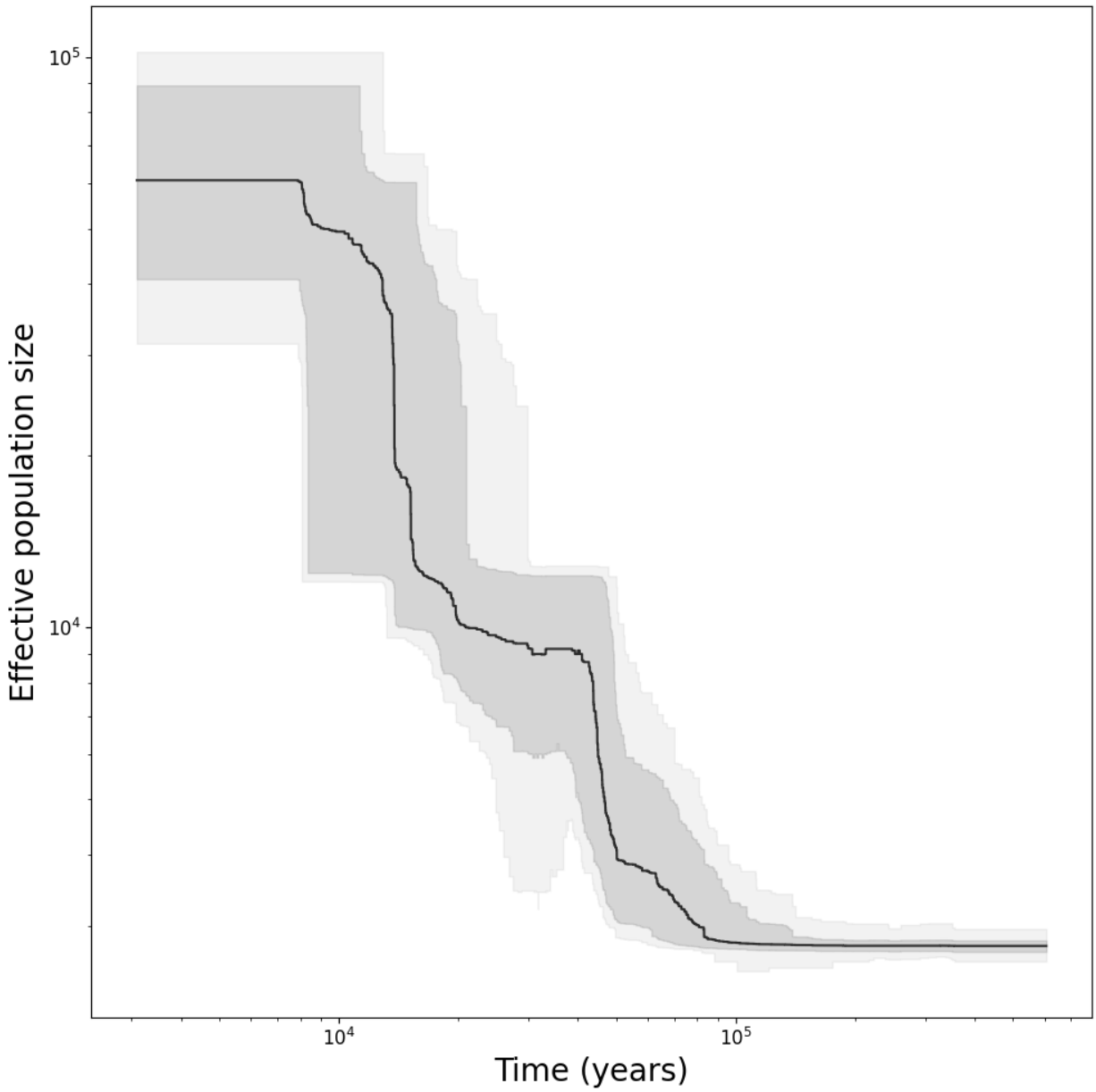

Figure B.18. *Zalophus californianus* (“Zalophus_californianus_GCal3”)

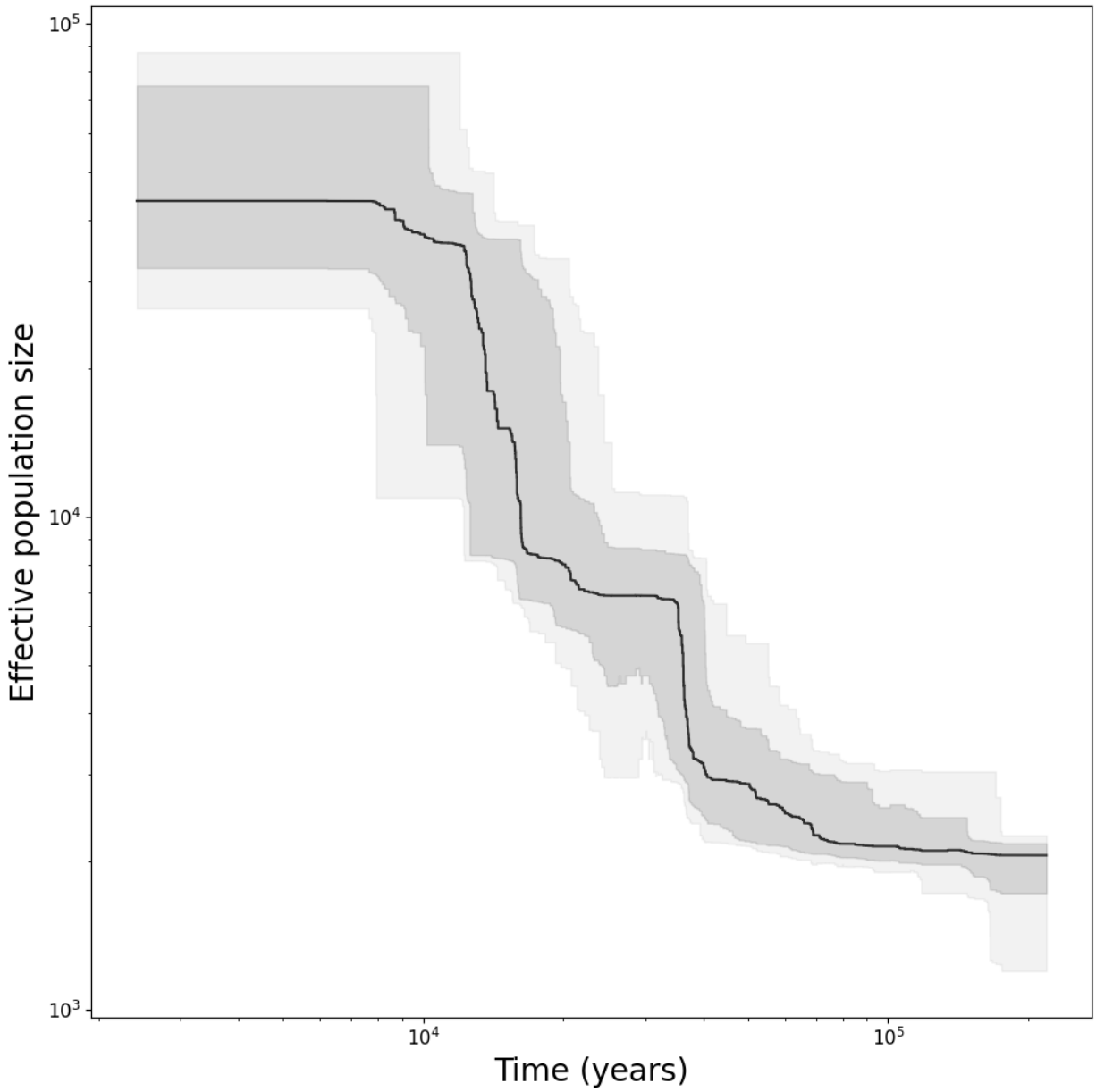

Figure B.19. *Zalophus californianus* (“Zalophus_californianus_GCal4”)

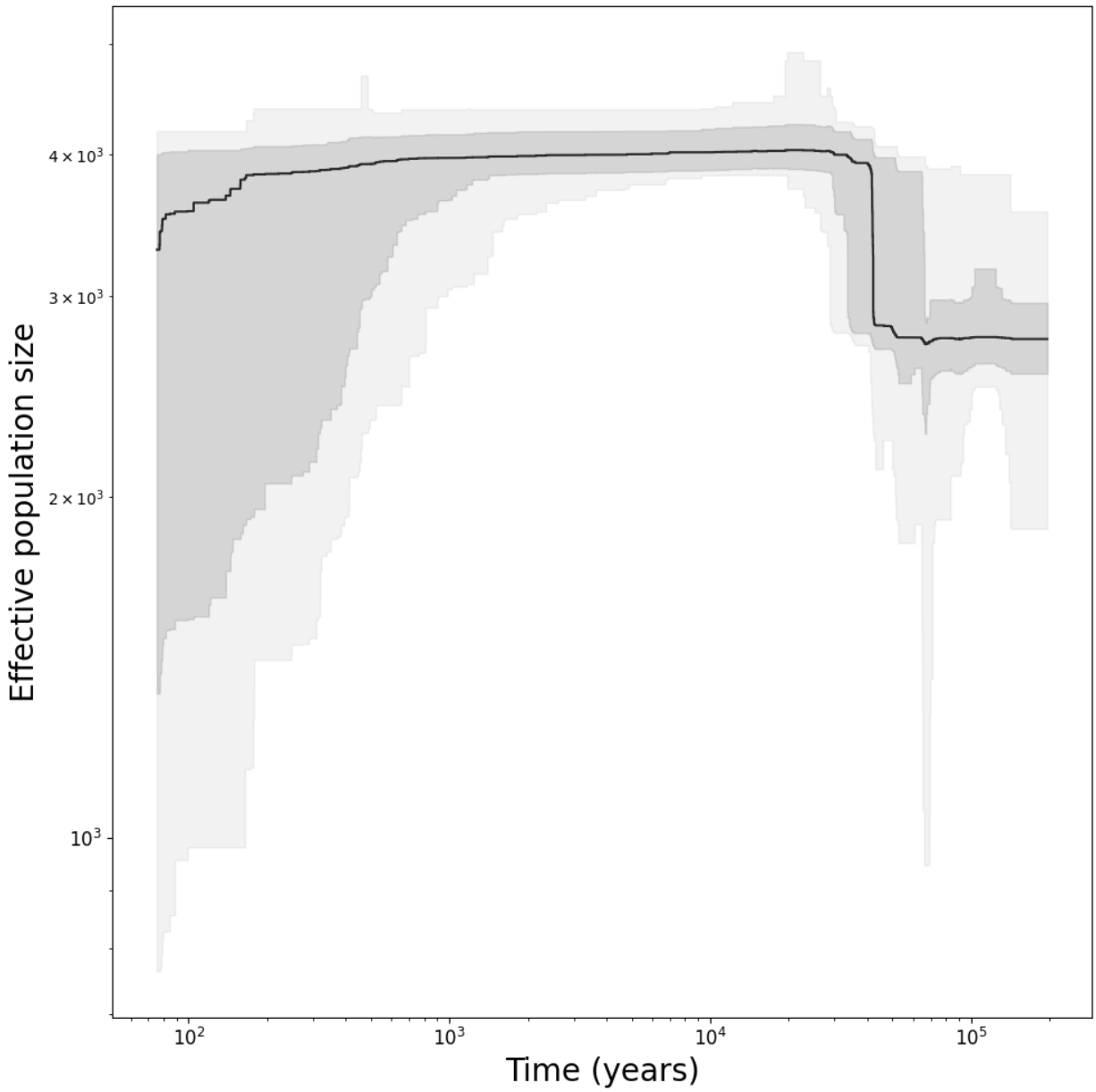

Figure B.20. *Zalophus californianus* (“Zalophus_californianus_SMargarita”)

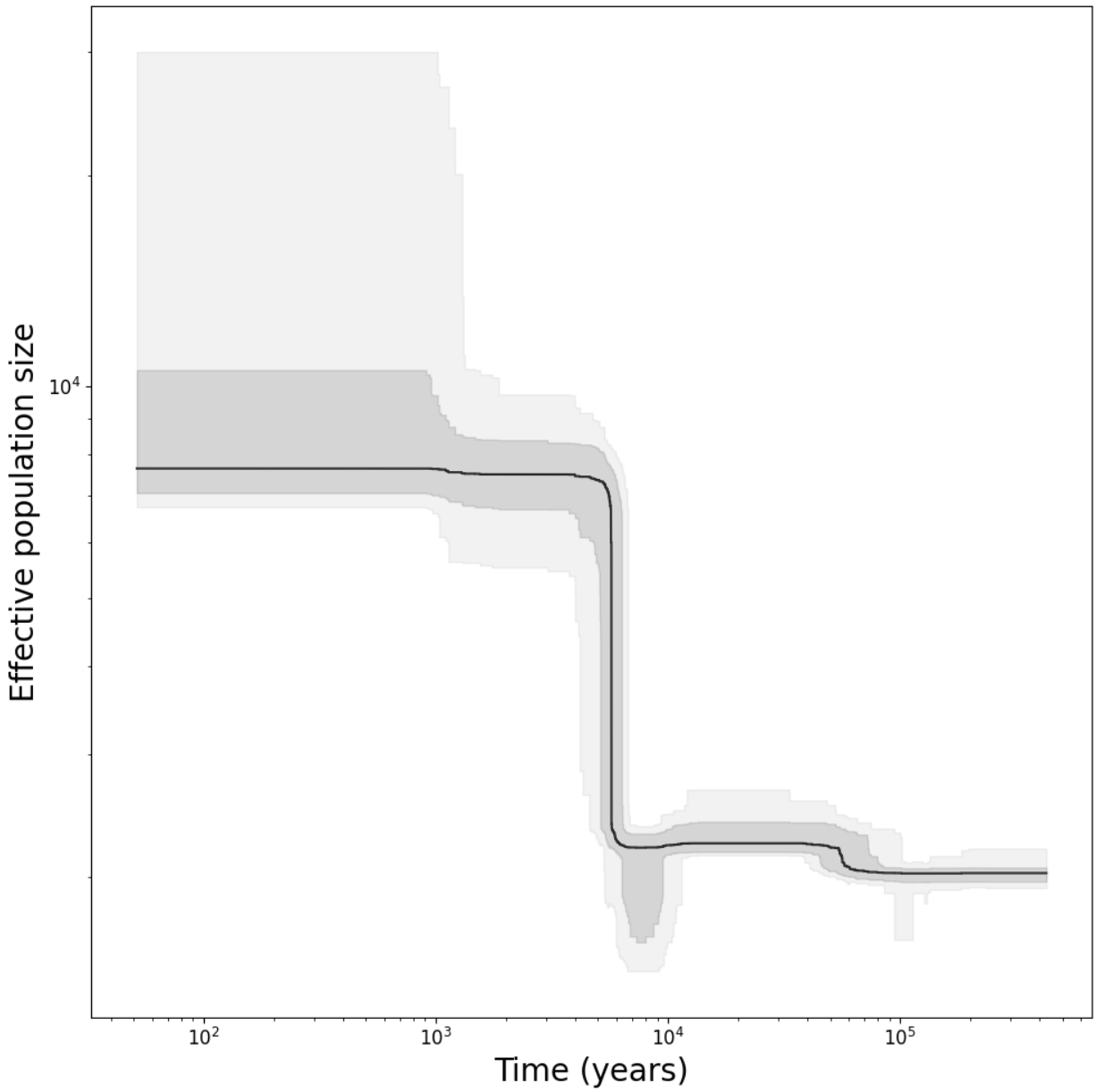

Figure B.21. *Zalophus wollabaeki* (“Zalophus_wollebaeki”)

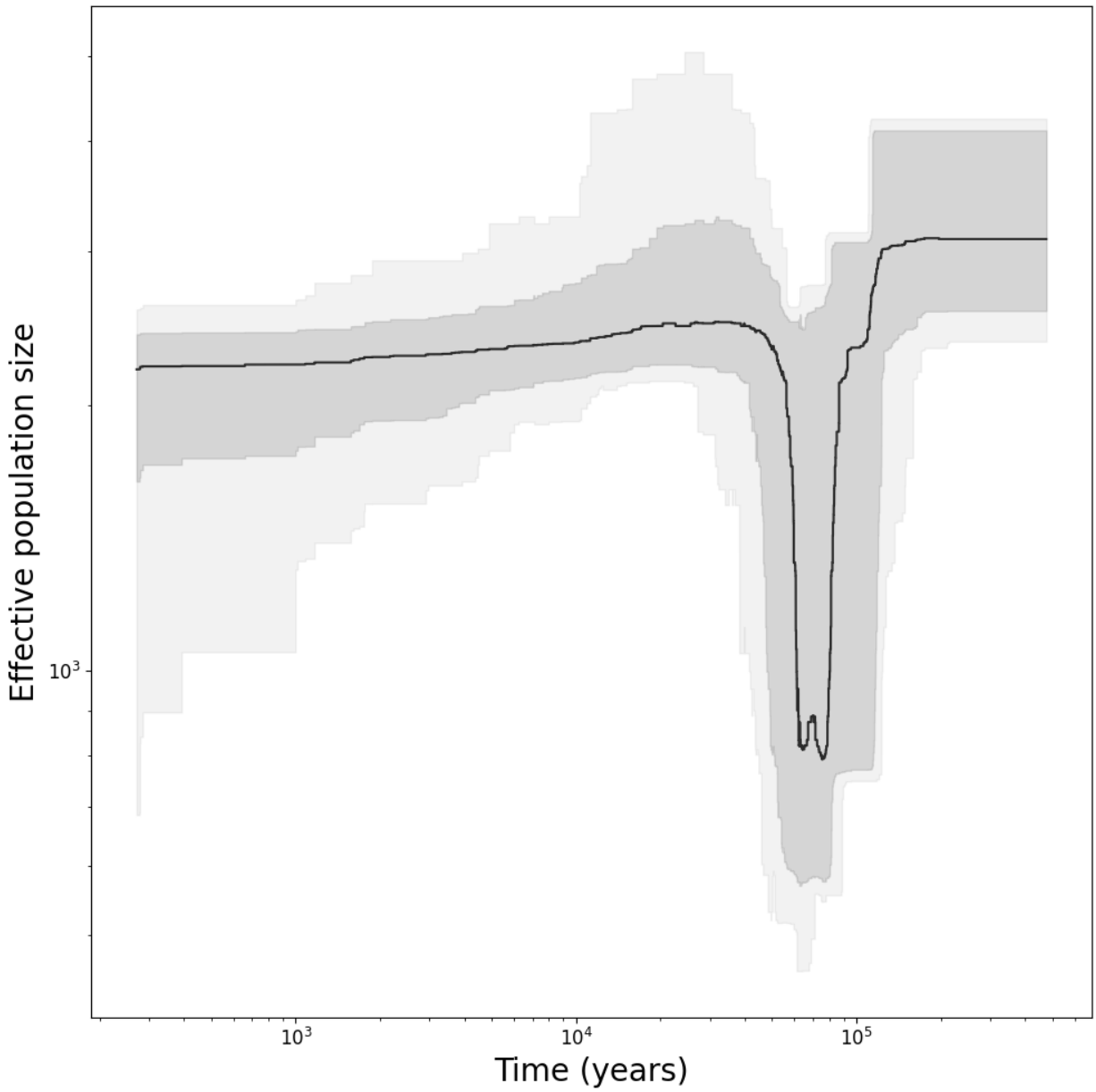

Figure B.22. *Zalophus wollabaeki* (“Zalophus_wollebaeki_Baltra”)

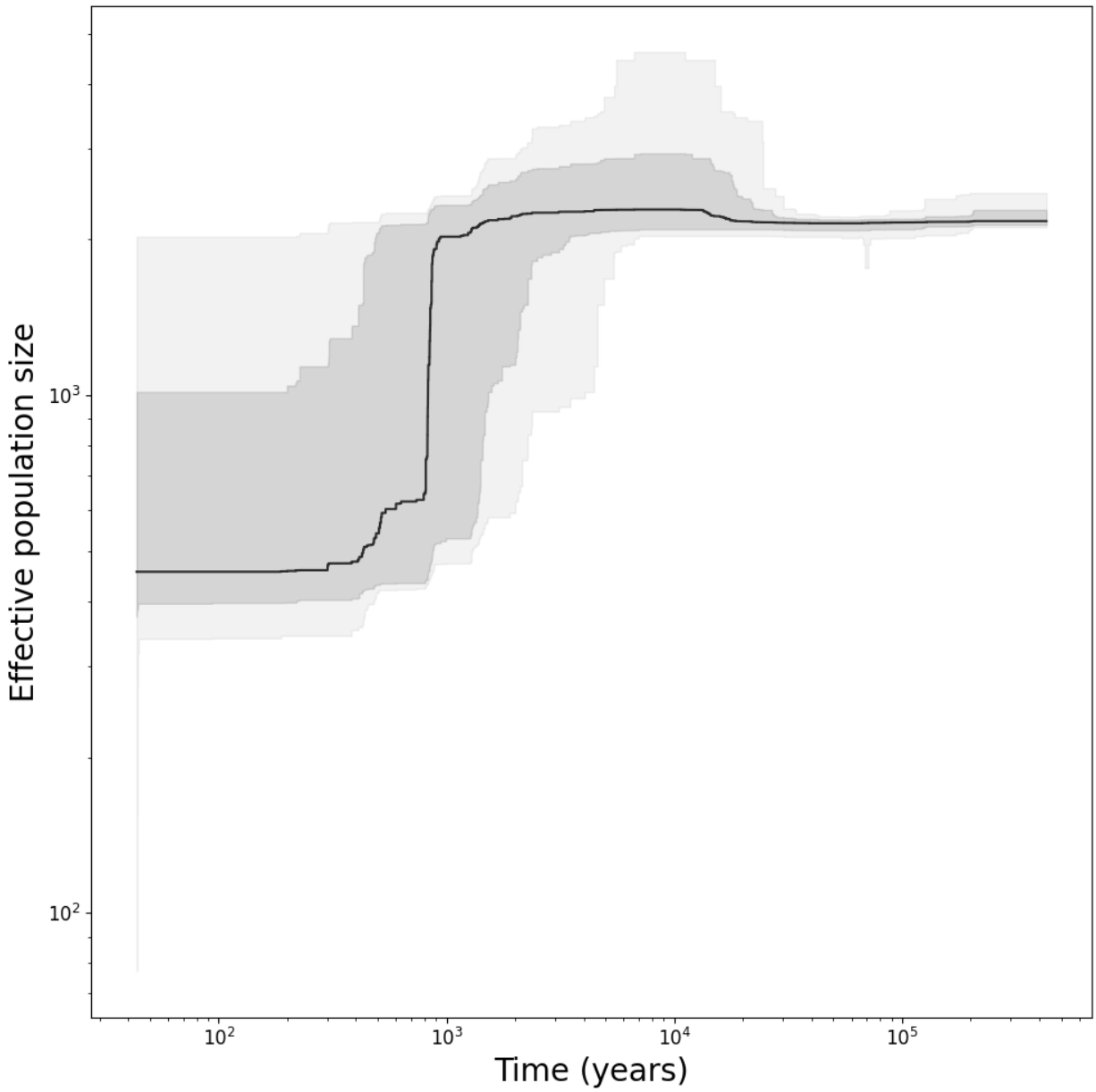

Figure B.23. *Zalophus wollabaeki* (“Zalophus_wollebaeki_Espanola”)

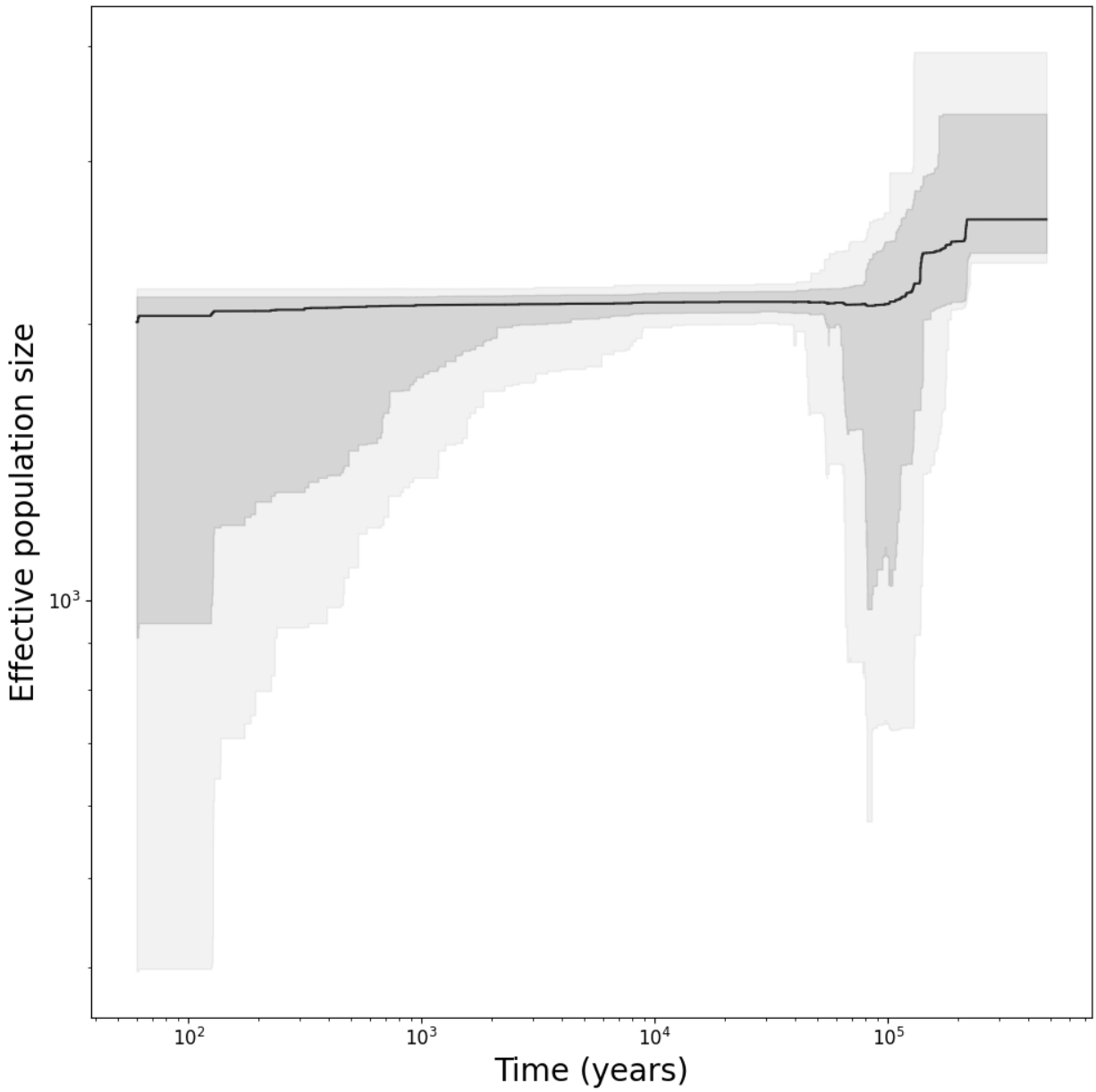

Figure B.24. *Zalophus wollabaeki* (“Zalophus_wollebaeki_Fernandina”)

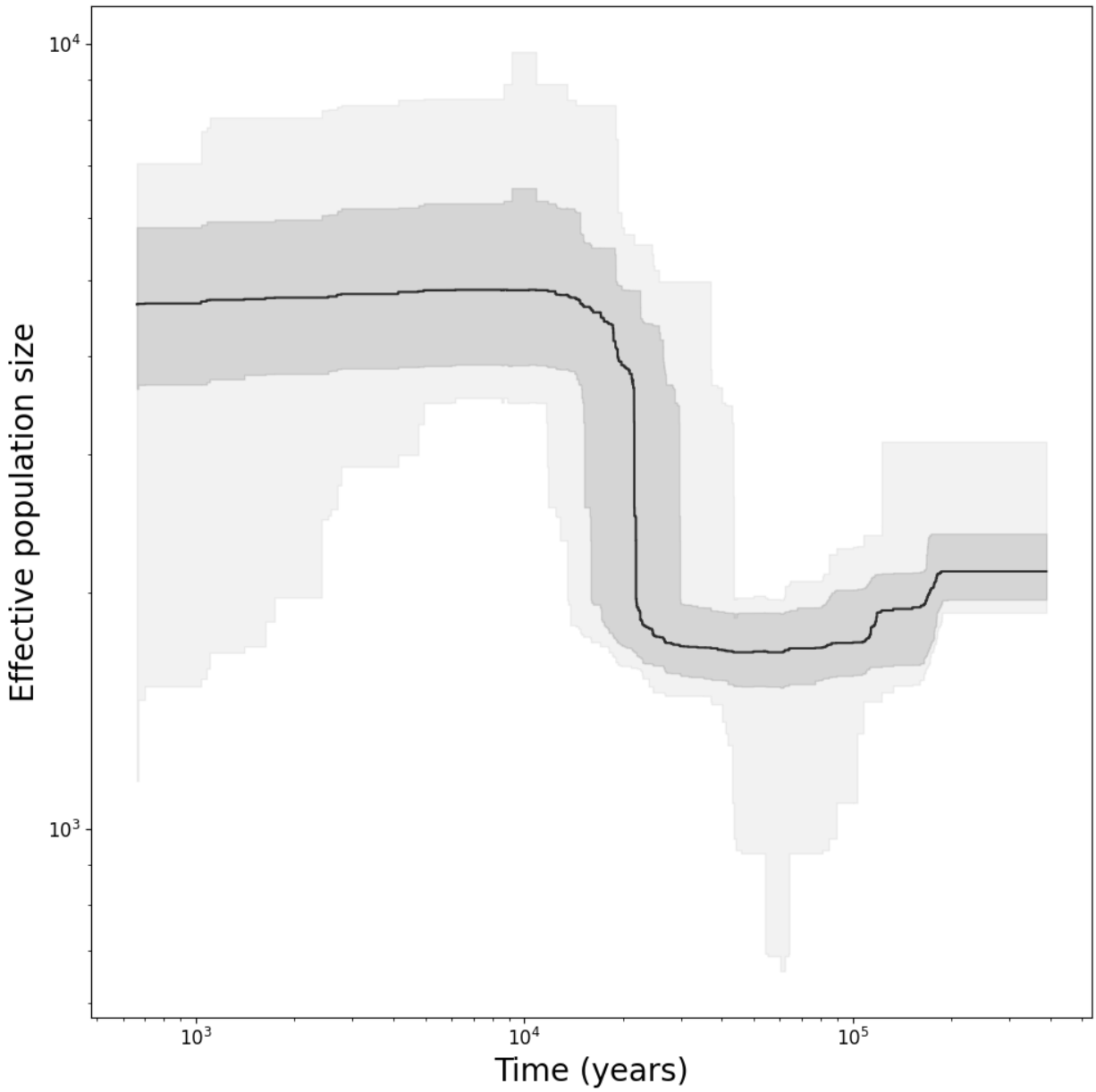

Figure B.25. *Zalophus wollabaeki* (“Zalophus_wollebaeki_Genovesa”)

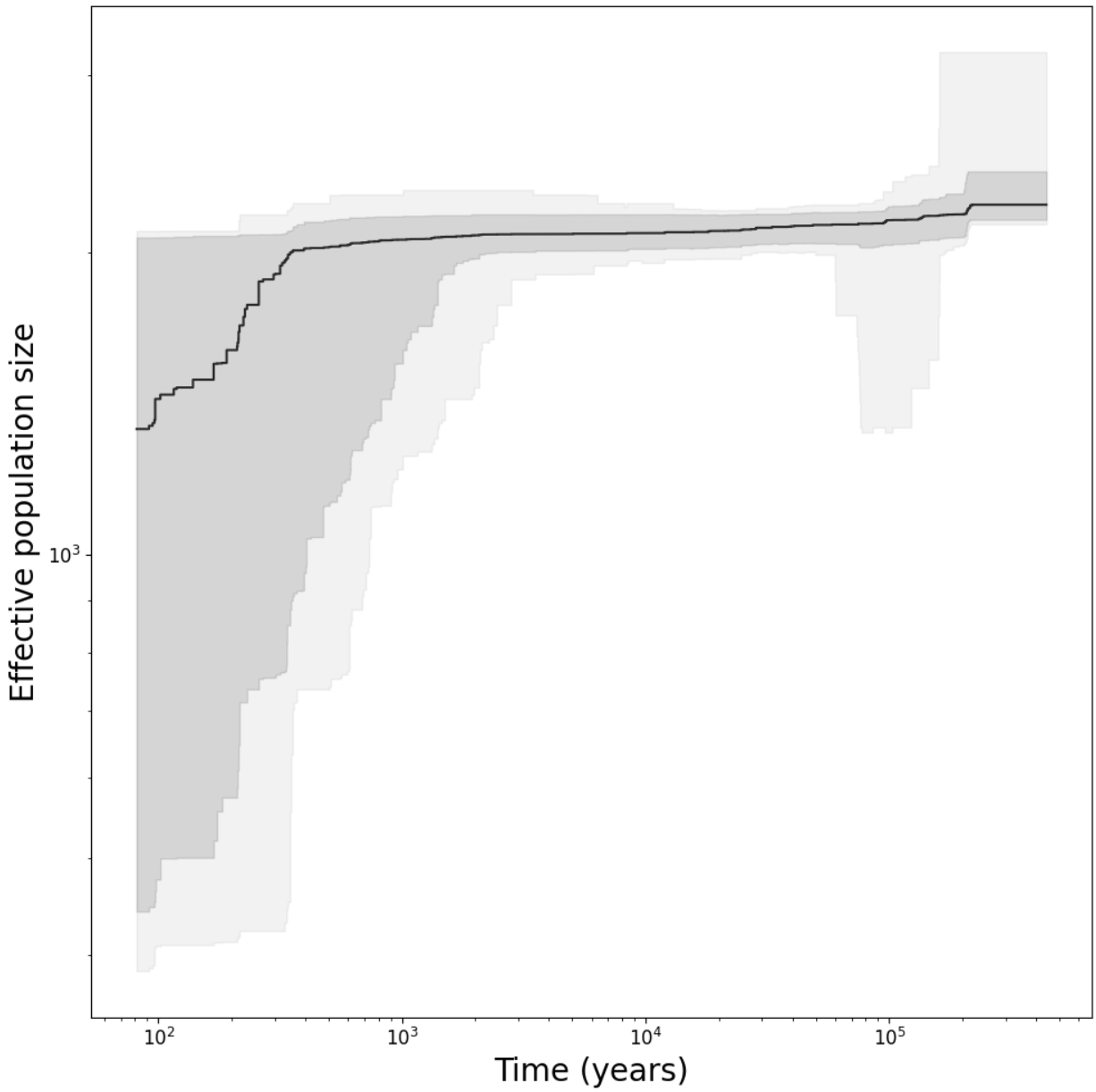

Figure B.26. *Zalophus wollabaeki* (“Zalophus_wollebaeki_IsabelaB”)

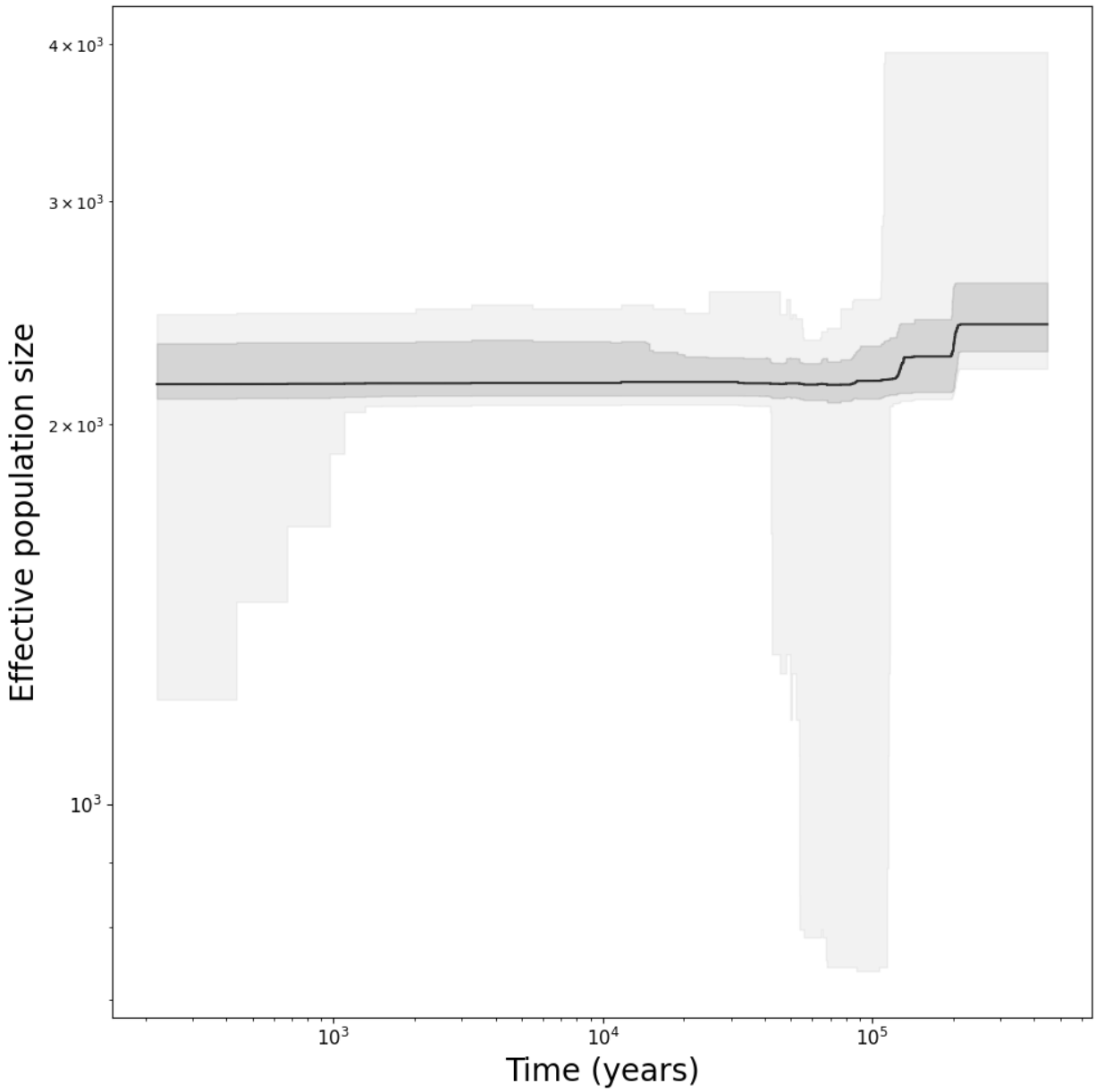

Figure B.27. *Zalophus wollabaeki* (“Zalophus_wollebaeki_IsabelaV”)

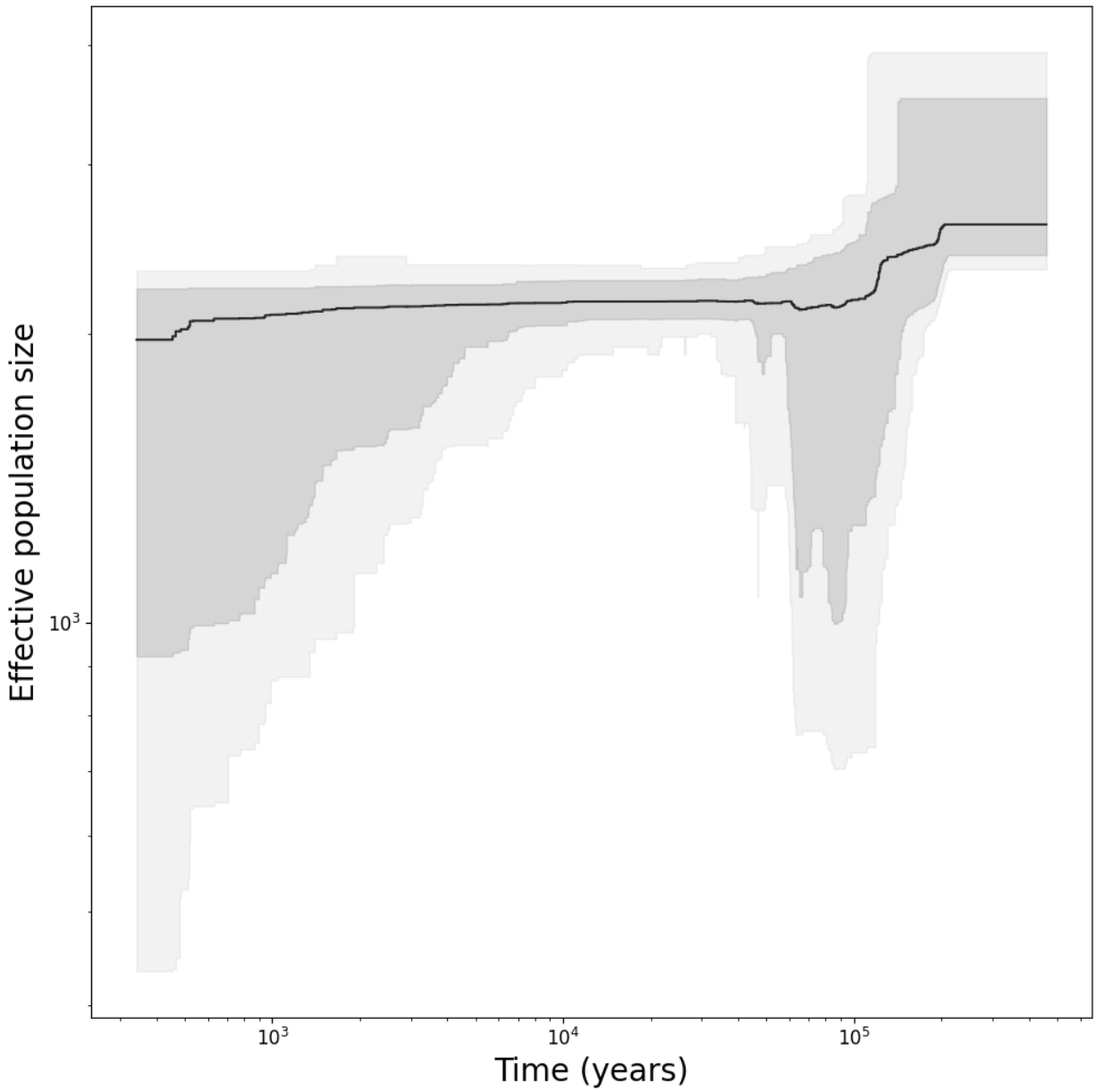

Figure B.28. *Zalophus wollabaeki* (“Zalophus_wollebaeki_Pinta”)

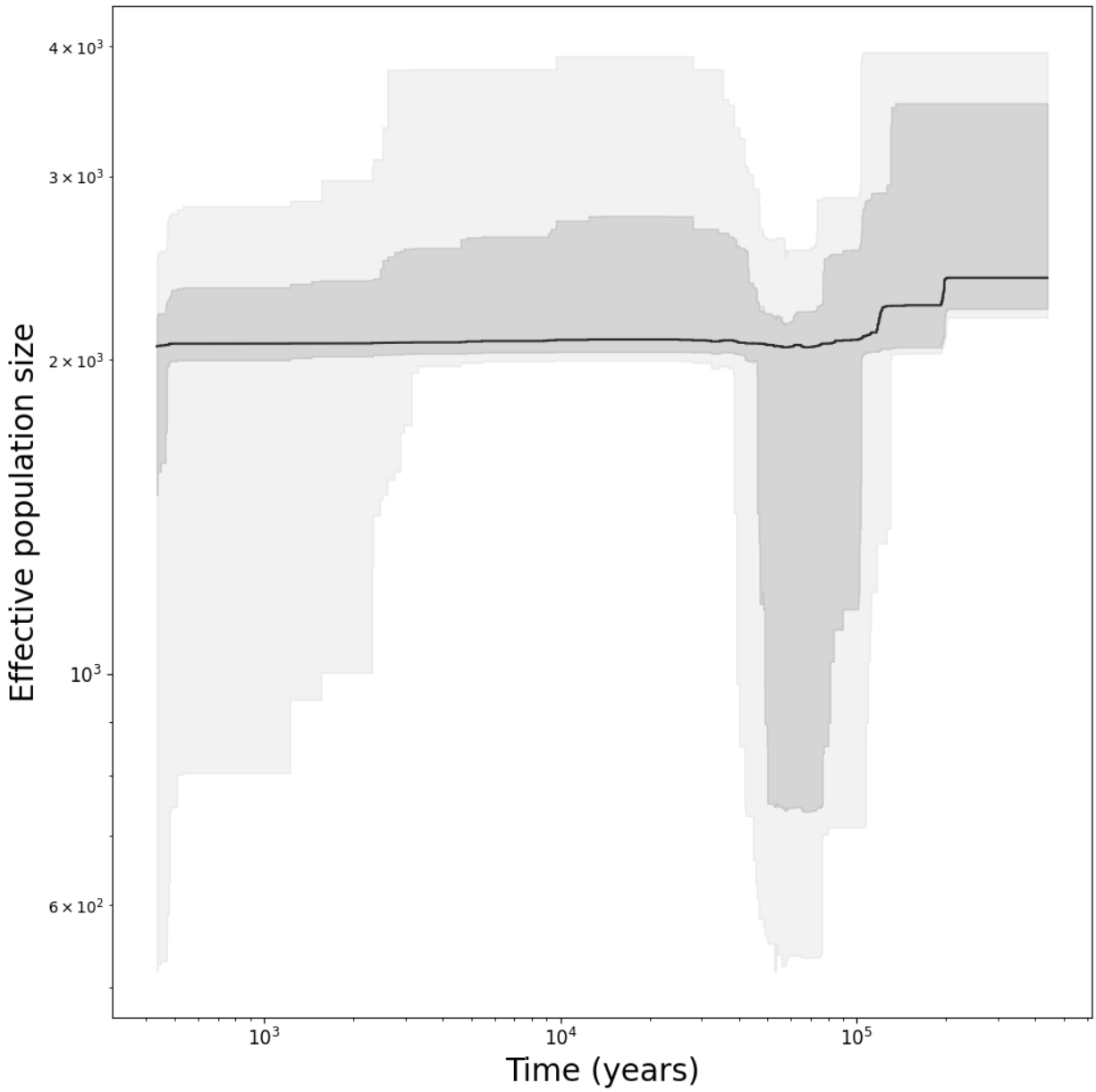

Figure B.29. *Zalophus wollabaeki* (“Zalophus_wollebaeki_SantaFe”)

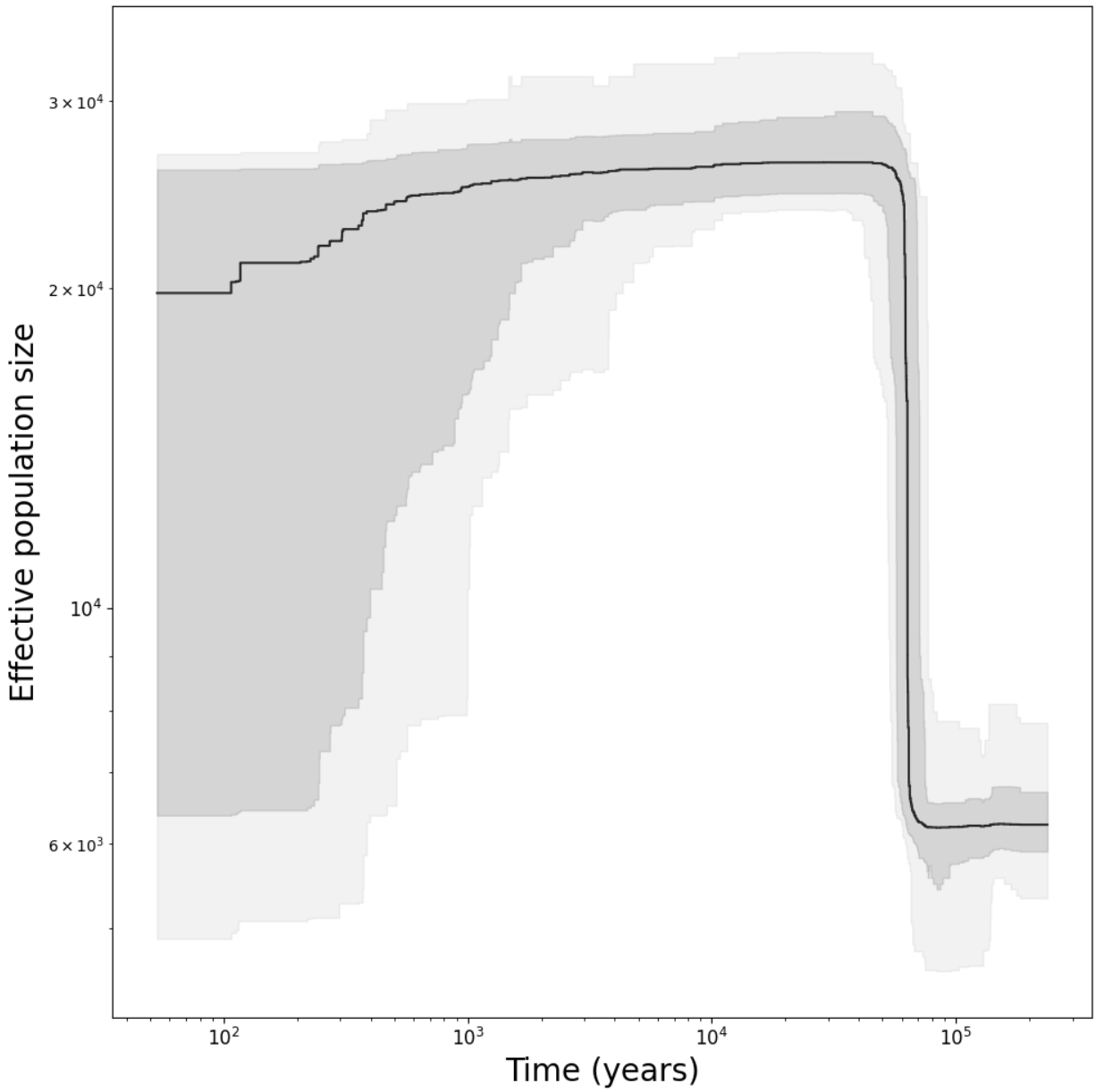

Figure B.30. *Leptonychotes weddellii* (“Leptonychotes_weddellii-Erebus_Bay”)

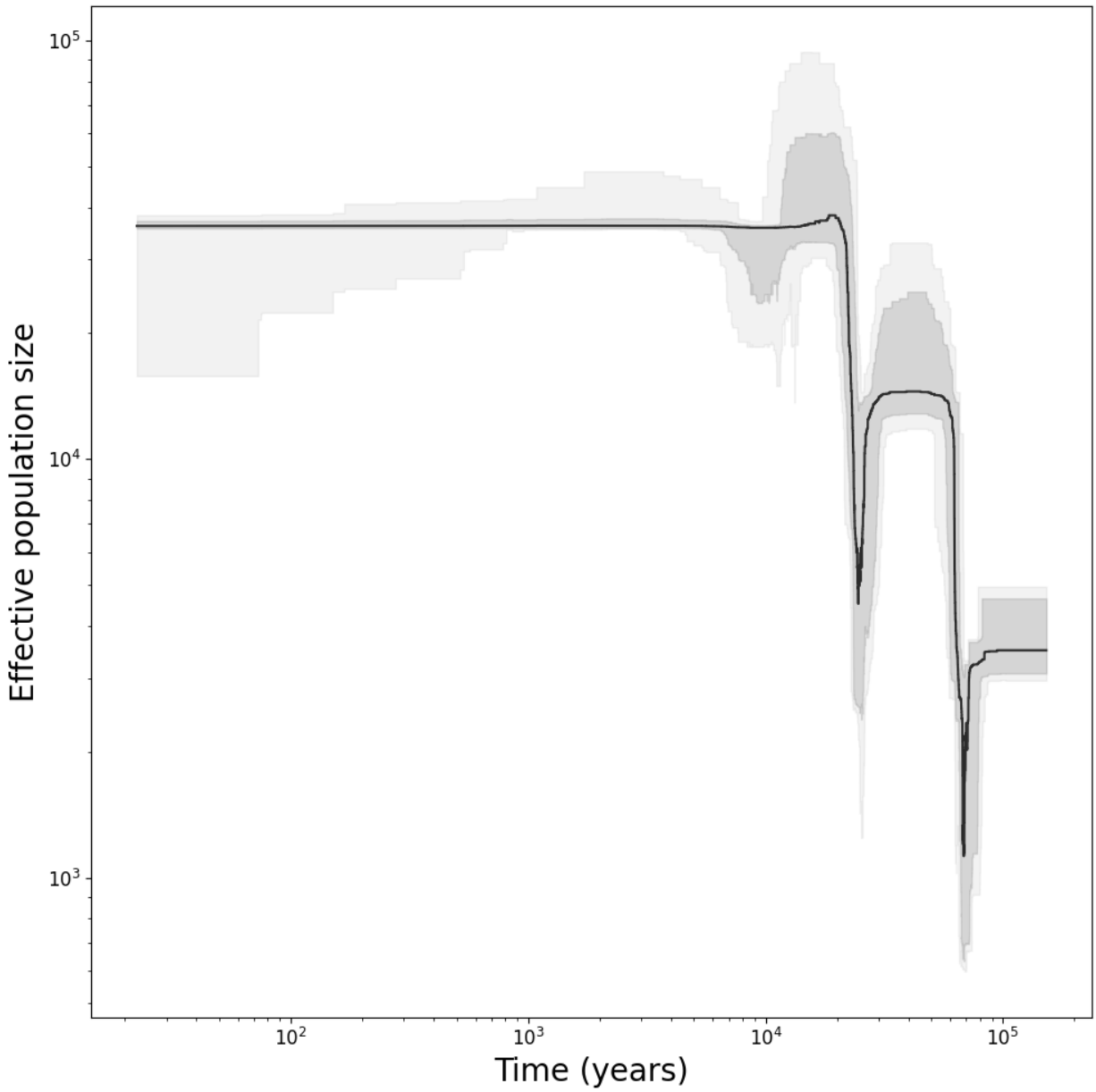

Figure B.31. *Aptenodytes patagonicus* (“King_penguin”)

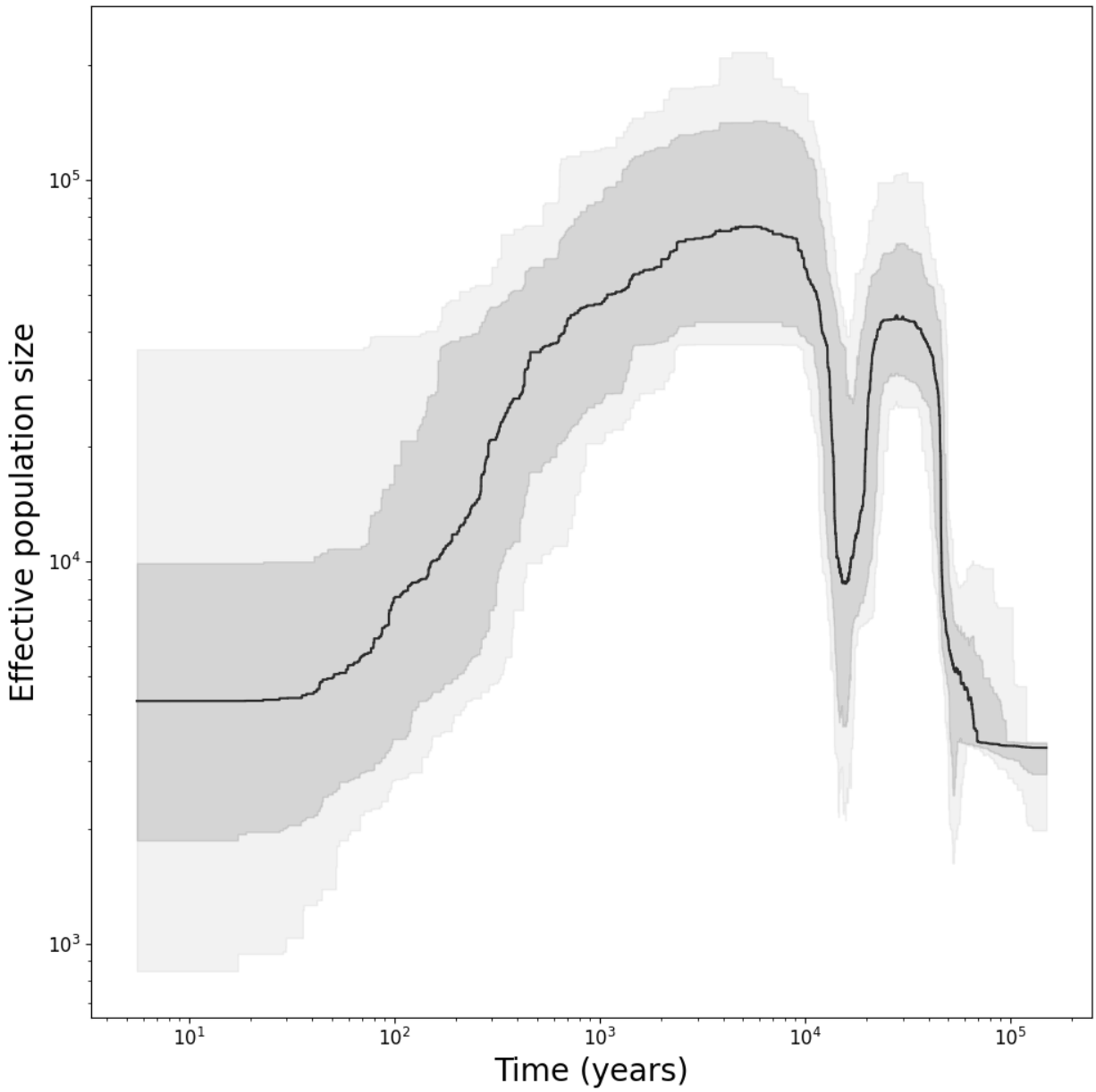

Figure B.32. *Aptenodytes patagonicus* (“King_penguin_Clucas2018-Falklands_Crozet”)

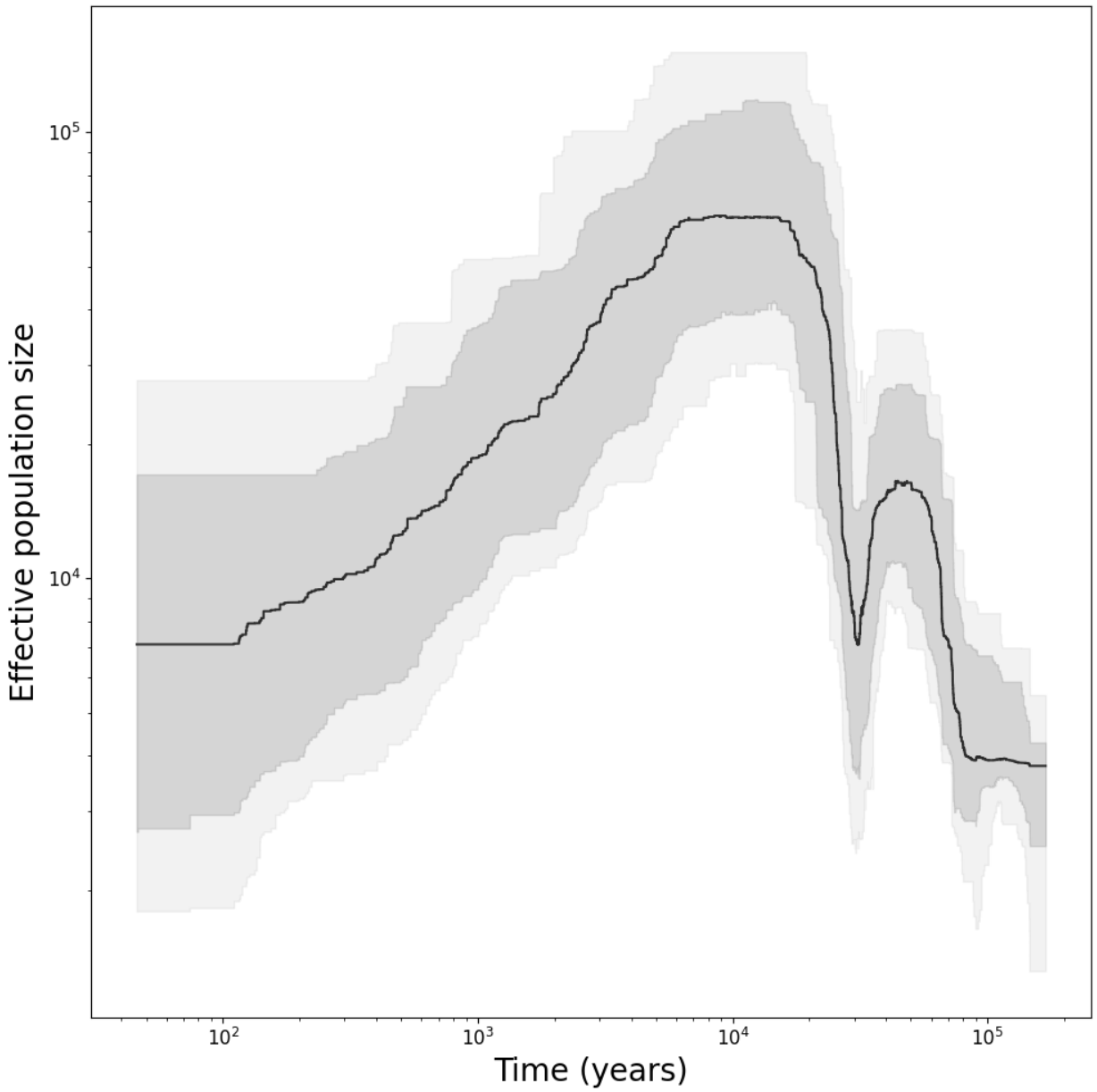

Figure B.33. *Aptenodytes patagonicus* (“King_penguin_Clucas2018-Macquarie”)

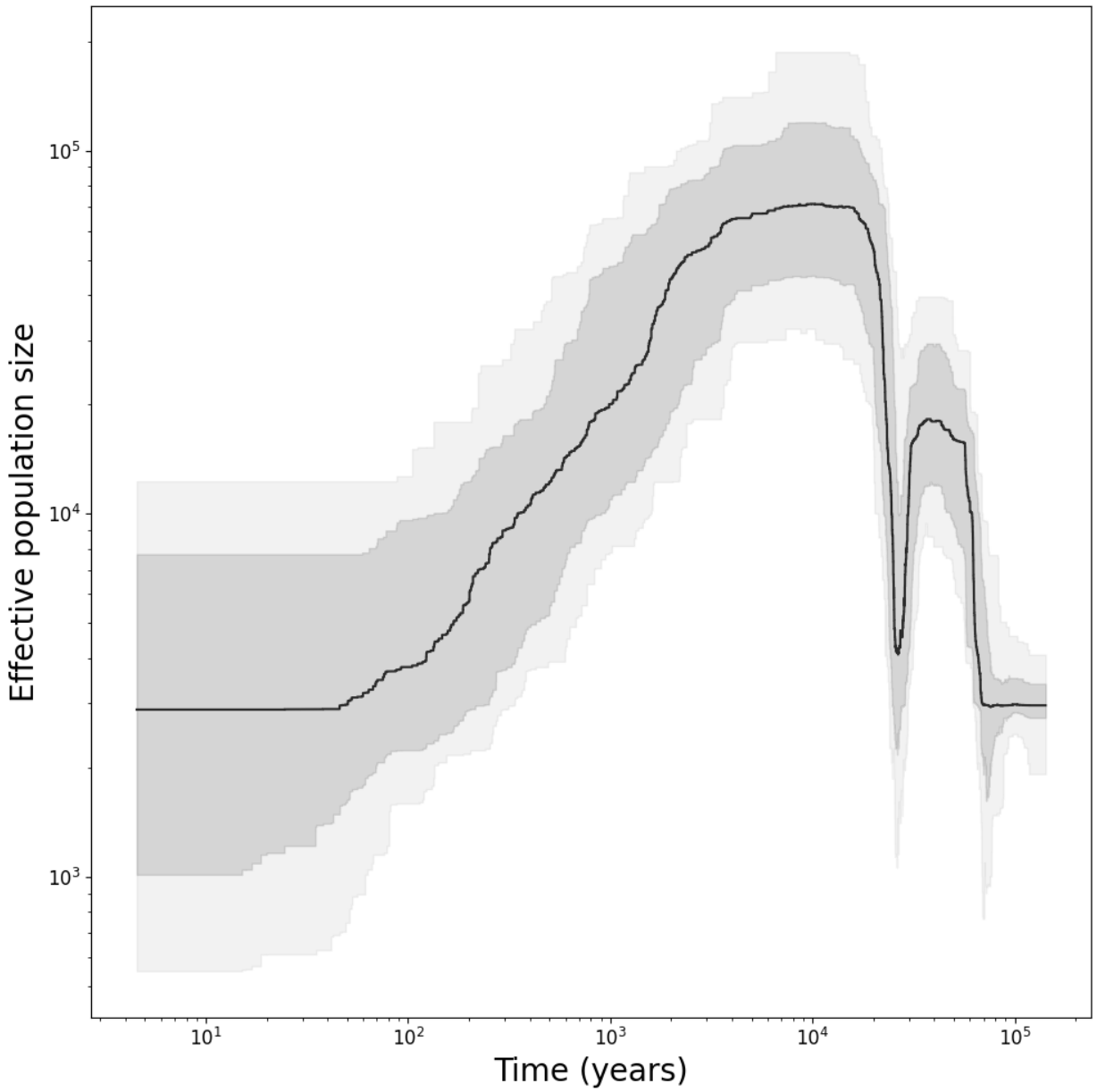

Figure B.34. *Aptenodytes patagonicus* (“King_penguin_Clucas2018-SouthGeorgia”)

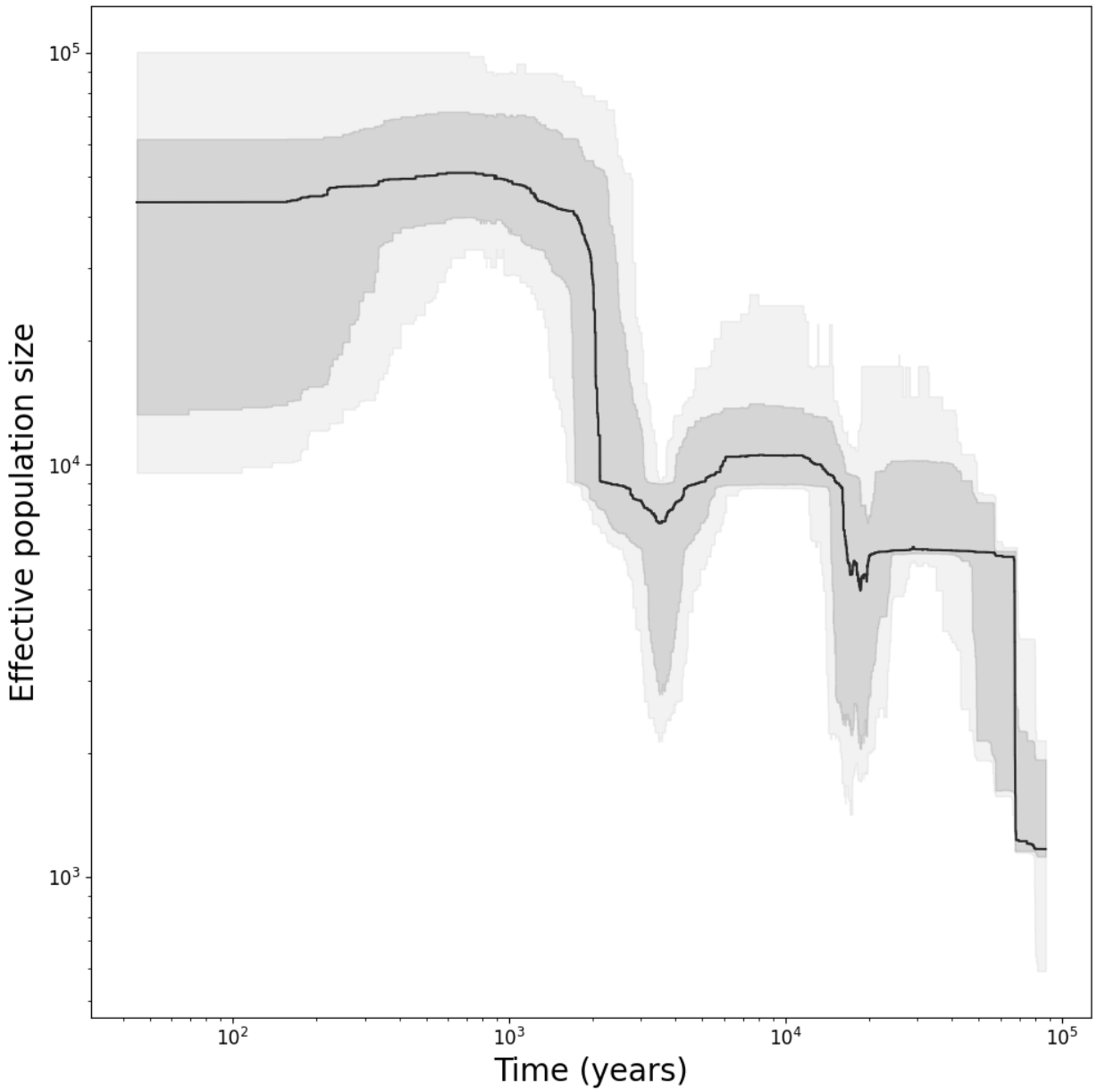

Figure B.35. *Pygoscelis antarcticus* (“Chinstrap_penguin”)

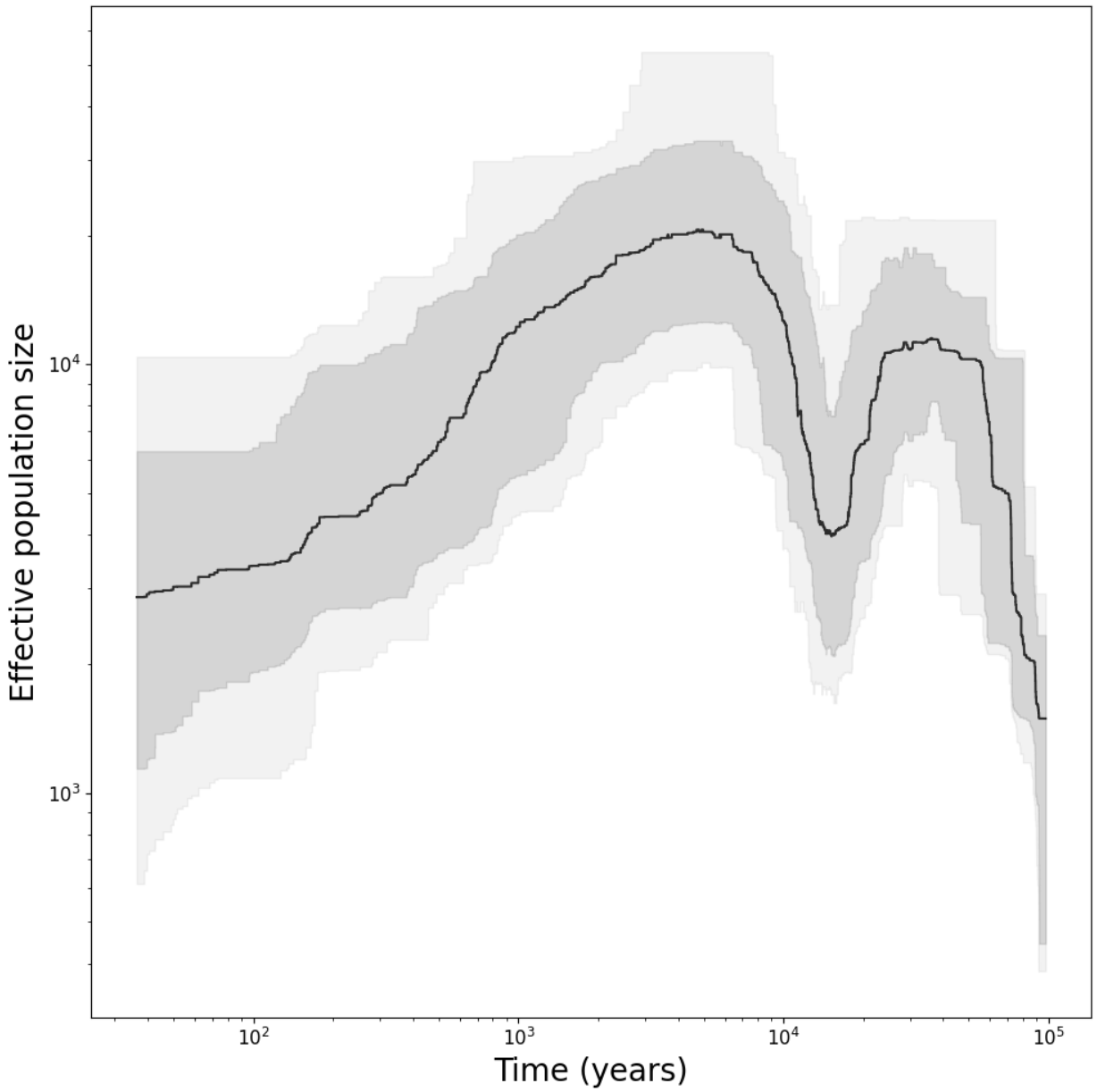

Figure B.36. *Pygooscelis antarcticus* (“Pygoscelis_antarcticus-Orne_Harbor”)

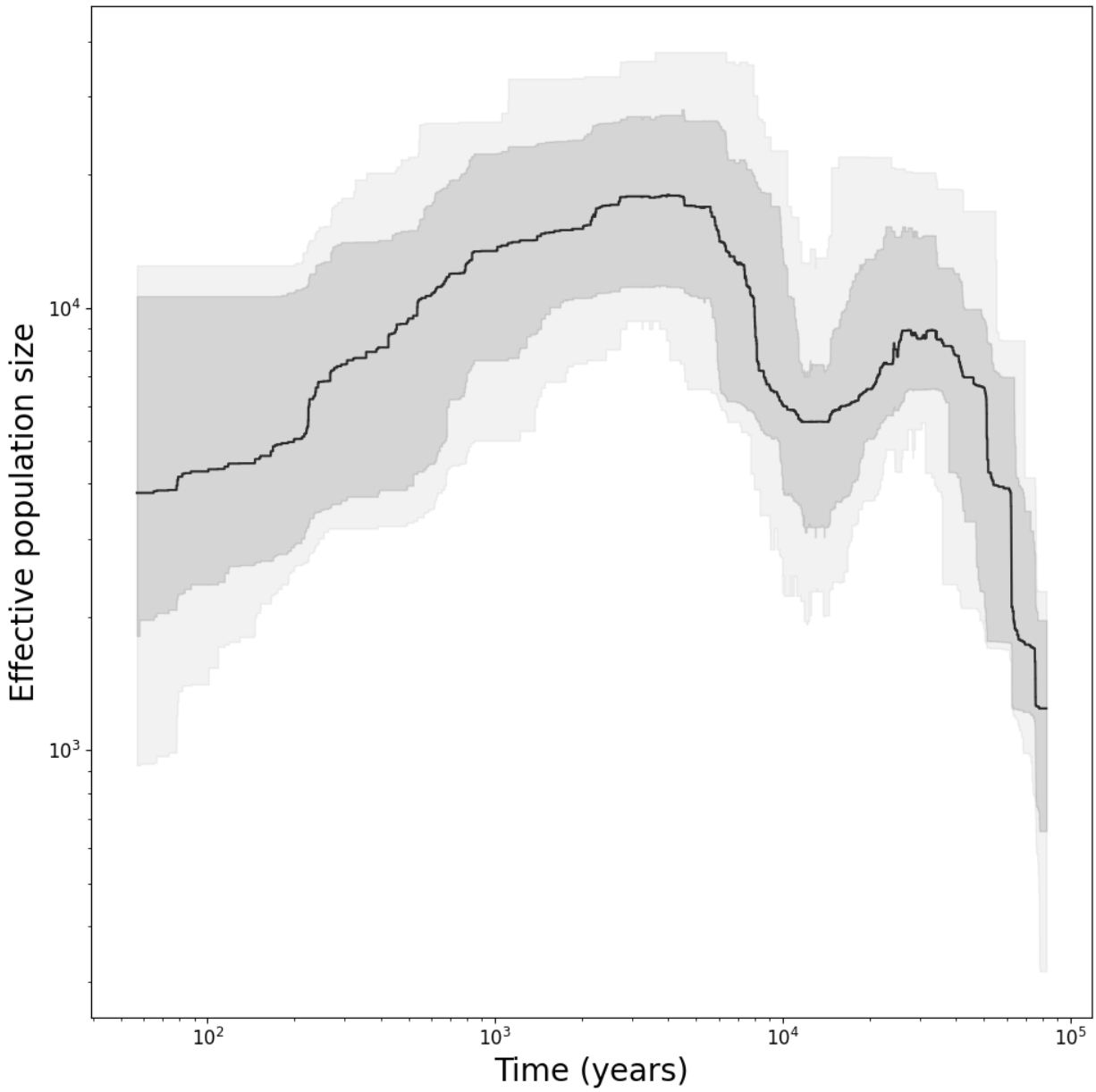

Figure B.37. *Pygooscelis antarcticus* (“Pygoscelis_antarcticus-Sandwich”)

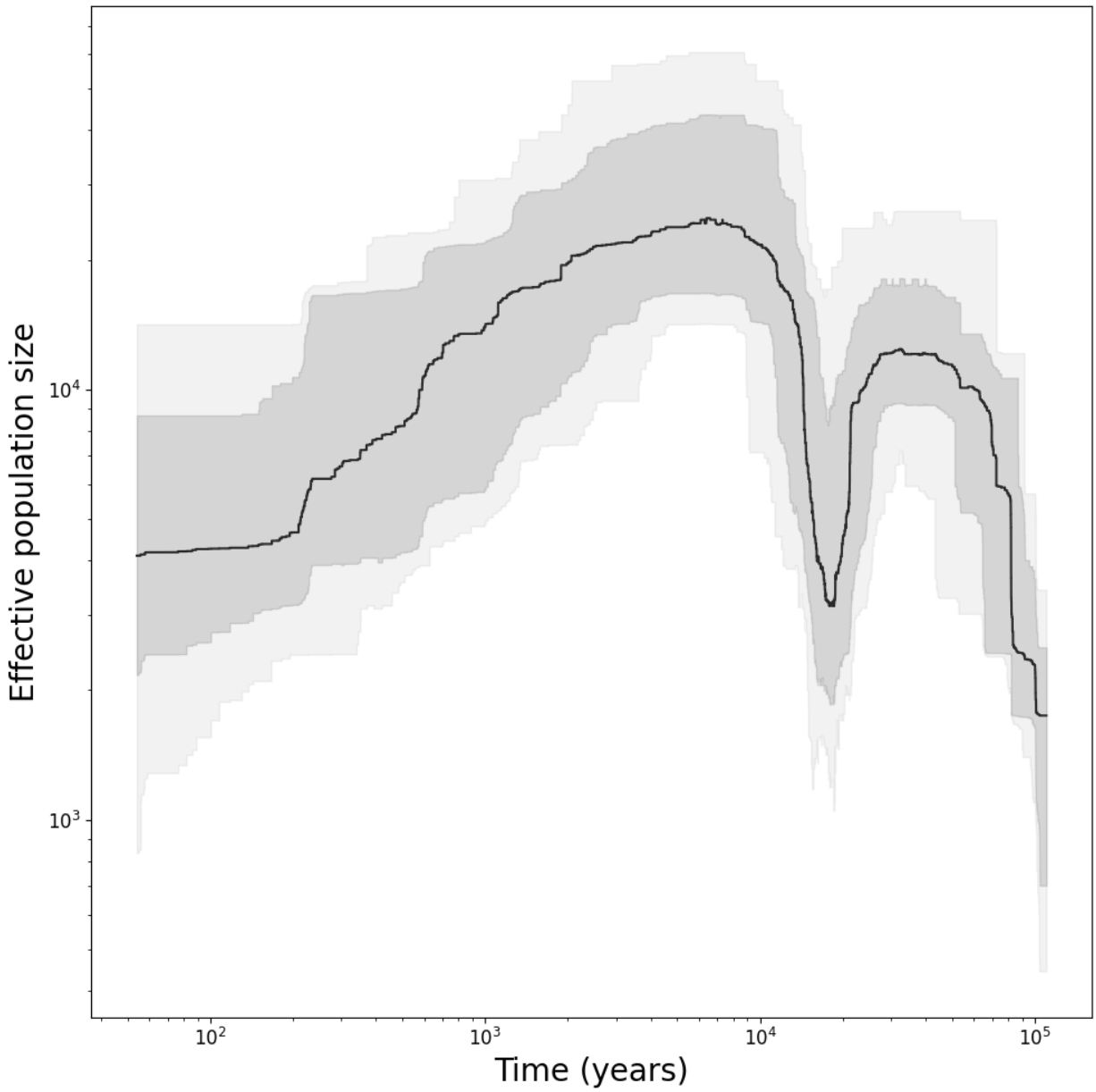

Figure B.38. *Pygooscelis antarcticus* (“Pygoscelis_antarcticus-South_Shetland”)

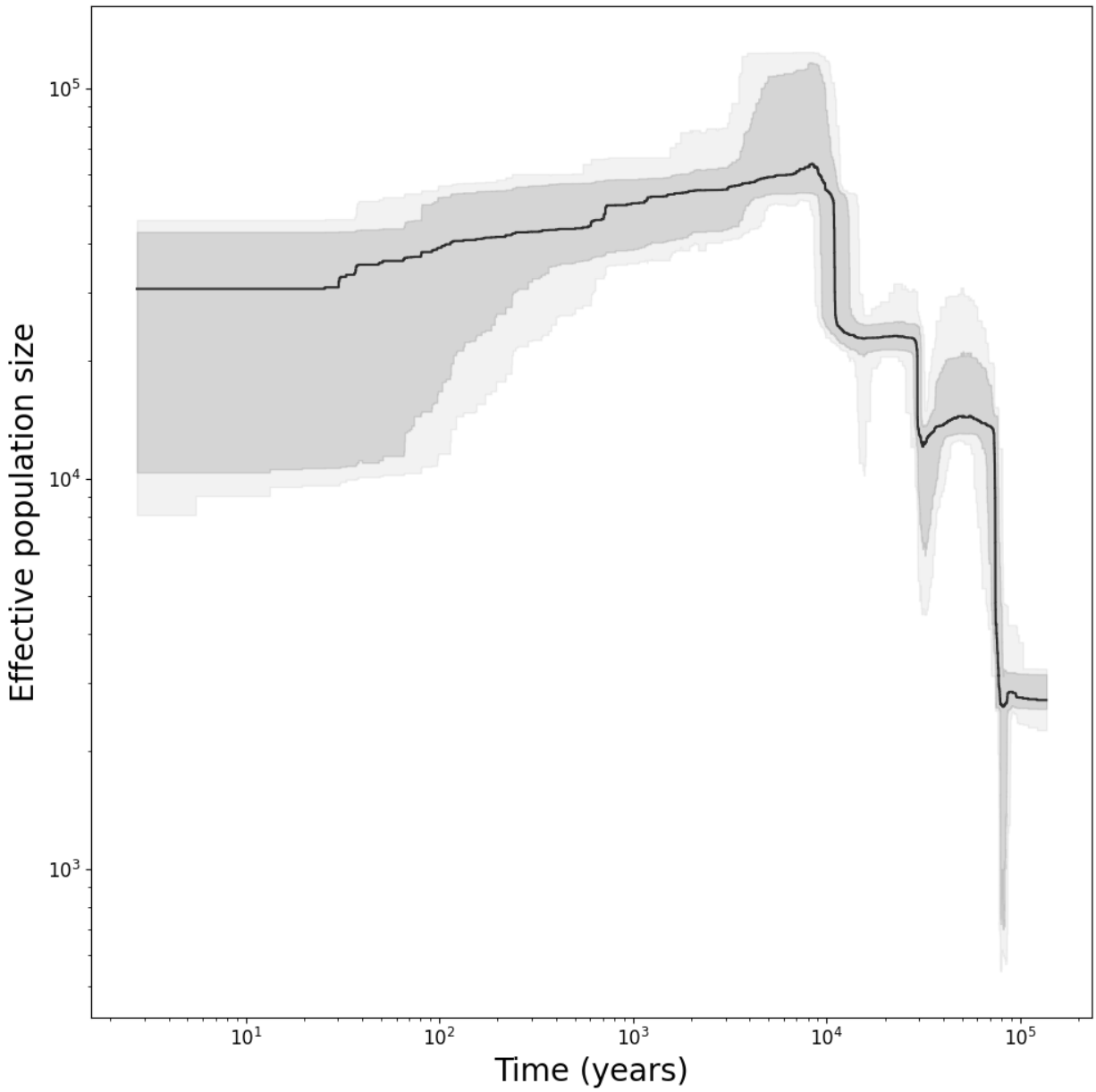

Figure B.39. *Pygoscelis adeliae* (“Adelie_penguin”)

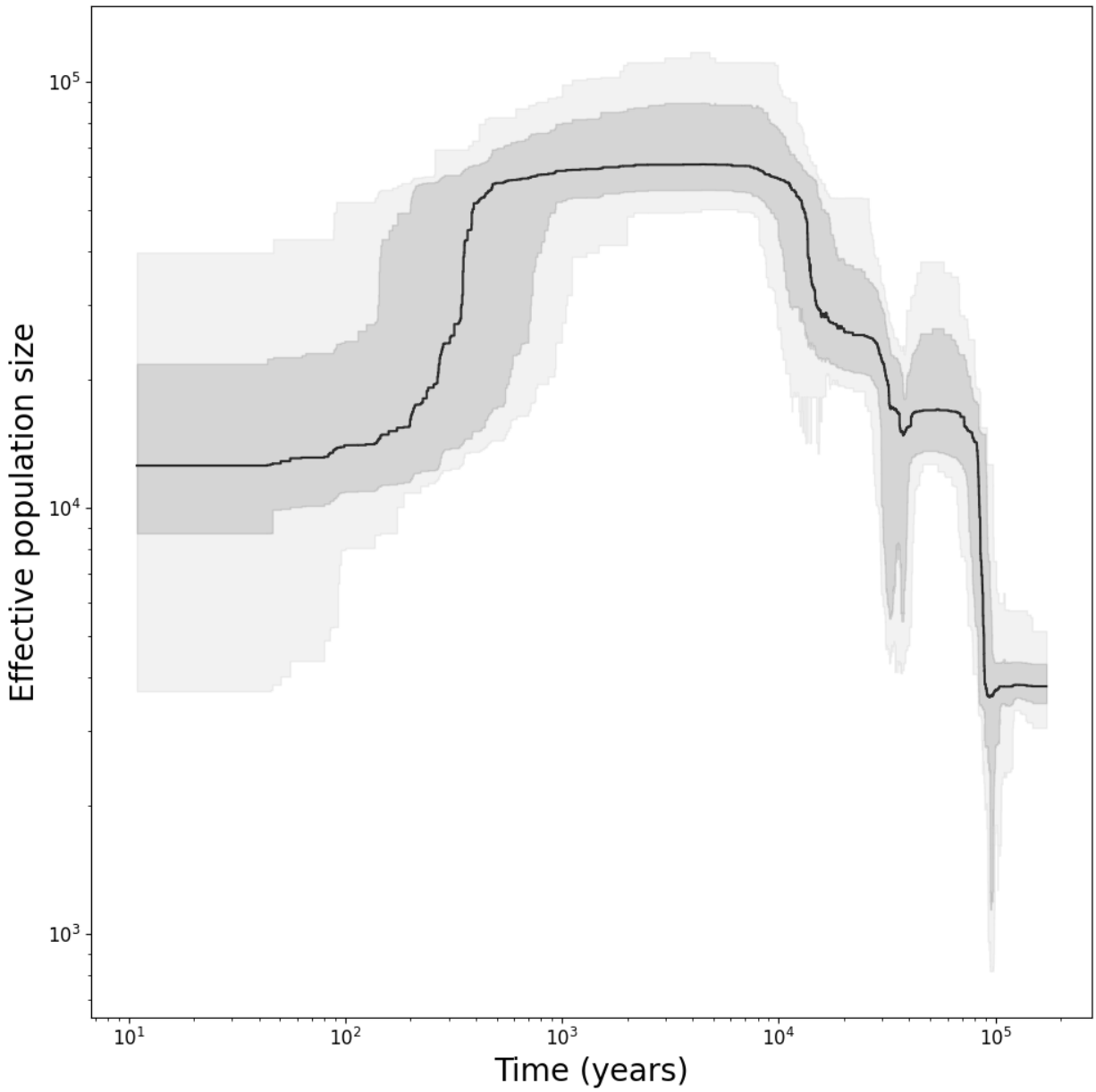

Figure B.40. *Pygooscelis adeliae* (“Pygoscelis_adeliae-West”)

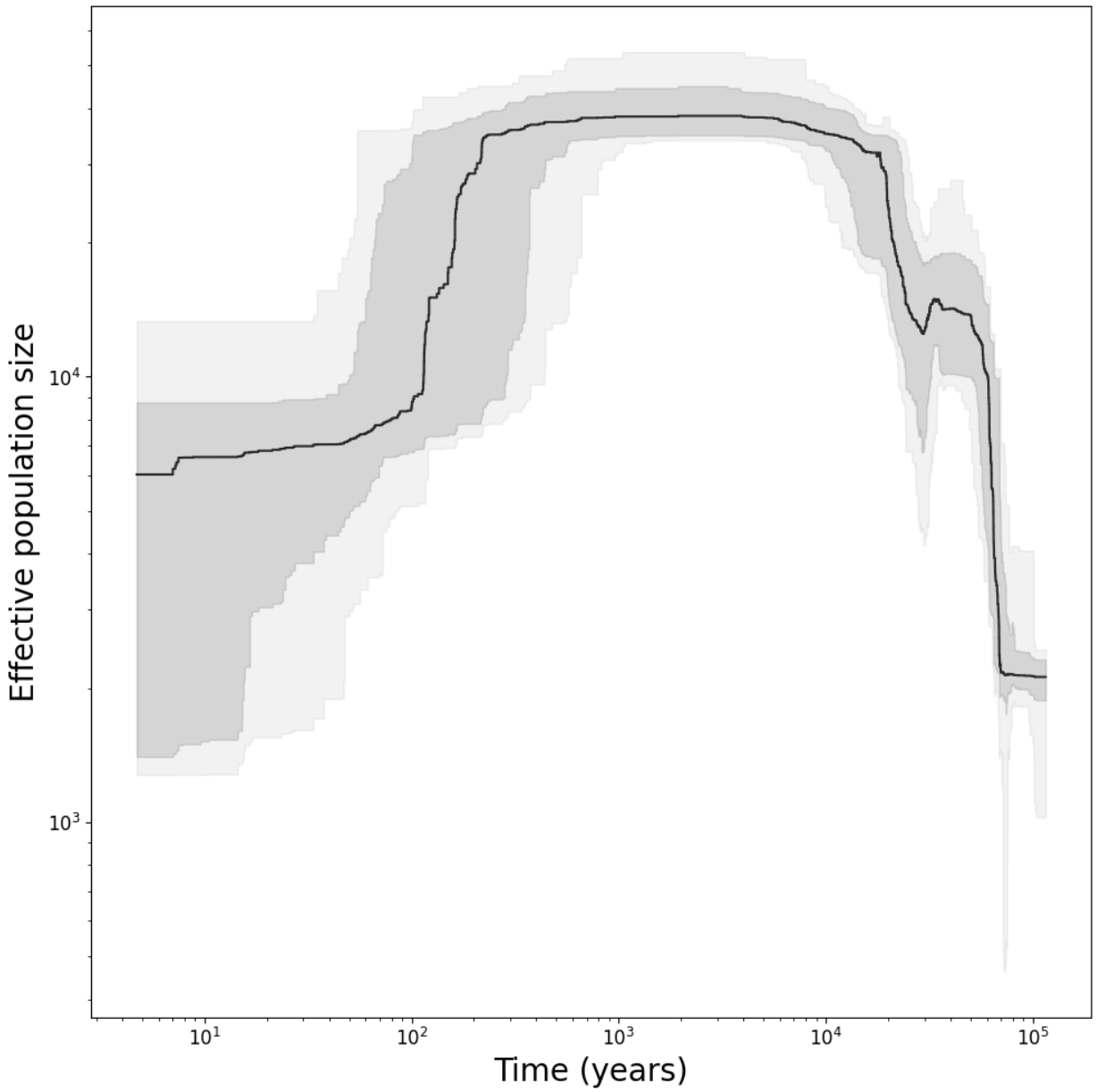

Figure B.41. *Pygooscelis adeliae* (“Pygoscelis_adeliae-East”)

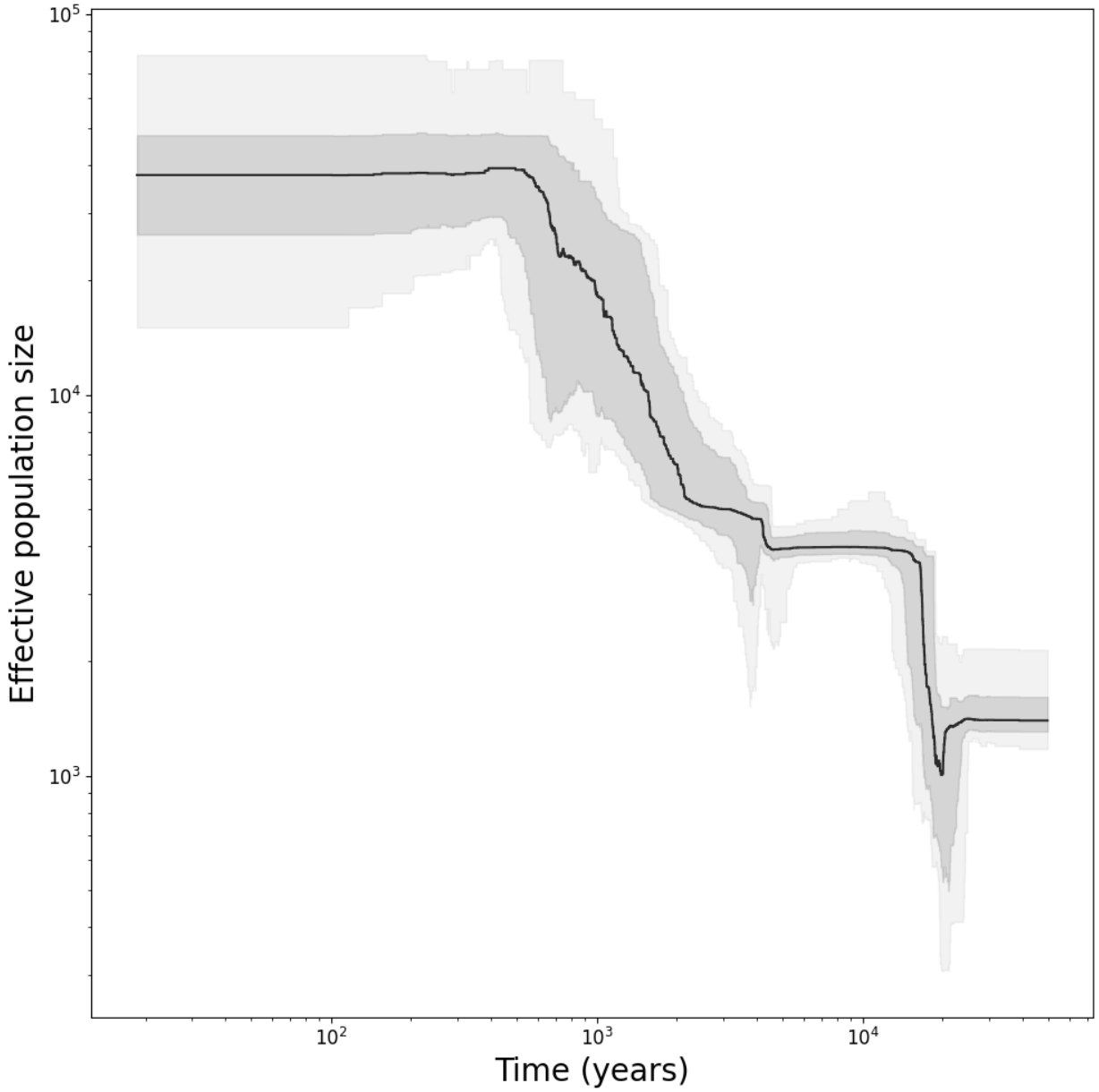

Figure B.42. *Pygoscelis papua* (“Gentoo_penguin”)

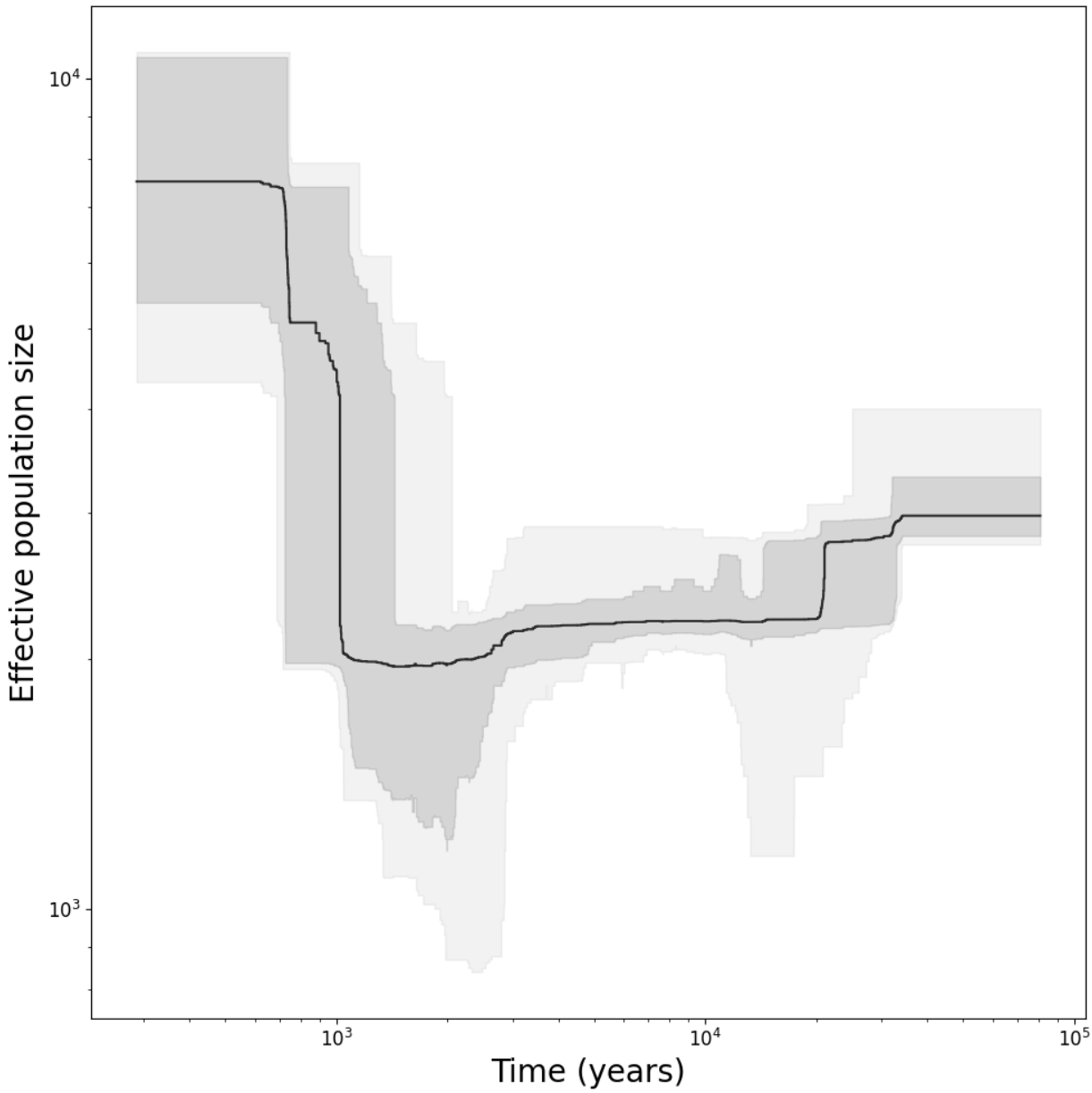

Figure B.43. *Pygooscelis papua* (“Pygoscelis_papua-Falklands”)

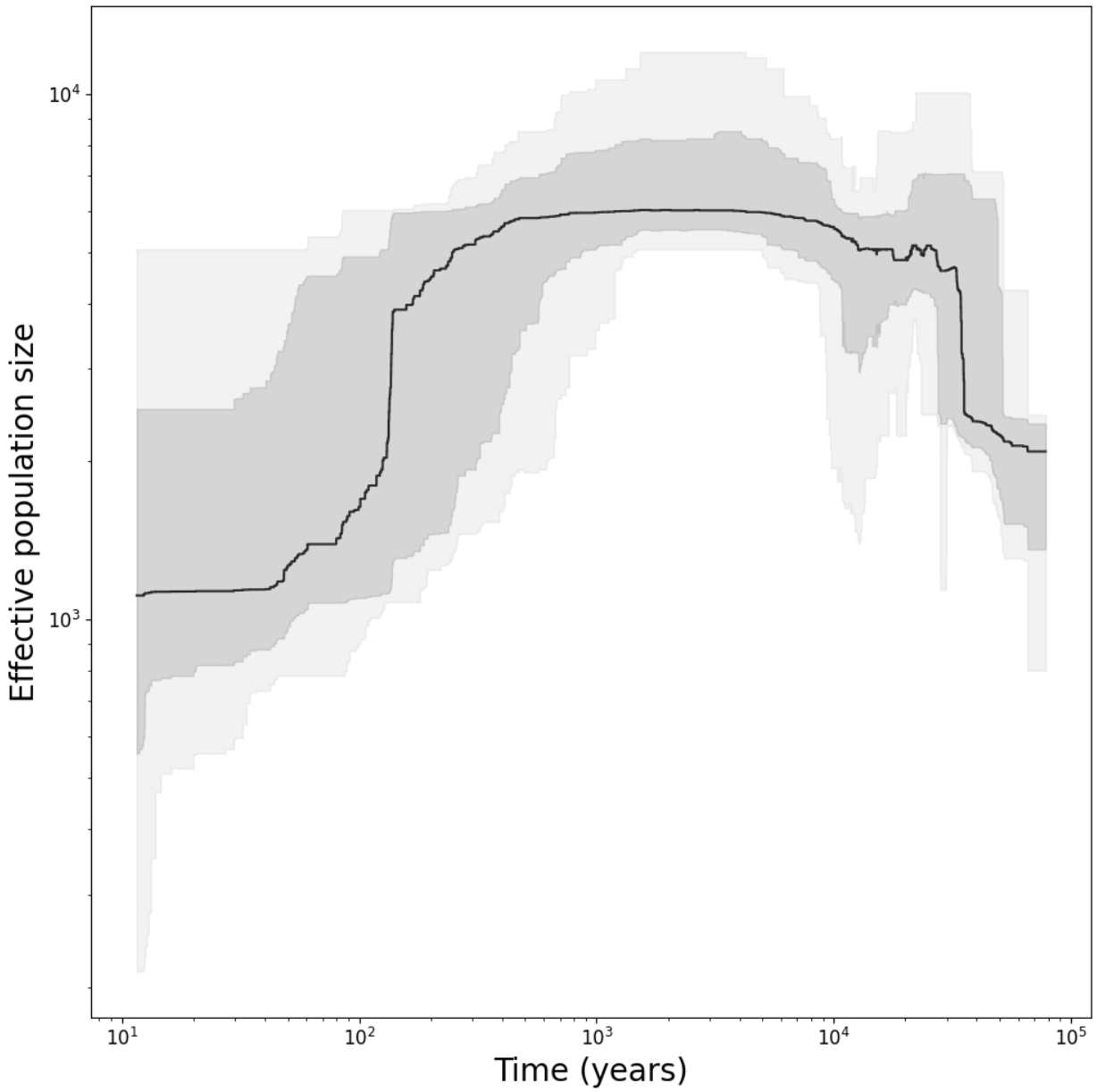

Figure B.44. *Pygooscelis papua* (“Pygoscelis_papua-Kerguelen”)

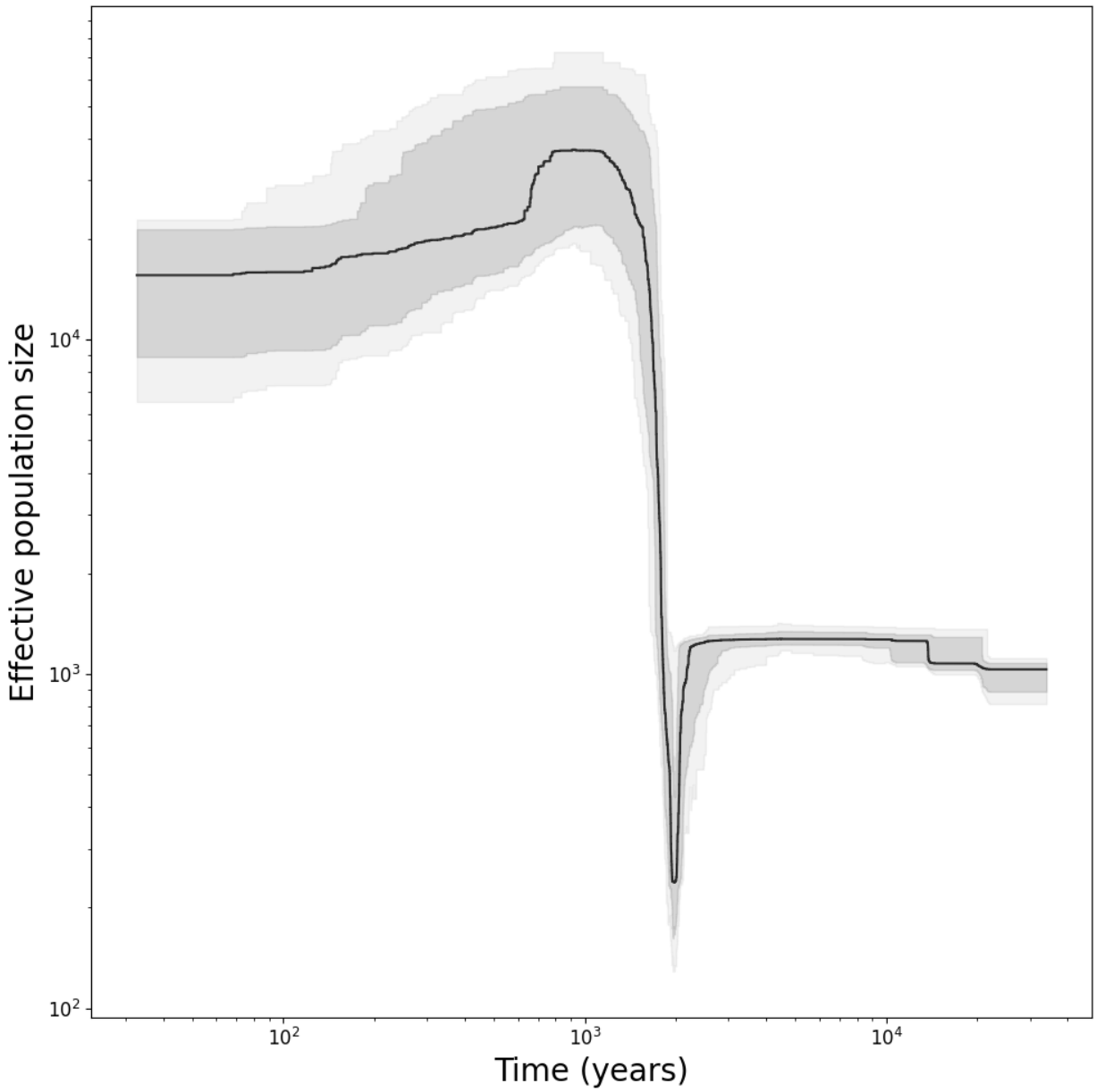

Figure B.45. *Pygooscelis papua* (“Pygoscelis_papua-Shetland_Georges_Jougla”)

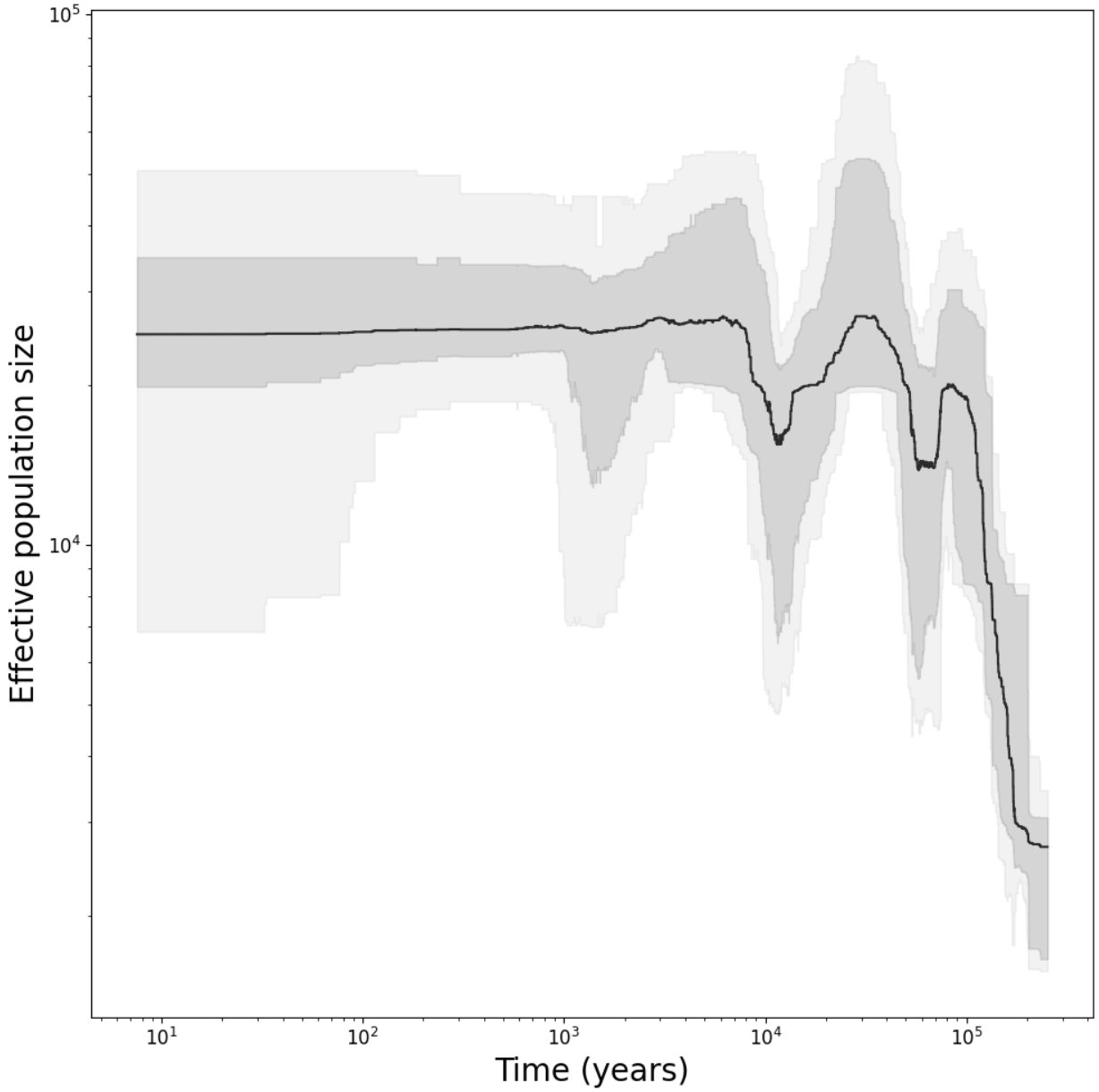

Figure B.46. *Aptenodytes forsteri* (“Emperor_penguin”)

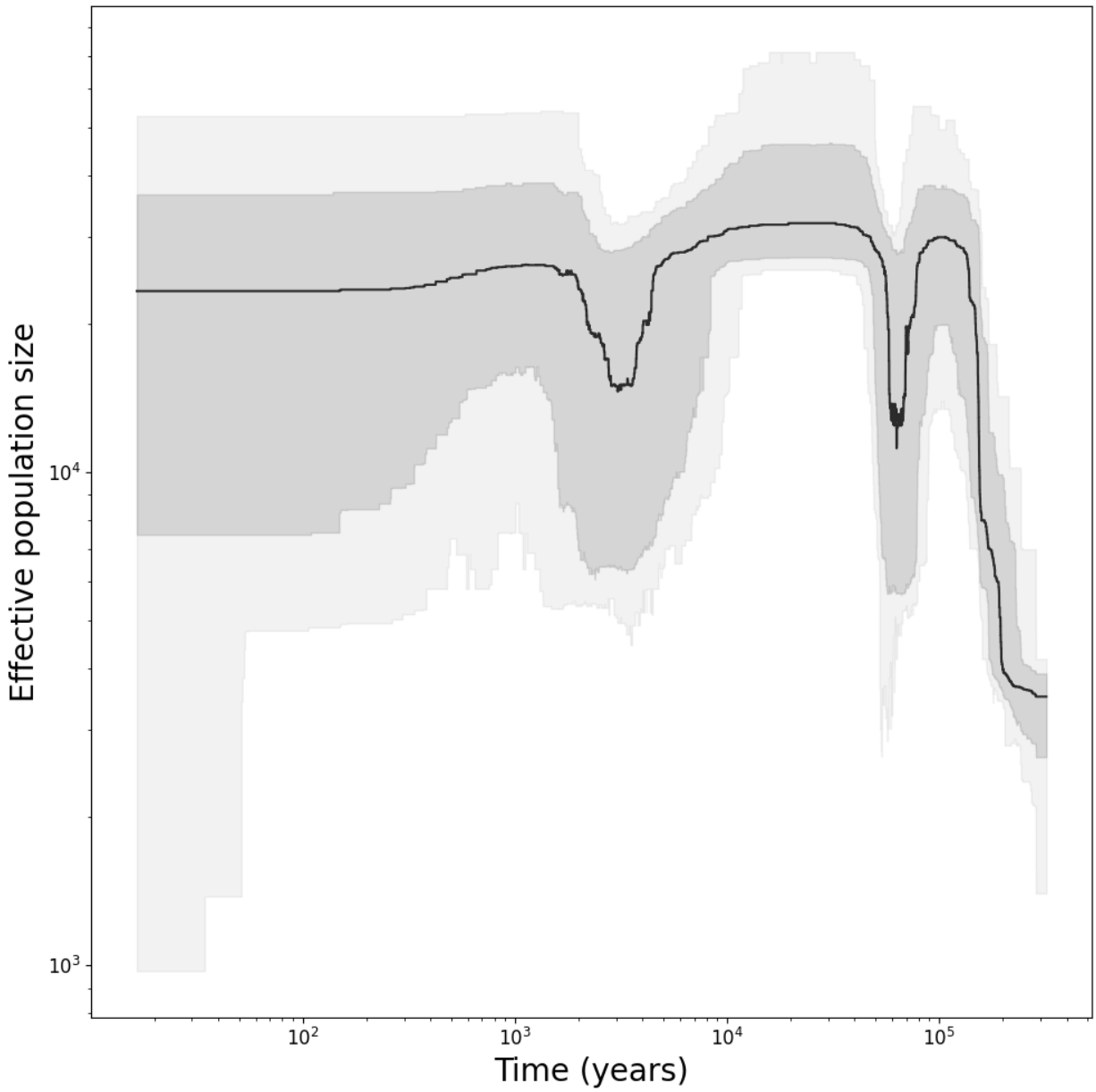

Figure B.47. *Aptenodytes forsteri* (“Emperor_penguin_Clucas2018-Amanda_Geologie”)

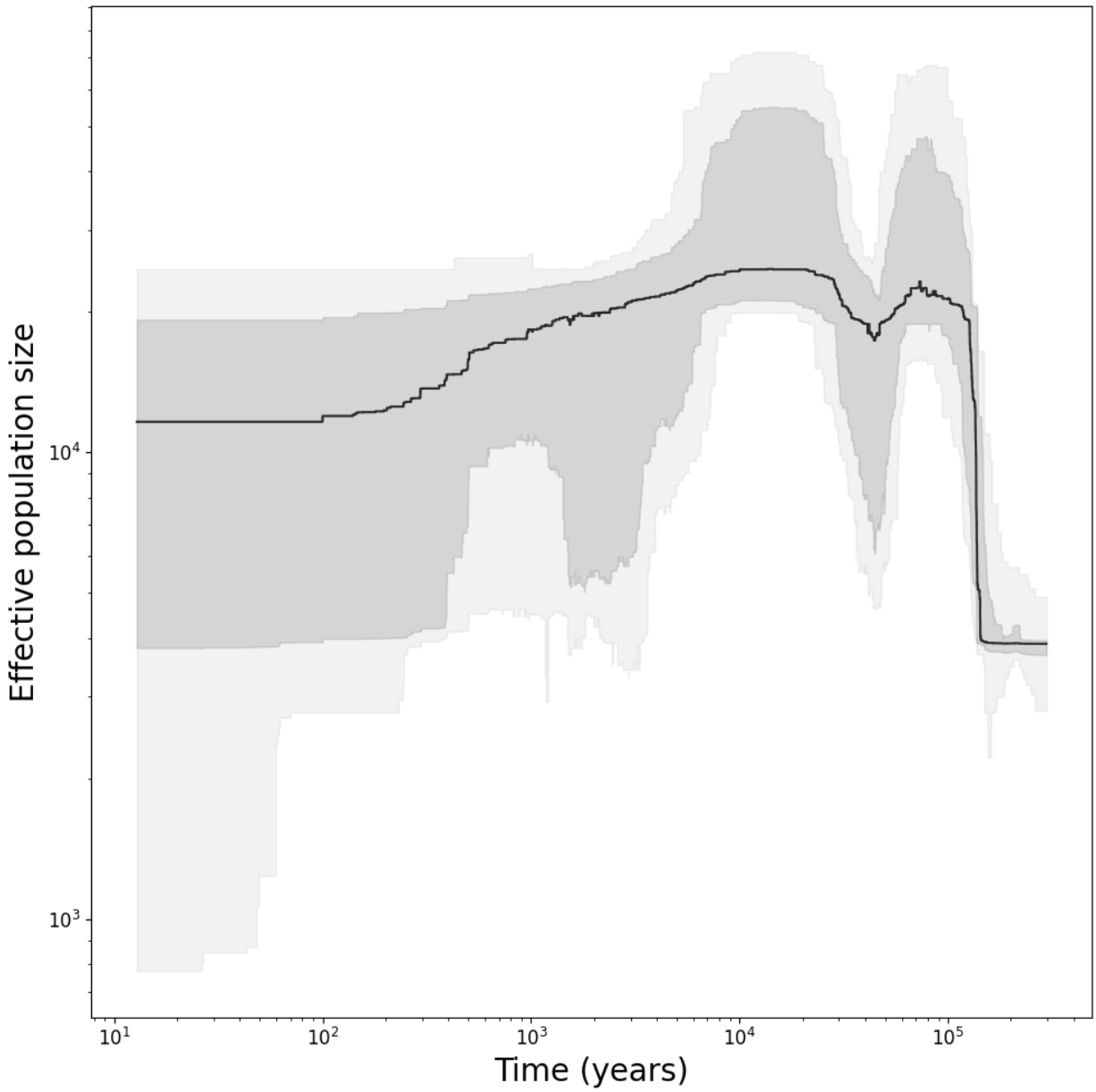

Figure B.48. *Aptenodytes forsteri* (“Emperor_penguin_Clucas2018-Fold_Auster”)

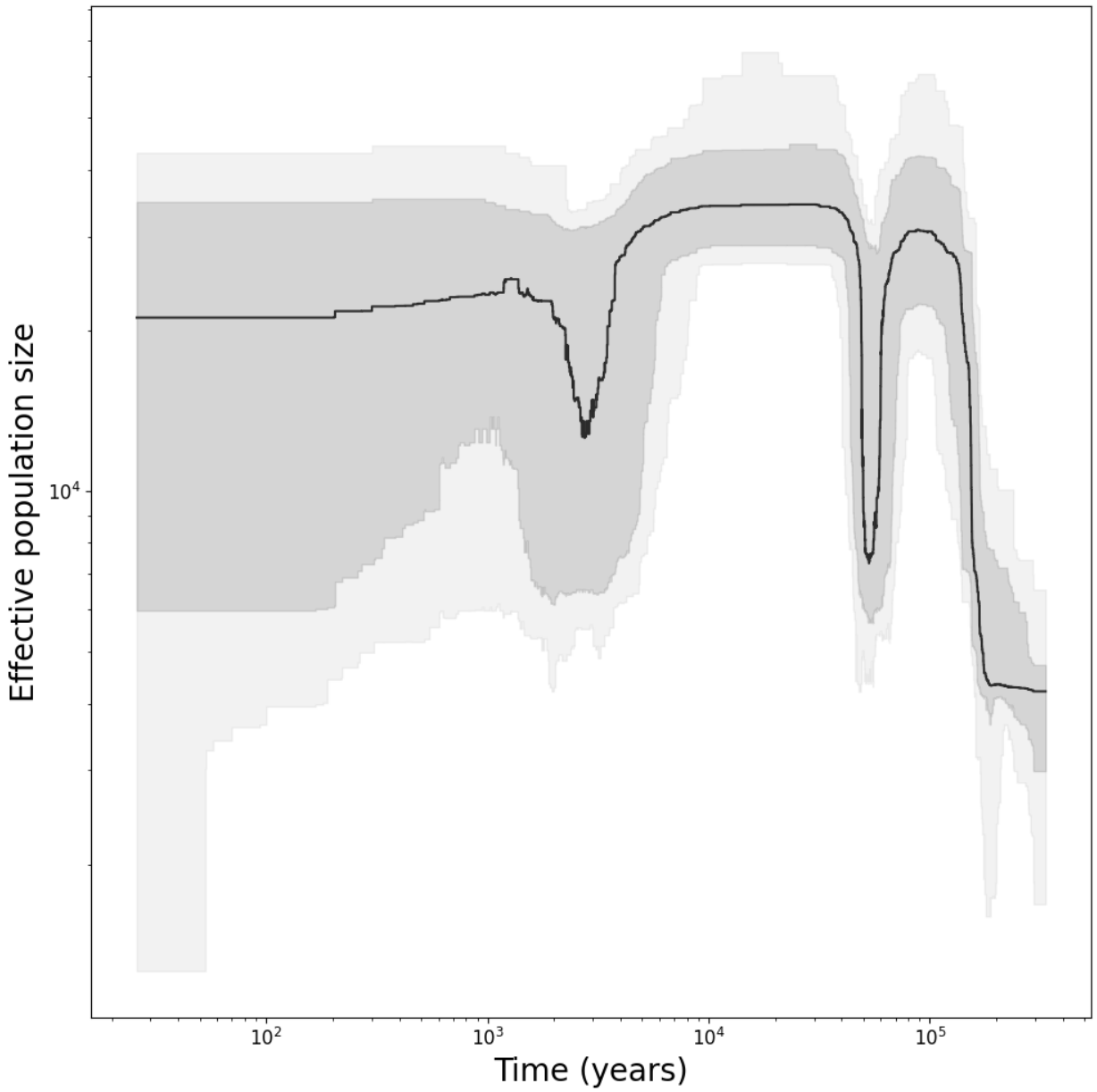

Figure B.49. *Aptenodytes forsteri* (“Emperor_penguin_Clucas2018-Gould_Halley”)

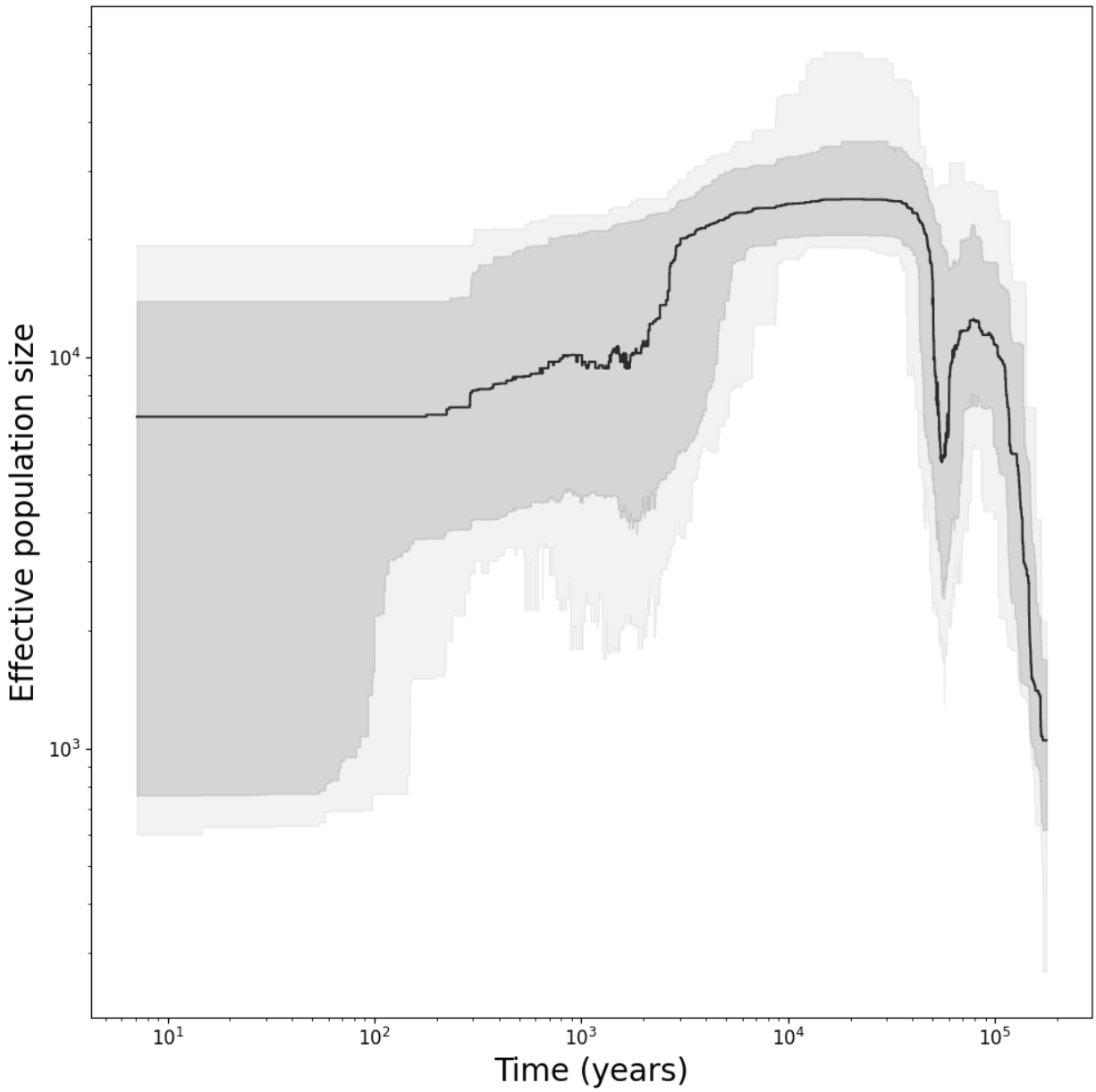

Figure B.50. *Aptenodytes forsteri* (“Emperor_penguin_Clucas2018-Roget_Washington”)

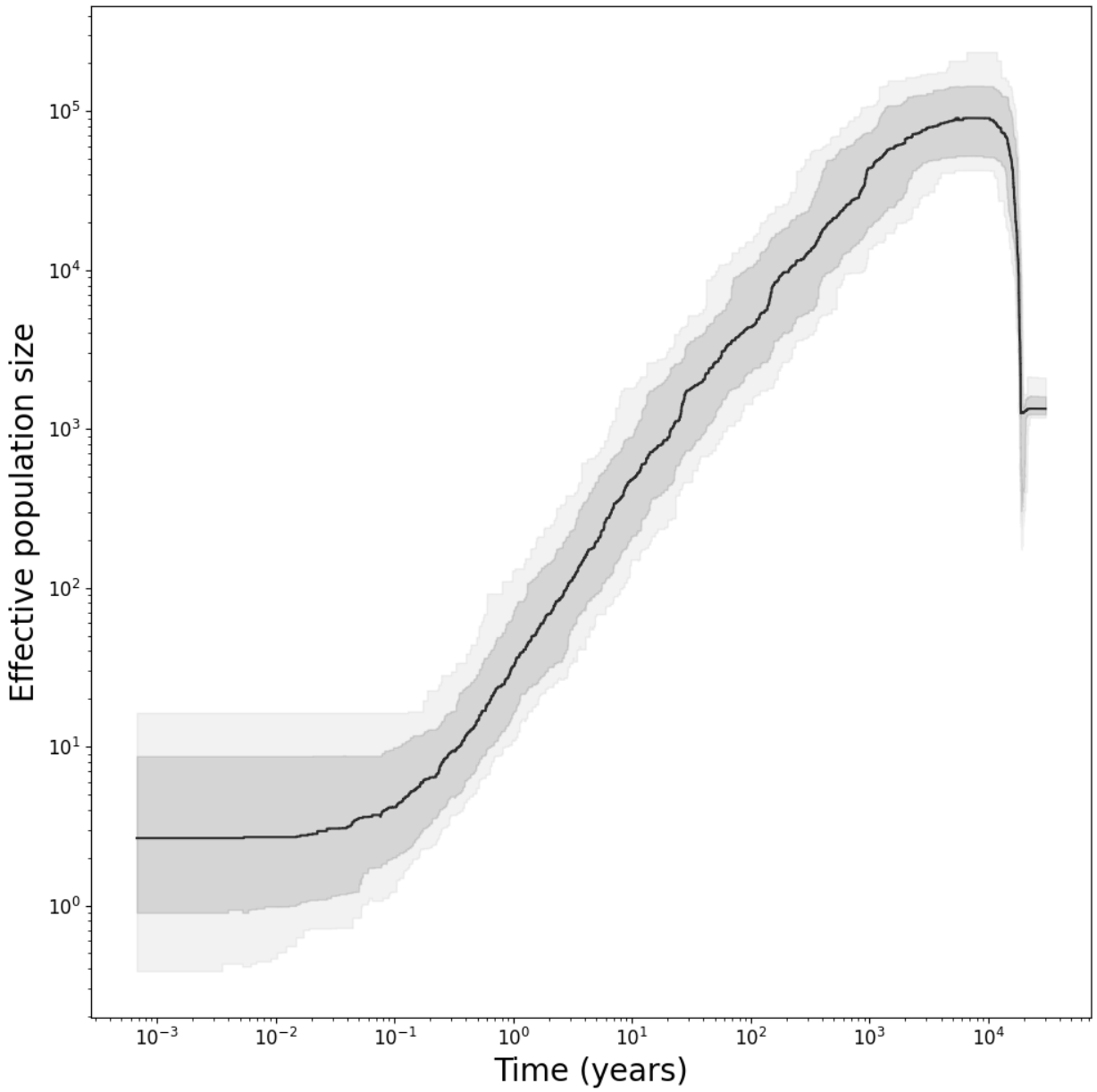

Figure B.51. *Odontesthes argentinensis* (“Oargentinensis”)

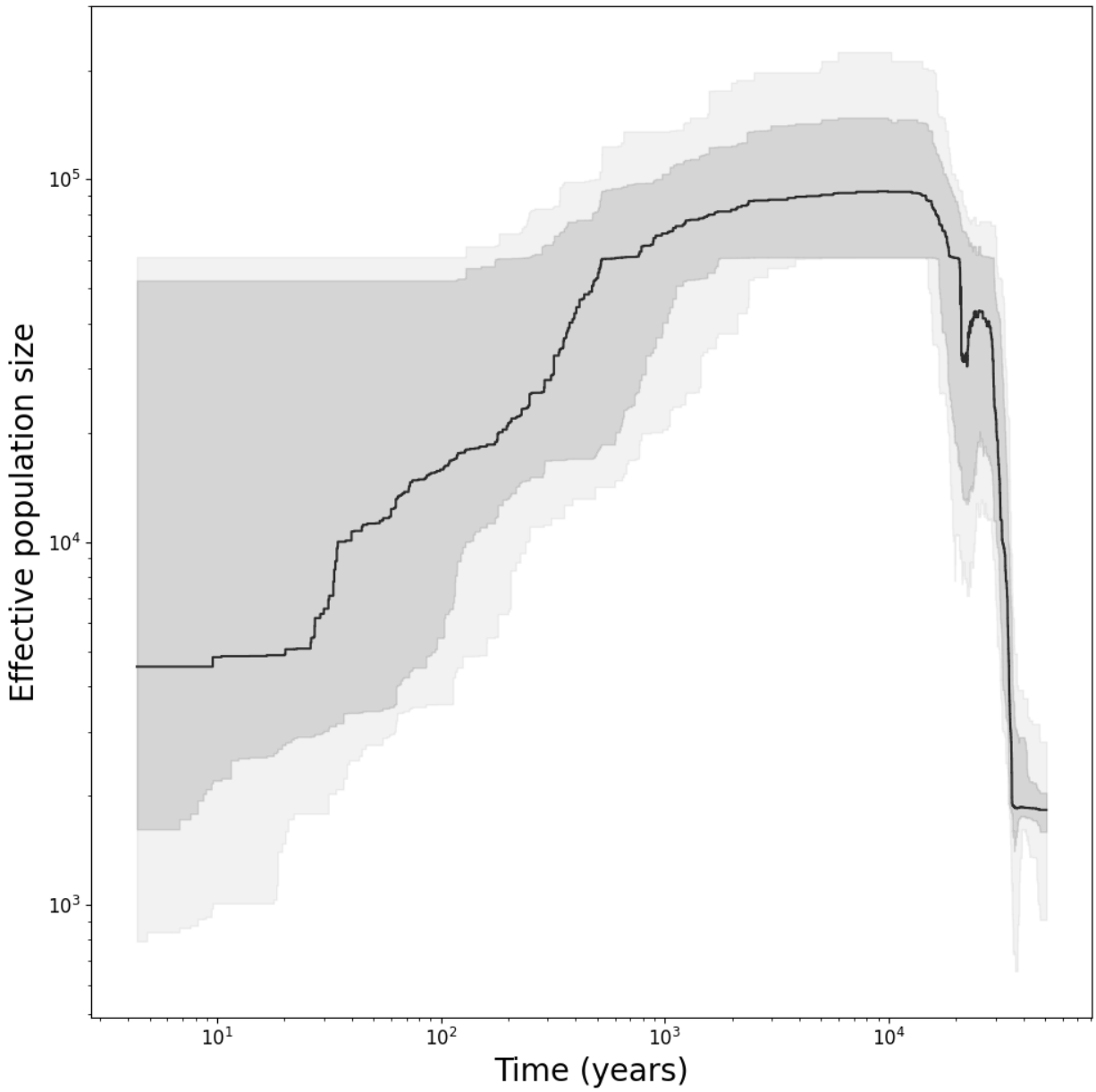

Figure B.52. *Odontesthes regia* (“Oregia”)

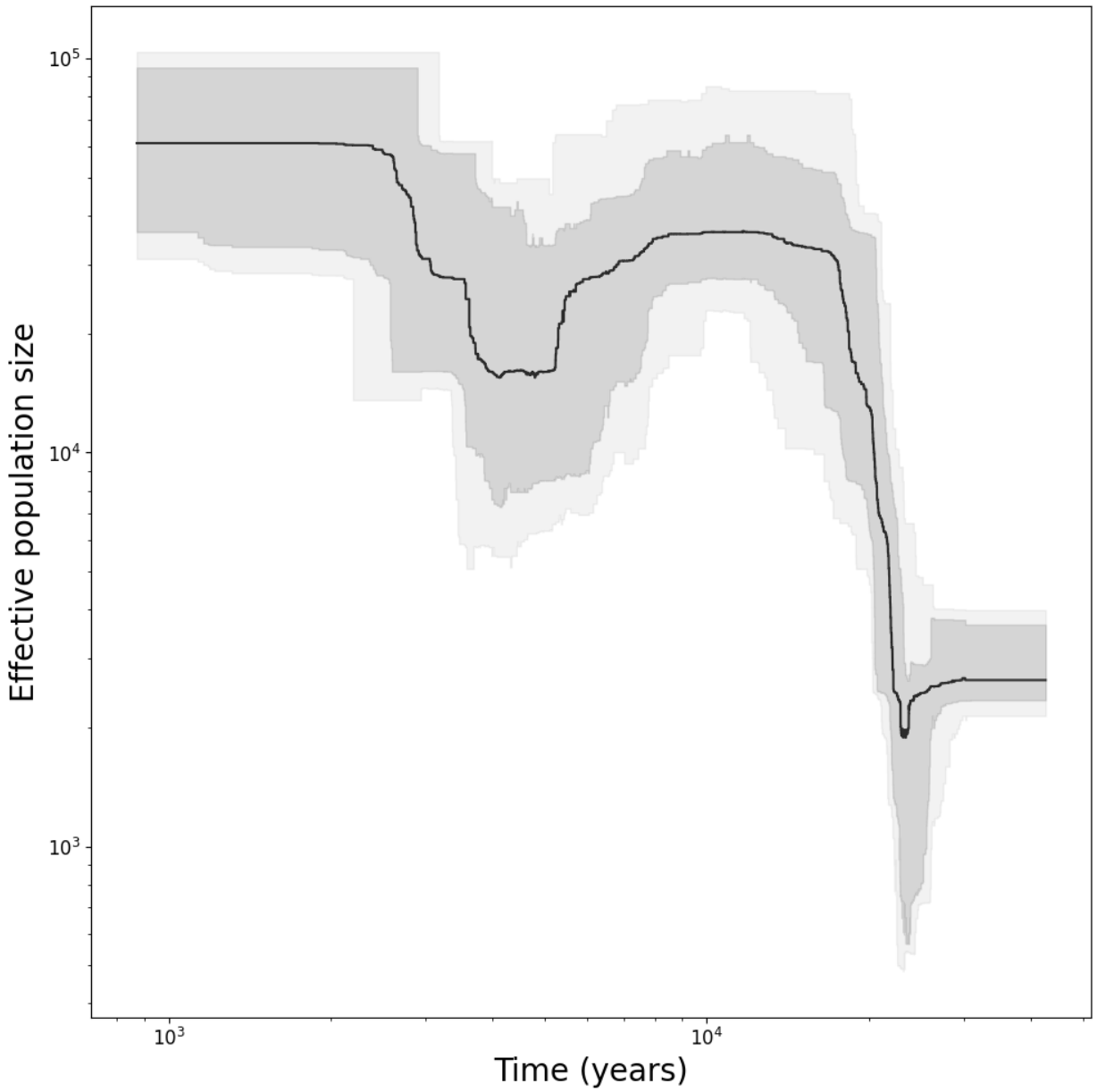

Figure B.53. *Odontesthes mirinensis* (“Omirinensis”)

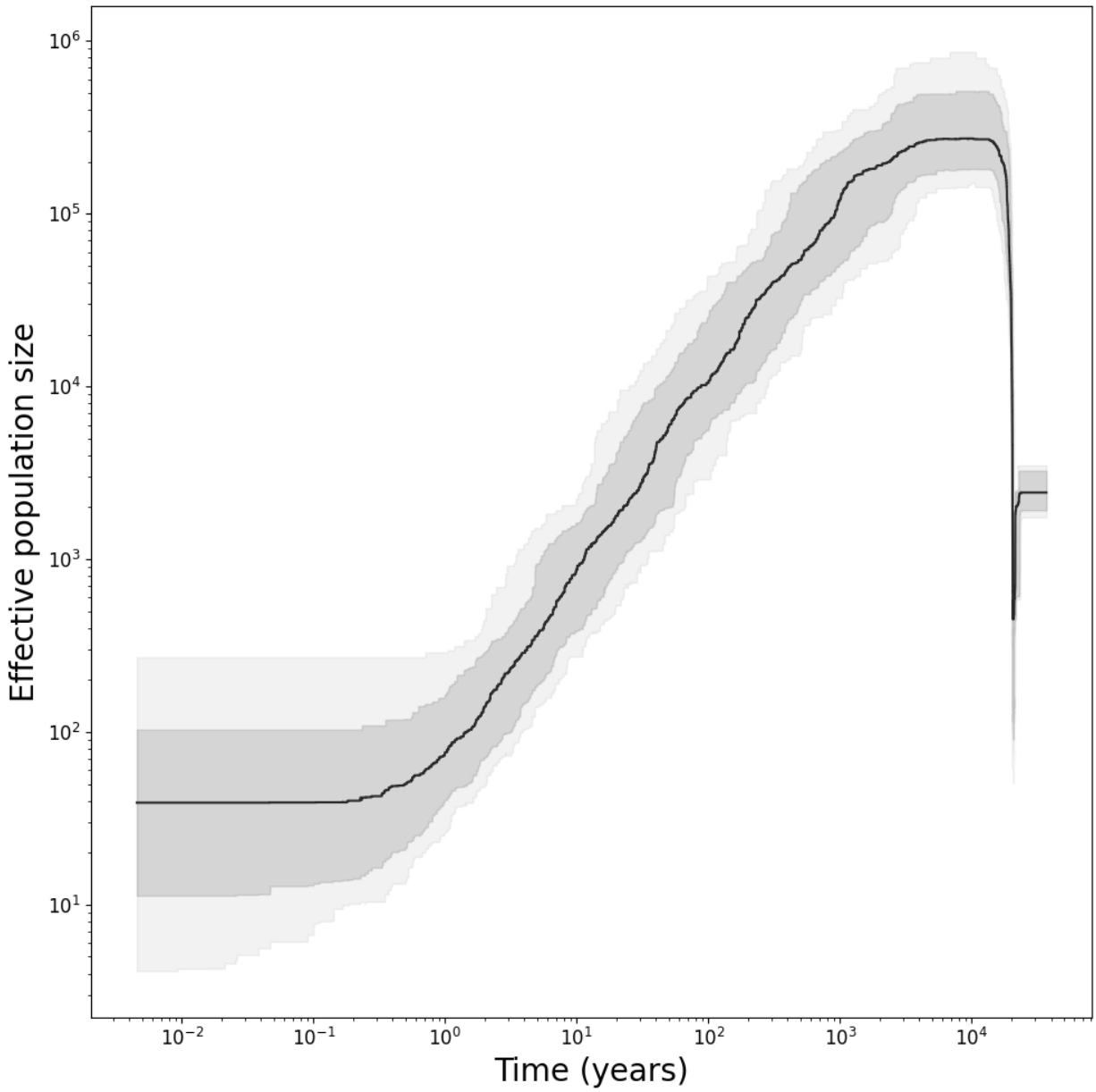

Figure B.54. *Odontesthes mauleanum* (“Omauleanum”)

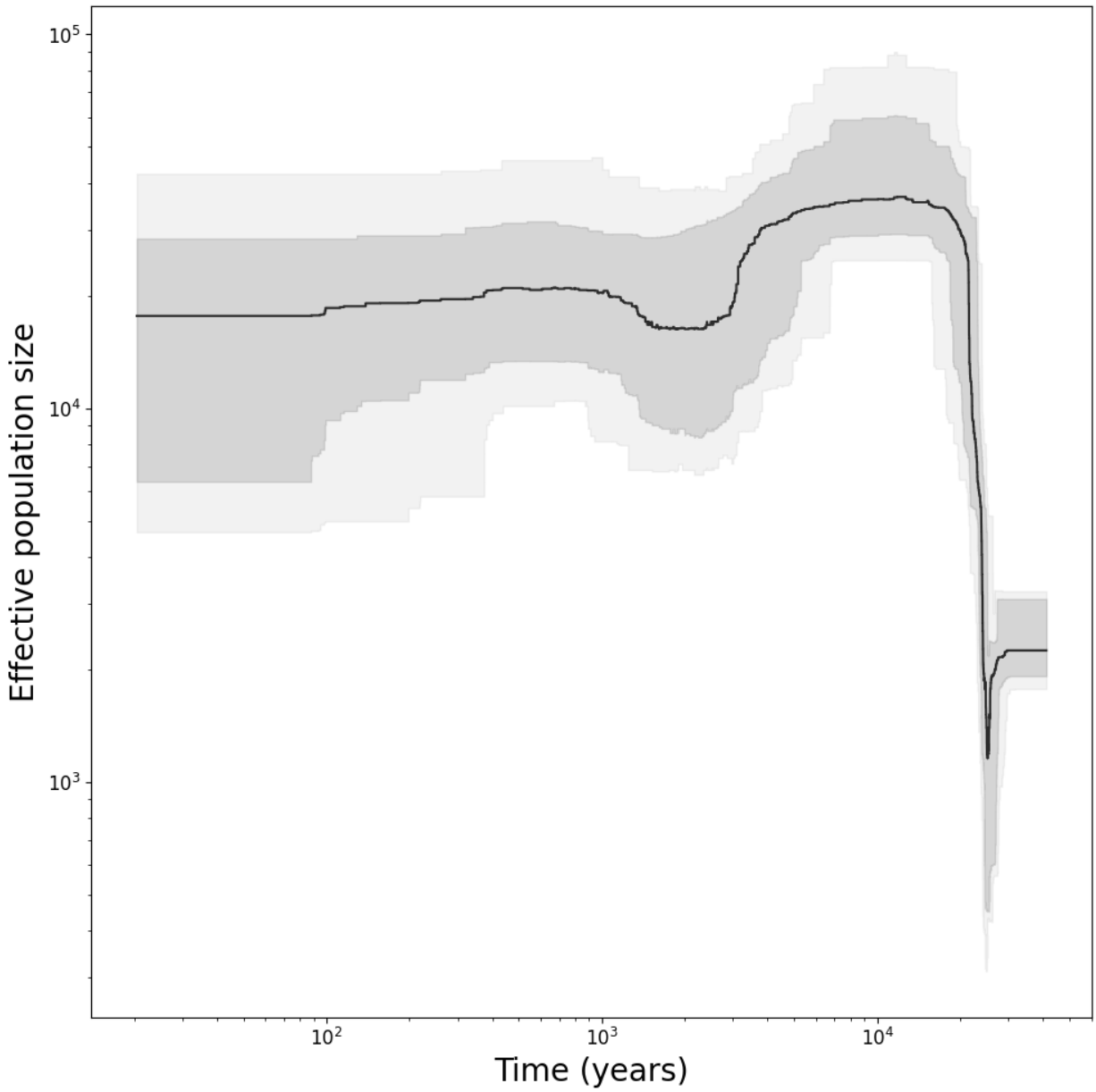

Figure B.55. *Odontesthes ledae* (“Oledae”)

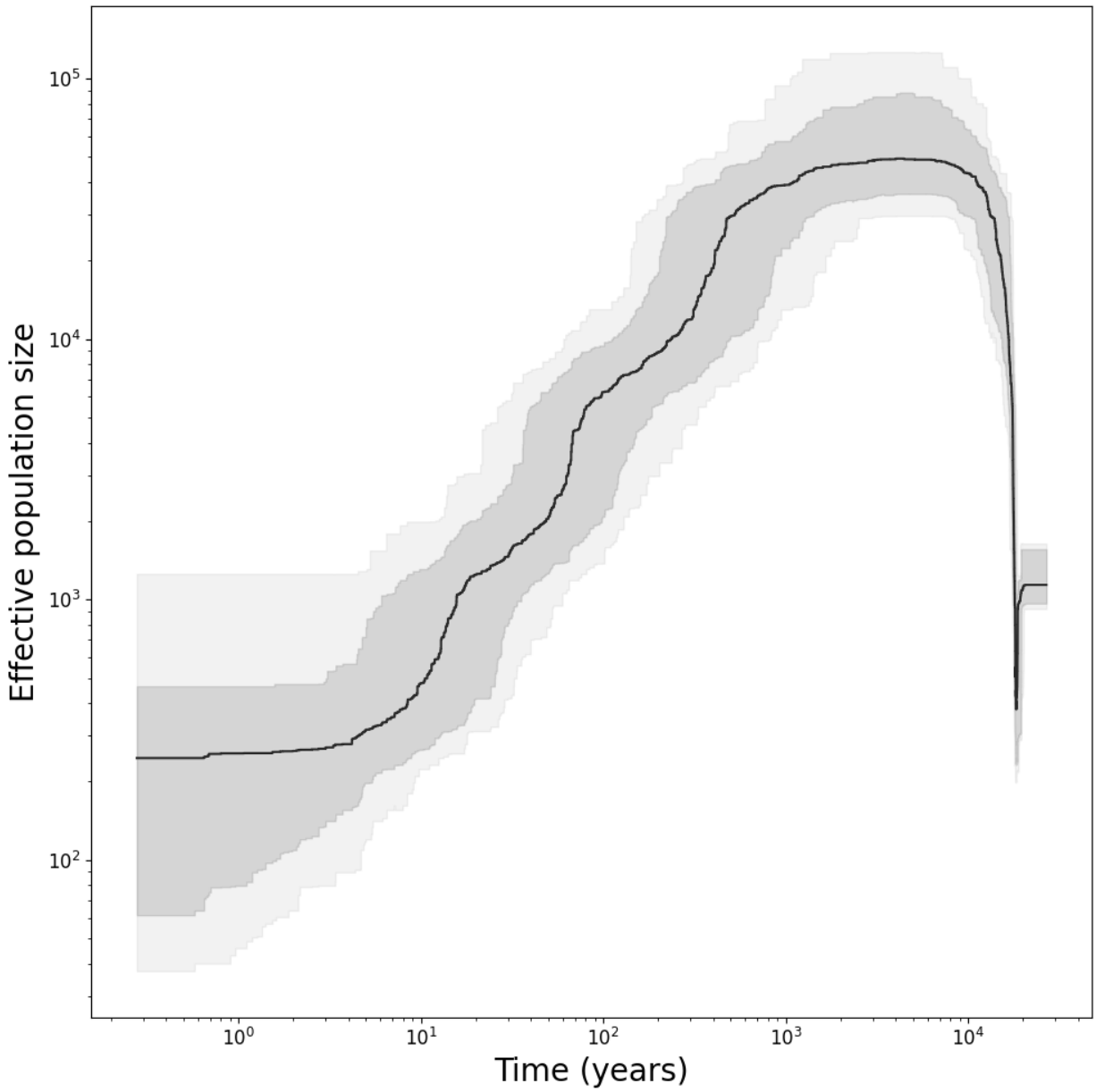

Figure B.56. *Odontesthes bonariensis* (“Obonariensis”)

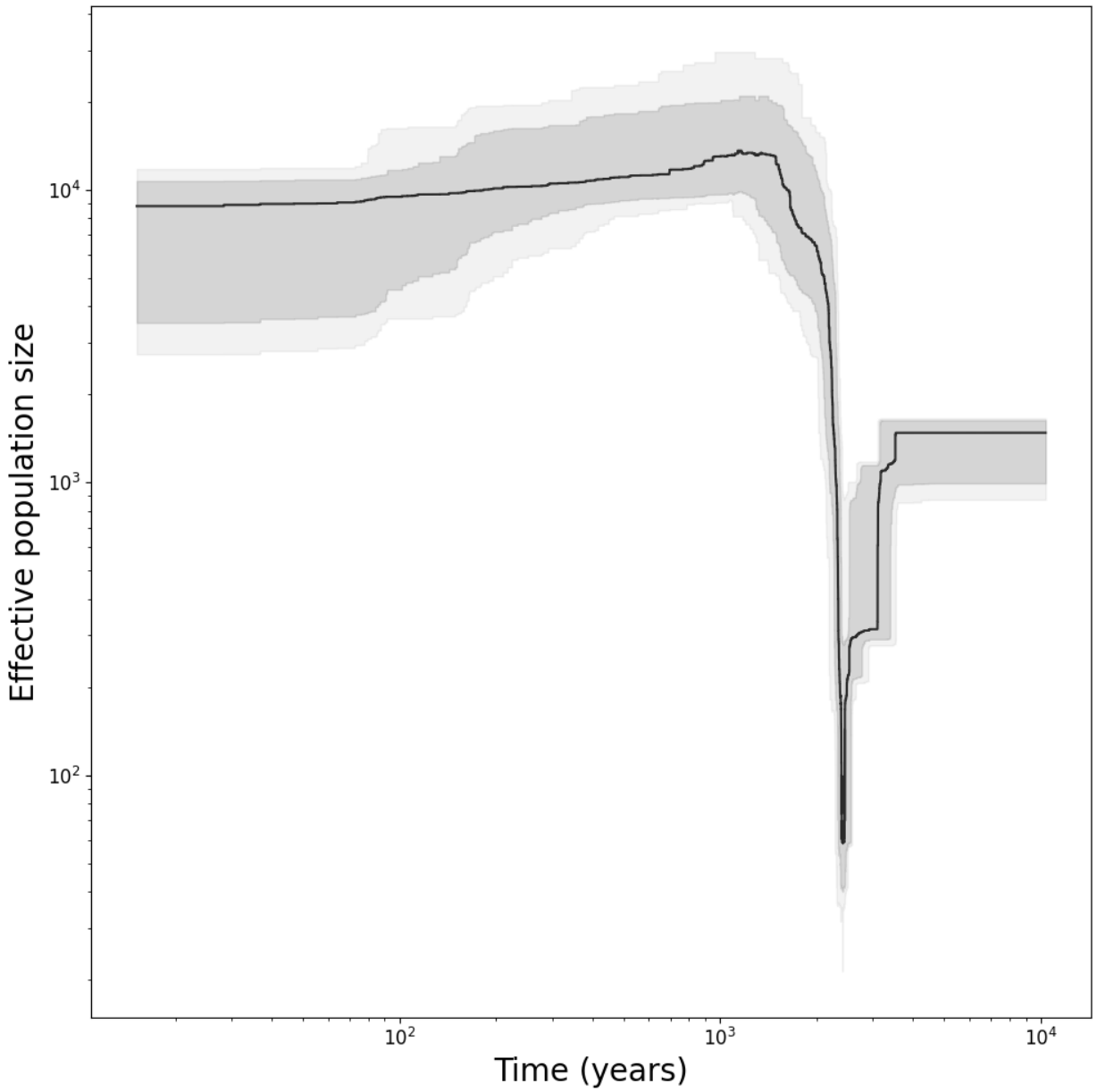

Figure B.57. *Odontesthes hatcheri* (“Ohatcheri”)

References:

1. Acha, E. M., Mianzan, H. W., Guerrero, R. A., Favero, M., & Bava, J. (2004). Marine fronts at the continental shelves of austral South America: Physical and ecological processes. *Journal of Marine Systems*, *44*(1), 83–105. https://doi.org/10.1016/j.jmarsys.2003.09.005
2. Adams, N. J., & Klages, N. T. (1987). Seasonal variation in the diet of the king penguin (Aptenodytes patagonicus) at sub-Antarctic Marion Island. *Journal of Zoology*, *212*(2), 303–324. https://doi.org/10.1111/j.1469-7998.1987.tb05992.x
3. Aguirre, M. L. (1993). Palaeobiogeography of the Holocene molluscan fauna from northeastern Buenos Aires Province, Argentina: Its relation to coastal evolution and sea level changes. *Palaeogeography, Palaeoclimatology, Palaeoecology*, *102*(1), 1–26. https://doi.org/10.1016/0031-0182(93)90002-Z
4. Ainley, D. G., Nur, N., & Woehler, E. J. (1995). Factors Affecting the Distribution and Size of Pygoscelid Penguin Colonies in the Antarctic. *The Auk*, *112*(1), 171–182. https://doi.org/10.2307/4088776
5. Alberto, F. J., Aitken, S. N., Alía, R., González-Martínez, S. C., Hänninen, H., Kremer, A., Lefèvre, F., Lenormand, T., Yeaman, S., Whetten, R., & Savolainen, O. (2013). Potential for evolutionary responses to climate change – evidence from tree populations. *Global Change Biology*, *19*(6), 1645–1661. https://doi.org/10.1111/gcb.12181
6. Alemany, D., Acha, E. M., & Iribarne, O. O. (2014). Marine fronts are important fishing areas for demersal species at the Argentine Sea (Southwest Atlantic Ocean). *Journal of Sea Research*, *87*, 56–67. https://doi.org/10.1016/j.seares.2013.12.006
7. Allio, R., Donega, S., Galtier, N., & Nabholz, B. (2017). Large Variation in the Ratio of Mitochondrial to Nuclear Mutation Rate across Animals: Implications for Genetic Diversity and the Use of Mitochondrial DNA as a Molecular Marker. *Molecular Biology and Evolution*, *34*(11), 2762–2772. https://doi.org/10.1093/molbev/msx197

8. Anderson, M. J. (2001). A new method for non-parametric multivariate analysis of variance. *Austral Ecology*, *26*(1), 32–46. https://doi.org/10.1111/j.1442-9993.2001.01070.pp.x

9. Anderson, M. J. (2014). Permutational multivariate analysis of variance (PERMANOVA). *Wiley Statsref: Statistics Reference Online*, 1-15. https://doi.org/10.1002/9781118445112.stat07841

10. Andreasen, A. M., Stewart, K. M., Longland, W. S., Beckmann, J. P., & Forister, M. L. (2012). Identification of source-sink dynamics in mountain lions of the Great Basin. *Molecular Ecology*, *21*(23), 5689–5701. https://doi.org/10.1111/j.1365-294X.2012.05740.x

11. Artico, L. O., Bianchini, A., Grubel, K. S., Monteiro, D. S., Estima, S. C., de Oliveira, L. R., Bonatto, S. L., & Marins, L. F. (2010). Mitochondrial control region haplotypes of the South American sea lion Otaria flavescens (Shaw, 1800). *Brazilian Journal of Medical and Biological Research*, *43*, 816–820. https://doi.org/10.1590/S0100-879X2010007500074

12. Axelsson, E., Willerslev, E., Gilbert, M. T. P., & Nielsen, R. (2008). The Effect of Ancient DNA Damage on Inferences of Demographic Histories. *Molecular Biology and Evolution*, *25*(10), 2181–2187. https://doi.org/10.1093/molbev/msn163

13. Barnosky, A. D. (1987). Punctuated Equilibrium and Phyletic Gradualism. In H. H. Genoways (Ed.), *Current Mammalogy* (pp. 109–147). Springer US. https://doi.org/10.1007/978-1-4757-9909-5_4

14. Barrionuevo, M., Ciancio, J., Marchisio, N., & Frere, E. (2018). Parental body condition and high energy value of fish determine nestling success in Magellanic penguin (Spheniscus magellanicus). *Marine Biology*, *165*(6), 105. https://doi.org/10.1007/s00227-018-3358-3

15. Barros, N. B., Ostrom, P. H., Stricker, C. A., & Wells, R. S. (2010). Stable isotopes differentiate bottlenose dolphins off west-central Florida. *Marine Mammal Science*, *26*(2), 324–336. https://doi.org/10.1111/j.1748-7692.2009.00315.x

16. Baylis, A. M. M., Kowalski, G. J., Voigt, C. C., Orben, R. A., Trillmich, F., Staniland, I. J., & Hoffman, J. I. (2016). Pup Vibrissae Stable Isotopes Reveal Geographic Differences in Adult

Female Southern Sea Lion Habitat Use during Gestation. *PLOS ONE*, *11*(6), e0157394. https://doi.org/10.1371/journal.pone.0157394

17. Baylis, A. M. M., Orben, R. A., Arnould, J. P. Y., Peters, K., Knox, T., Costa, D. P., & Staniland, I. J. (2015). Diving deeper into individual foraging specializations of a large marine predator, the southern sea lion. *Oecologia*, *179*(4), 1053–1065. https://doi.org/10.1007/s00442-015-3421-4

18. Ben-David, M., & Flaherty, E. A. (2012). Stable isotopes in mammalian research: A beginner's guide. *Journal of Mammalogy*, *93*(2), 312–328. https://doi.org/10.1644/11-MAMM-S-166.1

19. Bender, V. B., Hanebuth, T. J. J., & Chiessi, C. M. (2013). Holocene shifts of the Subtropical Shelf Front off southeastern South America controlled by high and low latitude atmospheric forcings. *Palaeoceanography*, *28*(3), 481–490. https://doi.org/10.1002/palo.20044

20. Berman, A. L., Silvestri, G. E., & Tonello, M. S. (2016). Differences between Last Glacial Maximum and present-day temperature and precipitation in southern South America. *Quaternary Science Reviews*, *150*, 221–233. https://doi.org/10.1016/j.quascirev.2016.08.025

21. Bhaskar, A., & Song, Y. S. (2014). Descartes' Rule Of Signs And The Identifiability Of Population Demographic Models From Genomic Variation Data. *Annals of Statistics*, *42*(6), 2469–2493. https://doi.org/10.1214/14-AOS1264

22. Boersma, P. D. (2008). Penguins as Marine Sentinels. *BioScience*, *58*(7), 597–607. https://doi.org/10.1641/B580707

23. Boersma, P. D., & Rebstock, G. A. (2014). Climate Change Increases Reproductive Failure in Magellanic Penguins. *PLOS ONE*, *9*(1), e85602. https://doi.org/10.1371/journal.pone.0085602

24. Boersma, P., & Rebstock, G. (2009). Foraging distance affects reproductive success in Magellanic penguins. *Marine Ecology Progress Series*, *375*, 263–275. https://doi.org/10.3354/meps07753

25. Bohling, J., Small, M., Von Bargen, J., Louden, A., & DeHaan, P. (2019). Comparing inferences derived from microsatellite and RADseq datasets: A case study involving threatened bull trout. *Conservation Genetics*, *20*(2), 329–342. https://doi.org/10.1007/s10592-018-1134-z

26. Bohonak, A. J., Holland, M. D., Santer, B., Zeller, M., Kearns, C. M., & Hairston, N. G. (2006). The population genetic consequences of diapause in Eudiaptomus copepods. *Archiv Für Hydrobiologie*, *167*(1–4), 183–202. https://doi.org/10.1127/0003-9136/2006/0167-0183

27. Bost, C. A., Cotté, C., Bailleul, F., Cherel, Y., Charrassin, J. B., Guinet, C., Ainley, D. G., & Weimerskirch, H. (2009). The importance of oceanographic fronts to marine birds and mammals of the southern oceans. *Journal of Marine Systems*, *78*(3), 363–376. https://doi.org/10.1016/j.jmarsys.2008.11.022

28. Bouckaert, R., Heled, J., Kühnert, D., Vaughan, T., Wu, C.-H., Xie, D., Suchard, M. A., Rambaut, A., & Drummond, A. J. (2014). BEAST 2: A Software Platform for Bayesian Evolutionary Analysis. *PLOS Computational Biology*, *10*(4), e1003537. https://doi.org/10.1371/journal.pcbi.1003537

29. Bouzat, J. L., Walker, B. G., & Boersma, P. D. (2009). Regional Genetic Structure in the Magellanic Penguin (Spheniscus magellanicus) Suggests Metapopulation Dynamics. *The Auk*, *126*(2), 326–334. https://doi.org/10.1525/auk.2009.07122

30. Boyd, I. L. (1993). Pup production and distribution of breeding Antarctic fur seals (Arctocephalus gazella) at South Georgia. *Antarctic Science*, *5*(1), 17–24. https://doi.org/10.1017/S0954102093000045

31. Brierley, A. S., Fernandes, P. G., Brandon, M. A., Armstrong, F., Millard, N. W., McPhail, S. D., Stevenson, P., Pebody, M., Perrett, J., Squires, M., Bone, D. G., & Griffiths, G. (2002).

Antarctic Krill Under Sea Ice: Elevated Abundance in a Narrow Band Just South of Ice Edge. *Science*, *295*(5561), 1890–1892. https://doi.org/10.1126/science.1068574

32. Bruyn, M. de, Hall, B. L., Chauke, L. F., Baroni, C., Koch, P. L., & Hoelzel, A. R. (2009). Rapid Response of a Marine Mammal Species to Holocene Climate and Habitat Change. *PLOS Genetics*, *5*(7), e1000554. https://doi.org/10.1371/journal.pgen.1000554

33. Bryant, D., Bouckaert, R., Felsenstein, J., Rosenberg, N. A., & Roy Choudhury, A. (2012). Inferring Species Trees Directly from Biallelic Genetic Markers: Bypassing Gene Trees in a Full Coalescent Analysis. *Molecular Biology and Evolution*, *29*(8), 1917–1932. https://doi.org/10.1093/molbev/mss086

34. Brzeziecki, B., Pommerening, A., Miścicki, S., Drozdowski, S., & Żybura, H. (2016). A common lack of demographic equilibrium among tree species in Białowieża National Park (NE Poland): Evidence from long-term plots. *Journal of Vegetation Science*, *27*(3), 460–469. https://doi.org/10.1111/jvs.12369

35. Bustos, R. L., Daneri, G. A., Volpedo, A. V., Harrington, A., & Varela, E. A. (2012). The diet of the South American sea lion (Otaria flavescens) at Río Negro, Patagonia, Argentina, during the winter-spring period. *Iheringia. Série Zoologia*, *102*, 394–400. https://doi.org/10.1590/S0073-47212012000400005

36. Bustos, R. L., Daneri, G. A., Volpedo, A. V., Harrington, A., & Varela, E. A. (2014). Diet of the South American sea lion Otaria flavescens during the summer season at Río Negro, Patagonia, Argentina. *Aquatic Biology*, *20*(3), 235–243. https://doi.org/10.3354/ab00557

37. Cammen, K. M., Schultz, T. F., Bowen, W. D., Hammill, M. O., Puryear, W. B., Runstadler, J., Wenzel, F. W., Wood, S. A., & Kinnison, M. (2018). Genomic signatures of population bottleneck and recovery in Northwest Atlantic pinnipeds. *Ecology and Evolution*, *8*(13), 6599–6614. https://doi.org/10.1002/ece3.4143

38. Campagna, C., Boeuf, B. J. L., Blackwell, S. B., Crocker, D. E., & Quintana, F. (1995). Diving behaviour and foraging location of female southern elephant seals from Patagonia. *Journal of Zoology*, *236*(1), 55–71. https://doi.org/10.1111/j.1469-7998.1995.tb01784.x

39. Campagna, C., & Le Boeuf, B. J. (1988). Reproductive Behaviour of Southern Sea Lions. *Behaviour*, *104*(3/4), 233–261.

40. Campagna, C., Le Boeuf, B. J., & Cappozzo, H. L. (1988). Pup Abduction and Infanticide in Southern Sea Lions. *Behaviour*, *107*(1/2), 44–60.

41. Campagna, C., Werner, R., Karesh, W., Marín, M. R., Koontz, F., Cook, R., & Koontz, C. (2001). Movements and location at sea of South American sea lions (Otaria flavescens). *Journal of Zoology*, *255*(2), 205–220. https://doi.org/10.1017/S0952836901001285

42. Cappozzo, H. L., Túnez, J. I., & Cassini, M. H. (2008). Sexual harassment and female gregariousness in the South American sea lion, Otaria flavescens. *Naturwissenschaften*, *95*(7), 625–630. https://doi.org/10.1007/s00114-008-0363-2

43. Carøe, C., Gopalakrishnan, S., Vinner, L., Mak, S. S. T., Sinding, M. H. S., Samaniego, J. A., Wales, N., Sicheritz-Pontén, T., & Gilbert, M. T. P. (2018). Single-tube library preparation for degraded DNA. *Methods in Ecology and Evolution*, *9*(2), 410–419. https://doi.org/10.1111/2041-210X.12871

44. Carroll, E. L., Hall, A., Olsen, M. T., Onoufriou, A. B., Gaggiotti, O. E., & Russell, D. J. (2020). Perturbation drives changing metapopulation dynamics in a top marine predator. *Proceedings of the Royal Society B: Biological Sciences*, *287*(1928), 20200318. https://doi.org/10.1098/rspb.2020.0318

45. Casaux, R., Baroni, A., & Ramón, A. (2006). The diet of the Weddell Seal Leptonychotes weddellii at the Danco Coast, Antarctic Peninsula. *Polar Biology*, *29*(4), 257–262. https://doi.org/10.1007/s00300-005-0048-7

46. Cassini, M. (1998). Inter-Specific Infanticide in South American Otariids. *Behaviour*, *135*(8), 1005–1012. https://doi.org/10.1163/156853998792913456

47. Castillo, J., Yorio, P., & Gatto, A. (2019). Shared dietary niche between sexes in Magellanic Penguins. *Austral Ecology*, *44*(4), 635–647. https://doi.org/10.1111/aec.12706

48. Catchen, J., Hohenlohe, P. A., Bassham, S., Amores, A., & Cresko, W. A. (2013). Stacks: An analysis tool set for population genomics. *Molecular Ecology*, *22*(11), 3124–3140. https://doi.org/10.1111/mec.12354

49. Catchen, J. M., Amores, A., Hohenlohe, P., Cresko, W., & Postlethwait, J. H. (2011). Stacks: Building and Genotyping Loci De Novo From Short-Read Sequences. *G3 Genes|Genomes|Genetics*, *1*(3), 171–182. https://doi.org/10.1534/g3.111.000240

50. Cayuela, H., Rougemont, Q., Prunier, J. G., Moore, J.-S., Clobert, J., Besnard, A., & Bernatchez, L. (2018). Demographic and genetic approaches to study dispersal in wild animal populations: A methodological review. *Molecular Ecology*, *27*(20), 3976–4010. https://doi.org/10.1111/mec.14848

51. Chang, D., & Shapiro, B. (2016). Using ancient DNA and coalescent-based methods to infer extinction. *Biology Letters*, *12*(2), 20150822. https://doi.org/10.1098/rsbl.2015.0822

52. Chapuis, M.-P., Loiseau, A., Michalakis, Y., Lecoq, M., Franc, A., & Estoup, A. (2009). Outbreaks, gene flow and effective population size in the migratory locust, Locusta migratoria: A regional-scale comparative survey. *Molecular Ecology*, *18*(5), 792–800. https://doi.org/10.1111/j.1365-294X.2008.04072.x

53. Cherel, Y., & Hobson, K. A. (2007). Geographical variation in carbon stable isotope signatures of marine predators: A tool to investigate their foraging areas in the Southern Ocean. *Marine Ecology Progress Series*, *329*, 281–287. https://doi.org/10.3354/meps329281

54. Cimino, M. A., Lynch, H. J., Saba, V. S., & Oliver, M. J. (2016). Projected asymmetric response of Adélie penguins to Antarctic climate change. *Scientific Reports*, *6*, 28785. https://doi.org/10.1038/srep28785

55. Clark, P. U., Dyke, A. S., Shakun, J. D., Carlson, A. E., Clark, J., Wohlfarth, B., Mitrovica, J. X., Hostetler, S. W., & McCabe, A. M. (2009). The Last Glacial Maximum. *Science*, *325*(5941), 710–714. https://doi.org/10.1126/science.1172873

56. Clucas, G. V., Dunn, M. J., Dyke, G., Emslie, S. D., Levy, H., Naveen, R., Polito, M. J., Pybus, O. G., Rogers, A. D., & Hart, T. (2014). A reversal of fortunes: Climate change 'winners' and 'losers' in Antarctic Peninsula penguins. *Scientific Reports*, *4*(1), 5024. https://doi.org/10.1038/srep05024

57. Clucas, G. V., Younger, J. L., Kao, D., Emmerson, L., Southwell, C., Wienecke, B., Rogers, A. D., Bost, C.-A., Miller, G. D., Polito, M. J., Lelliott, P., Handley, J., Crofts, S., Phillips, R. A., Dunn, M. J., Miller, K. J., & Hart, T. (2018). Comparative population genomics reveals key barriers to dispersal in Southern Ocean penguins. *Molecular Ecology*, *27*(23), 4680–4697. https://doi.org/10.1111/mec.14896

58. Cohen, J. (1988). *Statistical Power Analysis for the Behavioral Sciences* (2nd ed.). Routledge. https://doi.org/10.4324/9780203771587

59. Cole, T. L., Dutoit, L., Dussex, N., Hart, T., Alexander, A., Younger, J. L., Clucas, G. V., Frugone, M. J., Cherel, Y., Cuthbert, R., Ellenberg, U., Fiddaman, S. R., Hiscock, J., Houston, D., Jouventin, P., Mattern, T., Miller, G., Miskelly, C., Nolan, P., … Waters, J. M. (2019). Receding ice drove parallel expansions in Southern Ocean penguins. *Proceedings of the National Academy of Sciences*, *116*(52), 26690–26696. https://doi.org/10.1073/pnas.1904048116

60. Cristofari, R., Liu, X., Bonadonna, F., Cherel, Y., Pistorius, P., Le Maho, Y., Raybaud, V., Stenseth, N. C., Le Bohec, C., & Trucchi, E. (2018). Climate-driven range shifts of the king penguin in a fragmented ecosystem. *Nature Climate Change*, *8*(3), 245–251. https://doi.org/10.1038/s41558-018-0084-2

61. Curtis, C., Stewart, B. S., & Karl, S. A. (2009). Pleistocene population expansions of Antarctic seals. *Molecular Ecology*, *18*(10), 2112–2121. https://doi.org/10.1111/j.1365-294X.2009.04166.x

62. da Silva Cortinhas, M. C., Kersanach, R., Proietti, M., Dumont, L. F. C., D'Incao, F., Lacerda, A. L. F., Prata, P. S., Matoso, D. A., Noleto, R. B., Ramsdorf, W., Boni, T. A., Prioli, A. J., & Cestari, M. M. (2016). Genetic structuring among silverside fish (Atherinella brasiliensis) populations from different Brazilian regions. *Estuarine, Coastal and Shelf Science*, *178*, 148–157. https://doi.org/10.1016/j.ecss.2016.06.007

63. Dabney, J., Meyer, M., & Pääbo, S. (2013). Ancient DNA Damage. *Cold Spring Harbor Perspectives in Biology*, *5*(7), a012567. https://doi.org/10.1101/cshperspect.a012567

64. Dalerum, F., & Angerbjörn, A. (2005). Resolving temporal variation in vertebrate diets using naturally occurring stable isotopes. *Oecologia*, *144*(4), 647–658. https://doi.org/10.1007/s00442-005-0118-0

65. Danecek, P., Bonfield, J. K., Liddle, J., Marshall, J., Ohan, V., Pollard, M. O., Whitwham, A., Keane, T., McCarthy, S. A., Davies, R. M., & Li, H. (2021). Twelve years of SAMtools and BCFtools. *GigaScience*, *10*(2), giab008. https://doi.org/10.1093/gigascience/giab008

66. Dantas, G. P. M., Maria, G. C., Marasco, A. C. M., Castro, L. T., Almeida, V. S., Santos, F. R., Oliveira, L. R., Crespo, E., Frere, E., Milliones, A., González-Acuña, D., Morgante, J. S., & Vianna, J. A. (2018). Demographic history of the Magellanic Penguin (Spheniscus magellanicus) on the Pacific and Atlantic coasts of South America. *Journal of Ornithology*, *159*(3), 643–655. https://doi.org/10.1007/s10336-018-1538-z

67. Davey, J. W., & Blaxter, M. L. (2010). RADSeq: Next-generation population genetics. *Briefings in Functional Genomics*, *9*(5–6), 416–423. https://doi.org/10.1093/bfgp/elq031

68. Desprez, M., Gimenez, O., McMahon, C. R., Hindell, M. A., & Harcourt, R. G. (2018). Optimizing lifetime reproductive output: Intermittent breeding as a tactic for females in a

long-lived, multiparous mammal. *Journal of Animal Ecology*, *87*(1), 199–211. https://doi.org/10.1111/1365-2656.12775

69. Dickerson, B. R., Ream, R. R., Vignieri, S. N., & Bentzen, P. (2010). Population Structure as Revealed by mtDNA and Microsatellites in Northern Fur Seals, Callorhinus ursinus, throughout Their Range. *PLOS ONE*, *5*(5), e10671. https://doi.org/10.1371/journal.pone.0010671

70. Dodino, S., Riccialdelli, L., Polito, M. J., Pütz, K., & Rey, A. R. (2020). Inter-annual variation in the trophic niche of Magellanic penguins Spheniscus magellanicus during the pre-molt period in the Beagle Channel. *Marine Ecology Progress Series*, *655*, 215–225. https://doi.org/10.3354/meps13518

71. Drummond, A. J., Rambaut, A., Shapiro, B., & Pybus, O. G. (2005). Bayesian Coalescent Inference of Past Population Dynamics from Molecular Sequences. *Molecular Biology and Evolution*, *22*(5), 1185–1192. https://doi.org/10.1093/molbev/msi103

72. Dupanloup, I., Schneider, S., & Excoffier, L. (2002). A simulated annealing approach to define the genetic structure of populations. *Molecular Ecology*, *11*(12), 2571–2581. https://doi.org/10.1046/j.1365-294X.2002.01650.x

73. Elliott, K. H., Roth, J. D., & Crook, K. (2017). Lipid Extraction Techniques for Stable Isotope Analysis and Ecological Assays. In S. K. Bhattacharya (Ed.), *Lipidomics: Methods and Protocols* (pp. 9–24). Springer. https://doi.org/10.1007/978-1-4939-6996-8_2

74. Emmerson, L., Pike, R., & Southwell, C. (2011). Reproductive consequences of environment-driven variation in Adélie penguin breeding phenology. *Marine Ecology Progress Series*, *440*, 203–216. https://doi.org/10.3354/meps09265

75. Emslie, S. D., & Patterson, W. P. (2007). Abrupt recent shift in δ13C and δ15N values in Adélie penguin eggshell in Antarctica. *Proceedings of the National Academy of Sciences of the United States of America*, *104*(28), 11666–11669. https://doi.org/10.1073/pnas.0608477104

76. Eriksson, A., Mehlig, B., Rafajlovic, M., & Sagitov, S. (2010). The Total Branch Length of Sample Genealogies in Populations of Variable Size. *Genetics*, *186*(2), 601–611. https://doi.org/10.1534/genetics.110.117135

77. Excoffier, L., & Lischer, H. E. L. (2010). Arlequin suite ver 3.5: A new series of programs to perform population genetics analyses under Linux and Windows. *Molecular Ecology Resources*, *10*(3), 564–567. https://doi.org/10.1111/j.1755-0998.2010.02847.x

78. Fabiani, A., Hoelzel, A. R., Galimberti, F., & Muelbert, M. M. C. (2003). Long-Range Paternal Gene Flow in the Southern Elephant Seal. *Science*, *299*(5607), 676–676. https://doi.org/10.1126/science.299.5607.676

79. Feijoo, M., Lessa, E. P., Loizaga de Castro, R., & Crespo, E. A. (2011). Mitochondrial and microsatellite assessment of population structure of South American sea lion (Otaria flavescens) in the Southwestern Atlantic Ocean. *Marine Biology*, *158*(8), 1857–1867. https://doi.org/10.1007/s00227-011-1697-4

80. Fernández, D. A., Ciancio, J., Ceballos, S. G., Riva-Rossi, C., & Pascual, M. A. (2010). Chinook salmon (Oncorhynchus tshawytscha, Walbaum 1792) in the Beagle Channel, Tierra del Fuego: The onset of an invasion. *Biological Invasions*, *12*(9), 2991–2997. https://doi.org/10.1007/s10530-010-9731-x

81. Fernández, R., Almodóvar, A., Novo, M., Gutiérrez, M., & Díaz Cosín, D. J. (2013). Earthworms, good indicators for palaeogeographical studies? Testing the genetic structure and demographic history in the peregrine earthworm Aporrectodea trapezoides (Dugès, 1828) in southern Europe. *Soil Biology and Biochemistry*, *58*, 127–135. https://doi.org/10.1016/j.soilbio.2012.10.021

82. Fernández-Juricic, E., & Cassini, M. H. (2007). Intra-sexual female agonistic behaviour of the South American sea lion (Otaria flavescens) in two colonies with different breeding substrates. *Acta Ethologica*, *10*(1), 23–28. https://doi.org/10.1007/s10211-006-0024-4

83. Ferrer, M., & Negro, J. J. (2004). The Near Extinction of Two Large European Predators: Super Specialists Pay a Price. *Conservation Biology*, *18*(2), 344–349. https://doi.org/10.1111/j.1523-1739.2004.00096.x

84. Finkelstein, M. E., Doak, D. F., Nakagawa, M., Sievert, P. R., & Klavitter, J. (2010). Assessment of demographic risk factors and management priorities: Impacts on juveniles substantially affect population viability of a long-lived seabird. *Animal Conservation*, *13*(2), 148–156. https://doi.org/10.1111/j.1469-1795.2009.00311.x

85. Fisher, R. A. (1930). *The genetical theory of natural selection* (pp. xiv, 272). Clarendon Press. https://doi.org/10.5962/bhl.title.27468

86. Fleming, J., Sutherland, C., Sterrett, S. C., & Campbell Grant, E. H. (2020). A latent process model approach to improve the utility of indicator species. *Oikos*, *129*(12), 1753–1762. https://doi.org/10.1111/oik.07334

87. Foote, A. D., Hooper, R., Alexander, A., Baird, R. W., Baker, C. S., Ballance, L., ... & Morin, P. A. (2021). Runs of homozygosity in killer whale genomes provide a global record of demographic histories. *Molecular Ecology*, *30*(23), 6162-6177.

88. Forcada, J., & Trathan, P. N. (2009). Penguin responses to climate change in the Southern Ocean. *Global Change Biology*, *15*(7), 1618–1630. https://doi.org/10.1111/j.1365-2486.2009.01909.x

89. Fordham, D. A., Akçakaya, H. R., Alroy, J., Saltré, F., Wigley, T. M. L., & Brook, B. W. (2016). Predicting and mitigating future biodiversity loss using long-term ecological proxies. *Nature Climate Change*, *6*(10), 909–916. https://doi.org/10.1038/nclimate3086

90. Forero, M., Hobson, K., Bortolotti, G., Donázar, J., Bertellotti, M., & Blanco, G. (2002). Food resource utilisation by the Magellanic penguin evaluated through stable-isotope analysis: Segregation by sex and age and influence on offspring quality. *Marine Ecology Progress Series*, *234*, 289–299. https://doi.org/10.3354/meps234289

91. Franco-Trecu, V., Aurioles-Gamboa, D., Arim, M., & Lima, M. (2012). Prepartum and postpartum trophic segregation between sympatrically breeding female Arctocephalus australis and Otaria flavescens. *Journal of Mammalogy*, *93*(2), 514–521. https://doi.org/10.1644/11-MAMM-A-174.1

92. Franco-Trecu, V., Costa-Urrutia, P., Schramm, Y., Tassino, B., & Inchausti, P. (2015). Tide line versus internal pools: Mating system and breeding success of South American sea lion males. *Behavioral Ecology and Sociobiology*, *69*(12), 1985–1996. https://doi.org/10.1007/s00265-015-2010-1

93. Franco-Trecu, V., Botta, S., de Lima, R. C., Negrete, J., & Naya, D. E. (2022). Testing the niche variation hypothesis in pinnipeds. *Mammal Review*, *52*(4), 497-506. https://doi.org/10.1111/mam.12297

94. Fraser, C. I., Nikula, R., Ruzzante, D. E., & Waters, J. M. (2012). Poleward bound: Biological impacts of Southern Hemisphere glaciation. *Trends in Ecology & Evolution*, *27*(8), 462–471. https://doi.org/10.1016/j.tree.2012.04.011

95. Frichot, E., & François, O. (2015). LEA: An R package for landscape and ecological association studies. *Methods in Ecology and Evolution*, *6*(8), 925–929. https://doi.org/10.1111/2041-210X.12382

96. Frichot, E., Schoville, S. D., Bouchard, G., & François, O. (2013). Testing for associations between loci and environmental gradients using latent factor mixed models. *Molecular Biology and Evolution*, *30*(7), 1687–1699. https://doi.org/10.1093/molbev/mst063

97. Fu, Y.-X., & Li, W.-H. (1999). Coalescing into the 21st Century: An Overview and Prospects of Coalescent Theory. *Theoretical Population Biology*, *56*(1), 1–10. https://doi.org/10.1006/tpbi.1999.1421

98. Furrer, R. D., & Pasinelli, G. (2016). Empirical evidence for source–sink populations: A review on occurrence, assessments and implications. *Biological Reviews*, *91*(3), 782–795. https://doi.org/10.1111/brv.12195

99. Galbreath, K. E., Hafner, D. J., & Zamudio, K. R. (2009). When Cold Is Better: Climate-Driven Elevation Shifts Yield Complex Patterns of Diversification and Demography in an Alpine Specialist (american Pika, Ochotona Princeps). *Evolution*, *63*(11), 2848–2863. https://doi.org/10.1111/j.1558-5646.2009.00803.x

100. García, G., Ríos, N., Gutiérrez, V., Varela, J. G., Fernández, C. B., Pardo, B. G., & Portela, P. M. (2014). Promiscuous Speciation with Gene Flow in Silverside Fish Genus Odontesthes (Atheriniformes, Atherinopsidae) from South Western Atlantic Ocean Basins. *PLOS ONE*, *9*(8), e104659. https://doi.org/10.1371/journal.pone.0104659

101. Garner, A., Rachlow, J. L., & Hicks, J. F. (2005). Patterns of Genetic Diversity and Its Loss in Mammalian Populations. *Conservation Biology*, *19*(4), 1215–1221. https://doi.org/10.1111/j.1523-1739.2005.00105.x

102. Giardino, G. V., Mandiola, M. A., Bastida, J., Denuncio, P. E., Bastida, R. O., & Rodríguez, D. H. (2016). Travel for sex: Long-range breeding dispersal and winter haulout fidelity in southern sea lion males. *Mammalian Biology*, *81*(1), 89–95. https://doi.org/10.1016/j.mambio.2014.12.003

103. Górski, K., Habit, E. M., Pingram, M. A., & Manosalva, A. J. (2018). Variation of the use of marine resources by Galaxias maculatus in large Chilean rivers. *Hydrobiologia*, *814*(1), 61–73. https://doi.org/10.1007/s10750-015-2542-4

104. Gownaris, N. J., & Boersma, P. D. (2019). Sex-biased survival contributes to population decline in a long-lived seabird, the Magellanic Penguin. *Ecological Applications*, *29*(1), e01826. https://doi.org/10.1002/eap.1826

105. Grandi, M., Loizaga, R., Terán, E., Santos, M., Bailliet, G., & Crespo, E. (2017). Is recolonization pattern related to female philopatry? An insight into a colonially breeding mammal. *Mammalian Biology*, *89*. https://doi.org/10.1016/j.mambio.2017.12.002

106. Griffin, M. P. A., & Valiela, I. (2001). D15N isotope studies of life history and trophic position of Fundulus heteroclitus and Menidia menidia. *Marine Ecology Progress Series*, *214*, 299–305. https://doi.org/10.3354/meps214299

107. Gröcke, D. R., Treasure, E. R., Lester, J. J., Gron, K. J., & Church, M. J. (2021). Effects of marine biofertilisation on Celtic bean carbon, nitrogen and sulphur isotopes: Implications for reconstructing past diet and farming practices. *Rapid Communications in Mass Spectrometry*, *35*(5), e8985. https://doi.org/10.1002/rcm.8985

108. Groenen, M. A. M., Archibald, A. L., Uenishi, H., Tuggle, C. K., Takeuchi, Y., Rothschild, M. F., Rogel-Gaillard, C., Park, C., Milan, D., Megens, H.-J., Li, S., Larkin, D. M., Kim, H., Frantz, L. A. F., Caccamo, M., Ahn, H., Aken, B. L., Anselmo, A., Anthon, C., … Schook, L. B. (2012). Analyses of pig genomes provide insight into porcine demography and evolution. *Nature*, *491*(7424), 393–398. https://doi.org/10.1038/nature11622

109. Gu, F., Chiessi, C. M., Zonneveld, K. A. F., & Behling, H. (2019). Shifts of the Brazil-Falklands/Malvinas Confluence in the western South Atlantic during the latest Pleistocene–Holocene inferred from dinoflagellate cysts. *Palynology*, *43*(3), 483–493. https://doi.org/10.1080/01916122.2018.1470116

110. Guerrero, A. I., Pavez, G., Santos-Carvallo, M., Rogers, T. L., & Sepúlveda, M. (2020). Foraging behaviour of the South American sea lion (Otaria byronia) in two disparate ecosystems assessed through blubber fatty acid analysis. *Scientific Reports*, *10*(1), 5725. https://doi.org/10.1038/s41598-020-62178-6

111. Gutenkunst, R. N., Hernandez, R. D., Williamson, S. H., & Bustamante, C. D. (2009). Inferring the Joint Demographic History of Multiple Populations from Multidimensional SNP Frequency Data. *PLOS Genetics*, *5*(10), e1000695. https://doi.org/10.1371/journal.pgen.1000695

112. Hadley, G. L., RoTELla, J. J., Garrott, R. A., & Nichols, J. D. (2006). Variation in probability of first reproduction of Weddell seals. *Journal of Animal Ecology*, *75*(5), 1058–1070. https://doi.org/10.1111/j.1365-2656.2006.01118.x

113. Hadly, E. A., Ramakrishnan, U., Chan, Y. L., Tuinen, M. van, O'Keefe, K., Spaeth, P. A., & Conroy, C. J. (2004). Genetic Response to Climatic Change: Insights from Ancient DNA and Phylochronology. *PLOS Biology*, *2*(10), e290. https://doi.org/10.1371/journal.pbio.0020290

114. Hanski, I. (1998). Metapopulation dynamics. *Nature*, *396*(6706), 41–49. https://doi.org/10.1038/23876

115. Healy, K., Ezard, T. H. G., Jones, O. R., Salguero-Gómez, R., & Buckley, Y. M. (2019a). Animal life history is shaped by the pace of life and the distribution of age-specific mortality and reproduction. *Nature Ecology & Evolution*, *3*(8), 1217–1224. https://doi.org/10.1038/s41559-019-0938-7

116. Healy, K., Ezard, T. H. G., Jones, O. R., Salguero-Gómez, R., & Buckley, Y. M. (2019b). Animal life history is shaped by the pace of life and the distribution of age-specific mortality and reproduction. *Nature Ecology & Evolution*, *3*(8), 1217–1224. https://doi.org/10.1038/s41559-019-0938-7

117. Hecht, L. B. B., Thompson, P. C., & Rosenthal, B. M. (2018). Comparative demography elucidates the longevity of parasitic and symbiotic relationships. *Proceedings of the Royal Society B: Biological Sciences*, *285*(1888), 20181032. https://doi.org/10.1098/rspb.2018.1032

118. Hecht, L. B. B., Thompson, P. C., & Rosenthal, B. M. (2020). Assessing the evolutionary persistence of ecological relationships: A review and preview. *Infection, Genetics and Evolution*, *84*, 104441. https://doi.org/10.1016/j.meegid.2020.104441

119. Heled, J., & Drummond, A. J. (2008). Bayesian inference of population size history from multiple loci. *BMC Evolutionary Biology*, *8*(1), 289. https://doi.org/10.1186/1471-2148-8-289

120. Heller, R., Chikhi, L., & Siegismund, H. R. (2013). The Confounding Effect of Population Structure on Bayesian Skyline Plot Inferences of Demographic History. *PLOS ONE*, *8*(5), e62992. https://doi.org/10.1371/journal.pone.0062992

121. Hernández-Camacho, C. J., Aurioles-Gamboa, D., & Gerber, L. R. (2008). Age-specific birth rates of California sea lions (Zalophus californianus) in the Gulf of California, Mexico. *Marine Mammal Science*, *24*(3), 664–676. https://doi.org/10.1111/j.1748-7692.2008.00199.x

122. Hernández-Orts, J. S., Brandão, M., Georgieva, S., Raga, J. A., Crespo, E. A., Luque, J. L., & Aznar, F. J. (2017). From mammals back to birds: Host-switch of the acanthocephalan Corynosoma australe from pinnipeds to the Magellanic penguin Spheniscus magellanicus. *PLOS ONE*, *12*(10), e0183809. https://doi.org/10.1371/journal.pone.0183809

123. Hernández-Orts, J. S., Montero, F. E., García, N. A., Crespo, E. A., Raga, J. A., García-Varela, M., & Aznar, F. J. (2019). Transmission of Corynosoma australe (Acanthocephala: Polymorphidae) from fishes to South American sea lions Otaria flavescens in Patagonia, Argentina. *Parasitology Research*, *118*(2), 433–440. https://doi.org/10.1007/s00436-018-6177-z

124. Hinke, J. T., Trivelpiece, S. G., & Trivelpiece, W. Z. (2017). Variable vital rates and the risk of population declines in Adélie penguins from the Antarctic Peninsula region. *Ecosphere*, *8*(1), e01666. https://doi.org/10.1002/ecs2.1666

125. Ho, S. Y. W., Phillips, M. J., Cooper, A., & Drummond, A. J. (2005). Time Dependency of Molecular Rate Estimates and Systematic Overestimation of Recent Divergence Times. *Molecular Biology and Evolution*, *22*(7), 1561–1568. https://doi.org/10.1093/molbev/msi145

126. Ho, S. Y. W., & Shapiro, B. (2011). Skyline-plot methods for estimating demographic history from nucleotide sequences. *Molecular Ecology Resources*, *11*(3), 423–434. https://doi.org/10.1111/j.1755-0998.2011.02988.x

127. Hodel, R. G. J., Chen, S., Payton, A. C., McDaniel, S. F., Soltis, P., & Soltis, D. E. (2017). Adding loci improves phylogeographic resolution in red mangroves despite

increased missing data: Comparing microsatellites and RAD-Seq and investigating loci filtering. *Scientific Reports*, *7*(1), 17598. https://doi.org/10.1038/s41598-017-16810-7

128. Hodgkinson, A., & Eyre-Walker, A. (2011). Variation in the mutation rate across mammalian genomes. *Nature Reviews Genetics*, *12*(11), 756-766.

129. Hoelzel, A. R., Lopez, J. V., Dover, G. A., & O'Brien, S. J. (1994). Rapid evolution of a heteroplasmic repetitive sequence in the mitochondrial DNA control region of carnivores. *Journal of Molecular Evolution*, *39*(2), 191–199. https://doi.org/10.1007/BF00163807

130. Hoffman, J. I., Dasmahapatra, K. K., Amos, W., Phillips, C. D., Gelatt, T. S., & Bickham, J. W. (2009). Contrasting patterns of genetic diversity at three different genetic markers in a marine mammal metapopulation. *Molecular Ecology*, *18*(14), 2961–2978. https://doi.org/10.1111/j.1365-294X.2009.04246.x

131. Hoffman, J. I., Grant, S. M., Forcada, J., & Phillips, C. D. (2011). Bayesian inference of a historical bottleneck in a heavily exploited marine mammal. *Molecular Ecology*, *20*(19), 3989–4008. https://doi.org/10.1111/j.1365-294X.2011.05248.x

132. Holser, R. R., Crocker, D. E., Robinson, P. W., Condit, R., & Costa, D. P. (2021). Density-dependent effects on reproductive output in a capital breeding carnivore, the northern elephant seal (Mirounga angustirostris). *Proceedings of the Royal Society B: Biological Sciences*, *288*(1960), 20211258. https://doi.org/10.1098/rspb.2021.1258

133. Hückstädt, L. A., Rojas, C. P., & Antezana, T. (2007). Stable isotope analysis reveals pelagic foraging by the Southern sea lion in central Chile. *Journal of Experimental Marine Biology and Ecology*, *347*(1), 123–133. https://doi.org/10.1016/j.jembe.2007.03.014

134. Hückstädt, L. A., Tift, M. S., Riet-Sapriza, F., Franco-Trecu, V., Baylis, A. M. M., Orben, R. A., Arnould, J. P. Y., Sepulveda, M., Santos-Carvallo, M., Burns, J. M., & Costa, D. P. (2016). Regional variability in diving physiology and behavior in a widely distributed air-breathing marine predator, the South American sea lion (Otaria byronia). *Journal of Experimental Biology*, *219*(15), 2320–2330. https://doi.org/10.1242/jeb.138677

135. Hudson, R. R. (2002). Generating samples under a Wright–Fisher neutral model of genetic variation. *Bioinformatics*, *18*(2), 337–338. https://doi.org/10.1093/bioinformatics/18.2.337

136. Hughes, L. C., Cardoso, Y. P., Sommer, J. A., Cifuentes, R., Cuello, M., Somoza, G. M., González-Castro, M., Malabarba, L. R., Cussac, V., Habit, E. M., Betancur-R., R., & Ortí, G. (2020). Biogeography, habitat transitions and hybridization in a radiation of South American silverside fishes revealed by mitochondrial and genomic RAD data. *Molecular Ecology*, *29*(4), 738–751. https://doi.org/10.1111/mec.15350

137. Hume, F., Hindell, M. A., Pemberton, D., & Gales, R. (2004). Spatial and temporal variation in the diet of a high trophic level predator, the Australian fur seal (Arctocephalus pusillus doriferus). *Marine Biology*, *144*(3), 407–415. https://doi.org/10.1007/s00227-003-1219-0

138. James, J., & Eyre-Walker, A. (2020). Mitochondrial DNA Sequence Diversity in Mammals: A Correlation between the Effective and Census Population Sizes. *Genome Biology and Evolution*, *12*(12), 2441–2449. https://doi.org/10.1093/gbe/evaa222

139. Jarma, D., Romero, M. A., García, N. A., Svendsen, G., González, R., Dans, S. L., & Crespo, E. A. (2019). Small-scale variation in the diet of the South American Sea lion (Otaria flavescens) in northern Patagonia (Argentina). *Regional Studies in Marine Science*, *28*, 100592. https://doi.org/10.1016/j.rsma.2019.100592

140. Jeffries, D. L., Copp, G. H., Handley, L. L., Olsén, K. H., Sayer, C. D., & Hänfling, B. (2016). Comparing RADseq and microsatellites to infer complex phylogeographic patterns, an empirical perspective in the Crucian carp, Carassius carassius, L. *Molecular Ecology*, *25*(13), 2997–3018. https://doi.org/10.1111/mec.13613

141. Jenouvrier, S., Barbraud, C., & Weimerskirch, H. (2006). Sea ice affects the population dynamics of Adélie penguins in Terre Adélie. *Polar Biology*, *29*(5), 413–423. https://doi.org/10.1007/s00300-005-0073-6

142. Jentsch, A., & White, P. (2019). A theory of pulse dynamics and disturbance in ecology. *Ecology*, *100*(7), e02734. https://doi.org/10.1002/ecy.2734

143. Jeon, J. Y., Cho, S., Suk, H., Lee, C., Borzée, A., Song, J.-Y., & Min, M.-S. (2021). Resolving the taxonomic equivocacy and the population genetic structure of Rana uenoi—Insights into dispersal and demographic history. *Salamandra*, *57*, 529–540.

144. Jiang, N., Zhang, F., Wu, J., Chen, Y., Hu, X., Fang, O., Leach, L. J., Wang, D., & Luo, Z. (2016). A highly robust and optimized sequence-based approach for genetic polymorphism discovery and genotyping in large plant populations. *TAG. Theoretical and Applied Genetics. Theoretische Und Angewandte Genetik*, *129*, 1739–1757. https://doi.org/10.1007/s00122-016-2736-9

145. Jombart, T., & Ahmed, I. (2011). adegenet 1.3-1: New tools for the analysis of genome-wide SNP data. *Bioinformatics*, *27*(21), 3070–3071. https://doi.org/10.1093/bioinformatics/btr521

146. Jombart, T., Devillard, S., & Balloux, F. (2010). Discriminant analysis of principal components: A new method for the analysis of genetically structured populations. *BMC Genetics*, *11*(1), 94. https://doi.org/10.1186/1471-2156-11-94

147. Jones, C. G., Lawton, J. H., & Shachak, M. (1996). Organisms as Ecosystem Engineers. In F. B. Samson & F. L. Knopf (Eds.), *Ecosystem Management: Selected Readings* (pp. 130–147). Springer. https://doi.org/10.1007/978-1-4612-4018-1_14

148. Jönsson, K. I. (1997). Capital and Income Breeding as Alternative Tactics of Resource Use in Reproduction. *Oikos*, *78*(1), 57–66. https://doi.org/10.2307/3545800

149. Jouzel, J., Masson-Delmotte, V., Cattani, O., Dreyfus, G., Falourd, S., Hoffmann, G., Minster, B., Nouet, J., Barnola, J. M., Chappellaz, J., Fischer, H., Gallet, J. C., Johnsen, S., Leuenberger, M., Loulergue, L., Luethi, D., Oerter, H., Parrenin, F., Raisbeck, G., … Wolff, E. W. (2007). Orbital and Millennial Antarctic Climate Variability over the Past 800,000 Years. *Science*, *317*(5839), 793–796. https://doi.org/10.1126/science.1141038

150. Kaeuffer, R., Coltman, D. W., Chapuis, J.-L., Réale, D., & Pontier, D. (2007). The effects of cyclic dynamics and mating system on the effective size of an island mouflon population. *Molecular Ecology*, *16*(21), 4482–4492. https://doi.org/10.1111/j.1365-294X.2007.03501.x

151. Kaplan, M. R., Schaefer, J. M., Strelin, J. A., Denton, G. H., Anderson, R. F., Vandergoes, M. J., Finkel, R. C., Schwartz, R., Travis, S. G., Garcia, J. L., Martini, M. A., & Nielsen, S. H. H. (2016). Patagonian and southern South Atlantic view of Holocene climate. *Quaternary Science Reviews*, *141*, 112–125. https://doi.org/10.1016/j.quascirev.2016.03.014

152. Kelly, M. J. (2001). Lineage Loss in Serengeti Cheetahs: Consequences of High Reproductive Variance and Heritability of Fitness on Effective Population Size. *Conservation Biology*, *15*(1), 137–147. https://doi.org/10.1111/j.1523-1739.2001.99033.x

153. King, C. L., Millard, A. R., Gröcke, D. R., Standen, V. G., Arriaza, B. T., & Halcrow, S. E. (2017). A comparison of using bulk and incremental isotopic analyses to establish weaning practices in the past. *STAR: Science & Technology of Archaeological Research*, *3*(1), 126–134. https://doi.org/10.1080/20548923.2018.1443548

154. Kingman, J. F. C. (1982a). On the genealogy of large populations. *Journal of Applied Probability*, *19*(A), 27–43. https://doi.org/10.2307/3213548

155. Kingman, J. F. C. (1982b). The coalescent. *Stochastic Processes and Their Applications*, *13*(3), 235–248. https://doi.org/10.1016/0304-4149(82)90011-4

156. Kliman, R., Sheehy, B., & Schultz, J. (2008). Genetic drift and effective population size. *Nature Education*, *1*(3), 3.

157. Kochi, S., Pérez, S. A., Tessone, A., Ugan, A., Tafuri, M. A., Nye, J., Tivoli, A. M., & Zangrando, A. F. (2018). δ13C and δ15N variations in terrestrial and marine foodwebs of Beagle Channel in the Holocene. Implications for human palaeodietary reconstructions. *Journal of Archaeological Science: Reports*, *18*, 696–707. https://doi.org/10.1016/j.jasrep.2017.11.036

158. Koen Alonso, M., Crespo, E. A., Pedraza, S. N., Garcia, N. A., & Coscarella, M. A. (2000). *Food habits of the south american sea lion, Otaria flavescens, off Patagonia, Argentina*. https://ri.conicet.gov.ar/handle/11336/70210

159. Kohfeld, K. E., Graham, R. M., de Boer, A. M., Sime, L. C., Wolff, E. W., Le Quéré, C., & Bopp, L. (2013). Southern Hemisphere westerly wind changes during the Last Glacial Maximum: Palaeo-data synthesis. *Quaternary Science Reviews*, *68*, 76–95. https://doi.org/10.1016/j.quascirev.2013.01.017

160. Kovacs, K. M. (2018). Bearded Seal: Erignathus barbatus. In B. Würsig, J. G. M. Thewissen, & K. M. Kovacs (Eds.), *Encyclopedia of Marine Mammals (Third Edition)* (pp. 83–86). Academic Press. https://doi.org/10.1016/B978-0-12-804327-1.00063-7

161. Krebs, C. J., Boonstra, R., & Boutin, S. (2018). Using experimentation to understand the 10-year snowshoe hare cycle in the boreal forest of North America. *Journal of Animal Ecology*, *87*(1), 87–100. https://doi.org/10.1111/1365-2656.12720

162. Kuhner, M. K. (2009). Coalescent genealogy samplers: Windows into population history. *Trends in Ecology & Evolution*, *24*(2), 86–93. https://doi.org/10.1016/j.tree.2008.09.007

163. *Lack of demographic equilibrium indicates natural, large‐scale forest dynamics, not a problematic forest conservation policy – a reply to Brzeziecki et al.* (n.d.). https://doi.org/10.1111/jvs.12458

164. Lambert, D. M., Ritchie, P. A., Millar, C. D., Holland, B., Drummond, A. J., & Baroni, C. (2002). Rates of Evolution in Ancient DNA from Adélie Penguins. *Science*, *295*(5563), 2270–2273.

165. Lapierre, M., Lambert, A., & Achaz, G. (2017). Accuracy of Demographic Inferences from the Site Frequency Spectrum: The Case of the Yoruba Population. *Genetics*, *206*(1), 439–449. https://doi.org/10.1534/genetics.116.192708

166. *Lbbhecht/align_stairwayplot*. (n.d.). GitHub. Retrieved 16 September 2022, from https://github.com/lbbhecht/align_stairwayplot

167. Le Bohec, C., Durant, J. M., Gauthier-Clerc, M., Stenseth, N. C., Park, Y.-H., Pradel, R., Grémillet, D., Gendner, J.-P., & Le Maho, Y. (2008). King penguin population threatened by Southern Ocean warming. *Proceedings of the National Academy of Sciences*, *105*(7), 2493–2497. https://doi.org/10.1073/pnas.0712031105

168. Le Vaillant, M., Le Bohec, C., Prud'Homme, O., Wienecke, B., Le Maho, Y., Kato, A., & Ropert-Coudert, Y. (2013). How age and sex drive the foraging behaviour in the king penguin. *Marine Biology*, *160*(5), 1147–1156. https://doi.org/10.1007/s00227-013-2167-y

169. Leigh, J. W., & Bryant, D. (2015). POPART: Full-feature software for haplotype network construction. *Methods in Ecology and Evolution*, *6*(9), 1110–1116. https://doi.org/10.1111/2041-210X.12410

170. Lenton, T. M. (2013). Environmental Tipping Points. *Annual Review of Environment and Resources*, *38*(1), 1–29. https://doi.org/10.1146/annurev-environ-102511-084654

171. Lescroël, A., Ballard, G., Grémillet, D., Authier, M., & Ainley, D. G. (2014). Antarctic Climate Change: Extreme Events Disrupt Plastic Phenotypic Response in Adélie Penguins. *PLOS ONE*, *9*(1), e85291. https://doi.org/10.1371/journal.pone.0085291

172. Lewis, D. L., Breck, S. W., Wilson, K. R., & Webb, C. T. (2014). Modeling black bear population dynamics in a human-dominated stochastic environment. *Ecological Modelling*, *294*, 51–58. https://doi.org/10.1016/j.ecolmodel.2014.08.021

173. Li, C., Zhang, Y., Li, J., Kong, L., Hu, H., Pan, H., Xu, L., Deng, Y., Li, Q., Jin, L., Yu, H., Chen, Y., Liu, B., Yang, L., Liu, S., Zhang, Y., Lang, Y., Xia, J., He, W., … Zhang, G. (2014). Two Antarctic penguin genomes reveal insights into their evolutionary history and molecular changes related to the Antarctic environment. *GigaScience*, *3*(1), 27. https://doi.org/10.1186/2047-217X-3-27

174. Li, H., & Durbin, R. (2009). Fast and accurate short read alignment with Burrows-Wheeler transform. *Bioinformatics (Oxford, England)*, *25*(14), 1754–1760. https://doi.org/10.1093/bioinformatics/btp324

175. Li, H., & Durbin, R. (2011). Inference of human population history from individual whole-genome sequences. *Nature*, *475*(7357), 493–496. https://doi.org/10.1038/nature10231

176. Li, K., Zhang, S., Song, X., Weyrich, A., Wang, Y., Liu, X., Wan, N., Liu, J., Lövy, M., Cui, H., Frenkel, V., Titievsky, A., Panov, J., Brodsky, L., & Nevo, E. (2020). Genome evolution of blind subterranean mole rats: Adaptive peripatric versus sympatric speciation. *Proceedings of the National Academy of Sciences*, *117*(51), 32499–32508. https://doi.org/10.1073/pnas.2018123117

177. Liu, X., & Fu, Y.-X. (2015). Exploring population size changes using SNP frequency spectra. *Nature Genetics*, *47*(5), 555–559. https://doi.org/10.1038/ng.3254

178. Liu, X., & Fu, Y.-X. (2020). Stairway Plot 2: Demographic history inference with folded SNP frequency spectra. *Genome Biology*, *21*(1), 280. https://doi.org/10.1186/s13059-020-02196-9

179. Lopes, F., Hoffman, J. I., Valiati, V. H., Bonatto, S. L., Wolf, J. B. W., Trillmich, F., & Oliveira, L. R. (2015). Fine-scale matrilineal population structure in the Galapagos fur seal and its implications for conservation management. *Conservation Genetics*, *16*(5), 1099–1113. https://doi.org/10.1007/s10592-015-0725-1

180. Lou, R. N., Jacobs, A., Wilder, A. P., & Therkildsen, N. O. (2021). A beginner's guide to low-coverage whole genome sequencing for population genomics. *Molecular Ecology*, *30*(23), 5966–5993. https://doi.org/10.1111/mec.16077

181. Luikart, G., Sherwin, W. B., Steele, B. M., & Allendorf, F. W. (1998). Usefulness of molecular markers for detecting population bottlenecks via monitoring genetic change. *Molecular Ecology*, *7*(8), 963–974. https://doi.org/10.1046/j.1365-294x.1998.00414.x

182. Lynch, H. J., Naveen, R., Trathan, P. N., & Fagan, W. F. (2012). Spatially integrated assessment reveals widespread changes in penguin populations on the Antarctic Peninsula. *Ecology*, *93*(6), 1367–1377. https://doi.org/10.1890/11-1588.1

183. M, F. P., Poulin, E., Dantas, G. P. M., González-Acuña, D., Petry, M. V., & Vianna, J. A. (2014). Have Historical Climate Changes Affected Gentoo Penguin (Pygoscelis papua) Populations in Antarctica? *PLOS ONE*, *9*(4), e95375. https://doi.org/10.1371/journal.pone.0095375

184. Macavoy, S., Bacalan, V., Kazantseva, M., Rhodes, J., & Kim, K. (2014). Sulfur isotopes show importance of freshwater primary production for Florida manatees. *Marine Mammal Science*, *31*. https://doi.org/10.1111/mms.12166

185. Madenjian, C. P., Rutherford, E. S., Stow, C. A., Roseman, E. F., & He, J. X. (2013). Trophic Shift, Not Collapse. *Environmental Science & Technology*, *47*(21), 11915–11916. https://doi.org/10.1021/es404089y

186. Mak, S. S. T., Gopalakrishnan, S., Carøe, C., Geng, C., Liu, S., Sinding, M.-H. S., Kuderna, L. F. K., Zhang, W., Fu, S., Vieira, F. G., Germonpré, M., Bocherens, H., Fedorov, S., Petersen, B., Sicheritz-Pontén, T., Marques-Bonet, T., Zhang, G., Jiang, H., & Gilbert, M. T. P. (2017). Comparative performance of the BGISEQ-500 vs Illumina HiSeq2500 sequencing platforms for palaeogenomic sequencing. *GigaScience*, *6*(8), gix049. https://doi.org/10.1093/gigascience/gix049

187. Maniscalco, J. M., Springer, A. M., Adkison, M. D., & Parker, P. (2015). Population Trend and Elasticities of Vital Rates for Steller Sea Lions (Eumetopias jubatus) in the Eastern Gulf of Alaska: A New Life-History Table Analysis. *PLOS ONE*, *10*(10), e0140982. https://doi.org/10.1371/journal.pone.0140982

188. Marasco, A. C. M., Morgante, J. S., Barrionuevo, M., Frere, E., & de Mendonça Dantas, G. P. (2020). Molecular evidence of extra-pair paternity and intraspecific brood parasitism by the Magellanic Penguin (Spheniscus magellanicus). *Journal of Ornithology*, *161*(1), 125–135. https://doi.org/10.1007/s10336-019-01720-4

189. Marques, F. P., Cardoso, L. G., Haimovici, M., & Bugoni, L. (2018). Trophic ecology of Magellanic penguins (Spheniscus magellanicus) during the non-breeding period. *Estuarine, Coastal and Shelf Science*, *210*, 109–122. https://doi.org/10.1016/j.ecss.2018.06.001

190. Matthiopoulos, J., Harwood, J., & Thomas, L. (2005). Metapopulation consequences of site fidelity for colonially breeding mammals and birds. *Journal of Animal Ecology*, *74*(4), 716–727. https://doi.org/10.1111/j.1365-2656.2005.00970.x

191. Mauna, A. C., Botto, F., Franco, B., Schwartz, J. M., Acha, E. M., Lasta, M. L., & Iribarne, O. O. (2011). Shifts in an epibenthic trophic web across a marine frontal area in the Southwestern Atlantic (Argentina). *Journal of Sea Research*, *66*(3), 248–255. https://doi.org/10.1016/j.seares.2011.08.005

192. Mazet, O., Rodríguez, W., & Chikhi, L. (2015). Demographic inference using genetic data from a single individual: Separating population size variation from population structure. *Theoretical Population Biology*, *104*, 46–58. https://doi.org/10.1016/j.tpb.2015.06.003

193. Mazet, O., Rodríguez, W., Grusea, S., Boitard, S., & Chikhi, L. (2016). On the importance of being structured: Instantaneous coalescence rates and human evolution—lessons for ancestral population size inference? *Heredity*, *116*(4), 362–371. https://doi.org/10.1038/hdy.2015.104

194. McHuron, E. A., Costa, D. P., Schwarz, L., & Mangel, M. (2017). State-dependent behavioural theory for assessing the fitness consequences of anthropogenic disturbance on capital and income breeders. *Methods in Ecology and Evolution*, *8*(5), 552–560. https://doi.org/10.1111/2041-210X.12701

195. McKinney, G. J., Larson, W. A., Seeb, L. W., & Seeb, J. E. (2017). RADseq provides unprecedented insights into molecular ecology and evolutionary genetics: Comment on Breaking RAD by Lowry et al. (2016). *Molecular Ecology Resources*, *17*(3), 356–361. https://doi.org/10.1111/1755-0998.12649

196. Millar, C. D., Dodd, A., Anderson, J., Gibb, G. C., Ritchie, P. A., Baroni, C., Woodhams, M. D., Hendy, M. D., & Lambert, D. M. (2008). Mutation and Evolutionary Rates in Adélie Penguins from the Antarctic. *PLOS Genetics*, *4*(10), e1000209. https://doi.org/10.1371/journal.pgen.1000209

197. Miller, W., Schuster, S. C., Welch, A. J., Ratan, A., Bedoya-Reina, O. C., Zhao, F., Kim, H. L., Burhans, R. C., Drautz, D. I., Wittekindt, N. E., Tomsho, L. P., Ibarra-Laclette, E., Herrera-Estrella, L., Peacock, E., Farley, S., Sage, G. K., Rode, K., Obbard, M., Montiel, R., … Lindqvist, C. (2012). Polar and brown bear genomes reveal ancient admixture and demographic footprints of past climate change. *Proceedings of the National Academy of Sciences*, *109*(36), E2382–E2390. https://doi.org/10.1073/pnas.1210506109

198. *MODIS Aqua Level 3 SST Thermal IR 8 Day 4km Daytime V2019.0*. (2019). Physical Oceanography Distributed Active Archive Center (PO.DAAC). https://podaac.jpl.nasa.gov/dataset/MODIS_AQUA_L3_SST_THERMAL_8DAY_4KM_DAYTIME_V2019.0

199. Motro, U., & Thomson, G. (1982). On Heterozygosity and the Effective Size of Populations Subject to Size Changes. *Evolution*, *36*(5), 1059–1066. https://doi.org/10.2307/2408083

200. Mura-Jornet, I., Pimentel, C., Dantas, G. P. M., Petry, M. V., González-Acuña, D., Barbosa, A., Lowther, A. D., Kovacs, K. M., Poulin, E., & Vianna, J. A. (2018). Chinstrap penguin population genetic structure: One or more populations along the Southern Ocean? *BMC Evolutionary Biology*, *18*(1), 90. https://doi.org/10.1186/s12862-018-1207-0

201. Nabholz, B., Mauffrey, J.-F., Bazin, E., Galtier, N., & Glemin, S. (2008). Determination of Mitochondrial Genetic Diversity in Mammals. *Genetics*, *178*(1), 351–361. https://doi.org/10.1534/genetics.107.073346

202. Nachman, M. W., & Crowell, S. L. (2000). Estimate of the Mutation Rate per Nucleotide in Humans. *Genetics*, *156*(1), 297–304. https://doi.org/10.1093/genetics/156.1.297

203. NASA Ocean Biology Processing Group. (2018). *MODIS-Aqua Level 3 Mapped Chlorophyll Data Version R2018.0* [Data set]. NASA Ocean Biology DAAC. https://doi.org/10.5067/AQUA/MODIS/L3M/CHL/2018

204. Nei, M., Maruyama, T., & Chakraborty, R. (1975). The Bottleneck Effect and Genetic Variability in Populations. *Evolution*, *29*(1), 1–10. https://doi.org/10.2307/2407137

205. Nei, M., & Tajima, F. (1981). Genetic Drift and Estimation of Effective Population Size. *Genetics*, *98*(3), 625–640.

206. Noble, T. L., Piotrowski, A. M., Robinson, L. F., McManus, J. F., Hillenbrand, C.-D., & Bory, A. J.-M. (2012). Greater supply of Patagonian-sourced detritus and transport by the ACC to the Atlantic sector of the Southern Ocean during the last glacial period. *Earth and Planetary Science Letters*, *317–318*, 374–385. https://doi.org/10.1016/j.epsl.2011.10.007

207. Oaks, J. R., L'Bahy, N., & Cobb, K. A. (2020). Insights from a general, full-likelihood Bayesian approach to inferring shared evolutionary events from genomic data: Inferring shared demographic events is challenging*. *Evolution*, *74*(10), 2184–2206. https://doi.org/10.1111/evo.14052

208. O'Brien, S. J., Johnson, W. E., Driscoll, C. A., Dobrynin, P., & Marker, L. (2017). Conservation Genetics of the Cheetah: Lessons Learned and New Opportunities. *Journal of Heredity*, *108*(6), 671–677. https://doi.org/10.1093/jhered/esx047

209. Oksanen, Jari, F. Guillaume Blanchet, and Michael Friendly et al. (2019). vegan: Community Ecology Package. R package version 2.5-6. https://CRAN.R-project.org/package=vegan.

210. Oliveira, L. R. de, Fraga, L. D., & Majluf, P. (2012). Effective population size for South American sea lions along the Peruvian coast: The survivors of the strongest El Niño event in history. *Journal of the Marine Biological Association of the United Kingdom*, *92*(8), 1835–1841. https://doi.org/10.1017/S0025315411001871

211. Oliveira, L. R. de, Gehara, M. C. M., Fraga, L. D., Lopes, F., Túnez, J. I., Cassini, M. H., Majluf, P., Cárdenas-Alayza, S., Pavés, H. J., Crespo, E. A., García, N., Castro, R. L. de, Hoelzel, A. R., Sepúlveda, M., Olavarría, C., Valiati, V. H., Quiñones, R., Pérez-Alvarez, M. J., Ott, P. H., & Bonatto, S. L. (2017). Ancient female philopatry, asymmetric male gene flow, and synchronous population expansion support the influence of climatic oscillations on the evolution of South American sea lion (Otaria flavescens). *PLOS ONE*, *12*(6), e0179442. https://doi.org/10.1371/journal.pone.0179442

212. Orlando, L., Allaby, R., Skoglund, P., Der Sarkissian, C., Stockhammer, P. W., Ávila-Arcos, M. C., Fu, Q., Krause, J., Willerslev, E., Stone, A. C., & Warinner, C. (2021). Ancient DNA analysis. *Nature Reviews Methods Primers*, *1*(1), 1–26. https://doi.org/10.1038/s43586-020-00011-0

213. Orlando, L., & Cooper, A. (2014). Using Ancient DNA to Understand Evolutionary and Ecological Processes. *Annual Review of Ecology, Evolution, and Systematics*, *45*(1), 573–598. https://doi.org/10.1146/annurev-ecolsys-120213-091712

214. Ortiz, E. M. (2019). *vcf2phylip v2.0: Convert a VCF matrix into several matrix formats for phylogenetic analysis.* (v2.0). Zenodo. https://doi.org/10.5281/zenodo.2540861

215. Otley, H. M., Clausen, A. P., Christie, D. J., & Pütz, K. (2004). Aspects of the Breeding Biology of the Magellanic Penguin in the Falkland Islands. *Waterbirds*, *27*(4), 396–405. https://doi.org/10.1675/1524-4695(2004)027[0396:AOTBBO]2.0.CO;2

216. Overcast, I. (2022). *EasySFS* [Python]. https://github.com/isaacovercast/easySFS (Original work published 2016)

217. Parmesan, C. (2006). Ecological and Evolutionary Responses to Recent Climate Change. *Annual Review of Ecology, Evolution, and Systematics*, *37*(1), 637–669. https://doi.org/10.1146/annurev.ecolsys.37.091305.110100

218. Patton, A. H., Margres, M. J., Stahlke, A. R., Hendricks, S., Lewallen, K., Hamede, R. K., Ruiz-Aravena, M., Ryder, O., McCallum, H. I., Jones, M. E., Hohenlohe, P. A., & Storfer, A.

(2019). Contemporary Demographic Reconstruction Methods Are Robust to Genome Assembly Quality: A Case Study in Tasmanian Devils. *Molecular Biology and Evolution*, *36*(12), 2906–2921. https://doi.org/10.1093/molbev/msz191

219. Peart, C. R., Tusso, S., Pophaly, S. D., Botero-Castro, F., Wu, C.-C., Aurioles-Gamboa, D., Baird, A. B., Bickham, J. W., Forcada, J., Galimberti, F., Gemmell, N. J., Hoffman, J. I., Kovacs, K. M., Kunnasranta, M., Lydersen, C., Nyman, T., de Oliveira, L. R., Orr, A. J., Sanvito, S., … Wolf, J. B. W. (2020). Determinants of genetic variation across eco-evolutionary scales in pinnipeds. *Nature Ecology & Evolution*, *4*(8), 1095–1104. https://doi.org/10.1038/s41559-020-1215-5

220. Peralta, D. M., Cappozzo, H. L., Ibañez, E. A., Lucero, S., Failla, M., & Túnez, J. I. (2021). Phylogeography of Otaria flavescens (Carnivora: Pinnipedia): unravelling genetic connectivity at the southernmost limit of its distribution. *Biological Journal of the Linnean Society*, *blab053*. https://doi.org/10.1093/biolinnean/blab053

221. Peterson, B. K., Weber, J. N., Kay, E. H., Fisher, H. S., & Hoekstra, H. E. (2012). Double Digest RADseq: An Inexpensive Method for De Novo SNP Discovery and Genotyping in Model and Non-Model Species. *PLOS ONE*, *7*(5), e37135. https://doi.org/10.1371/journal.pone.0037135

222. Peyrégne, S., & Peter, B. M. (2020). AuthentiCT: A model of ancient DNA damage to estimate the proportion of present-day DNA contamination. *Genome Biology*, *21*(1), 246. https://doi.org/10.1186/s13059-020-02123-y

223. Peyrégne, S., & Prüfer, K. (2020). Present-Day DNA Contamination in Ancient DNA Datasets. *BioEssays*, *42*(9), 2000081. https://doi.org/10.1002/bies.202000081

224. Phillips, C. D., Trujillo, R. G., Gelatt, T. S., Smolen, M. J., Matson, C. W., Honeycutt, R. L., Patton, J. C., & Bickham, J. W. (2009). Assessing substitution patterns, rates and homoplasy at HVRI of Steller sea lions, Eumetopias jubatus. *Molecular Ecology*, *18*(16), 3379–3393. https://doi.org/10.1111/j.1365-294X.2009.04283.x

225. Pinsky, M. L., & Palumbi, S. R. (2014). Meta-analysis reveals lower genetic diversity in overfished populations. *Molecular Ecology*, *23*(1), 29–39. https://doi.org/10.1111/mec.12509

226. Pisoni, J. P., Rivas, A. L., & Piola, A. R. (2015). On the variability of tidal fronts on a macrotidal continental shelf, Northern Patagonia, Argentina. *Deep Sea Research Part II: Topical Studies in Oceanography*, *119*, 61–68. https://doi.org/10.1016/j.dsr2.2014.01.019

227. Polito, M. J., Lynch, H. J., Naveen, R., & Emslie, S. D. (2011). Stable isotopes reveal regional heterogeneity in the pre-breeding distribution and diets of sympatrically breeding Pygoscelis spp. Penguins. *Marine Ecology Progress Series*, *421*, 265–277. https://doi.org/10.3354/meps08863

228. Polito, M. J., Trivelpiece, W. Z., Patterson, W. P., Karnovsky, N. J., Reiss, C. S., & Emslie, S. D. (2015). Contrasting specialist and generalist patterns facilitate foraging niche partitioning in sympatric populations of Pygoscelis penguins. *Marine Ecology Progress Series*, *519*, 221–237. https://doi.org/10.3354/meps11095

229. Ponce, J. F., Rabassa, J., Coronato, A., & Borromei, A. M. (2011). Palaeogeographical evolution of the Atlantic coast of Pampa and Patagonia from the last glacial maximum to the Middle Holocene. *Biological Journal of the Linnean Society*, *103*(2), 363–379. https://doi.org/10.1111/j.1095-8312.2011.01653.x

230. Prieto, A. R., Mourelle, D., Peltier, W. R., Drummond, R., Vilanova, I., & Ricci, L. (2017). Relative sea-level changes during the Holocene in the Río de la Plata, Argentina and Uruguay: A review. *Quaternary International*, *442*, 35–49. https://doi.org/10.1016/j.quaint.2016.02.044

231. Pritchard, J. K., Stephens, M., & Donnelly, P. (2000). Inference of Population Structure Using Multilocus Genotype Data. *Genetics*, *155*(2), 945–959. https://doi.org/10.1093/genetics/155.2.945

232. Privé, F., Luu, K., Vilhjálmsson, B. J., & Blum, M. G. B. (2020). Performing Highly Efficient Genome Scans for Local Adaptation with R Package pcadapt Version 4. *Molecular Biology and Evolution*, *37*(7), 2153–2154. https://doi.org/10.1093/molbev/msaa053

233. Prost, S., Smirnov, N., Fedorov, V. B., Sommer, R. S., Stiller, M., Nagel, D., Knapp, M., & Hofreiter, M. (2010). Influence of Climate Warming on Arctic Mammals? New Insights from Ancient DNA Studies of the Collared Lemming Dicrostonyx torquatus. *PLOS ONE*, *5*(5), e10447. https://doi.org/10.1371/journal.pone.0010447

234. Rambaut, A., Ho, S. Y. W., Drummond, A. J., & Shapiro, B. (2009). Accommodating the Effect of Ancient DNA Damage on Inferences of Demographic Histories. *Molecular Biology and Evolution*, *26*(2), 245–248. https://doi.org/10.1093/molbev/msn256

235. Ramírez, F., Afán, I., Hobson, K. A., Bertellotti, M., Blanco, G., & Forero, M. G. (2014). Natural and anthropogenic factors affecting the feeding ecology of a top marine predator, the Magellanic penguin. *Ecosphere*, *5*(4), art38. https://doi.org/10.1890/ES13-00297.1

236. Ricotta, C., Acosta, A. T. R., Caccianiga, M., Cerabolini, B. E. L., Godefroid, S., & Carboni, M. (2020). From abundance-based to functional-based indicator species. *Ecological Indicators*, *118*, 106761. https://doi.org/10.1016/j.ecolind.2020.106761

237. Riet-Sapriza, F. G., Costa, D. P., Franco-Trecu, V., Marín, Y., Chocca, J., González, B., Beathyate, G., Louise Chilvers, B., & Hückstadt, L. A. (2013). Foraging behavior of lactating South American sea lions (Otaria flavescens) and spatial–temporal resource overlap with the Uruguayan fisheries. *Deep Sea Research Part II: Topical Studies in Oceanography*, *88–89*, 106–119. https://doi.org/10.1016/j.dsr2.2012.09.005

238. Ritchie, P. A., Millar, C. D., Gibb, G. C., Baroni, C., & Lambert, D. M. (2004). Ancient DNA Enables Timing of the Pleistocene Origin and Holocene Expansion of Two Adélie Penguin Lineages in Antarctica. *Molecular Biology and Evolution*, *21*(2), 240–248. https://doi.org/10.1093/molbev/msh012

239. Robbins, C. T., Ben-David, M., Fortin, J. K., & Nelson, O. L. (2012). Maternal condition determines birth date and growth of newborn bear cubs. *Journal of Mammalogy*, *93*(2), 540–546. https://doi.org/10.1644/11-MAMM-A-155.1

240. Robinson, P. W., Simmons, S. E., Crocker, D. E., & Costa, D. P. (2010). Measurements of foraging success in a highly pelagic marine predator, the northern elephant seal. *Journal of Animal Ecology*, *79*(6), 1146-1156. https://doi.org/10.1111/j.1365-2656.2010.01735.x

241. Roeder, A. D., Marshall, R. K., Mitchelson, A. J., Visagathilagar, T., Ritchie, P. A., Love, D. R., Pakai, T. J., McPartlan, H. C., Murray, N. D., Robinson, N. A., Kerry, K. R., & Lambert, D. M. (2001). Gene flow on the ice: Genetic differentiation among Adélie penguin colonies around Antarctica. *Molecular Ecology*, *10*(7), 1645–1656. https://doi.org/10.1046/j.0962-1083.2001.01312.x

242. Rogers, J., Raveendran, M., Harris, R. A., Mailund, T., Leppälä, K., Athanasiadis, G., Schierup, M. H., Cheng, J., Munch, K., Walker, J. A., Konkel, M. K., Jordan, V., Steely, C. J., Beckstrom, T. O., Bergey, C., Burrell, A., Schrempf, D., Noll, A., Kothe, M., … Baboon Genome Analysis Consortium. (2019). The comparative genomics and complex population history of Papio baboons. *Science Advances*, *5*(1), eaau6947. https://doi.org/10.1126/sciadv.aau6947

243. Romero, M. A., Grandi, M. F., Koen-Alonso, M., Svendsen, G., Ocampo Reinaldo, M., García, N. A., Dans, S. L., González, R., & Crespo, E. A. (2017). Analysing the natural population growth of a large marine mammal after a depletive harvest. *Scientific Reports*, *7*(1), 5271. https://doi.org/10.1038/s41598-017-05577-6

244. Romiguier, J., Gayral, P., Ballenghien, M., Bernard, A., Cahais, V., Chenuil, A., Chiari, Y., Dernat, R., Duret, L., Faivre, N., Loire, E., Lourenco, J. M., Nabholz, B., Roux, C., Tsagkogeorga, G., Weber, A. a.-T., Weinert, L. A., Belkhir, K., Bierne, N., … Galtier, N. (2014). Comparative population genomics in animals uncovers the determinants of genetic diversity. *Nature*, *515*(7526), 261–263. https://doi.org/10.1038/nature13685

245. Ropert-Coudert, Y., Bost, C., Handrich, Y., Bevan, R. M., Butler, P. J., Woakes, A. J., & Le Maho, Y. (2000). Impact of Externally Attached Loggers on the Diving Behaviour of the King Penguin. *Physiological and Biochemical Zoology*, *73*(4), 438–444. https://doi.org/10.1086/317743

246. Rosenberg, N. A., & Nordborg, M. (2002). Genealogical trees, coalescent theory and the analysis of genetic polymorphisms. *Nature Reviews Genetics*, *3*(5), 380–390. https://doi.org/10.1038/nrg795

247. Hoelzel, A.R. (1993). Evolution by DNA turnover in the control region of vertebrate mitochondrial DNA. *Current Opinion in Genetics & Development*, *3*(6), 891–895. https://doi.org/10.1016/0959-437X(93)90010-M

248. S, W. (1938). Size of population and breeding structure in relation to evolution. *Science*, *87*, 430–431.

249. Sabrina, H., Gabriela, S., Klemens, P., Thomas, M., & Andrea, R. R. (2020). Niche partitioning between coexisting gentoo Pygoscelis papua and Magellanic penguins Spheniscus magellanicus at Martillo Island, Argentina. *Marine Biology*, *167*(8), 105. https://doi.org/10.1007/s00227-020-03722-w

250. Santamaria, M., Lanave, C., Vicario, S., & Saccone, C. (2007). *Variability of the mitochondrial genome in mammals at the inter-species/intra-species boundary*. *388*(9), 943–946. https://doi.org/10.1515/BC.2007.121

251. Schneider, D. M., Martins, A. B., & de Aguiar, M. A. M. (2016). The mutation-drift balance in spatially structured populations. *Journal of Theoretical Biology*, *402*, 9–17. https://doi.org/10.1016/j.jtbi.2016.04.024

252. Schulz, T. M., & Bowen, W. D. (2005). The Evolution of Lactation Strategies in Pinnipeds: A Phylogenetic Analysis. *Ecological Monographs*, *75*(2), 159–177. https://doi.org/10.1890/04-0319

253. Scioscia, G., Raya Rey, A., Saenz Samaniego, R. A., Florentín, O., & Schiavini, A. (2014). Intra- and interannual variation in the diet of the Magellanic penguin (Spheniscus magellanicus) at Martillo Island, Beagle Channel. *Polar Biology*, *37*(10), 1421–1433. https://doi.org/10.1007/s00300-014-1532-8

254. Scolaro, J. A., Wilson, R. P., Laurenti, S., Kierspel, M., Gallelli, H., & Upton, J. A. (1999). Feeding Preferences of the Magellanic Penguin over Its Breeding Range in Argentina. *Waterbirds: The International Journal of Waterbird Biology*, *22*(1), 104–110. https://doi.org/10.2307/1521999

255. Sealy, J. C., van der Merwe, N. J., Thorp, J. A. L., & Lanham, J. L. (1987). Nitrogen isotopic ecology in southern Africa: Implications for environmental and dietary tracing. *Geochimica et Cosmochimica Acta*, *51*(10), 2707–2717. https://doi.org/10.1016/0016-7037(87)90151-7

256. Sepúlveda, M., & Oliva, D. (2005). Interactions between South American sea lions Otaria flavescens (Shaw) and salmon farms in southern Chile. *Aquaculture Research*, *36*(11), 1062–1068. https://doi.org/10.1111/j.1365-2109.2005.01320.x

257. Sepúlveda, M., Quiñones, R. A., Esparza, C., Carrasco, P., & Winckler, P. (2020). Vulnerability of a top marine predator to coastal storms: A relationship between hydrodynamic drivers and stranding rates of newborn pinnipeds. *Scientific Reports*, *10*(1), 12807. https://doi.org/10.1038/s41598-020-69124-6

258. Silva, A. B., Valls, F. C. L., Marques, F. P., & Bugoni, L. (2022). Movements of satellite tracked Magellanic penguins (Spheniscus magellanicus) in a wintering area in southern Brazil. *Ocean & Coastal Management*, *221*, 106120. https://doi.org/10.1016/j.ocecoaman.2022.106120

259. Silva, L., Saporit, F., Vales, D., Tavares, M., Gandini, P., Crespo, E. A., & Cardona, L. (2014). Differences in diet composition and foraging patterns between sexes of the Magellanic penguin (Spheniscus magellanicus) during the non-breeding period as revealed

by δ13C and δ15N values in feathers and bone. *Marine Biology*, *161*(5), 1195–1206. https://doi.org/10.1007/s00227-014-2410-1

260. Simmons, S., Crocker, D., Hassrick, J., Kuhn, C., Robinson, P., Tremblay, Y., & Costa, D. (2010). Climate-scale hydrographic features related to foraging success in a capital breeder, the northern elephant seal Mirounga angustirostris. *Endangered Species Research*, *10*, 233–243. https://doi.org/10.3354/esr00254

261. Smith, R. J., Hobson, K. A., Koopman, H. N., & Lavigne, D. M. (2011). Distinguishing between populations of fresh- and salt-water harbour seals (Phoca vitulina) using stable-isotope ratios and fatty acid profiles. *Canadian Journal of Fisheries and Aquatic Sciences*. https://doi.org/10.1139/f95-192

262. Soto, K. H., & Trites, A. W. (2011). South American sea lions in Peru have a lek-like mating system. *Marine Mammal Science*, *27*(2), 306–333. https://doi.org/10.1111/j.1748-7692.2010.00405.x

263. Soto, K. H., Trites, A. W., & Arias-Schreiber, M. (2004). The effects of prey availability on pup mortality and the timing of birth of South American sea lions (Otaria flavescens) in Peru. *Journal of Zoology*, *264*(4), 419–428. https://doi.org/10.1017/S0952836904005965

264. Southwell, C., Wotherspoon, S., & Emmerson, L. (2021). Emerging evidence of resource limitation in an Antarctic seabird metapopulation after 6 decades of sustained population growth. *Oecologia*. https://doi.org/10.1007/s00442-021-04958-z

265. Stephens, P. A., Houston, A. I., Harding, K. C., Boyd, I. L., & McNamara, J. M. (2014). Capital and income breeding: The role of food supply. *Ecology*, *95*(4), 882–896. https://doi.org/10.1890/13-1434.1

266. Stokes, D. L., & Boersma, P. D. (1991). Effects of Substrate on the Distribution of Magellanic Penguin (Spheniscus magellanicus) Burrows. *The Auk*, *108*(4), 923–933.

267. Sunde, J., Yıldırım, Y., Tibblin, P., & Forsman, A. (2020). Comparing the Performance of Microsatellites and RADseq in Population Genetic Studies: Analysis of Data for Pike (Esox

lucius) and a Synthesis of Previous Studies. *Frontiers in Genetics*, *0*. https://doi.org/10.3389/fgene.2020.00218

268. Szapkievich, V. B., Cappozzo, H. L., Crespo, E. A., Bernabeu, R. O., Comas, C., & Mudry, M. D. (1999). Genetic relatedness in two Southern sea lion (Otaria flavescens) rookeries in the southwestern Atlantic. *Zeitschrift Fur Saugetierkunde*, *64*(4), 246–250.

269. Szpak, P., & Buckley, M. (2020). Sulfur isotopes (δ34S) in Arctic marine mammals: Indicators of benthic vs. pelagic foraging. *Marine Ecology Progress Series*, *653*, 205–216. https://doi.org/10.3354/meps13493

270. Tagliaferro, M., Kelly, S. P., & Pascual, M. (2020). First study of food webs in a large glacial river: The trophic role of invasive trout. *Neotropical Ichthyology*, *18*. https://doi.org/10.1590/1982-0224-2020-0022

271. Tajima, F. (1983). Evolutionary Relationship Of Dna Sequences In Finite Populations. *Genetics*, *105*(2), 437–460. https://doi.org/10.1093/genetics/105.2.437

272. Tajima, F. (1989). Statistical method for testing the neutral mutation hypothesis by DNA polymorphism. *Genetics*, *123*(3), 585–595. https://doi.org/10.1093/genetics/123.3.585

273. Terhorst, J., Kamm, J. A., & Song, Y. S. (2017). Robust and scalable inference of population history from hundreds of unphased whole genomes. *Nature Genetics*, *49*(2), 303–309. https://doi.org/10.1038/ng.3748

274. Thatje, S., Hillenbrand, C.-D., Mackensen, A., & Larter, R. (2008). Life Hung by a Thread: Endurance of Antarctic Fauna in Glacial Periods. *Ecology*, *89*(3), 682–692. https://doi.org/10.1890/07-0498.1

275. Tian, J. S., Du, J., Lu, Z. C., Zhang, S. J., Song, X. R., & Han, J. B. (2019). Complete mitochondrial genome of South American sea lion Otaria byronia (Carnivora: Otariidae). *Mitochondrial DNA Part B*, *4*(1), 2065-2066.

276. Tian, J., Du, J., Han, J., Li, D., & Song, X. (2021). Complete Mitochondrial Genome of the South American Fur Seal Arctocephalus australis (Carnivora: Otariidae) and Its Phylogenetic Implications. *Russian Journal of Genetics*, *57*, 582-590.

277. Torchin, M. E., & Lafferty, K. D. (2009). Escape from Parasites. In G. Rilov & J. A. Crooks (Eds.), *Biological Invasions in Marine Ecosystems: Ecological, Management, and Geographic Perspectives* (pp. 203–214). Springer. https://doi.org/10.1007/978-3-540-79236-9_11

278. Torchin, M. E., Lafferty, K. D., Dobson, A. P., McKenzie, V. J., & Kuris, A. M. (2003). Introduced species and their missing parasites. *Nature*, *421*(6923), 628–630. https://doi.org/10.1038/nature01346

279. Trivelpiece, W. Z., Hinke, J. T., Miller, A. K., Reiss, C. S., Trivelpiece, S. G., & Watters, G. M. (2011). Variability in krill biomass links harvesting and climate warming to penguin population changes in Antarctica. *Proceedings of the National Academy of Sciences*, *108*(18), 7625–7628. https://doi.org/10.1073/pnas.1016560108

280. Trucchi, E., Gratton, P., Whittington, J. D., Cristofari, R., Le Maho, Y., Stenseth, N. C., & Le Bohec, C. (2014). King penguin demography since the last glaciation inferred from genome-wide data. *Proceedings of the Royal Society B: Biological Sciences*, *281*(1787), 20140528. https://doi.org/10.1098/rspb.2014.0528

281. Túnez, J. I., Cappozzo, H. L., & Cassini, M. H. (2008). Natural and anthropogenic factors associated with the distribution of South American sea lion along the Atlantic coast. *Hydrobiologia*, *598*(1), 191–202. https://doi.org/10.1007/s10750-007-9150-x

282. Túnez, J. I., Cappozzo, H. L., Nardelli, M., & Cassini, M. H. (2010). Population genetic structure and historical population dynamics of the South American sea lion, Otaria flavescens, in north-central Patagonia. *Genetica*, *138*(8), 831–841. https://doi.org/10.1007/s10709-010-9466-8

283. Túnez, J. I., Centrón, D., Cappozzo, H. L., & Cassini, M. H. (2007). Geographic distribution and diversity of mitochondrial DNA haplotypes in South American sea lions (Otaria flavescens) and fur seals (Arctocephalus australis). *Mammalian Biology*, *72*(4), 193–203. https://doi.org/10.1016/j.mambio.2006.08.002

284. Vianna, J. A., Fernandes, F. A. N., Frugone, M. J., Figueiró, H. V., Pertierra, L. R., Noll, D., Bi, K., Wang-Claypool, C. Y., Lowther, A., Parker, P., Le Bohec, C., Bonadonna, F., Wienecke, B., Pistorius, P., Steinfurth, A., Burridge, C. P., Dantas, G. P. M., Poulin, E., Simison, W. B., … Bowie, R. C. K. (2020). Genome-wide analyses reveal drivers of penguin diversification. *Proceedings of the National Academy of Sciences*, *117*(36), 22303–22310. https://doi.org/10.1073/pnas.2006659117

285. Vila, A. R., Campagna, C., Iñíguez, M., & Falabella, V. (2008). South American Sea Lions (Otaria flavescens) Avoid Killer Whale (Orcinus orca) Predation. *Aquatic Mammals*, *34*(3), 317–330. https://doi.org/10.1578/AM.34.3.2008.317

286. Vilata, J., Oliva, D., & Sepúlveda, M. (2010). The predation of farmed salmon by South American sea lions (Otaria flavescens) in southern Chile. *ICES Journal of Marine Science*, *67*(3), 475–482. https://doi.org/10.1093/icesjms/fsp250

287. Violante, R. A., Paterlini, C. M., Marcolini, S. I., Costa, I. P., Cavallotto, J. L., Laprida, C., Dragani, W., García Chapori, N., Watanabe, S., Totah, V., Rovere, E. I., & Osterrieth, M. L. (2014). Chapter 6 The Argentine continental shelf: Morphology, sediments, processes and evolution since the Last Glacial Maximum. *Geological Society, London, Memoirs*, *41*(1), 55–68. https://doi.org/10.1144/M41.6

288. Waldmann, N., Ariztegui, D., Anselmetti, F. S., Austin, J. A., Moy, C. M., Stern, C., Recasens, C., & Dunbar, R. B. (2010). Holocene climatic fluctuations and positioning of the Southern Hemisphere westerlies in Tierra del Fuego (54° S), Patagonia. *Journal of Quaternary Science*, *25*(7), 1063–1075. https://doi.org/10.1002/jqs.1263

289. Walker, M. J. C., Berkelhammer, M., Björck, S., Cwynar, L. C., Fisher, D. A., Long, A. J., Lowe, J. J., Newnham, R. M., Rasmussen, S. O., & Weiss, H. (2012). Formal subdivision of the Holocene Series/Epoch: A Discussion Paper by a Working Group of INTIMATE (Integration of ice-core, marine and terrestrial records) and the Subcommission on Quaternary Stratigraphy (International Commission on Stratigraphy). *Journal of Quaternary Science*, *27*(7), 649–659. https://doi.org/10.1002/jqs.2565

290. Waltoft, B. L., & Hobolth, A. (2018). Non-parametric estimation of population size changes from the site frequency spectrum. *Statistical Applications in Genetics and Molecular Biology*, *17*(3). https://doi.org/10.1515/sagmb-2017-0061

291. Wang, K., Lenstra, J. A., Liu, L., Hu, Q., Ma, T., Qiu, Q., & Liu, J. (2018). Incomplete lineage sorting rather than hybridization explains the inconsistent phylogeny of the wisent. *Communications Biology*, *1*(1), 1–9. https://doi.org/10.1038/s42003-018-0176-6

292. Webster, M. T., Axelsson, E., & Ellegren, H. (2006). Strong Regional Biases in Nucleotide Substitution in the Chicken Genome. *Molecular Biology and Evolution*, *23*(6), 1203–1216. https://doi.org/10.1093/molbev/msk008

293. Welch, B. L. (1947). The Generalization Of 'Student's' Problem When Several Different Population Varlances Are Involved. *Biometrika*, *34*(1–2), 28–35. https://doi.org/10.1093/biomet/34.1-2.28

294. White, T. A., Fotherby, H. A., Stephens, P. A., & Hoelzel, A. R. (2011). Genetic panmixia and demographic dependence across the North Atlantic in the deep-sea fish, blue hake (Antimora rostrata). *Heredity*, *106*(4), 690–699. https://doi.org/10.1038/hdy.2010.108

295. Wolf, J., Harrod, C., Brunner, S., Salazar, S., Trillmich, F., & Tautz, D. (2008). Tracing early stages of species differentiation: Ecological, morphological and genetic divergence of Galápagos sea lion populations. *BMC Evolutionary Biology*, *8*, 150. https://doi.org/10.1186/1471-2148-8-150

296. Wolff, E. W., Fischer, H., Fundel, F., Ruth, U., Twarloh, B., Littot, G. C., Mulvaney, R., Röthlisberger, R., de Angelis, M., Boutron, C. F., Hansson, M., Jonsell, U., Hutterli, M. A., Lambert, F., Kaufmann, P., Stauffer, B., Stocker, T. F., Steffensen, J. P., Bigler, M., … Gaspari, V. (2006). Southern Ocean sea-ice extent, productivity and iron flux over the past eight glacial cycles. *Nature*, *440*(7083), 491–496. https://doi.org/10.1038/nature04614

297. Wood, S. N. (2011). Fast stable restricted maximum likelihood and marginal likelihood estimation of semiparametric generalized linear models. *Journal of the Royal Statistical Society: Series B (Statistical Methodology)*, *73*(1), 3–36. https://doi.org/10.1111/j.1467-9868.2010.00749.x

298. Woodland, R. J., & Secor, D. H. (2013). Benthic-pelagic coupling in a temperate inner continental shelf fish assemblage. *Limnology and Oceanography*, *58*(3), 966–976. https://doi.org/10.4319/lo.2013.58.3.0966

299. Woolway, R. I., Dokulil, M. T., Marszelewski, W., Schmid, M., Bouffard, D., & Merchant, C. J. (2017). Warming of Central European lakes and their response to the 1980s climate regime shift. *Climatic Change*, *142*(3–4), 505–520. https://doi.org/10.1007/s10584-017-1966-4

300. Wright, J. P., & Jones, C. G. (2006). The Concept of Organisms as Ecosystem Engineers Ten Years On: Progress, Limitations, and Challenges. *BioScience*, *56*(3), 203–209. https://doi.org/10.1641/0006-3568(2006)056[0203:TCOOAE]2.0.CO;2

301. Xu, S., Zhao, L., Xiao, S., & Gao, T. (2019). Whole genome resequencing data for three rockfish species of Sebastes. *Scientific Data*, *6*(1), 97. https://doi.org/10.1038/s41597-019-0100-z

302. Xue, A. T., & Hickerson, M. J. (2017). multi-dice: R package for comparative population genomic inference under hierarchical co-demographic models of independent single-population size changes. *Molecular Ecology Resources*, *17*(6), e212–e224. https://doi.org/10.1111/1755-0998.12686

303. Yorio, P., González-Zevallos, D., Gatto, A., Biagioni, O., & Castillo, J. (2017). Relevance of forage fish in the diet of Magellanic penguins breeding in northern Patagonia, Argentina. *Marine Biology Research*, *13*(6), 603–617. https://doi.org/10.1080/17451000.2016.1273529

304. Younger, J., Emmerson, L., Southwell, C., Lelliott, P., & Miller, K. (2015b). Proliferation of East Antarctic Adélie penguins in response to historical deglaciation. *BMC Evolutionary Biology*, *15*(1), 236. https://doi.org/10.1186/s12862-015-0502-2

305. Younger, J. L., Clucas, G. V., Kooyman, G., Wienecke, B., Rogers, A. D., Trathan, P. N., Hart, T., & Miller, K. J. (2015a). Too much of a good thing: Sea ice extent may have forced emperor penguins into refugia during the last glacial maximum. *Global Change Biology*, *21*(6), 2215–2226. https://doi.org/10.1111/gcb.12882

306. Yuan, Y., Zhang, Y., Zhang, P., Liu, C., Wang, J., Gao, H., Hoelzel, A. R., Seim, I., Lv, M., Lin, M., Dong, L., Gao, H., Yang, Z., Caruso, F., Lin, W., Fonseca, R. R. da, Wang, D., Wang, X., Rasmussen, M. H., … Li, S. (2021). Comparative genomics provides insights into the aquatic adaptations of mammals. *Proceedings of the National Academy of Sciences*, *118*(37). https://doi.org/10.1073/pnas.2106080118

307. Yurkowski, D. J., Ferguson, S., Choy, E. S., Loseto, L. L., Brown, T. M., Muir, D. C., ... & Fisk, A. T. (2016). Latitudinal variation in ecological opportunity and intraspecific competition indicates differences in niche variability and diet specialization of Arctic marine predators. *Ecology and Evolution*, *6*(6), 1666-1678. https://doi.org/10.1002/ece3.1980

308. Zangrando, A. F. J., & Tivoli, A. M. (2015). Human use of birds and fish in marine settings of southern Patagonia and Tierra del Fuego in the Holocene: A first macro-regional approach. *Quaternary International*, *373*, 82–95. https://doi.org/10.1016/j.quaint.2014.11.047

309. Zenteno, L., Borella, F., Otero, J. G., Piana, E., Belardi, J. B., Borrero, L. A., Saporiti, F., Cardona, L., & Crespo, E. (2015b). Shifting niches of marine predators due to human exploitation: The diet of the South American sea lion (Otaria flavescens) since the late

Holocene as a case study. *Palaeobiology*, *41*(3), 387–401. https://doi.org/10.1017/pab.2015.9

310. Zenteno, L., Crespo, E., Goodall, N., Aguilar, A., Oliveira, L. de, Drago, M., Secchi, E. R., Garcia, N., & Cardona, L. (2013). Stable isotopes of oxygen reveal dispersal patterns of the South American sea lion in the southwestern Atlantic Ocean. *Journal of Zoology*, *291*(2), 119–126. https://doi.org/10.1111/jzo.12051

311. Zenteno, L., Crespo, E., Vales, D., Silva, L., Saporiti, F., Oliveira, L. R., Secchi, E. R., Drago, M., Aguilar, A., & Cardona, L. (2015a). Dietary consistency of male South American sea lions (Otaria flavescens) in southern Brazil during three decades inferred from stable isotope analysis. *Marine Biology*, *162*(2), 275–289. https://doi.org/10.1007/s00227-014-2597-1

312. Zhou, B., Wen, S., Wang, L., Jin, L., Li, H., & Zhang, H. (2017). AntCaller: An accurate variant caller incorporating ancient DNA damage. *Molecular Genetics and Genomics*, *292*(6), 1419–1430. https://doi.org/10.1007/s00438-017-1358-5

313. Zhou, X., Wang, B., Pan, Q., Zhang, J., Kumar, S., Sun, X., Liu, Z., Pan, H., Lin, Y., Liu, G., Zhan, W., Li, M., Ren, B., Ma, X., Ruan, H., Cheng, C., Wang, D., Shi, F., Hui, Y., … Li, M. (2014). Whole-genome sequencing of the snub-nosed monkey provides insights into folivory and evolutionary history. *Nature Genetics*, *46*(12), 1303–1310. https://doi.org/10.1038/ng.3137